

The Oxidation of Organic Films on Cloud Droplets

Claire Olivia Mary Lucas

M.Sci. (Hons.)

A thesis submitted for the degree of Doctor of Philosophy at the
University of London.

Department of Earth Sciences

Royal Holloway College

University of London

May 2012

This thesis was funded by a studentship from the Natural Environment Research Council (NERC): NE/F007116/1. The neutron reflectometry experimental work was funded by the Science and Technology Facilities Council (STFC) with training partly funded by the Royal Holloway Department of Earth Sciences research committee.



Cloud Formation at the ILL Grenoble, France

‘An understanding of the natural world and what's in it is a source of not only a great curiosity but great fulfilment.’ David Attenborough

The work in this thesis was a collaboration between the author (conducting experiments, fitting of the neutron data and running the kinetic fitting regimes on the experimental data, subsequent data analysis and writing of the thesis), Martin King (deciphering the kinetic mechanisms and author of the kinetic fitting algorithms), Christian Pfrang (calibration of ozoniser and experimental support) and Adrian Rennie (experimental support and author of the neutron data fitting programs used, structural data fitting in chapter 3) and is therefore not exclusively the authors own work. Where a contribution is made by another individual other than the author, this is pointed out in the text. The writing of the thesis was completed solely by the author.

Signature: *C. Lucas*

Date: 21/05/2012

Abstract

Cloud droplets in the atmosphere have an organic component which has been shown to form a monolayer film at the air-water interface of the cloud droplet and the atmosphere. The process by which a cloud droplet film will oxidise and the persistence or loss of an oxidised organic film from the air-liquid interface of a cloud droplet is not well quantified. To determine the surface properties of a cloud droplet film during atmospheric oxidation a measurement of a kinetic variable, the concentration of material comprising an organic film, during reaction with atmospheric radicals was required. The coupling of a Langmuir trough with a neutron reflectometer allows the measurement of the surface coverage of a monolayer in unison with measurement of the monolayer surface pressure. The technique of coupling a Langmuir trough with neutron reflectometry is used extensively for research into the properties of surfactants for industrial and medicinal use. This thesis builds on the work of King et al., (2009) and King et al., (2010), whom produced the first neutron reflectivity measurements of atmospheric proxy monolayers reacting with ozone. This is the first thesis detailing the neutron reflectometry measurement from an atmospheric perspective. Measurements were taken of representative fatty acid molecules which have atmospheric relevance (stearic acid, oleic acid and methyl oleate) as well as measurements of phospholipid molecules which are potential parent species for the fatty acids found in atmospheric waters (1,2-dipalmitoyl-*sn*-glycero-3-phosphocholine). The monolayers were reacted with aqueous phase OH radical and with gas-phase ozone to assess the kinetics of the oxidation of the monolayers at the air-water interface.

Title Page	1-2
Abstract	3
Table of Contents	4-15
List of Figures	16-31
List of Tables	32-34
Acknowledgements	35
Chapter 1: <i>The Oxidation of Cloud Droplet Films</i>	
1.1 Outline and Aims of the Thesis	36
1.2 The Role of Atmospheric Aerosol in Climate and Cloud Formation	37
1.3 The Nucleation of Cloud Droplets on Atmospheric Aerosol Particles	41
1.4 The Physical and Chemical Composition of Cloud Droplets	45
1.5 Cloud Droplet Organic Films	46
1.5.1 Evidence for Coated Droplets	48
1.5.2 Proposed Models of Cloud Droplet Films	51
1.5.3 Experiments on Atmospheric Films	53
1.5.4 The Climatic Effect of Cloud Droplet Film Oxidation	58
1.6 Using the Neutron Reflectometry Technique to Study Atmospheric Monolayers	59
References	62
Chapter 2: <i>Hydroxyl Radical Oxidation of Stearic Acid Monolayers</i>	
2.0 Abstract	69
2.1 Introduction	69
2.2 Aims	70
2.3 Background	70

2.3.1	Stearic Acid and Cloud Droplet Films	71
2.3.2	Oxidation of Cloud Droplet Films	72
2.3.3	Hydroxyl Radical Formation in Cloud Droplets	74
	1. Hydrogen Peroxide Photolysis and the Haber-Weiss Cycle	75
	2. Gas-Phase OH Radical Uptake into a Cloud Droplet	76
	3. Nitrate Photolysis	76
	4. The Photo-Fenton Cycle	77
	5. Photosensitization of Natural Organic Molecules	78
2.3.4	The Reaction of OH and Stearic Acid	80
2.4	Experimental	81
2.4.1	Measurement Techniques	82
2.4.2	Measuring Surface Pressure. The Wilhelmy Plate Balance and the Langmuir Trough	82
2.4.3	Measuring the Monolayer Surface Coverage with Neutron Reflectometry	85
2.4.3.1	Neutron Sub-Atomic Particles as a Tool for Measurement	85
2.4.3.2	The Generation of Neutrons at ISIS, Rutherford Appleton Laboratory, UK	86
2.4.3.3	The Basic Principles of Neutron Reflectometry	87
2.4.3.4	Neutron Scattering Theory	87
2.4.3.5	The SURF Reflectometer: Neutron Reflectometry at the Air-Water Interface	90
2.4.3.6	The Time of Flight Principle	94
2.4.3.7	Fitting of Reflectivity Data to Determine the Surface Coverage	98

2.4.3.8	Measuring the Error in Neutron Reflectivity Data	101
2.4.4	Brewster Angle Microscopy	103
2.4.5	Generating Aqueous Phase OH Radical During an Experiment	104
2.4.5.1	Photolysis Lamp Calibration by Chemical Actinometry	105
2.4.5.2	Actinometry Procedure	107
2.4.5.3	Actinometry Materials	109
2.4.5.4	Actinometry Chemicals	109
2.4.5.5	Actinometry Solutions	110
2.4.6	Determining the OH Radical Concentration in the Subphase with Titrations and Numerical Modelling	111
2.4.6.1	Titration Procedure	111
2.4.6.2	Titration Materials	113
2.4.6.3	Titration Chemicals	114
2.4.6.4	Titration Solutions	114
2.4.7	Kinetic Modelling of the Aqueous OH Radical Concentration	115
2.4.7.1	Modelling the Subphase OH Concentration During a Photolysis Reaction with Hydrogen Peroxide	115
2.5	Kinetic Analysis Methodology	117
2.5.1	Exponential Decay	117
2.5.2	Degradation Mechanism	118
2.5.3	Rate Limitation	120
2.6	The Methodology of a Typical Combined Surface Coverage and Surface Pressure Measurement	121
2.6.1	Sample Environment	121

2.6.2	Cleaning the Langmuir Trough	121
2.6.3	Controlling the Temperature of the Subphase	122
2.6.4	Experimental Methodology	122
2.6.4.1	Methodology for Varied Subphase H ₂ O ₂ Concentrations	123
2.6.4.2	Methodology for Varied Subphase Temperature Experiments	123
2.6.4.3	Equipment	123
2.6.4.4	Chemicals	124
2.7	Results	125
2.7.1	Preliminary Experiments	125
2.7.1.1	Aims of the Preliminary Langmuir Trough Experiments	125
2.7.1.2	Results of the Preliminary Langmuir Trough Experiments	126
2.7.2	Neutron Surface Coverage and Surface Pressure Measurement of The Decay of Stearic Acid Monolayers on a Subphase of Varied OH Radical Concentration	128
2.7.3	Neutron Surface Coverage and Surface Pressure Measurement of The Decay of Stearic Acid Monolayers on a Subphase of Varied Temperature	135
2.7.4	Summary of the Experimental Results	144
2.7.5	The Kinetic Analysis of the Surface Coverage Data	145
2.7.6	Brewster Angle Microscopy Images of Stearic Acid Monolayers Before and During Oxidation	152
2.7.7	Summary of Kinetic Results	163
2.8	Discussion	163
2.8.1	Discussion of the Experimental Surface Pressure and Surface	

Coverage Results	164
2.8.2 Discussion of the Kinetic Results	164
2.8.3 Discussion of the Possible Chemical Mechanism for the Reaction Between Aqueous OH Radical and a Stearic Acid Monolayer	166
2.8.4 The Proposed Chemical Mechanism for the Oxidation of a Stearic Acid Monolayer by OH Radical	167
2.8.5 Atmospheric Implications: Chemical Lifetime	172
2.8.6 Discussion of the Atmospheric Implications of the Reaction and the Atmospheric Lifetime of a Stearic Acid Monolayer Exposed to Aqueous OH Radical	173
2.9 Conclusions	174
References	175
Chapter 3: <i>The Oxidation of Oleic Acid Monolayers with Gas Phase Ozone</i>	
3.0 Abstract	182
3.1 Introduction	182
3.2 Aims	183
3.3 Background	183
3.4 Oleic Acid and Cloud Droplets	184
3.5 Formation of Gas-Phase Ozone in the Troposphere	188
3.5.1 Photochemical Formation of Ozone from Oxides of Nitrogen	188
3.5.2 Ozone Concentrations in the Troposphere	189
3.5.3 The Effect of Aerosol and Clouds on Ozone Concentrations in the Troposphere	191
3.6 Previous Atmospheric Studies of Oleic Acid and Ozone	192

3.6.1	Laboratory Studies of Oleic Acid Aerosol and Droplets	
	Reacting with Ozone	192
	3.6.1.1 Particle Phase Experiments	192
	3.6.1.2 Surface Pressure and Surface Tension Measurements of Oleic Acid Monolayers Reacting with Ozone	194
3.6.2	Issues Identified in the Current Literature to be Investigated in This Work	197
3.7	Experimental Methodology	198
	3.7.1 Experimental Objectives	198
	3.7.2 Oleic Acid Samples	200
	3.7.3 Surface Measurement Techniques	201
	3.7.3.1 The Neutron Reflectometer FIGARO	202
	3.7.3.2 The Effect of Partial Deuteration of a Monolayer on Neutron Reflectivity Measurements	206
	3.7.3.3 Obtaining Structural Neutron Reflectometry Measurements	207
	3.7.4 Generating Gas-Phase Ozone	210
	3.7.4.1 Determining the Concentration of Ozone	211
	3.7.5 The Experimental Methodology of a Typical Neutron Reflectivity Experiment with a Gas-Phase Reactant	213
	3.7.6 Kinetics of the Reaction of an Oleic Acid Monolayer with Gas-Phase Ozone	214
	3.7.6.1 The Decay Mechanism	214
	3.7.6.2 The Method of Kinetic Analysis	215
3.8	Experimental Results	217

3.8.1	The Surface Pressure and Surface Coverage of Fully Deuterated Oleic Acid Monolayers Exposed to High Concentrations of Gas-Phase Ozone	218
3.8.2	The Surface Pressure and Surface Coverage of Fully Deuterated Oleic Acid Monolayers Exposed to Low Concentrations of Gas-Phase Ozone	225
3.8.3	The Surface Pressure and Surface Coverage of Fully and Partially Deuterated Oleic Acid Monolayers in Oxygen	236
3.8.4	The Surface Pressure and Surface Coverage of Fully and Partially Deuterated Oleic Acid Monolayers on a pH Adjusted Subphase Exposed to Gas-Phase Ozone	239
3.8.5	Summary of the Surface Coverage and Surface Pressure Measurement Results	244
3.8.6	Structural Neutron Reflectivity Measurements of Fully Deuterated and Partially Deuterated Oleic Acid Monolayers at the Air-Water Interface	245
3.8.7	Kinetic Analysis and Results for the Decay in the Surface Coverage of Oleic Acid Monolayers Reacting with Gas-Phase Ozone	248
3.9	Discussion	256
3.9.1	The Contamination of the Oxford Isotope Facility Fully Deuterated Oleic Acid Sample	257
3.9.2	Comparison to Previous Studies of Oleic Acid at the Air-Water Interface: Discussion of the Kinetic Results	259
3.9.3	The Mechanism of Ozonolysis of an Oleic Acid Monolayer	260
3.9.4	The Fate of the Potential Reaction Products	267

3.9.5	Discussion of the Mechanism	268
3.9.6	Discussion of the Ozone Uptake Coefficient	272
3.10	The Atmospheric Monolayer Lifetime	275
3.11	Conclusions	276
3.12	Suggestions for Further Work	276
	References	277
Chapter 4: <i>The Oxidation of Mixed Composition Monolayers</i>		
4.0	Abstract	285
4.1	Introduction	285
4.2	Aims	285
4.3	Background	286
4.4	Previous Studies of Mixed Composition Saturated with Unsaturated Molecular Constituent Monolayers Reacting with Ozone	289
4.5	Experimental Methodology	290
4.5.1	Experimental Objectives	290
4.5.2	The Oleic Acid and Stearic Acid Samples	291
4.5.3	Experimental Method	293
4.5.4	Ozone Generation	294
4.5.4.1	Calculating the Concentration of Gas-Phase Ozone	295
4.5.5	The Method of Kinetic Analysis	295
4.6	Results	297
4.6.1	A Deuterated Stearic Acid Monolayer Decaying in the Presence of Gas-Phase Ozone	297
4.6.2	A Deuterated Oleic Acid Monolayer Decaying in the Presence of	

Gas-Phase Ozone	298
4.6.3 Monolayers of Deuterated Stearic Acid Mixed with Non-Deuterated Oleic Acid	299
4.6.4 Monolayers of Deuterated Oleic-Acid Mixed with Non-Deuterated Stearic Acid	304
4.6.5 Summary of the Experimental Results	308
4.6.6 Kinetic Results	309
4.7 Discussion	310
4.7.1 Discussion of the Contribution of Hydrogen Scattering of Neutrons to the Surface Coverage Measurements	310
4.7.2 Discussion of the Results in the Context of Other Studies	313
4.8 Conclusions	316
References	317
Chapter 5: <i>The Oxidation of Methyl Oleate Monolayers by Ozone</i>	
5.0 Abstract	320
5.1 Introduction	320
5.2 Aims	320
5.3 Background	321
5.4 Methyl Oleate and Cloud Droplets	322
5.5 Previous Atmospheric Studies of Methyl Oleate Reacting with Ozone	323
5.6 Experimental Methodology	324
5.6.1 Experimental Objectives	324
5.6.2 The Deuterated Methyl Oleate Sample	324
5.6.3 Generating and Determining the Concentration of Gas-Phase Ozone	325

5.6.4	The Experimental Methodology	327
5.6.5	The Reaction Kinetics of a Methyl Oleate Monolayer Reacting with Gas-Phase Ozone	329
5.6.5.1	The Decay Mechanism	329
5.7	Experimental Results	333
5.7.1	The Surface Coverage and Surface Pressure of Methyl Oleate Monolayers Exposed to Gas-Phase Ozone	334
5.7.2	The Surface Coverage and Surface Pressure of Methyl Oleate Monolayers in an Oxygen Atmosphere	343
5.7.3	A Summary of the Surface Pressure and Surface Coverage Results	344
5.7.4	Kinetic Results	347
5.8	Discussion	352
5.8.1	Discussion of the Surface Coverage and Surface Pressure Results	352
5.8.2	Discussion of the Kinetic Results	353
5.8.3	A Proposed Mechanism for the Reaction of Ozone with a Methyl Oleate Monolayer	355
5.8.3.1	Reaction Products Formed by the Ozonolysis of Methyl Oleate	365
5.9	The Atmospheric Monolayer Lifetime	368
5.10	Suggested Further Research	368
5.11	Conclusions	369
	References	370
Chapter 6:	<i>The Oxidation of Phospholipid Monolayers</i>	
6.0	Abstract	373
6.1	Introduction	373

6.2	Aims	374
6.3	Background	374
6.3.1	Phospholipids and the Atmosphere	374
6.3.2	Lipid Oxidation	376
6.4	Experimental Methodology	378
6.4.1	Experimental Objectives	379
6.4.2	DPPC Samples	380
6.4.3	The Generation of Aqueous Hydroxyl Radical	382
6.4.4	The Neutron Reflectivity Experimental Method	383
6.4.4.1	Stability of the Neutron Beam	385
6.4.5	The Neutron Reflectivity Data Fitting	385
6.5	Results	387
6.5.1	The Decay of the Fully Deuterated DPPC Monolayers Reacting with Aqueous OH Radical	387
6.5.2	The Decay of the Head Group Deuterated DPPC Monolayers Reacting with Aqueous OH Radical	389
6.5.3	The Decay of the Tail Group Deuterated DPPC Monolayers Reacting with Aqueous OH Radical	391
6.5.4	The Photolysis Only Decay of a Fully Deuterated DPPC Monolayer on a Subphase of Null Reflective Water	393
6.5.5	The Decay of a Fully Deuterated DPPC Monolayer on a Subphase of H ₂ O ₂ Without Photolysis	394
6.5.6	Summary of Experimental Results	395
6.6	Discussion of the Atmospheric Implications of the Oxidation of Phospholipids	

At the Air-Water Interface	399
References	402
Chapter 7: <i>Synthesis of the Experimental Results</i>	
7.1 A Summary of the Key Results	404
7.1.1 The Oxidation of Stearic Acid Monolayers by Aqueous OH Radical	404
7.1.2 The Oxidation of Oleic Acid Monolayers Initiated by Gas-Phase Ozone	405
7.1.3 The Oxidation of Mixed Oleic and Stearic Acid Monolayers Initiated By Gas-Phase Ozone	406
7.1.4 The Oxidation of Methyl Oleate Monolayers Initiated by Gas-Phase Ozone	407
7.1.5 The Oxidation of Phospholipid Monolayers Initiated by Aqueous OH Radical	407
7.2 A Summary of the Kinetic Results	408
7.3 Atmospheric Implications of the Findings of this Work	409
7.4 Ideas for Further Development of the Work	411
7.5 Conclusions	412
References	413

Appendices

Appendices to Chapter 3

<i>Item 1</i>	<i>The Differential Equations Used to Calculate the Concentration of Gas-phase Ozone in the Reaction Chamber during an Experiment</i>	414
<i>Item 2</i>	<i>An Explanation of the Choice of Kinetic Fitting Regime for Oleic Acid Monolayers Reacting with Gas-Phase Ozone Absorbed to the Monolayer Region</i>	415
<i>Item 3</i>	<i>The Application of Mixing Time to the Decay of Oleic Acid Monolayers Exposed to Gas Phase Ozone</i>	416

Appendices to Chapter 5

<i>Item 4</i>	<i>The Derivation of the Rate Expression for a Methyl Oleate Monolayer Reacting with Gas-phase Ozone</i>	418
---------------	--	-----

List of Figures

Chapter 1:

<i>1.1</i>	<i>The Size and Number Distribution of Common Atmospheric Aerosol Particles</i>	39
<i>1.2</i>	<i>The Nucleation of Cloud Droplets on Atmospheric Aerosol Particles</i>	41
<i>1.3</i>	<i>The Growth of a Cloud Droplet Along a Curve of Supersaturation of an Air Parcel with Water Vapour versus Particle Radius as Modelled by King et al., (2009)</i>	43
<i>1.4</i>	<i>The Effect of Droplet Curvature on the Equilibrium Vapour Pressure, the Kelvin Effect</i>	45
<i>1.5</i>	<i>The Spreading of a Monolayer on an Atmospheric Droplet to Minimize the Surface Free Energy</i>	47
<i>1.6</i>	<i>The Organic Amphiphile-Aqueous Subphase Contact Angle</i>	48
<i>1.7</i>	<i>The Core-Shell Morphology of a Cloud Droplet with a Monolayer</i>	

	<i>at the Air-Water Interface</i>	51
1.8	<i>The Functionalized Head Groups of the Surface Active Components of Cloud Droplet Monolayers</i>	52
1.9	<i>Image of a Langmuir Trough with a Wilhelmy Plate Balance</i>	55
1.10	<i>The Wilhelmy Plate at the Air-Water Interface Showing the Perimeter and Contact Angles used to Calculate the Surface Pressure of a Monolayer</i>	56
Chapter 2:		
2.1	<i>The Structure of Stearic Acid</i>	71
2.2	<i>The Addition of OH to a Double Bond and the Abstraction of Hydrogen by OH from a Single Hydrocarbon Bond</i>	73
2.3	<i>Gas-Phase and Liquid-Phase Cycling of OH in the Atmosphere</i>	75
2.4	<i>The Photo-Fenton Cycle</i>	77
2.5	<i>The Photosensitization Reaction Cycle Which Contributes to OH Production</i>	79
2.6	<i>The Langmuir Trough</i>	83
2.7	<i>The Surface Pressure-Area Isotherm of Stearic Acid at the Air-Water Interface as Measured on a Langmuir Trough</i>	84
2.8	<i>The Reflection and Refraction of Neutrons at an Air-Monolayer-Liquid Interface</i>	90
2.9	<i>The Components of the Reflectometer SURF at ISIS</i>	91
2.10	<i>SURF with the Langmuir Trough in Situ, as Set Up for an Experiment</i>	93
2.11	<i>The Reflectivity Profile of a Stearic Acid Monolayer at the Air-water Interface on a Subphase of $2.35 \text{ mol dm}^{-3} \text{H}_2\text{O}_2$</i>	94
2.12	<i>The Compositional Profile of a Monolayer of Stearic Acid Normal to the Air-Water Interface</i>	96
2.13	<i>Reflectivity versus Momentum Transfer of an Oleic Acid Monolayer Exposed to Gas Phase Ozone Measured on the Neutron Reflectometer FIGARO</i>	98
2.14	<i>The Brewster Angle Microscope with the Langmuir Trough Positioned for Imaging</i>	104

2.15	<i>The Fe(II) Absorbance versus Fe(II) Concentration</i>	108
2.16	<i>The Intensity of the 254nm Photolysis Lamp over Time</i>	109
2.17	<i>The Subphase H₂O₂ Concentration as Measured by Titration, for Lamp Configuration A and Lamp Configuration B</i>	113
2.18	<i>The Modelled OH Concentration in a Subphase of 0.0882 mol dm⁻³ H₂O₂</i>	116
2.19	<i>The Aluminium Reaction Chamber Housing the Langmuir Trough</i>	121
2.20	<i>The Langmuir Trough within the Aluminium Reaction Chamber</i>	122
2.21	<i>The Kinetic Decay in the Surface Pressure of a 30μL Monolayer of 1mg/ mL Stearic Acid on an H₂O Subphase With and Without the Photolysis Lamp at 20°C Conducted on the Royal Holloway Langmuir Trough</i>	126
2.22	<i>The Kinetic Decay of a 30μL Monolayer of 1mg/ mL Stearic Acid on an H₂O₂ Subphase With and Without the Photolysis Lamp at 20°C Conducted on the Royal Holloway Langmuir Trough</i>	127
2.23	<i>A 30μL Monolayer of 1mg/ mL Stearic Acid on an H₂O₂ Subphase With Photolysis at 20°C Conducted on the Royal Holloway Langmuir Trough</i>	128
2.24	<i>The Surface Coverage and Surface Pressure Kinetic Decay of a Stearic Acid Monolayer on a Subphase of 0.294 mol dm⁻³H₂O₂ / 8.6 × 10¹² mol dm⁻³ OH with a Kinetic Degradation Fit of Equation 2.45 to the Surface Coverage Data</i>	129
2.25	<i>The Surface Coverage and Surface Pressure Kinetic Decay of a Stearic Acid Monolayer on a Subphase of 0.588 mol dm⁻³H₂O₂ / 8.7 × 10¹² mol dm⁻³ OH with a Kinetic Degradation Fit of Equation 2.45 to the Surface Coverage Data</i>	130
2.26	<i>The Surface Coverage and Surface Pressure Kinetic Decay of a Stearic Acid Monolayer on a Subphase of 1.176 mol dm⁻³H₂O₂ / 8.7 × 10¹² mol dm⁻³ OH with a Kinetic Degradation Fit of Equation 2.45 to the Surface Coverage Data.</i>	131
2.27	<i>The Surface Coverage and Surface Pressure Kinetic Decay of a Stearic Acid Monolayer on a Subphase of 2.352 mol dm⁻³H₂O₂ / 8.7 × 10¹² mol dm⁻³ OH with a Kinetic Degradation Fit of Equation 2.45 to the Surface Coverage Data</i>	132
2.28	<i>The Surface Coverage and Surface Pressure Kinetic Decay of a Stearic Acid Monolayer on a Subphase of 2.352 mol dm⁻³H₂O₂ Without Photolysis With an Exponential Fit to the Surface Coverage Data</i>	133

2.29	<i>The Surface Coverage and Surface Pressure Kinetic Decay of a Stearic Acid Monolayer on a Subphase of Null Reflective Water with photolysis, and an Exponential Fit to the Surface Coverage Data</i>	134
2.30	<i>A Comparison of the Kinetic Decay in the Surface Pressure of A Stearic Acid Monolayer Exposed to Varied Concentrations of Aqueous H₂O₂ / OH Radical</i>	135
2.31	<i>The Surface Coverage and Surface Pressure Kinetic Decay of a Stearic Acid Monolayer on a Subphase of 1.176 mol dm⁻³H₂O₂ / 8.7 × 10¹² mol dm⁻³ OH at a temperature of 6.7°C with a Kinetic Degradation Fit of Equation 2.45 to the Surface Coverage Data</i>	136
2.32	<i>The Surface Coverage and Surface Pressure Kinetic Decay of a Stearic Acid Monolayer on a Subphase of 1.176 mol dm⁻³H₂O₂ / 8.7 × 10¹² mol dm⁻³ OH at a Temperature of 8°C with a Kinetic Degradation Fit of Equation 2.45 to the Surface Coverage Data</i>	137
2.33	<i>The Surface Coverage and Surface Pressure Kinetic Decay of a Stearic Acid Monolayer on a Subphase of 1.176 mol dm⁻³H₂O₂ / 8.7 × 10¹² mol dm⁻³ OH at a Temperature of 19.4°C with a Kinetic Degradation Fit of Equation 2.45 to the Surface Coverage Data</i>	138
2.34	<i>The Surface Coverage and Surface Pressure Kinetic Decay of a Stearic Acid Monolayer on a Subphase of 1.176 mol dm⁻³H₂O₂ / 8.7 × 10¹² mol dm⁻³ OH at a Temperature of 27°C with a Kinetic Degradation Fit of Equation 2.45 to the Surface Coverage Data</i>	139
2.35	<i>The Surface Coverage and Surface Pressure Kinetic Decay of a Stearic Acid Monolayer on a Subphase of 1.176 mol dm⁻³H₂O₂ / 8.7 × 10¹² mol dm⁻³ OH at a Temperature of 31.5°C with a Kinetic Degradation Fit of Equation 2.45 to the Surface Coverage Data</i>	140
2.36	<i>The Surface Coverage and Surface Pressure Kinetic Decay of a Stearic Acid Monolayer on a Subphase of 1.176 mol dm⁻³H₂O₂ / 8.7 × 10¹² mol dm⁻³ OH at a Temperature of 40.5°C with a Kinetic Degradation Fit of Equation 2.45 to the Surface Coverage Data</i>	141
2.37	<i>The Surface Coverage and Surface Pressure Kinetic Decay of a Stearic Acid</i>	

	<i>Monolayer on a Subphase of $1.176 \text{ mol dm}^{-3} \text{H}_2\text{O}_2 / 8.7 \times 10^{12} \text{ mol dm}^{-3} \text{OH}$ at a Temperature of 50°C with a Kinetic Degradation Fit of Equation 2.45 to the Surface Coverage Data</i>	142
2.38	<i>The Surface Coverage and Surface Pressure Kinetic Decay of a Stearic Acid Monolayer on a Subphase of $1.176 \text{ mol dm}^{-3} \text{H}_2\text{O}_2$ Without Photolysis at a Temperature of 20°C with an Exponential Fit to the Surface Coverage Data</i>	143
2.39	<i>The Decay in the Surface Coverage of a Monolayer of Stearic Acid at Different Temperatures</i>	144
2.40	<i>Modelled Surface Coverage Data Showing the Build Up of Product A and Product B in Relation to the Experimental Surface Coverage Data Obtained from the Reaction of a Stearic Acid Monolayer with Aqueous OH Radical at an H_2O_2 Concentration of $1.176 \text{ mol dm}^{-3}$</i>	145
2.41	<i>Arrhenius Plot of the Rate Constants k_A, k_B and k_C at Varied Temperatures with a Line Fit to k_A</i>	151
2.42	<i>A Brewster Angle Microscopy Image of a Stearic Acid Monolayer in the Gas Like Configuration Prior to Compression</i>	153
2.43	<i>The Surface Pressure versus Area per Molecule Isotherm of a Stearic Acid Monolayer on a Subphase of $2.352 \text{ mol dm}^{-3} \text{H}_2\text{O}_2$</i>	154
2.44	<i>The Kinetic Decay of a Monolayer of Stearic Acid on a Subphase of $2.352 \text{ mol dm}^{-3} \text{H}_2\text{O}_2$ in H_2O With Photolysis from the Beginning of the Decay</i>	156
2.45	<i>The Kinetic Decay of a Monolayer of Stearic Acid at on a Subphase of $2.352 \text{ mol dm}^{-3} \text{H}_2\text{O}_2$ in H_2O Without Photolysis from the Beginning of the Decay</i>	158
2.46	<i>A Compression of the Stearic Acid Monolayer from Figure 2.44 Measured at a Compression Rate of $10 \text{ cm}^2 / \text{min}$ Taken after the Surface Pressure had Declined to Zero</i>	159
2.47	<i>The Kinetic Decay of a Monolayer of Stearic Acid Temperature Controlled at 20°C on a Subphase of H_2O Without Photolysis</i>	160
2.48	<i>The Kinetic Decay of a Monolayer of Stearic Acid Temperature Controlled at 20°C on a Subphase of H_2O with Photolysis</i>	162

2.49	<i>The Cyclic Degredation Mechanism Proposed for Stearic Acid and Aqueous OH Radical</i>	168
2.50	<i>Step 1 – Hydrogen Abstraction</i>	169
2.51	<i>Step 2 – Propagation</i>	169
2.52	<i>Step 3- The Fate of Peroxy Radical B</i>	170
2.53	<i>The Fate of the Alkoxy Radical (i)</i>	171
2.54	<i>The Fate of the Alkoxy Radical (ii)</i>	171
Chapter 3:		
3.1	<i>The Structure of an Oleic Acid Molecule</i>	186
3.2	<i>The Surface Pressure Versus Surface Area per Molecule Isotherm for an Oleic Acid Monolayer at the Air-water Interface</i>	187
3.3	<i>A Simplified Diagram of the Creation and Destruction of Ozone in the Troposphere</i>	188
3.4	<i>The Decay of Oleic Acid Reacting with Gas-phase Ozone as Proposed by King et al. (2009)</i>	199
3.5	<i>Structure of a D₃₃ Oleic Acid Molecule</i>	200
3.6	<i>Structure of a D₁₈ Oleic Acid Molecule</i>	201
3.7	<i>The FIGARO Aluminium Reaction Chamber which Houses the Langmuir Trough on the Neutron Reflectometer Beamline Depicted Without the Chamber Lid</i>	202
3.8	<i>The FIGARO Reflectometer</i>	204
3.9	<i>Reflectivity Versus Momentum Transfer (Q) for an Un-reacted Fully Deuterated Oleic Acid and Partially Deuterated Oleic Acid Monolayer in an O₂ Atmosphere</i>	206
3.10	<i>The Four Layer Model Which the Lipid Fitting Regime Fits the Reflectivity to for Both Contrasts of a D₂O Subphase and a Null Reflecting Water Subphase</i>	208
3.11	<i>A Comparison of the Surface Coverage Data from the High Ozone Concentration Experiments</i>	219
3.12	<i>The Surface Coverage and Surface Pressure Data for a D₁₈ Oleic Acid Monolayer Reacting with $(297 \pm 31.8) \times 10^{12}$ molecules cm⁻³ Gas-Phase Ozone</i>	220

3.13	<i>The Surface Coverage and Surface Pressure Data for a D_{18} Oleic Acid Monolayer Reacting with $(130 \pm 3.89) \times 10^{12}$ molecule cm^{-3} Gas-Phase Ozone at 24°C</i>	221
3.14	<i>The Surface Coverage and Surface Pressure Data for a D_{34} Oleic Acid Monolayer Reacting with $(130 \pm 3.89) \times 10^{12}$ molecule cm^{-3} Gas-Phase Ozone at 24°C</i>	222
3.15	<i>A Kinetic Fit of Equation 3.11 to the Kinetic Decay in the Monolayer Surface Coverage of D_{18} Oleic Acid Exposed to $(297 \pm 31.9) \times 10^{12}$ molecule cm^3 Ozone in the Gas-Phase and a Concentration of $(5.23 \pm 0.56) \times 10^8$ molecule cm^{-2} Ozone in the Monolayer Tail Region</i>	223
3.16	<i>A Kinetic Fit of Equation 3.11 to the Kinetic Decay in the Monolayer Surface Coverage of D_{18} Oleic Acid Exposed to $(130 \pm 3.89) \times 10^{12}$ molecule cm^3 Ozone in the Gas-Phase and a Concentration of $(2.29 \pm 0.07) \times 10^8$ molecule cm^{-2} Ozone in the Monolayer Tail Region</i>	224
3.17	<i>A Kinetic Fit of Equation 3.11 to the Kinetic Decay in the Monolayer Surface Coverage of D_{33} Oleic Acid Exposed to $(130 \pm 3.89) \times 10^{12}$ molecule cm^3 Ozone in the Gas-Phase and a Concentration of $(2.29 \pm 0.07) \times 10^8$ molecule cm^{-2} Ozone in the Monolayer Tail Region</i>	225
3.18	<i>The Kinetic Decay in the Surface Coverage of D_{33} and D_{18} Oleic Acid Monolayers Exposed to Low Concentrations of Gas-Phase Ozone</i>	226
3.19	<i>The Kinetic Decay of Fully Deuterated Oleic Acid in an Atmosphere of $(67.2 \pm 8.55) \times 10^{12}$ molecule cm^3 O_3</i>	227
3.20	<i>The Kinetic Decay in the Surface Coverage of a D_{33} Oleic Acid Monolayer Exposed to $(29.4 \pm 9.97) \times 10^{12}$ molecule cm^{-3} Ozone in the Gas-Phase</i>	228
3.21	<i>The Kinetic Decay in the Surface Coverage of a D_{33} Oleic Acid Monolayer Exposed to $(16.1 \pm 3.94) \times 10^{12}$ molecule cm^{-3} Ozone in the Gas-Phase</i>	229
3.22	<i>The Kinetic Decay in the Surface Coverage of a D_{33} Oleic Acid Monolayer Exposed to $(16.1 \pm 3.94) \times 10^{12}$ molecule cm^{-3} Ozone in the Gas-Phase</i>	229
3.23	<i>The Kinetic Decay in the Surface Coverage of a D_{33} Oleic Acid Monolayer Exposed to $(11.6 \pm 2.20) \times 10^{12}$ molecule cm^{-3} Ozone in the Gas-Phase</i>	230

3.24	<i>The Kinetic Decay in the Surface Coverage of a D₁₈ Oleic Acid Monolayer Exposed to $(16.1 \pm 3.94) \times 10^{12}$ molecule cm⁻³ Ozone in the Gas-Phase</i>	230
3.25	<i>The Kinetic Decay in the Surface Coverage of a D₁₈ Oleic Acid Monolayer Exposed to $(16.1 \pm 3.94) \times 10^{12}$ molecule cm⁻³ Ozone in the Gas-Phase</i>	231
3.26	<i>The Recompression of Fully Deuterated Oleic Acid Monolayers with Exposure to Ozone</i>	232
3.27	<i>The Kinetic Decay of a Monolayer of Fully Deuterated Oleic Acid (Oxford Isotope Facility sample) in an Atmosphere of $(16.1 \pm 3.94) \times 10^{12}$ molecule cm³ O₃</i>	233
3.28	<i>The Kinetic Decay of a Monolayer of Fully Deuterated Oleic Acid with an Exponential Fit of Equation 3.11 to the Decay Curve Showing the Effect of Recompressing the Monolayer Exposed to an Ozone Concentration of $(16.1 \pm 3.89) \times 10^{12}$ molecule cm⁻³ in the Gas Phase and $(0.284 \pm 0.069) \times 10^8$ molecule cm⁻² in the Tail Region of the Monolayer</i>	234
3.29	<i>The Kinetic Decay of a Monolayer of Fully Deuterated Oleic Acid with Exponential Fits of Equation 3.11 to the Decay Curve Showing the Effect of Recompressing the Monolayer Exposed to an Ozone Concentration of $(16.1 \pm 3.89) \times 10^{12}$ molecule cm⁻³ in the Gas-Phase and $(0.284 \pm 0.069) \times 10^8$ molecule cm⁻² in the Tail Region of the Monolayer</i>	235
3.30	<i>The Kinetic Decay of Partially and Fully Deuterated Oleic Acid in Oxygen</i>	236
3.31	<i>The Kinetic Decay of a Monolayer of Fully Deuterated Oleic Acid in an O₂ Atmosphere Fitted to an Exponential Decay Function</i>	237
3.32	<i>Partially Deuterated Oleic acid in an O₂ Atmosphere Fitted to an Exponential Decay Function</i>	238
3.33	<i>The Pressure-Area Isotherm of D₃₃ and D₁₈ Oleic Acid on a Subphase of pH 2</i>	239
3.34	<i>The Kinetic Decay of Fully and Partially Deuterated Oleic Acid Monolayers on a Subphase of pH 1.5- 2 in Comparison with a Kinetic Decay at pH 5.5</i>	240
3.35	<i>The Kinetic Decay of a Monolayer of a Fully Deuterated Oleic acid in an Atmosphere of $(16.1. \pm 3.89) \times 10^{12}$ molecule cm⁻³ O₃ in the Gas-Phase and $(2.29 \pm 0.069) \times 10^8$ molecule cm⁻² O₃ in the Monolayer as Fitted to Equation 3.11</i>	241

3.36	<i>The Kinetic Decay of a Monolayer of a Fully Deuterated Oleic Acid in an Atmosphere of $(16.1. \pm 3.89) \times 10^{12}$ molecule cm^{-3} in the Gas-Phase and $(2.29 \pm 0.069) \times 10^8$ molecule cm^{-2}O_3 in the Monolayer with a Kinetic Fit to Equation 3.11</i>	242
3.37	<i>The Kinetic Decay of a Monolayer of a Partially Deuterated Oleic Acid in an Atmosphere of $(16.1. \pm 3.89) \times 10^{12}$ molecule cm^{-3} in the Gas-Phase Above the Monolayer and $(2.29 \pm 0.069) \times 10^8$ molecule $\text{cm}^{-2} \text{O}_3$ in the Tail Region of the Monolayer as Fitted to Equation 3.11</i>	243
3.38	<i>The Reflectivity Curve for Deuterated Oleic Acid at a Surface Pressure of 19 mNm^{-1} at 24°C as Fitted to the Scattering Length of the Relevant Deuteration of Oleic Acid</i>	246
3.39	<i>The Reflectivity Curve for Deuterated Oleic Acid at a Surface Pressure of 19 mNm^{-1} at 24°C as Fitted to the Scattering Length of the Relevant Deuteration of Oleic Acid</i>	247
3.40	<i>The Second Order Plot of the Pseudo First Order Rate Constants with Increasing Ozone Concentration</i>	252
3.41	<i>The Second Order Plot of the Pseudo First Order Rate Constants for the Lower Decay after the Inflection Feature, for Oleic Acid at Low Ozone Concentrations</i>	253
3.42	<i>The Pressure-Area Isotherms of the Oleic Acid Samples used in this work. O.I.F stands for Oxford Isotope Facility and S.A. for Sigma Aldrich</i>	258
3.43	<i>Formation of a Primary Ozonide from Oleic Acid and Ozone</i>	260
3.44	<i>The Decomposition of the Primary Ozonide Adapted from Vollhardt and Shore, 2003</i>	261
3.45	<i>Pathway A. The Cleavage of the Primary Ozonide Produces a Criegee Intermediate (I) and 9-oxononanoic Acid</i>	262
3.46	<i>Pathway B. The Cleavage of the Primary Ozonide Produces a Criegee</i>	

	<i>Intermediate (II) and Nonanal</i>	263
3.47	<i>The Formation of Secondary Ozonides from Criegee Intermediates and a Stable Molecule</i>	265
3.48	<i>The Formation of Diperoxide from Two Stabilized Criegee Intermediate (II) Molecules. The Diperoxide Decomposes into 9-oxononanoic Acid and Oxygen</i>	266
3.49	<i>The Formation of Diperoxide from Two Stabilized Criegee Intermediate (I) Molecules. The Diperoxide Decomposes into Two Nonanal Molecules</i>	266
3.50	<i>Nonanoic Acid (C₉) [CH₃(CH₂)₇CO₂H]</i>	267
3.51	<i>9-oxononanoic Acid [OCH(CH₂)₇CO₂H]</i>	267
3.52	<i>Nonanal [CH₃(CH₂)₇CHO]</i>	268
3.53	<i>Azelaic Acid [HO₂C(CH₂)₇CO₂H]</i>	268
Chapter 4:		
4.1	<i>The Surface Pressure versus Surface Area per Molecule Isotherms of Oleic and Stearic Acid Mixed Monolayers</i>	288
4.2	<i>The POPC Molecule Used in the Work of Thompson et al., (2010)</i>	289
4.3	<i>The Kinetic Decay in the Surface Coverage of a Monolayer of Deuterated Stearic Acid in an Atmosphere of $(2.4 \pm 0.6) \times 10^{12}$ molecule cm⁻³ O₃ in the Gas-Phase ($(4.3 \pm 1.1) \times 10^6$ molecule cm⁻² O₃ in the Monolayer)</i>	297
4.4	<i>The Monolayer Thickness at the Air-water Interface of a Monolayer of Deuterated Stearic Acid Exposed to $(2.4 \pm 0.6) \times 10^{12}$ molecule cm⁻³ O₃ in the Gas-Phase ($(4.3 \pm 1.1) \times 10^6$ molecule cm⁻² O₃ in the Monolayer)</i>	298
4.5	<i>The Kinetic Decay in the Surface Coverage of a Monolayer of Deuterated Oleic Acid in an Atmosphere of $(2.4 \pm 0.6) \times 10^{12}$ molecule cm⁻³ O₃ in the Gas-Phase ($(4.3 \pm 1.1) \times 10^6$ molecule cm⁻² O₃ in the Monolayer)</i>	299

- 4.6** *The Kinetic Decay in the Surface Coverage of a Monolayer of Deuterated Stearic Acid and Non-deuterated Oleic Acid, Mole Fraction 0.5:0.5 in an Atmosphere of $(2.4 \pm 0.6) \times 10^{12}$ molecule cm^{-3} O_3 in the Gas-Phase $((4.3 \pm 1.1) \times 10^6$ molecule cm^{-2} O_3 in the Monolayer)* 300
- 4.7** *A Repeat Measurement of the Kinetic Decay in the Surface Coverage of a Monolayer of Deuterated Stearic Acid and Non-deuterated Oleic Acid, Mole Fraction 0.5:0.5 in an Atmosphere of $(2.4 \pm 0.6) \times 10^{12}$ molecule cm^{-3} O_3 in the Gas-Phase $((4.3 \pm 1.1) \times 10^6$ molecule cm^{-3} O_3 in the Monolayer)* 301
- 4.8** *A Further Repeat of the Kinetic Decay in the Surface Coverage of a Monolayer of Deuterated Stearic Acid and Non-deuterated Oleic Acid, Mole Fraction 0.5:0.5 in an Atmosphere of $(2.4 \pm 0.6) \times 10^{12}$ molecule cm^{-3} O_3 in the Gas-Phase $((4.3 \pm 1.1) \times 10^6$ molecule cm^{-3} O_3 in the Monolayer)* 302
- 4.9** *The Kinetic Decay in the Surface Coverage and the Thickness of a Monolayer of Deuterated Stearic Acid and Non-deuterated Oleic Acid, Mole Fraction 0.5:0.5 in an Atmosphere of $(2.4 \pm 0.6) \times 10^{12}$ molecule cm^{-3} O_3 in the Gas-Phase $((4.3 \pm 1.1) \times 10^6$ molecule cm^{-3} O_3 in the Monolayer)* 303
- 4.10** *The Kinetic Decay in the Surface Coverage of a Monolayer of Deuterated Oleic Acid and Non-deuterated Stearic Acid, Mole Fraction 0.76:0.24 in an Atmosphere of $(2.4 \pm 0.6) \times 10^{12}$ molecule cm^{-3} O_3 in the Gas-phase $((4.3 \pm 1.1) \times 10^6$ molecule cm^{-2} O_3 in the Monolayer)* 304
- 4.11** *A Repeat of the Kinetic Decay in the Surface Coverage of a Monolayer of Deuterated Oleic Acid and Non-deuterated Stearic Acid, Mole Fraction 0.76:0.24 in an Atmosphere of $(2.4 \pm 0.6) \times 10^{12}$ molecule cm^{-3} O_3 in the Gas-Phase $((4.3 \pm 1.1) \times 10^6$ molecule cm^{-2} O_3 in the Monolayer)* 305
- 4.12** *The Kinetic Decay in the Surface Coverage of a Monolayer of Deuterated Oleic*

	<i>Acid and Non-deuterated Stearic Acid, Mole Fraction 0.52:0.48 in an Atmosphere of $(2.4 \pm 0.6) \times 10^{12}$ molecule cm^{-3} O_3 in the Gas-Phase ($(4.3 \pm 1.1) \times 10^6$ molecule cm^{-2} O_3 in the Monolayer)</i>	306
4.13	<i>The Kinetic Decay in the Surface Coverage of a Monolayer of Deuterated Oleic Acid and Non-deuterated Stearic Acid, Mole Fraction 0.20:0.80 in an Atmosphere of $(2.4 \pm 0.6) \times 10^{12}$ molecule cm^{-3} O_3 in the Gas-Phase ($(4.3 \pm 1.1) \times 10^6$ molecule cm^{-2} O_3 in the Monolayer)</i>	307
4.14	<i>The χ 0.52:0.48 D-Oleic Acid: Stearic Acid Monolayer and the χ 0.50:0.50 D-Stearic Acid: Oleic Acid Monolayer Relative Surface Coverage Plotted with the D-Stearic Acid Only and the D-Oleic Acid Only Monolayer Relative Surface Coverage</i>	313
Chapter 5:		
5.1	<i>The Structure of the Methyl Oleate Molecule</i>	321
5.2	<i>A Comparison of the Surface Pressure Versus Surface Area per Molecule Isotherm for a Methyl Oleate Monolayer at the Air-water Interface</i>	322
5.3	<i>The Structure of the D_{36} Methyl Oleate Molecule</i>	325
5.4	<i>The Reflectivity Profile for an Un-reacted Monolayer of Fully Deuterated Methyl Oleate in an O_2 Atmosphere at a Surface Pressure of 7 mNm^{-1}</i>	329
5.5	<i>The Decay in Surface Coverage of a Monolayer of Methyl Oleate Exposed to $(16.7 \pm 2.3) \times 10^{12}$ molecule cm^{-3} Gas-Phase O_3 Versus the Modelled O_3 Concentration from Equation 5.10</i>	332
5.6	<i>The Kinetic Decay of a D_{36} Methyl Oleate Monolayer Exposed to a Gas-Phase Ozone Concentration of $(235 \pm 7) \times 10^{12}$ molecule cm^{-3}</i>	334
5.7	<i>The Kinetic Decay of a D_{36} Methyl Oleate Monolayer Exposed to a Gas-Phase</i>	

	<i>Ozone Concentration of $(177 \pm 34) \times 10^{12}$ molecule cm^{-3}</i>	335
5.8	<i>The Kinetic Decay of a D_{36} Methyl Oleate Monolayer Exposed to a Gas-Phase Ozone Concentration of $(121 \pm 15.4) \times 10^{12}$ molecule cm^{-3}</i>	336
5.9	<i>A Repeat of the Kinetic Decay of a D_{36} Methyl Oleate Monolayer Exposed to a Gas-Phase Ozone Concentration of $(121 \pm 15.4) \times 10^{12}$ molecule cm^{-3}</i>	337
5.10	<i>The Kinetic Decay of a D_{36} Methyl Oleate Monolayer Exposed to a Gas-Phase Ozone Concentration of $(94.3 \pm 4.1) \times 10^{12}$ molecule cm^{-3}</i>	338
5.11	<i>The Kinetic Decay of a D_{36} Methyl Oleate Monolayer Exposed to a Gas-Phase Ozone Concentration of $(53 \pm 18) \times 10^{12}$ molecule cm^{-3}</i>	339
5.12	<i>The Kinetic Decay of a D_{36} Methyl Oleate Monolayer Exposed to a Gas-Phase Ozone Concentration of $(40.8 \pm 11.6) \times 10^{12}$ molecule cm^{-3}</i>	340
5.13	<i>The Kinetic Decay of a D_{36} Methyl Oleate Monolayer Exposed to a Gas-Phase Ozone Concentration of $(29.1 \pm 7.1) \times 10^{12}$ molecule cm^{-3}</i>	341
5.14	<i>The Kinetic Decay of a D_{36} Methyl Oleate Monolayer Exposed to a Gas-Phase Ozone Concentration of $(16.7 \pm 2.3) \times 10^{12}$ molecule cm^{-3}</i>	342
5.15	<i>The Decay in the Surface Pressure (Π) and the Surface Coverage (Γ) of a D_{36} Methyl Oleate Monolayer at the Air–liquid Interface over Time in an Oxygen Atmosphere with an Exponential Fit to the Surface Coverage Data Plotted with a Low Ozone Concentration Experiment</i>	343
5.16	<i>The Decay in the Surface Pressure (Π) of a D_{36} Methyl Oleate Monolayer at the Air–Water Interface over Time in an Atmosphere of Varied Concentrations of Gas-Phase Ozone</i>	344
5.17	<i>The Kinetic Decay in the Surface Coverage of Methyl Oleate Monolayers Exposed to Varied Concentrations of Gas-phase Ozone</i>	345

5.18	<i>Reflectivity versus Momentum Transfer for a Methyl Oleate Monolayer at the Air-water Interface Exposed to a Gas-phase Ozone Concentration of $(16.7 \pm 2.3) \times 10^{12}$ molecule cm^{-3}</i>	346
5.19	<i>The 2nd Order Kinetic Plot for the Decay in the Surface Coverage of a Monolayer of D₃₆ Methyl Oleate Under Conditions of Ozonolysis</i>	349
5.20	<i>Formation of a Primary Ozonide from Methyl Oleate and O₃</i>	356
5.21	<i>The Decomposition of the Primary Ozonide Adapted from Vollhardt and Shore, (2003)</i>	357
5.22	<i>The Cleavage of the Primary Ozonide Produces a Criegee Intermediate (I) and 9-oxo-methyl Nonanone. The Criegee Intermediate (I) then Stabilizes or Isomerises</i>	359
5.23	<i>The Formation of Methyl-9-oxostearate and Nonanal from Criegee Intermediate (I) and Methyl Oleate</i>	360
5.24	<i>Pathway B. The Cleavage of the Primary Ozonide Produces a Criegee Intermediate (II) and Nonanal. The Excited Criegee Intermediate (II) can Stabilize or Isomerise to the Methyl Ester of Azelaic Acid</i>	361
5.25	<i>The Formation of Secondary Ozonides from Criegee Intermediates and a Stable Molecule</i>	363
5.26	<i>The Formation of Diperoxide from Two Stabilized Criegee Intermediate (II) Molecules. The Diperoxide Decomposes into Two 9-oxo-methyl Nonanone Molecules and Oxygen</i>	364
5.27	<i>The Formation of Diperoxide from Two Stabilized Criegee Intermediate Molecules (I). The Diperoxide Decomposes into Two Nonanal Molecules</i>	365

Chapter 6:

6.1	<i>Structure of the DPPC Molecule ($C_{40}H_{80}NO_8P$)</i>	375
6.2	<i>The Surface Pressure versus Surface Area Isotherm of DPPC at the Air Water Interface at 22°C on a Subphase of Pure Water</i>	375
6.3	<i>The Surface Pressure versus Surface Area Isotherm of DPPC at the Air Water Interface at Varied Temperatures on a Subphase of Pure Water</i>	376
6.4	<i>The Fully Deuterated (d75) DPPC Molecule ($C_{40}H_5NO_8PD_{75}$)</i>	380
6.5	<i>The Head Group Deuterated (d13) DPPC Molecule ($C_{40}H_{67}NO_8PD_{13}$)</i>	380
6.6	<i>The Tail Group Deuterated (d62) DPPC Molecule ($C_{40}H_{18}NO_8PD_{62}$)</i>	380
6.7	<i>Reaction Scenario I: Aqueous OH Radical Reacting with the Head Group. The Head Group Reflectivity Signal is Rapidly Lost from the Air-water Interface</i>	381
6.8	<i>Reaction Scenario II: Aqueous OH Radical Reacting with the Tail Group. The Head group Reflectivity Signal Persists at the Air-water Interface</i>	382
6.9	<i>Reflectivity versus Momentum Transfer Measurement of a DPPC Monolayers on a Subphase of Null Reflective Water Containing $0.32 \text{ mol dm}^{-3} \text{ H}_2\text{O}_2$ Prior to Exposure to OH</i>	384
6.10	<i>The Decay in the Surface Coverage of Fully Deuterated DPPC Monolayers Exposed to Aqueous-phase OH Radical</i>	388
6.11	<i>The Neutron Reflectivity versus Momentum Transfer Measurement of a Monolayer of Fully Deuterated DPPC at the Air-water Interface</i>	389
6.12	<i>The Decay in the Surface Coverage of Head Group Deuterated DPPC Monolayers Exposed to Aqueous-phase OH Radical</i>	390
6.13	<i>The Neutron Reflectivity versus Momentum Transfer Measurement of a Monolayer of Head Group Deuterated DPPC at the Air-water Interface</i>	390
6.14	<i>The Decay in the Surface Coverage of Tail Group Deuterated DPPC</i>	

<i>Monolayers Exposed to Aqueous-phase OH Radical</i>	392
6.15 <i>The Neutron Reflectivity versus Momentum Transfer Measurement of a Monolayer of Tail Group Deuterated DPPC at the Air-water Interface</i>	392
6.16 <i>The Decay of a Fully Deuterated DPPC Monolayer with Photolysis on a Subphase of Null Reflective Water with an Exponential Decay Fitted to the Surface Coverage over Time</i>	393
6.17 <i>The Decay of a Fully Deuterated DPPC Monolayer with No Photolysis on a Subphase of H₂O₂</i>	394
6.18 <i>A Comparison of the Kinetic Decay in the Relative Surface Coverage of DPPC Isotopologue Monolayers at the Air-water Interface Exposed to 15.8×10^{12} mol dm⁻³ Aqueous OH Radical</i>	395
6.19 <i>A Comparison of the Kinetic Decay in the Relative Surface Coverage of DPPC Isotopologue Monolayers at the Air-water Interface Exposed to 15.8×10^{12} mol dm⁻³ Aqueous OH Radical with an Interrupted Experiment Highlighted</i>	396
6.20 <i>Reaction Scenario One. OH Preferentially Reacting with the DPPC Head Group</i>	397
6.21 <i>Reaction Scenario Two. OH Diffusing into the DPPC Tails and Reacting and also Reacting with the Head Group</i>	398

Chapter 7:*No Figures*

List of Tables**Chapter 1:**

- 1.1 Common Species of Atmospheric Aerosol* 38

Chapter 2:

- 2.1 The Parameters Used to Fit the Area per Molecule at the Air-Water Interface from the Neutron Reflectivity Data* 100
- 2.2 The Modelled OH Concentrations in the Langmuir Trough Subphase During a Photolysis Reaction* 117
- 2.3 Pseudo 1st Order Rate Constants for Stearic Acid Reacting with OH Radical for Varied Concentrations of H₂O₂* 147
- 2.4 Pseudo 1st Order Rate Constants for Stearic Acid Reacting with OH Radical at Different Temperatures* 148
- 2.5 The Second Order Rate Constants for the Decay of a Stearic Acid Monolayer Exposed to Varied H₂O₂ / OH Concentrations* 149
- 2.6 The Second Order Rate Constants for the Decay of a Stearic Acid Monolayer as Oxidised by OH Radical at Varied Temperatures* 150
- 2.7 Values of E_A/R from Monod et al, (2005) for Oxygenated Organic Compounds Reacting with Gas-phase OH Radical* 166

Chapter 3:

- 3.1 A Comparison of the Neutron Reflectometer SURF and FIGARO* 205
- 3.2 The Fitting Parameters Used to Fit the D₁₈ and D₃₃ Oleic Acid Monolayer Structural Reflectivity Data* 209
- 3.3 The Ozone Concentration in the Monolayer Tail Region as Calculated From Equation 3.3, and the Calibration of the Ozoniser* 212
- 3.4 The Concentrations of Gas-Phase and Monolayer Region Ozone Used in the High Ozone Experiments* 218
- 3.5 The Gas-Phase and Monolayer Region Concentrations of Ozone Used in the Low*

<i>Ozone Experiments</i>	225
3.6^a <i>The Pseudo 1st Order Rate Constant k and the Bimolecular Rate Constant $k[O_3]$ for Fully and Partially Deuterated Oleic Acid</i>	249
3.6^b <i>The Pseudo 1st Order Rate Constant k and the Bimolecular Rate Constant $k[O_3]$ for Fully and Partially Deuterated Oleic Acid</i>	250
3.6^c <i>The Pseudo 1st Order Rate Constant k and the Bimolecular Rate Constant $k[O_3]$ for Fully and Partially Deuterated Oleic Acid</i>	251
3.7 <i>The Uptake Coefficients for Ozone to an Oleic Acid Monolayer Coated Droplet</i>	255
Chapter 4:	
4.1 <i>The Weight Percentage of the Stearic Acid and Oleic Acid Components of Common Cooking Fats and Oils</i>	287
4.2 <i>The Mole Fractions of Oleic and Stearic Acid in the Spreading Solutions</i>	292
4.3 <i>The Scattering Lengths to which the Neutron Reflectivity versus Momentum Transfer Data was Fitted</i>	293
4.4 <i>The Reaction Rate Constants for the Reaction of Deuterated Oleic Acid and Deuterated Oleic Acid with Non-deuterated Stearic Acid with Gas-Phase Ozone</i>	309
Chapter 5:	
5.1 <i>The Gas-Phase Ozone Concentration in the Reaction Chamber and the Corresponding Ozone Concentration in the Monolayer Region</i>	327
5.2 <i>The Pseudo First Order Rate Constants and Second Order Rate Constants for Methyl Oleate Monolayers Reacting with Gas-phase Ozone</i>	348
5.3 <i>Uptake Coefficients for Ozone into a Cloud Droplet/ Aerosol with a Methyl Oleate Monolayer at the Air-water Interface</i>	351

5.4	<i>The Gas-phase Ozone Diffusion and Uptake Characteristic Time for Oleic Acid and Methyl Oleate Monolayers</i>	354
5.5	<i>The Solubility and Volatility of the Possible Products from the Ozonolysis of a Methyl Oleate Monolayer at the Air-Water Interface</i>	366
Chapter 6:		
6.1	<i>The Scattering Length of the Different Isotopologues of DPPC used in the Neutron Reflectivity Experiments</i>	386
Chapter 7:		
7.1	<i>A Summary of the Reaction Rate Constants and Monolayer Atmospheric Lifetimes Resulting from the Experimental Work in this Thesis</i>	408
7.2	<i>Uptake Coefficients for Ozone by a Monolayer of Oleic Acid and a Monolayer of Methyl Oleate</i>	409

I wish to thank my supervisors Martin King and Arwel Hughes for their support and help throughout the project, Margaret Collinson for her assistance as Director of Graduate Studies and my advisor Dave Alderton. Many thanks to Christian Pfrang for allowing me to participate in experiments and for the use of data from his allocated neutron reflectometry experimental time in this thesis. The support staff at ISIS and the ILL, especially Simon Wood for mending equipment and going out to buy anti-freeze for an experiment in the middle of the night, the support staff at Royal Holloway Department of Earth Sciences especially Mick and Mike for making the reaction chambers used for the experiments. The experimental team: Martin King, Arwel Hughes, Christian Pfrang, Katherine Thompson, Adrian Rennie and Richard Campbell. Team Snow at Royal Holloway: James France, Amelia Marks, and Holly Reay for being lovely to work with and for tea and cake breaks. Amelia must be especially thanked for helping with neutron experiments.

Finally I must thank my family, Paula Lucas, Paul Lucas and my partner Paul Goubran-Keshta for putting up with my missing many holidays and occasionally being a bit of a dragon during the writing up period. I must thank my parents for encouraging me to be interested in science, especially my Father, Lawrence Lucas and Grandfather, Sidney Jenkinson who sadly did not see the completion of this thesis.

The Oxidation of Cloud Droplet Films

1.1 Outline and Aims of the Thesis

The work in this thesis is concerned with understanding the chemistry which takes place at the air-water interface of a droplet in the troposphere. The interface between an aqueous droplet and the surrounding air has been shown to host a monolayer (one molecule thick) film which consists of surface active organic material (Tervahattu et al. 2002^a, 2002^b, 2005; Peterson and Tyler, 2002, 2003; Gilman et al. 2006; Peterson et al. 2006). The monolayer film lowers the surface tension of the droplet which under certain conditions of relative humidity facilitates the uptake of water vapour allowing the droplet to grow (Donaldson and Vaida, 2006; Andreae and Rosenfeld, 2008), such effects on the droplet are not well understood. The atmosphere is an oxidising medium where cloud droplets are surrounded by air containing reactive gases such as ozone, nitrogen dioxide, nitrogen pentoxide, hydroxyl radical, and halogens (Finlayson-Pitts and Pitts, 2000). An aqueous cloud droplet or aerosol particle also contains reactive species in the condensed phase such as hydroxyl radical and ozone (Bertram et al. 2001; Rudich, 2003; Elaison et al. 2004; Mochida et al. 2006). Such reactive species from the gas phase and from the condensed phase could oxidise the monolayer surrounding an atmospheric droplet (Moise and Rudich, 2001; Smoydzin and von Glasow, 2007; Aumann and Tabazadeh, 2008; King et al. 2009, 2010). The aim of this thesis is to contribute to the understanding of the processes by which a cloud droplet thin film will chemically oxidise in the troposphere by creating proxy cloud droplet films in the laboratory and studying the behaviour of the proxy film under exposure to reactant species found in the troposphere. Much of the data produced in this thesis which is relevant to a cloud droplet is also relevant to organic aerosol particles and to inorganic particles with an aqueous phase which can also possess an organic film.

The aims of this thesis are as follows:

1. To study the oxidation of organic monolayers as proxies for cloud droplet organic films at the air-water interface.
2. To measure the loss of the monolayer material in real time as the monolayer is exposed to atmospherically relevant oxidising species.
3. To perform kinetic analysis of the experimental results in order to better understand the mechanism of such reactions at the air-water interface.

The purpose of this introductory chapter is to give a brief introduction and review of the current literature on the formation of cloud droplets, evidence for organic film formation and the properties of such a droplet film, the potential oxidation of cloud droplet films will be explained

as well as the experimental techniques used in this thesis. The nucleation of a cloud droplet can occur upon atmospheric aerosol particles; the thesis focusses on cloud droplets formed on aerosol particles. Cloud droplets and aerosol particles are closely linked, in that an aerosol particle can grow into a cloud droplet so both morphologies and their climatic effects are addressed within the text.

The introduction is structured in the following order:

- A brief summary of the role of atmospheric aerosol in climate and cloud formation.
- The nucleation of cloud droplets on atmospheric aerosol.
- The modification of cloud droplets by an organic film.
- The oxidation of cloud droplet films.

1.2 The Role of Atmospheric Aerosol in Climate and Cloud Formation

Atmospheric aerosol provides a site for cloud droplet nucleation in the atmosphere; such aerosols are referred to as cloud condensation nuclei (CCN). Atmospheric aerosols are the non-gaseous components of the atmosphere, liquid or solid particles suspended in the gaseous atmosphere (Kommalapati and Valsaraj, 2009). The term aerosol is used for the size profile of 10^{-2} to $10\ \mu\text{m}$, in contrast the size range of cloud droplets is from 10 to $10^2\ \mu\text{m}$ the upper limit being the size of a rain droplet (Kommalapati and Valsaraj, 2009).

The chemical composition of aerosol is initially determined by its origin, as the particle ages it can become chemically altered (Pöschl, 2005). Common sources of atmospheric aerosol are given in table 1.1, as adapted from the Intergovernmental Panel on Climate Change (IPCC), (2007) and Kommalapati and Valsaraj, (2009). Some aerosol also forms in the atmosphere from condensed low volatility products of gas-phase chemical reactions, as secondary organic aerosol (Pandis et al. 1992). The chemical composition of the aerosol determines its wettability; a hydrophobic aerosol is less likely to become a cloud condensation nucleus.

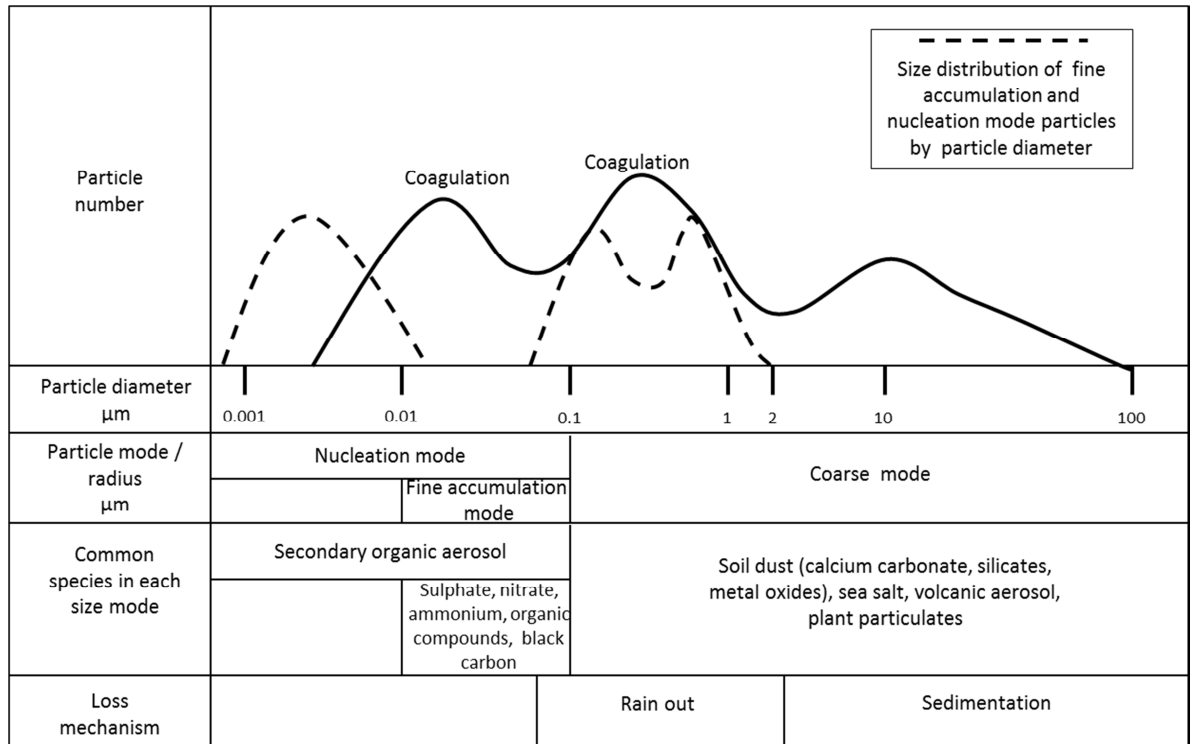
Table 1.1 *Common Species of Atmospheric Aerosol*

Aerosol Species	Aerosol Source	Role in Climate Relating to Cloud Formation
Sea salt	Oceans: sea salt enters the atmosphere through wave action creating sea spray and bubbles at the surface of the oceans which burst, propelling organic material from the ocean which is concentrated at the air-water interface into the atmosphere.	Primarily forms cloud condensation nuclei as most cloud formation occurs over the oceans. Sea salt aerosol is the most likely of the cloud condensation nuclei to have an organic film.
Anthropogenic Aerosols	Global: combustion of fossil fuels, biomass burning, waste incineration, manufacturing, mining, farming.	Climatic effect varies with chemistry. Predominantly cooling by absorption and scattering of solar radiation.
Carbonaceous Aerosols	Terrestrial global: organic and black carbon mainly emitted from biomass and fossil fuel combustion and the oxidation of volatile organic compounds (VOC).	Climatic effect varies with chemistry. Predominantly cooling by absorption and scattering of solar radiation. Black carbon is a poor CCN.
Sulphate and nitrate aerosols	Global: particulates can form as the product of chemical reactions in the atmosphere between gaseous species.	Predominantly cooling by absorption and scattering of solar radiation. Sulphate aerosol is an effective CCN*.
Volcanic aerosols	Mineral material and gaseous sulphur emitted during volcanic eruptions and degassing forms aerosol.	Climatic effect varies with chemistry. Predominantly cooling by absorption and scattering of solar radiation.
Eolian dust particles	Terrestrial global: windblown clays and silt particles [‡] .	Climatic effect varies with chemistry. Predominantly cooling by absorption and scattering of solar radiation.
Bio-aerosol	Global: emitted from organisms	Climatic effect not yet quantified

* O'Dowd et al., (1999), [‡] Johnson et al., (2004)

The size and radius of common aerosol particles are given in figure 1.1, the cloud condensation nuclei are predominantly coarse mode aerosol particles.

Figure 1.1 *The Size and Number Distribution of Common Atmospheric Aerosol Particles*



Atmospheric aerosol size ranges and common constituents as defined by Seinfeld and Pandis, (1998), and Finlayson-Pitts and Pitts, (2000).

The size and composition of the aerosol has several climatic effects, these effects are split into two broad categories of direct effects which are those determined by the aerosol particles direct interaction with radiation (McFiggans et al. 2005, Haywood and Boucher, 2000), and indirect effects which are those related to the effects of the aerosol on clouds and precipitation (IPCC, 2007).

Broadly summarized the aerosol indirect climatic affects are due to the ability of aerosol to:

- Absorb and convert solar energy to thermal energy throughout weather systems, a warming climatic effect.
- Act as Cloud Condensation Nuclei (CCN) providing a site for the formation of cloud droplets, a cooling climatic effect.

The work in this thesis is concerned with the effects involving warm clouds and precipitation, ice nuclei are beyond the scope of this work therefore the thesis concentrates on warm clouds and not mixed phase or cold clouds which contain ice nuclei.

The effects involving cloud droplets in warm clouds are summarized here after Haywood and Boucher (2000); Twomey (1974); Lohmann and Feichter (2005); IPCC (2007):

- The **cloud albedo or Twomey effect**, known as the first aerosol indirect effect where for a defined water content, introducing a greater number of CCN type aerosol particles, leads to a greater number of smaller cloud droplets as there are more sites for droplet nucleation. A greater number of smaller cloud droplets scatter solar radiation differently to larger droplets and reflect more solar radiation, thus the albedo of the cloud is increased by the smaller droplet size distribution (Twomey, 1974; IPCC, 2007.)
- The **cloud lifetime effect**, known as the secondary aerosol indirect effect where the smaller cloud droplets take longer to reach a sufficient mass to precipitate and the lifetime of the cloud in the atmosphere is increased (IPCC, 2007).
- The **semi direct effect** where energy adsorption by aerosols increases the local atmospheric temperature, reducing relative humidity (Johnson et al. 2004), and could lead to evaporation of cloud droplets and a reduction in cloud cover (IPCC, 2007). Atmospheric aerosol is dominated by non-absorbing compounds; the dominant energy adsorbing components of the atmospheric aerosol are black carbon and Aeolian dust (Johnson et al. 2004).

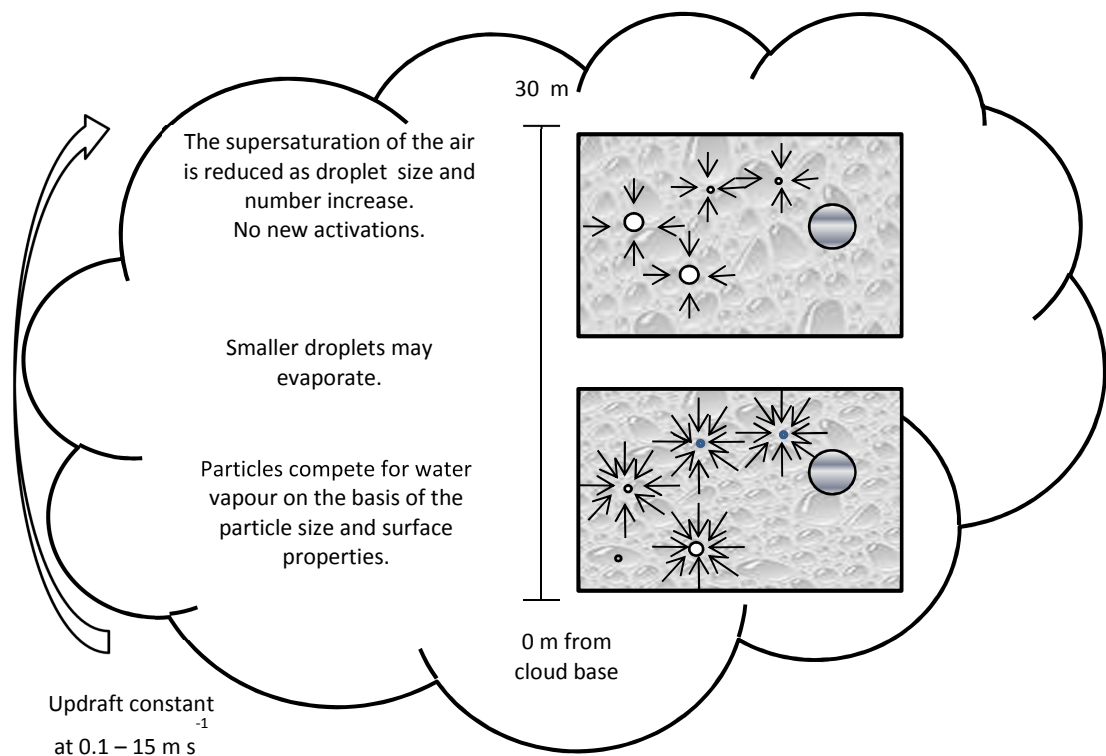
The indirect aerosol effects potentially influence the Earth's albedo, hydrological cycle and weather systems. In 2007 the IPCC rated the scientific understanding of the indirect effects of atmospheric aerosol on climate as very low. The process of cloud droplet formation and the chemical composition and structure of cloud droplets are poorly understood due to the difficulty in sampling an in situ cloud droplet with its structure and chemistry unaltered and intact which is not possible with current field sampling techniques.

Climate monitoring and weather forecasting rely on computer modelling of atmospheric circulation and processes (McFiggans, 2005.). Information on the detailed chemical processes which can influence cloud formation and the chemical lifetime of such species is required for greater accuracy of the modelling results. The data provided within this thesis may be of value to such climatic modelling.

1.3 The Nucleation of Cloud Droplets on Atmospheric Aerosol Particles

The process of cloud droplet nucleation when water vapour condenses on an atmospheric aerosol particle becoming a warm cloud droplet nuclei (CCN) without the presence of ice, takes place in the troposphere (Beard and Ochs, 1992), the region of the atmosphere from sea level to an altitude of approximately 20 km above sea level (Finlayson-Pitts and Pitts, 2000). The chemical and physical composition of the troposphere in which warm cloud droplet nucleation takes place it is locally and seasonally variable. The moisture content of the troposphere is controlled by evaporation from the oceans and land, water can be present in the troposphere as ice, water droplets and water vapour simultaneously in the same air mass, the vapour phase is always dominant even within a cloud, (Warneck, 1988) and its quantity is measured by radiosonde and lidar instrumentation (Mattis et al. 2002) as the saturation vapour pressure or relative humidity.

Figure 1.2 *The Nucleation of Cloud Droplets on Aerosol*



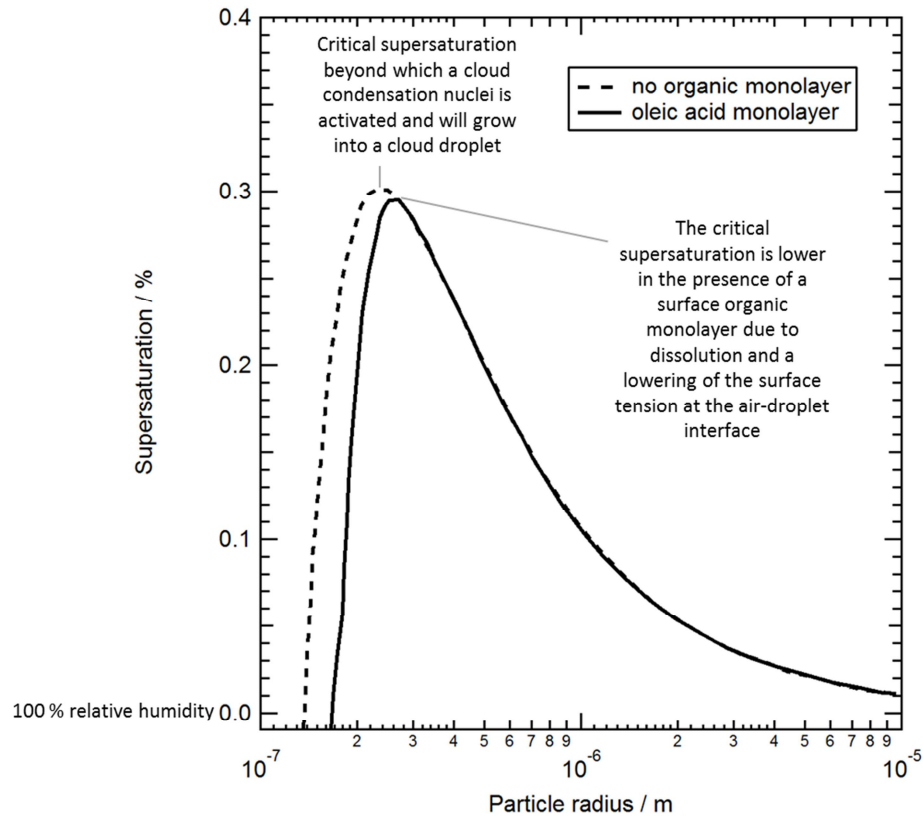
As an air parcel rises adiabatic cooling occurs, the air expands and cools, as it cools the relative humidity increases and the saturation vapour pressure is exceeded giving supersaturated conditions in which droplet nucleation occurs at cloud base height, as water vapour condenses onto particulate matter. The height of the cloud base is dependent on the temperature and pressure of the air and is highly variable

Figure 1.2 was created using information from Seinfeld and Pandis (1998).

The nucleation of a droplet on an aerosol particle is dependent on the composition of the aerosol. When the humidity (the quantity of water vapour) increases in a given parcel of air water vapour condenses onto hydrophilic aerosol particles which grow. As the relative humidity (the percentage saturation of the air with water vapour) increases deliquescence of water vapour onto particulate matter occurs (Centre for Atmospheric Science, 2011).

Deliquescence is the process by which the aerosol particle absorbs water and dissolves forming a droplet. At a relative humidity of 100% the air is saturated and nucleation occurs, beyond this the air is supersaturated and moisture readily condenses onto aerosol particles, the quantity of water vapour that an air parcel contains is dependent on temperature, at lower temperatures the air will reach supersaturation more rapidly. At the point of nucleation the droplets are in equilibrium with the surrounding air, with a further increase in relative humidity the droplets will grow as water vapour condenses from the air into the droplet. A point of critical supersaturation (the saturation ratio minus one), is reached at which the droplet will continue to grow until it reaches a critical size at which it can fall as rain. The average diameter of a cloud droplet is 10 to 20 μm , cloud droplets can range in size from several μm to 100 μm (Seinfeld and Pandis, 1998). The effect of an interfacial monolayer on the process of cloud droplet growth is shown in figure 1.3, it can be seen that the monolayer lowers the critical supersaturation required for droplet growth, however oxidation of a monolayer which resulted in removal of the film would increase the critical point of supersaturation to that modelled for a droplet without a film (King et al. 2009).

Figure 1.3 *The Growth of a Cloud Droplet Along a Curve of Supersaturation of an Air Parcel with Water Vapour versus Particle Radius as Modelled by King et al., (2009)*



The data plotted in figure 1.3 was taken from King et al., (2009) who modelled the growth of a cloud condensation nuclei into a cloud droplet with and without the presence of an organic monolayer.

The growth of the CCN into a cloud droplet of a sufficient mass to rain out of the cloud is dependent on many factors. A cloud droplet can grow, then shrink and evaporate if atmospheric conditions or the chemistry of the droplet changes. In turn the behaviour of the droplets determines the longevity of the cloud which they are a component of.

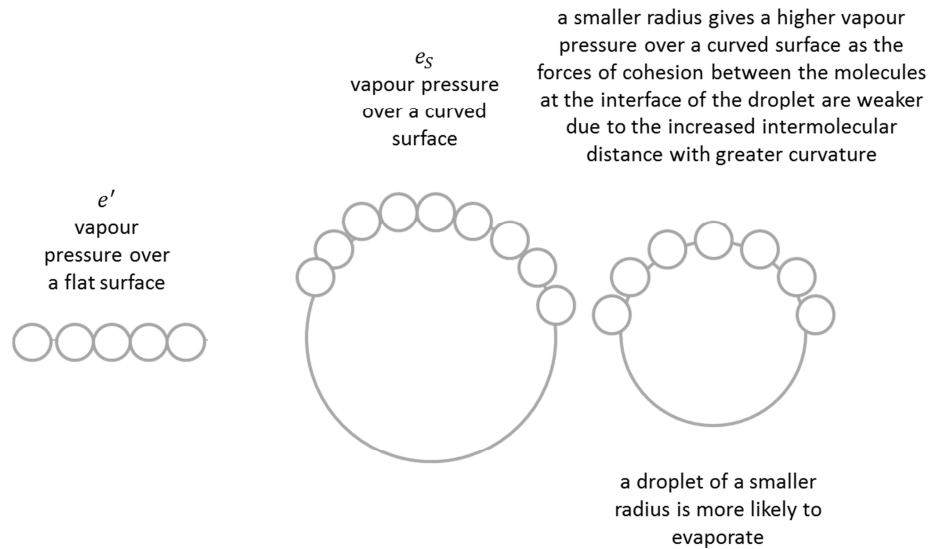
The process of droplet growth is described by Köhler theory (Köhler, 1936) which describes two factors governing the droplet growth and curvature of a hygroscopically generated cloud droplet, the solubility of the particle nuclei and its surface tension as it grows into a droplet through uptake of water vapour. A modified form of an equation expressing Köhler theory used by Shulman et al., (1996) which incorporates the effects of an organic compound on droplet surface tension and solubility is given in equation 1.1.

$$\frac{e'}{e_s} \cong 1 + \underbrace{\frac{2\sigma M_W}{kT\rho r}}_{\text{Kelvin effect}} - \underbrace{\frac{3M_W\Phi}{4\pi\rho r^3} \left(\frac{v_{dssc}X_{dssc}m_{ssc}}{M_{ssc}} + \frac{v_{sulf}m_{sulf}}{M_{sulf}} \right)}_{\text{Raoult effect}} \quad (E 1.1)$$

Equation 1.1 describes the equilibrium vapour pressure of water (e') over a curved droplet solution (of radius, r) in relation to the vapour pressure over a flat surface of water (e_s). The equation has two terms; the first relating to the effect of the solution comprising the droplet on surface tension, the Kelvin effect where the vapour pressure is enhanced over a curved surface (figure 1.4), and the latter describing the effect of dissolved species in the droplet solution in reducing the vapour pressure, the Raoult effect (Shulman et al. 1996). The Kelvin effect is calculated from the solution surface tension (σ), the molecular weight of water (M_W), the Boltzmann constant (k), the temperature (T), the solution density (ρ) and the radius (r) and the solution density (Φ). The Raoult effect is calculated from two terms. The first Raoult term uses the number of ions which the slightly soluble organic compound in solution disassociates into when it is dissolved (v_{dssc}), a modelled function of the solubility of the organic compound and sulphate concentration which is dissolved in the droplet (X_{dssc}), which is a quantity that changes with the droplet radius and takes into account that not all of the organic material will be dissolved, the molecular weight of the organic compound (m_{ssc}), and the mass of the sulphate salt in the solution (M_{ssc}). The second term of the Raoult effect takes into account the the sum of the number of ions which sulphate dissolves into (v_{sulf}), the mass of sulphate salt (m_{sulf}) and the molecular weight of the sulphate salt in the droplet (M_{sulf}) (Shulman et al. 1996).

Köhler theory is used in modelling the climatic effects of cloud droplet composition by calculating a curve which shows whether a droplet will at a certain relative humidity, grow into a rain droplet, to the right of the critical supersaturation point in figure 1.3, or evaporate, to the left of the critical supersaturation point in figure 1.3 depending on atmospheric conditions such as the availability of water vapour and the air temperature as well as the droplet radius (figure 1.4) and chemistry, thus the theory can be used in modelling cloud droplet and cloud lifetime.

Figure 1.4 *The Effect of Droplet Curvature on the Equilibrium Vapour Pressure, the Kelvin Effect*



The circles represent water molecules at the interface of the droplet with the surrounding air.

1.4 The Physical and Chemical Composition of Cloud Droplets

The chemical composition of a cloud droplet is initially governed by the composition of the aerosol onto which water vapour condensed forming a droplet. Any water soluble component of the aerosol will be present in solution and will influence the aqueous chemistry of the cloud droplet (Gourdeau, 2012). The insoluble components of the core aerosol will remain as a solid phase within the droplet which may subsequently react as the particle chemically ages in the atmosphere. Species from the gas phase surrounding the droplet can enter the aqueous droplet or condense onto the surface of a cloud droplet provided the Henry's Law equilibrium is maintained (Gourdeau, 2012). The Henry's Law expression which determines the concentration of a gas phase species, $[S_{(aq)}]$ diffusing into a cloud droplet is given by equation 1.2 from Schwartz (2003).

$$[S_{(aq)}] = H_S p_S = H_S \chi_S p_{atm} \quad (E 1.2)$$

H_S is the Henry's Law solubility for the gas phase species, χ is the molar mixing ratio of the gas phase species in air, p_{atm} is the atmospheric pressure and p_s is the partial pressure of substance S outside the droplet.

The pH and salinity of cloud droplets is variable, a typical cloud water pH value of ~ 4 to 6 is used for modelling based on cloudwater sampled from aircraft (Hegg and Hobbs, 1981), values of pH ~ 2 have been measured from ground based sampling of rainwater (Weathers et al. 1988) as the droplets generally acidify as they age in the atmosphere. Droplet salinity varies depending on the nuclei on which the droplet was formed and the chemistry of the atmosphere where the droplet is sampled, Weathers et al., (1988) measured a Cl⁻ content of 2 to 2257 µeq litres in cloudwater sampled in Puerto Rico, noting that the higher concentrations were found in stormy weather conditions where higher waves were generated increasing the flux of marine aerosol to the atmosphere (Weathers et al. 1988). Typical dissolved species found in solution in cloudwater include nitrates, magnesium, chloride and sodium salts, and sulfates (Weathers et al. 1988). King et al., (2009) showed that salinity did not influence the oxidation of a monolayer of oleic acid at the air-water interface so the experiments within this thesis were conducted on a subphase of purewater representing the aqueous component of the cloud droplet.

1.5 Cloud Droplet Organic Films

In addition to dissolved aqueous organic and inorganic species and solid particulate matter within a cloud droplet, the presence of insoluble surface active organic material has also been confirmed (Descesari et al. 2003). Several models of the configuration of the organic content of atmospheric droplets have been proposed. These were summarised by Aumann and Tabazadeh (2008) as follows:

1. The most simplistic model is of an external mixture where inorganic and organic aerosol are separated.
2. Complete miscibility where the organic and inorganic components of a droplet are totally mixed.
3. A colloidal system where the organic component forms small micelles within the droplet.
4. An organic coat or film of surface active organic material which surrounds the aqueous droplet, it is this model which the work in this thesis is based upon known as the core-shell model.

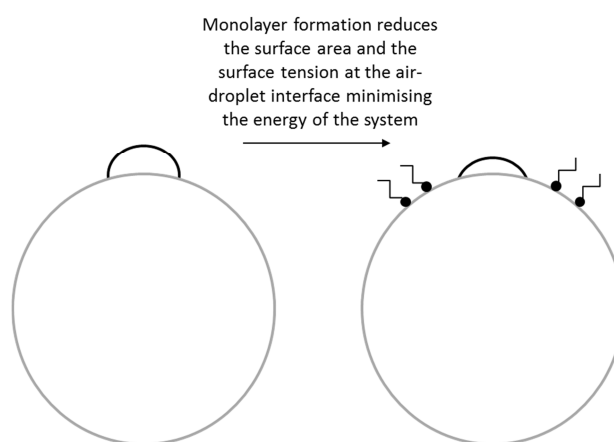
In addition Reid et al., (2011) proposed a partially coated model where a surface active organic component may exist as lenses at the surface of the droplet which are thicker than a monolayer and not evenly distributed around the droplet. This conclusion is based on a scenario of a water soluble organic compound mixed within the droplet that lowers the surface tension of the droplet so that film formation as a coating around the droplet is not thermodynamically favoured, thus lens formation by insoluble organic compounds occurs.

The formation of an organic coating on an aqueous droplet (the core-shell model) upon which this thesis focusses on, was demonstrated by Wyslouzil et al., (2006) using small angle neutron scattering (SANS) to measure the internal structure of multi component nanodroplets as a proxy for aerosol. An n-butanol shell was observed to form around and H₂O/D₂O core (Wyslouzil et al. 2006). Monolayers of amphiphiles were sprayed at the surface of acoustically levitated aqueous droplets by Tuckermann et al., (2007) showing that phase changes in the monolayer were evident as the droplet evaporated or increased in size as controlled by the relative humidity in which the droplet was studied.

The spreading of an organic at the air-water interface is described by thermodynamic equilibria. When considering a monolayer at the air-water interface of an atmospheric droplet the following physical phenomena apply to the spreading of the monolayer.

In order to minimize the surface free energy molecules leave a droplet of an amphiphile at the air-droplet interface and diffuse around the droplet (figure 1.5).

Figure 1.5 *The Spreading of a Monolayer on an Atmospheric Droplet to Minimize the Surface Free Energy*



For the surface to be considered wettable in order for the monolayer to spread the contact angle, θ , between the droplet of an organic amphiphile and the aqueous droplet must be $< 90^\circ$ (figure 1.6) (Barnes and Gentle, 2005).

Figure 1.6 *The Organic Amphiphile-Aqueous Subphase Contact Angle*

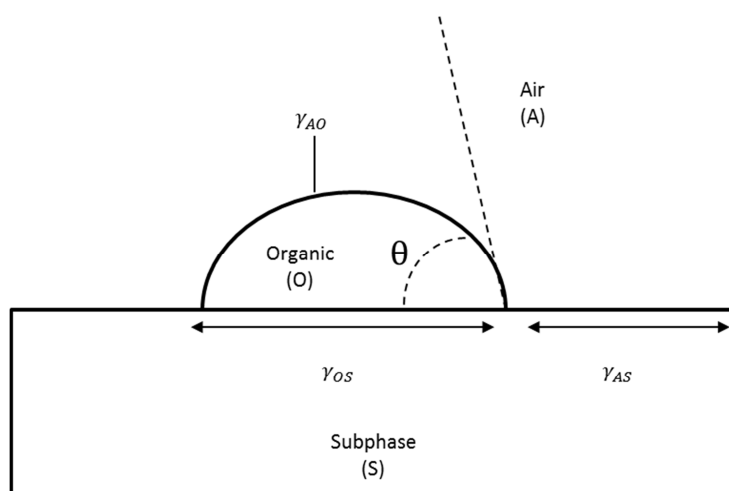


Figure 1.6 is adapted from Barnes and Gentle (2005)

When the contact angle between the organic and the aqueous droplet is low enough the spreading coefficient, S , can be determined by equation 1.3.

$$S = \gamma_{AS} - \gamma_{OS} - \gamma_{AO} \quad (E 1.3)$$

1.5.1 Evidence for Coated Droplets

There is evidence for the presence of film coated droplets in the atmosphere. Husar and Shu (1975) published electron microscopy images of continental aerosol from Los Angeles which had a shrivelled appearance at the surface. Husar and Shu (1975) interpreted the image as being the remains of an organic layer around an aqueous phase which had volatilized during the imaging process (Husar and Shu, 1975; Aumann and Tabazadeh, 2008). Aumann and Tabazadeh, (2008) note that the particle imaged by Husar and Shu (1975) had been heated to 250°C so was not a true reflection of an in-situ aerosol particle. Scanning Electron Microscope images of marine aerosol particles collected in Finland by Tervahattu et al., (2002^a) showed an actively reacting surface which bubbled when water was evaporated from the sample (Tervahattu et al. 2002^a; Aumann and Tabazadeh, 2008), the samples were from a polluted airmass and had a high content of dicarboxylic acids and fragmented aliphatic hydrocarbon material, the bubbling surface was found to be of an organic composition (Tervahattu et al. 2002^a).

The presence of fatty acids at the air-water interface of aerosols was confirmed by Tervahattu et al., (2002^b) and Tervahattu et al., (2005) by the analysis of marine aerosol samples and

continental sulphate and nitrate aerosol samples from Finland with analysis of aerosol samples collected on filters using time of flight secondary ion mass spectrometry (TOF-SIMS). Palmitic acid was detected at the particle surface of the marine aerosol (Tervahattu et al. 2002^b).

Continental aerosol collected following forest fires showed a dominance of *n*-alkanoic acids (C₁₄ to C₃₀) with the highest proportion of C₂₂, alkenoic acids were also detected and attributed to smoke from conifer tree combustion (Tervahattu et al. 2005). Tervahattu et al., (2005) note that the continental aerosol samples contained longer chain species than the marine aerosol in previous studies.

Russell et al., (2002) used soft X-ray spectromicroscopy at atmospheric pressure to measure the distribution of organic groups on dry particles collected from impactors mounted on aircraft which flew through a marine airmass in the Caribbean. Russel et al., (2002) mapped organic coatings surrounding crystalline carbonaceous aerosol particles noting that the particle surfaces were enhanced in shorter chain carboxylic acids and more oxygenated groups suggesting oxidation had taken place. The interior of the coated particles contained ketones and inorganic ions. The surface coating composition was a complex mixture of surface active organic material enriched in carboxylic carbonyl groups (R(C=O)OH) (Russell et al. 2002).

This thesis concentrates of the behaviour of polar organic molecules at the air-water interface, those with a hydrophilic head group and a hydrophobic portion which gives the overall behaviour of a surfactant which resides at the air-water interface. Such surface active organic compounds have been sampled in cloud waters, fog waters and in aerosol samples.

Emissions of surface active organic material to the atmosphere which could be the origin of cloud droplet monolayers occur from both natural and anthropogenic sources. Plants emit a range of organic compounds to the atmosphere including C₁₀ to C₁₇ *n*-alkanes, esters, alkenes, aromatics, ketones, aldehydes, alcohols and terpenes (Winer et al. 1992). The combustion of biomass also releases such compounds (Simoneit, 2002). The contribution of anthropogenic activities to organic aerosol monolayers must also be considered. Rogge et al., (1991) examined the composition of aerosol from meat grilling which contained aromatic hydrocarbons, *n* alkanes, *n*-alkanoic acids, *n*-alkenoic acids, and dicarboxylic acids. Palmitic acid, stearic acid and oleic acid were major components of meat grilling aerosol (Rogge at al. 1991) that could be surface active in the atmosphere. Combustion of fossil fuels also releases surface active organic compounds such as stearic and oleic acid to the atmosphere (Rogge et al. 1993). Increasingly traditional fuels are blended with biofuels which have a high organic content including surface active methyl esters (Knothe et al. 2006).

A natural source of surface active organic material such as lipids to the atmosphere is the sea surface microlayer (Simoneit et al. 2004). The oceans were identified as a likely source of surface active, monolayer film forming organic material to atmospheric droplets by Giddings and Baker (1977). The sea surface microlayer is of particular significance as the majority of warm cloud condensation nuclei originate in the marine atmosphere. The sea surface microlayer is present at the air-water interface of the oceans and is of a variable thickness from 1 to 1000 μm (Donaldson and Vaida, 2006), it is composed of algae, plankton, bacteria, and the chemical products of these organisms and the breakdown of detritus within the water column as well as anthropogenic pollution. Hardy (1982) suggested a structure of the sea surface microlayer as a monomolecular lipid film of a thickness of 10 to 20 \AA with a sublayer of proteins and other biological material beneath it, such films are also found at the surface of lakes (Sodergren, 1987). The lipid content of the sea surface microlayer includes phospholipids and fatty acids (Marty et al. 1979). Marty et al., (1979) found that the organic content of marine aerosol correlated with the composition of the sea surface microlayer. C_{14} to C_{32} fatty acids were sampled in aerosol collected by Mochida et al., (2002) over the North Pacific Ocean. The C_{14} to C_{19} saturated acids correlated with the concentration of sea salt and the authors suggest this is a result of the particles originating from the ocean surface. A typical marine aerosol structure consists of a basic saline core, containing smaller soluble organic species dissolved as salts (Gilman et al. 2004). The core can acidify during atmospheric transport (Gilman et al. 2004) and subsequently the dissolved organics would partition to the air-droplet interface as protonated acids (Gilman et al. 2004). Sea salt aerosol particles with an organic coating have been sampled from a ship sailing to the North of Iceland by Russel et al., (2010) which is considered to be a clean arctic marine region, the authors suggest the thin coatings are carbohydrates and dissolved organic carbon from seawater.

There is a lack of data on the fluxes of such material to the atmosphere or identification of the most significant sources for coated particles as this will be geographically variable. For warm cloud droplets the sea surface microlayer is likely to be the primary source of coated particles due to the proximity of the marine aerosol to cloud formation, and the high marine aerosol content of warm cloud. In heavily polluted continental areas and over large forests the sources may be dominated by surface active material of a continental origin. Levoglucosan, a tracer for biomass burning (Simoneit et al. 2002; Fu et al. 2009) has been found in aerosol samples from the Canadian High Arctic (Fu et al. 2009) at a great distance from any biomass burning source. High Arctic Aerosols showed a fatty acid content of predominantly even carbon numbered fatty acids, but also high quantities of C_9 , an oxidation product of oleic acid (Fu et al. 2009). Fu et al., (2009) attributed the organic content of aerosol sampled in the high arctic to six sources from

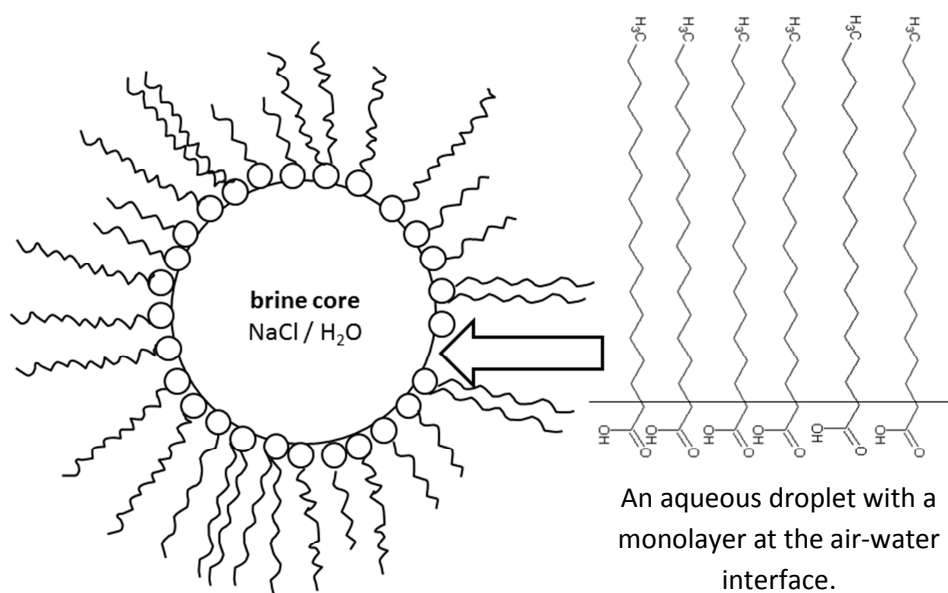
plant emissions, marine microbial lipids, biomass burning, fossil fuel combustion, soil re-suspension and secondary oxidation products.

1.5.2 Proposed Models of Coated Droplet Films

A model of an ‘inverted micelle’ was depicted by Ellison et al., (1999) after Gill et al., (1983) in which an aqueous marine aerosol would be coated in an insoluble monolayer of surface active organic material (Ellison et al. 1999; Aumann and Tabazadeh, 2008).

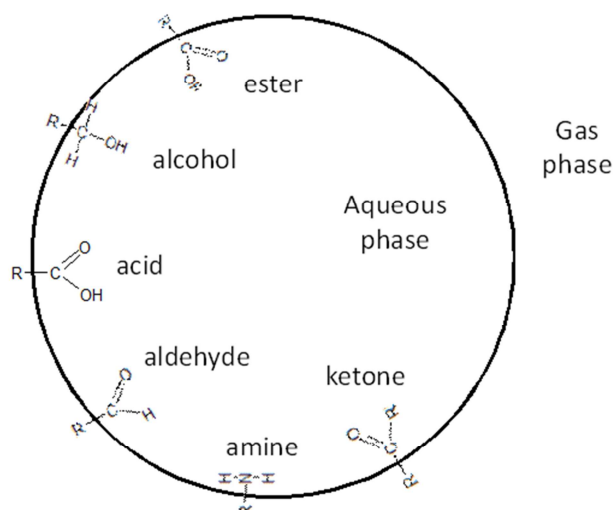
Aumann and Tabazadeh, (2008) proposed that droplets of lipid emitted for example from meat cooking, could coagulate onto an aqueous droplet and spread at the air-water interface. Droplets emitted from the surface of the oceans by wave action could have an organic film comprised of surface active lipid material from the sea surface microlayer, a concentrated layer of organic detritus at the surface of the oceans, which has been shown by Marty et al., (1979) to be reflected in the organic composition of marine aerosol samples. As deliquescence occurs and the aerosol is activated into a cloud droplet some of the lipid material would remain at the air-water interface. Such a coated droplet was illustrated as a core-shell morphology by Ellison et al., (1999) as depicted in figure 1.7.

Figure 1.7 *The Core-Shell Morphology of a Cloud Droplet with a Monolayer at the Air-Water Interface*



A monolayer system was studied rather than a multi-layer organic film as it was necessary to begin with a simple system from which to characterise the kinetics of film oxidation. The structure of the hydrophilic head groups of the monolayer forming molecules which could enable such a morphology at the air-water interface were listed by Gill et al., (1983) and is given in figure 1.8. An atmospheric monolayer would be composed of a mixture of many different surface active compounds with differing alkyl lengths. The portion of saturated organics are often sampled at higher levels than their unsaturated counterparts. This is due to aging as the unsaturated compounds are broken up faster by oxidants in the atmosphere (Zahardis and Petrucci, 2007).

Figure 1.8 *The Functional Head Groups of the Surface Active Components of Cloud Droplet Monolayers*



Monolayer formation occurs when the hydrophilic head group is polar or ionic or forms hydrogen bonds with the water within the droplet (Gill et al. 1983). The hydrophobic part of the molecule must be of a sufficient length (> 4 to 5 carbons) for the molecule to remain insoluble and persist at the interface (Gill et al. 1983).

The behaviour of a reaction in the interfacial region of a heterogeneous system such as a monolayer differs from a reaction in the bulk and the chemical mechanism and kinetics of a reaction vary from those taking place exclusively in the gas phase or the liquid phase (Vieceli et al. 2004). The reasons for the differences in reaction rate and mechanism are attributed to the orientation of the molecules exposing more or less reactive parts of a molecule to the reactant, and the trapping of gas phase species in the structure of the interface (Vieceli et al. 2004).

1.5.3 Experiments on Atmospheric Films

Traditional Köhler theory does not adequately describe the hygroscopic behaviour of organic CCN and atmospheric oxidation processes should also be considered when modelling the behaviour of CCN (Sun and Ariya, 2006). An organic monolayer at the air-water interface of a cloud droplet would be exposed to oxidation from atmospheric gases and from radical species dissolved in the aqueous phase of the cloud droplet or aerosol particle (Ellison et al. 1999). The primary oxidant species which could react with a cloud droplet organic film at the air-water interface are OH, NO, NO₂, Cl, O₃, and NO₃ (Vaida et al. 2000).

There are few experimental studies of the oxidation of monolayers at the air-water interface from an atmospheric perspective. A brief overview of the current state of knowledge based on laboratory experiments on the oxidation organic monolayer films in an atmospheric context will be given in the respective thesis chapters which contain further discussion of the relevant experiments together with relevant experiments on thick films such as those conducted on flow tube apparatus.

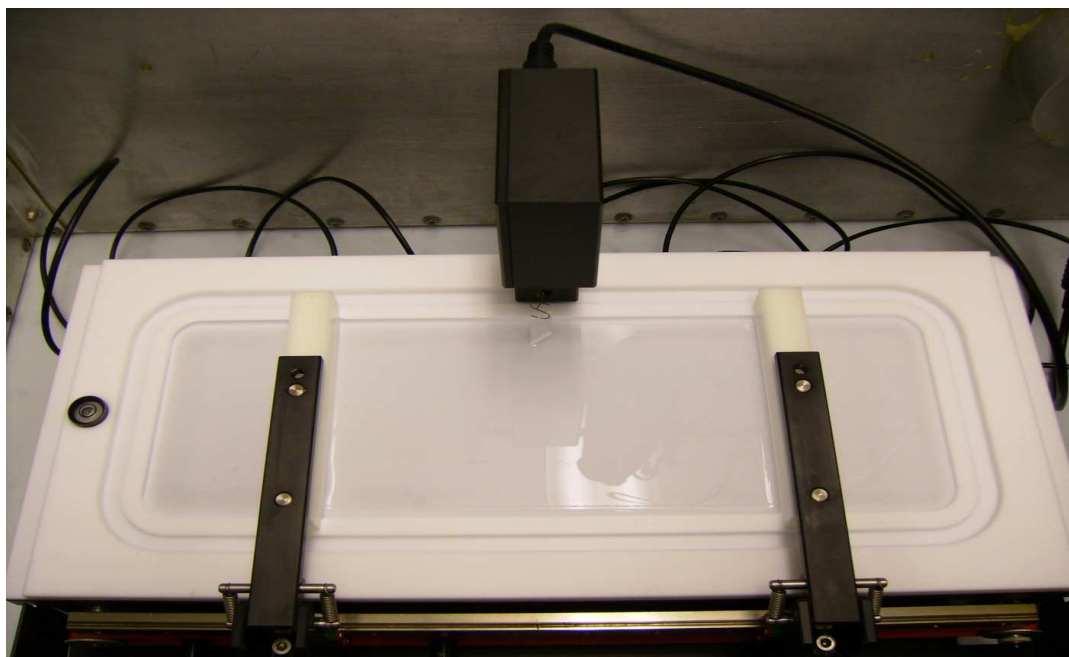
Oxidation of atmospheric monolayer forming materials has been investigated by several different laboratory methods. The degree of oxidation from the gas phase and from beneath an organic film at the air-water interface is poorly constrained. Graedel and Weschler (1981) and Gill et al., (1983) concluded that the organic monolayer would inhibit the uptake of oxidant gases into the droplet so solution oxidation within the droplet would be inhibited. The monolayer could alternatively be a more soluble medium than the droplet into which gas-phase species may accumulate (Donaldson and Vaida, 2006). Ellison et al., (1999) concluded that the organic film would be reactive to atmospheric gases and radical species and thus the coating would be processed and product formation would occur. Ellison et al., (1999) hypothesised that OH radical would react with the monolayer through hydrogen abstraction initiating an oxidising chain reaction leading to the presence of an array of functional groups a producing a 'functionalised' organic film.

Laser trapping of an oleic acid droplet using Raman tweezers was used by King et al., (2004) to probe the reaction products at the air-droplet interface of the oxidation of oleic acid initiated by gas phase ozone. King et al., (2004) found that oxidation initiated by gas phase ozone at the surface of an oleic acid droplet yielded nonanoic acid and nonanal and that the droplet grew as a result of oxidation as the relative humidity at which droplet growth could occur was lowered by the particle becoming more hydrophilic.

Voss et al., (2006) spread a monolayer of oleic acid (unsaturated) with palmitic acid (saturated) with deuterated acyl chains on a petri dish with an aqueous subphase then exposed the monolayer to gas phase ozone and measured the difference in the spectra before and after ozonolysis using a surface specific, broad-bandwidth, sum frequency generation spectroscopy technique which uses an infrared light beam of variable frequency and a fixed frequency laser beam. The two beams have different energies and the beam frequencies are tuned to match the vibrational order of the sample (Voss et al. 2006). The sum energy of the reflected beam is detected with a charge coupled device before and after interaction with the sample at a defined output angle giving a spectra of intensity versus incident infrared containing peaks which are characteristic to the vibrational order of groups present in the monolayer forming molecules. Prior to ozonolysis the oleic acid replaced the palmitic acid at the air-water interface as palmitic acid is more soluble, after ozonolysis the palmitic acid signal returned showing that the oleic acid had been lost from the interface as a result of exposure to gas phase ozone (Voss et al. 2006). The conclusion of this work was that it confirmed the theory of Tervahattu et al., (2002^{a,b}, 2005) that a monolayer on an atmospheric droplet would be oxidised by ozone and there could still be an absence of oxidised species at the interface as the products can be volatile or soluble (Voss et al. 2006) and that the least soluble species within the droplet would replace any more soluble oxidation products at the air-water interface (Voss et al. 2006).

The process by which photochemical oxidation by aqueous OH radical forms soluble dicarboxylic acids found in atmospheric waters was simulated by Tedetti et al., (2007) using irradiation of aqueous solutions of fatty acids with NO_3^- to generate aqueous OH radical. The samples were derivatized and analysed with gas chromatography and flame ionization detection demonstrating that the photooxidation of fatty acids produced the smaller soluble dicarboxylic acids found in atmospheric waters (Tedetti et al. 2007). Oleic acid in solution was cleaved at the double carbon-carbon bond followed by secondary photooxidation of the reaction products producing low molecular weight dicarboxylic acids (Tedetti et al. 2007).

It is a challenge to gain a high resolution measurement of an organic monolayer at the air-water interface of a droplet during oxidation. A flat air-water interface is commonly used as a simpler system for studying monolayers where the Kelvin effect of curvature does not affect the experiment as evaporation from a droplet will alter the packing of a monolayer which is difficult to constrain or characterize. The Langmuir trough, a shallow PTFE bath with PTFE barriers which run along the surface of the bath, allows the packing of a monolayer on an aqueous substrate to be controlled whilst providing a hydrophobic surface on which a monolayer can be studied with little interference from the containment apparatus; it is also relatively inexpensive in comparison to other techniques.

Figure 1.9 *Image of a Langmuir Trough with a Wilhelmy Plate Balance*

When an amphiphile is dissolved in a volatile solvent such as chloroform, then is spread onto the surface of a polar liquid such as water, the solvent evaporates leaving the amphiphile molecules orientated with their heads bonded into the water and their hydrophobic chains orientated into the air.

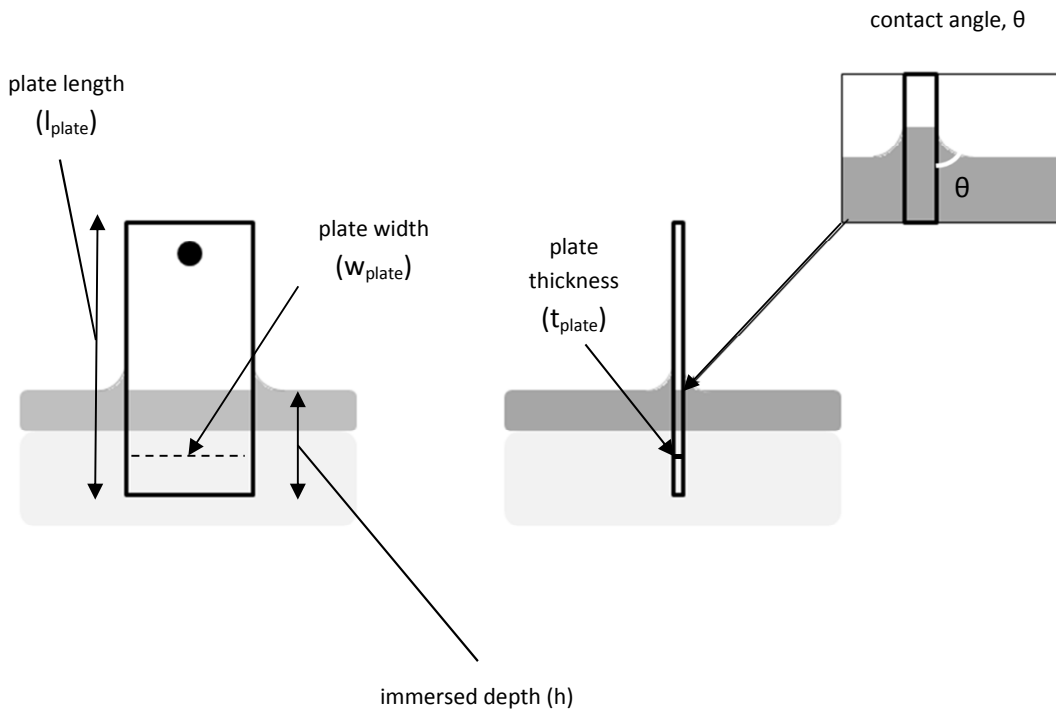
The Langmuir trough enables the monitoring of surface pressure, the change in surface tension due to molecular interactions at the air-water interface using a Wilhelmy plate balance. This consists of a plate suspended from a balance which when force is exerted on it turns a wire; the turn in the wire creates a current which is measured. A liquid surface exerts a mechanical force on a solid with which it is in contact (Sprackling, 1985), the surface pressure sensor fitted to the Langmuir trough measures this force by the submergence of a chromatography paper plate, the Wilhelmy plate, which is attached to a balance. A current is applied to an electromagnet to keep the filter paper level. The change in current is measured as the plate moves due to the force of surface tension at the air-water interface. Buoyancy acts in an upwards direction on the plate and gravity and surface tension act in a downwards direction normal to the interface. The surface pressure measurement is a product of the plate perimeter. The plate perimeter is calculated according to equation 1.4, the geometry of the Wilhelmy plate is shown in figure 1.10.

$$p = (w_{plate} t_{plate})^2 \quad (E 1.4)$$

The surface pressure (Π) is calculated from equation 1.5 where p is the plate perimeter and $\Delta\gamma$ is the change in the surface tension force pulling on the plate.

$$\Pi = \Delta\gamma p \quad (E 1.5)$$

Figure 1.10 *The Wilhelmy Plate at the Air-Water Interface Showing the Perimeter and Contact Angles used to Calculate the Surface Pressure of a Monolayer*



The figure is adapted from the manufacturer, KSV NIMA's website (KSV NIMA 2010) and the NIMA Langmuir Trough Manual

The net downwards force on the Wilhelmy plate is calculated according to equation 1.6 (KSV NIMA, 2011), where ρ_{plate} is the density of the plate, g is the gravitational constant ($6.673 \times 10^{-11} \text{ m}^3 \text{ kg}^{-1} \text{ s}^{-2}$), ρ_{liquid} is the density of the subphase (for water 1000 kg / m^{-3}) and h is the immersed depth of the plate.

$$F = \rho_{plate} g l_{plate} w_{plate} t_{plate} + 2\gamma(t_{plate} w_{plate})(\cos\theta) - \rho_{liquid} g t_{plate} w_{plate} h \quad (E 1.6)$$

Surface pressure (Π), is the difference between the surface tension of a clean liquid surface and the surface tension of a liquid surface with a surface active compound present. Surface pressure varies with the surface area per molecule. The calculation for the surface pressure of a monolayer on an aqueous subphase is shown in equation 1.7.

$$\Pi = \gamma_{water} - \gamma_{film} \quad (E 1.7)$$

An insoluble compound at the air-liquid interface will reduce the surface tension, thus increase the surface pressure. The higher the concentration (area per molecule), of the amphiphile, the greater the surface pressure. Insoluble monolayers were used to simplify the system for kinetic analysis of the oxidation process. Stearic acid and oleic acid form an insoluble monolayer and have been used as a standard model system for studying atmospheric organic film chemistry.

The use of the Langmuir Trough to study the surface pressure exerted by a monolayer of organic acid at the air-water interface from an atmospheric perspective is an established technique, some examples are given here. Gilman et al., (2006) studied the longevity of mixed fatty acid and hydrocarbon monolayers formed and aged on a Langmuir trough then sampled on a glass slide and characterized using NMR (nuclear magnetic resonance) showing that a long chain hydrocarbon such as nonacosane ($C_{29}H_{60}$) when mixed with teracosanoic acid ($CH_3(CH_2)_{22}COOH$) had a similar interfacial lifetime to a fatty acid at the air-water interface in ambient air. Eliason et al., (2003) also used a Langmuir trough housed in a thin film chamber to collect and analyse the products of ozonolysis of 2-octenoic acid and 10-undecenoic acid which were oxidised, hydrophilic shorter chain carboxylic acids. The competition between a surface active flourotelomer alcohol and stearic acid was studied as a proxy for an atmospheric droplet film on a Langmuir trough by Rontu and Vaida, (2007) showing that the alcohol had a greater longevity at the air-water interface when mixed with a fatty acid.

Voss et al., (2007) studied the aging of an oleic acid monolayer on a Langmuir trough housed in a reaction chamber in which the monolayer was exposed to gas phase ozone and the change in surface pressure over time was measured as the monolayer was oxidised. The same technique employed by Voss et al., (2007) is used in this thesis, the monitoring of the surface properties of the monolayer over time have been referred to as the measurement of a kinetic decay within my work to distinguish from compressional data referred to as an isotherm. Voss et al., (2007) found that the surface pressure of a monolayer of oleic acid at the air-water interface decayed to a value of zero $m Nm^{-1}$ over a time period of ~ 24 minutes when the monolayer was lost from the interface. For the work in this thesis the monolayer was compressed by closure of the barriers taking the monolayer into the liquid phase of the pressure-area isotherm as this is the most realistic configuration for a cloud droplet monolayer. When the monolayer reached the

required surface pressure, the Langmuir trough barriers were held in a fixed position and the surface pressure and area per molecule were monitored over time during a reaction with an atmospheric radical species.

King et al., (2009, 2010) were the first to observe the oxidation an atmospheric proxy monolayer film on a Langmuir Trough with neutron reflection showing a cleavage of the double bond in the tail of a monolayer comprised of the oleic acid molecule exposed to ozone (King et al. 2009) followed by the formation of surface active product molecules, and to NO₂ (King et al. 2010), which did not react with oleic acid other than isomerising the double bond from the *cis* configuration to *trans*. King et al., (2009, 2010), Thompson et al., (2010) and Voss et al., (2007) are the only studies of atmospheric monolayer oxidation to be performed in real time.

1.5.4 The Climatic Effect of Cloud Droplet Film Oxidation

The presence of an organic film at the air-water interface of a cloud droplet would increase the droplet lifetime by reducing the evaporation of water from the droplet (Gill et al. 1983). By lowering the surface tension of the droplet, the equilibrium size to which the droplet may grow is altered by the presence of a monolayer at the air-water interface (Seidl, 2000). The uptake of gaseous species to the droplet may also be inhibited (Decesari et al. 2003; Viccelli et al. 2004) thus the droplet chemistry will vary from an uncoated droplet. Oxidation which degrades the film would increase the surface tension taking its value closer to that of a pure aqueous droplet (King et al. 2009). The implications of the oxidation of the organic film are that:

- The monolayer area per molecule will be increased as material is lost from the air-water interface.
- Oxidation of a monolayer and loss of coverage at the air-water interface of an atmospheric aerosol particle would increase the equilibrium vapour pressure according to the Kelvin equation, requiring a higher supersaturation for droplet nucleation.
- The monolayer could be replaced by the least soluble organic component of the organics within the droplet phase as demonstrated by Voss et al., (2006).
- Oxygenated product species generated at the air-water interface by the reaction of insoluble organic monolayers could be better able to uptake water than the original monolayer (Cruz and Pandis, 1998; Elaison et al. 2004). A loss of the monolayer due to oxidation could lead to rapid evaporation of a droplet.
- King et al., (2009) showed that in terms of Köhler modelling, the growth curve of a CCN into a cloud droplet was more effected by the contribution of soluble reaction

products to the Raoult term than by the change in surface tension as a result of monolayer oxidation (the Kelvin term) (King et al. 2009), thus the reaction products regardless of their propensity for the interface will also have an effect on the growth of a CCN.

- The presence of a monolayer delays the adsorption of water vapour reducing the number of new cloud droplets in an air-mass of a given saturation (Feingold and Chuang, 2002; Decesari et al. 2003). Oxidation of the monolayer would increase the adsorption of water vapour and thus increase the number of new cloud droplets which could lead to enhancement of the Twomey effect.

The effect of the oxidation of a droplet monolayer on the chemistry at the air-water interface is poorly constrained, this thesis is an attempt to build on the work of King et al., (2009, 2010) by using the technique of neutron reflectometry to probe the effect of atmospheric oxidant species on the amount of labelled organic material residing at the air-water interface. Kinetic analysis of the persistence of surface active material at the interface will provide data on how long the reaction of an insoluble organic monolayer with a specific oxidant will take, when compared with the lifetime of an atmospheric droplet it can be seen which processes occur on a timescale that would affect the droplets' hygroscopicity.

1.6 Using the Neutron Reflectometry Technique to Study Atmospheric Monolayers

Following the studies of King et al., (2009, 2010) and Thompson et al., (2010) the work in this thesis utilizes the same neutron reflectometry technique to collect surface coverage measurements of an organic monolayer at the air-water interface over time during an oxidation reaction, coupled with surface pressure measurements which were obtained simultaneously. The measurement technique, methods of neutron generation and the geometry of the reflectometer instruments are given in the relevant experimental chapters.

The use of neutrons is complex and expensive when compared to other techniques in atmospheric science however several unique properties of the neutron facilitate measurements on a molecular level which can only be achieved with this technique.

- Unlike light neutrons only interact with the nucleus of an atom and not the electron cloud (Squires, 1978). The neutron does not react with the sample being investigated, in this case the monolayer as the neutron is electronically neutral (Squires, 1978) allowing kinetic measurements to be taken without changing the chemical outcome of a reaction.

- The wavelength of a thermal neutron is of the order of 0.1 to 30 Ångstrom (Eastoe, 2003). This wavelength is similar to the length of the spacing between atoms within a molecule (Squires, 1978).
- Each atom has a scattering length for neutrons. The scattering length (b) for hydrogen is -3.74 fm and for deuterium is 6.68 fm, vastly different, allowing the manipulation of scattering to determine structural information as the contrast affects the time of flight of a neutron through a sample (Penfold and Thomas, 1990).

In neutron reflectometry a beam of neutrons is directed at the sample. Neutrons within the beam will penetrate the atomic nuclei in the sample which scatter the incident neutrons. The scattering length of an organic molecule can be drastically changed by substituting deuterium for hydrogen. In the work in this thesis the experiments are designed so that the scattering of the neutrons is from the monolayer at the air-water interface within the Langmuir Trough giving a measurement from which the average amount of deuterated material at the air-water interface over reaction time (the surface coverage, Γ) can be constrained, providing a measurement suitable for kinetic analysis.

Isotopic substitution is used in this work to ensure that the scattering of neutrons takes place predominantly from the monolayer, by creating a subphase beneath the monolayer which scatters neutrons to the same degree as air. The substitution of hydrogen atoms with deuterium atoms within a molecule as a label will increase the reflectivity from specific part of a molecule which can give structural information about a monolayer and its changing composition during a reaction, this technique was also used.

The measurement of the monolayer surface coverage gives an advantage over measurement of the surface pressure alone as the surface coverage is a measurement of the amount of material present at the interface whereas the surface pressure is merely a product of the interaction between the molecules comprising the monolayer. A measure of quantity with time allows a kinetic analysis of the reaction of an atmospheric oxidant with a monolayer at the air-water interface which yields rate constants which can be used to model the effect of oxidation by a specific species on the lifetime of a cloud droplet or aqueous aerosol particle.

By placing the Langmuir trough in a controlled environment provided by an aluminium reaction chamber, the concentration of an oxidant gas in the air above the Langmuir trough can be controlled to probe the kinetics of any oxidising reactions. The reaction chamber was constructed from aluminium as aluminium does not activate and has a minimal effect on neutron scattering. Two reaction chambers were used for the majority of this work, each custom made to fit the neutron instruments sample areas and will be illustrated in the relevant

experimental chapters. A third reaction chamber was constructed in the laboratory at Royal Holloway University for running experiments in preparation for neutron measurements.

The thesis chapters are devoted to neutron experiments exploring the oxidation of monolayer organic films by different reactive species. Decay mechanisms describing the reaction occurring at the air-water interface were fitted to the neutron reflectivity data in the format of surface coverage over time to obtain rate constants for the reaction of OH generated in the aqueous phase and gas phase O₃ with various monolayers.

References

- Andreae, M.O. and Rosenfeld, D. 2008. Aerosol-cloud-precipitation interactions. Part 1. The nature and sources of cloud-active aerosol. *Earth-Science Reviews*, 89, 13-41.
- Aumann, E., and Tabazadeh, A. 2008. Rate of organic film formation and oxidation on aqueous drops. *Journal of Geophysical Research*, 113, D23205.
- Barnes, G.T. and Gentle, I.R. 2005. *Interfacial Science*. Oxford University Press. UK.
- Beard, K.V. and Ochs, H.T. (III). 1992. Warm-Rain Initiation. An Overview of Microphysical Mechanisms. *Journal of Applied Meteorology*, 32, pp. 608-625.
- Bertram, A.K., Ivanov, A.V., Hunter, M., Molina, L.T., Molina, M.J. 2001. The Reaction Probability of OH on Organic Surfaces of Tropospheric Interest. *The Journal of Physical Chemistry A*, 105, 41, pp. 9415-9421.
- Centre for Atmospheric Science (CAS), University of Manchester. 2011. Web pages on warm cloud characteristics. The University of Manchester.
<http://www.cas.manchester.ac.uk/resactivities/cloudphysics/background/warm/index.html>. As accessed on 13/09/11.
- Cruz, C.N., and Pandis, S.N. 1998. A Study of the Ability of Pure Secondary Organic Aerosol to Act as Cloud Condensation Nuclei. *Atmospheric Environment*, 31, 15, pp. 2205-2214.
- Descesari, S., Facchini, M.C., Mircea, M., Cavalli, F., Fuzzi, S. 2003. Solubility properties of surfactants in atmospheric aerosol and cloud/fog water samples. *Journal of Geophysical Research*, 108, D21, pp.4685-4694.
- Donaldson, D.J. and Vaida, V. 2006. The Influence of Organic Films at the Air-Aqueous Boundary on Atmospheric Processes. *Chemical Reviews*, 106, pp. 1445-1461.
- Eastoe, J. 2003. *Surfactant Chemistry, Scattering Techniques*. Available online at:
http://www.chm.bris.ac.uk/eastoe/Surf_Chem/ as accessed on 09/01/2012.
- Elaison, T.L., Gilman, J.B., Vaida, V. 2004. Oxidation of organic films relevant to atmospheric aerosols. *Atmospheric Environment*, 38, pp. 1367-1378.
- Ellison, G.B., Tuck, A.F., Vaida, V. 1999. Atmospheric processing of organic aerosols. *Journal of Geophysical Research*, 104, D9, pp. 11633-11641.

- Feingold, G., and Chuang, P.Y. 2002. Analysis of the Influence of Film-Forming Compounds on Droplet Growth: Implications for Cloud Microphysical Processes and Climate. *Journal of the Atmospheric Sciences*, 59, pp. 2006-2018.
- Finlayson-Pitts, B. Pitts J.N. 2000 Chemistry of the Upper and Lower Atmosphere, Theory, Experiments and Applications. Academic Press, California, USA.
- Fu, P., Kawamura, K., Barrie, L.A. 2009. Photochemical and Other Sources of Organic Compounds in the Canadian High Arctic Aerosol Pollution during Winter and Spring. *Environmental Science and Technology*, 43, 2, pp. 286-292.
- Giddings, W.P., and Baker, M.B. 1977. Sources and Effects of Monolayers on Atmospheric Water Droplets. *Journal of the Atmospheric Sciences*, December 1977, pp. 1957-1964.
- Gill, P.S., Greadel, T.E., Weshler, C.J. 1983. Organic Films on Atmospheric Aerosol Particles, Fog Droplets, Cloud Droplets, Raindrops and Snowflakes. *Reviews of Geophysics and Space Physics*, 21, 4, pp. 903-920.
- Gilman, J.B., Elaison, T.L., Fast, A., Vaida, V. 2004. Selectivity and stability of organic films at the air-aqueous interface. *Journal of Colloid and Interfacial Science*, 280, pp. 234-243.
- Gilman, J.B., Tervahattu, H., Vaida, V. 2006. Interfacial properties of mixed films of long-chain organics at the air-water interface. *Atmospheric Environment*, 40, pp. 6606-6614.
- Gourdeau, J. 2012. Web pages of the Max Planck Institute in Mainz Atmospheric Chemistry Department: http://www.atmosphere.mpg.de/enid/1__What_happens_in_clouds_-/_Cloud_chemistry_td.html accessed on 1/2/2012 author: J. Gourdeau. 1st scientific reviewer: M. Leriche, CNRS LaMP, France.
- Graedel, T.E., and Weshler, C.J. 1981. Chemistry within aqueous atmospheric aerosols and raindrops. *Reviews of Geophysics*, 19, 4, pp. 505-539.
- Hardy, J.T. 1982. The Sea Surface Microlayer: Biology, Chemistry and Anthropogenic Enrichment. *Progress in Oceanography*, 11, pp. 307-328.
- Haywood, J., and Boucher, O. 2000. Estimates of the direct and indirect radiative forcing due to tropospheric aerosols: A review. *Reviews of Geophysics*, 38, 4, pp. 513-542.
- Hegg, D.A., and Hobbs, P.V. 1981. Cloud Water Chemistry and the Production of Sulfates in Cloud. *Atmospheric Environment*, 15, 9, pp. 1597-1604.
- Husar, R.B., and Shu, W.R. 1975. Thermal Analysis of Los Angeles Smog Aerosol. *Journal of Applied Meteorology*, 14, pp. 1558-1565.

IPCC, 2007: Climate Change 2007: The Physical Science Basis. Contribution of Working Group I to the Fourth Assessment Report of the Intergovernmental Panel on Climate Change [Solomon, S., D. Qin, M. Manning, Z. Chen, M. Marquis, K.B. Averyt, M. Tignor and H.L. Miller (eds.)]. Cambridge University Press, Cambridge, United Kingdom and New York, NY, USA.

Johnson, B.T., Shine, K.P., Forster, P.M. 2004. The semi-direct aerosol effect: Impact of absorbing aerosols on marine stratocumulus. *Quarterly Journal of the Meteorological Society*, 130, pp. 1407-1422.

King, M.D., Thompson, K.C.T., Ward, A. 2004. Laser Tweezers Ramen Study of Optically Trapped Aerosol Droplets of Seawater and Oleic Acid Reacting with Ozone: Implications for Cloud-Droplet Properties. *Journal of the American Chemical Society*, 126, 51, pp. 16710-16711.

King, M.D., Rennie, A.R., Thompson, K.C., Fisher, F.N., Chaun Dong, C., Thomas, R.K., Pfrang, C., Hughes, A.V. 2009. Oxidation of oleic acid at the air-water interface and its potential effects on cloud critical supersaturations. *Physical Chemistry Chemical Physics*, 11, pp. 7699-7707.

King, M.D., Rennie, A.R., Pfrang, C., Hughes, A.V., Thompson, K.C. 2010. Interaction of nitrogen dioxide (NO₂) with a monolayer of oleic acid at the air-water interface – A simple proxy for atmospheric aerosol. *Atmospheric Environment*, 44, pp. 1822- 1825.

Köhler, H. 1936. The Nucleus In and the Growth of Hygroscopic Droplets. *Transactions of the Faraday Society*, 32, pp. 1152-1161.

Kommalapati, R.R., and Valsaraj, K.T. 2009. Atmospheric Aerosols and Their Importance. Chapter 1 in Atmospheric Aerosols edited by K.T. Valsaraj and R.R. Kommalapati published as part of the ACS Symposium Series, Volume 1005.

Knothe, G., Sharp, C.A., Ryan, T.W. 2006. Exhaust Emissions of Biodiesel, Petrodiesel, Neat Methyl Esters, and Alkanes in a New Technology Engine. *Energy and Fuels*, 20, 1, pp. 403-408.

KSV NIMA. 2010. <http://www.ksvnima.com/surface-pressure> as accessed on 2/12/2010.

Lohmann, U., and Feichter, J. 2005. Global indirect aerosol effects: a review. *Atmospheric Chemistry and Physics*, 5, pp. 715-737.

Marty, J.C., Saliot, A., Baut-Ménard, P., Chesselet, R., Hunter, K.A. 1979. Relationship Between the Lipid Compositions of Marine Aerosols, the Sea Surface Microlayer, and Subsurface Water. *Journal of Geophysical Research*, 84, C9, pp. 5707-5716.

Mattis, I., Ansmann, A., Althausen, D., Jaenisch, V., Wandinger, U., Müller, D., Arshinov, Y.F., Bobrovnikov, S.M., Serikov, I.B. 2002. Relative-Humidity Profiling in the Troposphere with a Ramen Lidar. *Applied Optics*, 41, 30, pp. 6451-6462.

McFiggans, G., Alfarra, M.R., Allan, J., Bower, K., Coe, H., Cubinson, M., Topping, D., Williams, P., Decesari, S., Facchini, C., Fuzzi, S. 2005. *Faraday Discussions*, 130, pp. 341-362.

Mochida, M., Kitamori, Y., Kawamura, K. 2002. Fatty acids in the marine atmosphere: Factors governing their concentrations and evaluation of organic films on sea-salt particles. *Journal of Geophysical Research*, 107, D17, pp. 4325-4335.

Mochida, M., Katrib, Y., Jayne, J.T., Worsnop, D.R., Martin, S.T. 2006. The relative importance of competing pathways for the formation of high-molecular weight peroxides in the ozonolysis of organic aerosol particles. *Atmospheric Chemistry and Physics Discussions*, 6, pp. 7137-7176.

Moise, T., and Rudich, Y. 2001. Uptake of Cl and Br by organic surfaces – A perspective on organic aerosols processing by tropospheric oxidants. *Geophysical Research Letters*, 28, 21, pp. 4083-4086.

O'Dowd, C.D., Lowe, J.A., Smith, M.H. 1999. Coupling sea-salt and sulphate interactions and its impact on cloud droplet concentration predictions. *Geophysical Research Letters*, 26, 9, pp. 1311-1314.

Pandis, S. N., Harley, R.A., Cass, G.R., Seinfeld, J.H. 1992. Secondary Organic Aerosol Formation and Transport. *Atmospheric Environment*, 26A, 13, pp. 2269-2282.

Penfold, J., and Thomas, R.K. 1990. The application of the specular reflection of neutrons to the study of surfaces and interfaces. *Journal of Physics: Condensed Matter*, 2, pp. 1369-1412.

Peterson, R.E., Nair, A., Dambach, S., Arlinghaus, H.F., Tyler, B.J. 2006. Characterization of individual atmospheric aerosol particles with SIMS and laser-SNMS. *Applied Surface Science*, 252, pp. 7006-7009.

Peterson, R.E., and Tyler, B.J. 2002. Analysis of organic and inorganic species on the surface of atmospheric aerosol using time-of-flight secondary ion mass spectrometry (TOF-SIMS). *Atmospheric Environment*, 36, pp. 6041-6049.

Peterson, R.E., and Tyler, B.J. 2003. Surface composition of atmospheric aerosol: individual particle characterization by TOF-SIMS. *Applied Surface Science*, 203-204, pp. 751-756.

Pöschl, U. 2005. Atmospheric Aerosols: Composition, Transformation and Health Effects. *Angewandte Chemie International Edition*, 44, pp. 7520-7540.

Reid, J.P., Dennis-Smith, B.J., Kwamena, N-O A., Miles, R.E.H., Hanford, K.L., Homer, C.J. 2011. The morphology of aerosol particles consisting of hydrophilic phases: hydrocarbons, alcohols, and fatty acids as the hydrophobic component. *Physical Chemistry Chemical Physics*, 13, pp. 15559-15572.

Rogge, W.F., Hildermann, L.M., Mazurek, M.A., Cass, G.R., Simoneit, B.R.T. 1991. Sources of Fine Organic Aerosol. 1. Charbroilers and Meat Cooking Operations. *Environmental Science and Technology*, 25, pp. 1112-1125.

Rogge, W.F., Hildemann, L.M., Mazurek, M.A., Cass, G.R., Simoneit, B.R.T. 1993. Sources of Fine Organic Aerosol. 2. Noncatalyst and Catalyst-Equipped Automobiles and Heavy-Duty Diesel Trucks. *Environmental Science and Technology*, 27, pp. 636-651.

Rontu, N., and Vaida, V. 2007. Miscibility of Perfluorododecanoic Acid with Organic Acids at the Air-Water Interface. *The Journal of Physical Chemistry C*, 111, 27, pp. 9975-9980.

Rudich, Y. 2003. Laboratory Perspectives on the Chemical Transformations of Organic Matter in Atmospheric Particles. *Chemical Reviews*, 103, 12, pp. 5097-5124.

Russell, L.M., Maria, S.F., Myneni, S.C.B. 2002. Mapping organic coatings on atmospheric particles. *Geophysical Research Letters*, 29, 16.

Russell, L.M., Hawkins, L.N., Frossard, A. A., Quinn, P.K., Bates, T.S. 2010. Carbohydrate-like composition of submicron atmospheric particles and their production from ocean bubble busting. *Proceedings of the National Academy of Sciences of the United States of America*, 107, 15, pp. 6657-6652.

Schwartz, S.E. 2003. Chapter 17 in the Handbook of Weather, Climate, and Water Edited by: T. D. Potter and B. R. Colman. Wiley –Interscience, pp. 331-345.

Seidl, W. 2000. Model for a surface film of fatty acids on rain water and aerosol particles. *Atmospheric Environment*, 34, pp. 4917-4932.

Seinfeld, J.H., and Pandis, S.N. 1998. Atmospheric Chemistry and Physics : From Air Pollution to Climate Change. John Wiley and Sons, New York.

Shulman, M.L., Jacobson, M.C., Carlson, R.J., Synovec, R.E., Young, T.E. 1996. Dissolution behaviour and surface tension effects of organic compounds in nucleating cloud droplets. *Geophysical Research Letters*, 23, 3, pp. 277-280.

Simoneit, B.R.T. 2002. Biomass burning- a review of organic tracers for smoke from incomplete combustion. *Applied Geochemistry*, 17, pp. 129-172.

Simoneit, B.R.T., Kobayashi, M., Mochida, M., Kawamura, K., Huebert, B.J. 2004. Aerosol particles collected on aircraft flights over the northwestern Pacific region during the ACE-Asia campaign:

Composition and major sources of the organic compounds. *Journal of Geophysical Research*, 109, D19S09.

Smoydzin, L., and von Glasow, R. 2007. Do organic surface films on sea salt aerosols influence atmospheric chemistry? – a model study. *Atmospheric Chemistry and Physics*, 7, pp. 5555-5567.

Sodergren, A. 1987. Origin and Composition of Surface Slicks in Lakes of Differing Trophic Status. *Limnology and Oceanography*, 32, 6, pp. 1307-1316.

Sprakling, M.T., 1985. Liquids and Solids. Kluwer Academic Publishers.

Squires, G.L., 1978. Introduction to the Theory of Thermal Neutron Scattering. Dover Publications.

Sun, J., and Ariya, P.A. 2006. Atmospheric organic and bio-aerosols as cloud condensation nuclei (CCN): A review. *Atmospheric Environment*, 40, pp. 795-820.

Tedetti, M., Kawamura, K., Narukawa, M., Joux, F., Charrière, B., Sempéré, R. 2007. Hydroxyl radical-induced photochemical formation of dicarboxylic acids from unsaturated fatty acid (oleic acid) in aqueous solution. *Journal of Photochemistry and Photobiology A: Chemistry*, 188, pp. 135-139.

Tervahattu, H., Hartonen, K., Kerminen, V-M., Kupiainen, K., Aarnio, P., Koskentalo, T., Tuck, A.F., Vaida, V. .2002^a. New evidence for an organic layer on marine aerosols. *Journal of Geophysical Research*, 107, D7.

Tervahattu, H., Juhanoja, J., Kupiainen, K. 2002^b. Identification of an organic coating on marine aerosol particles by TOF-SIMS. *Journal of Geophysical Research*, 107, D16.

Tervahattu, H., Juhanoja, J., Vaida, V., Tuck, A.F., Niemi, J.V., Kupiainen, K., Kumala, M., Vehkamäki, H. 2005. Fatty acids on continental sulphate aerosol particles. *Journal of Geophysical Research*, 110, D06207.

Thompson, K.C., Rennie, A.R., King, M.D., Hardman, S.J.O., Lucas, C.O.M., Pfrang, C., Hughes, B.R., Hughes, A.V. 2010. Reaction of a Phospholipid Monolayer with Gas-Phase Ozone at the Air-Water Interface: Measurement of Surface Excess and Surface Pressure in Real Time. *Langmuir*, 26, 22, pp. 17295-17303.

Tuckermann, R., Bauerecker, S., Cammenga, H.K. 2007. Generation and characterization of surface layers on acoustically levitated drops. *Journal of Colloid and Interface Science*, 310, pp. 559-569.

Twomey, S. 1974. The Influence of Pollution on the Shortwave Albedo of Clouds. *Journal of the Atmospheric Sciences*, 34, pp. 1149-1152.

Vaida, V., Tuck, A.F., Ellison, G.B. 2000. Optical and Chemical Properties of Atmospheric Organic Aerosols. *Physics and Chemistry of the Earth (C)*, 25, 3, pp. 195-198.

Vieceli, J., Ma, O.L., Tobias, D.J. 2004. Uptake and Collision Dynamics of Gas-phase Ozone at Unsaturated Organic Interfaces. *Journal of Physical Chemistry A*, 108, pp 5806-5814.

Voss, L.F., Hadad, C.M., Allen, H.C. 2006. Competition between Atmospherically Relevant Fatty Acid Monolayers at the Air/Water Interface. *The Journal of Physical Chemistry, B*, 110, 39, pp. 19487-19490.

Voss L.F., Bazerbashi M.F., Beekman C.P., Hadad C.M., Allen H.C., 2007. Oxidation of oleic acid at air/liquid interfaces. *Journal of Geophysical Research*, 112, D06209. pp.1-9.

Warneck, P. 1988. Chemistry of the Natural Atmosphere. International Geophysics Series. Volume 41. Academic Press Inc, San Diego, USA.

Weathers, K.C., Likens, G.E., Bormann, F.H., Bicknell, S.H., Bormann, B.T., Daube Jr, B.C., Eaton, J.S., Galloway, J.N., Keene, W.C., Kimball, K.D., McDowall, W.H., Siccama, T.G., Smlley, D., Tarrant, R.A. 1988. Cloudwater Chemistry from Ten Sites in North America. *Environmental Science and Technology*, 22, pp. 1018-1026.

Winer, A.M., Arey, J., Atkinson, R., Aschmann, S.M., Long, W.D., Morrison, C.L., Olszrk, D.M. 1992. Emission Rates of Organics From Vegetation in California's Central Valley. *Atmospheric Environment*, 26A, 14, pp. 2647-2659.

Wyslouzil, B.E., Wilemski, G., Strey, R., Heath, C.H., Dieregsweiler, U. 2006. Experimental evidence for internal structure in aqueous-organic nanodroplets. *Physical Chemistry Chemical Physics*, 8, pp. 54-57.

Zahardis, J. and Petrucci, G.A. 2007. The oleic acid-ozone heterogeneous reaction system: products, kinetics, secondary chemistry, and atmospheric implications of a model system – a review. *Atmospheric Chemistry and Physics*, 7, pp.1237-1274.

Hydroxyl Radical Oxidation of Stearic Acid Monolayers

2.0 Abstract

A monolayer of stearic acid, a naturally occurring insoluble organic amphiphile was oxidised with aqueous-phase hydroxyl radicals, generated by the photolysis of hydrogen peroxide. The rate of film oxidation at the air-water interface was monitored with neutron reflection on a Langmuir trough. The monolayer of deuterated stearic acid ($C_{18}D_{35}O_2H$) serves as a proxy for the organic film at the air-droplet interface of a cloud droplet. The surface pressure of the monolayer was measured with a Wilhelmy plate and the surface coverage of the deuterated material was measured with neutron reflection. The surface pressure and surface coverage declined with photolysis time. The kinetic decay of the surface coverage may be fitted to a degradation mechanism (species: stearic acid \rightarrow product A \rightarrow product B) with two surface-active products from the reaction between stearic acid and hydroxyl radical. We have shown that organic films at an air-water interface may initially resist aqueous-phase oxidation by hydroxyl radical; however continued oxidation will completely remove the film. The chemical lifetime of stearic acid and its product film from the reaction with aqueous hydroxyl radical exceeds 500 days and thus the chemical oxidation of stearic acid in aerosol and on cloud droplets in the atmosphere is unlikely.

2.1 Introduction

Atmospheric aerosol particles in the troposphere act as cloud condensation nuclei. The oxidation of atmospheric aerosols influences climate through cloud formation and precipitation effects, (Lohmann and Feichter, 2005; IPCC, 2007). Some cloud condensation nuclei have been shown to possess an organic film (Blanchard., 1964; Gill et al. 1983; Tervahattu et al. 2002^{a,b}, 2005). As a cloud droplet ages in the atmosphere it will be subject to oxidation by radical species from outside and within the droplet phase.

To investigate the process of the reaction of an insoluble organic layer at the air-water interface oxidised by a radical species from within a cloud droplet, aqueous phase hydroxyl radical (OH) was reacted with a monolayer of stearic acid formed at the surface of a Langmuir trough. By monitoring the surface pressure of the monolayer on an aqueous subphase, it was demonstrated that a reaction may be taking place. To study the kinetics and atmospheric relevance of this reaction the surface coverage of molecules at the air-water interface was measured using neutron reflection.

The experiment described here assesses the behaviour of a monolayer of stearic acid at the air-water interface as it reacts with OH.

2.2 Aims

1. To monitor the properties of surface pressure and surface coverage of a monolayer of stearic acid at the air-water interface in real time as the monolayer was oxidised with aqueous phase OH.
2. Kinetic analysis of the surface coverage of a monolayer of stearic acid over time to determine a rate constant for the reaction of stearic acid with aqueous phase OH.
3. To elucidate the mechanism for stearic acid removal from the air-water interface.
4. Calculation of the chemical lifetime of a stearic acid monolayer on a typical cloud droplet in the atmosphere in order to show the importance of the oxidation reaction of a monolayer of an insoluble amphiphile with aqueous phase hydroxyl radical in the atmosphere.

2.3 Background

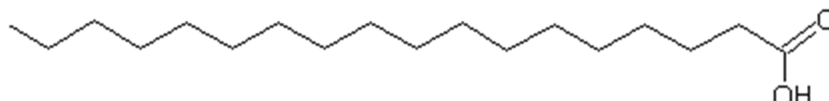
The chemical oxidation of cloud droplet films has not been widely studied. The presence of a cloud droplet film will increase the surface pressure (Π), thus decreasing the surface tension at the air-water interface. Oxidation of the organic surfactants in a cloud droplet film may have an effect on the surface pressure of the monolayer and its surface coverage (Γ) at the air-water interface. Alteration of the surface properties of a film as it ages chemically in the atmosphere will alter the critical supersaturation value according to the Köhler theory of cloud droplet formation and growth as explained in chapter 1.

The number and growth of cloud condensation nuclei (CCN) into cloud droplets has climatic implications. A chemical reaction at the air-water interface of atmospheric aerosol could activate a cloud condensation nuclei allowing hydrodynamic growth (the uptake of water), into a cloud droplet. A larger number of smaller cloud droplets in a defined parcel of air with a constant volume of water would scatter more radiation thus increasing the albedo of the cloud (Twomey, 1974). It should be noted that in reality the quantity of water vapour is not constant during cloud formation.

2.3.1 Stearic Acid and Cloud Droplet Films

Stearic acid is a saturated insoluble fatty acid, $(\text{CH}_3(\text{CH}_2)_{16}\text{COOH})$ with a straight chain of an even carbon number 18 which is present in the sea surface microlayer, a layer of organic material found at the surface of oceans formed from lipid membrane disintegration (Marty et al. 1979; Tervahattu et al. 2002^{a,b}).

Figure 2.1 *The Structure of Stearic Acid.*



The stearic acid molecule has a carboxylic acid head group with a saturated aliphatic hydrocarbon chain. The functional group is the (-COOH) carboxylic acid head which is hydrophilic. At the air-water interface the head group bonds to the hydrogen in the subphase and the chain is orientated into the air.

The amphiphilic structure of fatty acid molecules means that given a sufficient chain length the molecules will form a monolayer at the air-water interface. Stearic acid has a hydrophobic hydrocarbon chain length of 18 carbon atoms and orientates at surface pressures above $\sim 1 \text{ mNm}^{-1}$ with the hydrocarbon chain directed into the air whilst the carboxylic head group sits in the aqueous subphase of the droplet. Stearic acid provides an example of a saturated fatty acid which forms an insoluble monolayer at the air-water interface with which to explore the effect of OH oxidation as an example of an aqueous phase reaction that could produce secondary oxidation products.

In urban areas the majority of organics are primary in nature and hydrophobic (Saxena et al. 1995; Finlayson-Pitts and Pitts. 2000). Bi et al., (2008), sampled aerosol in the city of Guangzhou, South China detecting over 140 organic compounds many of which were secondary oxidation products, short chain dicarboxylic acids formed by the photo-oxidation of larger organic compounds. Photo-oxidation is an important process by which atmospheric aerosol is aged during transport.

The enriched layer of biological debris at the ocean air-water interface, the sea-surface microlayer, contributes organics to the atmosphere that are surface active, (Gill et al. 1983; Ellison et al. 1999; Donaldson and Vaida, 2006). The annual flux of marine aerosol to the atmosphere is approximately $3,300 \text{ Tg / yr}$ (Penner et al, 2001) based on the dry diameter of sea salt aerosol thus the amount of aerosol transmitted including wet organics would be higher than this figure. Stearic acid is a component of the sea-surface microlayer and its presence as a

constituent of marine aerosol (Tervahattu et al. 2002^{a,b}) indicates that stearic acid is transported into the atmosphere on aerosol which potentially act as cloud condensation nuclei. Stearic acid is also found in surface slicks on freshwater lakes (Meyers and Kawka, 1982; Södergren, 1987).

Rogge et al., (1991) estimated that meat cooking emissions accounted for up to 21% of the primary organic carbon particles in the area of Los Angeles and that stearic acid was emitted from grilling and frying of meat at a rate of 50.5 kg day⁻¹ or 70.6 kg day⁻¹ depending on the blends of processed meat being cooked. In the same study data from aerosol samples collected in 1982 was analysed and an ambient concentration of stearic acid of 106.2 ng m⁻³ was calculated for Western Los Angeles (Rogge et al. 1991). An increasing source of stearic acid in the troposphere is the combustion of biofuels (Khral et al. 2009).

Stearic acid provides a good proxy for an insoluble organic layer at the air-water interface as it is found in aerosol samples so is a genuine candidate for a cloud droplet film forming compound.

2.3.2 Oxidation of Cloud Droplet Films

The atmosphere is an oxidising environment (Finlayson Pitts and Pitts, 2000), where sunlight provides energy for reactions and radical chemistry provides the catalyst for oxidation of particulate, aqueous and gas-phase compounds. The organic film at the air-water interface of a cloud droplet is exposed to oxidants dissolved in and generated within the droplet (e.g. Bertram et al. 2001; King et al. 2004; Tedetti et al. 2007; Voss et al. 2007; Aumann and Tabazadeh, 2008), such as hydroxyl radical.

An organic film on a cloud droplet may react by the process of:

1. Gas-phase collisions of oxidant molecules with the surface of a cloud condensation nuclei or droplet.
2. Gas-phase oxidants that have dissolved into the droplet liquid phase and reacted with the film.
3. Oxidants generated in the droplet liquid phase which react with the film at the surface of the droplet.

Thus the film may be expected to oxidise. The lifetime of an oxidation reaction would need to be shorter than the lifetime of the cloud droplet to be a significant process to consider in climate modelling. The lifetime of a cloud droplet is controlled by many factors, such as fog formation, precipitation, entrainment of warm or dry air into the cloud which causes evaporation, and rates of mixing and uplift within a cloud. Measurement of the specific age of a cloud droplet in situ is

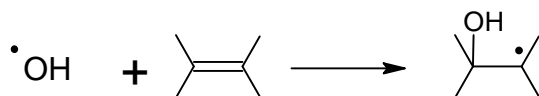
not possible, estimations are made based on modelling of the period of time an air parcel has spent in a cloud together with satellite images of the horizontal extent of the cloud and wind speed measurements (Colvile et al. 1997). Colvile et al., (1997) estimated an average cloud droplet age for orographic cloud at Great Dun Fell, UK during April and May 1993 of 1 to 30 minutes.

The lifetime of a cloud droplet within a cloud could be altered by the presence of a surfactant monolayer as this would decrease the droplets surface tension which would allow the droplet to uptake more water vapour and grow, however if such a monolayer was oxidised away then the droplets surface tension would be increased and the droplet would be more likely to evaporate. The effect of a surfactant film on cloud droplet growth is small and brief. Once a cloud droplet starts to grow the surface tension is not important, however the activation of cloud droplet nuclei is a component of climate modelling so investigation of the chemistry of atmospheric monolayer films will provide data for atmospheric modelling. Within this chapter I investigate the oxidation of a saturated fatty acid monolayer film by generating oxidants in the droplet liquid phase which may react with a film at the air-water interface by generating liquid phase OH beneath a stearic acid monolayer.

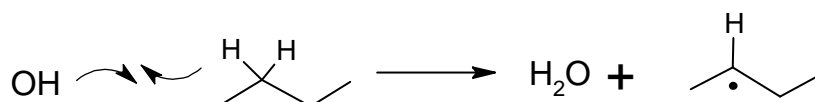
The experiments described in this chapter aim to assess the behaviour of a monolayer of stearic acid at the air-water interface as it reacts with hydroxyl radical. The following schemes show the two ways in which OH can react with an organic, film forming molecule.

Figure 2.2 *The Addition of OH to a Double Bond and the Abstraction of Hydrogen by OH from a Single Hydrocarbon Bond*

1. OH can add to double bonds



2. OH can abstract a hydrogen



In the case of an unsaturated molecule such as oleic acid hydroxyl radical (OH) can complete process 1 and 2. In stearic acid hydrogen abstraction of the hydrogen from the CH₂ groups by OH as in process 2 / figure 2.2 is predicted to lead to a series of shorter chain products. OH radical is oxidising in the presence of oxygen, the radical participates in the first step in a radical

chain reaction the overall process of which is oxidation. The oxidation reaction results in the following general reaction (R 2.1).



2.3.3 Hydroxyl Radical Formation in the Cloud Droplets

The OH radical in cloud water is generated by several different processes. Gas phase OH radical can partition into the droplet phase or aqueous phase OH can be generated by photolysis within the aqueous phase of a cloud droplet where in the presence of oxygen it acts as an oxidant. Photolysis of hydrogen peroxide is a prominent source of hydroxyl radical in atmospheric waters, (Zou and Hoigné, 1992, 1993; Faust et al. 1993; Anastasio et al. 1994; Arakaki and Faust, 1998; Yu and Barker, 2003).

OH radical in the aqueous phase of a cloud droplet can be formed by the following mechanisms:

1. Hydrogen peroxide photolysis and the Haber-Weiss cycle.
2. Uptake into the cloud droplet of gas phase OH radical.
3. Nitrate (NO_3^-) photolysis.
4. Photo-Fenton cycle.
5. Photosensitization of natural organic molecules.

These mechanisms are pictured schematically in figure 2.3.

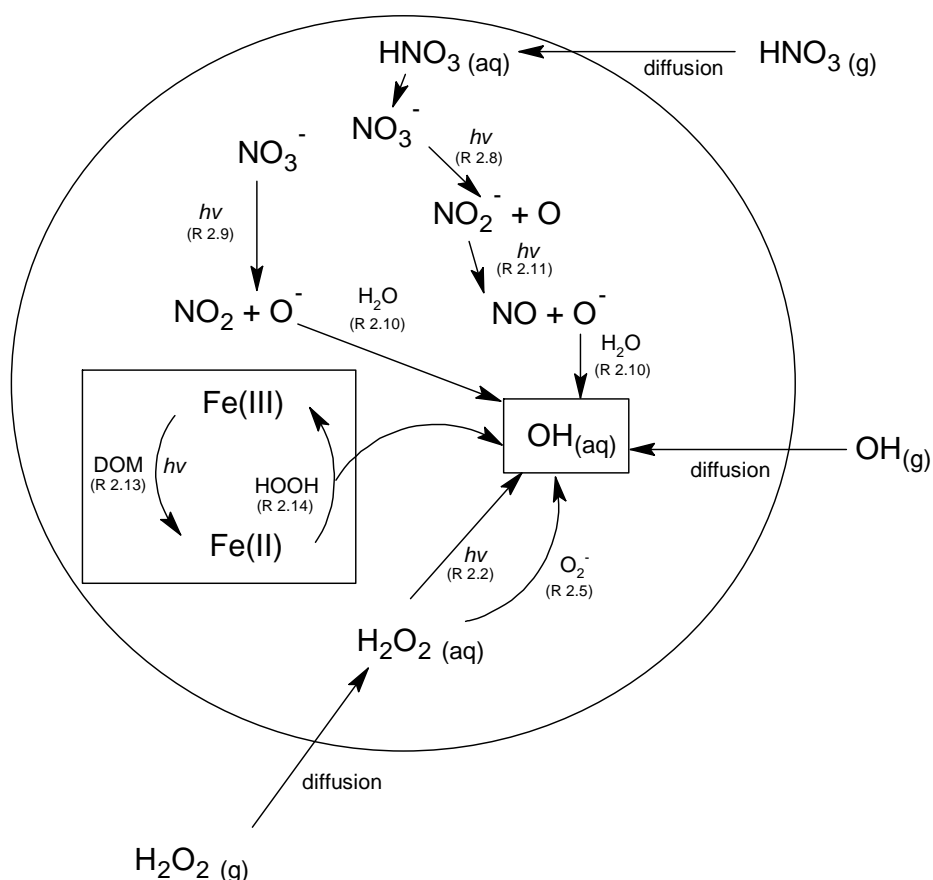
Figure 2.3 Gas-Phase and Liquid-Phase Cycling of OH in the Atmosphere

Figure 2.3 was adapted from Arakaki and Faust (1998).

1. Hydrogen Peroxide Photolysis and the Haber-Weiss Cycle

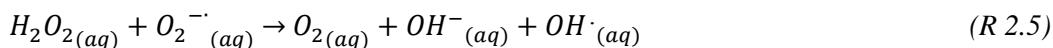
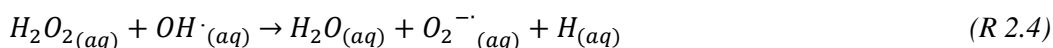
Hydrogen peroxide photolysis occurs within the cloud droplet by the following reaction:



Hydrogen peroxide is scavenged from the atmosphere by cloud droplets, after being formed in the gas phase from combination of hydroperoxyl radicals (HO_2), as shown in reaction 2.3 (Warneck, 1988). H_2O_2 is very soluble with a Henry's Law coefficient of $99000\ M\ atm^{-1}$ at 298.15 K based on data from Lind and Kok, (1986, 1994) as calculated by NIST (2012). The hydrogen peroxide then undergoes photolysis by sunlight producing two hydroxyl radicals within the aqueous phase (R 2.2).

The Haber-Weiss cycle (R 2.3 to 2.5) also produces OH radical in the aqueous phase. Secondary radical chemistry in solution effects the concentration of OH radical formed.





The third reaction in the Haber-Weiss cycle produces OH radicals (R 2.5). In the aqueous phase under experimental conditions there will be a high concentration of H₂O₂ and reaction 2.5 should proceed. Later I demonstrate with bulk kinetic modelling the relative concentrations of H₂O₂, HO₂, OH and O₂.

2. Uptake into the Cloud Droplet of Gas Phase OH Radical

The primary source of gas-phase hydroxyl radical is the photolysis of ozone into excited atomic oxygen (R 2.6), (Bahm and Khalil, 2004) which then reacts with water vapour to produce OH radicals in the gas phase (R 2.7). The gas phase OH radical can then diffuse into the droplet aqueous phase.



3. Nitrate (NO₃⁻) Photolysis

The nitrate photochemical cycle generates droplet phase OH radical from nitrate photolysis. Nitric acid (HNO₃) is scavenged from the atmosphere and nitrate (NO₃⁻) is photolysed releasing an oxygen radical anion. The oxygen radical anion reacts with H₂O to produce OH radical.



Nitrogen dioxide (NO₂) photolysis produces nitric oxide (NO) and excited oxygen. The excited oxygen then reacts with water producing OH radical (R 2.11 and 2.12). Photolysis of nitrite anion (NO₂⁻) produces nitric oxide (NO) and oxygen radical anion. The excited oxygen radical anion reacts with water producing OH radical.

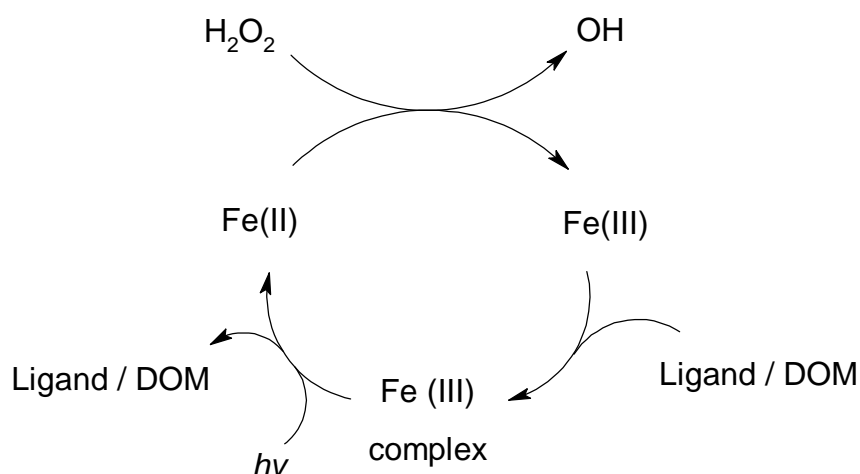


4. The Photo-Fenton Cycle

The photo-Fenton cycle of hydroxyl radical formation in solution catalysed by iron consists of two reactions progressing in unison and can occur within a cloud droplet. Iron is present in atmospheric particles such as fly ash and in clays within desert dust aerosols (Faust and Hoigné, 1990) which can act as cloud condensation nuclei. The iron present within the nuclei dissolves into the nucleated droplet. Rainwater samples from Leeds, UK analysed by Clark and Radojevic, (1987) had a mean iron concentration of $5 \mu\text{M}$, synthetic rainwater samples analysed by Weinstein-Lloyd and Schwartz, (1991) contained 0.02 to $0.3 \mu\text{M}$. The presence of iron leads to OH production via the Fenton mechanism.

The photo-Fenton reactions generate aqueous phase OH radical in two ways. Ferric oxide (Fe(III)) complexes with an organic molecule acting as a direct aqueous phase OH radical source. OH radicals are also formed indirectly by the re-oxidation of iron oxide (Fe(II)) to Fe(III) in the presence of hydrogen peroxide (HOOH), (Faust and Hoigné, 1990; Arakaki and Faust, 1998).

Figure 2.4 *The Photo-Fenton Cycle*



The chemistry in figure 2.4 is adapted from that detailed in Zepp, Faust and Hoigné (1992). DOM denotes dissolved organic matter within the cloud droplet.

Arakaki and Faust (1998) proposed that OH was generated through photolysis in cloudwater samples from Whiteface Mountain, New York and identified two photo-Fenton reaction sources of OH dependent on the aqueous HOOH concentration and independent of HOOH.

concentration. The HOOH dependent sources (R 2.14) were dominant. In acidic cloudwaters Fe(III) is photo chemically reduced to Fe(II) in minutes (R 2.13) (Arakaki and Faust, 1998).



The iron species involved in the Fenton reactions within a cloud droplet are $Fe(OH)^{2+}$ and $Fe(OH)^{4+}$ as both species absorb strongly in the UV region of 290 to 400 nm (Faust and Hoigné, 1990).

5. Photosensitization of Natural Organic Molecules

The photosensitization reaction of oxygen and dissolved organic matter in the aqueous phase of a cloud droplet produces hydroperoxyl radicals (HO_2) (Arakaki et al. 1995; Arakaki et al. 2006). The hydroperoxyl radicals form hydrogen peroxide which then produces OH radical through photolysis.

The basic process is described by reaction 2.15 (sourced from Wayne and Wayne, 1996) where the photosensitizer molecule for example dissolved organic matter in the cloud droplet in a triplet state (see Benzophenone in figure 2.5). The reaction results in the formation of superoxide oxygen radical which reacts with H_2O_2 producing the OH radical (R 2.3 to 2.5).

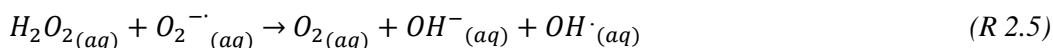
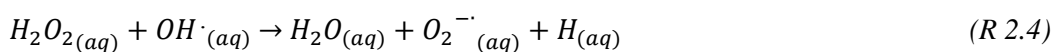
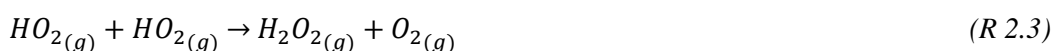
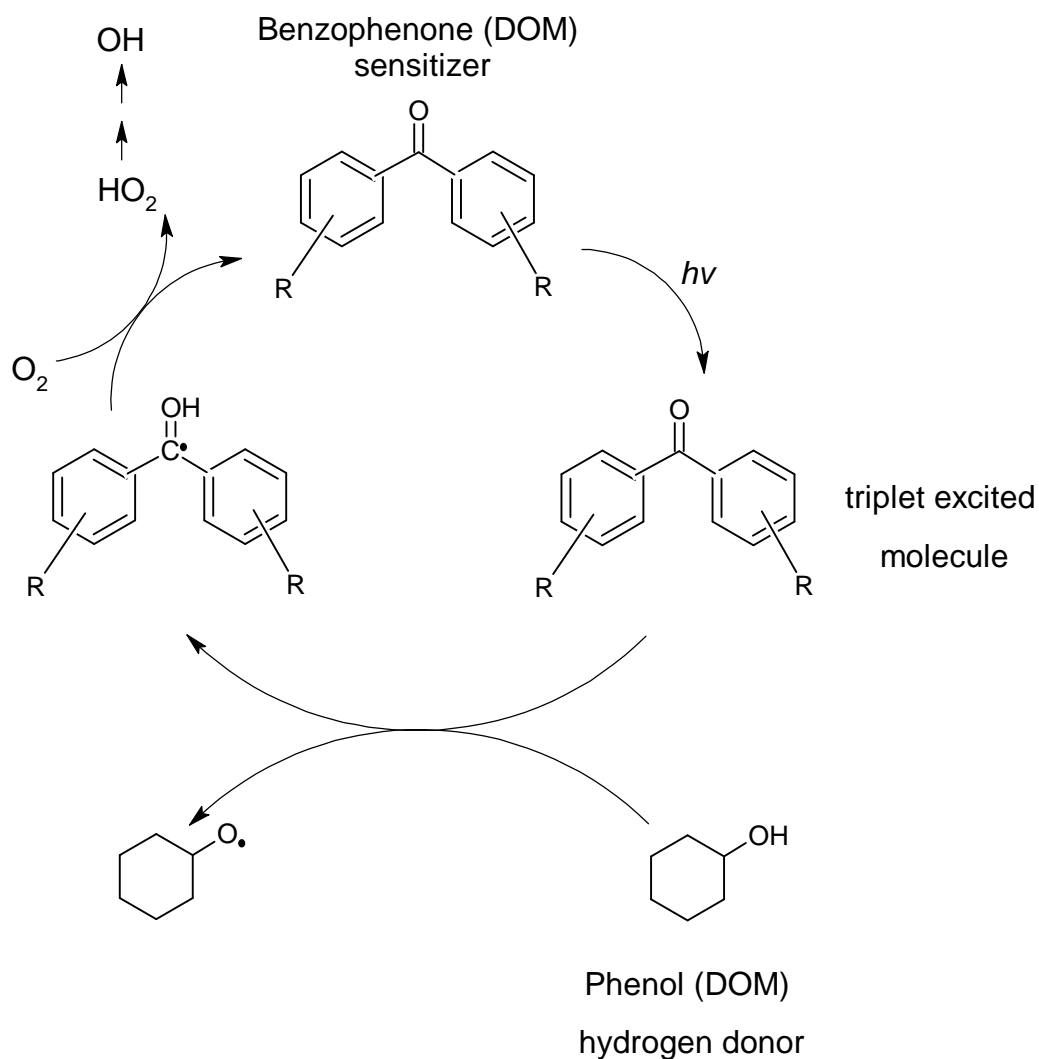


Figure 2.5 The Photosensitization Reaction Cycle Which Contributes to OH Production

The OH radical present in the cloud droplet formed by the above five processes will then go on to react with other species in the droplet including any surfactant film as represented by the monolayer in the experiments within this chapter.

The concentration of H_2O_2 in cloudwater is important as a source of OH radical in the aqueous phase. Concentrations of H_2O_2 in cloud water have been measured in many field campaigns as reviewed by Jackson and Hewitt (1999), and are commonly below $100 \mu M$ (Jackson and Hewitt, 1999). The FEBUKO experiment (Valverde-Canossa et al. 2005) measured cloud-water H_2O_2 concentrations at just under $2 \mu M$ during daylight hours in the Thuringian Forest, Germany. Sowka et al., (2001) measured aqueous H_2O_2 in cloud-water collected on Mount Szrenica,

Karkonosze mountains, Poland at an average concentration of $26.3\mu\text{M}$. Weinstein-Lloyd and Schwartz (1991) measured H_2O_2 yield from rainwater samples collected at Brookhaven National Laboratory, 100km East of New York and in synthetic samples of rainwater when irradiated with Cobalt-60 at differing intensities, in the presence of common cloud water constituents, in varying amounts. The findings of this work were that the initial concentration of H_2O_2 in the natural sample was measured at $50\mu\text{M}$, the yield was $40 - 65\mu\text{M}$ depending on the intensity of the Cobalt-60 irradiation which produces OH radicals from the H_2O_2 present in the sample. The presence of iron had a profound effect on the H_2O_2 yield from superoxide radical (O_2^-) and to accurately determine the yield it was vital to know the iron concentration (Weinstein-Lloyd and Schwartz, 1991).

Sources of the iron found in cloud droplets are the clays found in windblown (Eolian) dust and fuel fly ash (Faust and Hoignè, 1990). Iron concentrations from rainwater samples provide a concentration for cloud waters, Clarke and Radojevic (1987) measured Fe concentrations ranging from 0.3 to $23\mu\text{M}$ in rainwater samples from Leeds at pH 3-5, that of an acidified air-saturated cloud droplet (Faust and Hoignè, 1990). There is little data on the speciation of iron within cloud waters and it is thought to alter within the lifetime of a cloud droplet (Faust and Hoignè, 1990). Faust and Hoignè (1990) concluded that the dominant Fe(III)-hydroxy complex in cloud water was likely to be $\text{Fe}(\text{OH})^+$ which is a source of aqueous OH radical.

2.3.4 The Reaction of OH and Stearic Acid

OH radical is attributed as being the most reactive atmospheric radical species after ozone in the aqueous and gas-phase. It is the most reactive radical in atmospheric waters. Stearic acid is a proxy for an insoluble, surface active, film forming species. The stearic acid molecule is unsaturated and therefore will not react with ozone so if it was being oxidised then OH radical would be likely to be the radical responsible.

2.4 Experimental

To study the reaction of OH radical with stearic acid the surface coverage (Γ) and the surface pressure (Π) of a stearic acid film at the surface of a Langmuir trough were measured to monitor the amount of material at the air-water interface over reaction time. OH radicals were generated in solution beneath the stearic acid film to simulate oxidation of a film from within a cloud droplet.

A series of preliminary experiments were conducted to determine:

- The surface pressure behaviour of a stearic acid monolayer at the air-water interface during oxidation. The surface pressure of the stearic acid monolayer was measured over reaction time with a Langmuir trough and a Wilhelmy plate balance.
- Determination of the concentration of OH radical generated during a reaction through numerical modelling, the photolysis rate constant (J), for the numerical modelling was determined using titrations.
- Quantification of the intensity of the lamps used to generate OH radical using chemical actinometry.

Following the preliminary experiments, neutron reflectivity experiments were conducted to determine the kinetic behaviour of the reaction of aqueous OH radical with a stearic acid monolayer. There were three components to the neutron reflectivity experiments:

- To monitor the surface coverage of the stearic acid monolayer as a kinetic variable with reaction time as the monolayer reacted with aqueous OH radical. The aqueous OH radical was generated by the photolysis of hydrogen peroxide in the Langmuir trough subphase beneath the monolayer. The surface coverage of the monolayer was measured simultaneously to the surface pressure which was measured with a Wilhelmy plate balance.
- The concentration of H_2O_2 in the Langmuir trough subphase beneath the monolayer of stearic acid was varied to gauge the effect of varied OH radical production on the kinetic decay of the stearic acid monolayer. The monolayer surface coverage and surface pressure were monitored with neutron reflection and the Wilhelmy plate apparatus simultaneously.
- Experiments were conducted with a single concentration of H_2O_2 but at different temperatures to monitor the effect of temperature on the kinetics of the reaction between OH radical and a monolayer of stearic acid.

To gain an understanding of the changes in the monolayer morphology during a reaction with aqueous OH radical a Brewster angle microscope was used to take images of the monolayer during an H₂O₂ photolysis reaction.

The measurement techniques will be explained followed by the experimental methodology including the method of OH radical generation.

2.4.1 Measurement Techniques

The properties of surface pressure (Π) and surface coverage (Γ), were monitored versus reaction time to:

- To gain an understanding of the effect of OH radical on a stearic acid film at the air-water interface.
- To take measurements of a kinetic variable in order to calculate the rate coefficient for the decrease of stearic acid at the interface with time, and to calculate the chemical lifetime of the stearic acid under attack by hydroxyl radical relative to a cloud droplet lifetime.
- To observe any surface active products.

2.4.2 Measuring Surface Pressure. The Wilhelmy Plate Balance and the Langmuir Trough

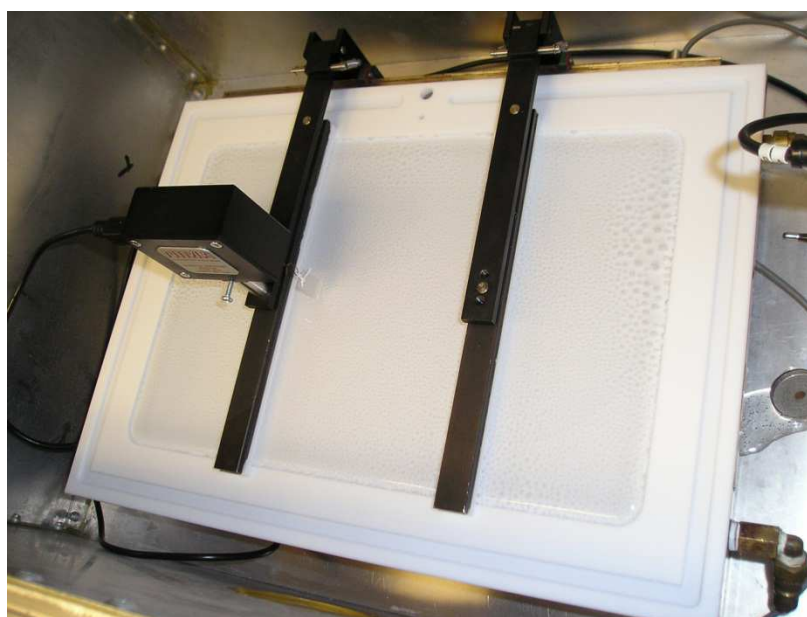
The monolayer surface pressure gives a measurement of the closeness in the packing together of the molecules forming a monolayer at the air-water interface, the closer the molecules, the stronger the surface pressure at the interface becomes. This measurement is a useful indication of loss of material from the interface as a reduction in the number of molecules present at the air-water interface weakens the surface pressure exerted by the monolayer. The Langmuir trough and Wilhelmy plate balance provide a cost effective method for determining whether a chemical reaction is causing a loss of material from the air-water interface. The equipment used to monitor the monolayer surface pressure will be explained in the following paragraphs.

To measure the surface pressure (Π), exerted by a stearic acid monolayer at the air-water interface during a reaction with OH radical the monolayer must be held in an apparatus which allows the interface to be accessible for measurements to be made, yet preserves the structure of the monolayer at the interface. The Langmuir trough, a PTFE bath with a shallow depth and large surface area is ideal. PTFE is very hydrophobic, when the trough is filled with water (the subphase), the contact angle with the PTFE produces a high meniscus at the surface of the trough and there is little disturbance of the liquid surface from the walls. When mixed with a

rapidly evaporating, volatile solvent such as chloroform, an amphiphile such as stearic acid can be spread at the air-liquid interface drop by drop from a syringe forming a one molecule thick organic layer across the surface of the subphase known as a monolayer. The Langmuir trough has moving barriers which compress the monolayer to achieve a closer packing of the molecules within the film, increasing the surface pressure.

The surface pressure of the monolayer is measured with a plate made of chromatography paper (the Wilhelmy plate), suspended through the monolayer into the subphase. The plate is suspended from a wire balance with an electronic current running through it to an electromagnet. The downward force of surface pressure exerted on the plate pulls on the balance increasing the current which counteracts the force maintaining the special position of the plate. The electrical current is related to the surface pressure.

Figure 2.6 *The Langmuir Trough*



Surface pressure at the air-liquid interface is the difference between the surface tension (γ) of a clean liquid surface ($\gamma_{\text{pure subphase}}$) and the surface tension of a liquid surface with a monolayer present ($\gamma_{\text{subphase with film}}$). The units for the measurement of surface pressure and surface tension are milli-Newton meters (mNm^{-1}).

$$\Pi = \gamma_{\text{pure subphase}} - \gamma_{\text{subphase with film}} \quad (E 2.1)$$

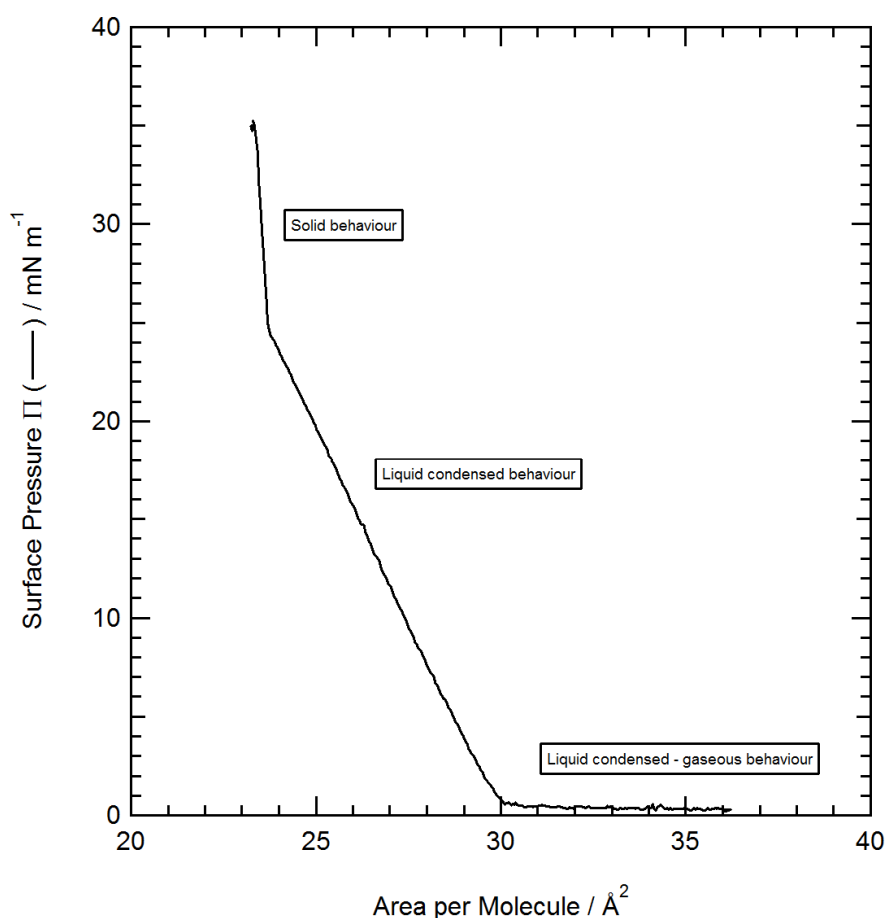
The surface pressure is an indication of the change in forces which are dependent on the intermolecular distance of the monolayer forming molecules at the air-water interface during a reaction. The surface pressure measurement does not give information on a kinetically variable

property such as the amount of monolayer material with reaction time as surface pressure is not proportional to surface coverage. The surface pressure data indicates the effect of the molecules and molecular packing on the surface tension of the air-water interface but not how the molecules themselves are altered during a chemical reaction.

The use of the Langmuir Trough and Wilhelmy plate balance to study a monolayer of organic acid from an atmospheric perspective is an established technique and has been used on stearic acid by Gilman et al., (2006). Eliason et al., (2003) used a Langmuir trough housed in a thin film chamber to collect and analyse the products of ozonolysis of 2-octenoic acid and 10-undecenoic acid which were oxidised, hydrophilic shorter chain carboxylic acids.

The surface pressure-area isotherm of a monolayer of stearic acid at the air-water interface measured on a Langmuir trough is shown in figure 2.7. The isotherm measurement of surface pressure is achieved by compression of the monolayer by closure of the Langmuir trough barriers.

Figure 2.7 *The Surface Pressure-Area Isotherm of Stearic Acid at the Air-Water Interface as Measured on a Langmuir Trough*



A 30 μL monolayer of 1mg / mL stearic acid in chloroform compressed at a rate of $20\text{cm}^2 \text{min}^{-1}$ to produce an isotherm performed at 20°C on the Royal Holloway Langmuir trough ($30 \times 10 \text{cm}^2$ surface area) showing the phases of the monolayer as the molecules are packed closer together.

2.4.3 Measuring the Monolayer Surface Coverage with Neutron Reflectometry

The measurement of surface pressure alone does not provide a quantitative surface concentration which can be used for kinetic analysis. To accurately measure the amount of surface active material present and its loss from the air-water interface a specular neutron reflectometry technique has been used. Neutron reflectometry determines, through the scattering of neutrons, how much material is present (the compositional profile) at the air-water interface over time. From this measurement a reaction scheme can be composed and fitted which gives a rate constant for the reaction of a stearic acid monolayer with aqueous OH radical. A chemical lifetime for the species of interest under conditions of oxidation can be calculated which will provide new data for climatic modelling.

Neutron reflectometry experiments require the use of a neutron source which consists of large particle generating plant which generates neutrons through the collision of atoms or through the decay of atoms in a nuclear reactor. The theory behind the neutron reflectometry technique is extensive; the key principles will be explained with regard to this experimental work in the following section.

2.4.3.1 Neutron Sub-Atomic Particles as a Tool for Measurement

The use of neutron reflectometry is complex and expensive when compared to other techniques in atmospheric science; however several unique properties of the neutron facilitate measurements on a molecular level which can only be achieved with this technique.

The neutron is a component of the nucleus of the atom held together with protons by the strong force. Experiments by Fermi showed that neutrons behaved as light when reflected from a flat surface (Fermi and Marshall, 1947). The manipulation of the scattering of neutrons from a surface to gain structural information normal to the interface, a technique known as neutron reflectometry has been practiced since the early 1990's. Neutrons are unique in that they only interact with the nucleus of an atom and not with the electron cloud as light does (Squires, 1978). Neutrons behave as a particle and as a wave according to quantum mechanics in much the same way as light does; therefore many optical phenomena used for measurements are also exhibited by neutrons (Penfold and Thomas, 1990). The neutron does not react with the sample

as the neutron is electronically neutral, allowing kinetic measurements to be taken without changing the chemical outcome of a reaction.

The wavelength of a neutron is of the order of 1 Ångstrom or 0.1 nm. This wavelength is similar to the length of the spacing between atoms within a molecule (Squires, 1978). The technique of reflectometry is reliant on the interference in the wavelength of a neutron reflecting from an interface, the measurable interference effect is only achieved when the spacing of the atomic nuclei which scatter the neutrons are at a distance close to that of the neutron wavelength (Hughes, 2010).

The neutron wavelength (λ) is dependent on the velocity of the neutron according to the de Broglie relation (equation 2.2) where h is Planck's constant (6.636×10^{-34} J s) m is the neutron mass (1.675×10^{-27} kg) and v is the velocity of the particle.

$$\lambda = \frac{h}{mv} \quad (E. 2.2)$$

The dependence of neutron velocity on the neutron wavelength allows time of flight measurements to reveal information about a material as the neutrons velocity changes due to scattering. For a pulse of neutrons the particles spread out over the distance travelled so that the high energy, low wavelength neutrons arrive at the instruments detector first (Campbell, 2011). It is the interference patterns of the scattering events between the neutron and a material of interest which give information about the sample (Beddington, 2008).

2.4.3.2 The Generation of Neutrons at ISIS, Rutherford Appleton Laboratory, UK

The experimental work for this chapter was performed at ISIS Pulsed Neutron and Muon Source at the Rutherford Appleton Laboratory, Oxfordshire, UK. ISIS produces neutrons through the acceleration of protons in a synchrotron, which are then fired at a heavy metal target producing a pulse of neutrons with varying wavelengths. A simplified account of the generation of neutrons is given in the following section based on information from publicity material and the websites of the neutron institutions with literature references where available.

The production of neutrons at ISIS is a several stage process of injection, acceleration, and spallation before the neutrons are channelled to the instruments. The process begins with H^+ ions sourced from an electric discharge plasma of hydrogen gas and caesium vapour (ISIS, 2009^a). The H^+ ions are directed by a Radio Frequency Quadrupole accelerator that groups the ions into pulses before further acceleration down tanks filled with copper drift tube electrodes in the linear accelerator (ISIS, 2009^a). The H^+ ions then enter a ring of tubular magnets, the synchrotron. The function of the synchrotron is to remove the electrons creating a proton beam

and to accelerate the protons, which form two groups of protons due to electric fields. The electrons are removed by a thin aluminium oxide foil (ISIS, 2009^b), and the protons are gathered until a sufficient number is reached then they are spun repeatedly (10,000 revolutions) before being exposed to radio frequency electric fields (ISIS, 2009^b).

When the 2 proton groups have separated kicker electro-magnets are activated which extract the protons and send them into the target stations. This cycle is repeated 50 times a second (ISIS, 2010). Each proton incident of the target releases approximately 12 neutrons (Beddington, 2008).

There are two target stations which receive protons at ISIS. The work in this thesis has been conducted on the reflectometer 'SURF' in target station one. At the centre of the experimental hall there is a small block of tungsten into which the protons are accelerated, this is the target. Bombardment of the tungsten with the high energy proton beam releases neutrons from the tungsten atoms nuclei (ISIS, 2009^b). Moderators slow down the neutrons to the desired wavelength giving a pulse of neutrons with a range of momentum transfer (Q) values which is directed to the reflectometer instrument SURF (Beddington, 2008).

2.4.3.3 The Basic Principles of Neutron Reflectometry

Neutron reflectometry is the measurement at a low incident angle of a beam of neutrons passing through and being scattered by atomic nuclei in a sample. The scattering is dependent on the effective neutron refractive index (Lu et al. 2000). For this work the neutrons are scattered by the organic monolayer held at the air-water interface of a Langmuir trough as it reacts with atmospheric oxidant species. The reflectometer is essentially a series of devices for measurement of the scattering of neutrons at a defined angle which are arranged to accommodate a sample from which the scattering is measured.

In neutron reflectometry a beam of neutrons is directed through a material of interest to a detector. The elastic reflection of neutrons occurs when the neutron particles energy is preserved during this interaction. The nuclei in the sample scatter neutrons without losing energy thus the chemistry of the sample is un-altered making this technique ideal for investigating kinetics. The neutron reflectivity is related to the number and efficiency of the scattering nuclei.

2.4.3.4 Neutron Scattering Theory

Each atom has a scattering length for neutrons which are published in tabulated form (Sears, 1992). The scattering length for a neutron from an atomic nucleus is a product of the shift in phase of the neutron wave as it is scattered from the nucleus compared to that of a free, un-

scattered neutron wave. The scattering length of an atomic nucleus can be positive or negative depending on the phase shift the neutron experiences when scattered. The neutron scattering length (b) for hydrogen is -3.74 fm and for deuterium is 6.68 fm, vastly different, allowing the manipulation of scattering to determine structural information as the contrast affects the time of flight of a neutron through the sample (Penfold and Thomas, 1990).

Large differences in scattering lengths of a molecule or a system of surfaces can be created by replacing hydrogen atoms with deuterium atoms. This manipulation of hydrogen isotopes is unique to neutron techniques and cannot be achieved with X-ray reflectivity as hydrogen does not scatter X-rays (Squires, 1978).

Isotopic substitution is used in this work to ensure that the scattering of neutrons takes place predominantly from the monolayer at the air-water interface, by creating a subphase beneath the monolayer which scatters neutrons to the same degree as air. The substitution of hydrogen atoms with deuterium atoms within a molecule as a label will increase the reflectivity from specific part of a molecule which can give structural information about a monolayer and its changing composition during a reaction.

Neutrons scatter elastically from atomic nuclei, different isotopes scatter neutrons at different efficiencies. The scattering efficiency is determined by a calculated scattering length (b). The scattering length of a substance is dependent on the refractive index. Refractive index (n) is the measure of the speed of a neutron in a material. At the interface of two media this is determined by the wave vectors (magnitude and direction of travel denoted k) of the neutron outside the material of interest, for this work in air (k_{air}) and within the material of interest, for this work the monolayer (k_{film}) according to equation 2.3, (Penfold and Thomas, 1990).

$$n = \frac{k_{air}}{k_{film}} \quad (E. 2.3)$$

It is more useful to consider the refractive index (n) in its relationship to the bound coherent scattering length of the monolayer material for neutrons (b) as in Equation 2.4 (Penfold and Thomas, 1990).

$$n = 1 - \left(\lambda^2 \left(\frac{Nb}{2\pi} \right) \right) \quad (E. 2.4)$$

λ *neutron wavelength*

N *the atomic number density of the monolayer material*

b *the scattering length, that is the summation of the component scattering nuclei scattering lengths in the volume of one molecule, see equation 2.10.*

To calculate the scattering length of stearic acid (b), the following calculations must be performed. The volume of a single molecule (V_M) of the amphiphile is calculated from equation 2.5 where M_r is the relative molecular mass calculated by the addition of the mass numbers of the constituent atoms, ρ_m is the mass density as calculated from equation 2.6 and N_A is Avogadro's number.

$$V_M = \frac{M_r}{\rho_m N_A} \quad (E 2.5)$$

The molecular density of the deuterated molecule (ρ_m), is calculated by equation 2.6 where ρ_{mH} is the density of the hydrogenated molecule, RMM_D is the relative molecular mass of the deuterated molecule and RMM_H is the relative molecular mass of the hydrogenated molecule. The relative molecular mass is calculated in g mol^{-1} by addition of the molecular weights of the constituent atoms in the compound.

$$\rho_m = \frac{\rho_{mH} RMM_D}{RMM_H} \quad (E 2.6)$$

The number of moles of a deuterated compound in a defined volume (N_{mol}) is calculated by dividing the relative molecular mass of the deuterated molecule (RMM_D) by the density of the deuterated molecule (ρ_m).

$$N_{mol} = \frac{RMM_D}{\rho_m} \quad (E 2.7)$$

Calculation of the volume per mole of the deuterated molecule (V_M) is by the division of the number of moles in a defined volume of $\text{cm}^3 \text{ mol}^{-1}$ (N_{mol}), by Avogadro's number (N_A).

$$V_M = \frac{N_{mol}}{N_A} \quad (E 2.8)$$

The scattering length density (ρ) is calculated by the scattering length of the deuterated molecule (b) divided by the molecular volume (V_M).

$$\rho = \frac{b}{V_M} \quad (E 2.9)$$

The scattering length (b) is then calculated by dividing the scattering length density of the deuterated molecule (ρ), by the volume per mole (V_M).

$$b = \frac{\rho}{V_M} \quad (E 2.10)$$

The value of scattering length (b), converted from centimetres to femto meters is then used as a fixed parameter in the neutron data fitting which will be explained in section 2.4.3.7.

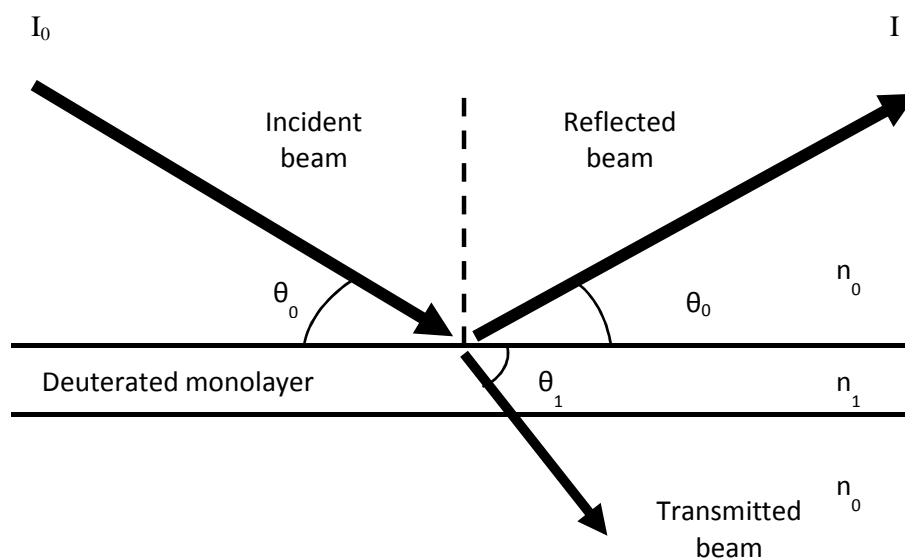
The neutron scattering length density (ρ) defines the scattering length (b) of the atomic nuclei within the volume of a stearic acid molecule in this experiment. D_{35} stearic acid ($C_{18}D_{35}O_2H$) has an observed neutron scattering length density (ρ) of $7.19 \times 10^{-2} \text{ fm}^2$.

A scattering event in an atomic nucleus can have three outcomes; the neutron will be reflected at the same angle of incidence or will scatter at an altered trajectory, or the neutron will be refracted and will not reach the instrument's detector. In an experiment with a monolayer at the air-liquid interface the majority of the beam of neutrons is transmitted through the monolayer into the subphase, this is known as the transmitted beam and is not detected or measured. The neutrons reflected at the angle of incidence reach a detector and are counted.

2.4.3.5 The SURF Reflectometer: Neutron Reflectometry at the Air-Water Interface

The geometry of the reflection of neutrons by a monolayer at the air-water interface is shown in figure 2.8. A schematic diagram of the reflectometer SURF is shown in figure 2.9.

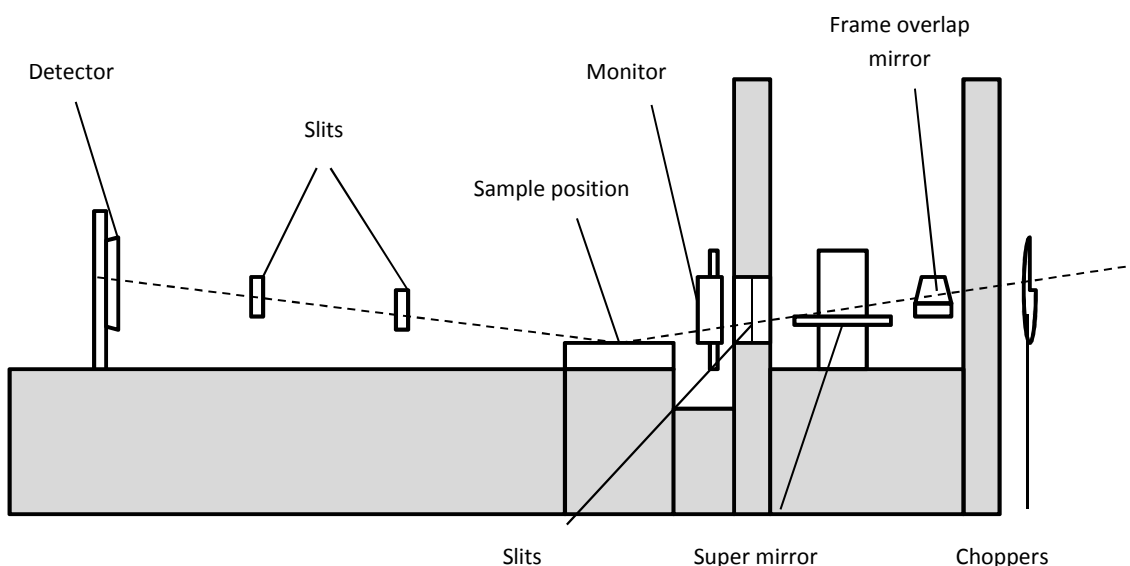
Figure 2.8 *The Reflection and Refraction of Neutrons at an Air-Monolayer-Liquid Interface*



The dashed line in figure 2.8 represents the geometry normal to the interface at which the surface coverage measurement is valid. To obtain neutron measurements of a monolayer at the air-water interface concurrently with surface pressure measurements during a reaction the Langmuir trough was fitted to the neutron reflectometer instrument SURF. The neutron instrument is essentially a frame into which a sample environment can be fitted to enable the passage of neutrons through a material of choice. By housing a Langmuir trough in an aluminium chamber which is transparent to neutrons and does not interfere with the signal, the

temperature and atmospheric composition around a monolayer at the air-water interface could be controlled whilst keeping the surface undisturbed and clean (figure 2.10).

Figure 2.9 *The Components of the Reflectometer SURF at ISIS*



The dashed line represents the path of the neutron beam. The grey areas are concrete shielding. Figure 2.9 was Adapted from Penfold et al., (1997).

For the SURF instrument the incident neutron beam from the ISIS target is collimated to an angle of 1.5° to the horizontal plane, (Penfold et al. 1997). When the beam hits the target a burst of fast neutrons and gamma rays are produced, the high energy neutrons are removed from the beam to the instrument by a chopper spinning at 50Hz (ISIS, 2011^a). A double disc chopper selects the wavelength of 0.55 to 6.8 Å by altering the time frame / phase of the pulse of neutrons that is allowed to pass through, (Wilson, 1990; ISIS, 2011^b). The beam is defined after the choppers with further collimation to a height of 60mm x width 10mm (ISIS, 2010). The range of momentum transfer denoted as Q on SURF is 0.048 to 1.1 Å⁻¹.

There are slits beyond the collimation which further restrict the beam so that the sampling area / footprint of the beam on the surface of the Langmuir trough can be defined. The beam is focussed on the sample position at 1.5° using a super mirror. The frame overlap mirror removes the fast neutrons from the next pulse appearing at the end of the former pulse of neutrons (Hughes, 2011).

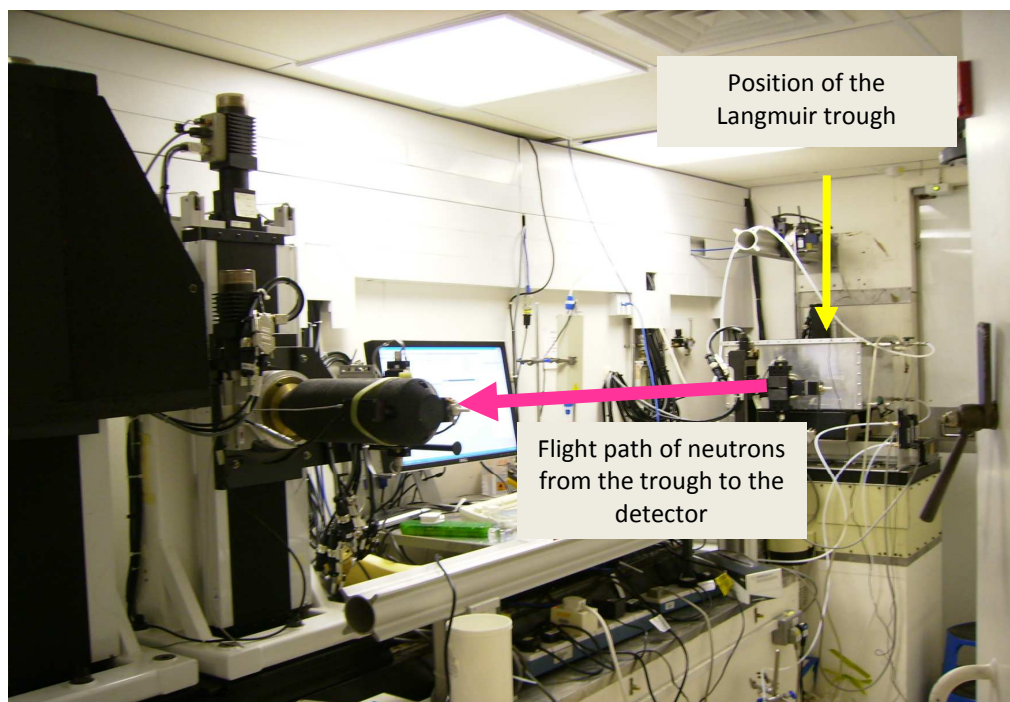
The distance from the sample to the detector was set to approximately 2 meters for this work. The humidity and temperature of the instrument enclosure are controlled throughout an experiment.

The Langmuir Trough is positioned on a mobile platform which can be height adjusted to position the neutron beam in the centre of the trough using a guiding laser to check the beams incidence on the trough and that the positioning of the slits is adequate. The beam on SURF was adjusted to a footprint of 8 by 6 cm² on the surface of the Langmuir trough.

The reflectivity signal is the intensity of energy produced by neutrons hitting the detector and producing a current. SURF utilises a single ³He gas detector (Penfold et al. 1997). The detector is comprised of two metal plates with a cavity between them containing ³He. The ionization of He₃ by incoming neutrons produces energy / electrons which produce an electrical current on a wire which acts as an anode. The detector measures the arrival time of the neutron and its spatial location. The signal is measured in the unit of KeV. This is then recorded as the number of counts (kHz / mm²) versus pulse height / energy. The neutron creates a charged particle in reaction 2.16 (ISIS, 2008).

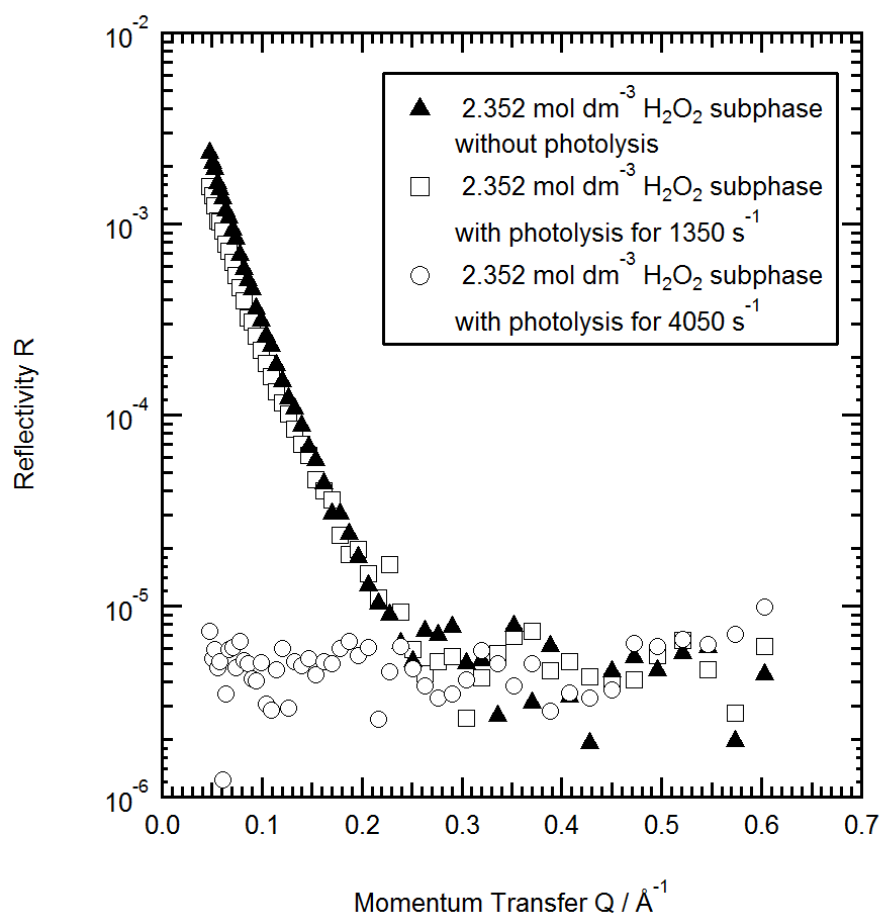


The detector measures the count of neutrons over a specified time period as counts per milli second against the time of flight of the neutron. The time of flight is the neutron velocity measured as mm/ μ sec. A relaxed resolution leads to higher flux (Penfold et al. 2007), so taking a longer measurement increases the number of counts on the detector. A measurement time of 10 to 15 minutes gives adequate signal to noise statistics for kinetic measurements on SURF. The background signal on SURF is approximately $1 \times 10^{-5} R(Q)$, for a 20 minute measurement period.

Figure 2.10 *SURF with the Langmuir Trough in Situ, as Set Up for an Experiment*

The neutron detector measures the specular reflection (R), of neutron particles which have passed through the monolayer and exited the atomic nuclei of the molecules in the monolayer at the same angular trajectory as the particles entered at. This angle is termed the angle of incidence and for the SURF reflectometer used in the experiments detailed in this chapter the angle of incidence (θ) was 1.5° .

Figure 2.11 *The Reflectivity Profile of a Stearic Acid Monolayer at the Air-water Interface on a Subphase of $2.35 \text{ mol dm}^{-3} \text{H}_2\text{O}_2$*



In the reflectivity profile displayed in figure 2.11 neutrons were counted for 90 seconds at a beam current of $43 \mu\text{A}$. The value of surface coverage at this point was $5.18 \times 10^{18} \pm 9.41 \times 10^{17}$ molecule m^2 without photolysis, $4.10 \times 10^{18} \pm 4.24 \times 10^{17}$ molecule m^2 with photolysis for 1350 s^{-1} and $5.10 \times 10^{18} \pm 3.18 \times 10^{16}$ molecule m^2 with photolysis for 4050 s^{-1} . It can be seen that the reflectivity signal decreases with reaction time for a D_{35} stearic acid monolayer.

2.4.3.6 The Time of Flight Principle

The time taken for a neutron to undergo specular reflection from an interface and reach a detector at a fixed angle (θ), on an atomic scale to be refracted, when compared to the time taken for reflectance from a surface giving total reflection with no refraction (liquid deuterium oxide, D_2O) is related to the refractive index and scattering length density of the material through which the neutron travels. This is the neutrons time of flight. The time of flight

reflectivity measurement is in the format of $R(Q)$, R being reflected beam intensity and Q being the momentum transfer in direction z , normal to the interface, Q is the scattering vector, perpendicular to the monolayer.

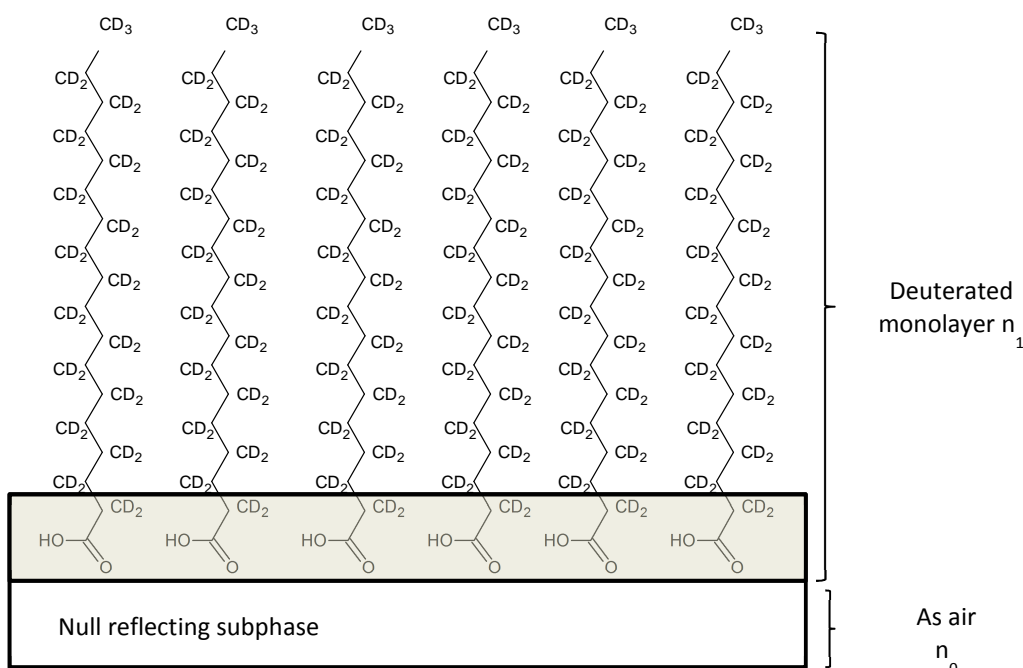
The neutron beam is pulsed to achieve a measurable time gap which forms the time zero measurement which allows the change in distance over time vector (velocity/ momentum transfer Q) to be measured.

To the instruments detector, all neutrons appear the same, the detector merely count neutrons over a prescribed period of time. It is the time of arrival of the neutron at the detector which gives the measurable property as the time of flight of a neutron to the detector is known in absence of a sample and the velocity of a neutron which has travelled through a sample is altered to a degree determined by the refractive index of that sample (Hughes, 2010). As the refractive index is altered as a molecule reacts the time of flight changes affecting the number of counts on the detector in a set measurement time which gives a lower signal of reflectivity (R).

The compositional reflectivity profile of a monolayer of deuterated stearic acid is shown in figure 2.12 with the head group of the molecule sitting in the subphase and the tail group orientated normal to the interface. The reflectivity signal comes from the head group and the tail group for a fully deuterated (D_{35}), stearic acid molecule. Fully deuterated molecules were used for this chapter as it was the persistence of the monolayer at the interface is being studied and not its structure. To perform a structural study different isotopologues of a molecule are used which are deuterated to different degrees as will be explained in subsequent chapters.

For the experiments in this chapter the monolayer was deuterated so that it dominated the neutron reflectivity signal. The surrounding sample environment was positioned and designed so as to give the minimum possible contribution to reflectivity. By adding deuterium oxide (D_2O), to the aqueous subphase of the Langmuir trough at a mole fraction of 0.088 mole D_2O in H_2O (Penfold and Thomas, 1990), the subphase was isotopically “tuned” to scatter neutrons to the same degree as air (with the same scattering length (n)) rendering the subphase invisible to neutrons with a scattering length of zero (Lu et al. 2000) this is known as null reflective water.

Figure 2.12 *The Compositional Profile of a Monolayer of Stearic Acid Normal to the Air-Water Interface*



The scattering by the monolayer determines the intensity at the detector (I_D). The intensity of the neutron beam channelled to the neutron reflectometer instrument is measured, and the intensity of the beam after interaction with a sample is measured at a critical angle of incidence (θ). The reflected beam intensity (R), is equivalent to the beam intensity at the instruments detector (I_D), divided by the beam intensity at the instruments monitor (I_M), prior to reflection from the sample (equation 2.11). The reflected intensity is a function of the momentum transfer scattering vector (Q) (equation 2.12). For a monolayer at the air-water interface the scattering vector Q is the one dimensional change in the momentum of a neutron after it is reflected from the sample and is calculated according to equation 2.12 where n is the refractive index, λ is the wavelength and θ is the angle of incidence. Intensity is measured in units of counts per mm on the instruments detector so a signal is obtained from a period of counting which when taken in series produces a time resolved measurement of reflectivity. The detector measures the counts per millimetre. R is a measure of the intensity of the reflected beam and is dimensionless. Q is a measure of the momentum transfer (distance, time vector, equivalent to velocity) of the neutrons arriving at the detector (Jacrot, 1976, Penfold and Thomas, 1990).

$$R = \frac{I_D}{I_M} \quad (E 2.11)$$

$$Q = \frac{4\pi n}{\lambda} \sin\theta \quad (E 2.12)$$

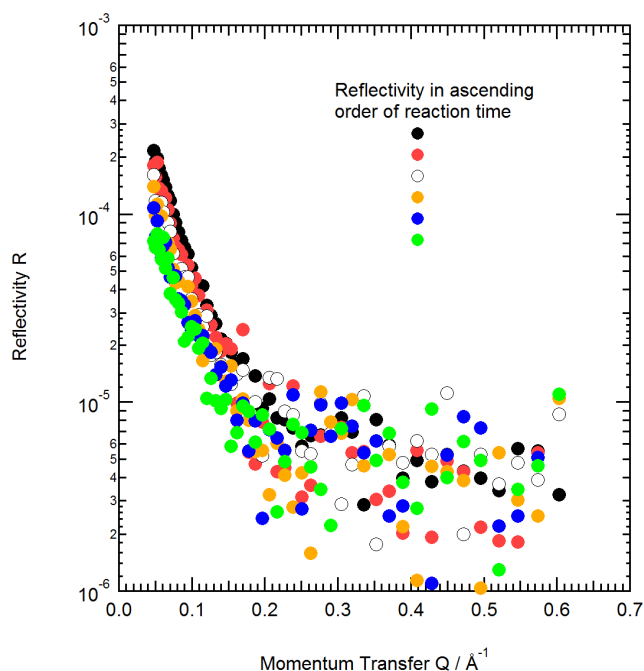
Equation 2.12 is a form of Braggs law relating the ration of the reflected beam intensity to the intensity of the neutron beam, the term 4π is related to the shift in phase of the neutron when it is scattered (Hughes, 2010).

From a surface of deuterium oxide (D_2O) all the incident neutrons of varied wavelengths are reflected to the detector at a time of arrival at the detector (t_D). Measurement of the reflectivity from a deuterium oxide subphase in the Langmuir trough gives the maximum intensity of the reflected beam. To ensure the detector is not saturated by rapidly counting the highest energy portion of the spectrum of neutron wavelengths comprising the neutron beam a region of an adequate wavelength to allow measurement of the sample is selected by adjusting the slits which determine the size of the sample area and the flux of the incident beam. Opening the slits allows shorter measurement times but can lead to saturation of the detector. The deuterium oxide calibration of the instrument is known as the scale factor. The scale factor is subtracted from the reflectivity data prior to analysis so that the scattering which is analysed is only that from the monolayer.

$$R(Q)_{monolayer} = R(Q)_{D_2O} - R(Q)_{experiment} \quad (E 2.13)$$

The resulting reflectivity data can be seen in figure 2.13 for a monolayer of oleic acid reacting with gas phase ozone. Each colour represents measurements of R versus Q taken for a prescribed period of counting at the instruments detector which by the fitting process described in section 2.4.3.7 becomes a single surface coverage measurement.

Figure 2.13 Reflectivity versus Momentum Transfer of an Oleic Acid Monolayer Exposed to Gas Phase Ozone Measured on the Neutron Reflectometer FIGARO



The positioning of the reaction chamber windows is checked by running a zero transmission, which is directing the neutron beam through the chamber without the Langmuir trough. It is necessary to correct the measurement of reflectivity for any neutron scattering from the sample environment. The loss in the intensity of reflectivity at the detector through scattering by the sample environment is quantified by running the beam through the chamber, with the Langmuir trough in situ but without a subphase present. This value is recorded as the background scattering and is input when fitting the reflectivity data to obtain a surface coverage measurement.

2.4.3.7 Fitting of Reflectivity Data to Determine the Surface Coverage

The reflectivity data (R versus Q) data in units of \AA^{-1} , can be fitted to, to obtain information on the surface coverage (Γ) that is the compositional profile of the organic monolayer film normal to the air-water interface, a kinetic variable equivalent to a surface concentration. The surface coverage measurement is presented in units of deuterated molecules per square meter at the interface. The reflectivity can also give an indication of the thickness of the deuterated component of a monolayer and the interfacial roughness between the molecules and the aqueous subphase. The surface coverage is equal to the scattering length density (ρ) multiplied by the

thickness (τ) which is equal to the scattering length per unit area, which is divided by the scattering length per molecule (b) giving the number of molecules per unit area (E 2.14). The product of equation 2.14 is the same as one divided by the area per molecule (APM) which is a product of fitting the reflectivity data (E 2.15).

$$\Gamma = \frac{\rho\tau}{b} \quad (E\ 2.14)$$

$$\Gamma = \frac{1}{APM} \quad (E\ 2.15)$$

The reflectivity data was fitted using the MONO program written by Adrian Rennie. MONO was chosen as it does not require an experimentally measured value of thickness to calculate the area per molecule, simply an accurate estimate, meaning that it was more suitable for the kinetic measurements which are not a structural measurement and are simply of the scattering from the deuterated portion of the molecule at a single angle. MONO uses the Abelès equivalent optical matrix method (Abelès, 1950) where the monolayer is divided into several parallel layers with parameters describing the scattering of neutrons. The parameters are varied until an energy function reaches a minimum (van der Lee et al. 2007).

Table 2.1 *The Parameters Used to Fit the Area per Molecule at the Air-Water Interface from the Neutron Reflectivity Data*

Parameter	Symbol	Unit	Input Value
Scattering length density of air	ρ_{air}	10^{-6} \AA^{-2}	0
Scattering length density of subphase	ρ_{subphase}	10^{-6} \AA^{-2}	0
Experimental scale factor	F_s	no unit	0 as this has been subtracted prior to fitting
Roughness between the monolayer and the air	ξ_{air}	\AA	0 to 4, this is adjusted to improve the fit, it is usually 0
Experimental background	B	no unit	Approximately 0.1×10^{-6}
Thickness of the monolayer layer	τ	\AA	The length of the monolayer forming molecule (oleic acid was treated as purely cis bonded)
Scattering length of the monolayer forming molecule	b	fm (10^{-15} m)	The scattering length of the monolayer forming molecule. For D ₃₅ stearic acid 361 fm
Roughness between the monolayer and the subphase	ξ_{subphase}	\AA	4 for an aqueous subphase
Area per molecule at the interface	APM	\AA^2	Obtained from the fit, an initial guess is entered

Table adapted from Rennie. 2011

It is common experimental practice is to take measurements at several angles to reveal structural information about an interface, time not being a crucial element of the data. However to obtain kinetic information the timings are vital and the reflectivity technique is used with a single angle to obtain a thickness.

The surface coverage is an indication of the presence of a monolayer. If there is no monolayer material remaining due to oxidation the reflectivity signal will decrease and a value of zero surface coverage would be obtained, conversely if the monolayer is not reacting the surface coverage will not decline. Incoherent scattering of neutrons contributes to a background signal that is subtracted from the data during fitting.

2.4.3.8 Measuring the Error in Neutron Reflectivity Data

The error in the R versus Q data is the product of counting statistics, the longer the period of counting the smaller the error in the counting.

When neutrons are counted on the detector, some times of flight will occur more frequently than others. The average value best describes the sample. The final data point produced for a period of counting at the detector is an average of the counts collected (Hughes, 2011). The standard deviation of the counts on the detector is the square root of the mean number of recorded counts.

$$\text{standard deviation} = \sqrt{\text{measured value}} \quad (E 2.16)$$

If more neutrons are counted at the detector during a measurement the value of the standard deviation increases however when the standard deviation is expressed as a percentage of the total number of counts then the value of the error range decreases for the measurement of reflectivity.

To minimise error in the measurement the smallest scale is used giving a small innate error which is equal to half of the smallest unit of measurement for example 0.5 Angstrom.

$$\text{minimum error} = \left(\frac{\text{innate error}}{\text{number of counts}} \right) \quad (E 2.17)$$

The minimum error is equal to the innate error in the unit that the detector counts in, divided by the count rate, the number of counts on the detector in specified counting time. The longer the counting time the smaller the minimum error becomes, (Monk, 2006).

$$\text{count rate} = \frac{\text{number of counts}}{\text{time counted}} \quad (E 2.18)$$

The effect of re-defining the time bins in which the neutron count data is distributed for example by co-addition of two original measurement periods of for example ten minutes making a twenty minute measurement is to lower the error. This is a practice used when the reflectivity signal becomes weaker as the monolayer is lost from the interface.

The process of background subtraction of a measurement of off specular scattering from the experimental sample environment ($sd^{background}$), from that of an experimental measurement ($sd^{experiment}$), requires the consideration of a range of possible errors (Sprawls, 2011).

$$standard\ deviation = \sqrt{sd^{background}sd^{experiment}} \quad (E\ 2.19)$$

When the error is expressed as a percentage the range increases when the difference is taken between two measurements for example by subtracting the background. Towards the end of an experiment as the signal is weaker then subtracting the background puts the measurement in the region of noise so adding measurements together decreases the size of the error bar making the measurement distinguishable from the noise.

The reduced reflectivity data (that normalised for the scale factor) which is fitted for SURF is in a 3 column format (.asc) of R , error in R and Q . The error in reflectivity from the instrument is calculated as a counting statistic. The greater the number of neutrons counted, the smaller the error in the measurements.

The error in the fit is given as the uncertainty in the fit, which is the percentage deviation between the measured data and the fit by the simple model to known parameters. A good fit minimises this difference to one standard deviation, twice this is the 95th percentile.

The error in the fitted data is given as a relative error (equation 2.20), the absolute error in the area per molecule divided by the fitted value of area per molecule, as calculated from equation 2.21.

$$Relative\ error = \frac{\sigma_{APM}}{APM} \quad (E\ 2.20)$$

The program MONO calculates the percentage error in the area per molecule (Rennie., 2009) according to equation 2.41.

$$\% \sigma_{APM} = \frac{APM_{mod} - APM_{calc}}{APM_{calc}} \quad (E\ 2.21)$$

Where the modelled area per molecule (APM_{mod}), is the value obtained by the fit and the calculated area per molecule (APM_{calc}) as calculated from the scattering data. To get the absolute error, the error in the modelled value obtained by the fit and the value calculated from the scattering data, the percentage error in area per molecule is divided by one hundred and multiplied by the value of area per molecule.

$$\sigma_{APM} = \frac{\% \sigma_{APM}}{100} APM_{mod} \quad (E\ 2.22)$$

The error in the calculated surface coverage (Γ), is

$$\sigma\Gamma = \frac{1}{(APM)^2} \sigma APM \quad (E 2.23)$$

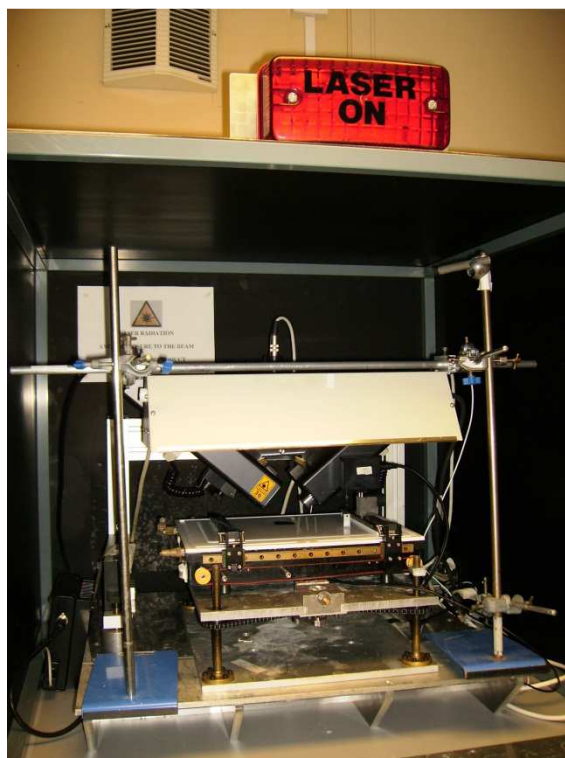
The experimental method employed in this thesis is based on the work of King et al. (2009), which was the first study to observe the oxidation of an oleic acid monolayer by gas-phase ozone on a Langmuir Trough with neutron reflection as a proxy for a cloud droplet system. King et al. (2009) showed a cleavage of the double bond in the tail of the oleic acid molecule generated surface active product formation. For the work in this chapter the same measurement technique was employed. For this chapter the neutron reflectivity measurements were fitted to obtain the surface coverage of deuterated material at the air-water interface during a reaction with aqueous phase OH radical.

The production of OH radical during the neutron and Langmuir trough experiments is described in section 2.4.5.

2.4.4 Brewster Angle Microscopy

The Brewster angle microscope (BAM) can image a monolayer in-situ on a Langmuir trough by the manipulation the angle of 53° at which there is no reflectivity from a clean surface of pure water. The reflected light parallel to the plane of incidence is zero at 53° . When a monolayer is present at the air-water interface light is reflected. The intensity of the reflected light is dependent on the thickness of the monolayer, the interfacial roughness and the directional dependence of the monolayer at different values of surface area per molecule (Webster and Langridge, 1999). Brewster angle microscopy was useful only as a visual confirmation of the decay of the film as the data obtained was not quantitative, only a small area of the surface, approximately 1 mm^2 is imaged.

Figure 2.14 *The Brewster Angle Microscope with the Langmuir Trough Positioned for Imaging*



To capture images of a stearic acid monolayer during the reaction with OH aqueous radical the subphase was made up with H_2O_2 as explained in section 2.4.5. The 254 nm photolysis lamps were fitted at a 45° angle so that the light was incident of the surface of the Brewster microscopy Langmuir trough. A black silicon wedge shaped block was placed in the Langmuir trough prior to spreading the monolayer, to provide a dark background for the image as the Langmuir trough is white and reflects the laser light to too high a degree to get an image of the monolayer.

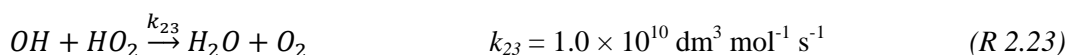
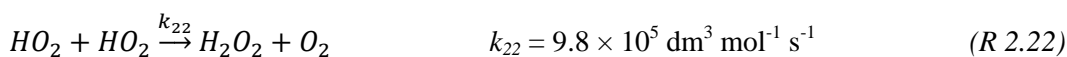
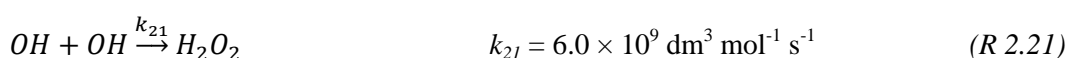
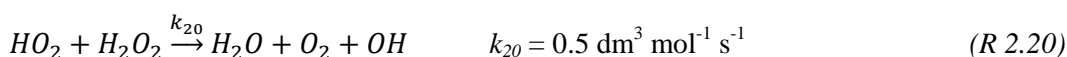
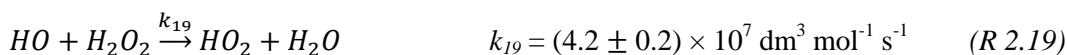
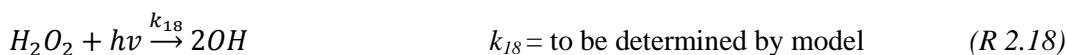
2.4.5 Generating Aqueous Phase OH Radical During an Experiment

To mimic the aqueous phase OH radical production in atmospheric droplets as shown in figure 2.3, aqueous phase OH radicals were generated from photolysis of H_2O_2 in the subphase of the Langmuir trough. A lamp was fitted to the reaction chamber lid which contained two 254 nm UVC strip bulbs which extended above the full length of the trough to give an even distribution of light. Each bulb was labelled so that it could be identified when the bulbs were changed and calibrated accordingly. Hydroxyl radical was generated by reaction R.17.



The production and subsequent secondary chemistry of aqueous hydroxyl radicals in the subphase in this study, and the relevant rate constants after Yu and Barker (2003) are given below

The reactions contributing to the OH radical concentration in the subphase were as follows:



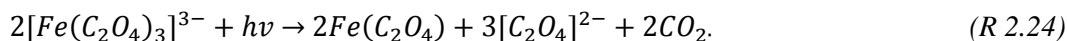
To quantify the concentration of OH radical generated in the Langmuir trough subphase several experiments were necessary:

- Chemical actinometry of Fe(II) to determine the time taken for the lamp to give a stable output of photons was measured.
- Titrations of H_2O_2 to determine the loss in the concentration of H_2O_2 in the subphase over time due to the production of OH through photolysis. The photolysis rate constant was calculated from the H_2O_2 decay and the H_2O_2 concentration was also used to kinetically model the OH concentration in the subphase.
- Kinetic modelling of reaction 2.18 to 2.23 to determine the OH concentration in the subphase during the neutron experiments.

2.4.5.1 Photolysis Lamp Calibration by Chemical Actinometry

The photolysis lamp was calibrated using actinometry to quantify the photon flux, that is the number of photons per cm^2 incident on the surface of the Langmuir trough. An actinometer is a substance with a known quantum yield as a function of wavelength (Pilling and Seakins, 1995) that behaves in a known and predictable manner. Using a potassium ferrioxalate solution containing Fe(III) as an actinometrical subphase, actinometry was carried out following the method of Hatchard and Parker (1956).

As the photons incident on the Langmuir trough react with a subphase of potassium ferrioxalate solution (Fe(III)), a complex of iron in the 2+ oxidation state (Fe(II)) is generated according to reaction 2.24.



Each Fe^{2+} produced represents the interaction of one photon. The reaction of the Fe^{2+} with phanathroline added to the sample produces an orange colouration of the subphase potassium ferrioxalate solution which provides a measurable change in the adsorption of light by a sample of the subphase from which the concentration of Fe(II) can be measured on an ultra violet visible spectrometer and calculated using the Beer-Lambert law (E 2.24).

$$A = \ln \frac{I_T}{I_0} = -\sigma[c]l \quad (E\ 2.24)$$

According to Beer-Lambert law the absorption (A) of light by a sample is equivalent to the change in light intensity that is, the intensity of light that has passed through the sample as transmitted light (I_T), divided by the intensity of light before interaction with a sample (I_0). The change in the intensity of transmitted light ($\frac{I_T}{I_0}$) is dependent on the extinction coefficient (σ) the path length (l) and the concentration of Fe(II). The path length and the extinction coefficient are kept constant so the loss in the intensity of transmitted light is a result in a change in the Fe (II) concentration (E 2.25).

$$[c] = \frac{\ln \frac{I_T}{I_0}}{\sigma l} \quad (E\ 2.25)$$

The change in the concentration of Fe(II) over exposure time (t_e) gives the warm up time for the lamps to give a stable output of photons.

The photon flux (q_p) was calculated by dividing the measured quantum yield (y) of Fe(II) in the sample by the time that the sample was exposed to the photolysis lamp (E 2.26). The photon flux divided by the surface area of the Langmuir trough gives the intensity of the light (I_0) falling on the surface of the Langmuir trough (E 2.27).

$$q_p = \frac{y}{t_e} \quad (E\ 2.26)$$

$$I_0 = \frac{q_p}{600\ cm^2} \quad (E\ 2.27)$$

2.4.5.2 Actinometry Procedure

The actinometry was performed under dark room conditions with only red light. The spectrometer measures the absorption of light at a single wavelength of 510 nm. A value of absorption for a solution containing no iron (I_0) was measured initially.

The Langmuir trough was set up as if for a neutron experiment within the aluminium reaction chamber with the photolysis lamp fitted to the lid. The trough was filled with the actinometer solution.

Two 2.5 mL samples of the actinometer solution were taken with a pipette from the Langmuir trough under dark room conditions prior to any illumination. One sample was immediately stored in a dark cupboard, the second aliquot of sample was pipetted into a 50mL volumetric flask with 5 mL phenanthroline solution and 2.5mL of the buffer solution, then was made up to volume with H_2O . A sample of this solution was then pipetted into a cuvette. The cuvette was stored in darkness for 30 minutes for a complex to form between the Fe(II) and the phenanthroline.

The remaining actinometer solution in the Langmuir trough was irradiated with the 254 nm photolysis lamp for set time intervals of 0, 5, 10, 30, 60, 120 and 300 seconds. After illumination a 2.5mL sample was taken from just beneath the surface of the subphase by pipette. This irradiated sample of actinometer solution was then transferred into a 50mL volumetric flask. 5 mL of phenanthroline solution and 2.5mL of buffer solution were added and the flask was filled to volume with H_2O . The solution was placed in a dark cupboard for 30 minutes for a complex to form between the Fe(II) and the phenanthroline.

Phenanthroline solution was added to the sample. Phenanthroline has a strong absorption cross section at 510 nm and can be used to quantify the Fe^{2+} production from photolysis of Fe(III).

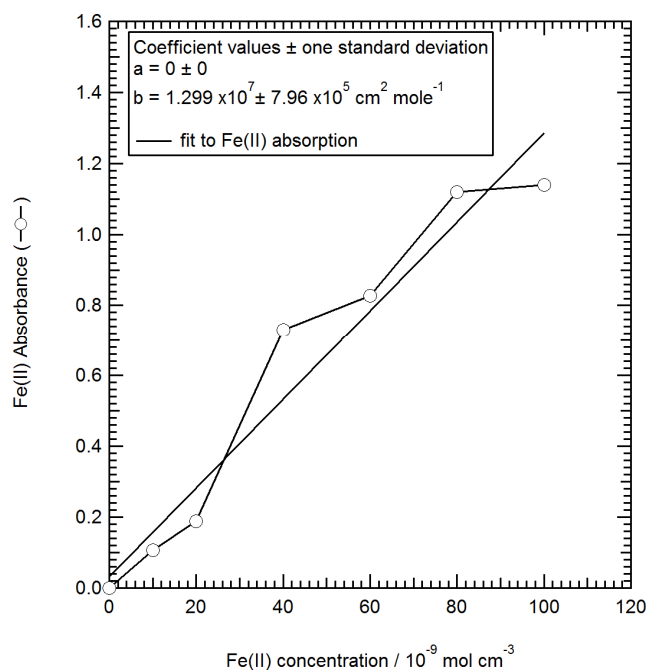
The Fe(II) forms a complex with phenanthroline which is bright orange in colour. Fe(III) does not complex with phenanthroline. The ratio of Fe(II) to Fe(III) determines the intensity of the orange colour formed. The absorption cross section of Fe(II), ϕ , is equivalent to the absorbance of light by the Fe(II) solution, φ , measured on the spectrometer divided by the path length, l .

$$\phi = \frac{\varphi}{l} \quad (E 2.28)$$

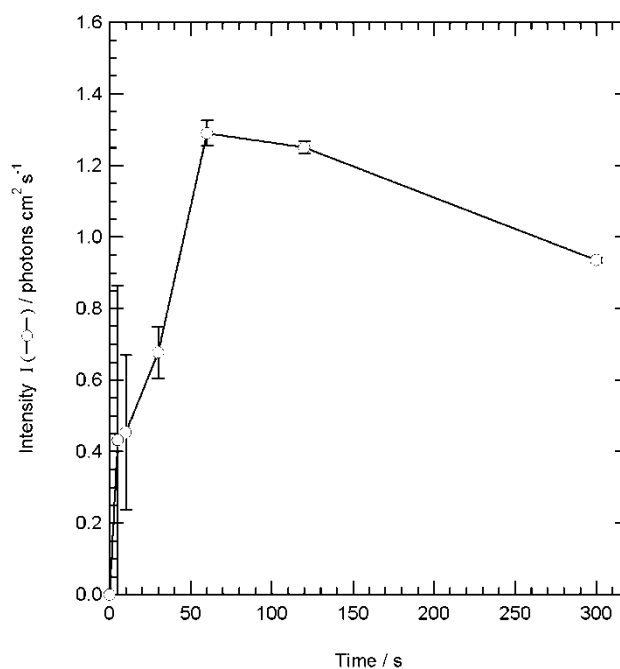
After 30 minutes a 1 mL sample of each solution was pipetted into cuvettes. The absorbance was measured with the spectrometer at 510nm and corrected for the absorbance of the I_0

solution with no iron present. The absorption cross section (Φ) for Fe(II) molecules to absorb a photon at 510 nm was $1.3 \times 10^7 \pm 8.0 \times 10^5 \text{ cm}^2 \text{ mole}^{-1}$.

Figure 2.15 *The Fe(II) Absorbance versus Fe(II) Concentration*



The time taken for the bulbs to produce a stable output of photons was determined by measuring the yield of Fe(II) which was produced by the photolysis of Fe(III). The lamp took 100 seconds to reach the maximum output of photons, the lamp intensity reached 7.7×10^{17} photons per second incident on the trough in <100 seconds. Ideally this experiment would have been repeated as the final point at 300 seconds is outlying. It was not possible to repeat this experiment as it required the beam line Langmuir trough which is in constant use.

Figure 2.16 *The Intensity of the 254nm Photolysis Lamp over Time*

2.4.5.3 Actinometry Materials

- Langmuir trough (the ISIS Langmuir trough as used for the neutron experiments)
- 2L 1L, 250 mL and 50 mL volumetric flasks
- UV visible single wavelength spectrometer with appropriate cuvettes
- Automatic pipette and tips
- Pasteur pipettes
- Pure water wash bottle

2.4.5.4 Actinometry Chemicals

- Sulphuric acid (H₂SO₄)
- Phenanthroline monohydrate solution (C₁₂H₈N₂·H₂O)
- Sodium acetate (C₂H₃O₂Na·3H₂O)
- Potassium oxalate (K₂C₂O₄·H₂O)
- Ferriin Indicator Solution: Sigma Aldrich-Fluka, redox indicator 0.025 M [Fe(C₁₂H₈N₂)₃]SO₄, (1,10-Phenanthroline iron(II) sulfate complex), catalogue number: 46270

2.4.5.5 Actinometry Solutions

Seven ferrous sulphate solutions were made up at concentrations of 0, 1.25, 2.5, 5, 7.5, 10 and 12.5 mL of solution F in 50 mL volumetric flasks with the addition of 12.5 mL of solution A, 5 mL of solution B, and 12.5 mL of solution C, then made up to volume with H₂O.

A. Buffer solution

Buffer solution composed of 0.6M sodium acetate (C₂H₅O₂Na·3H₂O) and 0.18M sulphuric acid (H₂SO₄). 20.41g of sodium acetate and 4.41g of sulphuric acid weighed into a 250 mL volumetric flask and made up to volume with water. The sodium acetate must be added first followed by a little water then the sulphuric acid followed by the remaining water.

B. 5 × 10⁻³ M 1:10-phenanthroline monohydrate solution (C₁₂H₈N₂·H₂O)

0.25g of 1:10-phenanthroline monohydrate weighed into a 250 mL volumetric flask made up to volume with H₂O.

C. 0.5 M Sulphuric acid solution (H₂SO₄)

49.04g of sulphuric acid in a 1L volumetric flask made up to volume with H₂O.

D. 0.18 M Potassium oxalate solution (K₂C₂O₄·H₂O)

8.29g of potassium oxalate in a 250 mL volumetric flask made up to volume with the 0.5M sulphuric acid solution.

E. 0.03 M Ferric(III) sulphate solution (Fe₂(SO₄)₃)

3g of ferric(III) sulphate weighed into a 250 mL volumetric flask made up to volume with 0.5M sulphuric acid solution.

F. 4.0 × 10⁻⁴ M Ferrous sulphate solution (FeSO₄·2H₂O)

0.0188g of FeSO₄·2H₂O and 1.23g of H₂SO₄ weighed into a 250 mL volumetric flask made up to volume with H₂O.

A solution of 2.5 mL of the 0.5M sulphuric acid and 12.5 mL of the buffer solution was made up to 50 mL with pure water. This solution was used to determine the I₀ value for the spectrometer.

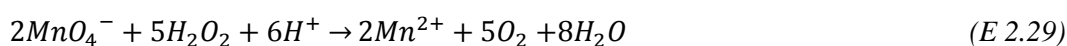
A subphase solution to fill the Langmuir trough was made up under dark room conditions using red light only to illuminate the laboratory. The potassium ferrioxalate actinometer solution was made up in a 1L volumetric flask with 200 mL of each of solutions (C, D and E) and filled to capacity with H₂O:

The 1L potassium ferrioxalate actinometer solution was subsequently transferred into a 2L volumetric flask and filled to volume again with H₂O.

2.4.6 Determining the OH Radical Concentration in the Subphase with Titrations and Numerical Modelling

To produce absolute rate constants for the decline of the monolayer surface coverage at the air-water interface from the pseudo-first-order rate constants for the reaction of hydroxyl radical with stearic acid, the concentration of hydroxyl radicals in the Langmuir trough must be quantified. To determine the concentration of OH in the subphase over time an experiment was undertaken where a sample of the Langmuir trough subphase containing H₂O₂ was taken after a measured period of photolysis time. The sample was titrated with standardized potassium permanganate solution for hydrogen peroxide. The titration data of the decay in H₂O₂ with photolysis time was then fitted to obtain a concentration of hydrogen peroxide in the subphase during a photolysis experiment.

The following equation describes the consumption of H₂O₂ during titration with potassium permanganate.



2.4.6.1 Titration Procedure

The Langmuir trough was set up as for a neutron experiment, within the aluminium reaction chamber. The trough was filled with 400 mL of 0.088 ± 0.002 mol dm⁻³ H₂O₂ in H₂O subphase solution. Each 400 mL sample provided two samples without the depth of the solution affecting the OH production.

A 50 mL burette was fixed to a clamp stand and filled with potassium permanganate solution. The reaction end point between H₂O₂ and the potassium permanganate solution was established by mixing in a 250 mL Erlenmeyer flask, 10 mL of the 4M sulphuric acid solution, and 50 mL pure water. 1 drop of potassium permanganate solution was added with a Pasteur pipette and the mixture was agitated in a circular direction until the mixture became a pale pink which was the end point colour to titrate the samples to.

A standardisation was performed to calculate the amount of sodium oxalate required to react with 30 mL of the potassium permanganate solution. The sodium oxalate solution (D, section 2.4.6.4) was heated to 80°C on a hotplate. The hot solution was then placed beneath the potassium permanganate burette, the level of potassium permanganate solution in the burette was recorded and the tap of the burette was opened so that a slow trickle of potassium permanganate solution entered the sodium oxalate solution. The Erlenmeyer flask was agitated with a swirling motion continuously. When the solution of potassium oxalate reached the reaction end point colour the level of potassium permanganate remaining in the burette was recorded.

The titration of H₂O₂ samples was conducted on a 25 mL sample of the subphase H₂O₂ solution after exposure to the photolysis lamp for a measured period of time. The 25 mL subphase sample was pipetted into a 250 mL Erlenmeyer flask and 10 mL of sulphuric acid solution was slowly added. The level of potassium permanganate solution in the burette was recorded and the Erlenmeyer flask was then held beneath the burette containing the potassium permanganate solution and the tap was opened to allow a slow trickle of potassium permanganate to enter the flask. The flask was continually agitated in a swirling motion until the end point colour was reached. The level of potassium permanganate in the burette was recorded at the end point and the sample calculation was performed.

A 25 mL sample of the subphase was taken using a pipette prior to any photolysis. This sample was titrated with the potassium permanganate solution to determine the initial H₂O₂ concentration to compare to the irradiated samples.

The following set of equations (R 2.30 to 2.32) form the sample calculation used to determine the H₂O₂ concentration in the titrated samples. The number of moles of KMnO₄ titrated to reach the reaction end point was calculated according to equation 2.30 where V_{titrated} is the volume of KMnO₄ titrated in micro litres, multiplied by the molarity of the KMnO₄ solution used for titration.

$$[KMnO_4]_{\text{titrated}} = (V_{\text{titrated}})[KMnO_4]_{\text{solution}} \quad (E 2.30)$$

The number of moles of KMnO₄ solution taken to reach the reaction end point multiplied by a factor of 2.5 gives the number of moles of H₂O₂ titrated ($[H_2O_2]_{\text{titrated}}$).

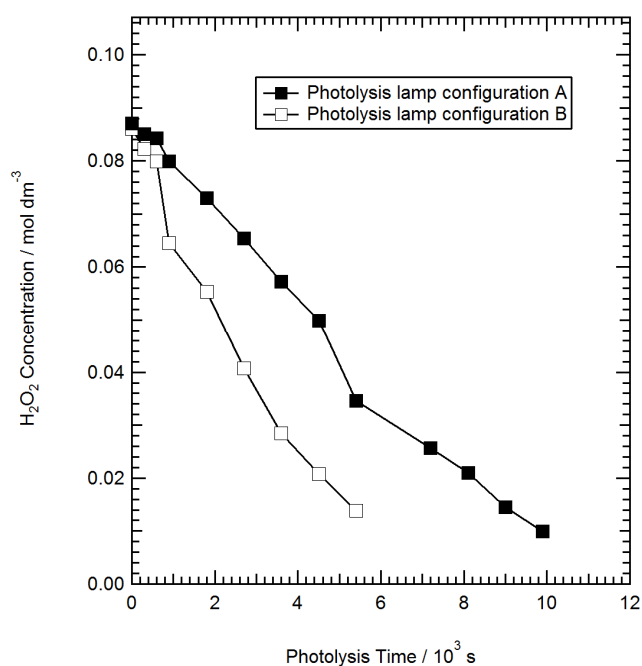
$$[H_2O_2]_{\text{titrated}} = ([KMnO_4]_{\text{titrated}}) 2.5 \quad (E 2.31)$$

$$[H_2O_2]_{\text{mol dm}^{-3}} = \frac{[H_2O_2]_{\text{titrated}}}{RMM_{H_2O_2}} \quad (E 2.32)$$

The concentration of H_2O_2 in the titrated sample was calculated using equation 2.32, the relative molecular mass of H_2O_2 ($RMM_{\text{H}_2\text{O}_2}$) is 34.1.

The titration experiment was performed twice for different bulb configurations, to allow the calculation of an accurate photolysis rate constant when the bulbs had been changed.

Figure 2.17 *The Subphase H_2O_2 Concentration as Measured by Titration, for Lamp Configuration A and Lamp Configuration B*



2.4.6.2 Titration Materials

- Pasteur pipettes
- 20 mL glass graduated pipette for extracting the subphase from the Langmuir trough to be titrated.
- 1 mL glass graduated pipette for measuring out the H_2O_2 to make up the H_2O_2 subphase solution.
- 2 1L volumetric flasks, one for the H_2O_2 subphase, one for the potassium permanganate solution.
- Erlenmeyer flasks (250 mL) to titrate into.
- Hotplate (80°C)
- Burette (50mL)
- Clamp stand
- Measuring cylinder (25 mL) for the potassium permanganate solution.

2.4.6.3 Titration Chemicals

- Pure water purified by a Millipore machine to a conductivity of 18 Ω M.
- H_2O_2 : 30% NormaPur for trace analysis purchased from VWR, product code: 23615.261.
- Potassium permanganate (KMnO_4) purchased from Sigma Aldrich in dry granular form. Catalogue number: 223468
- Sulphuric Acid (H_2SO_4) purchased from Sigma Aldrich.
- Sodium oxalate ($\text{Na}_2\text{C}_2\text{O}_4$) purchased from Sigma Aldrich

2.4.6.4 Titration Solutions

- A. 0.0882 mol dm^{-3} Hydrogen peroxide (H_2O_2) solution.
The solution was made up by volume using 10 mL 30% H_2O_2 in 1L H_2O . The solution concentration was 0.3 % H_2O_2 .
- B. 4 M Sulphuric acid (H_2SO_4) solution
98.08g in 250mL H_2O .
- C. 0.025 M Potassium permanganate (KMnO_4) solution
3.95g KMnO_4 in 1L H_2O .
- D. Sodium oxalate ($\text{Na}_2\text{C}_2\text{O}_4$) solution for standardisation
0.345g of sodium oxalate powder was weighed out into a 250 mL Erlenmeyer flask. 60 mL of pure water and 10 mL of the sulphuric acid solution were added to the sodium oxalate. The mixture was agitated until the sodium oxalate dissolved.

A low concentration of H_2O_2 was used so that the reservoir concentration of H_2O_2 would decline allowing the modelling of the photolysis rate constant from the decay in H_2O_2 concentration. For the neutron experiments a high concentration of H_2O_2 was used in the subphase so that the OH concentration remained near constant during a reaction with stearic acid.

2.4.7 Kinetic Modelling of the Aqueous OH Radical Concentration

The aqueous OH radical concentration in the subphase was determined through modelling based on the titration data which gave the decay in the concentration of H₂O₂ with photolysis time.

The kinetic modelling of the OH concentration showed that:

- OH diffused to the interface more rapidly than it was destroyed.
- The concentration of H₂O₂ made little difference to the concentration of OH. The OH concentration was much more sensitive, to the number of photons incident on the surface of the Langmuir trough.
- Secondary chemistry was not responsible for the radical reaction with the monolayer as OH diffused to the air-water interface rapidly and was the dominant reactive chemical species in the subphase.

2.4.7.1 Modelling the Subphase OH Concentration during a Photolysis Reaction with Hydrogen Peroxide

To calculate the concentration of OH radical in the subphase the photolysis rate constant (J) was calculated using a kinetic model which modelled reaction 18 to 23 within the subphase. The photolysis rate constant (J) governs the dissociation of H₂O₂ into OH radicals. The box model took into account the penetration depth of the UVC light into the subphase and the mixing with depth.

In order to model the photolysis rate constant the subphase concentration of H₂O₂ with reaction time needed to be measured as the model calculated [OH] based on the decay of H₂O₂ as measured in the titration experiment. The kinetic model ran reaction 18 to 23 as a kinetic system of first-order differential equations which were solved using a Runge-Kutta solver to predict the concentration of H₂O₂ and OH radical in the subphase. The k_{18} value was varied to obtain an accurate fit to the temporal decay in the hydrogen peroxide concentration due to photolysis. The modelled OH concentrations are given in table 2.1. Yu and Barker (2003) measured the quantum yield of hydroxyl radicals from photolysis of aqueous hydrogen peroxide solutions and its secondary reactions (R 2.18 to 2.23), this was input into the model.

J was modelled according to equation 2.33.

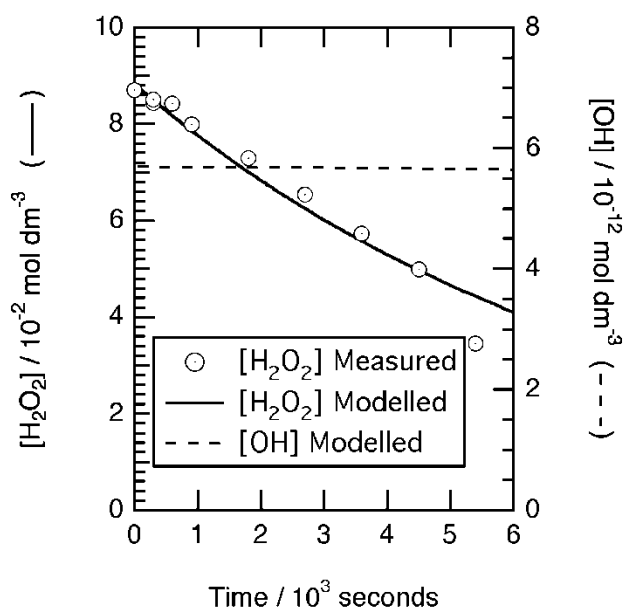
$$J = \int \sigma \phi F d\lambda \quad (E 2.33)$$

J is defined as the integral of the absorption cross section (σ) of H_2O_2 for light at a wavelength (λ) of 254 nm $\sim 25 \text{ M}^{-1} \text{ cm}^{-1}$ multiplied by the quantum yield of OH production events per photon (ϕ), which is 1, multiplied by the photon flux (F) and the wavelength ($d\lambda$).

The J rate for a $0.882 \text{ mol dm}^{-3} \text{ H}_2\text{O}_2$ solution was $(1.8 \pm 0.2) \times 10^{-4} \text{ s}^{-1}$, for the lamp configuration A with older bulbs in the lamp, when one bulb was replaced (lamp configuration B) the J rate increased to $(3.4 \pm 0.4) \times 10^{-4} \text{ s}^{-1}$. The error in J is the upper and lower limit of J within which a fit of the H_2O_2 modelled concentration data to the titration H_2O_2 versus photolysis time experimental data is valid.

The temporal decay of hydrogen peroxide due to the photolysis of $0.0882 \text{ mol dm}^{-3}$ hydrogen peroxide solution in the absence of a stearic acid monolayer is shown in figure 2.18 together with the predicted kinetically modelled hydrogen peroxide and hydroxyl radical concentrations.

Figure 2.18 *The Modelled OH Concentration in a Subphase of $0.0882 \text{ mol dm}^{-3} \text{ H}_2\text{O}_2$*



The modelling showed that the OH concentration in the top box of the model in the subphase region immediately beneath the monolayer, stays constant at approximately 8.4 to $8.7 \times 10^{-12} \text{ mol dm}^{-3}$ throughout the timescale of a neutron experiment. When a new bulb was fitted to the lamp the OH concentration increased to $16 \times 10^{-12} \text{ mol dm}^{-3}$ showing that the intensity of light had more influence on the OH radical concentration than the starting concentration of H_2O_2 .

Table 2.2 *The Modelled OH Concentrations in the Langmuir Trough Subphase During a Photolysis Reaction According to Reactions 18 to 23*

H₂O₂ subphase concentration mol dm ⁻³	OH subphase concentration (10 ⁻¹² mol dm ⁻³)
0.029	8.4
0.294	8.6
0.588	8.7
1.176	8.7
1.470	*16
2.352	8.7

**Note that the OH concentration of 16 mol dm⁻³ is valid for the experiments in section 2.7.3 where the subphase temperature was varied. The higher value was a result of a new bulb being used in the photolysis lamp.*

From table 2.2 it can be seen that a large change in the initial hydrogen peroxide concentration leads to a small change in the concentration of OH in the subphase.

2.5 Kinetic Analysis Methodology

The decay in the surface coverage measurements from the neutron reflectivity data for the reaction between OH radical and a stearic acid monolayer were fitted to a degradation mechanism.

Blank experiments to check for the effect of the photolysis lamp on the monolayer surface coverage without OH radical production and with no photolysis to measure the decay in ambient air of the stearic acid monolayer were fitted to an exponential decay. The two decay mechanisms will be explained here.

2.5.1 Exponential Decay

The blank experiments with no photolysis, or with photolysis and no H₂O₂ were fit to an exponential decay where the rate of decrease at the surface is related to the amount at the surface at the start of the experiment.

The reaction scheme for the loss of stearic acid over time is:

$$\Gamma_{stearic}^{t=0} \xrightarrow{k} \Gamma_{stearic}^t \quad (E 2.34)$$

The rate expression for the decay in the surface coverage, Γ , of the stearic acid monolayer is:

$$\frac{d[\Gamma_{stearic}]}{dt} = -k_{stearic}[\Gamma_{stearic}] \quad (E 2.35)$$

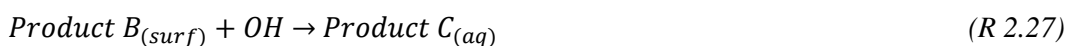
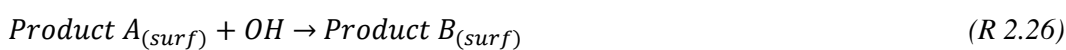
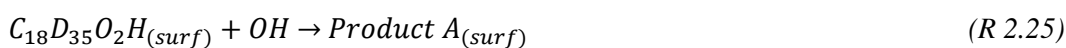
A simple exponential as shown below can be fitted to the surface coverage data giving the rate of decay of surface coverage therefore the loss of the stearic acid monolayer over time.

A fitting regime was used which follows the form of equation 2.36 allowing time zero for the fit to be prescribed as the start of the reaction, the point in time where the lamp was engaged for the photolysis blank experiments.

$$\Gamma_t = \Gamma_{unreacted} + \Gamma_{t=0} e^{-\frac{(t-t_0)}{\tau}} \quad (E 2.36)$$

2.5.2 Degradation Mechanism

A sequential decay mechanism was fitted to the measured kinetic variation of surface coverage (Γ_{total}), as recorded by neutron reflection. The measured surface coverage is the sum of all the deuterated species at the air-water interface i.e. deuterated stearic acid and any deuterated products of the reaction between stearic acid and hydroxyl radical. The following scheme is suggested;



Where stearic acid, and its shorter chain length products A, and B, are surface active (surf), thus contribute to the surface coverage Γ_{total} at the air-water interface. Product C is denoted as (aq) and partitions into the bulk aqueous solution as it has no propensity to be found at the air-water interface. The neutron reflection technique as employed in these experiments measures the coverage of deuterium atoms at the surface and no distinction is made between stearic acid and products A and B (C is dissolved in the bulk therefore does not contribute to the reflection signal). The total surface coverage would depend on stearic acid, product A, and product B. It is assumed that the OH radical initiates a series of reactions removing four CD_2 groups in each

reaction, 2.25, 2.26 and 2.27. There are likely to be more steps, and this is a simplified model.

Thus the total surface coverage Γ_{total} depends on:

$$\Gamma_{total} = 35\Gamma_{stearic} + N_A\Gamma_A + N_B\Gamma_B \quad (E 2.37)$$

Where $\Gamma_{stearic}$, Γ_A , Γ_B , are the surface coverage measurements of stearic acid, product A and product B respectively and N_A and N_B are the number of deuteriums found in product A and B respectively. To account for the cleaving of four CD_2 groups from the stearic acid chain in each reaction, (R2.23 to 2.25) arbitrary values of 27 and 21 are assigned to N_A and N_B .

$$\Gamma_{total} = 35\Gamma_{stearic} + 27\Gamma_A + 21\Gamma_B \quad (E 2.38)$$

Fitting the above scheme to the Γ data yielded the pseudo first order rate constants.

The rate equations for reactions 2.25 to 2.27 are:

$$\frac{d\Gamma_{stearic}}{dt} = -k_{39}\Gamma_{stearic}[OH] \quad (E 2.39)$$

$$\frac{d\Gamma_A}{dt} = k_{39}\Gamma_{stearic}[OH] - k_{40}\Gamma_A[OH] \quad (E 2.40)$$

$$\frac{d\Gamma_B}{dt} = k_{40}\Gamma_A[OH] - k_{41}\Gamma_B[OH] \quad (E 2.41)$$

Assuming first-order conditions with $[OH]$ constant as photolysis does not consume H_2O_2 rapidly, and defining 2nd order rate constants:

$$k_{stearic} = k_{39}[OH] \quad (E 2.42)$$

$$k_A = k_{40}[OH] \quad (E 2.43)$$

$$k_B = k_{41}[OH] \quad (E 2.44)$$

By solving equations 2.39 to 2.41 (Laidler, 1995) and substituting the answers into equation 2.38 the following equation is produced:

$$\begin{aligned} \Gamma_{total} = & \left(35\Gamma_{stearic}^{t=0} + \frac{27\Gamma_{stearic}^{t=0} k_{stearic}}{(k_A - k_{stearic})} + \frac{21\Gamma_{stearic}^{t=0} k_{stearic} k_A}{(k_A - k_{stearic})(k_B - k_{stearic})} \right) e^{-k_{stearic}t} \\ & + \left(\frac{27\Gamma_{stearic}^{t=0} k_{stearic}}{(k_A - k_{stearic})} + \frac{21\Gamma_{stearic}^{t=0} k_{stearic} k_A}{(k_A - k_{stearic})(k_B - k_{stearic})} \right) e^{-k_A t} \\ & + \left(\frac{21\Gamma_{stearic}^{t=0} k_{stearic} k_B}{(k_A - k_{stearic})(k_B - k_{stearic})} + \frac{21\Gamma_{stearic}^{t=0} k_{stearic} k_A}{(k_A - k_{stearic})(k_B - k_A)} \right) e^{-k_B t} \end{aligned} \quad (E 2.45)$$

Where $\Gamma^{t=0}$ is the surface coverage at time zero and Γ^t is the surface coverage at a later time, t . Equation 2.45 describes the temporal behaviour of Γ_{total} and can be fitted to the experimental data by varying the value of $k_{stearic}$, k_A and k_B . Rate constants for k_{39} , k_{40} and k_{41} can be determined by knowledge of $[OH]$.

The reaction initiating the mechanism is hydrogen peroxide and $h\nu$ producing 2 OH radicals. This mechanism fits the experimental observations and has been proposed on the basis of current literature. The proposed mechanism is a cyclic radical driven process that :

- (a) shortens the amphiphile at the air-water interface and
- (b) regenerates an amphiphile meaning that material stays at the surface.

The rate constants obtained by fitting to equation 2.45 to the surface coverage data from each neutron experiment are set out in the results section.

2.5.3 Rate Limitation

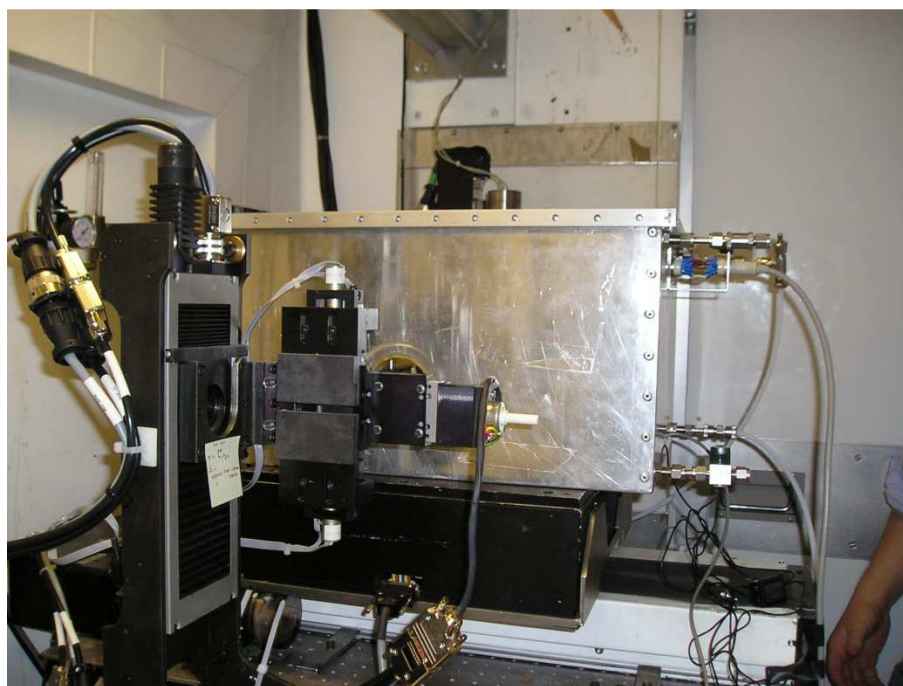
The rate limiting process for the reaction of stearic acid as a cloud droplet film component in the atmosphere and aqueous OH radical would be the OH concentration. In the experiment the rate limiting step was the process of OH attacking the stearic acid molecules in the film, which is in turn governed by the J rate of the lamps which determines the OH production rate, see equation 2.33. J was a constant value as the lamps were used when in a warmed up state only so it is not investigated further here.

2.6 The Methodology of a Typical Combined Surface Coverage and Surface Pressure Measurement

2.6.1 Sample Environment

The Langmuir trough was housed in a custom made aluminium reaction chamber as shown in figure 2.19.

Figure 2.19 *The Aluminium Reaction Chamber Housing the Langmuir Trough*



The reaction chamber was fitted to the SURF reflectometer sample environment and the beam was adjusted using a laser as a trace so that the neutrons would reflect from the surface of the Langmuir trough.

2.6.2 Cleaning the Langmuir Trough

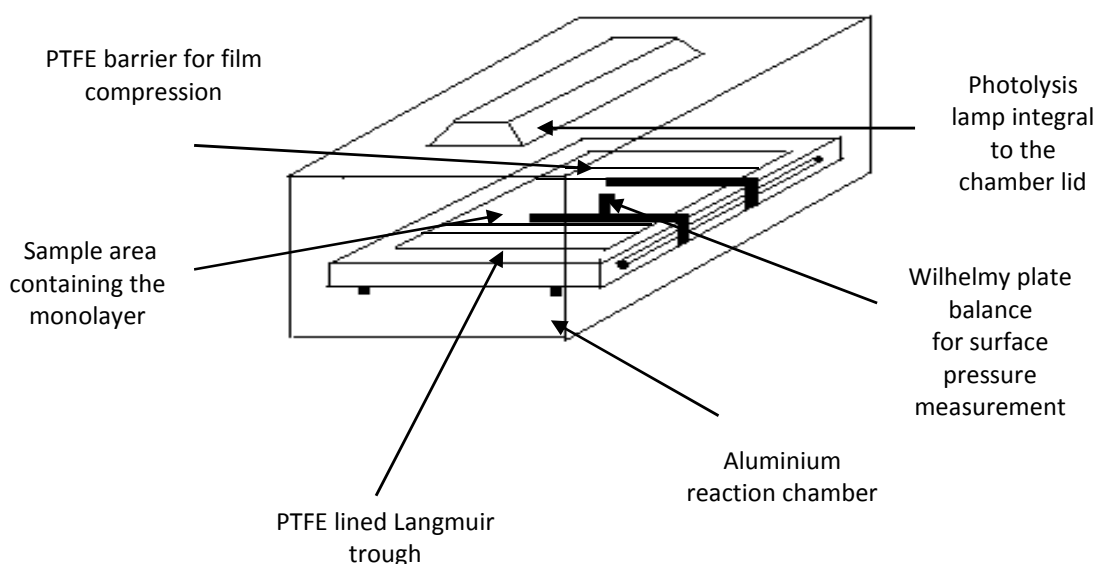
The Langmuir trough was cleaned with hydrochloric acid and then rinsed with pure water seven times. The trough was then wiped down with chloroform and rinsed a further seven times to remove any trace organics from the PTFE surface. The aluminium reaction chamber was also wiped down with chloroform and then wiped over seven times with pure water on a lint free tissue. The Langmuir trough was placed within the aluminium reaction chamber from which the surface pressure sensor can be connected and powered through a series of serial ports. The surface pressure sensor was calibrated using a weight at the beginning of the experiment. All glassware was washed with decontaminant (Decon 90) and rinsed seven times with pure water. The syringe was cleaned with chloroform seven times before use and immediately after use.

2.6.3 Controlling the Temperature of the Subphase

The temperature of the Langmuir trough subphase was controlled using a circulating water bath which pumped glycol into a system of tubing integral to the base of the trough which cools through heat exchange. The temperature was set to two degrees above the desired subphase temperature, and at the point where the photolysis lamp was switched on, the temperature was dropped by two degrees to counteract the warming effect of the lamp.

2.6.4 Experimental Methodology

Figure 2.20 *The Langmuir Trough within the Aluminium Reaction Chamber*



The Langmuir trough was filled with 400 mL of null reflective water containing H_2O_2 . The organic film at the air-water interface was created by adding 100 μl of 1 mg mL^{-1} deuterated stearic acid ($\text{C}_{18}\text{D}_{35}\text{O}_2\text{H}$), with a Hamilton syringe, drop by drop at the air-water interface on the Langmuir trough.

The reaction chamber lid with the integral photolysis lamp was placed onto the chamber. Once the stearic acid monolayer was spread the Langmuir trough barriers were closed to compress the monolayer to a surface pressure (Π) of $\sim 30 \text{ mNm}^{-1}$ in the solid region of the stearic acid isotherm at a velocity of $40 \text{ cm}^2 \text{ min}^{-1}$ and subsequently relaxed to 20 mNm^{-1} into the liquid region of the stearic acid isotherm to prevent phase change interference in the measurement. Upon reaching the desired surface pressure the trough barriers were stopped and the area was held constant, the surface pressure was monitored to record a kinetic decay as the photolysis lamps illuminated the trough. The neutron reflectivity measurements were initiated

simultaneously. The photolysis lamp was also switched on to generate OH radical within the subphase.

2.6.4.1 Methodology for Varied Subphase H₂O₂ Concentration Experiments

The H₂O₂ concentration in the subphase was varied at values of 0.0294, 0.2940, 0.588, 1.470, 1.176, and 2.352 mol dm⁻³, in order to vary the concentration of aqueous OH radical in order to observe whether a greater OH concentration would lead to a more rapid decay in the surface coverage of a stearic acid monolayer.

All runs were maintained at a temperature of 17°C as this temperature was achievable rapidly to maximise measurement time and was within the standard temperature range of 15°C to 20°C commonly used in atmospheric experiments for relevance to the temperature of the lower Troposphere at cloud base.

Neutron reflectivity data was collected over ~5 minute periods of measurement per surface coverage measurement data point.

2.6.4.2 Methodology for Varied Subphase Temperature Experiments

The subphase H₂O₂ concentration was kept constant at 0.588 mol dm⁻³ to determine if the subphase temperature (6.7 to 50°C), had an effect on the kinetic decay of the stearic acid monolayer. The trough was cleaned and re-filled with a new subphase and monolayer before each temperature experiment. The subphase temperature was altered by setting the circulating temperature controlling bath for cold runs at 5°C less than the desired temperature and for warm runs at 2°C more than the desired temperature. The subphase temperature within the Langmuir trough was observed by fitting a thermocouple to the Langmuir trough barrier with the tip immersed in the subphase behind the trough barrier to avoid interference with the monolayer.

Neutron reflectivity data was collected in 5 minute and 30 second, periods of measurement.

2.6.4.3 Equipment

- Neutron Reflectometer, SURF at the ISIS Pulsed Neutron and Muon Facility, Rutherford Appleton Laboratory, Oxfordshire, UK.
- Langmuir trough suitable for use on the neutron reflectometer SURF, with the Wilhelmy plate pressure sensor positioned on the barrier, out of the path of flight of the neutron beam. Measurements: 37.2cm x 32cm x 15cm custom model, Nima Technology.
- Surface Pressure Sensor: model IU4, Nima Technology.
- 50 µL Hamilton syringe

- Julabo Circulating temperature controlling bath model: FP50-MH with insulated tubing and connectors which will fit to the base of the Langmuir trough.
- Pre-cut Wilhelmy plates made from Whatman chromatography paper for Wilhelmy plates: Whatman 1cm width reel, catalogue number: 3001604.
- Gold wire for construction of oxidation resistant hooks to connect the Wilhelmy plate to the balance. Alpha Aesar, catalogue number 45084, 0.0138 inch diameter, 99.9% purity.
- Steel plated tweezers for placing the Wilhelmy plates and hooks onto the balance.
- Kimwipe lint free tissues.
- Aluminium reaction chamber custom made to house the Langmuir trough, with quartz windows to allow laser alignment of the neutron beam path onto the surface of the Langmuir trough.
- Germicidal ($\lambda_{\text{max}} \sim 254 \text{ nm}$) photolysis lamp. Photolysis Lamp: UVP XX_15BLB UV Bench Lamp. Photolysis lamp bulbs: Sylvania UVC (wavelength centred on 254nm)
- 1L volumetric flask with glass stopper for storing subphase.
- 10mL volumetric flask with glass stopper for making up the 1mg/mL spreading solution of D₃₅ stearic acid.
- Decon 90 detergent.

2.6.4.4 Chemicals

- H₂O₂: 30% NormaPur for trace analysis, VWR, product code: 23615.261
- Deuterated Stearic Acid: d35, Sigma Aldrich Isotech, catalogue number: 448249
- Non deuterated Stearic Acid: Sigma Aldrich-Fluka, puriss p.a. (standard for GC), catalogue number: 85679 used for test experiments.
- Deuterium Oxide: Sigma Aldrich, catalogue number: 661643
- Pure water: Millipore conductivity of $>18\Omega\text{M}$
- Chloroform: Sigma Aldrich, Chromasolv plus for HPLC 99.9% with ethanol stabilizer, catalogue number: 650471

2.7 Results

The experimental results are presented in the following order.

2.7.1) Preliminary surface pressure measurements

2.7.2) Neutron surface coverage and surface pressure measurements of the decay of stearic acid monolayers on a subphase of varied OH radical concentration.

2.7.3) Neutron surface coverage and surface pressure measurements of the decay of stearic acid monolayers on a subphase of varied temperature.

The results of the kinetic analysis and imaging of the monolayer will then be presented.

2.7.4) The results of the kinetic analysis of the surface coverage data.

2.7.5) Brewster angle microscopy images of stearic acid monolayers before and during oxidation.

2.7.1 Preliminary Experiments

2.7.1.1 Aims of the Preliminary Langmuir Trough Experiments

Before time on the neutron reflectometer can be obtained evidence of the need to use the instrument must be submitted to the neutron facility. A Langmuir trough at Royal Holloway University was used to run test experiments to determine whether a reaction was taking place that required surface coverage data in addition to surface pressure data to establish the kinetic behaviour of the reaction. A brief description of this preliminary data is given here.

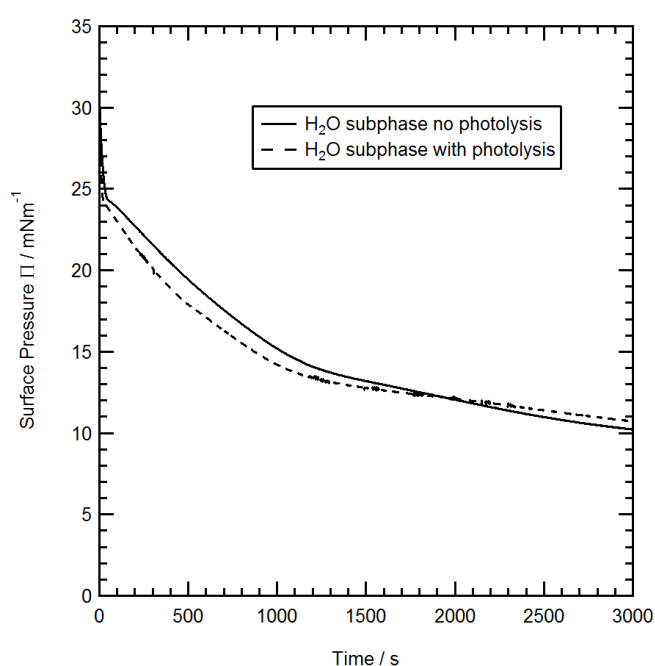
The aims of the preliminary experiments were

- To ensure the concentrations of reactants were sufficient to produce a reaction on a time order suitable to facilitate neutron reflectivity measurements of the monolayer surface coverage.
- To ensure that the reaction was initiated by the aqueous chemistry and not by the ambient air.
- The stearic acid monolayer was monitored with and without the photolysis lamps used to generate OH radical from aqueous H₂O₂ to ensure that the stearic acid monolayer was not photolysed (figure 2.20).

2.7.1.2 Results of the Preliminary Langmuir Trough Experiments

On a subphase of H_2O at 20°C the decay in the monolayer surface pressure was not greatly altered by photolysis as shown in figure 2.21. The phase transition at $\sim 13 \text{ mN m}^{-1}$, from liquid to liquid condensed like behaviour was less pronounced under photolysis conditions. The surface pressure decayed from 30 mN m^{-1} to 10 mN m^{-1} over 3000 seconds / 50 minutes.

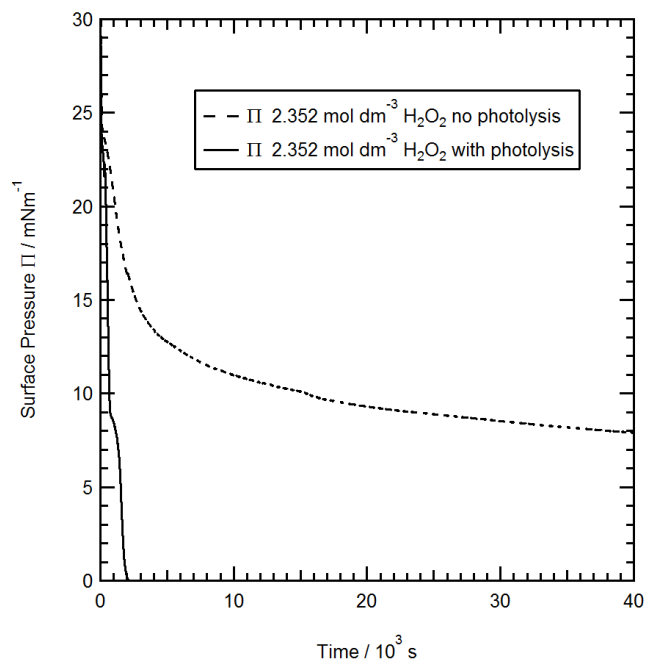
Figure 2.21 *The Kinetic Decay in the Surface Pressure of a $30\mu\text{L}$ Monolayer of 1 mg/mL Stearic Acid on an H_2O Subphase With and Without the Photolysis Lamp at 20°C Conducted on the Royal Holloway Langmuir Trough*



The interference in the surface pressure data was caused by groundwork adjacent to the laboratory which was on-going throughout the project causing vibrations despite the use of a laser table to minimise interference.

To ensure that the production of OH radical in the subphase had a measurable effect on the stearic acid monolayer the surface pressure of the monolayer on a high concentration of H_2O_2 ($2.352 \text{ mol dm}^{-3}$) subphase was monitored at 20°C with and without photolysis (figure 2.22). The effect of the OH radical on the kinetic decay of the monolayer surface pressure can be clearly seen with the surface pressure reaching zero within 2000 seconds. In the presence of H_2O_2 alone without photolysis the surface pressure decayed to just 18 mN m^{-1} over 40000 seconds/ >11 hours.

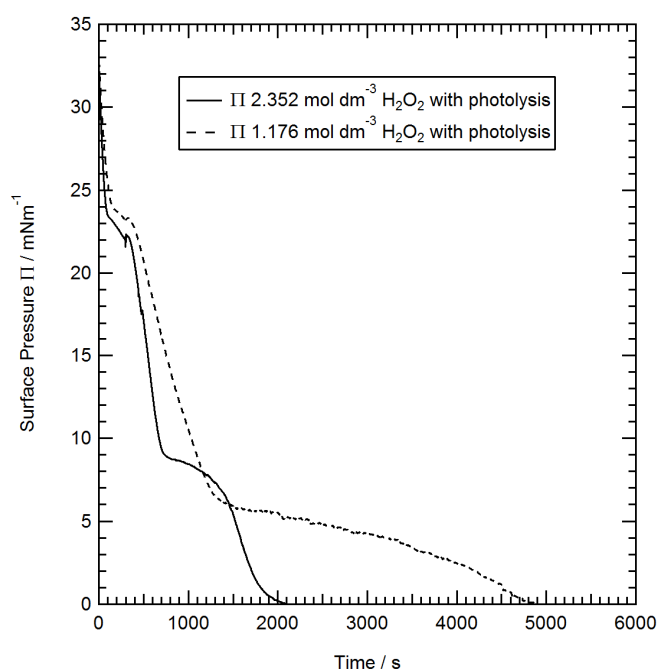
Figure 2.22 *The Kinetic Decay of a 30 μ L Monolayer of 1mg/mL Stearic Acid on an H₂O₂ Subphase With and Without the Photolysis Lamp at 20°C Conducted on the Royal Holloway Langmuir Trough*



The lamp was initiated at time zero.

To test whether changing the H₂O₂ concentration had an effect on the kinetic decay in the surface pressure of the stearic acid monolayer; the surface pressure was monitored at different H₂O₂ concentrations (figure 2.23). The slope of the decay in surface pressure in the liquid region appeared steeper at a higher H₂O₂ concentration. The difference in the surface pressure decay over time on subphases of different H₂O₂ concentrations was the basis of the neutron experiment described in section 2.7.2.

Figure 2.23 A 30 μ L Monolayer of 1mg/ mL Stearic Acid on an H₂O₂ Subphase With Photolysis at 20°C Conducted on the Royal Holloway Langmuir Trough



The photolysis lamp was initiated at 400 seconds. Firing the lamp made heat which produced a small rise in the surface pressure data. The surface pressure rise was eliminated by reducing the temperature by 2°C when the lamp was switched on.

2.7.2 Neutron Surface Coverage and Surface Pressure Measurement of the Decay of Stearic Acid Monolayers on a Subphase of Varied OH Radical Concentration

The kinetic decay in the surface coverage and surface pressure of a stearic acid monolayer due to a reaction with aqueous OH radical was measured simultaneously on the Langmuir trough and the SURF neutron reflectometer. The H₂O₂ concentration and therefore the OH radical concentration was altered to investigate the effect of concentration on the reaction and to assess rate limitations on the reaction of the stearic acid monolayer with aqueous OH radical.

The H₂O₂ concentrations and the corresponding OH concentrations deduced from the kinetic modelling are explained in section 2.4.7 are given in table 2.2 in section 2.4.7.1.

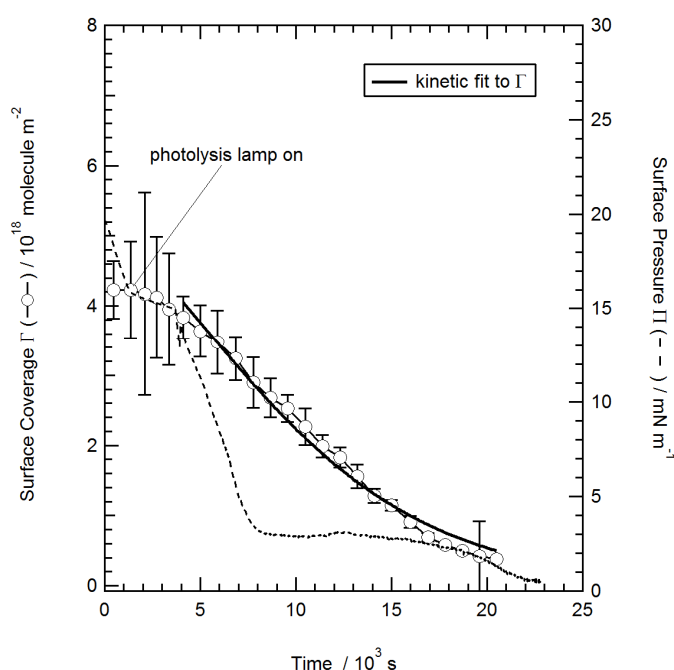
The results of the OH reaction experiments are presented in order of increasing OH concentration. The kinetic decay in the surface coverage of a stearic acid monolayer on a subphase of null reflective water with photolysis showed that the stearic acid monolayer does not photolyse (figure 2.28). The kinetic decay in the surface pressure and surface coverage of a stearic acid monolayer on a subphase of H₂O₂, without photolysis (figure 2.28) was measured to show the effect on the monolayer decay due to H₂O₂ for comparison to a photolysis experiment

in which OH reacts with the monolayer showing that the surface reaction with OH is distinguishable (figure 2.24).

The graphs are presented with fits of the kinetic decay mechanism (equation 2.45) to the surface coverage data as explained in section 2.5.2, the results of which are given in section 2.7.5.

At an OH concentration of $8.6 \times 10^{12} \text{ mol dm}^{-3}$ the surface coverage decayed to $0.5 \times 10^{18} \text{ molecule m}^{-2}$ over 21000 seconds (figure 2.24). The surface pressure decayed to 2.5 mN m^{-1} over 7500 seconds. The decay in the surface coverage did not follow the decay in the surface pressure thus if kinetic calculations were based on the decay in the surface pressure the rate constant would not be valid for the amount of material at the air-water interface.

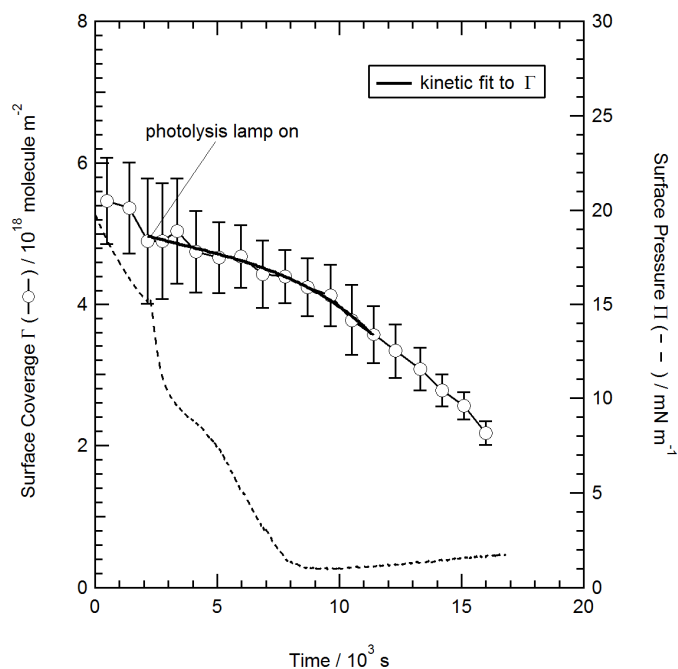
Figure 2.24 *The Surface Coverage and Surface Pressure Kinetic Decay of a Stearic Acid Monolayer on a Subphase of $0.294 \text{ mol dm}^{-3} \text{H}_2\text{O}_2 / 8.6 \times 10^{12} \text{ mol dm}^{-3} \text{OH}$ with a Kinetic Degradation Fit of Equation 2.45 to the Surface Coverage Data.*



The subphase temperature was 20°C .

At an OH concentration of $8.7 \times 10^{12} \text{ mol dm}^{-3}$ the surface coverage decayed to $2.1 \text{ molecule m}^{-2}$ over 16000 seconds (figure 2.24). The surface pressure decayed to the lowest value of 1 mN m^{-1} over 9000 seconds.

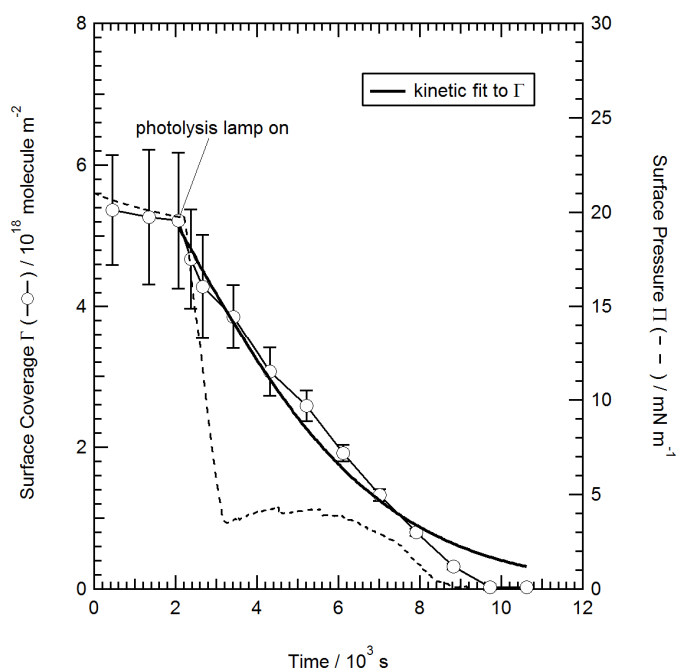
Figure 2.25 *The Surface Coverage and Surface Pressure Kinetic Decay of a Stearic Acid Monolayer on a Subphase of $0.588 \text{ mol dm}^{-3} \text{H}_2\text{O}_2 / 8.7 \times 10^{12} \text{ mol dm}^{-3} \text{OH}$ with a Kinetic Degradation Fit of Equation 2.45 to the Surface Coverage Data*



The subphase temperature was 6°C .

At a modelled OH concentration of $8.7 \times 10^{12} \text{ mol dm}^{-3}$, but a higher H_2O_2 concentration of $1.176 \text{ mol dm}^{-3}$ (figure 2.25), the surface coverage decayed to zero over 9600 seconds. The surface pressure decayed to zero over 9000 seconds. A rise in the surface pressure and a subsequent decay can be seen from 3100 onwards. The feature in the surface pressure data can also be seen as a change in the slope of the surface coverage data at 5200 seconds / $2.5 \times 10^{18} \text{ molecule m}^{-2}$.

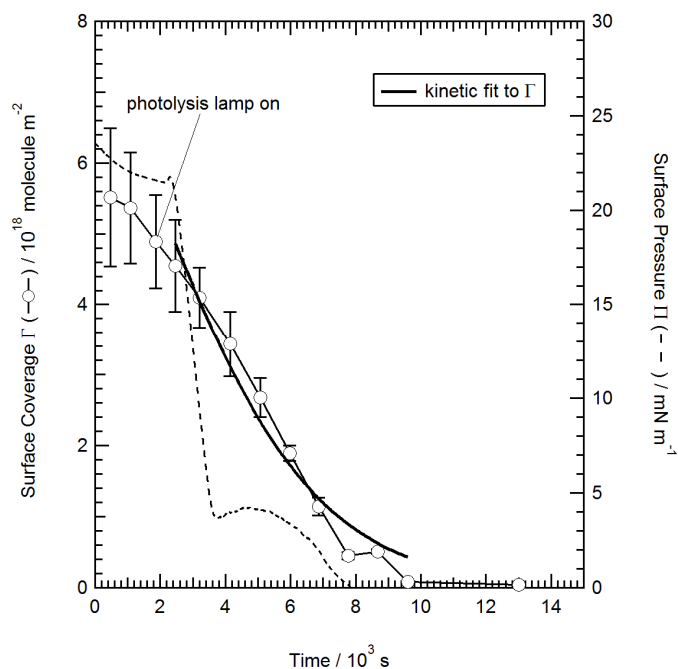
Figure 2.26 *The Surface Coverage and Surface Pressure Kinetic Decay of a Stearic Acid Monolayer on a Subphase of $1.176 \text{ mol dm}^{-3} \text{H}_2\text{O}_2 / 8.7 \times 10^{12} \text{ mol dm}^{-3} \text{OH}$ with a Kinetic Degradation Fit of Equation 2.45 to the Surface Coverage Data. The subphase temperature was 20°C*



The subphase temperature was 20°C .

At a modelled OH concentration of $8.7 \times 10^{12} \text{ mol dm}^{-3}$ and an initial H_2O_2 concentration of $2.352 \text{ mol dm}^{-3}$ the surface coverage decayed to zero over 9600 seconds, and the surface pressure decayed to zero over 8000 seconds (figure 2.27). As in figure 2.26 a pronounced rise in the surface pressure can be seen at 3000 seconds / 3 mN m^{-1} onwards, with a subsequent decay to zero. A change in the decay slope of the surface coverage can also be seen from 2500 seconds at a surface coverage of $4 \times 10^{18} \text{ molecule m}^{-2}$.

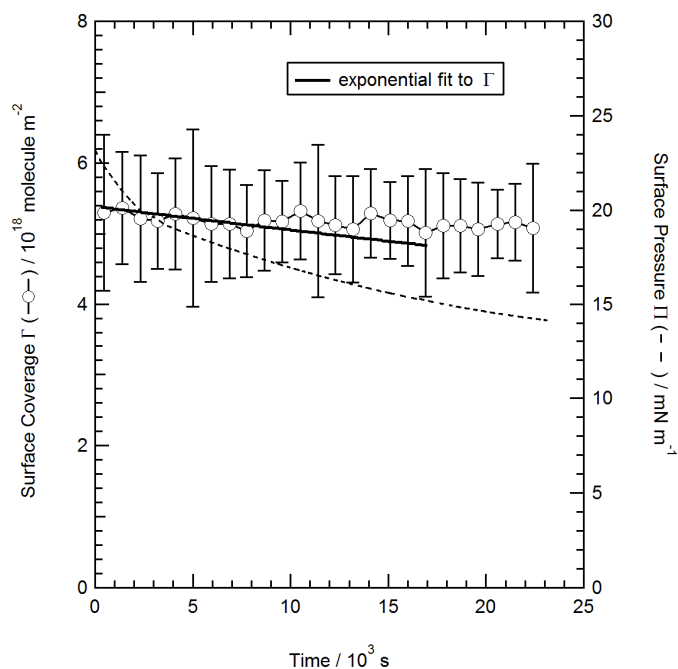
Figure 2.27 *The Surface Coverage and Surface Pressure Kinetic Decay of a Stearic Acid Monolayer on a Subphase of $2.352 \text{ mol dm}^{-3} \text{H}_2\text{O}_2 / 8.7 \times 10^{12} \text{ mol dm}^{-3} \text{OH}$ with a Kinetic Degradation Fit of Equation 2.45 to the Surface Coverage Data*



The subphase temperature was 20°C .

The surface coverage was constant at $\sim 5.1 \times 10^{18} \text{ molecule m}^{-2}$ within error over 23000 seconds on a subphase of $2.352 \text{ mol dm}^{-3} \text{H}_2\text{O}_2$ with no photolysis or production of OH radical (figure 2.28). The surface pressure decayed from 23 mN m^{-1} to 14 mN m^{-1} over 23000 seconds at a slower rate than in the presence of aqueous OH radical.

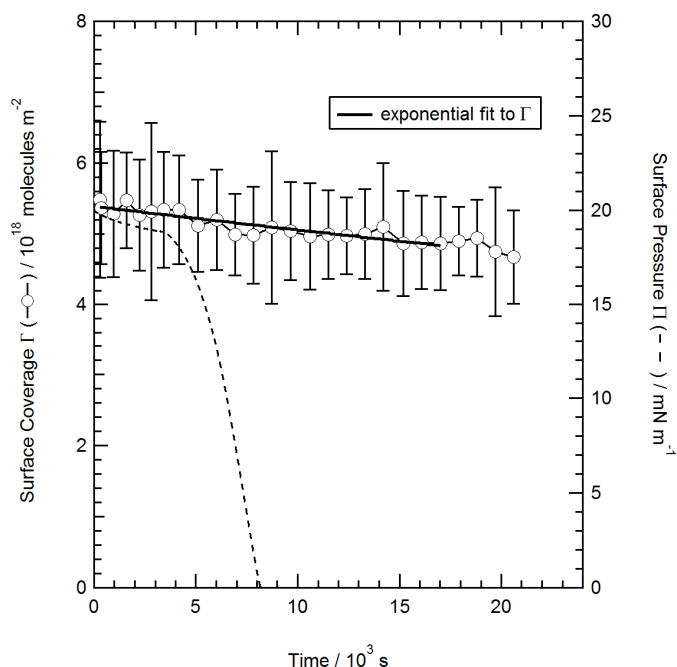
Figure 2.28 *The Surface Coverage and Surface Pressure Kinetic Decay of a Stearic Acid Monolayer on a Subphase of $2.352 \text{ mol dm}^{-3} \text{H}_2\text{O}_2$ Without Photolysis with an Exponential Fit to the Surface Coverage Data*



The subphase temperature was 20°C.

To ensure that the decay in the surface coverage and surface pressure of the stearic acid monolayer was not caused by photolysis of the stearic acid measurements were taken in the absence of H_2O_2 on a subphase of null reflective water. The surface coverage remained constant at $\sim 5 \times 10^{18} \text{ molecule m}^{-2}$ within error over 21000 seconds. The surface pressure rapidly decayed from 20 mN m^{-1} to zero over 8000 seconds.

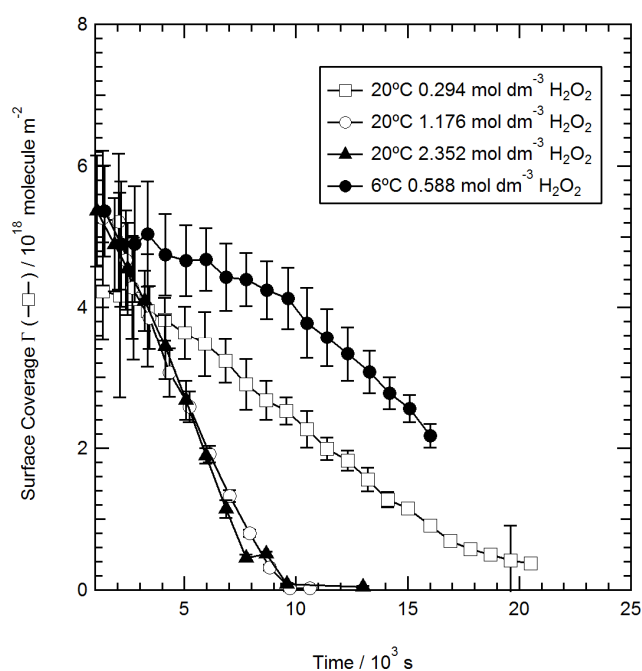
Figure 2.29 *The Surface Coverage and Surface Pressure Kinetic Decay of a Stearic Acid Monolayer on a Subphase of Null Reflective Water with photolysis, and an Exponential Fit to the Surface Coverage Data*



The photolysis lamp was initiated at time zero. The subphase temperature was 20°C.

The difference in the slope of the decay in surface coverage with increasing H₂O₂ concentration can be seen in figure 2.30. There was not enough data collected to quantify the effect and this experiment would need repeating to do so. The neutron beam was lost for a total of half the experimental time granted on SURF due to a mechanical failure at ISIS, therefore the data set is not ideal however some kinetic information can be gained from this work. The experiment at 6°C showed a more shallow decay in surface coverage which was investigated further in the following neutron reflectivity experiment described in section 2.7.3.

Figure 2.30 A Comparison of the Kinetic Decay in the Surface Pressure of A Stearic Acid Monolayer Exposed to Varied Concentrations of Aqueous H_2O_2 / OH Radical

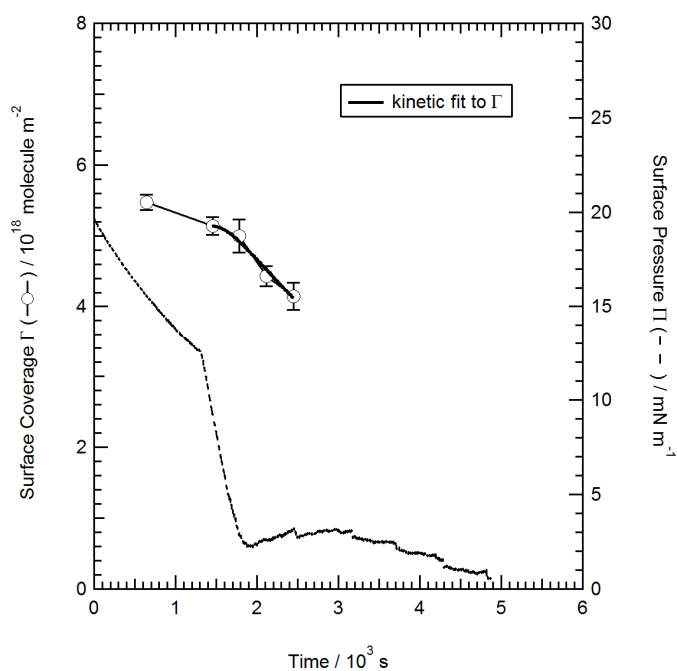


2.7.3 Neutron Surface Coverage and Surface Pressure Measurement of the Decay of Stearic Acid Monolayers on a Subphase of Varied Temperature

Measurements of the surface pressure and surface coverage of a stearic acid monolayer at the air-water interface were taken at a single H_2O_2 / OH concentration at different temperatures. The subphase temperature was varied to show whether the rate constant would decrease with at higher temperatures. Measuring a range of temperatures allowed the creation of an Arrhenius plot to show if there was a relationship between temperature and reaction rate. The results are presented in order of temperature from 6.7°C to 50°C.

At 6.7°C (figure 2.31) the surface pressure measurement repeated the behaviour seen in figure 2.25 and 2.26 where the surface pressure decayed then rises before decaying again. The neutron beam was lost during this experiment after 3000 seconds / 50 minutes, thus there is only surface coverage data for the decay from 5.5 to 4×10^{18} molecule m^{-2} .

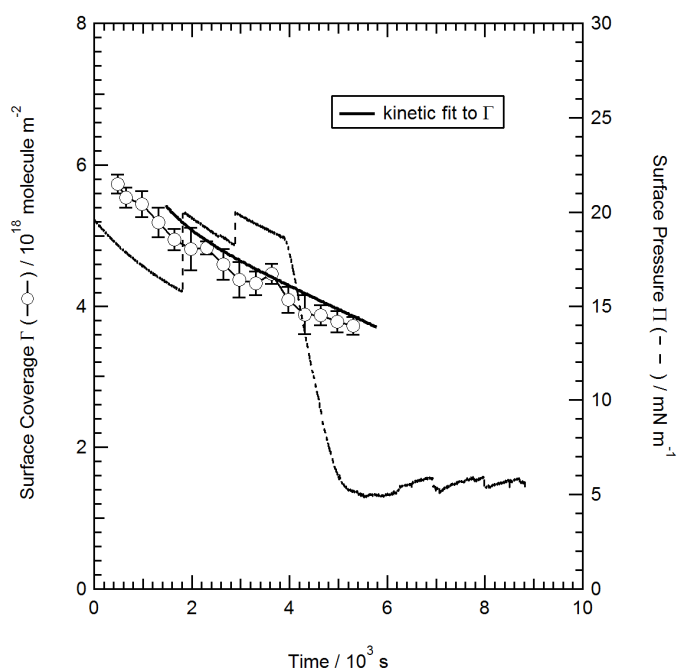
Figure 2.31 *The Surface Coverage and Surface Pressure Kinetic Decay of a Stearic Acid Monolayer on a Subphase of $1.176 \text{ mol dm}^{-3} \text{H}_2\text{O}_2 / 8.7 \times 10^{12} \text{ mol dm}^{-3} \text{OH}$ at a temperature of 6.7°C with a Kinetic Degradation Fit of Equation 2.45 to the Surface Coverage Data*



The photolysis lamp was initiated at reaction time zero for all the varied temperature experiments.

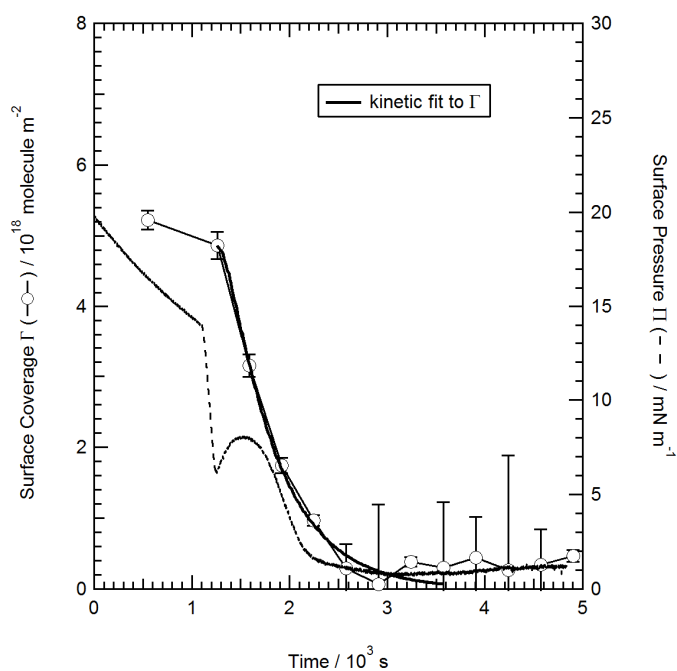
At 8°C (figure 2.32) the surface pressure data was distorted by a bubble forming in the subphase beneath the Wilhelmy plate. The surface coverage decayed from 5.9 to $3.8 \times 10^{18} \text{ molecule m}^{-2}$ over 4500 seconds after which the neutron beam was lost and the measurements of surface coverage were stopped.

Figure 2.32 *The Surface Coverage and Surface Pressure Kinetic Decay of a Stearic Acid Monolayer on a Subphase of $1.176 \text{ mol dm}^{-3} \text{H}_2\text{O}_2 / 8.7 \times 10^{12} \text{ mol dm}^{-3} \text{OH}$ at a Temperature of 8°C with a Kinetic Degradation Fit of Equation 2.45 to the Surface Coverage Data*



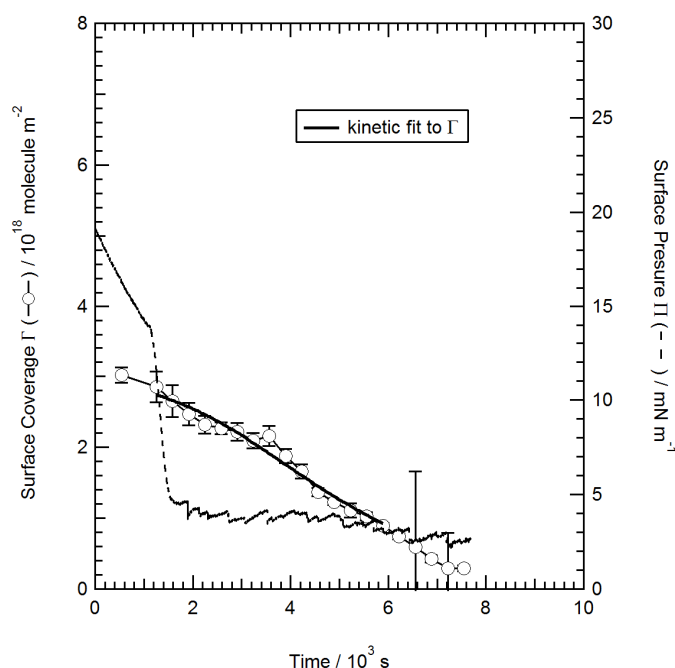
At 19.4°C the surface pressure decayed from 20 mN m^{-1} to zero over 3600 seconds. The surface pressure can be seen to rise from a value of 6 mN m^{-1} at 1300 seconds reaching a value of 8 mN m^{-1} at 1600 seconds then falling again as was observed in previous experiments. The surface coverage decayed to zero over 2900 seconds. The feature seen as a rise in surface pressure was not reflected in the decay of surface coverage but the neutron beam was of a poor flux initially in this experiment so the period of counting per point was long and the feature may not have been seen on this time order.

Figure 2.33 *The Surface Coverage and Surface Pressure Kinetic Decay of a Stearic Acid Monolayer on a Subphase of $1.176 \text{ mol dm}^{-3} \text{H}_2\text{O}_2 / 8.7 \times 10^{12} \text{ mol dm}^{-3} \text{OH}$ at a Temperature of 19.4°C with a Kinetic Degradation Fit of Equation 2.45 to the Surface Coverage Data*



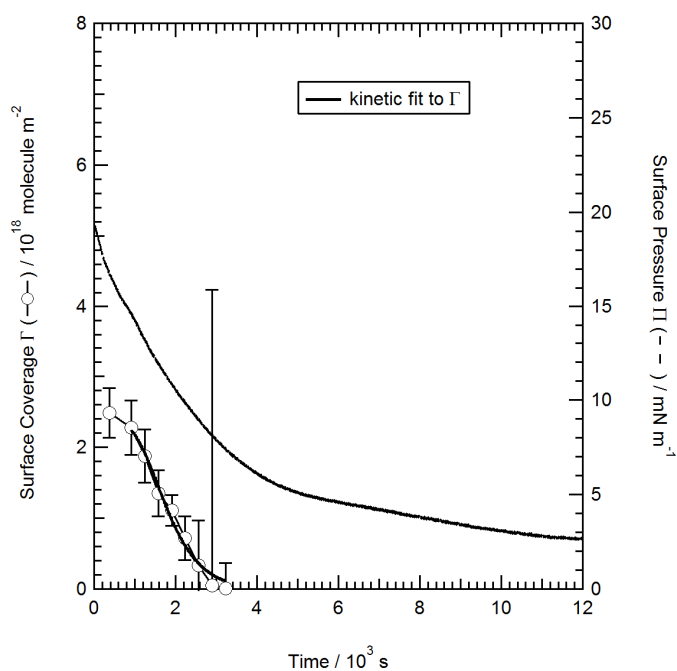
At a temperature of 27°C the surface pressure data suffered interference from a bubble beneath the Wilhelmy plate. The surface coverage declined from $3 \times 10^{18} \text{ molecule m}^{-2}$ to $0.2 \times 10^{18} \text{ molecule m}^{-2}$ over 6800 seconds.

Figure 2.34 *The Surface Coverage and Surface Pressure Kinetic Decay of a Stearic Acid Monolayer on a Subphase of $1.176 \text{ mol dm}^{-3} \text{H}_2\text{O}_2 / 8.7 \times 10^{12} \text{ mol dm}^{-3} \text{OH}$ at a Temperature of 27°C with a Kinetic Degradation Fit of Equation 2.45 to the Surface Coverage Data*



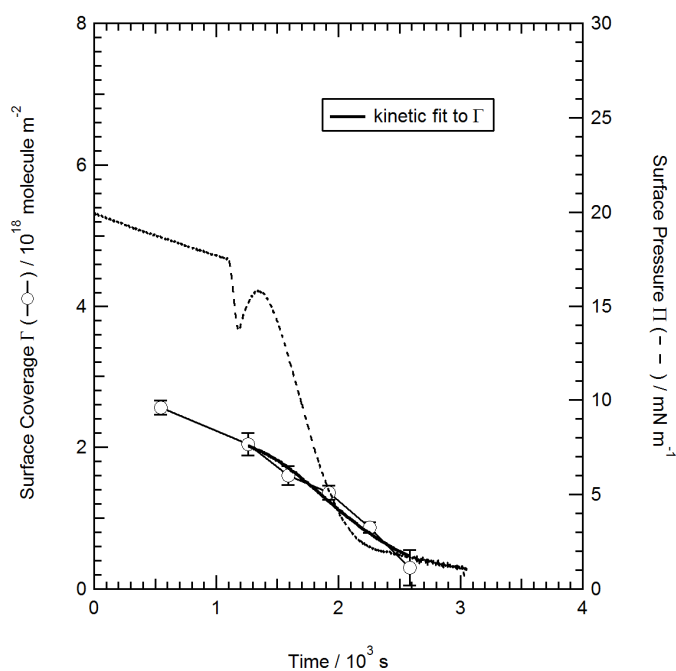
At a temperature of 31.5°C the surface pressure decayed from 20 to 2.7 mN m^{-1} without rising again. The starting value of surface coverage was low at $2.5 \times 10^{18} \text{ molecule m}^{-2}$, the variance in the starting surface coverage in each experiment is due to two factors, when the beam had been lost prior to starting the photolysis lamps the film was recompressed to 20 mN m^{-1} when the beam was recovered and the experiment was started, a small loss in the amount of material at the air-water interface occurs with time whilst the film sits in the Langmuir trough, also the monolayer was spread at the interface by different members of the experimental team, a technique was agreed to make this as uniform as possible however the surface coverage values at the start are different. The surface coverage decayed to zero over 3200 seconds.

Figure 2.35 *The Surface Coverage and Surface Pressure Kinetic Decay of a Stearic Acid Monolayer on a Subphase of $1.176 \text{ mol dm}^{-3} \text{H}_2\text{O}_2 / 8.7 \times 10^{12} \text{ mol dm}^{-3} \text{OH}$ at a Temperature of 31.5°C with a Kinetic Degradation Fit of Equation 2.45 to the Surface Coverage Data*



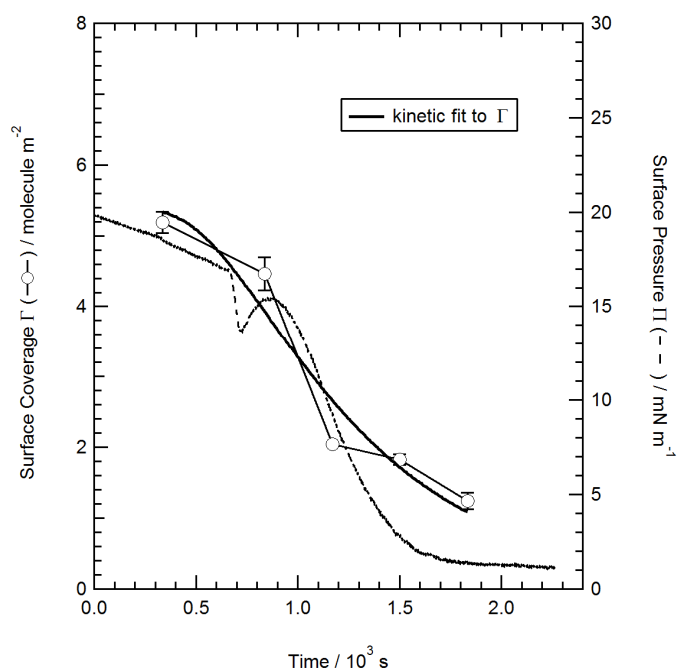
At a temperature of 40.5°C the surface pressure decayed from 20 mN m^{-1} to 0.1 mN m^{-1} over 3010 seconds. A rise in surface pressure from 14 to 15.1 mN m^{-1} occurred after 1100 seconds. The surface coverage decayed from $2.5 \times 10^{18} \text{ molecule m}^{-2}$ to $2 \times 10^{18} \text{ molecule m}^{-2}$ over 2600 seconds.

Figure 2.36 *The Surface Coverage and Surface Pressure Kinetic Decay of a Stearic Acid Monolayer on a Subphase of $1.176 \text{ mol dm}^{-3} \text{H}_2\text{O}_2 / 8.7 \times 10^{12} \text{ mol dm}^{-3} \text{OH}$ at a Temperature of 40.5°C with a Kinetic Degradation Fit of Equation 2.45 to the Surface Coverage Data*



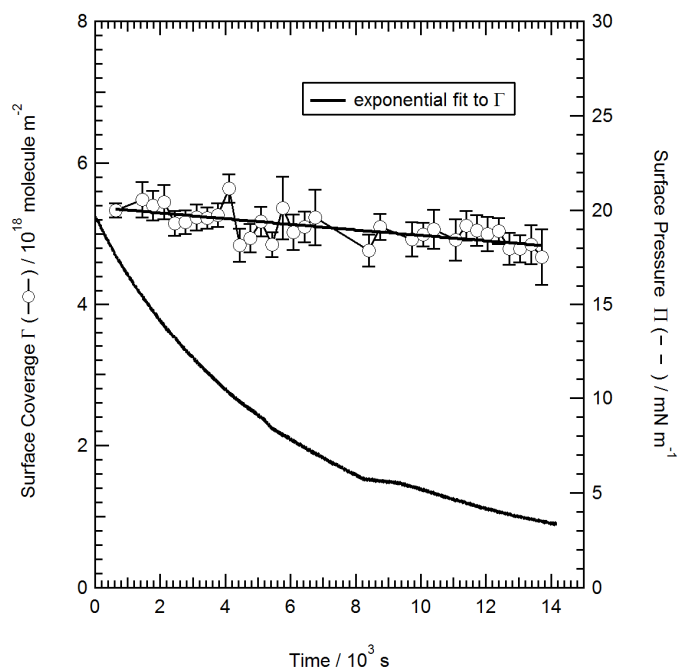
At a temperature of 50°C the monolayer surface coverage declined from 19 mN m^{-1} to 0.1 mN m^{-1} over 2350 seconds. A rise in the surface pressure by 2 mN m^{-1} occurred after 0.7 seconds. The surface coverage decayed from 5.1 to $1.2 \times 10^{18} \text{ molecule m}^{-2}$ over 1850 seconds. Due to a low flux neutron beam the data points for the surface coverage measurement were once again far apart and the time resolution of the measurement was poor so it could not be said whether the surface pressure rise was reflected in the neutron data.

Figure 2.37 *The Surface Coverage and Surface Pressure Kinetic Decay of a Stearic Acid Monolayer on a Subphase of $1.176 \text{ mol dm}^{-3} \text{H}_2\text{O}_2 / 8.7 \times 10^{12} \text{ mol dm}^{-3} \text{OH}$ at a Temperature of 50°C with a Kinetic Degradation Fit of Equation 2.45 to the Surface Coverage Data.*



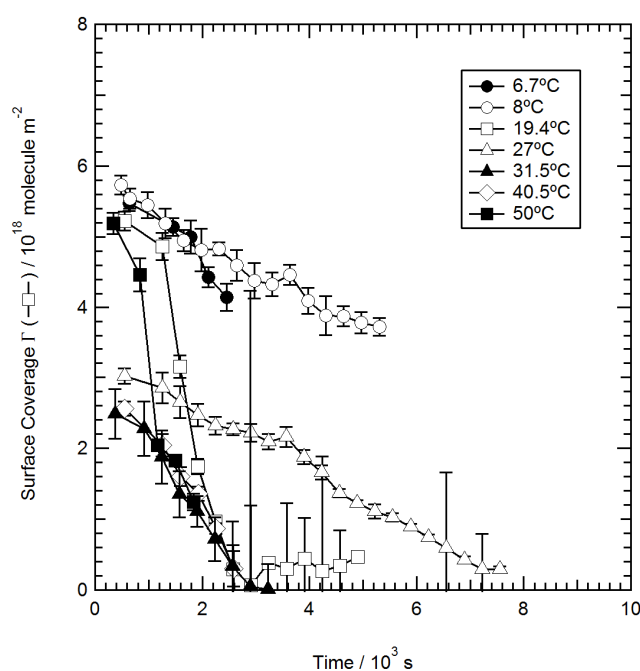
On a subphase of H_2O_2 without photolysis the surface coverage decayed $< 1 \times 10^{18} \text{ molecule m}^{-2}$ within error over 14000 seconds. The surface pressure decayed from 19 mN m^{-1} to 0.4 mN m^{-1} over 14000 seconds.

Figure 2.38 *The Surface Coverage and Surface Pressure Kinetic Decay of a Stearic Acid Monolayer on a Subphase of $1.176 \text{ mol dm}^{-3} \text{H}_2\text{O}_2$ Without Photolysis at a Temperature of 20°C with an Exponential Fit to the Surface Coverage Data*



When the surface coverage measurements at different temperatures were plotted together (figure 2.39) the decay slope appeared to increase with temperature, the 19.4°C data being an exception to that observation.

Figure 2.39 *The Decay in the Surface Coverage of a Monolayer of Stearic Acid at Different Temperatures*



2.7.4 Summary of the Experimental Results

- The decay in surface pressure does not follow the decay in surface coverage.
- There is a repeatable feature of a surface pressure rise of $\sim 2 \text{ mN m}^{-1}$ at a range of surface coverage values from $0.3 \times 10^{18} \text{ molecule m}^{-2}$ to $3.5 \times 10^{18} \text{ molecule m}^{-2}$. The surface pressure rise appears at a range of surface pressures from 2 to 14 mN m^{-1} suggesting that the feature is related to the chemistry and not to the structure of the monolayer such as a phase transition or the molecules lying at a lower angle than 90° to the interface.
- The surface coverage decays to zero or to a low value with reaction time for each experiment.
- Varying the concentration of aqueous OH radical did not appear to be affecting the reaction kinetics.
- Varying the subphase temperature did appear to affect the reaction kinetics; this will be investigated in section 2.7.5.

2.7.5 The Kinetic Analysis of the Surface Coverage Data

Based on the degredated chain mechanism described in section 2.5.2, the reaction of hydrogen peroxide and UV radiation creates two OH radicals which then react with the stearic acid monolayer. The kinetic decay mechanism (equation 2.45) was fitted to the surface coverage data to obtain three rate constants which describe the abstraction of hydrogen from the stearic acid molecule (species A) tail and the formation of a shorter chain surface active product (species B) followed by the formation of a shorter chain product molecule (species C) which is soluble and would dissolve into the Langmuir trough subphase.

The rise in surface pressure and the corresponding change in the slope of the surface coverage measurements are hypothesised to be a result of the mixing of stearic acid and surface active product B at the air-water interface.

Figure 2.40 *Modelled Surface Coverage Data Showing the Build Up of Product A and Product B in Relation to the Experimental Surface Coverage Data Obtained from the Reaction of a Stearic Acid Monolayer with Aqueous OH Radical at an H_2O_2 Concentration of $1.176 \text{ mol dm}^{-3}$*

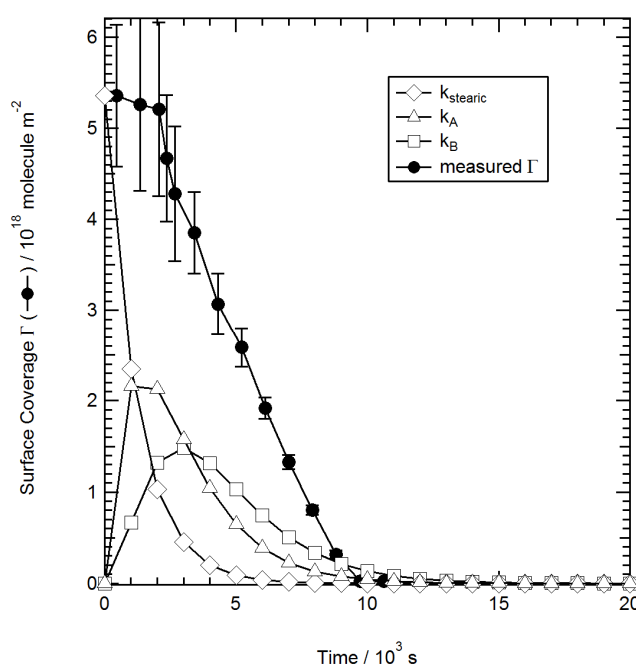


Figure 2.40 shows how the observed surface coverage could be contributed to by the decay build-up of stearic acid and its reaction products formed as OH radical shortens the molecule. The decay is modelled as three exponentials. It can be seen that product k_A builds up at the air-water interface, followed by product k_B as the reaction proceeds, product k_B is more soluble.

It is inferred that the radical driven reaction shortens the amphiphile at the air-water interface and regenerates an amphiphile meaning that material persists at the air-water interface. A proposed chemical mechanism for the oxidation of a stearic acid monolayer initiated by OH radical is described in detail in section 2.8.4.

The rate constants from the fitting of equation 2.45 are set out in the following tables.

- Table 2.3 *Pseudo 1st Order Rate Constants for Stearic Acid Reacting with OH Radical for Varied Concentrations of H₂O₂*
- Table 2.4 *Pseudo 1st Order Rate Constants for Stearic Acid Reacting with OH Radical at Different Temperatures*
- Table 2.5 *The Second Order Rate Constants for the Decay of a Stearic Acid Monolayer Exposed to Varied H₂O₂ / OH Concentrations*
- Table 2.6 *The Second Order Rate Constants for the Decay of a Stearic Acid Monolayer as Oxidised by OH Radical at Varied Temperatures*

The tables are followed by an Arrhenius plot showing the temperature dependence of the reaction between OH radical and stearic acid.

Table 2.3 Pseudo 1st Order Rate Constants for Stearic Acid Reacting with OH Radical for Varied Concentrations of H₂O₂

[OH] / 10 ¹² mol dm ⁻³	Photolysis (λ=254 nm)	Exponential fit rate coefficient k / 10 ⁻⁶ s ⁻¹	Degradation mechanism fit rate coefficient k _{stearic} / 10 ⁻⁴ s ⁻¹	Degradation mechanism fit rate coefficient k _A / 10 ⁻⁴ s ⁻¹	Degradation mechanism fit rate coefficient k _B / 10 ⁻⁴ s ⁻¹	T / °C
8.4	Yes		4.93 ± 6.28	19.1 ± 166	0.25 ± 0.28	17
8.6	Yes		2.42 ± 1.25	3.16 ± 10.3	3.44 ± 11.3	17
8.7	Yes		1.93 ± 4.31	2.69 ± 53	3.14 ± 67	17
8.7	Yes		1.05 ± 2.43	2.51 ± 67	3.16 ± 97	6
8.7	Yes		8.23 ± 9.16	6.08 ± 54.4	6.75 ± 69.2	17
8.7	Yes		6.03 ± 19.9	8.57 ± 266	9.85 ± 332	17
H ₂ O ₂	No	1.44 ± 0.449	-	-	-	17
2 Average k at 17°C	Yes		4.71	7.92	4.68	17
0	Yes	6.35 ± 0.691	-	-	-	17
2 Standard deviations at 17°C	No		2.61	6.67	3.69	-

Table 2.4 Pseudo 1st Order Rate Constants for Stearic Acid Reacting with OH Radical at Different Temperatures

Neutron experiment	[H ₂ O ₂] / 10 ¹² mol dm ⁻³	[OH] × 10 ¹² mol dm ⁻³	Photolysis (λ=254 nm)	Exponential fit rate coefficient k / 10 ⁻⁶	Degradation mechanism fit rate coefficient $k_{stearic} / 10^{-4} s^{-1}$	Degradation mechanism fit rate coefficient $k_A / 10^{-4} s^{-1}$	Degradation mechanism fit rate coefficient $k_B / 10^{-4} s^{-1}$	T / °C
3	1.47	16	Yes	-	2.8 ± 6.6	71.49 ± 14000	92.80 ± 25100	6.7
3	1.47	16	Yes	-	12 ± 5.4	1.47 ± 3	1.01 ± 0.7	8
3	1.47	16	Yes	-	19.23 ± 5.2	103.52 ± 759	457.69 ± 14900	19.4
3	1.47	16	Yes	-	7.63 ± 17	6.11 ± 49.2	6.28 ± 46	27
3	1.47	16	Yes	-	30.39 ± 75	24.12 ± 176	24.24 ± 150	31.5
3	1.47	16	Yes	-	28.75 ± 76	28.93 ± 221	27.28 ± 279	40.5
3	1.47	16	Yes	-	14.1 ± 136	49 ± 21200	59 ± 32600	50
3	1.47	16	No	7.73 ± 1.45	-	-	-	20

Table 2.5 The Second Order Rate Constants for the Decay of a Stearic Acid Monolayer Exposed to Varied H_2O_2 / OH Concentrations

[OH] / 10^{12} mol dm^{-3}	Photolysis ($\lambda=254$ nm)	k_{39} / 10^7 dm^3 mol $^{-1}$ s $^{-1}$	k_{40} / 10^7 dm^3 mol $^{-1}$ s $^{-1}$	k_{41} / 10^7 dm^3 mol $^{-1}$ s $^{-1}$	T / °C
8.4	Yes	5.87 ± 7.5	22.7 ± 198	29.8 ± 0.3	17
8.6	Yes	2.81 ± 1.5	3.67 ± 12	4 ± 13	17
8.7	Yes	2.21 ± 2.8	3.10 ± 77	3.61 ± 111	17
8.7	Yes	1.21 ± 5	2.88 ± 60	3.63 ± 77	6
8.7	Yes	9.46 ± 11	6.99 ± 63	7.75 ± 80	17
8.7	Yes	6.93 ± 23	9.85 ± 306	11.3 ± 382	17
2 Average k at 17°C = bimolecular k		5.5	9.3	5.4	-
2 Standard deviations at 17°C		3.2	7.6	4	-

Table 2.6 *The Second Order Rate Constants for the Decay of a Stearic Acid Monolayer as Oxidised by OH Radical at Varied Temperatures*

[OH] / 10^{12} mol dm ⁻³	Photolysis ($\lambda=254$ nm)	k_{39} / 10^7 dm ³ mol ⁻¹ s ⁻¹	k_{40} / 10^7 dm ³ mol ⁻¹ s ⁻¹	k_{41} / 10^7 dm ³ mol ⁻¹ s ⁻¹	T / °C
16	Yes	1.76 ± 4.14	45 ± 8750	58 ± 15700	6.7
16	Yes	7.5 ± 3.4	25.9 ± 1.8	0.63 ± 0.44	8
16	Yes	12 ± 3.2	64.7 ± 474	286 ± 9310	19.4
16	Yes	3.97 ± 10	4.51 ± 31	4.77 ± 29	27
16	Yes	19 ± 47	15.1 ± 110	15.2 ± 94	31.5
16	Yes	18 ± 48	18.1 ± 138	17 ± 174	40.5
16	Yes	88.1 ± 85	360000 ± 133000	370000 ± 204000	50

Figure 2.41 Arrhenius Plot of the Rate Constants k_A , k_B and k_C at Varied Temperatures with a Line Fit to k_A .

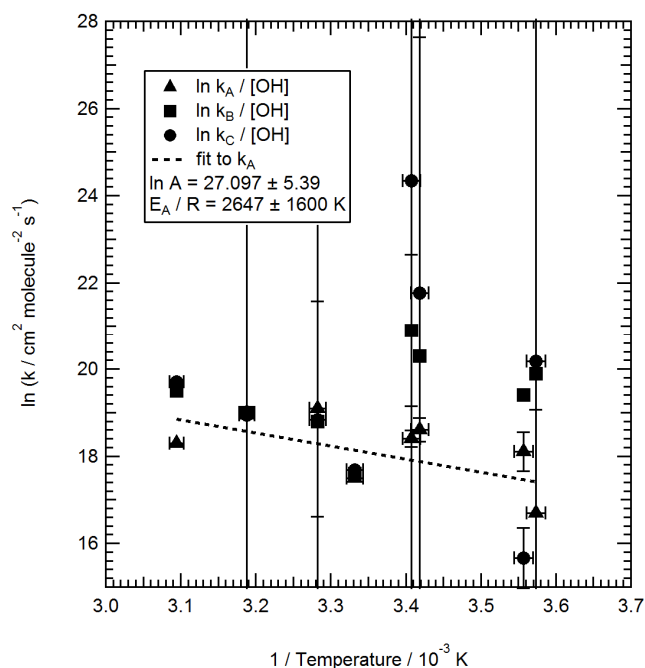


Figure 2.41 shows that the reaction of stearic acid and OH radical has some temperature dependence. The error bars in figure 2.41 were statistical and describe how well the model fitted the data, the data fitted well visually but statistically the model predicts that there are better outcomes and produces a large error bar. In figures 2.30, 2.31, 2.33 and 2.36 the model was not constrained well enough for a perfect fit for error calculation. The straight line fit shows a single rate limited thermally activated process. To determine the activation energy the Arrhenius equation is applied.

$$k = A \exp\left(-\frac{E_{\text{expt}}}{RT}\right) \quad (\text{E 2.46})$$

$$\ln k = \ln A - \frac{E_A}{RT} \quad (\text{E 2.47})$$

The slope of the rate constant k versus temperature is equivalent to the activation energy (E_A) divided by the gas constant multiplied by the absolute temperature (RT). The activation energy was $22.0 \pm 13.3 \text{ kJ mol}^{-1}$.

2.7.6 Brewster Angle Microscopy Images of Stearic Acid Monolayers Before and During Oxidation

Brewster angle microscopy images show the tilt of the molecular chains at the air-subphase interface on the Langmuir trough. When the tilt is normal there is little reflection and the surface appears grey and featureless, the same is true when the molecules are lying flat. When the molecules are tilted from the normal plane then features can be seen as a function of the azimuthal tilt orientation of the molecules comprising domains at the air-water interface (Katholy et al., 2000).

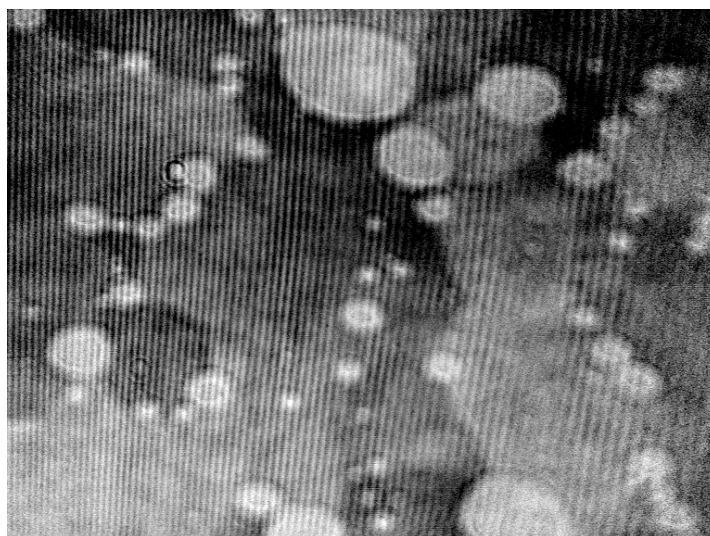
The following pages contain plots of the kinetic decay in the monolayer surface pressure with images taken at regular intervals shown along the plot to give an indication of the morphology of the monolayer.

The Brewster angle microscopy image plots are given in the following order:

- The pressure-area isotherm of a stearic acid monolayer on a subphase of $2.352 \text{ mol dm}^{-3} \text{ H}_2\text{O}_2$ in H_2O without photolysis. The Brewster angle microscopy images were taken during the compression of the monolayer. (Figure 2.43).
- The kinetic decay of a monolayer of stearic acid on a subphase of $2.352 \text{ mol dm}^{-3} \text{ H}_2\text{O}_2$ in H_2O :
 1. With photolysis from the beginning of the decay (Figure 2.44).
 2. Without photolysis (Figure 2.45).
- The kinetic decay of a monolayer of stearic acid temperature controlled at 20°C on a subphase of H_2O :
 1. Without photolysis (Figure 2.47).
 2. With photolysis (Figure 2.48).

Figure 2.47 shows a stearic acid monolayer spread onto a subphase of $2.352 \text{ mol dm}^{-3} \text{ H}_2\text{O}_2$ in a gas like configuration before closure of the Langmuir trough barriers to compress the film. There are several phases visible. The lighter coloured blobs are patches of one phase of liquid stearic acid and in the background another phase is visible with tilted domains which appear as angular 'plates'. The surface pressure was 0 mN m^{-1} at this point prior to compression.

Figure 2.42 *A Brewster Angle Microscopy Image of a Stearic Acid Monolayer in the Gas Like Configuration Prior to Compression*



As the stearic acid monolayer was compressed at $10 \text{ cm}^2 / \text{minute}$ the round domains seen in figure 2.43 appear as angular plate like domains as the monolayer enters the liquid expanded region of the isotherm. In the liquid condensed phase the plates appear more rounded and of a smaller area per domain at 15 mN m^{-1} , at 19 mN m^{-1} it became difficult to distinguish one phase from another, in the solid phase of the isotherm the monolayer becomes featureless indicating the tilt of the molecules is normal to the air-water interface.

Figure 2.43 *The Surface Pressure versus Area per Molecule Isotherm of a Stearic Acid Monolayer on a Subphase of $2.352 \text{ mol dm}^{-3} \text{ H}_2\text{O}_2$*

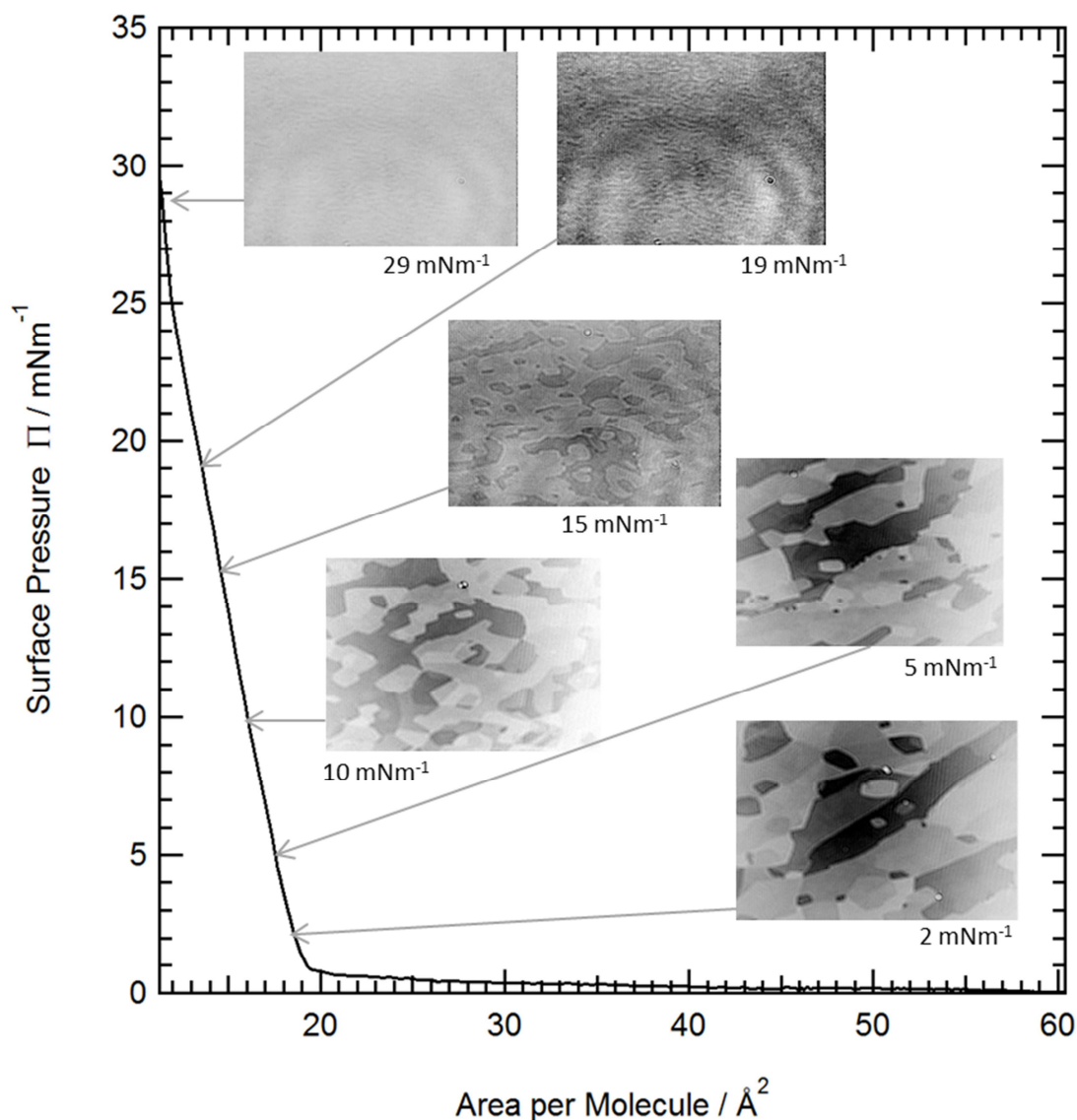


Figure 2.44 overleaf shows Brewster angle microscopy images plotted onto a kinetic decay measurement of surface pressure with photolysis to produce OH radical in the Langmuir trough subphase beneath the stearic acid monolayer as it was imaged. The aim was to take images where there was a rise in the surface pressure to see if there was evidence of the presence of reaction products or mixing at the air-water interface. Brewster angle microscopy cannot confirm the chemical composition of material at the air-water interface but it did show at a surface pressure of 18 mN m^{-1} that there were two distinct domain formations, one which

resembled the stearic acid images shown in figure 2.43 as angular plate like domains, the other had a fibrous like appearance composed of tiny circles which broke up into islands during exposure to OH. Both domain formations disappeared from the interface and the background grey image dominated with reaction time.

Figure 2.44 *The Kinetic Decay of a Monolayer of Stearic Acid on a Subphase of $2.352 \text{ mol dm}^{-3} \text{ H}_2\text{O}_2$ in H_2O With Photolysis from the Beginning of the Decay*

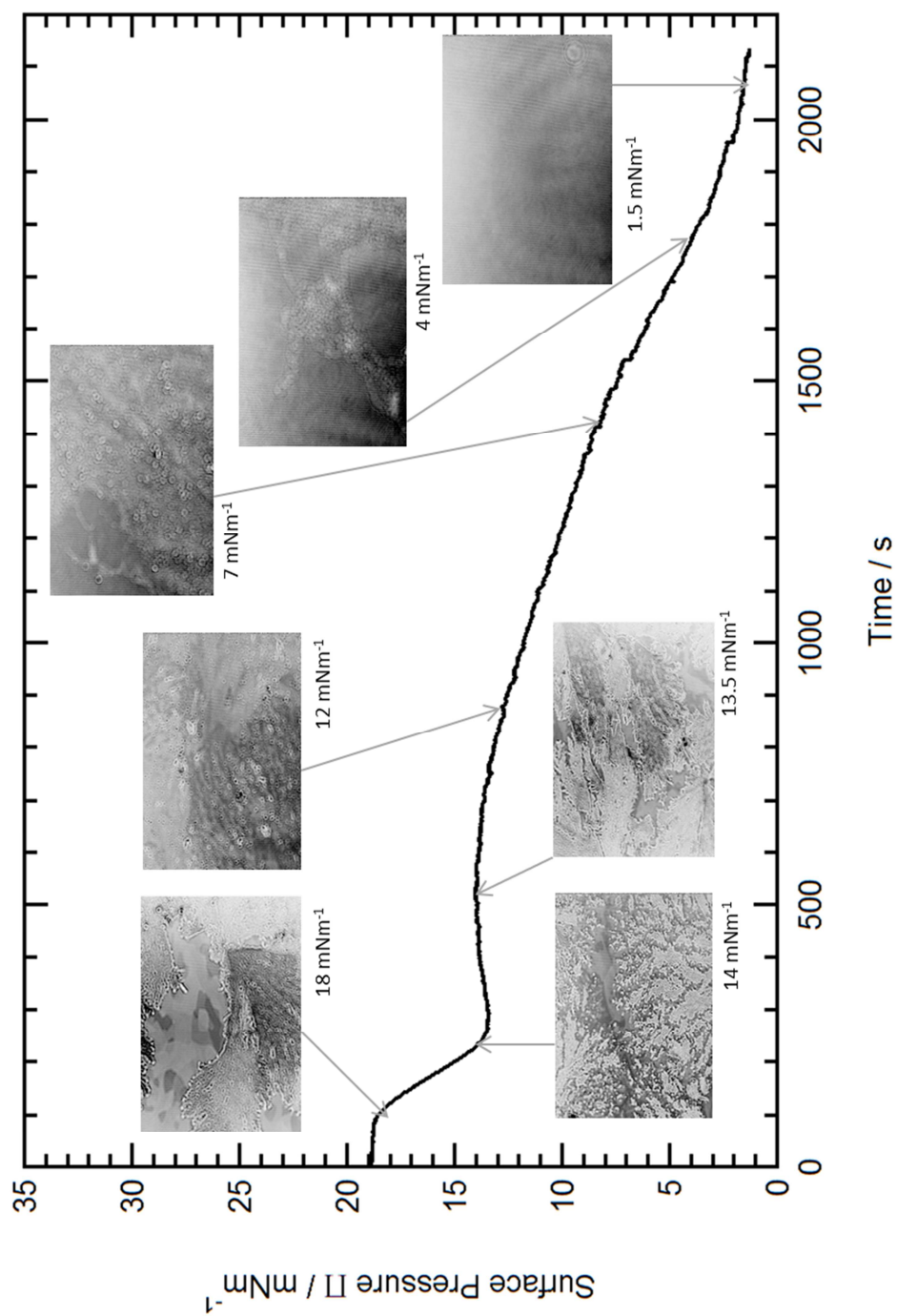


Figure 2.45 shows images taken during a surface pressure kinetic decay of a stearic acid monolayer on a subphase containing hydrogen peroxide without photolysis, so that OH radical was not produced. The image taken at a surface pressure of 18 mN m^{-1} was very different to that shown in figure 2.44 at the same surface pressure in the presence of OH radical. Large plate like domains can be seen with what are inferred by the author to be small lathe shaped crystals which were more concentrated at the edges of the plate like domains; these features could be stearic acid crystals. As the surface pressure decreased the plate like domains softened at the edges and appeared to elongate and appeared as a swirl shaped pattern of domains, the number of the crystalline features increased with reaction time.

Figure 2.45 *The Kinetic Decay of a Monolayer of Stearic Acid at on a Subphase of $2.352 \text{ mol dm}^{-3} \text{ H}_2\text{O}_2$ in H_2O Without Photolysis from the Beginning of the Decay*

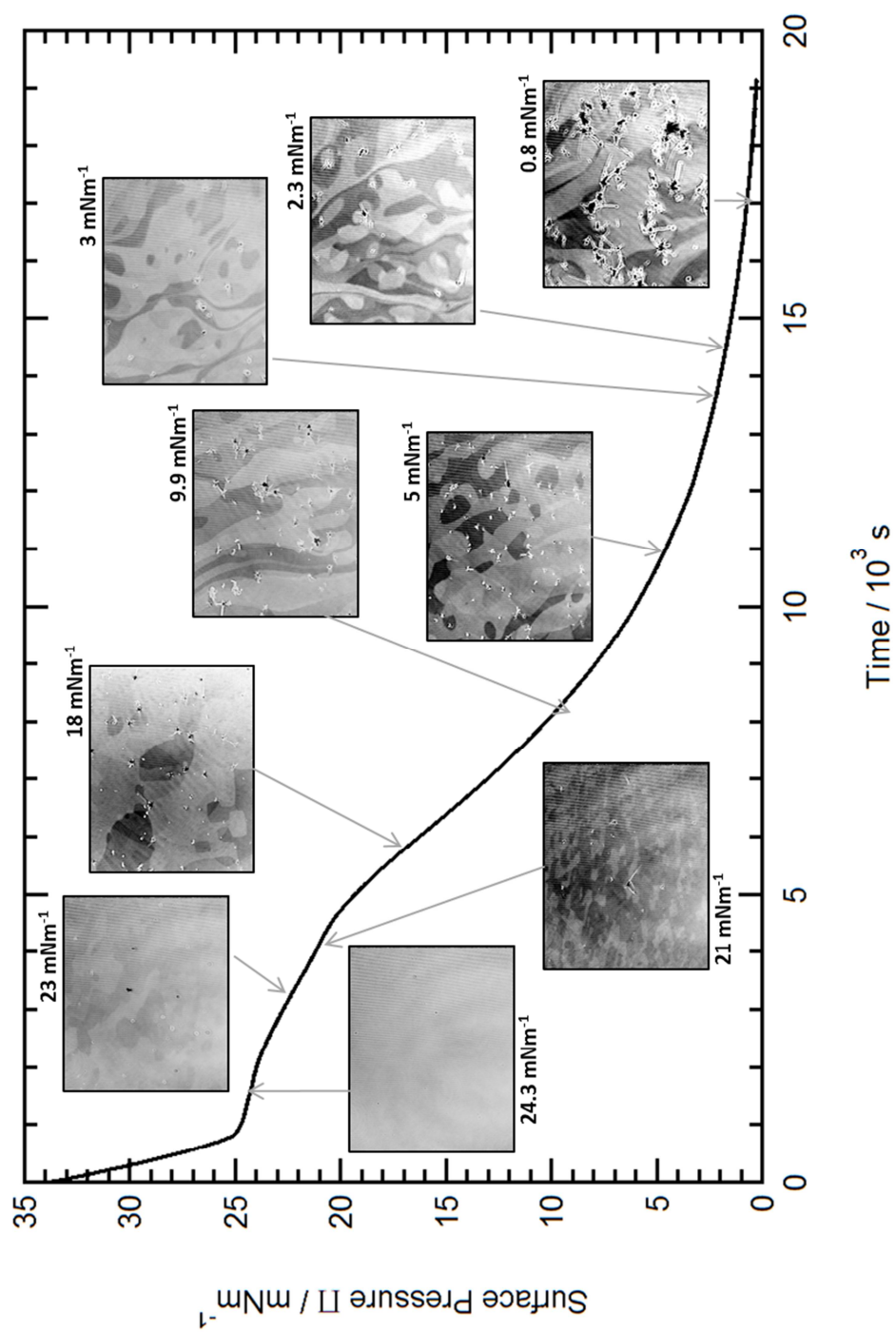
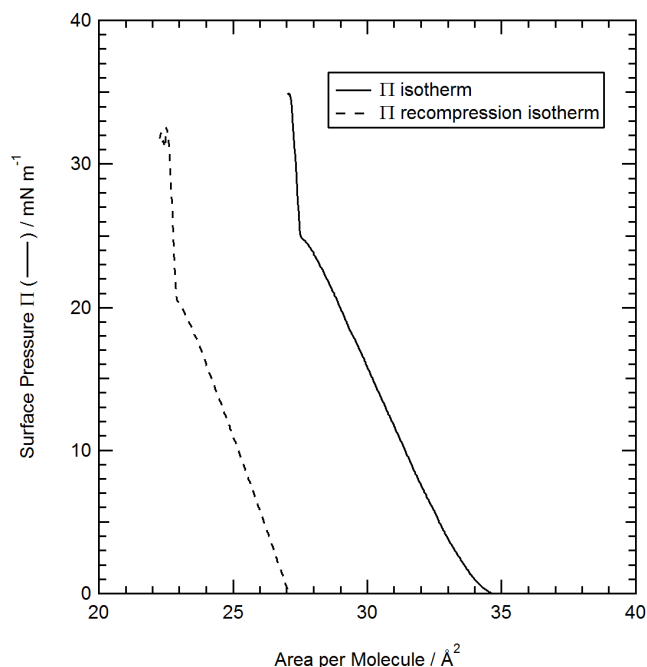


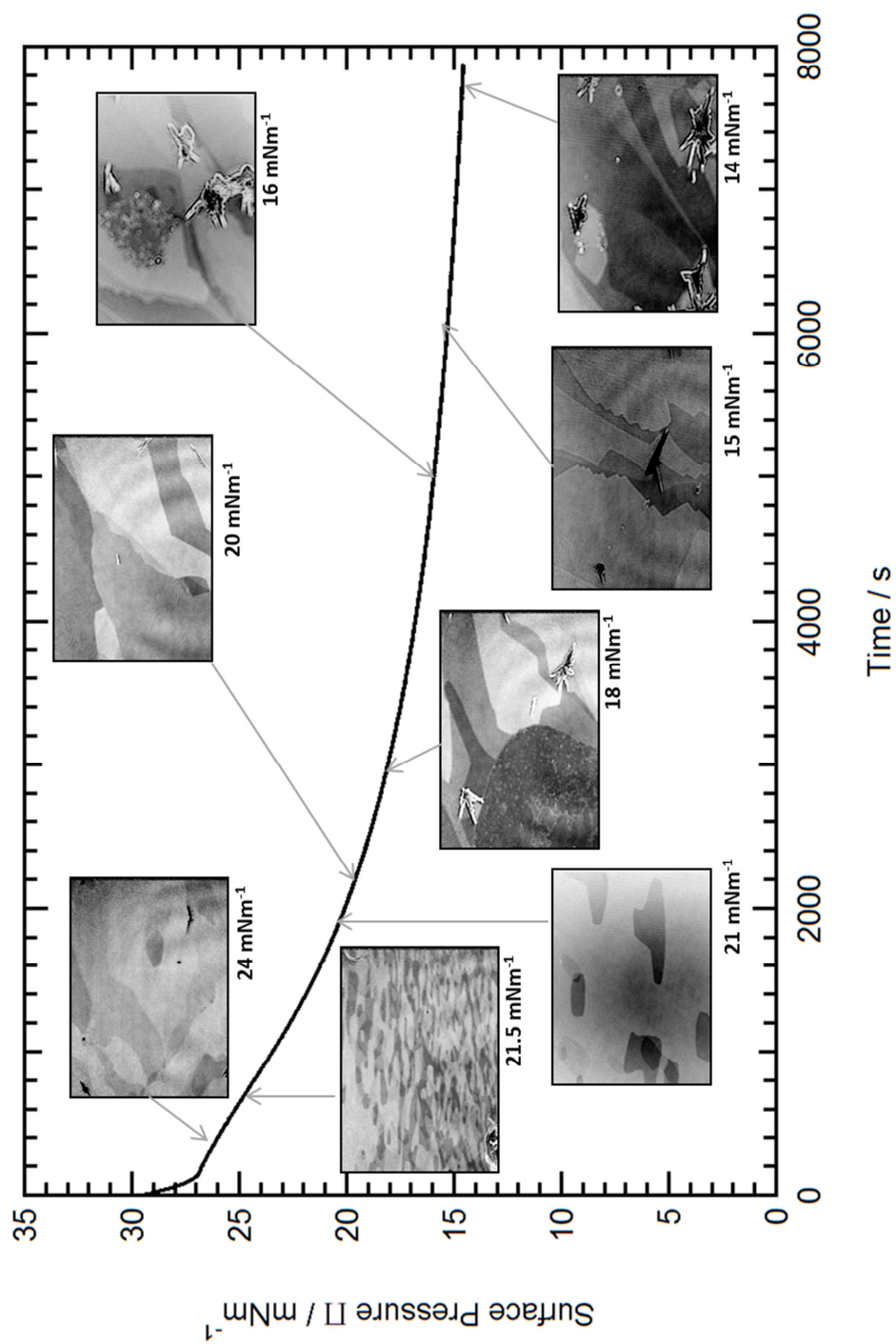
Figure 2.46 A Compression of the Stearic Acid Monolayer from Figure 2.44 Measured at a Compression Rate of $10 \text{ cm}^2 / \text{min}$ Taken After the Surface Pressure Had Declined to Zero



The surface pressure decay of a stearic acid monolayer with time was measured and imaged on a subphase of $2.352 \text{ mol dm}^{-3} \text{ H}_2\text{O}_2$ in H_2O without photolysis to show any differences in the monolayer morphology due to temperature (figure 2.45). After the surface pressure had decayed to zero the trough barriers were closed to recompress any material left at the surface of the Langmuir trough, this produced an isotherm (figure 2.46) which was very similar to stearic acid showing that without photolysis the monolayer is not greatly reacted and is still composed of a majority of stearic acid molecules.

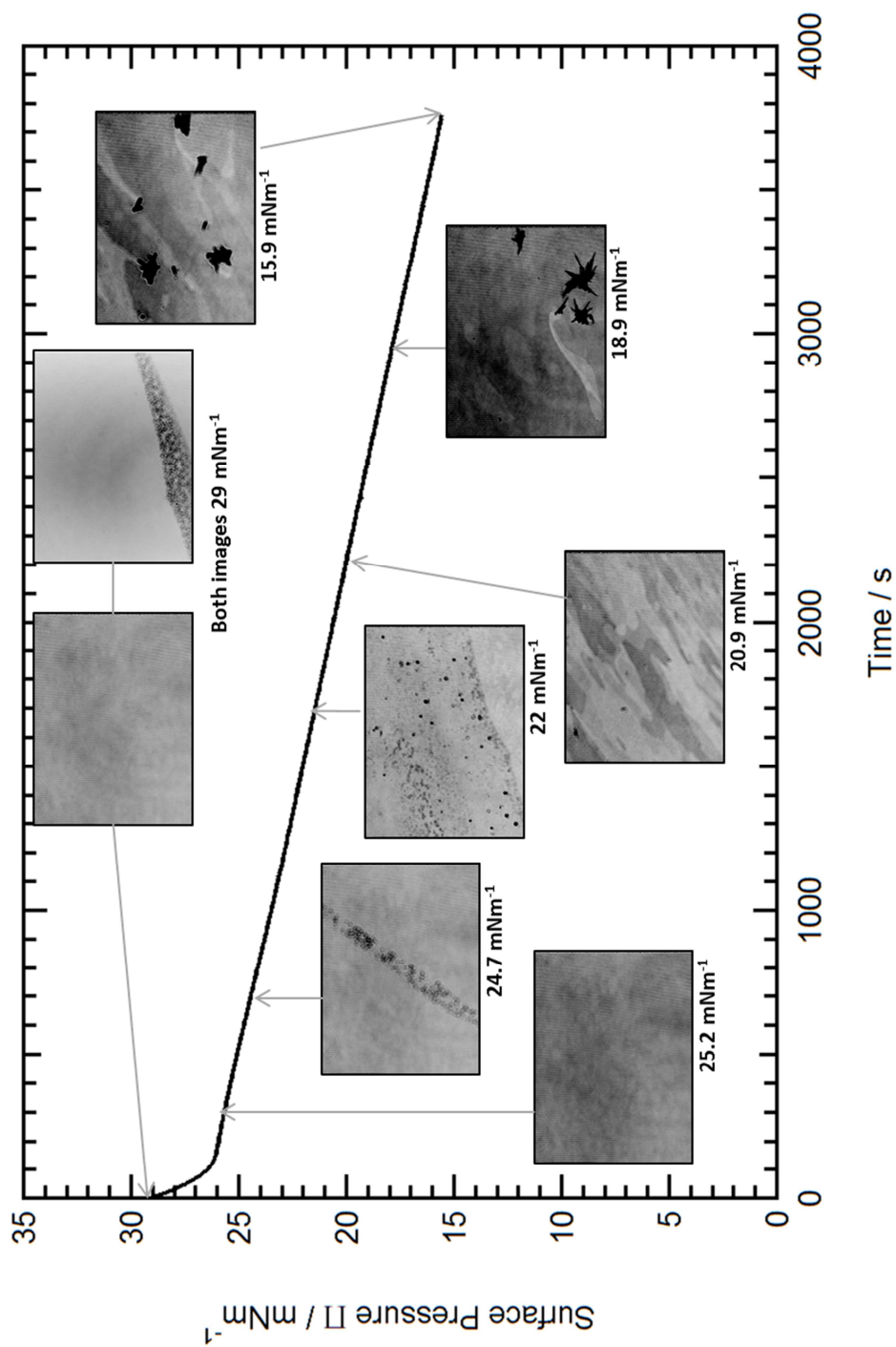
To show differences in the monolayer appearance on varied compositions of subphase images were taken of a stearic acid monolayer on an H_2O subphase (figure 2.46). The plate like domains appear larger but the morphology was similar to the stearic acid monolayer decaying on a subphase of H_2O_2 supporting the notion that the surface reaction is predominantly caused by OH radical and not H_2O_2 . The crystalline features can also be seen on the H_2O subphase.

Figure 2.47 *The Kinetic Decay of a Monolayer of Stearic Acid Temperature Controlled at 20°C on a Subphase of H₂O Without Photolysis*



To study the effect of the photolysis lamp on a stearic acid monolayer without H_2O_2 or OH images were taken during the surface pressure kinetic decay of a stearic acid monolayer on a subphase of H_2O with the photolysis lamp on (figure 2.48). At a surface pressure of 20.9 mN m^{-1} the angular plate like domains were observed which were also seen without photolysis in figure 2.42. At 30 mN m^{-1} to 22 mN m^{-1} domains consisting of a coagulation of tiny circles were seen, these were mobile and floated around rapidly then broke apart. With decreasing surface pressure the crystalline features appeared at the air-water interface which were observed on a subphase of H_2O without photolysis and on a subphase of H_2O_2 without photolysis. The images of the decay of the stearic acid monolayer with photolysis on a subphase of H_2O were different to those observed without photolysis but not as significantly so as the images taken in the presence of OH radical.

Figure 2.48 *The Kinetic Decay of a Monolayer of Stearic Acid Temperature Controlled at 20°C on a Subphase of H₂O with Photolysis*



2.7.7 Summary of Experimental Results

In summary the results of this experimental work are that;

- The reaction of a stearic acid monolayer and aqueous OH radical occurs at the air-water interface. The reaction can be measured with neutron reflectometry in order to perform a kinetic analysis.
- The reaction reduces the surface pressure until a point of what is hypothesised to be the mixing of surface active reaction products creating a brief rise in the surface pressure followed by a subsequent continuation in the decay of the surface pressure of the monolayer as the products react.
- The mixing feature is reflected in the surface coverage data where the slope of the decay in surface coverage shallows.
- A degraded chain mechanism can be fit to the temporal decay in the monolayer surface coverage measurement.

2.8 Discussion

The neutron reflectivity measurements give new insight into the reaction of stearic acid with hydroxyl radical at the air-water interface as this is the first study of the kinetics of the reaction of stearic acid with aqueous hydroxyl radical to be conducted using neutron reflectometry. The neutron reflectometry technique has been successful in producing kinetic data for a reaction with an aqueous radical in this work and for the reaction of an oleic acid monolayer with gas phase ozone as studied by King et al., (2009) and the reaction of oleic acid and NO₂ as studied by King et al., (2010).

The discussion will focus on literature related to the reaction of stearic acid with OH radical and the atmospheric implications of the reaction. There have been several structural neutron reflectometry studies of stearic acid monolayers at the air-water interface however these studies did not measure the kinetics of the decay of the monolayer over time so are not included in the discussion.

The discussion will be ordered as follows;

- Discussion of the experimental surface pressure and surface coverage results.
- Discussion of the kinetic results.
- Discussion of the chemical mechanism of the reaction between aqueous OH radical and a stearic acid monolayer.

- Presentation of a hypothesised chemical mechanism for the oxidation of a stearic acid monolayer by OH radical.
- Presentation of a calculated atmospheric lifetime for a stearic acid cloud droplet film at the air-water interface based on the kinetic results of this study.
- Discussion of the atmospheric implications of the reaction and the atmospheric lifetime of a stearic acid monolayer.

2.8.1 Discussion of the Experimental Surface Pressure and Surface Coverage Results

The experimental results show that the saturated stearic acid monolayer clearly reacts with aqueous OH radical. The reaction of stearic acid with gas phase OH radical at the air-water interface has been investigated by Bertram et al., (2001). Bertram et al., (2001) conducted coated wall flow tube experiments exposing a thick film of a stearic-palmitic acid mixture to gas phase OH radical carried in a helium gas flow through the flow tube reactor. Stearic acid and palmitic acid are both saturated molecules, palmitic acid has a shorter hydrocarbon chain ($C_{16}H_{32}O_2$). The OH was detected with a chemical ionization mass spectrometer. The stearic-palmitic acid mixture was melted and the pyrex flow tube was dipped into the melted solution, the film was then crystallised by dipping it in liquid nitrogen. The measured OH signal decreased with reaction time showing that the OH was reacting with the saturated film in agreement with the results presented in this chapter. The author could not find comparable surface pressure measurements of the decay of a stearic acid monolayer exposed to OH radical. The surface pressure measurement did not reflect the amount of material at the interface which may have implications for future kinetic studies utilizing Langmuir troughs.

2.8.2 Discussion of the Kinetic Results

The surface coverage measurements for the dark reaction of a stearic acid monolayer on a subphase of H_2O_2 gave a first order loss rate constant, k , of $(1.44 \pm 0.45) \times 10^{-6} s^{-1}$. Under conditions of photolysis on a subphase which did not contain H_2O_2 the first order loss rate constant, k , was $(6.35 \pm 0.69) \times 10^{-6} s^{-1}$. Under conditions of photolysis on an H_2O subphase the decay in the monolayer surface coverage was more rapid than on a subphase of H_2O_2 without photolysis however it is still two orders of magnitude slower than the first order loss owing to the reaction of stearic acid with aqueous OH radical (table 2.3). The average first order loss rate constant, k_{stearic} , for the reaction of aqueous OH radical with a stearic acid monolayer at $17^\circ C$ is $4.71 \times 10^{-4} s^{-1}$. There are no other kinetic studies of this reaction in the aqueous phase. Vlasenko et al., (2008) measured the yield of volatile organic compounds from the oxidation of condensed

phase organic films by gas-phase OH radical measuring a yield of 0.34 ± 0.14 relative to OH loss. The change in size of palmitic acid particles exposed to gas phase OH radical in a flow tube was monitored with a particle size analyser and a chemical ionization mass spectrometer by McNeill et al., (2008). An average pseudo first order rate constant k , for the loss of palmitic acid ($C_{16}H_{32}O_2$) of 0.45 s^{-1} was modelled to be diffusion limited. The value obtained by McNeill et al., (2008) was much larger than the average pseudo first order rate constant measured in this chapter for the decay in the surface concentration of stearic acid exposed to aqueous phase OH radical.

George et al., (2007) measured an average rate constant for the reaction of 150 nm particles comprised of saturated Bis(2-ethylhexyl)sebacate molecules ($C_{26}H_{50}O_4$, BES), reacted with gas phase OH radical in a flow tube. The average rate constant for the decay in Bis(2-ethylhexyl) sebacate with OH exposure was $(7.6 \pm 1.6) \times 10^7 \text{ atm}^{-1} \text{ s}^{-1}$.

The degradation sequential decay kinetic mechanism presented for the reaction of stearic acid and OH radical is proposed for the reaction of aqueous phase OH radical at the air-water interface. The reaction would occur through the Langmuir-Hinshelwood mechanism whereby the OH radical is absorbed and then reacts with the species at the air-water interface (George and Abbatt, 2010). The reacto-diffusive length of OH radical in the gas-phase of a nano meter scale is such that it does not penetrate the bulk before reaction in studies using pure substances making reactions at the air-water interface favourable (George and Abbatt, 2010), in this chapter the OH radical is diffusing from the bulk aqueous phase into the monolayer and reacting suggesting that in a multicomponent system the interface is accessible to radical reactants from the bulk of a droplet.

George and Abbatt, (2010) commented on the difference in the reaction mechanisms observed between gas-phase OH radical reacting with liquid particles and those obtained from reaction with solid particles and well-ordered monolayers which show enhanced volatilization of products, observing that with the current state of knowledge organic molecules in liquid particles would endure less functionalization due to the faster diffusion time for OH radical to the C-H bonds closer to the air-water interface in a well ordered monolayer which would be functionalised as opposed to a disordered liquid where the OH radical would encounter collisions with C-H bonds at a variety of positions along the chain leaving fewer volatile product molecules than in the well-ordered system. The results showed a build-up of product molecules from the reaction of OH with a liquid phase monolayer at the air-water interface, showing that OH from the aqueous phase could travel up the chain and react leaving some molecules with sufficient chain length to remain surface active.

The Arrhenius plot analysis gave an activation energy of $22 \pm 13.3 \text{ k J mol}^{-1}$ and a value of the activation energy divided by the gas constant (E_A/R) of $2647 \pm 5.39 \text{ K}$. Monod et al, (2005) measured lower values of E_A/R which are listed in table 2.7 for oxygenated organic compounds reacting with gas-phase OH radical. The higher activation energy for a stearic acid monolayer reacting with aqueous OH radical at the air-water interface could result from the OH radical having to penetrate the film before reacting with the stearic acid molecular chain, a process which would require more energy than a gas phase OH radical reacting would.

Table 2.7 Values of E_A/R from Monod et al, (2005) for Oxygenated Organic Compounds Reacting with Gas-phase OH Radical

Compound	$\frac{E_A}{R}$ / K
Ethyl ter-butyl ether	580 ± 560
<i>n</i> -butyl acetate	1000 ± 200
acetone	1400 ± 500
Methyl ethyl ketone	1200 ± 200
methylglyoxyl	1100 ± 300
Methyl iso-butyl ketone	1200 ± 300

The data in the table is taken from Monod et al., (2005).

2.8.3 Discussion of the Possible Chemical Mechanism for the Reaction between Aqueous OH Radical and a Stearic Acid Monolayer

The kinetics and mechanisms by which atmospheric OH radical oxidises alkanes was reviewed by Atkinson (1986), Atkinson (1986), stated that for gas phase OH radical reacting with an alkane hydrogen abstraction was occurring from the C-H bonds, for molecules with hydrocarbon chains longer than C_3 multiple alkyl radicals were formed.

Bertram et al., (2001) attribute the loss of OH to hydrogen abstraction from the stearic-palmitic film and subsequent formation of H_2O and an alkyl radical at the interface. O_2 addition would then form a peroxy radical. Bertram et al., (2001) hypothesised that given the proposed mechanism the film would become more hydrophilic, this was tested by exposing a methyl terminated monolayer of octadecyltrichlorosilane ($CH_3(CH_2)_{17}SiCl_3$), to gas phase OH and observing the contact angle of water droplets at the air-water interface which was greatly reduced post OH exposure showing an increased wettability as a result of OH radical reaction

with a monolayer. The sequential decay mechanism fitted to the surface coverage data in this study is based upon the same decay mechanism as that described by Bertram et al., (2001), the findings of this experimental work support the hypothesis of Bertram et al., (2001). A detailed suggested mechanism for the oxidation of a stearic acid monolayer by aqueous OH radical is given in section 2.8.4.

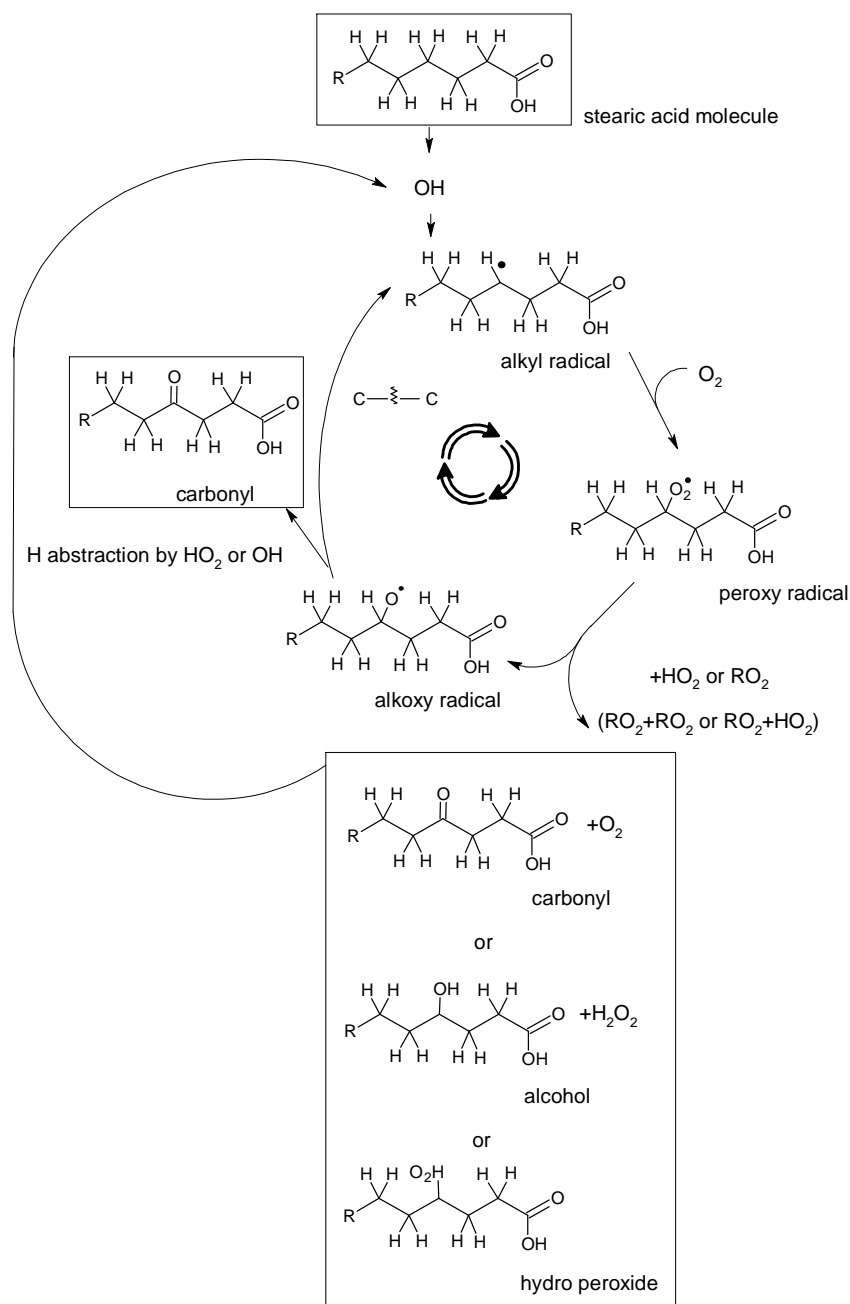
Tedetti et al., (2007) produced low molecular weight dicarboxylic acids from OH radical reacting with oleic acid in solution. The oleic acid molecule differs from stearic acid in that it has a cis form double bond in its chain however as OH is a highly reactive indiscriminate radical it reacts along the chain as well as at the double bond site producing multiple product species. It could be expected that low molecular weight dicarboxylic acids could be an eventual product of the reaction of OH with stearic acid.

The OH radical initiated oxidation of 2-butoxyethanol ($C_4H_9OCH_2CH_2OH$) in aqueous solution studied by Stemmler and von Gunten., (2000^a) produced esters, ketones, aldehydes and hydroperoxides. Stemmler and von Gunten., (2000^a) note that the initial step in the reaction of aqueous OH radical with a saturated oxygenated compound is the abstraction of a hydrogen atom forming a carbon centred radical. The radical subsequently reacts with oxygen to form peroxy radical (Neta et al., 1990; Stemmler and von Gunten., 2000^a). Stemmler and von Gunten., (2000^a) assess that in atmospheric waters the product formation would be determined by decomposition of peroxy radicals, H abstraction reactions occurring as intermolecular reactions, addition of peroxy radicals to double bonds on other organic molecules and the reduction of peroxy radicals within the aqueous phase. Stemmler and von Gunten., 2000^a conclude that the stable reaction products were predominantly carbonyl derivatives and carbonyl compounds which were fragments of the parent organic molecule with a minor organic hydroperoxide product fraction which is increased in the presence of iron and copper ions (Stemmler and von Gunten., 2000^b).

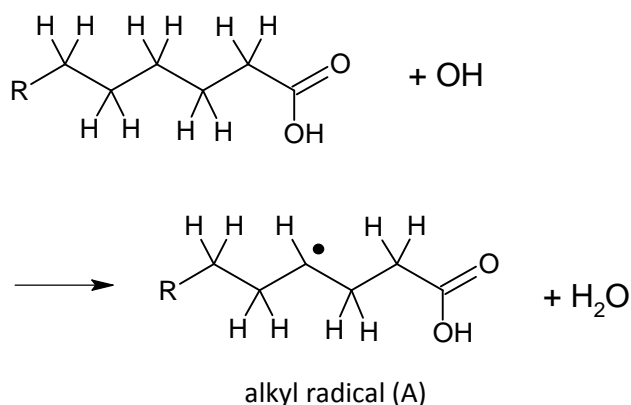
2.8.4 The Proposed Chemical Mechanism for the Oxidation of a Stearic Acid Monolayer by OH Radical.

A reaction scheme for the degradation mechanism responsible for the decay of a stearic acid monolayer as it reacts with aqueous OH radical is given based on the work by Alfassi et al., (1997). Figure 2.49 is a summary of the process followed by the individual steps which are detailed in figure 2.50 to 2.54.

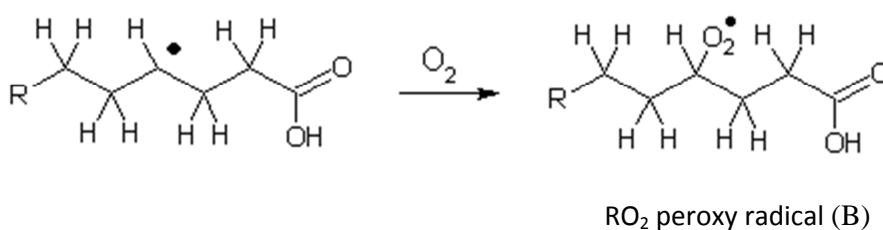
Figure 2.49 *The Cyclic Degradation Mechanism Proposed for Stearic Acid and Aqueous OH Radical*



The first step of oxidation is the initiation reaction between OH and stearic acid. We start with a stable stearic acid molecule. The OH radical abstracts a hydrogen atom leaving an alkyl radical (figure 2.50). The abstracted hydrogen forms water.

Figure 2.50 Step 1 – Hydrogen Abstraction

In the presence of oxygen, which is abundant in the cloud droplet system and in the experimental system, an oxygen molecule bonds to radical A. A peroxy radical, radical B is formed (figure 2.51).

Figure 2.51 Step 2 – Propagation

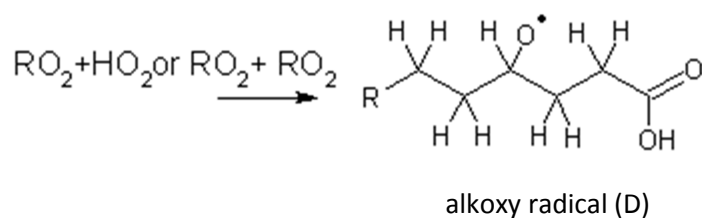
Steps 1 and step 2 are widely reported in literature (Von Sonntag and Schuchmann, 1997; Frankel, 1998). Step 3 is more complex and is not always clearly elucidated in the literature.

There are two different potential pathways for the peroxy radical.

- i) Termination where the peroxy radical reacts with another radical.
- ii) Reaction with HO₂ giving:
 - Stable surface active products with the same chain length. The head group may be considered larger but this will not increase the deuterium signal at the interface.
 - Alkoxy radicals (radical D)

Process i is unlikely as lots of RO₂ is required to self-react and terminate making this a slow process unless there is an abundance of RO₂ which there is not in this system.

It is proposed that the RO₂ peroxy radical becomes an alkoxy radical (D) through H abstraction.

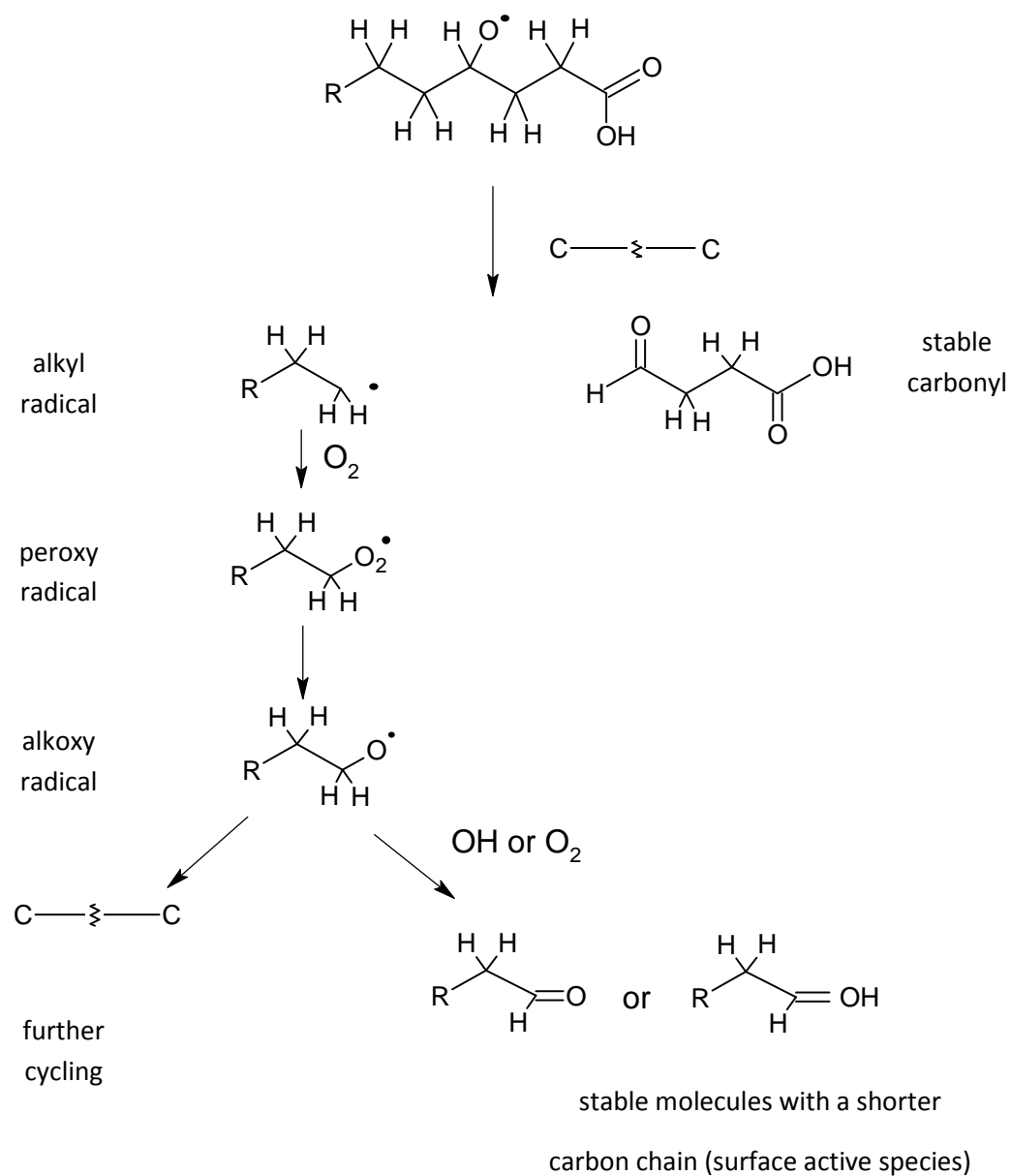
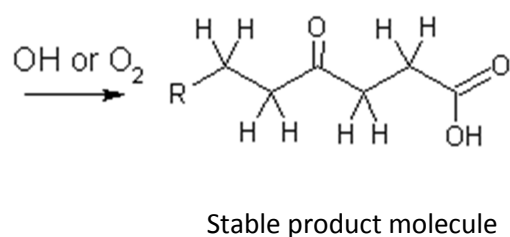
Figure 2.52 Step 3- The Fate of Peroxy Radical B

The alkoxy radical could then have another hydrogen abstracted by OH or O₂, adjacent to the singlet oxygen and form a stable product molecule with a bigger head group (product C).

The fate of the alkoxy radical could be that C-C scission occurs forming a stable oxygenated carbonyl acid and an alkyl radical (i) or step 2 (ii) could be repeated.

- i) C – C scission producing a stable oxygenated carbonyl acid which is soluble and enters the bulk subphase and an alkyl radical.
- ii) H abstraction by OH or O₂ and subsequent oxygen bonding as per step 2 forming a stable carbonyl (figure 2.49).

Process ii is more likely where H abstraction occurs as there is an abundance of HO₂ in the experimental system meaning this process could happen quickly or the alkoxy radical could undergo further C – C scission forming either a shorter stable molecule which enters the bulk subphase or the scission could produce an alkyl radical which is shorter and undergoes further chain degradation.

Figure 2.53 *The Fate of the Alkoxy Radical (i)***Figure 2.54** *The Fate of the Alkoxy Radical (ii)*

The persistence of the reaction products at the air-water interface would be dependent on the length of the molecules hydrocarbon chain.

2.8.5 Atmospheric Implications: Chemical lifetime

The atmospheric lifetime of the stearic acid film at the air-water interface reacting with hydroxyl radical from within the subphase/droplet can be calculated from the bimolecular rate constants for the reaction between OH and stearic acid (equation 2.48).

$$\tau_{stearic} = \frac{1}{k[OH]} \quad (E. 2.48)$$

Where k is the bimolecular rate constant for the reaction between [OH] and stearic acid, $5.5 \times 10^7 \text{ dm}^3 \text{ mol}^{-1} \text{ s}^{-1}$. By rearranging equation 2.45, assuming that:

$$\frac{\Gamma_{stearic}}{\Gamma_{stearic}^{t=0}} = \frac{1}{e} \quad (E. 2.49)$$

When calculated with the rate constants at one temperature for an [OH] concentration of $3.80 \times 10^{-16} \text{ mol dm}^{-3}$ as measured in aqueous extracts of sea salt aerosol (1.6-15 μm), under photolysis (Anastasio and Newburg, 2007), the first order loss of stearic acid corresponds to an atmospheric lifetime of 553 days. The lifetime of an aerosol in the atmosphere is dependent on the particle type. The modelled lifetime for a sea salt aerosol is half a day, sulphate and dust particles 3 days and particulate and organic matter 6 to 7 days (Textor et al. 2006). George and Abbatt, (2010) modelled the lifetime of saturated surfactant organic molecules at the surface of a 100 nm aerosol as less than a day under oxidation by the global mean gas phase OH concentration of $10^6 \text{ molecules cm}^{-3}$. The atmospheric lifetime of 553 days for the reaction of aqueous phase OH radical with stearic acid was surprising given how rapidly gas-phase OH radical could remove an atmospheric film. The lifetime of the multi-component film comprised of stearic acid and the products of oxidation would be longer than that calculated for the stearic acid component alone, suggesting that aqueous phase oxidation of the organic film on aerosol particles and on cloud droplets is not important at the air water interface in the atmosphere as it is not removed by the process studied here during the atmospheric lifetime of the aerosol.

2.8.6 Discussion of the Atmospheric Implications of the Reaction and the Atmospheric Lifetime of a Stearic Acid Monolayer Exposed to Aqueous OH Radical

The effect of a stearic acid monolayer on the evaporation of an aqueous droplet was investigated by Tuckermann et al., (2007). Tuckermann et al., (2007), generated acoustically levitated water droplets (1.5 to 2 mm radius) with a stearic acid / hexane solution spread as a monolayer at the air-water interface by the evaporation of the hexane from the solution which was sprayed onto the water droplet as a burst of microdroplets. As the water droplet evaporates the molecules in the monolayer are packed closer together. The surface area of the coated droplet reduced with time by 3 mm² over 1300 seconds when levitated in ambient air. The relative permeation resistance of the surface layer which is a measure of the difference in the evaporation rate of the aqueous droplet with and without the monolayer was 100 ± 20 s / m.

Bertram et al., (2001) observed that the reaction of gas phase OH radical with saturated films at the air-water interface of modelled atmospheric aerosol was not a significant tropospheric loss mechanism for OH as the gas phase reaction of OH with NO₂ would dominate loss in the troposphere under high NO₂ conditions. Bertram et al., (2001) modelled the oxidation of atmospheric aerosol particles by gas phase OH radical at an average atmospheric gas phase concentration of 1×10^6 molecule cm⁻³ (Prinn et al. 1992; Bertram et al. 2001) showing that to oxidise 90% of a non-aqueous organic aerosol surface would take under 7 days. Bertram et al conclude that it can be expected that most atmospheric aerosol which is chemically aged will have an oxidised hydrophilic surface and that in a liquid aerosol the oxidation could be more extensive than just at the surface of the droplet. The results of the work in this thesis chapter shows that the oxidation from within the droplet by aqueous OH radical is not as efficient and takes place over a longer timescale than the gas phase reaction at the air-water interface.

The formation of water soluble product molecules from the oxidation of stearic acid by aqueous OH radical would result in the addition of water soluble organic compounds to the aqueous phase of a cloud droplet which would increase the hygroscopicity of the droplet as the surface tension would be lowered allowing a greater uptake of water to the cloud droplet however at atmospheric OH concentrations the aqueous OH radical would not be a significant source of such material over a relevant timescale.

2.9 Conclusions

The reaction of aqueous hydroxyl radical with stearic acid at the air-water interface follows a sequential decay mechanism with $\sim\text{C}_4\text{H}_8$ being removed as a result of each interaction. Surface active product molecules are produced which decay with similar decay kinetics to stearic acid.

A monolayer of stearic acid at the air-water interface of a cloud droplet could have considerable longevity as it is resistant to gas phase ozone and although stearic acid reacts with aqueous OH radical, at atmospheric concentrations this reaction would not be significant in removing a monolayer from the surface of a cloud droplet. Gas phase OH radical would dominate the oxidation of a stearic acid cloud droplet monolayer as oxidation by gas phase OH has been shown by Bertram et al., (2001) to be on a timescale which is relevant to the lifetime of a cloud droplet. This work shows that there would be oxidation from within the droplet to a lesser degree.

Of the products of the reaction between stearic acid and OH radical some are surface active and some are soluble so the reaction would have an effect on both the Raoult term and the Kelvin term of the Köhler equation for predicting cloud droplet activation and growth.

References

- Abelès F., 1950. Recherches sur la propagation des ondes électromagnétiques sinusoïdales dans les milieux stratifiés. Applications aux couches minces. *Ann. de Physique* 5, pp. 596-640.
- Alfassi, Z.B., Huie, R.E., Neta, P. 1997. Kinetic studies of organic peroxy radicals in aqueous solution and mixed solvents. In: Alfassi, Z.B. (Ed.), *Peroxy Radicals*, Wiley, Chichester, England, pp. 235-281.
- Anastasio, C., Faust, B.C., Allen, J.M. 1994. Aqueous phase photochemical formation of hydrogen peroxide in authentic cloud waters. *Journal of Geophysical Research*, 99, D4, pp. 8231–8248.
- Anastasio, C and Newberg J.T. 2007. Sources and sinks of hydroxyl radical in sea-salt particles. *Journal of Geophysical Research*, 112, D10306.
- Arakaki, T., Anastasio, C., Shu, P.G., Faust, B.C. 1995. Aqueous-phase photoproduction of hydrogen peroxide in authentic cloud waters: Wavelength dependence and the effects of filtration and freeze thaw cycles. *Atmospheric Environment*, 29, 14, pp. 1697-1703.
- Arakaki, T., Kuroki, Y., Okada, K., Nakama, Y., Ikota, H., Kinjo, M., Higuchi, T., Uehara, M., Tanahara, A. 2006. Chemical composition and photochemical formation of hydroxyl radicals in aqueous extracts of aerosol particles collected in Okinawa, Japan. *Atmospheric Environment*, 40, 25, pp. 4764-4774.
- Arakaki, T. and Faust, B.C. 1998. Sources, sinks, and mechanisms of hydroxyl radical ($\cdot\text{OH}$) photoproduction and consumption in authentic acidic continental cloud waters from Whiteface Mountain, New York: The role of the Fe(II, III) photochemical cycle. *Journal of Geophysical Research*, 103, D3, pp. 3487-3504.
- Atkinson, R. 1986. Kinetics and mechanisms of the gas-phase reactions of the hydroxyl radical with organic compounds under atmospheric conditions. *Chemical Reviews*, 86, 1, pp. 69-201.
- Aumann, E and Tabazadeh, A. 2008. Rate of organic film formation and oxidation on aqueous drops. *Journal of Geophysical Research*, 113, D23205.
- Bahm, K. and Khalil, M.A.K. 2004. A new model of tropospheric hydroxyl radical concentrations. *Chemosphere*, 54, 2, pp. 143-166.
- Beddington, S. 2008. The ISIS Neutron Training Course, lecture notes.
- Bertram, A.K., Ivanov, A.V., Hunter, M., Molina, L.T., Molina, M.J. 2001. The Reaction Probability of OH on Organic Surfaces of Tropospheric Interest. *Journal of Physical Chemistry. A*, 105, 41, pp. 9415-9421.
- Bi, X., Simoneit, B.R.T., Sheng, G., Ma, S., Fu, J. 2008. Composition of major compounds in urban aerosols. *Atmospheric Research*, 88, 3-4, pp. 256-265.

- Blanchard, D.C. 1964. Sea-to-Air Transport of Surface Active Material. *Science*, 146, 3642, pp. 396-397.
- Campbell, R. 2011. Personal communication: email.
- Clarke, A.G. and Radojevic, M. 1987. Oxidation of SO₂ in rainwater and its role in acid rain chemistry. *Atmospheric Environment*, 21, 5, pp.1115-1123.
- Colvile, R.N., Bower, K.N, Choularton, T.W., Gallagher, M.W., Beswick, K.M., Arends, B.G., Kos, G.P.A., Wobrock, W., Schell, D., Hargreaves, K.J., Storeton-West, R.L., Cape, J.N., Jones, B.M.R., Weidensohler, A., Hannson, H-C., Wendisch, M., Acker, K., Wieprechtj, W., Pahl, S., Winkler, P., Berner, A., Krusiz, C., Gieray, R. 1997. Meteorology of the great dun fell cloud experiment 1993. *Atmospheric Environment*, 31, 16, pp. 2407-2420.
- Donaldson, D.J. and Vaida, V. 2006. The Influence of Organic Films at the Air-aqueous Boundary on Atmospheric Processes. *Chemical Reviews*, 106, 4, pp. 1445-1461.
- Eliason, T.L., Aloisio, S., Donaldson, D.J., Cziczo, D.J., Vaida, V. 2003. Processing of unsaturated organic acid films and aerosols by ozone. *Atmospheric Environment*, 37, pp. 2207-2219.
- Ellison, G.B, Tuck, A.F., Vaida, V. 1999. Atmospheric processing of organic aerosols. *Journal of Geophysical Research*, 104, D9, pp. 11633-11641.
- Faust, B.C. and Hoigné, J.1990. Photolysis of Fe(III)-hydroxy complexes as sources of OH radicals in clouds, fog and rain. *Atmospheric Environment, Part A, General Topics*, 24,1, pp. 79-89.
- Faust, B.C., Anastasio, C, Allen, J.M., Arakaki, T. 1993. Aqueous-phase photochemical formation of peroxides in authentic cloud and fog waters. *Science*, 260, 5104, pp. 73-75.
- Fermi, E. and Marshall, L. 1947. Interference Phenomena of Slow Neutrons. *Physical Review*, 71, pp. 666-677.
- Finlayson-Pitts B., and Pitts J., 2000. Chemistry of the Upper and Lower Atmosphere. Academic Press. pp 61-63.
- George, I.J. and Abbatt J.P.D. 2010. Heterogeneous Oxidation of Atmospheric Aerosol Particles by Gas-phase Radicals. *Nature Chemistry*, 2, pp. 2713-2722.
- George, I.J., Vlasenko, A., Slowik, J.G., Broekhuizen, K., Abbatt, J.P.D. 2007. Heterogeneous oxidation of saturated organic aerosols by hydroxyl radicals: uptake kinetics, condensed-phase products, and particle size change. *Atmospheric Chemistry and Physics*, 7, 16, pp. 4187-4201.
- Gill, P.S., Grael, T.E., Weschler, C.J. 1983. Organic films on atmospheric aerosol particles, fog droplets, cloud droplets, raindrops and snowflakes. *Reviews of Geophysics*, 21, 4, pp. 903-920.
- Gilman, J.B., Tervahattu, H., Vaida, V. 2006. Interfacial properties of mixed films of long chain organics at the air-water interface. *Atmospheric Environment*, 40, 34, pp. 6606-6614.

- Hatchard, C.G. and Parker, C.A. 1956. A New Sensitive Chemical Actinometer. II. Potassium Ferrioxalate as a Standard Chemical Actinometer. *Proceedings of the Royal Society, A*, 235, 1203, pp. 518-536.
- Hughes, A. 2010. Personal Communication: verbal (meeting).
- Hughes, A. 2011. Personal Communication: verbal (meeting).
- IPCC, 2007: Climate Change 2007: The Physical Science Basis. Contribution of Working Group I to the Fourth Assessment Report of the Intergovernmental Panel on Climate Change [Solomon, S., D. Qin, M. Manning, Z. Chen, M. Marquis, K.B. Averyt, M. Tignor and H.L. Miller (eds.)]. Cambridge University Press, Cambridge, United Kingdom and New York, NY, USA.
- ISIS. 2008. Neutron course notes.
- ISIS. 2009^a. Webpage on the production of neutrons at ISIS. Available at <http://www.isis.stfc.ac.uk/about-isis/how-isis-works6313.html> as accessed on 12/01/2009.
- ISIS. 2009^b. Webpage on the ISIS accelerator and target. Available at <http://www.isis.stfc.ac.uk/groups/accelerator-science/accelerators-and-targets3389.html> as accessed on 20/01/2009.
- ISIS. 2010. Webpages containing video clips of neutron generation at ISIS. Available at <http://www.isis.stfc.ac.uk/science/a-video-tour-of-the-isis-facility4469.html> as accessed on 20/01/2010.
- ISIS. 2011^a Webpages on the function of choppers at ISIS. Available at <http://www.isis.rl.ac.uk/archive/usersupport/choppers.htm>, as accessed on 07/07/2011
- ISIS. 2011^b Webpages on the technical specifications of the reflectometer SURF. Available at <http://www.isis.stfc.ac.uk/instruments/surf/technical/surf-technical-information7308.html>, as accessed on 12/07/2011.
- Jackson, A.V. and Hewitt, C.N. 1999. Atmospheric Hydrogen Peroxide and Organic Hydroperoxides: A Review. *Critical Reviews in Environmental Science and Technology*, 29, 2, pp. 175-228.
- Jacrot, B. 1976. The study of biological structures by neutron scattering from solution. *Reports on Progress in Physics*, 39, pp. 911-953.
- Katholy, S., Reiche, J., Brehmer, L. 2000. Texture of fatty acid Langmuir films studied by means of Brewster angle reflectometry. *Colloids and Surfaces, A: Physicochemical and Engineering Aspects*, 171, pp. 87-95.
- Khral., J., Knothe, G., Munak, A., Ruschel, Y., Schröder, O., Hallier, E., Westphal, G., Bünger, J. 2009. Comparison of exhaust emissions and their mutagenicity from the combustion of biofuel, vegetable oil, gas-to-liquid and petrodiesel fuels. *Fuel*, 88, pp. 1064- 1069.
- King M.D., Thompson K.C., Ward A.D., 2004. Laser tweezers Ramen study of optically trapped aerosol droplets of seawater and oleic acid reacting with ozone: Implications for cloud-droplet properties. *Journal of the American Chemical Society*, 126, pp. 16710-16711.

- King, M.D., Rennie, A.R., Thompson, K.C., Fisher, F.N., Chuan Dong, C., Thomas, R.K., Pfrang C., Hughes A.V., 2009. Oxidation of oleic acid at the air-water interface and its potential effects on cloud critical supersaturations. *Physical Chemistry Chemical Physics*, 11, pp. 7699-7707.
- King, M.D., Rennie, A.R., Pfrang, C., Hughes, A.V., Thompson, K.C., 2010. Interaction of nitrogen dioxide (NO₂) with a monolayer of oleic acid at the air-water interface – A simple proxy for atmospheric aerosol. *Atmospheric Environment*, 44, pp. 1822-1825.
- Laidler K.J. 1995. *Chemical Kinetics*. 3rd Edition. Prentice Hall, New Jersey.
- Lind, J.A. and Kok, G.L. 1986. Henry's Law Determinations for Aqueous Solutions of Hydrogen Peroxide, Methylhydroperoxide and Peroxyacetic Acid. *Journal of Geophysical Research*, 91, D7, pp. 7889- 7895.
- Lind, J.A. and Kok, G.L. 1994. Erratum 'Henry's Law Determinations for Aqueous Solutions of Hydrogen Peroxide, Methylhydroperoxide and Peroxyacetic Acid'. *Journal of Geophysical Research*, 99, D10, pp.21119.
- Lohmann, U. and Feichter, J. 2005. Global Indirect Aerosol Effects: A Review. *Atmospheric Chemistry and Physics*, 5, 3, pp. 715-737.
- Lu J.R., Thomas R.K., Penfold J., 2000. Surfactant layers at the air / water interface: structure and composition. *Advances in Colloid and Interface Science*, 84, pp. 143-304.
- Marty J.C., Saliota A., Buatmenard P., Chesselet R., Hunter K.A. 1979. Relationship between lipid compositions of marine aerosols, the sea surface microlayer and subsurface water. *Journal of Geophysical Research-Oceans and Atmospheres*, 84, NC9, pp.5707-5716.
- Mc Neill, V.F., Yatavelli, R.L.N., Thornton, J.A., Stipe, C.B., Landgrebe, O. 2008. Heterogeneous OH oxidation of palmitic acid in single component and internally mixed aerosol particles: vaporization and the role of particle phase. *Atmospheric Chemistry and Physics*, 8, pp. 5465-5476.
- Meyers, P.A. and Kawka, O.E. 1982. Fractionation of Hydrophobic Organic Materials in Sea Surface Microlayers. *Journal of Great Lakes Research*, 8, 2, pp. 288-298.
- Monk, P. 2006. *Maths for Chemistry*. Oxford University Press, Oxford.
- Monod, A., Poulain, L., Grubert, D., Voisin, D., Wortham, H. 2005. Kinetics of OH-initiated oxidation of oxygenated organic compounds in the aqueous phase: new rate constants, structure-activity relationships and atmospheric implications. *Atmospheric Environment*, 39, pp. 7667 – 7688.
- Neta, P., Huie, R.E., Ross, A.B. 1990. Rate constants for reactions of peroxy radicals in fluid solutions. *Journal of Physical Chemical Reference Data*, 19, pp. 413-505
- NIST (2012) web pages on Henrys law coefficient of H₂O₂

- Pilling M.J., and Seakins P.W., 1995. Reaction Kinetics. Oxford Science Publications, Oxford, UK. pp. 279.
- Penfold, J. and Thomas, R.K. 1990. The application of the specular reflection of neutrons to the study of surfaces and interfaces. *Journal of Condensed Matter*, 2, pp. 1369-1412.
- Penfold, J., Richardson, R.M., Zorbakhsh, A., Webster, J.R.P., Bucknall, D.G., Rennie, A.R., Jones, R.A.L., Cosgrove, T., Thomas, R.K., Higgins, J.S., Fletcher, P.D.I., Dickinson, E., Roser, S.J., McLure, I.A., Hillman, A.R., Richards, R.W., Staples, E.J., Burgess, A.N., Simister, E.A., White, J.W. 1997. Recent advances in the study of chemical surfaces and interfaces by specular neutron reflection. *Journal of the American Chemical Society, Faraday Transactions*, 93, 22, pp. 3899-3917.
- Penner, J.E., Hegg, D., Leaitch, R. 2001. Unravelling the Role of Aerosols in Climate Change. *Environmental Science and Technology*, 35, 15, pp. 332-340.
- Prinn, R., Cunnold, D., Simmonds, P., Alyea, F., Boldi, R., Crawford, A., Fraser, P., Gutzler, D., Hartley, D., Rosen, R., Rasmussen, R. 1992. Global Average Concentrations and Trend for Hydroxyl Radicals Deduced From ALE/GAGE Trichloroethane (Methyl Chloroform) Data for 1978-1990. *Journal of Geophysical Research*, 97, D2, pp. 2445-2461.
- Rennie, A. 2009. Personal Communication: verbal.
- Rennie, A. 2011. Webpages on neutron reflectivity data fitting available at : http://material.fysik.uu.se/Group_members/adrian/mono.htm. As accessed on 23/10/11.
- Rogge, W.F., Hildermann, L.M., Mazurek, M.A., Cass, G.R., 1991. Sources of fine organic aerosol. 1. Charbroilers and meat cooking operations. *Environmental Science and Technology*, 25, 6, pp. 1112-1125.
- Saxena P., Hildemann L.M., Mc Murry P.H., Seinfeld J.H., 1995. Organics alter hygroscopic behaviour of atmospheric particles. *Journal of Geophysical Research*. 100, D9, pp. 18755-18770.
- Sears V.F. 1992. Neutron scattering lengths and cross sections. *Neutron News* 3,3.
- Sprawls, P. 2011. The Physical Principles of Medical Imaging, online text book published by Medical Physics Publishing Wisconsin. Available at www.sprawls.org as accessed on 01/10/2011.
- Stemmler, K. and von Gunten, U. 2000^a. OH radical-initiated oxidation of organic compounds in atmospheric water phases: part 1. Reactions of peroxy radicals derived from 2-butoxyethanol in water. *Atmospheric Environment*, 34, 25, pp. 4241-4252.
- Stemmler, K. and von Gunten, U. 2000^b. OH radical-initiated oxidation of organic compounds in atmospheric water phases: part 2. *Atmospheric Environment*, 34, 25, 4253-4264.
- Södergren, A. 1987. Origin and composition of surface slicks in lakes of differing trophic status. *Limnology and Oceanography*, 32, 6, pp. 1307-1316.

- Sówka I., Zwoźdzaik J., Zwoźdzaik A., Kmeić G.K., 2001. Observation of hydrogen peroxide concentrations in cloudwater. *Abstracts of the European Aerosol Conference* S483.
- Squires G.L. 1978. Introduction to the Theory of Thermal Neutron Scattering. Dover Publications Inc, New York. As reprinted in 1996.
- Tedetti, M., Kawamura, K., Narukawa, M., Joux, F., Charrière, B., Sempéré, R., 2007. Hydroxyl radical-induced photochemical formation of dicarboxylic acids from unsaturated fatty acid (oleic acid) in aqueous solution. *Journal of Photochemistry and Photobiology A: Chemistry*, 188, pp. 135-139.
- Tervahattu^a H., Hartonen K., Kerminen V., Kupiainen K., Aarnio P., Koskentalo T., Tuck A. F., Vaida V., 2002. New evidence of an organic layer on marine aerosols. *Journal of Geophysical Research* 107, D7, pp. 1-9.
- Tervahattu^b H., Juhanoja J., Kupiainen K., 2002. Identification of an organic coating on marine aerosol particles by TOF-SIMS. *Journal of Geophysical Research, Atmospheres*, 107, 4319, pp. 1-7.
- Tervahattu, H., Juhanoja, J., Vaida, V., Tuck, A.F., Niemi, J.V., Kupiainen, K., Kulmala, M., Vehkamäki, H. 2005. Fatty acids on continental sulfate aerosol particles. *Journal of Geophysical Research*, 110, D06207.
- Textor C., Schulz M., Guilbert S., Kinne S., Balkanski Y., Bauer S., Berntsen T., Berglen T., Boucher O., Chin M., Dentener F., Diehl T., Easter R., Feichter H., Fillmore D., Ghan S., Ginoux P., Gong S., Grini A., Hendricks J., Horowitz L., Huang P., Isaksen I., Iverson T., Kloster S., Koch D., Kirkevåg A., Kristjansson J.E., Krol M., Lauer A., Lamarque J.F., Lui X., Montanaro V., Myhre G., Penner J., Pitari G., Reddy S., Seland Ø., Stier P., Takemura T., Tie X., 2006. Analysis and quantification of the diversities of aerosol life cycles within AeroCom. *Atmos. Chem. Phys.* 6, pp. 1777-1813.
- Tuckermann, R., Bauerecker, S., Cammenga, H.K. 2007. Generation and characterization of surface layers on acoustically levitated drops. *Journal of Colloid and Interface Science*, 310, pp. 559-569.
- Twomey, S. 1974. Pollution and the planetary albedo. *Atmospheric Environment*, 8, 12, pp. 1251-1256.
- Valverde-Canossa, J., Wieprecht, W., Acker, K., Moortgat, G.K. 2005. H₂O₂ and organic peroxide measurements in an orographic cloud: The FEBUKO experiment. *Atmospheric Environment*, 39, 23-24, pp. 4279-4290.
- Van der Lee, A., Salah, F., Harzallah, B. 2007. A comparison of modern data analysis methods for X-ray and neutron specular reflectivity data. *Journal of Applied Crystallography*, 40, pp. 820-833.
- Vlasenko, A., George, I.J., Abbatt, J.P.D. 2008. Formation of Volatile Organic Compounds in the Heterogeneous Oxidation of Condensed-Phase Organic Films by Gas-Phase OH. *The Journal of Physical Chemistry, A*, 112, 7, pp. 1552-1560.
- Von Sonntag, C., and Schuchmann, H-P. 1997. Peroxyl radicals in aqueous solutions. In Alfassi, Z.B. (Ed.), *Peroxyl Radicals*, Wiley, Chichester, England.

- Voss L.F., Bazerbashi M.F., Beekman C.P., Hadad C.M., Allen H.C., 2007. Oxidation of oleic acid at air/liquid interfaces. *Journal of Geophysical Research*, 112, D06209. pp.1-9.
- Warneck P., 1988. Chemistry of the Natural Atmosphere. International Physics Series. Volume 41. Academic Press.
- Wayne. C.E. and Wayne. R.P.1996. Photochemistry. Oxford University Press.
- Webster, J. and Langridge, S. 1999. Applications of index matching in reflectometry, SANS and Brewster angle microscopy. *Current Opinion in Colloid and Interface Science*, 4, 3, pp. 186-189.
- Weinstein-Lloyd, J. and Schwartz, S.E. 1991. Low-intensity radiolysis study of free-radical reactions in cloudwater: hydrogen peroxide production and destruction. *Environmental Science and Technology*, 25, 4, pp. 791-800.
- Wilson, C.C. 1990. ISIS, the UK Spallation Neutron Source – a Guided Tour. *Neutron News*, 1, 1, pp. 14-19.
- Yu, X-Y. and Barker, J.R. 2003. Hydrogen Peroxide Photolysis in Acidic Aqueous Solutions Containing Chloride Ions. I. Chemical Mechanism. *Journal of Physical Chemistry, A*, 107, 9, pp. 1313-1324.
- Zepp, R.G., Faust, B.C. and Hoigné, J. 1992. Hydroxyl radical formation in aqueous reactions (pH 3-8) of iron(II) with hydrogen peroxide: the photo-Fenton reaction. *Environmental Science and Technology*, 26, 2, pp. 313- 319.
- Zou, Y. and Hoigné, J. 1992. Formation of hydrogen peroxide and depletion of oxalic acid in atmospheric water by photolysis of iron(III)-oxalato complexes. *Environmental Science and Technology*, 26, 5, pp. 1014-1022.
- Zou, Y. and Hoigné, J. 1993. Evidence for Photochemical Formation of H₂O₂ and Oxidation of SO₂ in Authentic Fog Water. *Science*, 260, 5104, pp. 71-73.

The Oxidation of Oleic Acid Monolayers with Gas Phase Ozone

3.0 Abstract

A monolayer of oleic acid, a naturally occurring insoluble organic amphiphile was oxidised with gas-phase ozone, generated by the photolysis of oxygen. The rate of film oxidation at the air-water interface was monitored with neutron reflection on a Langmuir trough. The monolayer of deuterated oleic acid ($C_{18}D_{33}O_2H$) serves as a proxy for the organic film at the air-droplet interface of a cloud droplet. The surface pressure of the monolayer was measured with a Wilhelmy plate and the surface coverage of the deuterated material was measured with neutron reflection. The surface pressure and surface coverage declined with reaction time. The kinetic decay of the surface coverage was complex. Continued oxidation completely removed the film showing inconsistency with the present work on this system.

3.1 Introduction

Atmospheric aerosol particles in the troposphere act as cloud condensation nuclei. The oxidation of atmospheric aerosols influences climate through cloud formation and precipitation effects, (Lohmann and Feichter, 2005; IPCC, 2007). Some cloud condensation nuclei have been shown to possess an organic film (Blanchard, 1964; Gill et al. 1983; Tervahattu et al. 2002^{a,b};2005). As a cloud droplet/aerosol ages in the atmosphere it will be subject to oxidation by radical species from outside and within the droplet phase. One of the primary oxidant species in the troposphere is ozone and it is a precursor to the formation of OH radical in the gas phase (Finlayson-Pitts and Pitts. 1997). Ozone readily reacts with the double carbon-carbon bond in unsaturated organic molecules in the atmosphere, contributing to the aging process of atmospheric aerosols and cloud droplet organic films (Zahardis and Petrucci, 2007; Rudich et al. 2007 and references therein).

To investigate the process of the reaction by a gas phase oxidant species from outside a cloud droplet, and an insoluble organic layer at the air-liquid interface, gas-phase ozone (O_3) was reacted with a monolayer of oleic acid formed at the surface of a Langmuir trough. Oleic acid was chosen because:

- The reaction of oleic acid with ozone has been studied with a range of spectroscopic techniques giving information on product composition but not about the surface physical and chemical characteristics on a molecular level.
- Oleic acid is one of the most commonly sampled fatty acids in aerosol field samples and there have been other studies of oleic acid monolayers at the air-water interface.
- Oleic acid serves as a model system for an unsaturated aerosol surface film.

By monitoring the surface pressure (Π) of the monolayer on an aqueous subphase, it was demonstrated that a reaction was taking place. To study the kinetics and atmospheric relevance of this reaction the surface coverage (Γ) of molecules at the air-water interface was measured using neutron reflection.

The experiment described here attempts to assess the behaviour of a monolayer of oleic acid at the air-water interface as it reacts with gas phase ozone. The heterogeneous oleic acid-ozone reaction system has been reviewed by Zahardis and Petrucci (2007) as a proxy for the heterogeneous oxidation of unsaturated organics, the review highlighted the need to gain more detailed chemical descriptions of the ozonolysis process and secondary reactions in order to better understand the climatic effect of ozonolysis of atmospheric organic films. The experimental work in this chapter contributes to a better understanding of ozonolysis as it is the second study of oleic acid ozonolysis of an oleic acid organic film and the results highlighted a flaw in the first study by King et al., (2009).

3.2 Aims

1. To monitor the properties of surface pressure and surface coverage of a monolayer of oleic acid ($C_{18}H_{33}COOH$), at the air-water interface in real time as the monolayer was oxidised with gas-phase ozone.
2. To conduct a kinetic analysis of the surface coverage of a monolayer of oleic acid over time to determine a rate constant for the reaction of oleic acid with gas-phase ozone.
3. To elucidate the presence of a mechanism for oleic acid removal from the air-water interface.
4. To calculate a chemical lifetime for a monolayer of oleic acid reacting with ozone in the atmosphere.

3.3 Background

The chemical oxidation of cloud droplet films has not been widely studied. Oleic acid is a constituent of the sea-surface microlayer (Kattner and Brockmann, 1978) and has been sampled as a component of atmospheric marine aerosol (Tervahattu et al, 2002^b) so is a candidate molecule for cloud droplet film formation. The presence of a cloud droplet film will increase the surface pressure (Π), thus decreasing the surface tension at the air-water interface however oxidation of the film would increase the surface tension of a host droplet closer to that of its core composition (Voss et al., 2007). Tropospheric ozone (O_3), is an oxidant gas, the concentration of which can be 50 ppb in unregulated urban environments (Finlayson-Pitts and

Pitts, 2000), the annual mean background concentration of tropospheric ozone is from 23 to 45 ppb in the Northern Hemisphere (Vingarzan, 2004).

Alteration of the surface properties of a film as it reacts with atmospheric oxidants and is degraded; a process known as oxidative aging, in the atmosphere will alter the critical supersaturation value according to the Köhler theory of cloud droplet formation and growth as explained in chapter 1. To assess the impact of oxidation by gas phase ozone on an unsaturated cloud droplet film, an oleic acid monolayer was exposed to gas-phase ozone and the surface pressure and surface coverage were monitored in order to determine the kinetic behaviour of the reaction between an unsaturated film at the air-water interface and gas-phase ozone.

The growth of cloud condensation nuclei (CCN) into cloud droplets, and the number density of such droplets in a cloud have climatic implications. A larger number of smaller cloud droplets in a defined parcel of air with a constant volume of water would scatter less incoming solar radiation in the forward direction relative to larger cloud droplets according to the theory of Mie scattering, thus increasing the albedo of the cloud (Twomey, 1974).

3.4 Oleic Acid and Cloud Droplets

There are many sources of oleic acid to the atmosphere, the most significant are;

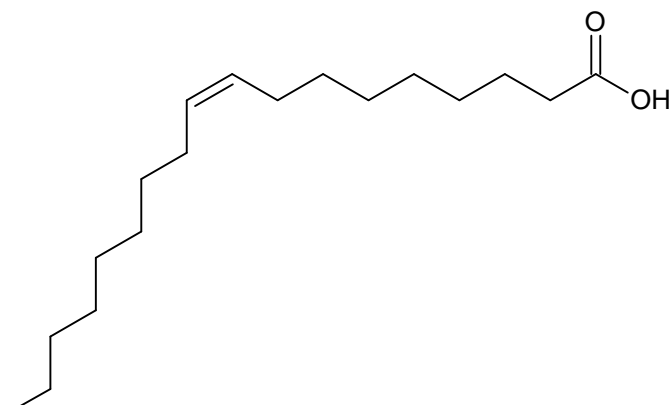
- Aerosol emissions from the sea surface microlayer (Simoneit et al. 2004).
- Grilling and other methods of meat cooking (Rogge et al. 1991).
- Land plant emissions, combustion of land plants and use of plant oils and waxes (Rogge et al. 1993^a).
- Exhaust emissions from vehicles possessing a catalytic converter (Rogge et al. 1993^b) which increases the oleic acid emission per petrol car from 1.2 µg/km to 5 µg/km (Rogge et al. 1993^b).

The fatty acid, oleic acid is emitted to the atmosphere from both natural and anthropogenic sources (Limbeck and Puxbaum, 1999; Cheng et al. 2004; Zahardis and Petrucci, 2007). Oleic acid has been found on marine aerosol (Fang et al. 2002) and as a component of the sea surface microlayer (Larsson et al. 1974). The sea surface microlayer is a film of organic chemicals found at the surface of oceans; it forms from polar organic molecules released by the photosynthesis, death and decomposition of vegetation and sea creatures such as phytoplankton, the detritus collects at the surface enriching the content of organic immiscible chemicals (fatty acids, *n*-alkanes, and hydrocarbons) by a factor of 2 to 5 (Marty et al. 1979), at the surface of the water (Marty, et al. 1979; Zahrdis and Petrucci, 2007). The oceans are rich in phospholipids

such as phosphatidylglycerol, phosphatidylethanolamine, and phosphatidylcholine produced by plankton (Popendorf et al. 2011) which decompose to form fatty acids. Aerosol is created by sea spray, bubbles bursting at the surface when waves break and from the wind blowing over the surface of the ocean (Blanchard, 1963, 1964; Barger and Garret, 1970, 1976; Bezdek and Carlucci, 1974; Tseng et al. 1992; Zahardis and Petrucci, 2007), the marine aerosol can have a coating of organic chemicals from the sea surface microlayer (Tervahattu et al. 2002^{a,b}) as surfactant material concentrates at the air-water interface of bursting bubbles and of sea spray produced by waves (O'Dowd et al., 2007). Marine aerosol sampled from onboard ships have a lower concentration of unsaturated fatty acids than saturated fatty acids such as stearic acid, the coating organic films contain a mixture of both saturated and unsaturated compounds (Zahardis and Petrucci, 2007; Mochida et al. 2002; Fang et al. 2002; Kawamura and Gagosian, 1987), it is suggested that the unsaturated fatty acids are more readily oxidised in the atmosphere than saturated fatty acids accounting for the lower concentrations in aerosol samples, photolysis of unsaturated compounds can also occur, (Mochida et al. 2002; Kawamura and Gagosian, 1987). The mixture of saturated and unsaturated fatty acids will be explored in chapter 5. The same process of microlayer formation takes place at the surface of lakes (Södergren, 1987).

In terrestrial environments plants emit biogenic fatty acids, vascular plants, those which have a vascular structure for transporting water and nutrients and have multiple chromosome sets per cell are responsible for emitting a range of saturated and unsaturated fatty acids (Zahardis and Petrucci, 2007; Cheng et al. 2004; Pio et al. 2001; Simoneit et al. 1988, 1991; Simoneit and Mazurek, 1982). In urban terrestrial locations traffic emissions of fatty acids are higher from vehicles with catalytic converters installed, 53.4% of the identifiable organic mass, in vehicles lacking a catalytic converter the predominant organic component of the emissions are polyaromatic hydrocarbons (Zahardis and Petrucci, 2007; Rogge et al. 1993^b).

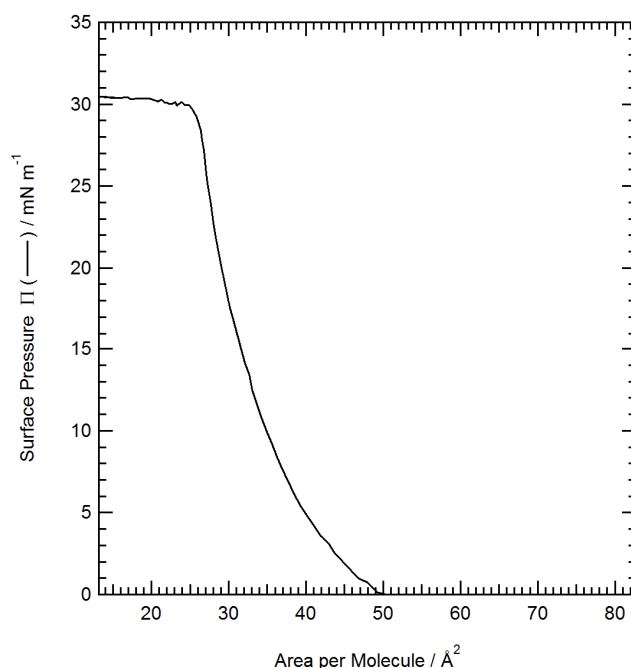
Mochida et al., (2002) measured the fatty acid content of marine aerosols collected quarterly from the Northern Pacific region from autumn 1996 to summer 1997. The saline aerosol correlated with higher fatty acid content suggesting a marine source of the fatty acids. The fatty acid concentrations were greater in the spring and summer when the Pacific experiences a period of high biological productivity indicating a marine biological source for fatty acids which are then transmitted to the atmosphere (Mochida et al. 2002). Average C₁₈ fatty acid concentrations were highest in April 1997 at 1400 pg m⁻³ and lowest in October 1996 at 450 pg m⁻³.

Figure 3.1 *The Structure of an Oleic Acid Molecule*

The oleic acid molecule has a carboxylic acid head group with an unsaturated aliphatic hydrocarbon chain. The functional group is the (-COOH) carboxylic acid head which is hydrophilic. At the air-water interface the head group forms a hydrogen bond with the water molecules in the subphase (the droplet phase or in the experiment the liquid in the Langmuir trough beneath the surface film), and the hydrocarbon chain is orientated into the air. The chain is kinked at the double bond affecting its orientation; this structure reduces the density at which a monolayer film of unsaturated molecules can be packed to at the air-liquid interface. A typical value of area per molecule for an oleic acid monolayer in the liquid phase is 42 to 47 Å² per molecule⁻¹ (Gaines, 1966) compared to that of stearic acid which is the same carbon number but does not possess a double bond which has an area per molecule of 27 to 21 Å² per molecule⁻¹ in the liquid phase (Gilman et al. 2004).

As with stearic acid, oleic acid does not dissolve in water; it is insoluble and forms a monolayer at the air-liquid interface with the molecules' hydrophilic, acidic, head group in the liquid cloud droplet and the hydrocarbon chain orientated into the air. The kink created by the double bond in the oleic acid molecule affects the surface pressure area isotherm as shown in figure 3.2.

Figure 3.2 *The Surface Pressure Versus Surface Area per Molecule Isotherm for an Oleic Acid Monolayer at the Air-water Interface*



The isotherm in figure 3.2 was adapted from Voss et al., (2007) as measured at 23°C and compressed at 5mm / min⁻¹.

The packing of the film is affected by the double bond in oleic acid which alters the orientation of the hydrocarbon chain. Stearic acid with its straight chain will pack in a monolayer very closely with other straight chain molecules into a condensed monolayer. The oleic acid film will not pack as closely as the stearic acid film; the oleic acid monolayer is in the expanded phase (Gaines, 1966) and does not exhibit the distinct phase changes seen in a saturated monolayer. Oleic acid is liquid at room temperature whereas its saturated equivalent in carbon number, stearic acid is crystalline. It was suggested by Adam, (1968) that an oleic acid monolayer would not be in a condensed state until it reached a temperature of -30°C, so in a cloud/ aerosol setting it is unlikely to be condensed. The surface pressure isotherm of an unsaturated monolayer is less affected by temperature than that of a saturated compound (Adam and Jessop, 1926; Gaines, 1966).

3.5 Formation of Gas-Phase Ozone in the Troposphere

The majority of ozone in the troposphere is a secondary product of photochemical reactions occurring during daylight hours (Finlayson Pitts and Pitts, 2000). Major sources of tropospheric gas-phase ozone in urban environments are primary pollutants such as the NO_x and VOC compounds from vehicle emissions which are photolysed producing O_3 (Finlayson Pitts and Pitts, 2000). Ozone production from traffic emissions is often lower during the morning when there is a higher NO concentration, the O_3 concentration increases in the afternoon and into the evening. Production of O_3 is dependent on sunlight thus its formation ceases after dark but its lifetime means it can be transported as a component of an airmass (Finlayson Pitts and Pitts, 2000). The lifetime for ozone in the troposphere is hours to days (Blasing, 2011).

Figure 3.3 A Simplified Diagram of the Creation and Destruction of Ozone in the Troposphere

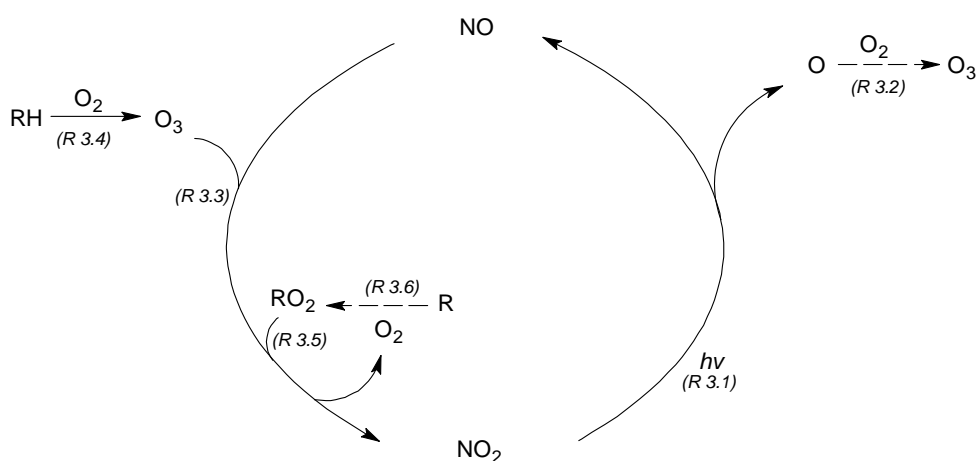


Figure 3.3 was adapted from the United Kingdom Photochemical Oxidants Review Group, 1997, figure 2.4.

3.5.1 Photochemical Formation of Ozone from Oxides of Nitrogen

The NO_x chemistry directly producing or removing ozone involves the photo-dissociation of nitrogen dioxide (NO_2), in air producing nitric oxide (NO) and atomic oxygen (O), (reaction 3.1 to 3.3). The molecular oxygen then combines with oxygen (O_2), in the presence of a third body forming ozone (O_3). The levels of the NO_x species determine the lifetime of ozone, as nitric oxide (NO), rapidly destroys ozone producing nitrogen dioxide (NO_2) and oxygen (O_2), (reaction 3.3). In high nitric oxide conditions ozone levels do not build up.



A saturated hydrocarbon (alkene), RH can react with oxygen generating ozone (R 3.4).



Gas phase NO_2 levels are influenced by reaction 3.5 where alkyl peroxy radical (RO_2) and nitric oxide (NO) react producing alkoxy radical (RO) and nitrogen dioxide (NO_2).



Alkyl peroxy radical (RO_2) is formed from (R) in the presence of oxygen in the presence of a third body molecule.



In addition to the processes described here the influence of particle phase reactions involving precursor species to ozone on the reaction rates and yields is not well quantified (United Kingdom Photochemical Oxidants Review Group., 1997).

3.5.2 Ozone Concentrations in the Troposphere

The concentration of gas-phase O_3 is highly variable by geographical location due the varied emission of precursor species (Finlayson Pitts and Pitts, 2000), in the remote marine regions there are lower concentrations of precursor species (Lelieveld and Crutzen, 1994). However concentrations of tropospheric ozone are naturally higher at certain oceanic locations, Chandra et al., (2004) suggest this is due to a higher downward flux of ozone from the stratosphere into the troposphere over the Atlantic and Pacific oceans at Northerly latitudes.

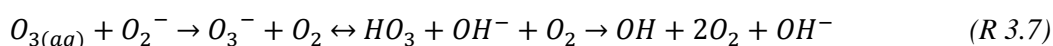
Tropospheric ozone concentrations are measured by balloon sounding, aircraft instrumentation and surface measurements and are reported as a mixing ratio typically as parts per billion volume which is 1 molecule of ozone in 10^9 molecules of air or 1 ppb (Warneck, 1988).

Lelieveld and Crutzen, 1990 give the following values for the mixing ration of O_3 in summer and winter at $45^\circ S$, $45^\circ N$ and at the equator. The equatorial mixing ratio of O_3 was 30 ppb at an altitude of 1.5 to 5 km. At 45° South, the summer mixing ratio was 15 ppb at an altitude of 1.5 to 3 km and the winter value was 25 ppb O_3 at an altitude of 1.5 to 3 km. At $45^\circ N$ the summer

mixing ratio was 30 ppb and the winter mixing ratio of O₃ was 40 ppb at an altitude of 1.5 to 3 km.

Finlayson-Pitts and Pitts, (1997) give figures for different land use types, giving a peak O₃ concentration calculated from data collected in rural to suburban areas of 80 to 150 ppb and in remote locations such as the Baltic Sea island Arkona concentrations are 30-40ppb (Finlayson-Pitts and Pitts 1997). The highest O₃ concentrations are found in urban locations with no emissions regulation where levels can reach 500 ppb (Finlayson-Pitts and Pitts, 2000). Over the Atlantic Ocean ozone concentrations from 30 to 35 ppb were measured in May 2007 from aircraft at altitudes of 500 to 2,250 m (Read et al., 2008). Remote location measurements of the background level of ozone at Antarctica at the South Pole at an elevation of 2835 m and at Arrival Heights at sea level gave annual means of 26 to 30 ppb (1992 to 2001) and 23 to 26 ppb (1997 to 1999), (CMDL, 2004; Vingarzan, 2004). The background concentration of ozone in the troposphere is 30 to 40 ppb.

The effect of cloud formation on tropospheric ozone levels has been noted. Monod and Carlier (1999) used a box model approach to study the multiphase photochemistry taking place in clouds with the presence of soluble organic compounds. The aqueous phase photochemistry taking place in cloud droplets effects the gas phase concentration of ozone (Jacob, 2000; Jacob et al. 1989; Lelieveld and Crutzen, 1990; Walcek et al. 1997; Monod and Carlier, 1999). The effect of cloud droplets on the gas phase ozone concentration when compared to clear sky conditions is to reduce the net production of ozone (Monod and Carlier, 1999). The reduction occurs because the highly soluble peroxy radical (HO₂) enters the aqueous phase decreasing the gaseous phase HO₂ available for ozone formation (Monod and Carlier, 1999). Monod and Carlier predict a reduction in the formation of ozone of up to 50% in cloudy conditions. More directly ozone is scavenged by cloud droplets as NO and NO₂ have low solubility so do not contribute to ozone production within the droplet and ozone which dissolves from the gas phase into the droplet is consumed by reactions with oxygen radicals (O₂⁻) at a more rapid rate than the ozone can diffuse (Monod and Carlier, 1999).



The potential products of the oxidation of an insoluble monolayer can be soluble organic compounds. The work of Monod and Carlier (1999), where methanol was modelled as a soluble organic compound in cloud water showed that ozone production was reduced in cloudy conditions in the presence of soluble organic compounds.

3.5.3 The Effect of Aerosol and Clouds on Ozone Concentrations in the Troposphere

Tropospheric ozone measurements are taken with aircraft based spectrometers, ozonesondes, ground based lidar, airborne lidar and satellite observations. At present the lidar and ozonesonde techniques work only for cirrus/ice clouds, the resolution of these techniques in cloud is poor due to scattering effects, therefore there are few in cloud ozone measurements. It is standard practice to use ambient ozone concentrations in atmospheric modelling for in cloud systems in the troposphere. Warneck, (1988) stated a calculated in-cloud liquid phase dissolved O_3 concentration of 6.4×10^{-10} mol/kg based on a gas phase mixing ratio of 4×10^{-8} (40 ppb) which is the accepted background level for gas phase ozone in the troposphere.

There are indications that aerosol can act as a sink for ozone in the troposphere through scavenging. Modelling and field studies show a reduction in tropospheric ozone levels in the presence of dust aerosol, which is rich in minerals originating from soils and desert sands (Reus et al. 2000) and is of a large particle size as demonstrated by continental dust storms which contain visible aerosol particles. Rues et al., (2000) took airborne measurements of ozone mixing ratios during ascent from Tenerife, the Canary Islands showing at 2km and ozone mixing ratio of 45 ppbv, 2.5 to 5.8 km a steady mixing ratio of 30 ppbv and at 6 to 11.8 km a fluctuating concentration of between 50 and 70 ppb. The steady, lower mixing ratio for ozone from 2.5 to 5.8 km was found to coincide with high levels of accumulation mode particles (diameter 0.11 to 3.5 μm), these are large aerosol particles. In the region containing the dust aerosol the relative humidity increased from 4% to 35%. If the relative humidity reached 60 to 80 % this aerosol could form droplets, if they contained dissolved species which react with ozone, then the droplets could scavenge ozone leading to the lower concentration of ozone measured in the dust layer, however in this case the air was drier and Rues et al., (2000) suggest that the ozone is reacting with trace metals (manganese, iron) or oxidising organic material from the dust aerosol.

The ozone concentrations around a warm aqueous cloud droplet are those in the lower troposphere at that given location. The experiments in this thesis are concerned with warm aqueous clouds such as orographic clouds, maritime cumuli and continental cumuli (Squires, 1958) in the lower atmosphere within the atmospheric boundary layer at altitudes of up to 6km (Warneck, 1988). Vertical mixing, a process in which clouds play a role by venting, can lead to layers enriched in O_3 when compared to the surface concentration at sea level (Finlayson Pitts and Pitts, 2000). Cloud venting is the process by which gaseous matter and aerosol are transported from the lower troposphere into mid to upper troposphere cloud layer where the transported matter is scavenged by the surface of cloud droplets (Cotton et al. 1995). The effect

of cloud on ambient ozone concentrations is poorly constrained, particularly the role of the particles and droplets in ozone processing through oxidation. There will also be oxidation by ozone dissolved within cloud droplets.

3.6 Previous Atmospheric Studies of Oleic Acid and Ozone

Here the current literature regarding oleic acid and ozone by atmospheric chemists is reviewed in brief. There is a large body of experimental work on oleic acid films on laboratory synthetic aerosol particles and thick oleic acid films yet there are few studies of oleic acid monolayers, there are two oleic acid monolayer studies utilising neutron reflectometry by King et al., (2009), and King et al., (2010) which were conducted with a custom synthesised fully deuterated oleic acid molecule as deuterated oleic acid was not commercially available until late 2010.

3.6.1 Laboratory Studies of Oleic Acid Aerosol and Droplets Reacting with Ozone

Zahardis and Petrucci, (2007) reviewed the experimental data on the ozonolysis of oleic acid from an atmospheric perspective. The current state of knowledge is based upon particle phase studies of aqueous and mixed phase aerosol and studies of oleic acid films reacting with ozone at the air-water interface.

3.6.1.1 Particle Phase Experiments

Ziemann, (2005) used a thermal desorption particle beam mass spectrometer (TDPBMS) to analyse the composition of the reaction products from the ozonolysis of pure oleic acid particles, liquid particles of oleic acid mixed with dioctyl sebacate and oleic acid as a component of a solid liquid mixtures with hexadecanoic acid and heptadecanoic acid. High performance liquid chromatography (HPLC) coupled with selected ion monitoring (SIM) or mass spectral analysis (MS) was also used to characterize the reaction products which were primarily volatile. The loss of oleic acid due to reaction initiated by ozone was faster in the liquid mixed particles than in the liquid-solid mixed particles (Ziemann, 2005).

King et al., (2004) used laser tweezers to hold a droplet of synthetic seawater and oleic acid and subjected it to Raman spectroscopy to monitor the size of the droplet and the signal given by the composition of the droplet. The oleic acid was inferred to be present at the surface of the droplet, with a saline liquid core. The droplet was oxidised with gas phase ozone. As the droplet reacted it grew from 6.5 to 8 μm owing to hygroscopic growth, nonanal and nonanoic acid were detected in the droplet. The loss of the Raman signal for oleic acid from the droplet over 900 seconds was attributed to the reaction of oleic acid and ozone and the subsequent break down of oleic acid allowing the ozone to penetrate to the saline core of the droplet which reacted with

Br^- initiating the formation of radical species which would rapidly remove the organic component from the droplet phase (King et al. 2004). King et al., (2004) concluded that the oxidation of a coating of oleic acid on a droplet by ozone lowered the critical supersaturation required for droplet growth in the atmosphere and that as the oleic acid was oxidised the droplet became more hydrophilic so a previously inert droplet or particle could become an active cloud condensation nuclei.

Katrib et al., (2004) studied the reaction products of oleic acid films coatings on polystyrene latex spheres. The film was formed by condensation of vaporised oleic acid. The coated films ranged in thickness from 2 to 30 nm (Katrib et al. 2004). It was observed that a 20 nm film was reduced to 15 nm following oxidation and that the products of the reaction of oleic acid with ozone were volatile. There is broad agreement in the literature that the reaction of oleic acid with ozone proceeds by the scission of the double bond followed by the formation of Criegee intermediates leading to decomposition into shorter chain organic acids and secondary ozonides. The mechanism of the reaction of oleic acid with ozone will be presented in section 3.7.6.

Kinetic measurements of the loss of sodium oleate due to reaction with gas-phase ozone were taken by McNeill et al., (2007) who conducted aerosol flow tube experiments where submicron aqueous aerosols composed of a mixture of sodium oleate and water were atomized and flowed in a nitrogen at a controlled relative humidity of 62-67 % to a flow tube or photochemical reactor containing 4 ppm ozone. The aerosols were sampled with a differential mobility analyser (DMA) and an ultrafine condensation particle counter (CPC). Kinetic measurements were achieved by varying the flow rate of the reactant gas. The oleate was detected as oleic acid using a chemical ionization mass spectrometer (CIMS). The reaction time was proportional to the position along the flow tube where the aerosol was injected. The sodium oleate particles were oxidised at the surface and the reaction kinetics followed Langmuir Hinshelwood behaviour where adsorption occurs at surface sites. McNeill et al., (2007) calculated a reactive uptake coefficient for ozone of $\sim \times 10^{-5}$ to 6×10^{-5} concluding that the lifetime of a thin film of unsaturated organic molecules on a liquid aerosol would be ~ 10 minutes due to oxidation by atmospheric ozone at 50 ppb. McNeill et al., (2007) also note that the effect of the substrate mineralogical composition of the solid fraction of an aerosol particle could lengthen the lifetime from minutes to days.

3.6.1.2 Surface Pressure and Surface Tension Measurements of Oleic Acid Monolayers Reacting with Ozone

The reaction of an oleic acid monolayer with gas phase ozone was studied from a health perspective by Srisankar and Patterson, (1979) using a Langmuir trough and Wilhelmy plate balance housed in a reaction chamber. Srisankar and Patterson, (1979) observed the film contracting; to maintain a given surface pressure of 7 mN m^{-1} the barriers on the Langmuir trough reduced the surface area by compression. The observation was made that there was a decay of the monolayer in air which was not as pronounced in an oxygen only atmosphere in which the surface pressure could be maintained for 90 minutes without compression of the monolayer, the decay in air was attributed to the presence of trace quantities of ozone.

González-Labrada et al., (2007) studied the change in the surface pressure of pendant aqueous drops covered with an oleic acid monolayer spread by syringe within a solution of chloroform which evaporates. Pendant drop apparatus are an alternative way of measuring surface pressure and surface tension to the use of a Wilhelmy plate apparatus and a Langmuir trough. The surface pressure was measured as a function of reaction time. The surface area per molecule can be monitored by changing the volume of the droplet, decreasing the volume is the equivalent of compressing or releasing a monolayer on a Langmuir trough. The change in surface tension was monitored with a tensiometer. The ozone exposure took place in a reaction chamber. González-Labrada et al., (2007) also measured droplets of the reaction products nonanal and nonanoic acid but no increase in surface pressure with compression was observed using the droplet apparatus or a Langmuir trough so it can be inferred that these species are not present at the interface. The kinetic results obtained by González-Labrada et al., (2007) will be discussed in section 3.9.2.

The kinetics of the reaction of a monolayer of the unsaturated phospholipid 1-oleoyl-2-palmitoyl-*sn*-glycero-3-phosphocholine, (OPPC) with gas phase ozone was conducted by Wadia et al., (2000) by monitoring the gas-phase reaction products. OPPC has one saturated and one unsaturated chain. The OPPC monolayer was held on a Langmuir trough housed in a reaction chamber from which the air was directed into an atmospheric pressure ionization mass spectrometer (API-MS) which measured the gas phase products of the reaction at the air-liquid interface, the condensed phase kinetics were not determined. Nonanal was detected in the air above the monolayer after reaction with 0.25 to 1ppm O_3 . The area per molecule did not affect the yield of nonanal in a predictable manner which Wadia et al., (2000) collate with the packing of the monolayer not greatly affecting the availability of the double bond to ozone. The rate constant for the reaction of the monolayer with ozone was faster than that of a supposed gas

phase reaction of ozone with OPPC (Wadia et al. 2000). Wadia et al., (2000) propose that the monolayer is porous and that the ozone molecules are trapped in the region of the hydrocarbon chains of the monolayer, these trapped molecules react more rapidly with the OPPC than gas phase ozone molecules colliding with a flat, impenetrable surface (Wadia et al. 2000). Wadia et al., (2000) also note that the reaction product nonanal is soluble in water so the experiment only detects nonanal that enters the gas phase and not that which is dissolved into the subphase, the net yield for the production of nonanal was $54 \pm 11\%$.

King et al., (2009) oxidised a monolayer of deuterated oleic acid on a Langmuir trough housed in a teflon bag for some early experiments and an aluminium reaction chamber for later experiments, with a flow of gas-phase ozone. Simultaneous neutron reflectivity measurements of the surface coverage of the monolayer were taken together with surface pressure measurements. The sub-phase beneath the film was varied from pure water to a salinity of 33g L^{-1} NaCl. King et al., (2009) showed that after 250 minutes exposure to 4.2×10^{12} molecule cm^{-3} of ozone, on a sub-phase of 33g L^{-1} NaCl, a monolayer with a surface pressure of 14 mN m^{-1} and a surface coverage of 1.1×10^{18} molecule m^{-2} remained at the air-liquid interface. A value of the rate constant for the reaction of ozone and oleic acid was taken from fitting the surface coverage to a scheme with two reaction pathways, one yielding one soluble or volatile product and one surface active product, another pathway giving only soluble or volatile products. The kinetic analysis showed that the kinetics for the production of products from the reaction of oleic acid with ozone, was not affected by the composition of the subphase. It is for this reason that the experiments in this thesis are conducted on pure water subphase and not saline. The values of the rate constants from the work of King et al., (2009) will be re-visited in the discussion section 4.14. King et al., (2009) conclude that the remaining material at the interface after sustained exposure to ozone was likely to be nonanoic acid; this is the least soluble of the known products from the reaction of oleic acid thin films with ozone which is surface active (McNeill et al. 2007).

Voss et al., (2007) compressed a monolayer of oleic acid on a Langmuir trough from starting area per molecule of 83 \AA^2 . A phase transition was observed at 51 \AA^2 per molecule and prior to collapse at 28 \AA^2 per molecule. Voss et al., (2007) took broad-bandwidth sum frequency generation spectroscopy (BBSFG) spectra of the intensity of the output beam of infrared radiation versus incident infrared radiation for the monolayer. Broad-bandwidth sum frequency generation (BBSFG) spectroscopy is a vibrational spectroscopy technique. The signal is dependent on the number density and orientation of the molecules at the interface. Its limitations are that it does not give a measure of the amount of a material present so cannot yield kinetic information. It was used in-situ with the Langmuir trough for studying the compression of an

oleic acid monolayer however it was not coupled with the Langmuir trough during oxidation; instead the monolayers were prepared in petri dishes. Measurements at 83, 51 and 28 Å² per molecule showed that at 83 Å² per molecule, at 0 mNm⁻¹ surface pressure, the spectra was relatively flat and featureless. The BBSFG spectra shows peaks for the CH groups within the monolayer which for oleic acid on an aqueous substrate occur at 2846 cm⁻¹ (CH₂ symmetric stretch), 2876 cm⁻¹ (CH₃ symmetric stretch), from 2923 (CH₂ Fermi resonance) to 2941 (CH₃ Fermi resonance) and at 3014 (CH olefinic stretch/ double bond). At 51 Å² per molecule and the monolayer undergoes a phase transition from a liquid-gas state to the liquid phase, this is evident as a series of peaks at 2850 cm⁻¹, 2880 cm⁻¹ and a broader peak at 2945 cm⁻¹ on the spectra which are characteristic of oleic acid, the spectra of oleic acid appeared as the surface pressure exceeded 0 mNm⁻¹. At 28 Å² per molecule at a surface pressure of 28 mN m⁻¹ the spectra shows a higher intensity peak at 2880 cm⁻¹ and a broader peak at 2945 cm⁻¹ than was observed at 51 Å² per molecule. The disordered structure of the monolayer at 83 Å² was shown by the absence of peaks characteristic of the C-H bonds as the sparse configuration of molecules in a gas phase monolayer is below the detection limit of the technique. Compressing the monolayer, packing the molecules into a more ordered state intensified the C-H peaks in the spectra, for a well ordered film the CH₃ peak at 2876 cm⁻¹ is the largest (Voss et al. 2007).

For oxidation experiments the monolayer was spread to 32 Å² (the equilibrium spreading pressure, 30 mNm⁻¹) in a petri dish contained in a closed cell and exposed to a flow of 20ppm ozone. After 1 minute of exposure to ozone the CH₃ peak at 2876 cm⁻¹ observed optically decreased in intensity (Voss et al. 2007). As the exposure time is increased the peaks in the spectra reduced until after an exposure time of 30 minutes there was no signal from the monolayer which had been oxidised and completely lost from the interface (Voss et al. 2007). Voss et al., (2007) used a complimentary technique of infrared reflection absorption spectroscopy (IRRAS), to show that the commonly observed reaction products from the oxidation of oleic acid by ozone were not present at the interface after the oxidation of oleic acid. In addition to the spectroscopy, Voss et al., (2007) observed the decline referred to in this thesis as a kinetic decay in surface pressure as the oleic acid monolayer on the Langmuir trough was oxidised. In contrast to the work of King et al., (2009) the surface pressure of the oleic acid monolayer declined to zero mN m⁻¹ under sustained exposure to 190 ±80 ppm ozone for 23 minutes. No information is given in Voss et al., (2007) as to how the Langmuir trough was enclosed for oxidation surface pressure experiments or of the ozone concentration at the interface.

Monolayers of oleic acid oxidation products, nonanoic acid, azalaic acid and nonanal were prepared in petri dishes by Voss et al., (2007) to see if a measurement could be obtained or if

the product had dissolved into the subphase or evaporated. BBSFG spectra could only be produced from nonanal when a quantity equivalent to three monolayers was spread at the air-water interface; this signal was not comparable to that of a partially oxidised oleic acid film (Voss et al. 2007). Voss et al., (2007) conclude that there was no organic material remaining at the air-water interface after the oxidation of an oleic acid monolayer with ozone, and that the changes in the BBSFG spectra during oxidation are comparable to the changes observed when the monolayer was compressed so are a product of the films packing and not caused by the production of surface active product molecules. Wadia et al, (2000) observed gas-phase nonanal above the Langmuir trough suggesting that this product would not be present at the air-water interface post reaction. Voss et al., (2007) saw complete removal of the oleic acid film under ozonolysis, King et al., (2009) did not.

3.6.2 Issues Identified in the Current Literature to be Investigated in This Work

The experiment described in this chapter may contribute further understanding of the following issues cited in the current literature.

- The conflicting results of Voss et al., (2007) and King et al., (2009) as to the presence of a monolayer following the exposure of oleic acid to ozone. King et al., (2009) concluded there was a significant surface coverage of material remaining at the air-water interface post reaction, Voss et al., (2007) concluded there was no monolayer remaining.
- The structural change in the orientation of the molecules at the air-liquid interface as the monolayer of oleic acid is oxidised.
- In chapter 2 it was demonstrated that the surface pressure and surface coverage were giving different information about the material at the interface. The amount of material present was not reflected in the surface pressure measurement, when the two measurements are correlated there is less need to use the expensive neutron reflectometry technique.

3.7 Experimental Methodology

It should be noted that the author was not present for the experiments detailed in this chapter. The methodology is based on the notes taken by the experimental team (Martin King, Adrian Rennie, Amelia Marks, Christian Pfrang and Richard Campbell). The author processed the data, conducted the analysis and drew conclusions following the data processing. The experimental section is presented in the following order:

- Experimental aims (3.7.1).
- A description of the oleic acid samples used for the neutron reflectometry experiments (3.7.2).
- A description of the FIGARO reflectometer at the Institut Laue Langevin, Grenoble, France used for the experimental work (3.7.3). A description is given of the surface measurement techniques (3.7.3.1) with an explanation of the effect of partial deuteration on the neutron reflectivity measurement (3.7.3.2) and the method of structural neutron reflectometry measurements (3.7.3.3).
- The generation of gas-phase ozone (3.7.4) and the modelling of the ozone reactant concentration in the gas-phase and in the monolayer (3.7.4.1).
- The methodology of a typical neutron reflectivity measurement of a kinetic decay in surface pressure of a monolayer reacting with a gas-phase reactant is given (3.7.5) and the materials used to conduct the experimental work are listed (3.7.5).
- An explanation of the kinetic fitting regime which was applied to the surface coverage data is given (3.7.6).

3.7.1 Experimental Objectives

The experiment was designed to monitor the properties of the surface pressure and the surface coverage of a monolayer of oleic acid ($C_{18}H_{33}COOH$), at the air-water interface in real time as the monolayer was oxidised with varied concentrations of gas-phase ozone.

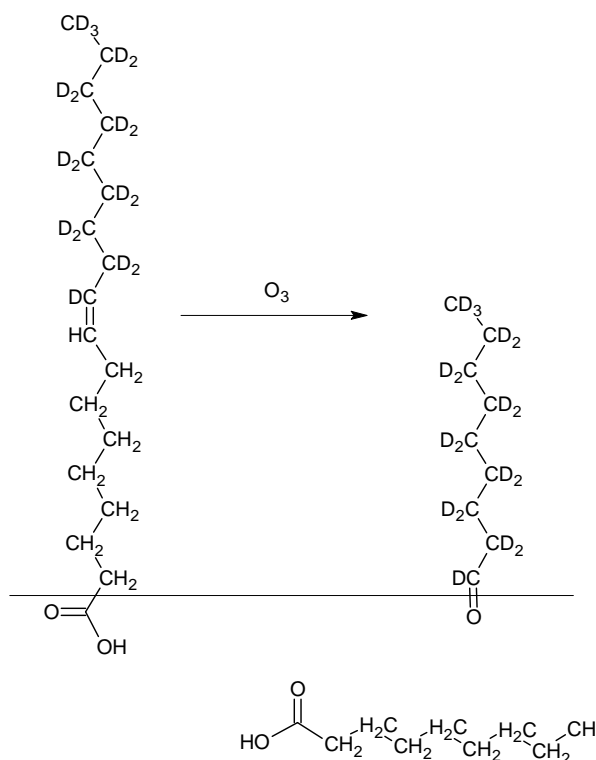
The objectives of the experiment conducted on FIGARO were;

1. To measure the decay in the surface coverage and the surface pressure of an oleic acid monolayer at the air-water interface simultaneously during a reaction with gas-phase ozone.
2. To ascertain whether an oleic acid monolayer persist at the air-water interface under sustained exposure to gas-phase ozone.

- To measure the decay of a monolayer comprised of oleic acid molecules which were deuterated from the double bond to the terminal CH_3 group (in this case CD_3), to show if the deuterated tail group remained at the air-water interface after ozone has reacted with the double bond in the oleic acid molecule.
- To subsequently conduct a kinetic analysis of the surface coverage of a monolayer of oleic acid over time to determine a rate constant for the reaction of oleic acid with gas-phase ozone.
- To model the lifetime of an oleic acid monolayer at the air-water interface of a cloud droplet under atmospheric conditions.

The aims were based on the hypothesis by King et al., (2009) that the cleavage of oleic acid at the double bond would leave a surface active monolayer comprised of shorter chain length product molecules which would be persistent to further reaction with ozone. This mechanism is illustrated in figure 3.4.

Figure 3.4 *The Decay of Oleic Acid Reacting with Gas-phase Ozone as Proposed by King et al. (2009)*



3.7.2 Oleic Acid Samples

In order to achieve the second experimental aim there were three oleic acid chemical samples used for this experiment. Deuterated oleic acid was not commercially available until 2010. Previous experiments on fully deuterated oleic acid (King et al. 2009;2010), used fully deuterated oleic acid ($C_8D_{17}CD=CDC_7D_{14}CO_2H$), synthesised by the Isotope Facility at Oxford University (named D_{33} fully deuterated oleic acid^a for simplicity). When deuterated oleic acid became commercially available from Sigma Aldrich a fully deuterated D_{33} sample was purchased for comparison to the King et al., (2009) sample, upon which to conduct further experiments. The Oxford University Isotope Facility synthesised a sample of partially deuterated ($C_8D_{17}CD=CHC_7H_{14}CO_2H$) oleic acid, (named D_{18} for simplicity), the sample provided the opportunity to see which half of the molecule persisted at the air-liquid interface during ozonolysis, and to show if the ozone attacked the double bond as expected. Each sample was made up to a concentration of 1 mg/mL^{-1} in chloroform as a spreading solution.

- D_{33} oleic acid, fully deuterated: custom synthesised by Robert Thomas at the Isotope Facility at Oxford University. The structure is shown in figure 3.4.
- D_{33} oleic acid, fully deuterated: Sigma Aldrich, product number 683582, lot number EW0201. The structure is shown in figure 3.5.
- D_{18} oleic acid, partially deuterated; custom synthesised by the Isotope Facility at Oxford University. The structure is shown in figure 3.6.

Figure 3.5 Structure of a D_{33} Oleic Acid Molecule

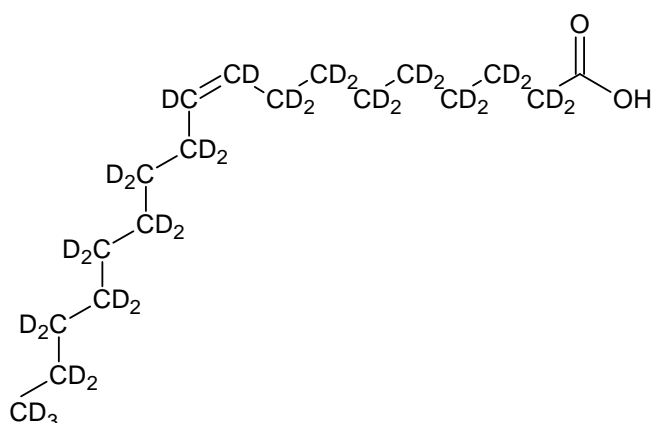
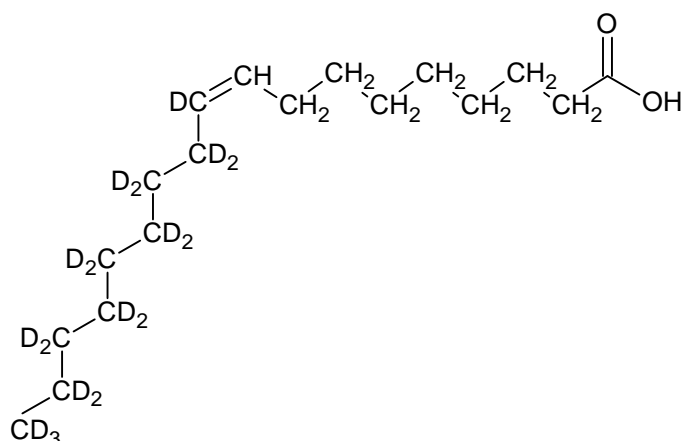
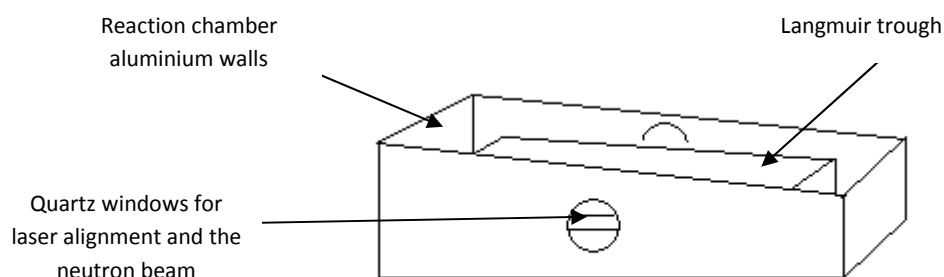


Figure 3.6 Structure of a D_{18} Oleic Acid Molecule

3.7.3 Surface Measurement Techniques

Both surface measurements of surface pressure and of surface coverage at the air-water interface were undertaken on a Langmuir trough simultaneously as explained in chapter 2. The neutron reflectivity measurement of reflectivity which is fitted to give a value of surface coverage (Γ) was required as the work of King et al., (2009) showed that when modelling the effects of surface tension and that of dissolved solutes in a cloud droplet according to Köhler theory, the dissolved product material from a reaction at the surface of the droplet has a greater effect on the critical supersaturation at which the droplet will grow than the surface tension effect on this process. Neutron reflectivity is the only technique by which a measure can be made of the hydrogen/deuterium composition of a monolayer at the air-liquid interface over time. By substituting hydrogen atoms with deuterium atoms one can highlight a portion of a molecule to see where the molecule breaks in a reaction, and whether that material persists at the air-liquid interface. The operation, calibration and cleaning of the Langmuir trough were as explained in chapter 2. The reaction chamber housing the Langmuir trough was custom made by the University of Reading to fit the neutron reflectometer FIGARO and is shown in figure 3.7. The chamber was designed as a prism trapezoid shape to reduce the chamber volume, therefore reducing the mixing time of reactant gases.

Figure 3.7 *The FIGARO Aluminium Reaction Chamber which Houses the Langmuir Trough on the Neutron Reflectometer Beamline Depicted Without the Chamber Lid*



3.7.3.1 The Neutron Reflectometer FIGARO

The surface coverage measurement of the deuterated oleic acid monolayer was determined from reflectivity measurements from the neutron reflectometer, FIGARO (Fluid Interfaces Grazing Angle Reflectometer) at the Institut Laue-Langevin (ILL), in Grenoble, France. The FIGARO reflectometer differs from the SURF reflectometer as SURF at ISIS uses a pulsed beam of neutrons produced by spallation as explained in chapter 2. At the Institut Laue-Langevin a beam of neutrons of a steady flux is produced from a nuclear reactor by nuclear fission of uranium-235. The data is comparable from both instruments as the measurement of reflectivity is a product of the momentum transfer (Q) of a pulse of neutrons of varying wavelengths. Both instruments measure the time of flight of a pulse, at ISIS this comes from the target as a pulse, at the ILL the pulse is created from the beam of neutrons by choppers which produce a gap in the beam. The reflectivity is measured on FIGARO as the change in intensity as on SURF; once the raw measurement is converted to R versus Q the measurements are comparable.

The flux of the transmitted neutron beam and its wavelength distribution are tuned to the experiment by the adjustment of two frame overlap mirrors which remove neutrons with a wavelength above 20 or 30 Å and four disc choppers which control the wavelength resolution (Campbell et al. 2011) creating a pulse of neutrons for time of flight measurements. The beam then travels through two deflector mirrors which determine the transmitted beam angle, between 0.62° and 3.8° , for this work an angle of 0.62° was used for measuring the kinetic decay in the surface coverage of the monolayer during a reaction. For structural measurements 2 angles were used (0.62° and 3.8°). A collimation guide removes off specular scattering of neutrons caused by the mirrors which are set to give the beam an orientation close to horizontal to the sample, in

this case the surface of the Langmuir trough. Before reaching the sample, the beam travels through a monitor which measures the intensity of the transmitted beam. The reflected beam intensity is then measured on a 2D ^3He aluminium mono-block multi tube detector which is positioned depending on the angle of incidence of the beam (Hall, 2010). The neutrons position along the tube is measured by charge division which causes the emission of a photon from the electrons (charge) produced reacting with the He_3 gas. The distance from the sample to the detector is 3 m (Campbell, 2010); a vacuum tube reduces interference over this distance as shown in figure 3.8.

The measurement of reflectivity versus momentum transfer is achieved by the time of flight method which is made possible by the choppers which make a gap in the beam so that time of arrival at the detector can be measured. The range in time of arrival of neutrons travelling at different speeds at the detector is converted into a range of momentum transfer statistics (Q). The momentum transfer data is plotted against reflectivity (R) data obtained from the change in intensity of the beam due to reflection from the sample. The data was then fitted to obtain a value of surface coverage (Γ) as explained in chapter 2.

The measurement of the surface coverage of the monolayer was as described in chapter 2. The technical set up of the instrument for example the settings of the beam choppers is different for each instrument but the experiment as conducted by the users of the instrument is essentially the same for both SURF and FIGARO for this work.

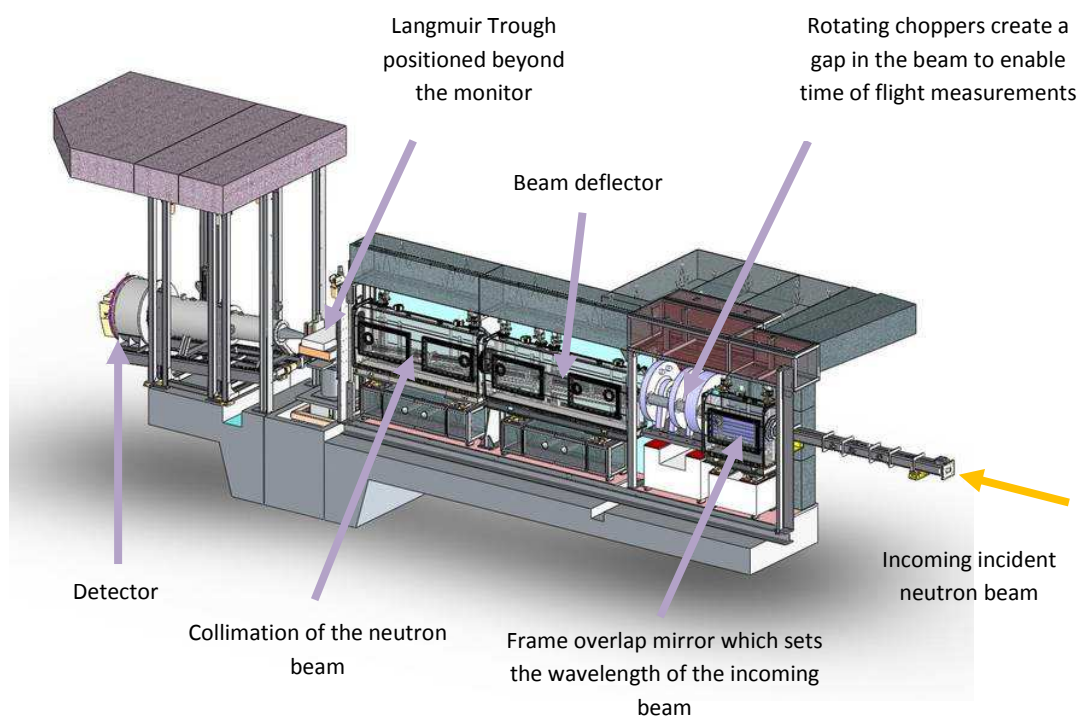
Figure 3.8 *The FIGARO Reflectometer*

Figure 3.8 was used with the permission of Richard Campbell (Dec 2010) from <http://www.ill.eu/instruments-support/instruments-groups/instruments/figaro/>. The figure has been modified to describe the set-up of the instrument for a Langmuir trough experiment. The labels were adapted from a similar figure from a Neutron News article by Harrison and Martinez (2009).

A brief comparison of the neutron reflectometers FIGARO and SURF is given in table 3.1 overleaf.

Table 3.1 *A Comparison of the Neutron Reflectometer SURF and FIGARO*

Specification	SURF	FIGARO
Angle of the incident beam (θ)	1.5°	0.62 and 3.8° *
Beam size at sample	60 x 10mm ²	40 x 10mm ²
Incoming beam wavelength	0.55 – 6.8 Å	2 -30 Å
Detector	He ³ scintillation detector	He ³ tubular aluminium monoblock
Distance detector to sample	2m	1 to 2.85 m
Q range	0.048 to 1.1 Å ⁻¹	0.005 to 0.3 Å ⁻¹
Volume of aluminium reaction chamber available to gas	45 L	26 L or 13.3 L with aluminium volume reducing inserts

Information in the table was taken from ISIS (2011^b), Campbell (2010), Campbell et al., (2011).

*FIGARO was operated at an incident beam angle θ of 0.62° for the kinetic measurements. Where structural measurements were taken for chapter 4 the 3.8° angle was also used. Both angles are used to determine the scale factor from the D₂O reflectivity measurement where a range of θ values are used.

The main difference in obtaining the kinetic decay of surface coverage measurements over time on FIGARO is that each measurement requires a shorter counting time of 60 to 300 seconds than on SURF where neutrons were counted for 300 up to 1200 seconds.

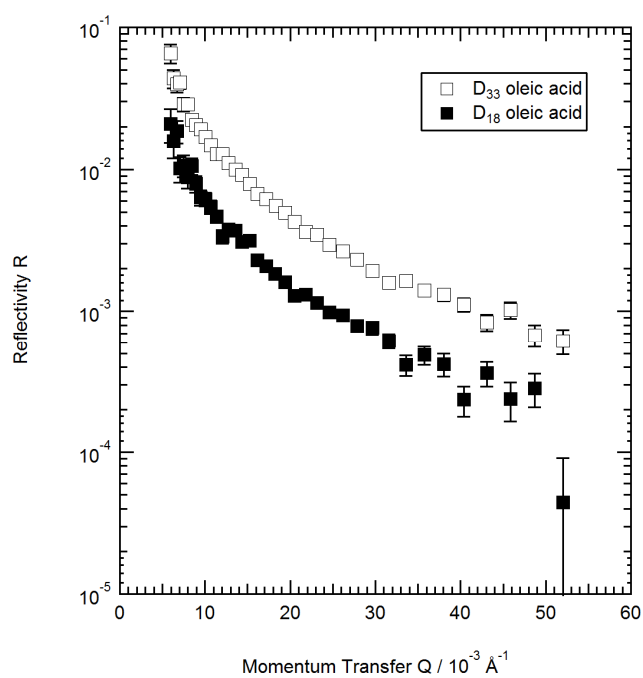
The background signal on FIGARO is approximately $1 \times 10^{-6} R(Q)$. Having the instruments collimation slits opened wider allowed a faster measurement period but increased the background signal from incoherent scattering. The treatment of the reflectivity data to obtain a value of surface coverage was as described in chapter 2 using the same Abelès fitting regime (Abelès, 1950).

3.7.3.2 The Effect of Partial Deuteration of a Monolayer on Neutron Reflectivity Measurements

A partially deuterated molecule produces less positive scattering of neutrons as it contains fewer deuterium atoms and more negative scattering as it contains more hydrogen atoms contributing to a lower reflectivity signal than the fully deuterated molecule as shown in figure 3.9.

The partially deuterated oleic acid molecule which is shown in figure 3.6 was used to show whether the molecule cleaving at the double bond would be visible to neutrons and if so how long the deuterated tail persisted at the air-liquid interface.

Figure 3.9 Reflectivity Versus Momentum Transfer (Q) for an Un-reacted Fully Deuterated Oleic Acid and Partially Deuterated Oleic Acid Monolayer in an O_2 Atmosphere



3.7.3.3 Obtaining Structural Neutron Reflectometry Measurements

To determine the effect of ozone exposure on the thickness of an oleic acid monolayer, reflectivity measurements were taken and the reflectivity data was fitted to a model describing the head group region and the hydrocarbon chain or tail region of the oleic acid molecule.

The incident angle of the neutron beam to the sample (θ), or the neutron wavelength determines the range of momentum transfer (Q). In order to measure a larger range of momentum transfer the incident angle of the beam to the horizontal sample is increased which gives a range of higher momentum transfer neutrons reaching the detector allowing measurement at lower reflectivity. For a spallation source such as ISIS the pulse of neutrons contains particles with different values of momentum transfer (Q). At the ILL the neutron beam is continuous so rotating discs with a gap; called choppers are used to create a time zero, gap in the beam for time of flight measurements. Both instruments operate in time of flight mode measuring a reflectivity spectrum of the energy of the neutrons reaching the detector versus the momentum transfer, $r(Q_z)$, of the neutrons.

When obtaining structural measurements a D_2O subphase is used as opposed to null reflective water in order to increase the reflectivity signal as D_2O acts like a mirror and reflects all the incident neutrons giving a larger number of counts on the detector. This optimises the scattering from the partially deuterated monolayer, using a D_2O subphase and measuring at a higher incident angle gives the reflectivity at higher values of momentum transfer which allows a more accurate structural fit to be obtained as the scattering length density of the deuterated sample can be better constrained. Measurements were taken at an incident angle (θ) of 0.62° and 3.8° .

The structural neutron reflectivity data was fitted in the program 'Lipid' that allows the head and tails of the molecule to be treated separately when inputting fitting parameters to the model which can fit several data sets simultaneously. Specifically the scattering length density for the head and tail can be fit individually taking into account mixing with the solvent / subphase (Rennie, 2011). The fully deuterated (D_{33}) oleic acid sample was measured on a subphase of null reflective water; the D_{18} sample was measured on a subphase of deuterium oxide (D_2O) to obtain a higher signal as this molecule contained fewer deuterium atoms therefore scatters neutrons less efficiently.

Figure 3.10 *The Four Layer Model Which the Lipid Fitting Regime Fits the Reflectivity to for Both Contrasts of a D₂O Subphase and a Null Reflecting Water Subphase*

Air	Air
Deuterated layer (hydrocarbon chain above the double bond)	Deuterated layer (hydrocarbon chain above the double bond)
Hydrogenated layer (head group and chain below the double bond)	Hydrogenated layer (head group and chain below the double bond)
D ₂ O subphase	Null Reflecting Water subphase

For structural measurements reflectivity data was collected at a constant surface pressure of 19 mNm⁻¹ and temperature of 24°C showing a comparison of the reflectivity of the Oxford Isotope Facility fully deuterated oleic acid and the partially deuterated sample synthesised at the same laboratory. The reflectivity data were fitted globally (all data sets fit simultaneously) using the physical properties of the molecule shown in table 3.2 to gain information on the thickness of the film (head and tail combined), the variation in the fit was in the parameter: scattering length density (head). The resulting fits to the reflectivity data are shown in figures 3.38 and 3.39 in the results section (3.8).

Table 3.2 *The Fitting Parameters Used to Fit the D_{18} and D_{33} Oleic Acid Monolayer Structural Reflectivity Data*

Fitting Parameter	Units	Value D_{18}	Step D_{18}	% Deviation D_{18}	Value D_{33}	Step D_{33}	% Deviation D_{33}
Scattering length density	Å	0	0	0	0	0	0
Scale factor	-	1	0	0	1	0	0
Fraction of air mixed with tails	-	0	0	0	0	0	0
Interfacial roughness	Å	2.5	0	0	2.5	0	0
Thickness (tail)	Å	7.803	0.1	7.61	7.803	0.1	7.61
Scattering length density tail	Å ² (1×10^{-6})	6.970	0.1	4.52	6.970	0.1	4.52
Interfacial roughness (tail)	Å	2.5	0	0	2.5	0	0
Scattering length density head	Å ² (1×10^{-6})	6.350	0	0	6.350	0	0
Thickness (head)	Å	5.593	0.1	3.77	5.593	0.1	3.77
Scattering length density (head)	Å ² (1×10^{-6})	-0.37	0	0	6.970	-107	4.52
Interfacial roughness (head)	Å	2	0	0	2	0	0
Fraction of solvent mixed with head group	-	0.4872×10^{-1}	-3.0	0	0.4872×10^{-1}	-3.0	0

3.7.4 Generating Gas-phase Ozone

The chloroform used for the spreading solutions and cleaning of the Langmuir trough was Sigma Aldrich, Chromasolv plus for HPLC 99.9% with ethanol stabilizer, catalogue number: 650471.

The Langmuir trough liquid subphase was made up from deuterium oxide which is recovered from the nuclear reactor at the ILL and from Millipore 18M Ω cm resistivity pure water to form null reflecting water (NRW) which has mole ratio of 0.088 mole D₂O in H₂O (Penfold and Thomas, 1990). This solution produces no specular reflection (Lu et al. 2000), so does not contribute to the change in signal produced by the deuterated monolayer during a reaction. Null reflecting water has a scattering length of zero to neutrons.

Bottled oxygen manufactured by Air Products of 99.5% purity was flowed rate of 5 L/min⁻¹ as monitored with a ball and valve flow meter, through Teflon tubing and stainless steel Swagelok connectors to an ozoniser creating a dilute flow of O₃ in O₂. The ozone / oxygen mixture flowed into the reaction chamber housing the Langmuir trough.

A UVP mercury pen ray discharge light source ozone generator, model 97-0067-02 was used to generate ozone. The ozoniser functions by emitting short wave 185nm radiation which photolyses the oxygen flowing past the lamp generating ozone, by reaction 3.8 and 3.9. The concentration of ozone was varied by shielding sections of the lamp reducing the intensity of radiation that the flow of oxygen was exposed to. The ozoniser and flow meter were calibrated by Christian Pfrang of the Department of Chemistry at the University of Reading. The ozoniser was calibrated by measuring the absorbance at 254 nm on a U.V. visible spectrometer, of the ozone produced at different levels of shielding in a cell. Royal Holloway University did not possess a U.V. visible spectrometer of adequate sensitivity to calibrate the ozoniser for these low concentrations of ozone.



3.7.4.1 Determining the Concentration of Ozone

The concentration of ozone in the reaction chamber was determined by calculating the flux of ozone into and out of the reaction chamber allowing calculation of the concentration within the chamber. The concentration of gas phase ozone in the chamber was then used to calculate a mixing time for ozone in the reaction chamber.

Calculating the volume of the reaction chamber available to the gas phase ozone requires the subtraction of the volume of the Langmuir Trough and its fittings. For the FIGARO beam line Langmuir trough the volume of the trough was estimated to be 20 L and the volume of the chamber available to the gas phase ozone was 26.2 L. The flow of gas within the chamber could not be assumed to be plug flow where the concentration would build up across the chamber from the entry point, instead the flow was considered to be a well-mixed reactor where the flow out of the chamber produces a well-mixed scenario where there is no significant concentration gradient within the chamber. The chemical reaction between the ozone and the monolayer consumes very little ozone so was not included in estimating the gas phase ozone concentration. The first order differential equations for calculating the ozone concentration within the reaction chamber are included in the appendix; item 1, solving these equations results in equation 3.1.

It was assumed that the gas phase ozone reacts with the monolayer rather than dissolved ozone which has entered the subphase. The air-water exchange of a gas is slow without agitation which was not present in this system. When the ozoniser is not engaged the reaction observed in the surface pressure data ceases in less than one minute suggesting that any dissolved ozone in the subphase is not contributing to the decay of the monolayer. To calculate the concentration of O_3 in the reaction chamber the following equation was used from Smith et al, (2002):

$$[O_3]_{chamber} = [O_3]_{ozonizer} \left(1 - e^{-\frac{Ft}{V}} \right) \quad (E 3.1)$$

Where F is the flow rate of O_3 into and out of the chamber (5 L min^{-1}). F was kept constant for each experiment. $[O_3]_{ozonizer}$ is the concentration of ozone in the flow F taken from the ozonizer calibration, which was varied for different experiments. V is the volume of the reaction chamber minus the volume of the Langmuir trough and fittings (26.2 L).

The time taken for the concentration of O_3 in the chamber to reach 38%, the characteristic mixing time (t_{mix}) was determined by dividing the volume of the chamber (less the volume of the Langmuir trough) of 26.2 L divided by the flow rate which was 5 L min^{-1} (equation 3.2). The characteristic mixing time was 314 seconds. This value is important for the kinetics as fits

should be taken after the characteristic mixing time. 314 seconds is a long mixing time suggesting that for future work it would be best to aid the mixing process, for the work detailed in chapter 5 the volume of the chamber was reduced using hollow aluminium boxes which fitted around the Langmuir trough, reducing the characteristic mixing time.

$$t_{mix} = \frac{V}{F_{rate}} \quad (E 3.2)$$

For the kinetic analysis the concentration of ozone within the film region was calculated by equation 4.11.

$$O_{3\ film} = [O_{3\ chamber}]H\delta_{film} \quad (E 3.3)$$

The ozone concentration in the film region $O_{3\ film}$ is equal to the gas phase ozone concentration in the chamber ($O_{3\ chamber}$) multiplied by H , the Henrys law constant for ozone (11.75 molecule cm^{-3} (molecule $\text{cm}^{-3})^{-1}$), multiplied by the thickness of the monolayer (δ_{film}), 15 Å. The ozone concentrations in the film region are listed in table 3.3

Table 3.3 *The Ozone Concentration in the Monolayer Tail Region as Calculated From Equation 3.3, and the Calibration of the Ozoniser.*

Ozone Concentration from the Ozoniser [O ₃] _{ozonizer} / ppb	Gas Phase Ozone Concentration [O ₃] _{chamber} / ppb	Gas Phase Ozone Concentration [O ₃] _{chamber} / (10 ¹² molecules cm ⁻³)	Ozone Concentration in the Monolayer Region [O ₃] _{film} / (10 ⁸ molecules cm ⁻²)
26.6 ± 5.04	4.62 ± 0.88	11.6 ± 2.20	0.204 ± 0.039
37 ± 9.03	6.43 ± 1.57	16.1 ± 3.94	0.284 ± 0.069
51.9 ± 14.75	9.02 ± 2.56	22.6 ± 6.43	0.399 ± 0.113
67.4 ± 22.86	11.7 ± 3.97	29.4 ± 9.97	0.518 ± 0.176
119.9 ± 5.19	20.83 ± 0.90	52.3 ± 2.26	0.921 ± 0.040
154.1 ± 19.61	26.77 ± 3.41	67.2 ± 8.55	1.18 ± 0.151
225.5 ± 43.22	39.18 ± 7.51	98.3 ± 18.8	1.73 ± 0.332
298.5 ± 8.92	51.86 ± 1.55	130 ± 3.89	2.29 ± 0.069
384.8 ± 83.91	66.85 ± 14.6	168 ± 36.6	2.96 ± 0.645
680.3 ± 73.22	118.19 ± 12.7	297 ± 31.9	5.23 ± 0.563

The gas-phase ozone concentrations in parts per billion are provided for comparison to atmospheric ozone concentrations.

3.7.5 The Experimental Methodology of a Typical Neutron Reflectivity Experiment with a Gas-phase Reactant

As explained in chapter 2 the neutron surface coverage and Wilhelmy plate surface pressure measurements were collected simultaneously using a Langmuir trough housed in an aluminium reaction chamber which was fitted to the neutron beamline. The Langmuir trough used for the experiments was the FIGARO beamline Langmuir trough, which is a custom model manufactured by Nima Technology. Its dimensions were: depth 0.5 cm, width 20 cm, length 50 cm. The aluminium reaction chamber is shown in figure 3.7, its dimensions were: maximum height 18.5 cm, width 39 cm, length 64 cm.

The Langmuir trough was cleaned and calibrated according to the procedures explained in chapter 2. The Langmuir trough was filled with 600 mL of null reflective water and a 40 μL monolayer of deuterated oleic acid was spread at the air-water interface using a 50 μL capacity Hamilton syringe. The film was spread drop by drop at different points across the surface by placing the needle very close to the surface but not touching it and allowing the drop (at the end of the needle) to make contact with the surface, the initial surface pressure reading was 12 mNm^{-1} . The area per molecule was 43.7 \AA^2 prior to compression for a monolayer of 40 μL of fully deuterated oleic acid.

The subphase temperature was maintained at 24-25°C using a temperature controlled circulating water bath which was attached to an integrated cooling system in the base of the Langmuir trough. pH papers were used to monitor the pH of the null reflective water (pH 5.5). Oxygen was flowed at 5L min^{-1} from a bottle through Teflon tubing via the UVP pen-ray ozoniser which at this point had its lamp fully shielded so was not producing ozone. The oxygen flowed from the ozonizer into the reaction chamber through tubing with Swagelok connectors. The flow entered the chamber through a tube which was positioned above the Langmuir trough facing away from the monolayer.

The monolayer was spread and then compressed to a surface pressure of 25 mN m^{-1} . When the monolayer was at the desired surface pressure the barriers were held, the chamber lid was fixed on to provide a gas tight seal and the neutron instrument was started ready to take measurements of surface coverage. There is a short delay between the start of the surface pressure measurement and the time when the first neutrons reach the sample to accrue a surface coverage measurement whilst the radiation shielding interlock is engaged prior to the neutron beam reaching the sample.

Once the initial surface coverage had been recorded for a monolayer the ozone supply was activated by reducing the shielding covering the lamp. The ozone was flowed through the same tubing as the oxygen at the same rate, into the reaction chamber to react with the oleic acid monolayer.

3.7.6 Kinetics of the Reaction of an Oleic Acid Monolayer with Gas Phase Ozone

3.7.6.1 The Decay Mechanism

The decay in the surface coverage of a monolayer of deuterated oleic acid at the air-water interface follows exponential behaviour whereby the decay curve shallows exponentially as observed by King et al., (2009).

The rate expression for the reaction of a deuterated oleic acid monolayer with gaseous phase O_3 is;



$$\frac{-d[C_{18}D_{33}O_2H]}{dt} = k[C_{18}D_{33}O_2H]^\alpha [O_3]^\beta \quad (E 3.5)$$

Where α and β are exponents which are determined experimentally, the sum of which determines the order of the reaction. The reaction was pseudo first order. The same expression is appropriate to the partially deuterated molecule as the kinetics were not affected by the deuteration. The change in the surface concentration (surface coverage) of oleic acid is described by equations 3.6 to 3.8:

$$\frac{d[oleic\ acid]}{dt} = \frac{dr}{dt} \quad (E 3.6)$$

$$\frac{dr}{dt} = k[\Gamma][O_3] \quad (E 3.7)$$

$$\frac{dr}{dt} = k\Gamma[O_3] \quad (E 3.8)$$

It is assumed that the concentration of ozone is constant during the reaction. Solving equation 3.9 gives the rate of change in the surface coverage with time.

$$k' = k[O_3] \quad (E 3.9)$$

$$\frac{dr}{dt} = k'\Gamma \quad (E 3.10)$$

$$\Gamma_t = \Gamma_{final} + \Gamma_0 e^{-k'(t-t_0)} \quad (E 3.11)$$

3.7.6.2 The Method of Kinetic Analysis

The surface coverage data was fitted to an exponential decay mechanism which allows the start point of the reaction to be defined after the mixing time for ozone in the reaction chamber had been reached. The kinetic decay data of the surface coverage of the deuterated monolayer material with reaction time was fitted to equation 3.11.

$$\Gamma_t = \Gamma_{final} + \Gamma_0 e^{-k'(t-t_0)} \quad (E\ 3.11)$$

Where Γ_t was the surface coverage at the air-liquid interface at time t , Γ_{final} was the surface coverage at the air-liquid interface at the end of the reaction, Γ_0 was the surface coverage at the air-liquid interface before the reaction and k' was the first order rate constant for the decay in the surface coverage of the deuterated material at the air-liquid interface. In chapter 5 for the reaction between a methyl oleate monolayer and gas phase ozone an alternative kinetic regime was used which incorporated an estimation of the mixing time for ozone in the reaction chamber. The reasoning for using a different fitting regime for the data in this chapter to that used for the experiments in chapter 5 is given in appendix item 3.

From the results of the neutron reflectivity experiments it was decided that the behaviour of the system was pseudo first order where oleic acid reacted with ozone producing reaction products which were soluble or volatile and did not persist at the air-liquid interface so an exponential decay could be fit to the data. This was in contrast to the kinetic analysis of King et al., (2009) where there was material remaining at the air-liquid interface after the reaction of ozone with the monolayer.

A simple exponential was fitted to the decay in the surface coverage of d-oleic acid at the air-liquid interface, these fits fall into three categories.

1. A simple exponential fit to the decay curve of deuterated oleic acid with time as deuterated oleic acid is lost from the interface.
2. At low ozone concentrations a shallowing of the decay curve occurred mid decay which is referred to as an inflection feature herein. An exponential fit was made to the first part of the decay curve prior to the inflection feature in the surface coverage data. A subsequent exponential was fitted to the decay curve after the region of inflection.
3. The oleic acid monolayer was allowed to decay in the presence of ozone and was subsequently recompressed to show whether the inflection feature was related to a chemical change or a structural phenomenon. An initial exponential fit was taken of the first decay curve, and then after recompression as the surface coverage decayed again

an exponential fit was taken before and after the region of inflection in the surface coverage data.

The exponential kinetic fitting to the surface coverage data is plotted over the surface coverage data in the results section (3.8).

3.8 Experimental Results

The experiments were conducted at a range of gas-phase ozone concentrations to facilitate the calculation of a bimolecular rate constant from the surface coverage measurements. The decay in the surface coverage and surface pressure of fully deuterated and partially deuterated oleic acid samples were monitored in order to determine whether the decay kinetics were significantly different enough to show whether the oleic acid molecule was broken at the double bond leaving a product film that was persistent at the air-water interface as hypothesised by King et al., (2009).

Surface coverage data was collected for fully and partially deuterated monolayers on a pH altered subphase to show whether OH radical forming as a result of ozone dissolving into the subphase was causing the observed loss of oleic acid. Structural neutron reflectivity measurements were also taken of each oleic acid sample for comparison between samples and to measure the monolayer thickness.

The simultaneous neutron surface coverage (Γ) and monolayer surface pressure measurements (Π), will be presented in the following order with kinetic fits of the surface coverage measurements to equation 3.11 shown with the relevant neutron reflectometry data.

The surface pressure and surface coverage data is presented together in the following order:

- Fully deuterated (D_{33}) and partially deuterated (D_{18}) oleic acid monolayers with high gas-phase ozone concentrations of $(130 \pm 3.89) \times 10^{12}$ molecules cm^{-3} to $(297 \pm 31.9) \times 10^{12}$ molecules cm^{-3} representative of a polluted urban air mass (3.8.1).
- Fully deuterated and partially deuterated oleic acid monolayers with low gas-phase ozone concentrations of $(11.6 \pm 2.20) \times 10^{12}$ molecules cm^{-3} to $(98.3 \pm 18.8) \times 10^{12}$ molecules cm^{-3} representative of a marine or rural environment (3.8.2).
- The decay of fully and partially deuterated oleic acid monolayers in oxygen (3.8.3).
- The surface pressure and surface coverage of fully and partially deuterated oleic acid monolayers on a pH adjusted subphase exposed to gas-phase ozone (3.8.4).
- A summary of the surface coverage and surface pressure measurement results (3.8.5).
- The results of structural neutron reflectivity measurements of fully deuterated and partially deuterated oleic acid monolayers at the air-water interface (3.8.6).
- Kinetic analysis and results (3.8.7).

3.8.1 The Surface Pressure and Surface Coverage of Fully Deuterated Oleic Acid Monolayers Exposed to High Concentrations of Gas-phase Ozone

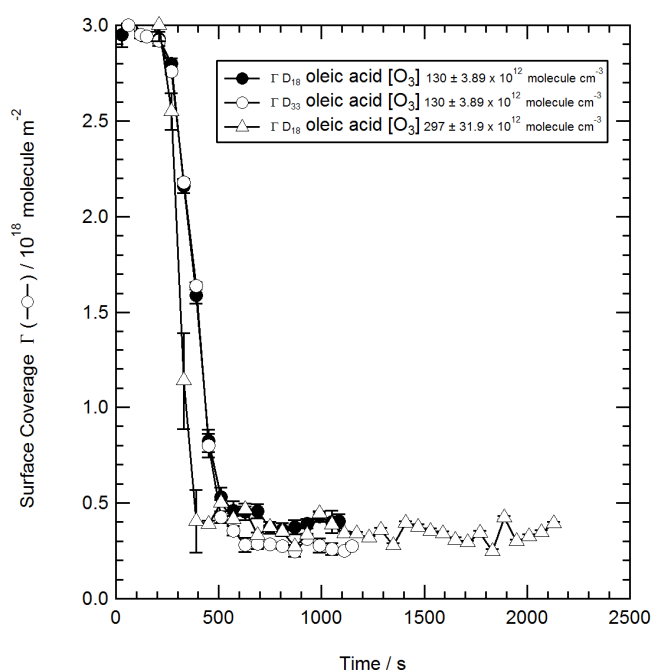
Three experiments were conducted on fully deuterated oleic acid monolayers at high gas phase ozone concentrations in order to measure the decay in the surface pressure and surface coverage of the monolayer. The surface coverage and surface pressure data for these experiments are shown in figures 3.11 to 3.14. The corresponding gas phase ozone concentration and the concentration of ozone in the tail region of the monolayer are listed in table 3.4.

Table 3.4 *The Concentrations of Gas-Phase and Monolayer Region Ozone Used in the High Ozone Experiments*

Gas Phase Ozone Concentration / 10^{12} molecule cm^{-3}	Ozone Concentration in the Monolayer / 10^8 molecule cm^{-2}
130 ± 3.89	2.29 ± 0.069
297 ± 31.9	5.23 ± 0.563

The kinetic fits to the surface coverage data are given in figures 3.15 to 3.17.

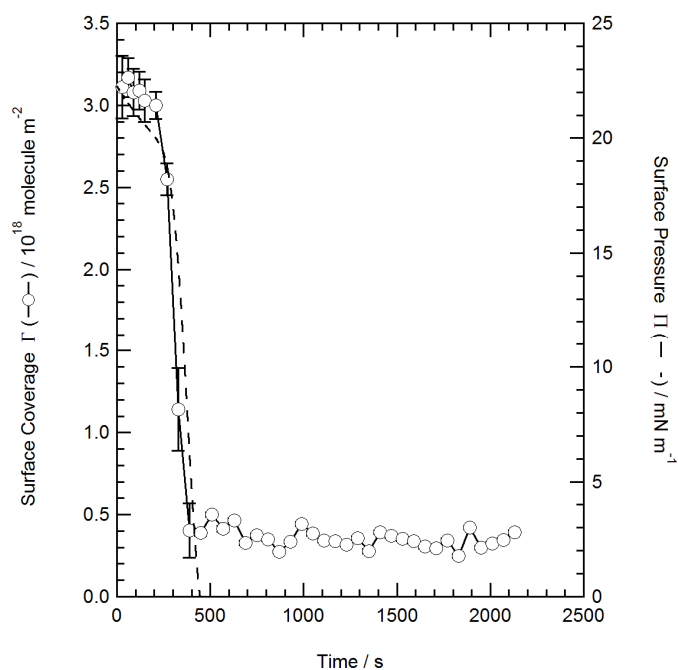
Figure 3.11 A Comparison of the Surface Coverage Data from the High Ozone Concentration Experiments



At high ozone concentrations the decay of the D₃₃ (Sigma Aldrich) monolayer exposed to $297 \pm 31.8 \times 10^{12}$ molecules cm^{-3} decayed to a surface coverage of 0.5×10^{18} molecule m^{-2} approximately 110 seconds faster than the D₃₃ monolayer exposed to the slightly lower ozone concentration of $130 \pm 3.89 \times 10^{12}$ molecules cm^{-3} .

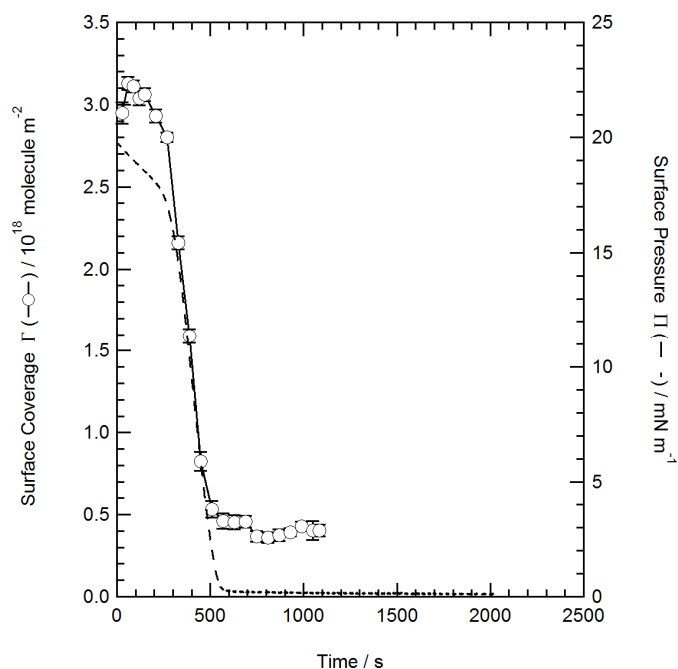
The D₁₈ oleic acid (Oxford Isotope Facility) monolayer exposed to a gas phase ozone concentration of $130 \pm 3.89 \times 10^{12}$ molecules cm^{-3} decayed in an identical fashion to the D₃₃ monolayer until the surface coverage reached 0.4×10^{18} molecule m^{-2} at which the D₃₃ monolayer decayed slightly further to a lower residual surface coverage of 0.3×10^{18} molecule m^{-2} . The deuterated products of the reaction may vary causing the decay curve from 500 seconds onwards differ where the partially deuterated oleic acid has decayed but there is still a signal above zero, so there is still deuterated material present at the air-liquid interface.

Figure 3.12 *The Surface Coverage and Surface Pressure Data for a D_{18} Oleic Acid Monolayer Reacting with $(297 \pm 31.8) \times 10^{12}$ molecules cm^{-3} Gas-Phase Ozone*



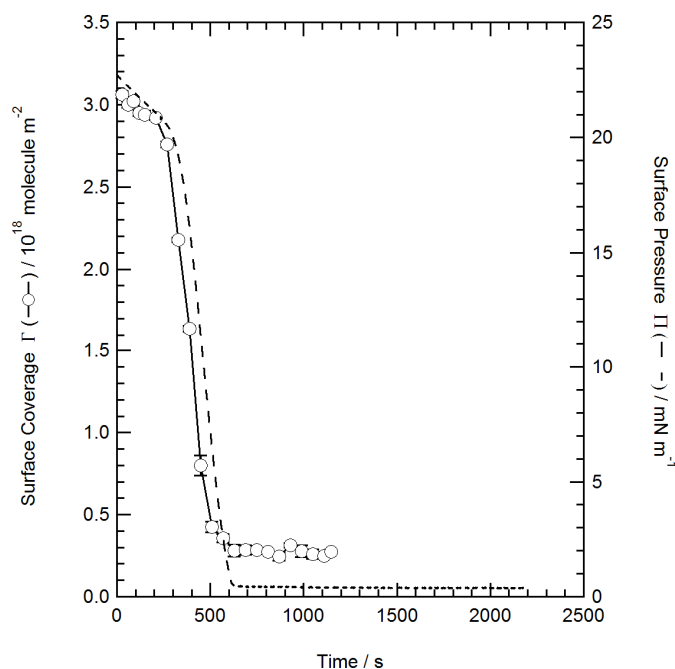
The most rapid decay in the surface pressure and surface coverage of an oleic acid monolayer was measured at the highest ozone concentration shown in figure 3.12. The partially deuterated oleic acid monolayer left a residual surface coverage of $\sim 0.4 \times 10^{18}$ molecule m^{-2} even when reacting with a very high concentration of ozone.

Figure 3.13 *The Surface Coverage and Surface Pressure Data for a D_{18} Oleic Acid Monolayer Reacting with $(130 \pm 3.89) \times 10^{12}$ molecule cm^{-3} Gas-Phase Ozone at 24°C*



At an ozone concentration of $(130 \pm 3.89) \times 10^{12}$ molecules cm^{-3} the surface pressure data appeared to follow the decay in surface coverage. The slope in the decay of surface pressure and surface coverage is very similar at this concentration for both isotopologues of oleic acid. Both the fully deuterated and partially deuterated monolayer leave a residual surface coverage of deuterated material at the air-water interface which is not reflected in the surface pressure data.

Figure 3.14 *The Surface Coverage and Surface Pressure Data for a D_{34} Oleic Acid Monolayer Reacting with $(130 \pm 3.89) \times 10^{12}$ molecule cm^{-3} Gas-Phase Ozone at 24°C*



In both the surface pressure and the surface coverage data it can be seen that a steeper decay occurred at the highest ozone concentration. Recompressing the Langmuir trough barriers after a reaction did not produce a rise in the surface pressure which remained at zero.

It was concluded that the ozone concentration used here was not ideal for kinetic analysis as there were few points to fit to before the reaction of ozone with the oleic acid monolayer was over. Kinetic fits of equation 3.11 to the surface coverage data are shown in the following plots. As shown in figure 3.15 to 3.17 the kinetic fit could only be achieved for part of the decay curve which consisted of few measurements as the reaction proceeded too rapidly at high ozone concentrations to achieve a good kinetic fit.

Figure 3.15 A Kinetic Fit of Equation 3.11 to the Kinetic Decay in the Monolayer Surface Coverage of D_{18} Oleic Acid Exposed to $(297 \pm 31.9) \times 10^{12}$ molecule cm^3 Ozone in the Gas-Phase and a Concentration of $(5.23 \pm 0.56) \times 10^8$ molecule cm^{-2} Ozone in the Monolayer Tail Region

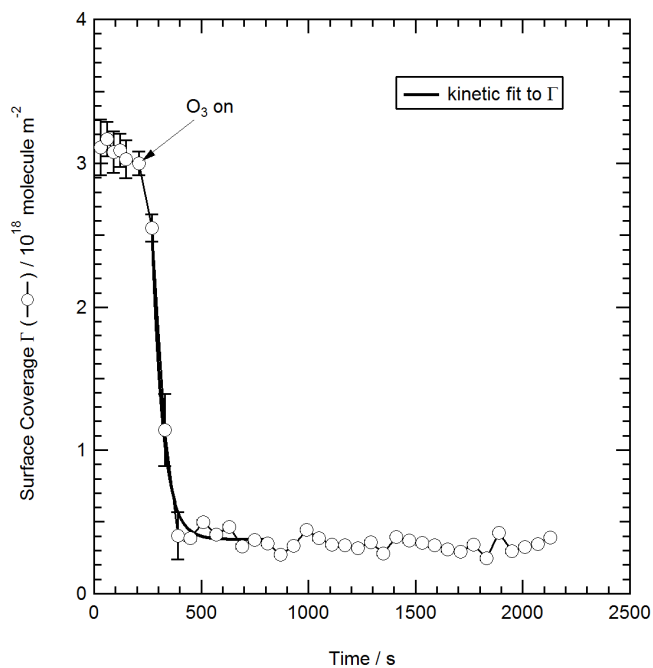


Figure 3.16 A Kinetic Fit of Equation 3.11 to the Kinetic Decay in the Monolayer Surface Coverage of D_{18} Oleic Acid Exposed to $(130 \pm 3.89) \times 10^{12}$ molecule cm^3 Ozone in the Gas-Phase and a Concentration of $(2.29 \pm 0.07) \times 10^8$ molecule cm^{-2} Ozone in the Monolayer Tail Region

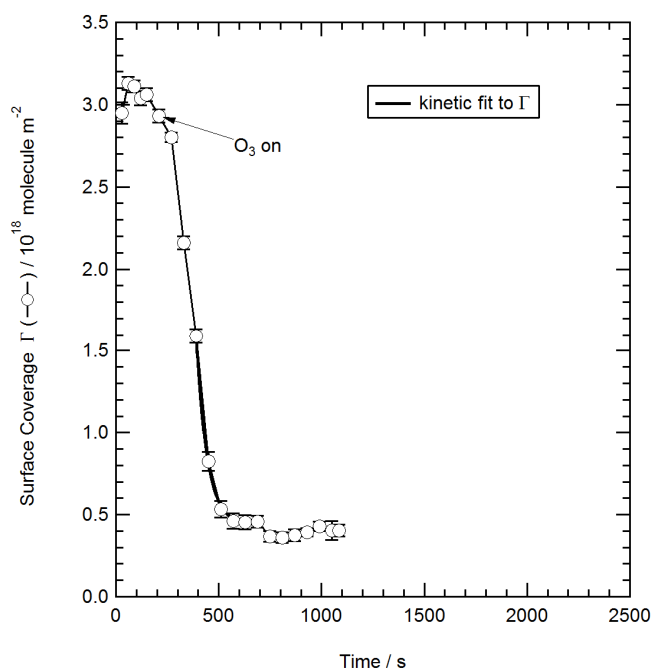
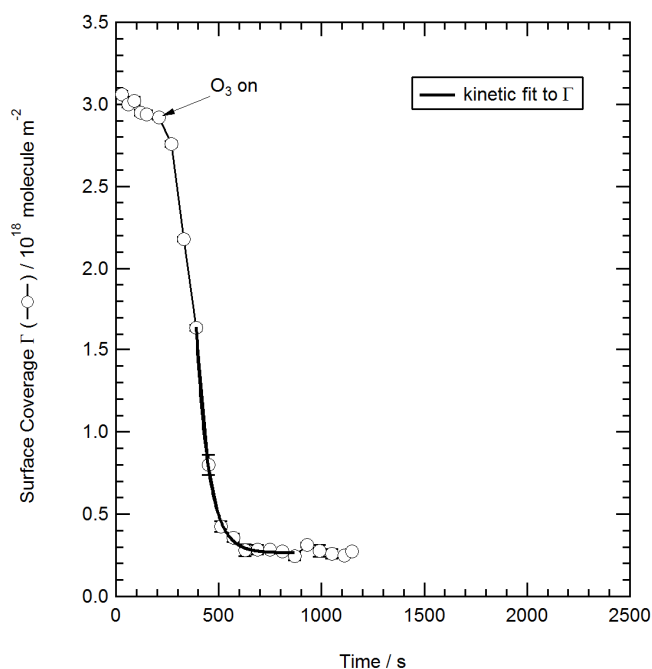


Figure 3.17 A Kinetic Fit of Equation 3.11 to the Kinetic Decay in the Monolayer Surface Coverage of D_{33} Oleic Acid Exposed to $(130 \pm 3.89) \times 10^{12}$ molecule cm^3 Ozone in the Gas-Phase and a Concentration of $(2.29 \pm 0.07) \times 10^8$ molecule cm^{-2} Ozone in the Monolayer Tail Region



3.8.2 The Surface Pressure and Surface Coverage of Fully and Partially Deuterated Oleic Acid Monolayers Exposed to Low Concentrations of Gas-phase Ozone

The lower experimental ozone concentrations used for experiments of fully deuterated and partially deuterated oleic acid are given in table 3.5. In total for both D_{33} and D_{18} oleic acid monolayers seven experiments were undertaken at low gas phase concentrations of ozone. The surface coverage and surface pressure data is shown in figure 3.18.

Table 3.5 The Gas-Phase and Monolayer Region Concentrations of Ozone Used in the Low Ozone Experiments

Gas Phase Ozone Concentration / 10^{12} molecule cm^{-3}	Ozone Concentration in the Monolayer Region / 10^8 molecule cm^{-2}
11.6 ± 2.20	0.204 ± 0.039
16.1 ± 3.94	0.284 ± 0.069
29.4 ± 9.97	0.518 ± 0.176

The decay of the fully deuterated monolayer appears to be faster with increasing gas phase ozone concentration. In figure 3.18 the surface coverage data for both the partially and fully deuterated oleic acid monolayer are shown together for comparison. The rate of the kinetic decay is explained and discussed in section 3.8.7.

Figure 3.18 *The Kinetic Decay in the Surface Coverage of D_{33} and D_{18} Oleic Acid Monolayers Exposed to Low Concentrations of Gas-Phase Ozone*

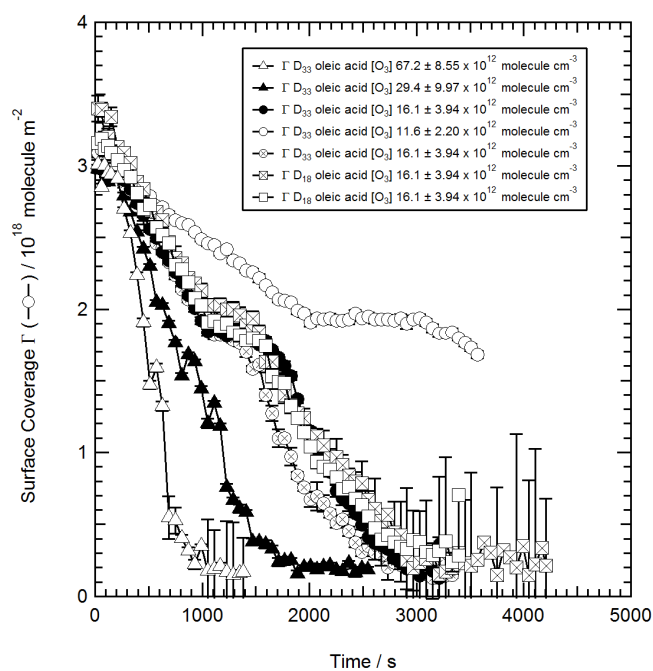


Figure 3.18 shows at a surface coverage of $\sim 2 \times 10^{18}$ molecule m^{-2} a shallowing of the kinetic decay in the monolayer surface coverage for a short period followed a subsequent continuation of the decay of the monolayer. The feature is most pronounced at the lowest ozone concentration and is referred to as an inflection feature in the analysis of these results. It can be seen in figure 3.18 that the inflection feature was repeatable at low ozone concentrations. The individual experiments are shown over the following pages with kinetic fitting of equation 3.11 to the surface coverage data.

Figure 3.19 *The Kinetic Decay of Fully Deuterated Oleic Acid in an Atmosphere of $(67.2 \pm 8.55) \times 10^{12}$ molecule cm^{-3} O_3*

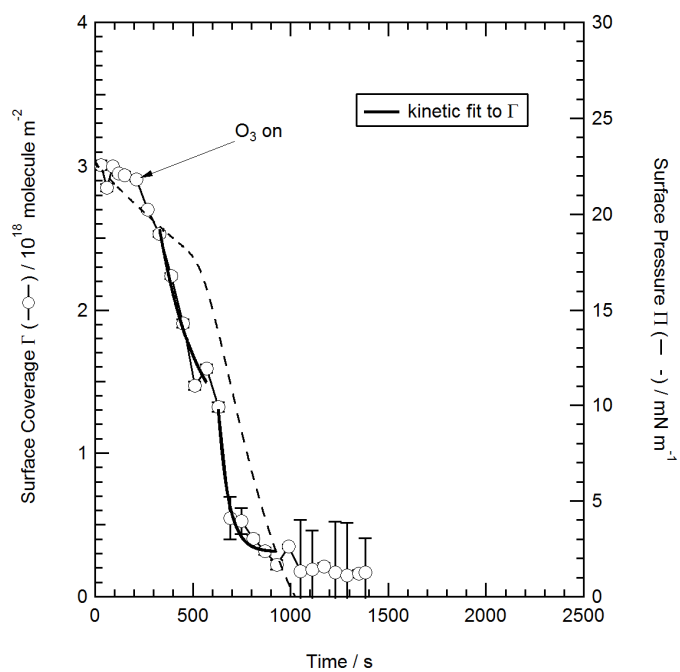
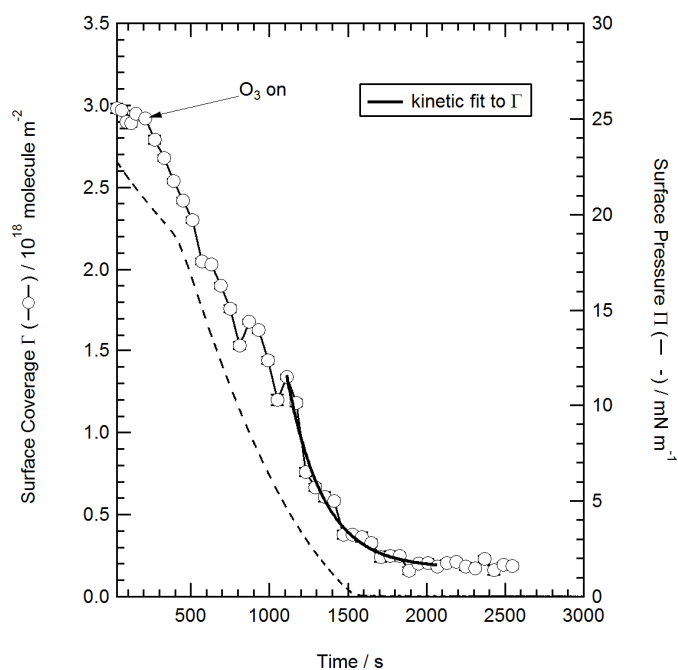


Figure 3.20 *The Kinetic Decay in the Surface Coverage of a D_{33} Oleic Acid Monolayer Exposed to $(29.4 \pm 9.97) \times 10^{12}$ molecule cm^{-3} Ozone in the Gas-Phase*



At a gas -phase ozone concentration of $29.4 \pm 9.97 \times 10^{12}$ molecule cm^{-3} a kinetic fit of equation 3.11 could only be achieved for the region of the decay curve beneath the inflection feature.

Figure 3.21 *The Kinetic Decay in the Surface Coverage of a D₃₃ Oleic Acid Monolayer Exposed to $(16.1 \pm 3.94) \times 10^{12}$ molecule cm⁻³ Ozone in the Gas-Phase*

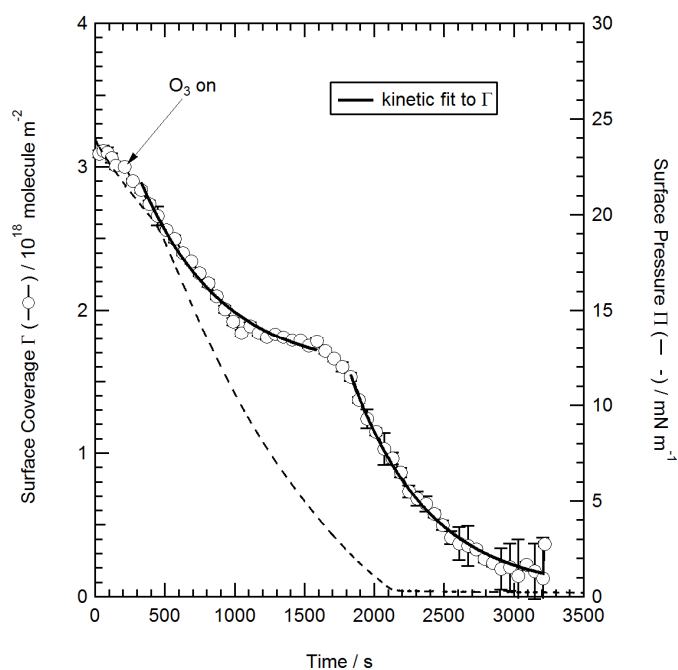


Figure 3.22 *The Kinetic Decay in the Surface Coverage of a D₃₃ Oleic Acid Monolayer Exposed to $(16.1 \pm 3.94) \times 10^{12}$ molecule cm⁻³ Ozone in the Gas-Phase*

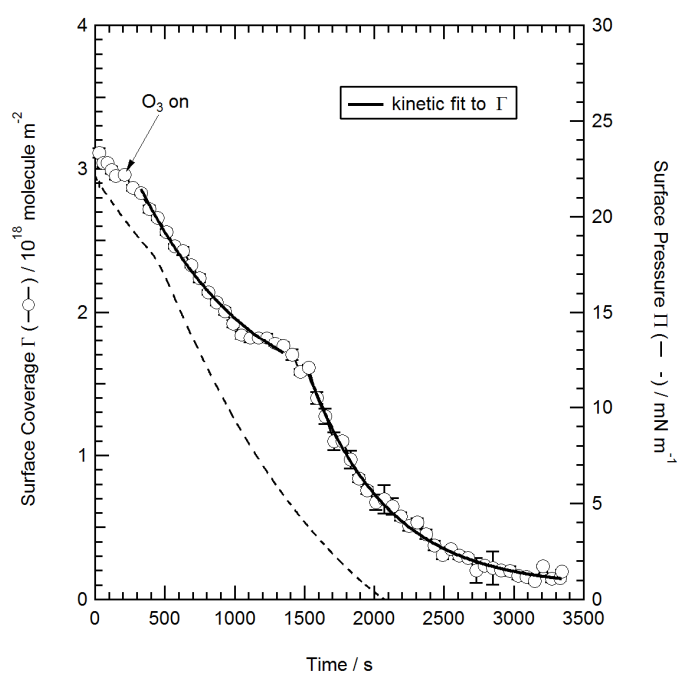


Figure 3.23 *The Kinetic Decay in the Surface Coverage of a D_{33} Oleic Acid Monolayer Exposed to $(11.6 \pm 2.20) \times 10^{12}$ molecule cm^{-3} Ozone in the Gas-Phase*

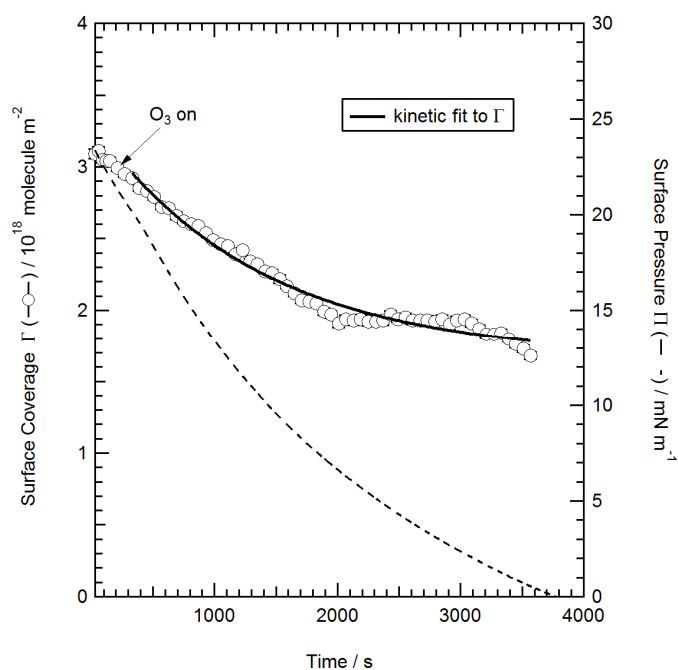


Figure 3.24 *The Kinetic Decay in the Surface Coverage of a D_{18} Oleic Acid Monolayer Exposed to $(16.1 \pm 3.94) \times 10^{12}$ molecule cm^{-3} Ozone in the Gas-Phase*

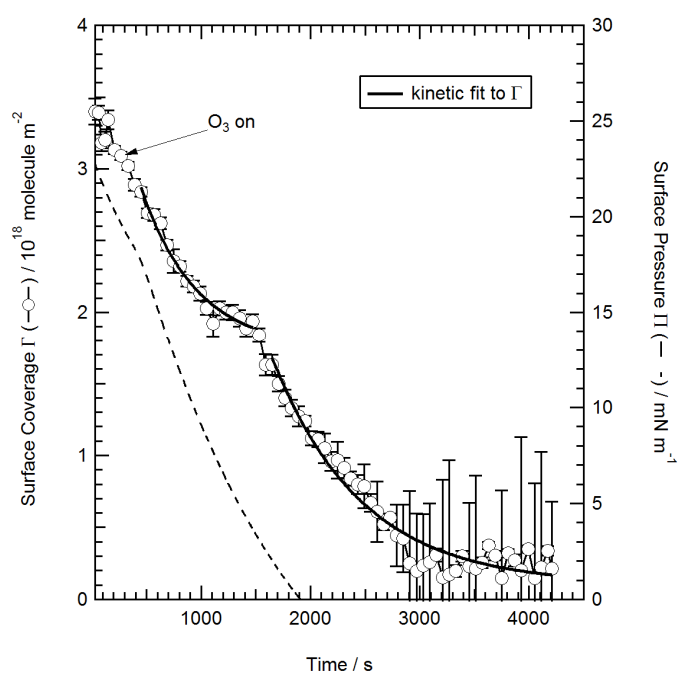
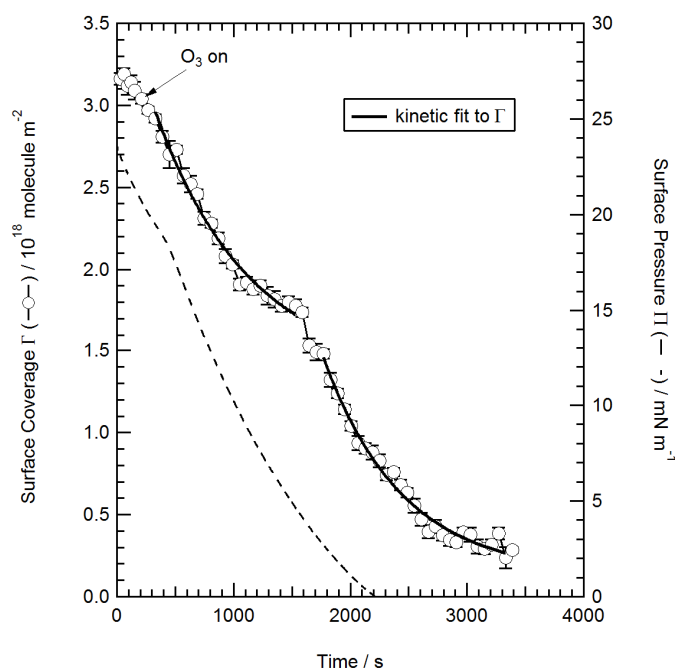


Figure 3.25 *The Kinetic Decay in the Surface Coverage of a D_{18} Oleic Acid Monolayer Exposed to $(16.1 \pm 3.94) \times 10^{12}$ molecule cm^{-3} Ozone in the Gas-Phase*

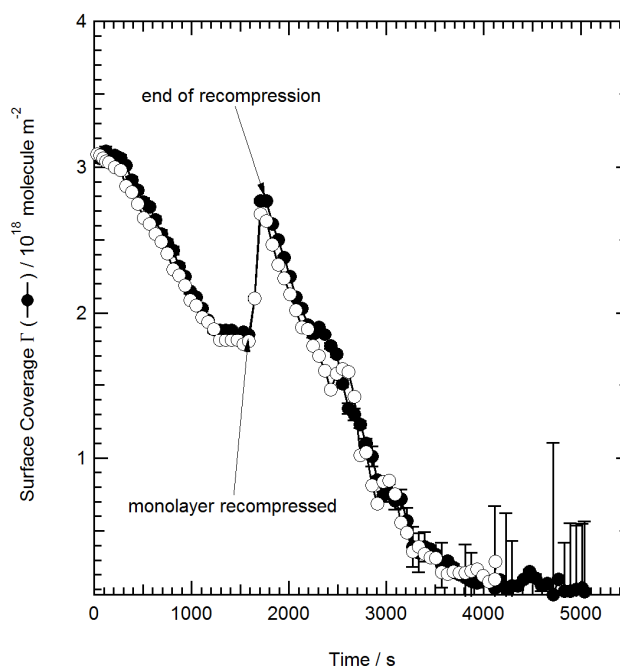


With decreasing ozone levels the behaviour of the surface pressure was very different to that of the surface coverage, the surface pressure showed a more rapid, smooth featureless decay than the surface coverage. At $(11.6 \pm 2.20) \times 10^{12}$ molecule cm^{-3} ozone the surface coverage showed a longer inflection feature appearing later in the kinetic decay from 2000 to 3700 seconds, than at $(16.1 \pm 3.94) \times 10^{12}$ molecule cm^{-3} ozone where the plateau appeared at 1100 seconds to 1600 and 1800 seconds. The repeat measurement of a fully deuterated oleic acid monolayer exposed to $(16.1 \pm 3.94) \times 10^{12}$ molecule cm^{-3} ozone showed more variability in the length of the inflection than the partially deuterated monolayer which repeatedly lasted for 800 seconds. It would be desirable to obtain further repeats of this measurement but this was not possible in the time allocated on the FIGARO instrument.

The fully deuterated monolayer was recompressed to see whether the inflection of the kinetic decay as seen at an ozone concentration of $(16.1 \pm 3.94) \times 10^{12}$ molecule cm^{-3} was a feature of the oleic acid molecule breaking up or whether the molecules were lying horizontally at the surface producing the change in the rate of decay of the surface coverage in the middle of the experiments. By recompressing by closing the Langmuir trough barriers, the molecules in the monolayer are re-orientated with the chain into the air as an ordered monolayer. If the chain had been broken by ozone oxidation then the decay post recompression could be expected to be different in shape to that of the initial decay of the oleic acid monolayer. The decay of the

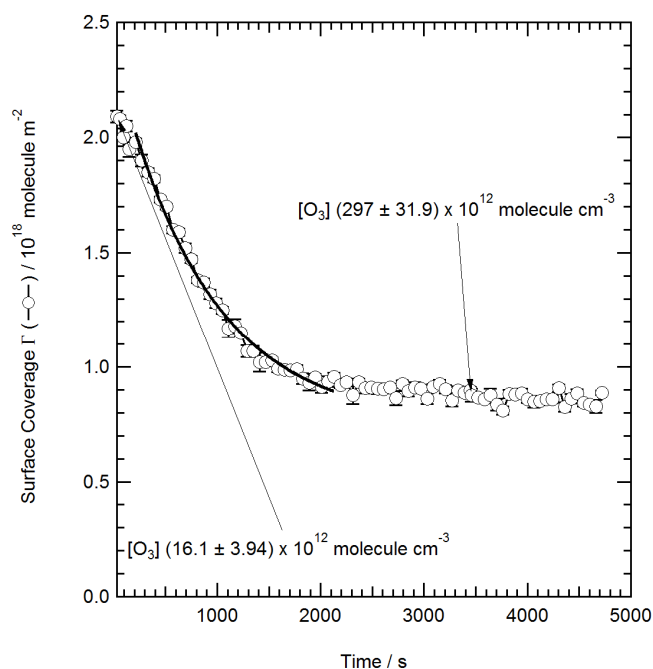
recompressed oleic acid monolayer was similar to that prior to recompression and the pattern in the surface coverage of two distinct slopes in the kinetic decay was repeated as shown in figure 3.26.

Figure 3.26 *The Recompression of Fully Deuterated Oleic Acid Monolayers with Exposure to Ozone*



The recompression was started when the surface pressure reached 0 mNm^{-1} and the monolayer was recompressed up to 18 mNm^{-1} at a speed of 50 cm^2 a minute. The first five surface coverage measurements were taken with an O_2 gas flow in to the chamber. From the sixth point onwards the monolayer was exposed to $(16.1 \pm 3.94) \times 10^{12} \text{ molecule cm}^{-3} \text{ O}_3$.

Figure 3.27 *The Kinetic Decay of a Monolayer of Fully Deuterated Oleic Acid (Oxford Isotope Facility sample) in an Atmosphere of $(16.1 \pm 3.94) \times 10^{12}$ molecule cm^{-3} O_3*



The fully deuterated Oxford Isotope facility sample was exposed to $(16.1 \pm 3.94) \times 10^{12}$ molecule cm^{-3} ozone in the gas phase, which was a concentration of $(0.284 \pm 0.069) \times 10^8$ molecule cm^{-3} in the tail region of the monolayer. As in the work of King et al., (2009) the surface coverage did not decay to zero. The ozone concentration was increased to $(297 \pm 31.9) \times 10^{12}$ molecule cm^{-3} in the gas phase above the monolayer and $(5.23 \pm 0.563) \times 10^8$ molecule cm^{-3} in the tail region of the monolayer, the surface coverage did not decrease indicating that the remaining molecule was not oxidised by ozone therefore would be a saturated molecule. The kinetic exponential fit was taken to the decay at the lower ozone concentration.

Figure 3.28 *The Kinetic Decay of a Monolayer of Fully Deuterated Oleic Acid with an Exponential Fit of Equation 3.11 to the Decay Curve Showing the Effect of Recompressing the Monolayer Exposed to an Ozone Concentration of $(16.1 \pm 3.89) \times 10^{12}$ molecule cm^{-3} in the Gas Phase and $(0.284 \pm 0.069) \times 10^8$ molecule cm^{-2} in the Tail Region of the Monolayer*

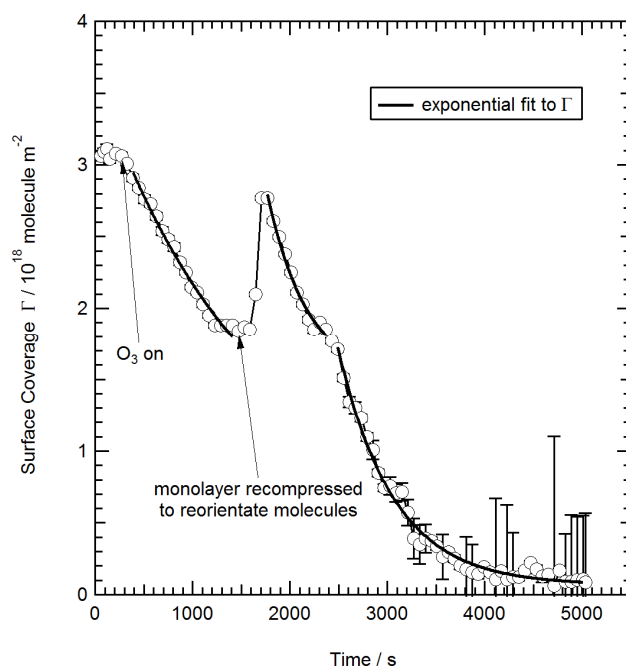
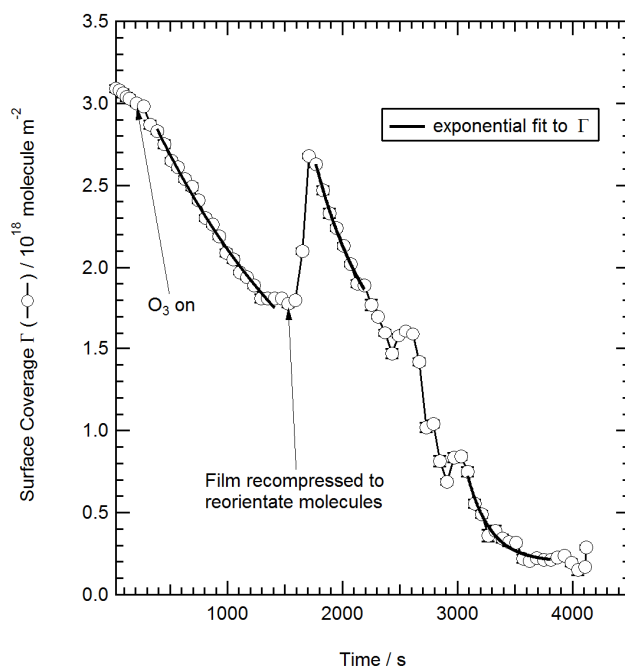


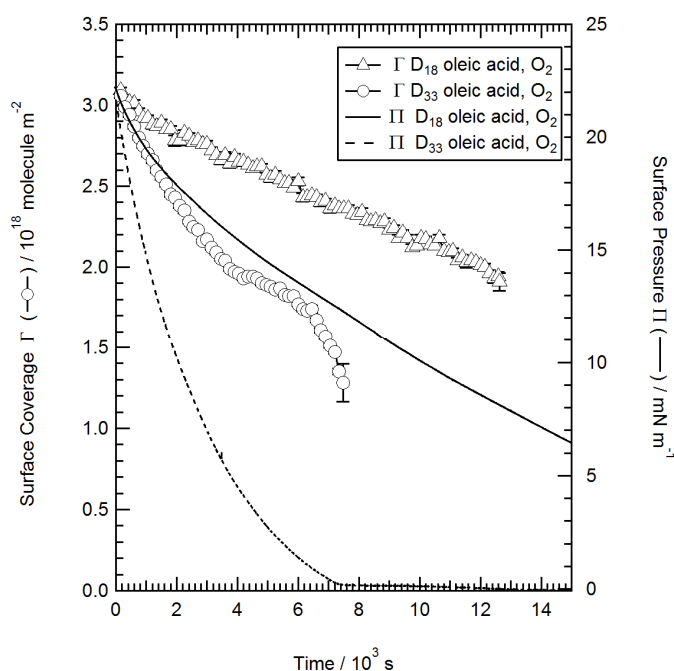
Figure 3.29 *The Kinetic Decay of a Monolayer of Fully Deuterated Oleic Acid with Exponential Fits of Equation 3.11 to the Decay Curve Showing the Effect of Recompressing the Monolayer Exposed to an Ozone Concentration of $(16.1 \pm 3.89) \times 10^{12} \text{ molecule cm}^{-3}$ in the Gas-Phase and $(0.284 \pm 0.069) \times 10^8 \text{ molecule cm}^{-2}$ in the Tail Region of the Monolayer*



A repeat of the recompression shown in figure 3.29 shows a rise in surface coverage between two slopes in the decay post recompression. From this behaviour it was concluded that the inflection feature seen in the low ozone concentration kinetic decays was a result of the packing of the molecules in the monolayer and not the result of a chemical effect of product molecules building up at the air-liquid interface.

3.8.3 The Surface Pressure and Surface Coverage of Fully and Partially Deuterated Oleic Acid Monolayers in Oxygen

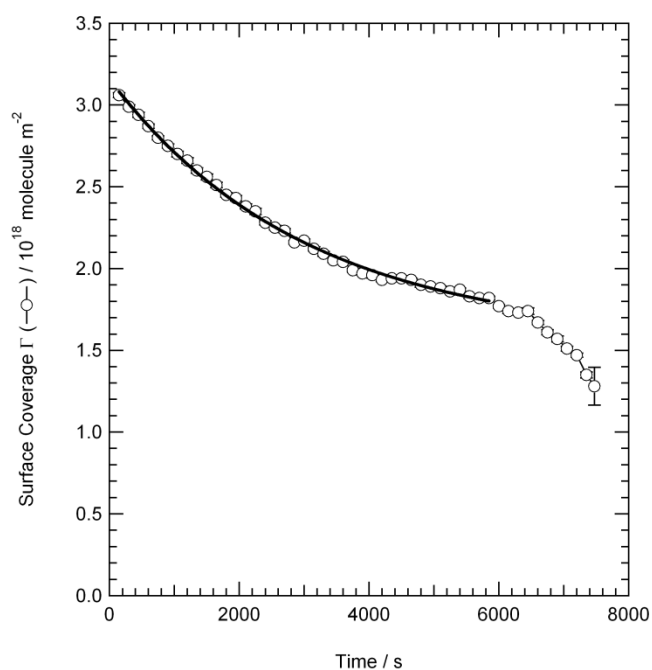
Figure 3.30 *The Kinetic Decay of Partially and Fully Deuterated Oleic Acid in Oxygen*



The fully deuterated oleic acid monolayer appeared to react with oxygen. This was in contrast to the results of King et al., (2009). This result led to the conclusion that there was a problem with the sample used by King et al., (2009) and the possibility of contamination was investigated by the comparison of the three samples used for this experimental work as shown in section 3.9.1. The decay of the oleic acid monolayer in oxygen was slower than when the monolayer was exposed to the lowest concentration of ozone (figure 3.23) showing that ozone was also oxidising the monolayer and in a different way to oxygen. Following the decay measurement the Langmuir trough barriers were closed to see if there was any material left on the surface. After the decay of fully deuterated oleic acid in oxygen a surface pressure rise was from 0 to $0.5 mN m^{-1}$ when the barriers were closed to the minimum surface area of $336.31 cm^2$ was observed.

Unsaturated compounds can undergo autoxidation by oxygen in the air as the spread monolayer is vulnerable to this (Gaines, 1966) this explains the rapid initial loss in surface pressure of approximately $3 mN m^{-1}$ when the oleic acid is spread at the air-water interface in air. It was the experience of the author that this initial loss stabilized and was distinct from the decay in surface pressure caused by the reactant ozone.

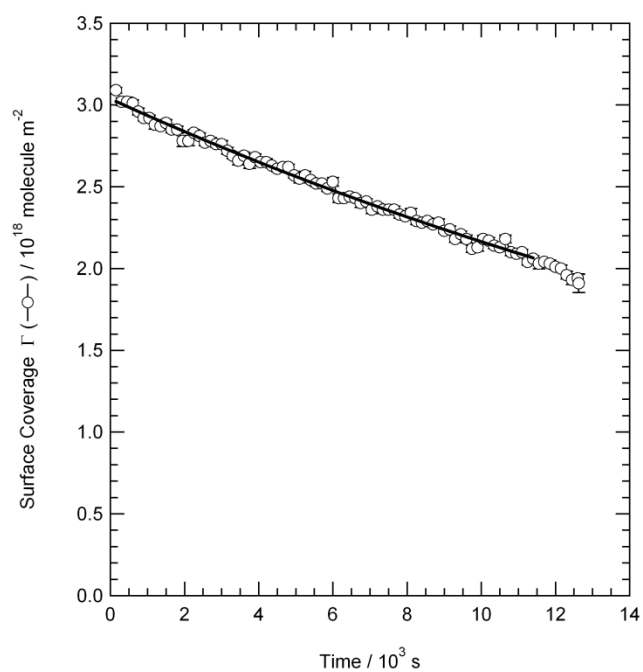
Figure 3.31 *The Kinetic Decay of a Monolayer of Fully Deuterated Oleic Acid in an O₂ Atmosphere Fitted to an Exponential Decay Function*



The kinetic fits were made to as much of the curve as possible whilst maintaining a reasonable margin of error for the fit. The data in figure 3.31 and 3.32 was fit to the exponential decay mechanism.

The decay is visibly different between fully deuterated oleic acid in O₂ where there is an inflection at 4100 seconds and for partially deuterated oleic acid where there is no inflection during a decay of 12400 seconds. This implies that the oxygen reaction involves the head group or the hydrocarbon chain up to the double bond and that is why the inflection can only be seen for the fully deuterated molecule.

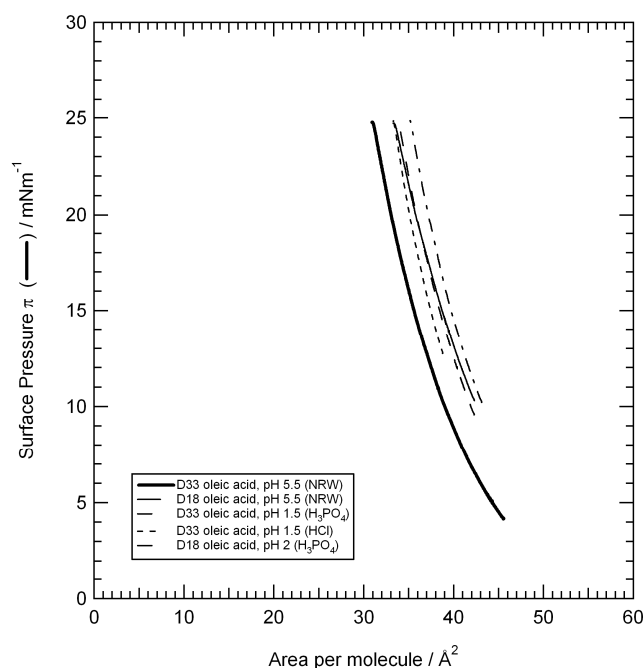
Figure 3.32 *Partially Deuterated Oleic acid in an O₂ Atmosphere Fitted to an Exponential Decay Function*



3.8.4 The Surface Pressure and Surface Coverage of Fully and Partially Deuterated Oleic Acid Monolayers on a pH Adjusted Subphase exposed to Gas-phase Ozone

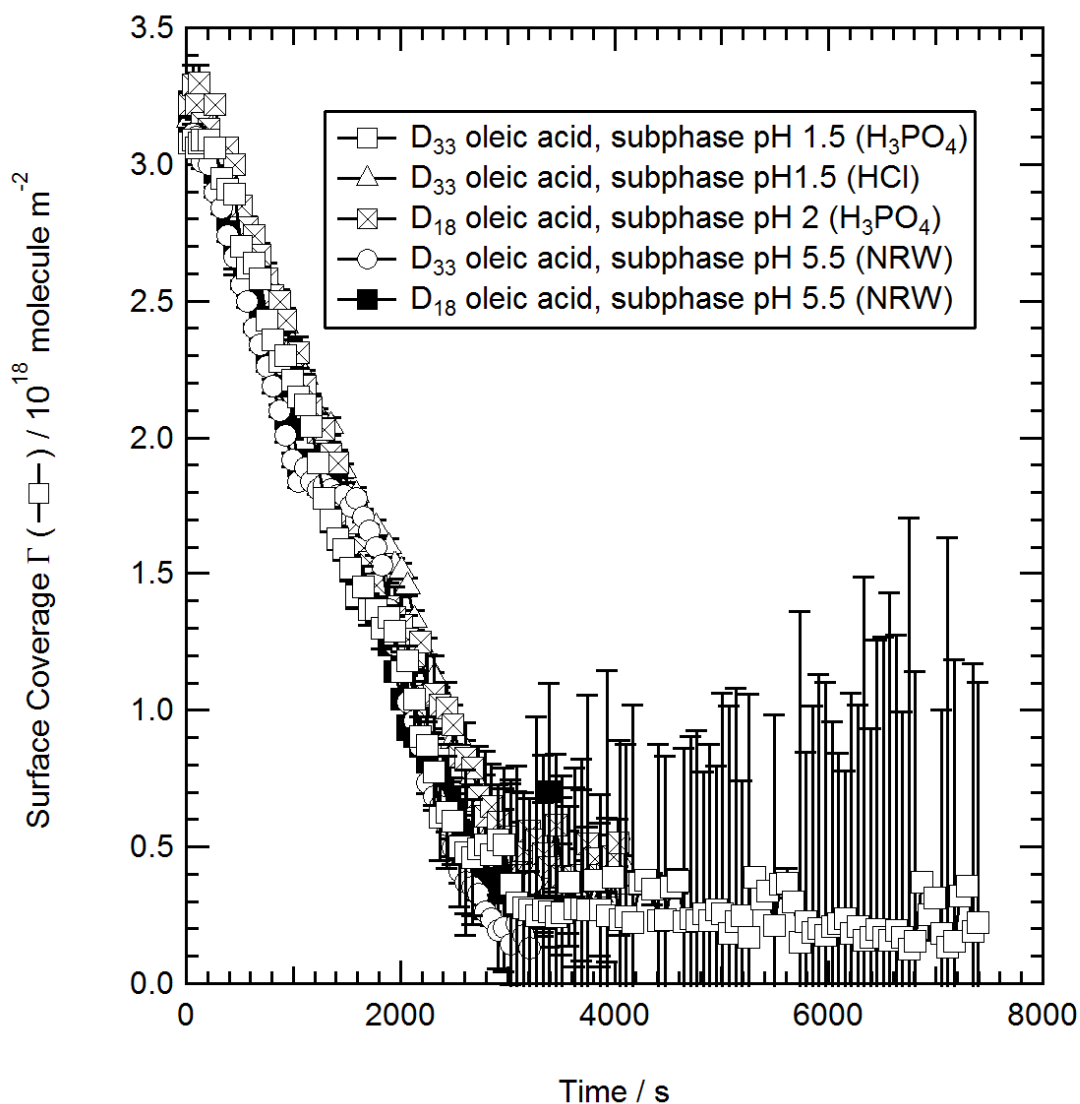
The pH of the null reflecting water subphase was 5.5, this was measured using pH papers as the wet bulb pH meters give a slightly elevated reading when deuterium oxide is present. The pH was lowered to 2 by the addition of phosphoric acid (H_3PO_4) and for a further experiment it was altered with hydrochloric acid (HCl), also to a pH value of 2. The purpose of altering the pH was to eliminate the formation of hydroxyl radical (OH) in the subphase which could if present be responsible for the decay of the oleic acid monolayer. If the monolayer decayed despite the pH being highly acidic then this would show that it was ozone which was oxidising the oleic acid monolayer.

Figure 3.33 The Pressure-Area Isotherm of D_{33} and D_{18} Oleic Acid on a Subphase of pH 2



The pressure-area isotherm of the Sigma Aldrich fully deuterated oleic acid oleic acid had a slightly larger area per molecule on a pH 1.5 to 2 subphase than on a pH 5.5 subphase. The pressure area isotherm of the partially deuterated oleic acid sample from the Oxford Isotope Facility on a subphase of pH 2 was near identical to that on a pH 5.5 subphase.

Figure 3.34 *The Kinetic Decay of Fully and Partially Deuterated Oleic Acid Monolayers on a Subphase of pH 1.5- 2 in Comparison with a Kinetic Decay at pH 5.5. The Monolayers Were Exposed to a Gas-phase Ozone Concentration of $(16.1 \pm 3.94) \times 10^{12} \text{ molecule cm}^{-3}$*



It can be seen in figure 3.34 that the kinetic decay of fully deuterated oleic acid was not altered significantly by the elimination of OH radical at pH 1.5 to 2, thus it can be assumed that the reaction observed is primarily the result of the oleic acid monolayer reacting with gas phase ozone molecules. The kinetic decay in the surface coverage of the partially deuterated molecule was also not significantly different on a subphase of pH 1.5 to 2 compared to a subphase of pH 5.5.

Figure 3.35 *The Kinetic Decay of a Monolayer of a Fully Deuterated Oleic acid in an Atmosphere of $(16.1. \pm 3.89) \times 10^{12}$ molecule cm^{-3} O_3 in the Gas-Phase and $(2.29 \pm 0.069) \times 10^8$ molecule cm^{-2} O_3 in the Monolayer as Fitted to Equation 3.11. The Subphase pH was Adjusted to 1.5 with HCl.*

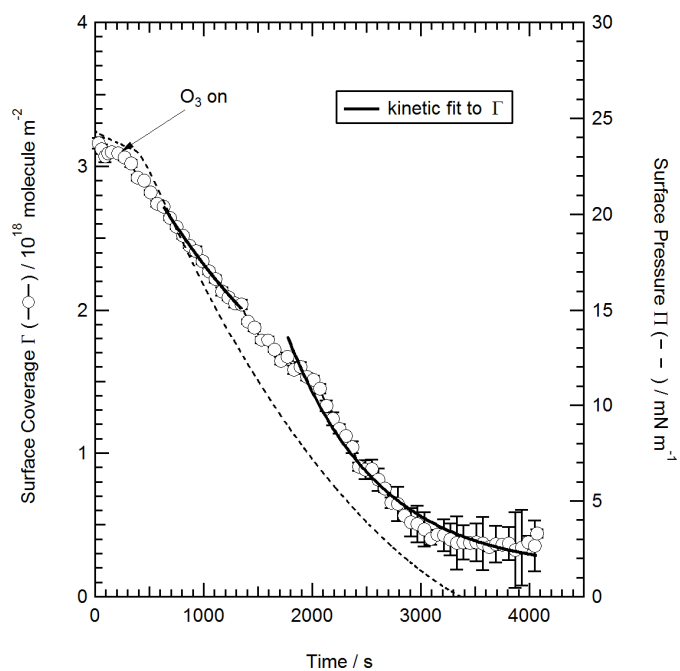


Figure 3.36 *The Kinetic Decay of a Monolayer of a Fully Deuterated Oleic Acid in an Atmosphere of $(16.1. \pm 3.89) \times 10^{12}$ molecule cm^{-3} in the Gas-Phase and $(2.29 \pm 0.069) \times 10^8$ molecule cm^{-2} O_3 in the Monolayer with a Kinetic Fit to Equation 3.11. The Subphase pH was Adjusted to 1.5 with H_3PO_4 .*

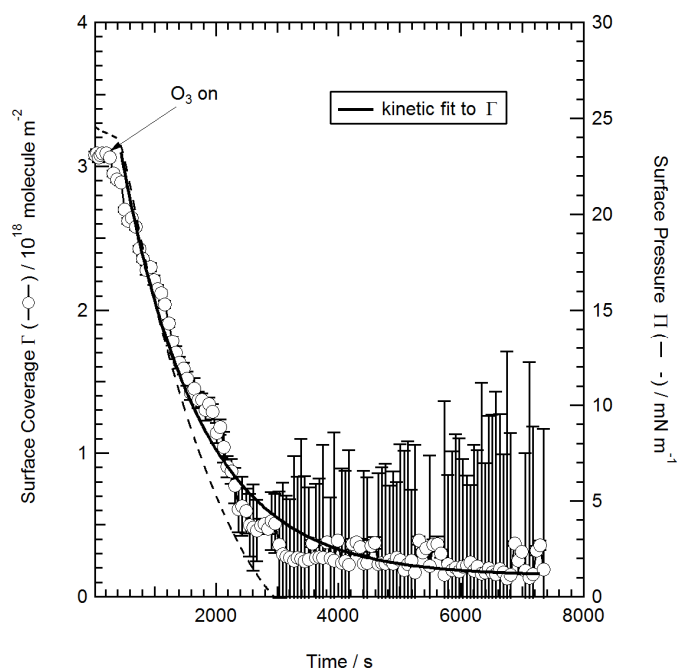
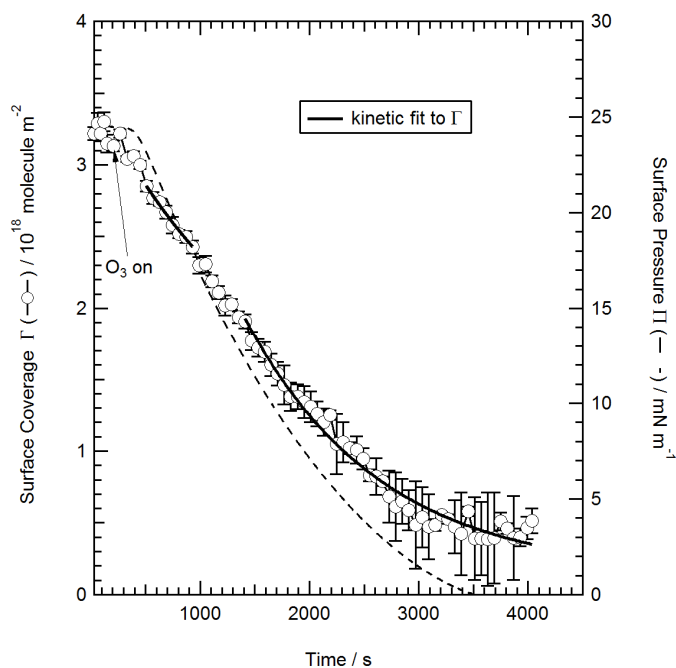


Figure 3.37 *The Kinetic Decay of a Monolayer of a Partially Deuterated Oleic Acid in an Atmosphere of $(16.1 \pm 3.89) \times 10^{12}$ molecule cm^{-3} in the Gas-Phase Above the Monolayer and $(2.29 \pm 0.069) \times 10^8$ molecule cm^{-2} O_3 in the Tail Region of the Monolayer as Fitted to Equation 3.11. The Subphase pH was Adjusted to 2 with H_3PO_4 .*



The decay of an oleic acid monolayer on a pH 2 subphase was not measured without ozone due to time constraints as the kinetic measurements of the different deuterations of oleic acid were the priority within the limited neutron time available.

3.8.5 Summary of the Surface Coverage and Surface Pressure Measurement Results

At higher ozone concentrations the surface pressure data followed the surface coverage data however at lower ozone concentrations an inflection feature was observed which was not reflected in the surface pressure measurement. This was unknown before as the deuterated oleic acid has only recently become commercially available so there are few neutron reflectometry studies of its behaviour.

In summary the experimental results are;

- Both deuterations of oleic acid show the same decay behaviour. The oleic acid film is lost from the interface almost completely when exposed to ozone and the double bond is known to be reacting and breaking first on the time order measured in this experiment. The ozone is selective and reacts at the double bond site.
- The decay in surface coverage and surface pressure due to ozone reacting is visibly faster than the decay of an oleic acid monolayer in an atmosphere of oxygen, however the oleic acid monolayer is not stable at the interface in an oxygen atmosphere so there is a reaction taking place between oleic acid and oxygen.
- At a concentration of $16.1 \pm 3.89 \times 10^{12}$ molecule cm^{-3} ozone in the gas-phase a flattening of the surface coverage value or area of inflection can be seen mid decay, behaviour which when the film is recompressed, is repeated suggesting that this is a structural phenomenon.
- Area per head group increases as a result of the reaction with ozone.
- The surface coverage versus time decay for ozone and oleic acid is dependent on the ozone concentration with a change in the surface coverage related to the packing of the monolayer at the air-liquid interface.
- Altering the pH of the subphase did not alter the kinetic behaviour of the decay in surface coverage showing that OH radical production was not influencing the kinetic decay.
- As expected from the literature the oleic acid monolayer was removed from the air-liquid interface during the reaction with ozone. This result is in contrast to the results of King et al., (2009).

The implications of these results will be discussed in section 3.9

3.8.6 Structural Neutron Reflectivity Measurements of Fully Deuterated and Partially Deuterated Oleic Acid Monolayers at the Air-Water Interface

Structural reflectivity measurements were taken by the method explained in section 3.7.3.3. The thickness of the monolayer is equal to the monolayer surface coverage per molecule (Γ) multiplied by the total scattering length of the molecule (b), divided by the molecules scattering length density (ρ) (equation 3.12).

$$\delta = \frac{\Gamma b}{\rho} \quad (E 3.12)$$

From the global fit to the neutron reflectivity data conducted by Adrian Rennie the monolayer thickness was calculated as 15 Å.

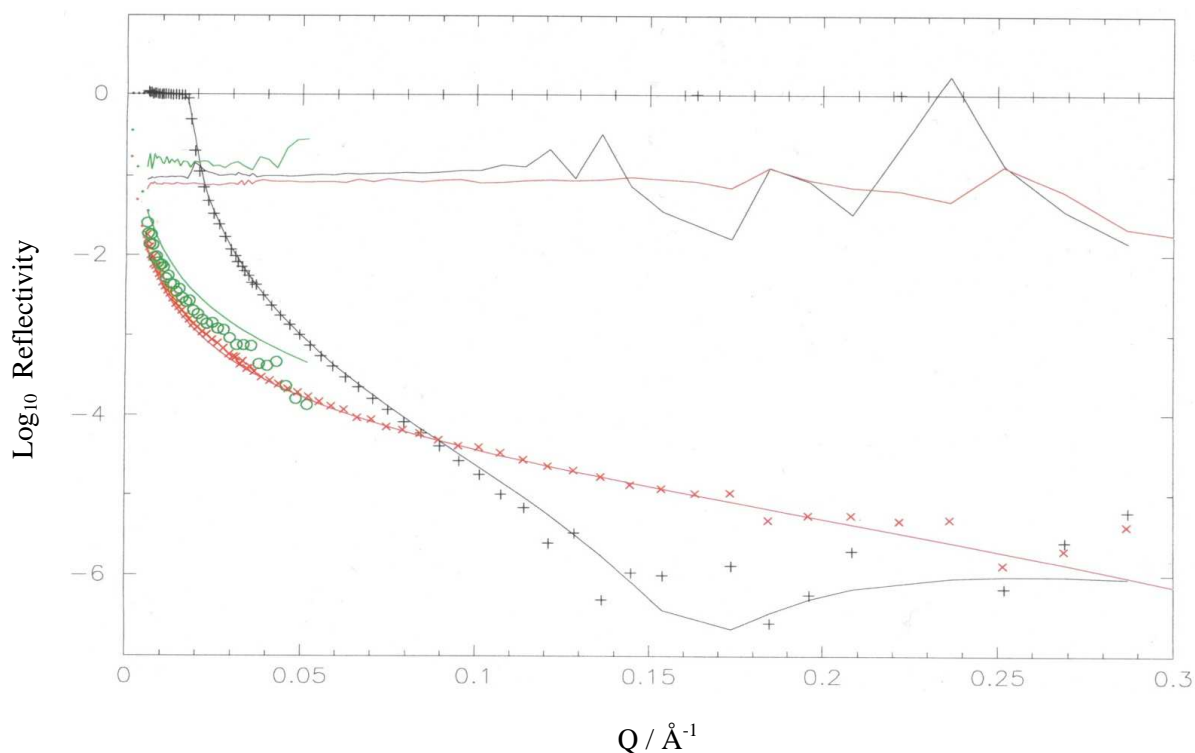
To elucidate whether the fully deuterated oleic acid sample from the Oxford Isotope Facility was contaminated, neutron reflectivity data at constant surface pressure at 25°C, was fitted using the ‘lipid’ fitting program which is a more detailed model than the program ‘mono’ and allows the head and tail group scattering to be treated separately and for modelling of mixing between the defined layers in the model. The reflectivity curves are shown in figure 3.38 and figure 3.39.

Three structural reflectivity measurements were undertaken:

1. Fully deuterated oleic acid (Oxford Isotope Facility) on a subphase of null reflecting water at 19 mNm⁻¹ at an incident beam angle of 0.62°.
2. Fully deuterated oleic acid (Sigma Aldrich) on a subphase of null reflecting water at a surface pressure of 19 mNm⁻¹ and at an incident beam angle of 0.62°.
3. Measurements of the reflectivity of a monolayer of partially deuterated oleic acid (Oxford Isotope Facility) on a subphase of D₂O at 19 mNm⁻¹ at an incident beam angle of 0.6° and at 3.8° in comparison to a contrasting measurement of the same sample on a subphase of null reflecting water at 0.62° and 3.8°.

Adrian Rennie ran two global fits, the first incorporating the partially deuterated monolayer data on two different contrasts of subphase (D₂O and NRW) with no ozone. This fit gave a monolayer thickness of 12 to 13 Å. The second fit incorporated the D₁₈ partially deuterated data from the two contrasts as well as the D₃₃ fully deuterated monolayer data from the Oxford Isotope Facility sample, when fitting the three data set simultaneously the thickness of the monolayer was 15 Å with a slightly lower scattering length density showing a difference in the properties of the molecules comprising the monolayer. The fitting parameters are shown in table 3.3.

Figure 3.38 *The Reflectivity Curve for Deuterated Oleic Acid at a Surface Pressure of 19 mNm⁻¹ at 24°C as Fitted to the Scattering Length of the Relevant Deuteration of Oleic Acid*



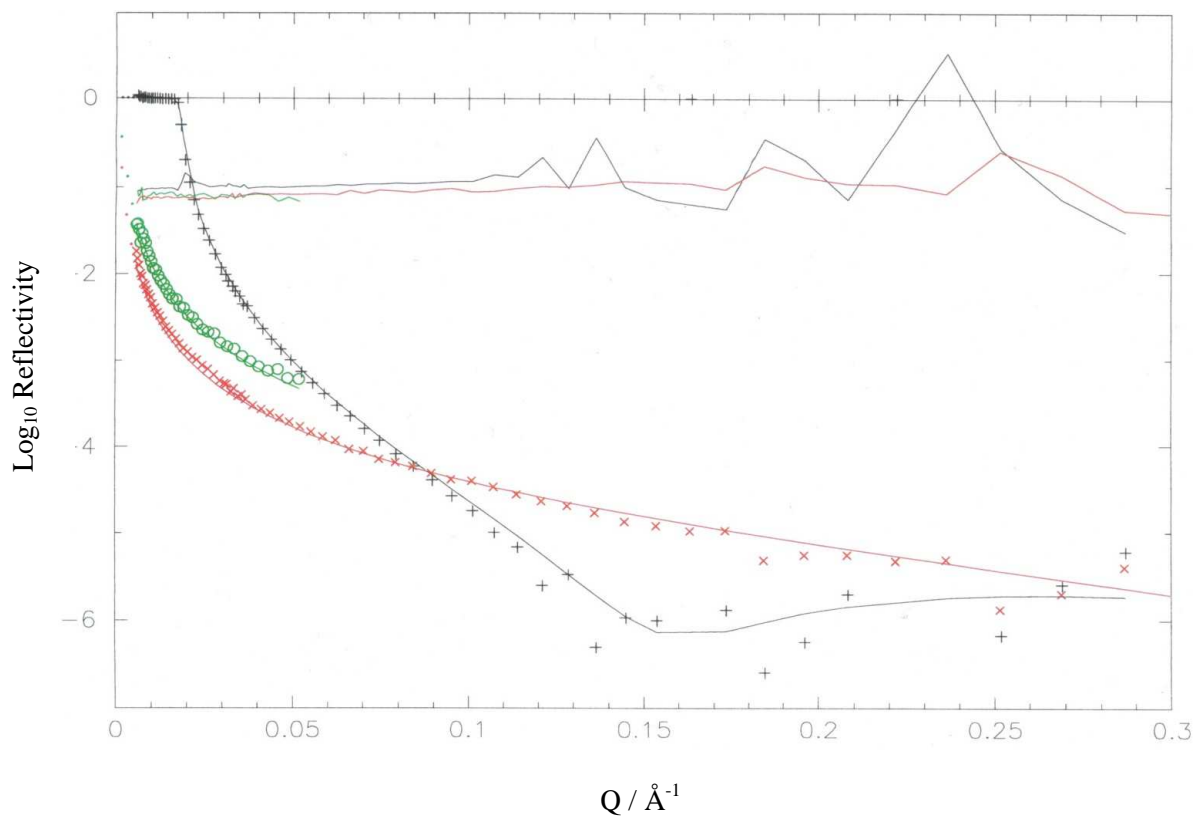
× denotes the partially deuterated Oxford Isotope Facility sample on a subphase of null reflective water measured at two incident beam angles (0.62 and 3.8°).

° denotes the fully deuterated Oxford Isotope Facility sample measured on a subphase of null reflective water measured at one incident beam angle (0.62°).

+ denotes the partially deuterated Oxford Isotope Facility sample on a subphase of D₂O measured at two incident beam angles (0.62 and 3.8°).

The green line in figure 3.38 is where the reflectivity of a monolayer fully deuterated oleic acid should plot according to the reflectivity values predicted by the lipid program model. In figure 3.39 it can be seen that the reflectivity of the fully deuterated oleic acid sample purchased from Sigma Aldrich did plot on this line. This result shows that the fully deuterated Oxford Isotope Facility sample is not oleic acid and given the results of King et al., (2009) where a residual film was left after the reaction with ozone and the same sample, the sample may contain a saturated deuterated molecule which was not as reactive to ozone.

Figure 3.39 *The Reflectivity Curve for Deuterated Oleic Acid at a Surface Pressure of 19 mNm⁻¹ at 24°C as Fitted to the Scattering Length of the Relevant Deuteration of Oleic Acid*



+ denotes the reflectivity of the Oxford Isotope Facility partially deuterated oleic acid sample on a subphase of D₂O at an incident beam angle of 0.62 and 3.8°.

° denotes the Sigma Aldrich fully deuterated oleic acid sample on a subphase of null reflective water at an incident beam angle of 0.62°.

× denotes the Oxford Isotope Facility partially deuterated oleic acid sample on a subphase of null reflective water at an incident beam angle of 0.62 and 3.8°.

When the reflectivity curve at a surface pressure of 19 mN m⁻¹ is contrasted between the three structural reflectivity measurements it can be seen that the fully deuterated Oxford Isotope Facility sample reflectivity sits close to that of the partially deuterated monolayer. The reflectivity of a fully deuterated oleic acid sample should produce a higher curve on the same subphase as a partially deuterated oleic acid molecule due to the higher deuterium content.

3.8.7 Kinetic Analysis and Results for the Decay in the Surface Coverage of Oleic Acid Monolayers Reacting with Gas-Phase Ozone

The pseudo first order rate constants (k) determined by fitting equation 3.11 to the surface coverage data as displayed on the plots in the experimental results section, and the resulting bimolecular rate constants (k') from the division of k by the ozone concentration in the monolayer are given in table 3.6^{a-c}.

From table 3.6 it can be seen that the blank experiment on partially deuterated oleic acid with a 5 L min^{-1} flow of oxygen into the chamber produced rate constants of 1 to 2 orders of magnitude slower than the experiments conducted with exposure to the lowest O_3 concentration. Where the decay in the monolayer surface coverage was slower at low ozone concentrations the kinetic fits are labelled upper and lower or upper, middle and lower depending on the regime.

The surface coverage of the fully deuterated (Sigma Aldrich), oleic acid film declined faster with higher concentrations of ozone. The surface coverage of the partially deuterated oleic acid film declined at similar rates for different ozone concentrations, the fastest decay of 0.0255 s^{-1} was achieved through doubling the ozone concentration. An extreme change in the ozone concentration was necessary to alter the decay rate significantly.

When comparing the rate of decay in the surface coverage of D_{18} and D_{33} oleic acid monolayers exposed to ozone it can be seen in figure 3.34 that the rate of loss of deuterated material from the air-water interface is roughly the same for both deuterations of oleic acid. When reacting with ozone the whole molecule is lost from the interface, if a deuterated reaction product had remained at the interface then the rate of decay of the D_{18} oleic acid monolayer would be different to that of the D_{33} oleic acid monolayer. The rate was the same thus it can be confirmed that the reaction product(s) produced by ozone reacting with oleic acid are not surface active and are lost from the air-water interface.

Table 3.6^a *The Pseudo 1st Order Rate Constant k and the Bimolecular Rate Constant $k'[\text{O}_3]$ for Fully and Partially Deuterated Oleic Acid*

Deuteration	Subphase	pH	O ₃ regime	$[\text{O}_{3(\text{g})}] \times 10^{12}$ molecule cm ⁻³	$[\text{O}_{3(\text{org})}] \times 10^8$ molecule cm ⁻²	$\frac{\Gamma_{\text{final}}}{\Gamma_{\text{initial}}}$	$k' (\times 10^{-2} \text{ s}^{-1})$	$k'/[\text{O}_3] (\times 10^{12} \text{ s}^{-1})$
D ₃₃	Null Reflective Water	5.5	O ₂ only			0.418	0.0035 ± 0.00072	
D ₁₈	NRW	5.5	O ₂ only	–	–	0.628	0.0332 ± 0.00124	–
D ₁₈	NRW	5.5	high O ₃	297 ± 31.9	5.23 ± 0.563	0.126	2 ± 0.24	38.3 ± 8.77
D ₁₈	NRW	5.5	high O ₃	130 ± 3.89	2.29 ± 0.069	0.137	1.89 ± 0.11	82.5 ± 7.22
D ₃₃	NRW	5.5	high O ₃	130 ± 3.89	2.29 ± 0.069	0.0895	1.64 ± 0.065	71.3 ± 4.97

Table 3.6^b *The Pseudo 1st Order Rate Constant k and the Bimolecular Rate Constant $k[O_3]$ for Fully and Partially Deuterated Oleic Acid*

Deuteration	Subphase	pH	O ₃ regime	[O _{3(g)}] × 10 ¹² molecule cm ⁻³	[O _{3(org)}] × 10 ⁸ molecule cm ⁻²	$\frac{\Gamma_{final}}{\Gamma_{initial}}$	k' (×10 ⁻² s ⁻¹)	$k'[O_3]$ (×10 ⁻¹² s ⁻¹)
D ₃₃	NRW	5.5	low O ₃	67.2 ± 8.55	1.18 ± 0.151	upper: 0.528 lower: 0.129	upper: 0.508 ± 0.562 lower: 1.89 ± 0.625	upper: 160 ± 73.1 lower: 42.9 ± 52.9
D ₃₃	NRW	5.5	low O ₃	29.4 ± 9.97	0.518 ± 0.176	0.0624	0.431 ± 0.0443	83.2 ± 37
D ₃₃	NRW	5.5	low O ₃	16.1 ± 3.94	0.284 ± 0.069	upper: 0.576 lower: 0.0843	upper: 0.169 ± 0.0196 lower: 0.18 ± 0.0167	upper: 59.3 ± 21.4 lower: 63.5 ± 21.4
D ₃₃	NRW	5.5	low O ₃	16.1 ± 3.94	0.284 ± 0.069	upper: 0.546 lower: 0.0925	upper: 0.121 ± 0.0021 lower: 0.176 ± 0.0851	upper: 42.4 ± 17.6 lower: 61.8 ± 18.1
D ₁₈	NRW	5.5	low O ₃	16.1 ± 3.94	0.284 ± 0.069	upper: 0.541 lower: 0.130	upper: 0.197 ± 0.033 lower: 0.123 ± 0.013	upper: 69.3 ± 28.7 lower: 43.3 ± 15
D ₁₈	NRW	5.5	low O ₃	16.1 ± 3.94	0.284 ± 0.069	upper: 0.551 lower: 0.192	upper: 0.125 ± 0.02 lower: 0.1479 ± 0.014	upper: 43.8 ± 17.7 lower: 52 ± 17.7
D ₃₃	NRW	5.5	low O ₃	11.6 ± 2.20	0.204 ± 0.039	0.544	0.2 ± 0.06	36.2 ± 9.72
D ₃₃	NRW	5.5	low O ₃	16.1 ± 3.94	0.284 ± 0.069	upper: 0.601 middle: 0.067 lower: 0.006	upper: 0.0633 ± 0.02 middle: 0.242 ± 0.053 lower: 0.175 ± 0.008	upper: 22.3 ± 12.66 middle: 85.1 ± 39.3 lower: 61.7 ± 17.9
D ₃₃	NRW	5.5	low O ₃	16.1 ± 3.94	0.284 ± 0.069	upper: 0.586 middle: 0.559 lower: 0.2	upper: 0.0617 ± 0.015 middle: 0.20 ± 0.057 lower: 0.49 ± 0.085	upper: 21.7 ± 10.5 middle: 70.5 ± 37.5 lower: 175 ± 72.6
D ₃₃ OIF *	NRW	5.5	low O ₃	16.1 ± 3.94	0.284 ± 0.069	0.425	0.113 ± 0.0071	39.7 ± 12.2

* OIF denotes Oxford Isotope Facility

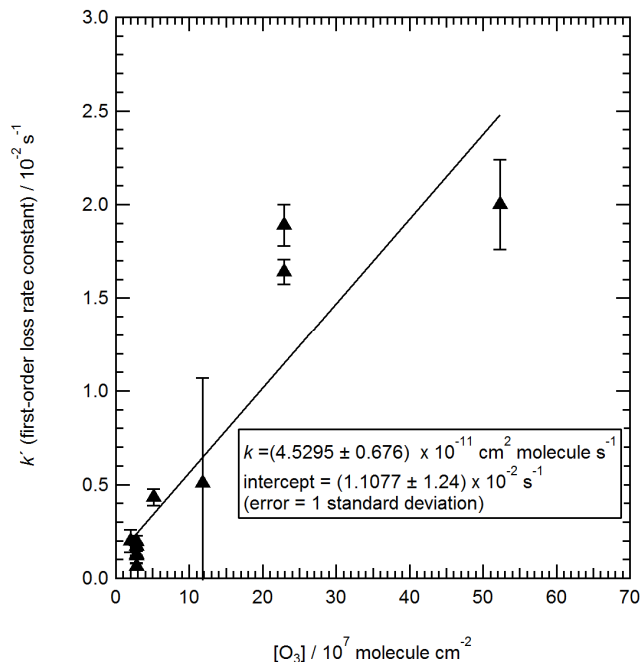
Table 3.6 The Pseudo 1st Order Rate Constant k and the Bimolecular Rate Constant $k[O_3]$ for Fully and Partially Deuterated Oleic Acid

Deuteration	Subphase	pH	O ₃ regime	$[O_{3(g)}] \times 10^{12}$ molecule cm ⁻³	$[O_{3(org)}] \times 10^8$ molecule cm ⁻²	$\frac{\Gamma_{final}}{\Gamma_{initial}}$	$k' (\times 10^{-2} \text{ s}^{-1})$	$k'[O_3] (\times 10^{12} \text{ s}^{-1})$
D ₃₃	NRW/HCl	1.5	low O ₃ /acidic	16.1 ± 3.94	0.284 ± 0.069	0.062	0.0779 ± 0.0028	27.4 ± 7.68
D ₃₃	NRW/H ₃ PO ₄	1.5	low O ₃ /acidic	16.1 ± 3.94	0.284 ± 0.069	upper: 0.649 lower: 0.221	upper: 0.0563 ± 0.022 lower: 0.119 ± 0.01	upper: 19.8 ± 12.6 lower: 41.7 ± 13.7
D ₁₈	NRW/H ₃ PO ₄	2	low O ₃ /acidic	16.1 ± 3.94	0.284 ± 0.069	upper: 0.714 lower: 0.269	upper: 0.0634 ± 0.08 lower: 0.081 ± 0.007	upper: 22.3 ± 33.4 lower: 28.5 ± 9.71

To assess whether there was a relationship between the concentration of ozone reacting with the monolayer and the rate of the reaction between ozone and oleic acid as shown by the decay in surface coverage, the pseudo first order rate constants were plotted against the concentration of ozone in the monolayer tail region and a line was fitted to the plot (figure 4.41). The gradient of the line is the rate of change in the surface coverage k' during the reaction of a monolayer of oleic acid with ozone over a range of ozone concentrations.

A second order plot of the rate constant k' for the first order loss of the surface coverage of deuterated material versus the ozone concentration in the monolayer was produced to find k from $k'=k[O_3]$. As shown in figure 3.40 the value of k' fitted to the entire decay at high ozone concentrations and to the initial region of decay prior to the inflection feature at low ozone concentrations was $(4.5295 \pm 0.676) \times 10^{-11} \text{ cm}^2 \text{ molecule s}^{-1}$. The rate constants measured from the Oxford Isotope Facility D_{33} sample were not included in the plots as the structural reflectivity measurements showed the sample behaved differently to the D_{33} oleic acid sample from Sigma Aldrich and the D_{18} oleic acid sample.

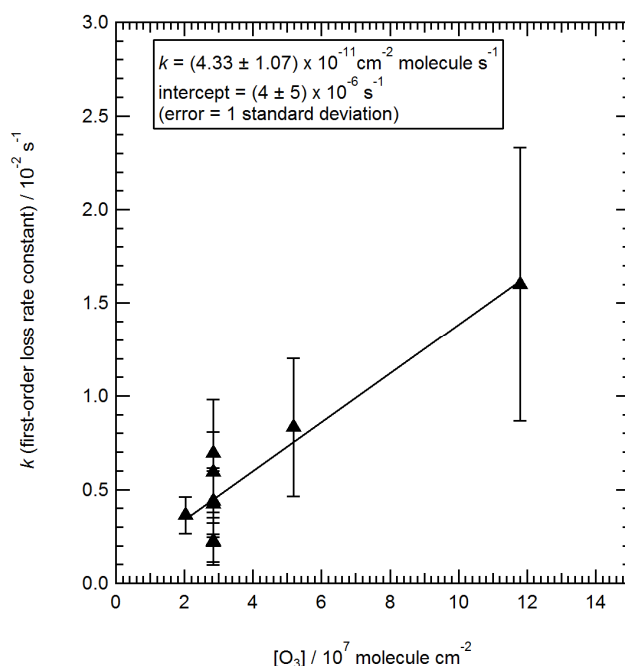
Figure 3.40 *The Second Order Plot of the Pseudo First Order Rate Constants with Increasing Ozone Concentration*



The errors on the points are the statistical error from the fitting of equation 3.11 to the surface coverage decay experimental data. The restricted range of concentrations was a result of the limited amount of time available on the neutron reflectometer.

A further second order plot of k' fitted to the post inflection decay in surface coverage at lower ozone concentrations is shown in figure 3.41.

Figure 3.41 *The Second Order Plot of the Pseudo First Order Rate Constants for the Lower Decay after the Inflection Feature, for Oleic Acid at Low Ozone Concentrations*



The bimolecular rate constant for the surface reaction of the oleic acid monolayer with gas-phase ozone, k is defined as k' divided by the concentration of ozone in the monolayer, $[O_3]_{(film)}$ (equation 3.13).

$$k = \frac{k'}{[O_3]_{(film)}} \quad (E 3.13)$$

The bimolecular rate constant k was obtained from fitting a line to the second order plot (figure 3.40) and taking the gradient of the line to give bimolecular k , the rate of decay of surface coverage. Bimolecular k was $4.53 \pm 0.68 \times 10^{-11} \text{ cm}^2 \text{ molecule}^{-1} \text{ s}^{-1}$. Fitting to the low ozone concentration rate constants gives a value of bimolecular k of $4.33 \pm 1.07 \times 10^{-11} \text{ cm}^2 \text{ molecule}^{-1} \text{ s}^{-1}$ as shown in figure 3.41. Fitting to the lower decay which occurs after the inflection feature in the low ozone experiments was not possible as the data was collected at only two ozone concentrations of $1.18 \times 10^8 \text{ molecule cm}^2 \text{ O}_3$ and $0.284 \times 10^8 \text{ molecule cm}^2 \text{ O}_3$, taking an average of the rate constant pseudo first order k gave bimolecular k for the decay in the surface coverage of the film post inflection as $5.27 \pm 2.50 \times 10^{-11} \text{ cm}^2 \text{ molecule}^{-1} \text{ s}^{-1}$ which within error is that same as that obtained from the decay prior to the inflection feature. In the discussion,

section 3.9.2, a comparison of this value will be made to those obtained in other studies of oleic acid reacting with ozone.

The reaction of an oleic acid monolayer with oxygen gave a reaction rate constant of $(0.0035 \pm 0.00072) \times 10^{-2} \text{ s}^{-1}$ which was two orders of magnitude slower than that of the lowest ozone concentration reacting with an oleic acid monolayer.

In summary the results of the kinetic analysis are that:

- The decay rate constants (k') for an oleic acid monolayer reacting with gas-phase ozone observed at higher ozone concentrations were the same as those observed under low ozone conditions within error.
- At lower ozone concentrations the decay featured two distinct regions of decay with an inflection region between them. It was concluded that this was a structural feature; the rate constant k' for the decay post recompression of the monolayer was very slightly slower than the decay prior to recompression. The rate constant for the decay after the inflection was within error, the same as the rate constant prior to the inflection however the rate constant for the post inflection decay was based on only two ozone concentrations so further work would be required to confirm this.

To consider if the surface coverage measurements are for the reaction of ozone with oleic acid or if transport of ozone is contributing to the kinetics the time taken for ozone to diffuse to the monolayer and to reach a stable concentration (for mixing to complete) was calculated. The characteristic time for the diffusion of ozone ($\tau_{diffusion}$) in the gas phase was calculated from equation 3.14 (Seinfeld and Pandis, 2006; King et al. 2009) where d is the thickness of the monolayer, (15 Å) also known as the characteristic distance, D_g is the gas phase diffusion constant for ozone ($1.80 \times 10^{-5} \text{ m}^2 \text{ s}^{-1}$) (Seinfeld and Pandis, 2006; King et al. 2009).

$$\tau_{diffusion} = \frac{d^2}{4D_g} \quad (E. 3.14)$$

The characteristic diffusion time for ozone to diffuse to the monolayer was $3.13 \times 10^{-14} \text{ s}$.

The characteristic time taken for the accommodation of ozone at the interface or interfacial equilibrium was calculated according to equation 3.15 where D_l denotes the diffusion constant for ozone in an organic liquid ($1 \times 10^{-9} \text{ m}^2 \text{ s}^{-1}$) (Seinfeld and Pandis, 2006; King et al. 2009).

$$\tau_{interfacial} = \frac{d^2}{\pi^2 D_l} \quad (E. 3.15)$$

The accommodation time was $2.28 \times 10^{-10} \text{ s}$.

The characteristic time taken for the reaction of ozone with oleic acid, $\tau_{reaction}$ was determined by the following equation 3.16, where k is the bimolecular surface reaction rate constant between oleic acid and ozone, the value k was taken as $4.5 \times 10^{-11} \text{ cm}^2 \text{ molecule}^{-1} \text{ s}^{-1}$. The surface concentration of oleic acid (surface coverage) Γ_{oleic} of $3 \times 10^{18} \text{ molecules m}^{-2}$ was taken from the experimental data.

$$\tau_{reaction} = \frac{1}{k \Gamma_{oleic}} \quad (E 3.16)$$

As equation 3.16 is dependent on the starting value of Γ which was not consistent it has been calculated for a surface coverage of oleic acid (Γ_{oleic}) of $2 \times 10^{18} \text{ molecules m}^{-2}$ and for $3 \times 10^{18} \text{ molecules m}^{-2}$ giving results of $1 \times 10^{-4} \text{ s}$ and $6.8 \times 10^{-5} \text{ s}$ respectively.

The uptake coefficient (γ) for ozone on a cloud droplet or aerosol particle possessing a monolayer of oleic acid can be estimated using equation 3.17 from Hearn et al., (2005). Where H is the Henry's law constant of $480 \text{ mol m}^{-3} \text{ atm}^{-1}$, R is the gas constant of $8.204 \times 10^{-5} \text{ atm m}^3 \text{ mol}^{-1} \text{ K}^{-1}$, T is the temperature, \bar{c} is the average molecular speed of gas phase ozone (360 m s^{-1}), δ is the thickness of the film ($15 \times 10^{-10} \text{ m}$). For this equation k is taken in units of concentration over time at a value of $2.7 \times 10^9 \text{ mol}^{-1} \text{ s}^{-1}$ ($4.5 \times 10^{-11} \text{ cm}^2 \text{ molecule}^{-1} \text{ s}^{-1}$).

$$\gamma = \frac{4HRT}{\bar{c}} \delta k \Gamma_{oleic} \quad (E 3.17)$$

The uptake coefficients, γ , are given in table 3.7

Table 3.7 *The Uptake Coefficients for Ozone to an Oleic Acid Monolayer Coated Droplet*

$\Gamma \times 10^{18}$ molecule m^{-2}	$\Gamma \times 10^{-6}$ mol m^{-2}	$\delta / \text{\AA}$	γ at T = 293 K (~ 20°C) / $\times 10^{-6}$	γ at T = 278 K (~ 5°C) / $\times 10^{-6}$	γ at T = 293 K (~ 0°C) / $\times 10^{-6}$
2	3.32	15	1.7	1.6	1.6
2	3.32	20	2.3	2.2	2.2
3	4.98	15	2.6	2.5	2.4
3	4.98	20	3.5	3.3	3.2

What this analysis shows is that the characteristic lifetime of the reaction of an oleic acid monolayer with gas-phase ozone is much slower than the diffusion of ozone to the air-water interface and the interfacial accommodation of ozone therefore the measured results of surface coverage are valid for the reaction between the monolayer and ozone and are not measuring the process of diffusion or accommodation rather than the reaction of the ozone with the monolayer.

3.9 Discussion

The discussion will focus on the following aspects of my work;

- The experimental surface coverage and surface pressure results for an oleic acid monolayer reacting with gas-phase ozone at the air-water interface compared to other studies.
- The contamination of the fully deuterated oleic acid sample used by King et al., (2009).
- Discussion of the kinetic results.
- Discussion of the ozone uptake coefficient.
- Discussion of the reaction mechanism for an oleic acid monolayer reacting with gas-phase ozone.

The plateau and slight surface coverage rise seen in an atmosphere of 16.1 ± 2.20 molecule cm^{-3} O_3 was interpreted as a structural phenomenon where the molecules comprising the film would be in a more 'gas-like' configuration, potentially lying down thus increasing their area at the interface and the film thickness which leads to a greater value of Γ . To test this theory the film was recompressed to a higher surface pressure in order to observe whether the decay of the film from a liquid compression state would repeat the same behaviour. The behaviour was repeated.

From the results of this work the following conclusions were inferred;

1. The presence of ozone causes the oleic acid molecules comprising the film to change orientation leading to the appearance of a surface coverage rise as effectively in laying horizontally the molecule has increased what we refer to as its area per head group, which is used to calculate the surface coverage measurement. This was shown not to affect the kinetics as when the monolayer was recompressed following this feature the subsequent decay in the surface coverage was not significantly different.
2. Sustained ozone exposure causes the oleic acid monolayer at the air-liquid interface to nearly all decay away, reaching surface coverage values of approximately 0.5×10^{18} molecules per m^2 . Recompression does not produce a surface pressure reading. At a surface coverage of 0.5×10^{18} molecules per m^2 the monolayer is unlikely to be intact.

The second result is in contrast to the findings of King et al., (2009) whom using the Oxford Isotope Facility fully deuterated sample showed that the surface coverage of D_{33} oleic acid almost halved, decaying to a surface coverage of 1×10^{18} molecule per m^2 under sustained ozone exposure, a coverage at which it was inferred that there was an intact product monolayer. The work of King et al., (2009) also stated that the oleic acid monolayer did not react with

oxygen in contrast to the findings presented here using the Sigma Aldrich sample. The rate constants however are in agreement within two standard deviations in this study ($4.5 \pm 0.7 \times 10^{-11} \text{ cm}^2 \text{ molecule}^{-1} \text{ s}^{-1}$), and the King et al., (2009) study which reported a bimolecular rate constant of $7.3 \pm 0.9 \times 10^{-11} \text{ cm}^2 \text{ molecule}^{-1} \text{ s}^{-1}$.

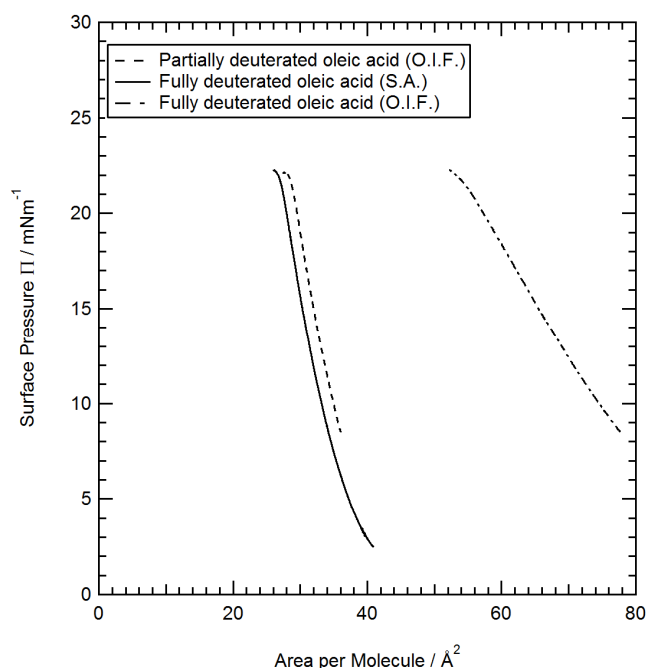
The difference in the two sets of experimental results from the experiment shown here and the experiment detailed in King et al., (2009) showed that one of the samples was contaminated, a deuterated impurity was found in the sample synthesised for the King et al., (2009) work. The genuine result for the reaction of oleic acid with gaseous phase ozone is that detailed in this work, where the monolayer rapidly decays to a very low value of surface coverage or entirely away when exposed to gas phase ozone.

The atmospheric implications of the results of this work with the Sigma Aldrich deuterated oleic acid are that a thin organic film of an unsaturated amphiphile on a cloud droplet would be oxidised away by ozone from the air surrounding the droplet. The products from this reaction must be volatile or soluble as they are not observed at the air-liquid interface (Voss et al. 2007; Wadia et al. 2000); the signal from the deuterated molecule is lost from the interface in this work.

3.9.1 The Contamination of the Oxford Isotope Facility Fully Deuterated Oleic Acid Sample

The D_{33} fully deuterated oleic acid was found to be contaminated with a deuterated impurity present from its synthesis. The surface pressure versus area isotherm for the three samples of oleic acid used in this work is shown in figure 3.4. Although the surface pressure-area isotherm is featureless in that the phase transitions are not visible in the surface pressure data, a contrast can be seen between the area per molecule of the fully deuterated (D_{33}) monolayer synthesised by the Oxford Isotope Facility and that purchased from Sigma Aldrich. The partially deuterated (D_{18}) oleic acid sample synthesised by the Oxford Isotope Facility was in agreement with the fully deuterated Sigma Aldrich sample.

Figure 3.42 *The Pressure-Area Isotherms of the Oleic Acid Samples used in this work. O.I.F stands for Oxford Isotope Facility and S.A. for Sigma Aldrich*



From figure 3.42 it can be observed that the fully deuterated sample obtained from the Oxford Isotope Facility did not follow the isotherm for oleic acid whereas the partially deuterated sample from the same facility and the Sigma Aldrich sample were in agreement. When compressed from the same starting pressure as the partially deuterated sample, at the same barrier speed of $25 \text{ cm}^2 / \text{min}$ the slope of the isotherm was shallower indicating that the molecules were not packing in the same way. The Oxford Isotope Facility D_{33} sample had previously been used by King et al., (2009) to monitor the kinetic decay in the surface coverage of oleic acid monolayers at the air-water interface when exposed to gas-phase ozone. When conducting isotherms King et al., (2009) had not noticed the isotherm to be different to that of non-deuterated oleic acid (King, 2012) so it is thought that the sample had deteriorated between their experimental work and this. Further differences were observed in the neutron reflectivity data. The effect of this impurity can be seen in figure 3.18 where that surface coverage does not decay to zero during a reaction with ozone.

To further investigate the Oxford Isotope Facility, fully deuterated sample composition an NMR profile and GC-MS spectra was taken by Chu Chaun Dong at the Oxford Isotope Facility of the fully deuterated oleic acid sample produced there. It was found to have a surface active deuterated impurity that was inert to ozone as it did not contain a double bond.

3.9.2 Comparison to Previous Studies of Oleic Acid at the Air-Liquid Interface: Discussion of the Kinetic Results

The oxidation of oleic acid at the air-water interface has been studied by several authors (Voss et al. 2007, González-Labrada et al. 2006;2007, King et al. 2009). The findings of King et al., (2009) with regard to the persistence of a monolayer after the reaction of oleic acid with ozone were juxtaposed to the work of Voss et al.,(2007), however the conclusions of King et al., (2009) were based on a contaminated sample so have now been discounted.

In this chapter a bimolecular rate constant of $4.5 \pm 0.7 \times 10^{-11} \text{ cm}^2 \text{ molecule}^{-1} \text{ s}^{-1}$ was taken from the change in surface coverage during the reaction of an oleic acid monolayer at the air-liquid interface with gas phase ozone. González-Labrada et al., (2006) studied the reaction of a monolayer of oleic acid with gas phase ozone obtaining a bimolecular rate constant of $4.9 \times 10^{-11} \text{ cm}^2 \text{ molecule}^{-1} \text{ s}^{-1}$; this figure is in agreement with that obtained from the experiments in this chapter. In the work of González-Labrada et al., (2006) the oleic acid monolayer was spread on a pendant droplet of water and the change in surface pressure, surface area of the droplet and the droplet volume were monitored; the surface pressure was converted to a surface concentration of oleic acid. The monolayer was exposed to 7 to $615 \times 10^{12} \text{ molecule cm}^{-3}$ gas phase ozone.

From the experimental results it can be seen that there appears to be a reaction with oxygen occurring (figures 3.31 and 3.32). Although the decay is faster in the presence of O_3 , the oleic acid monolayer is not stable in the presence of a flow of oxygen under dark conditions. The decay in oxygen gave a rate constant k of $(0.0035 \pm 0.00072) \times 10^{-2} \text{ s}^{-1}$ compared to $(0.2 \pm 0.06) \times 10^{-2} \text{ s}^{-1}$ with the lowest concentration of ozone ($(0.204 \pm 0.039) \times 10^8 \text{ molecule cm}^{-3}$ in the monolayer) reacting with the fully deuterated oleic acid film. As the value of k for the reaction of the oleic acid monolayer with ozone was two orders of magnitude larger the oxygen decay was ignored for the purpose of kinetic analysis and was not modelled as part of the monolayer atmospheric lifetime calculation given in section 3.10.

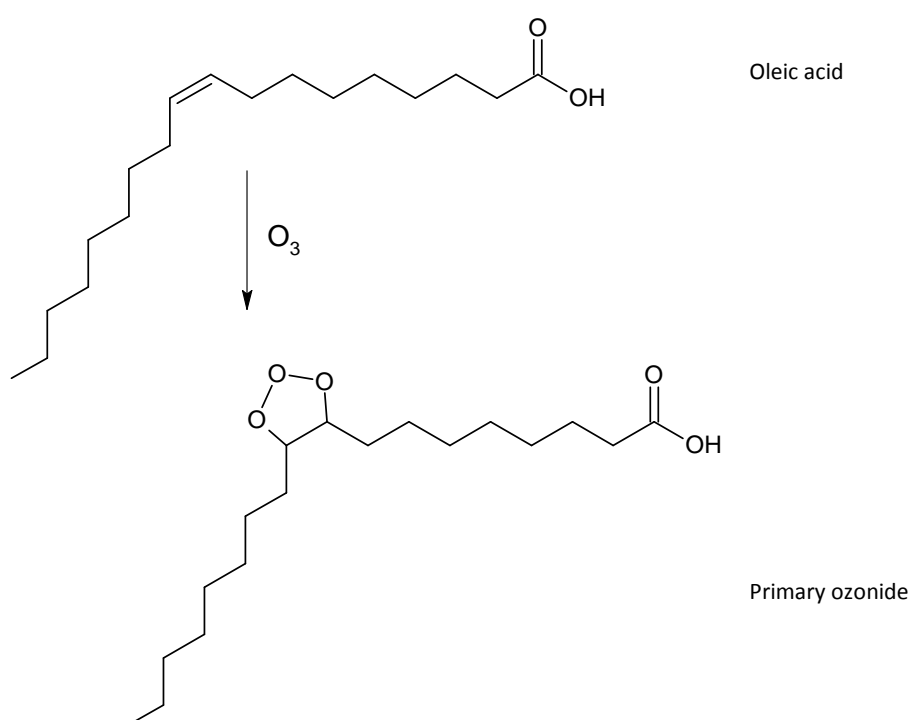
3.9.3 The Mechanism of Ozonolysis of an Oleic Acid Monolayer

A chemical mechanism for the ozonolysis of an oleic acid monolayer at the air-water interface is given which is based on this work and the findings of other studies (Ziemann, 2005, Zahardis and Petrucci, 2007) of oleic acid reacting with ozone at the air-liquid interface.

The proposed reaction would take place in several steps.

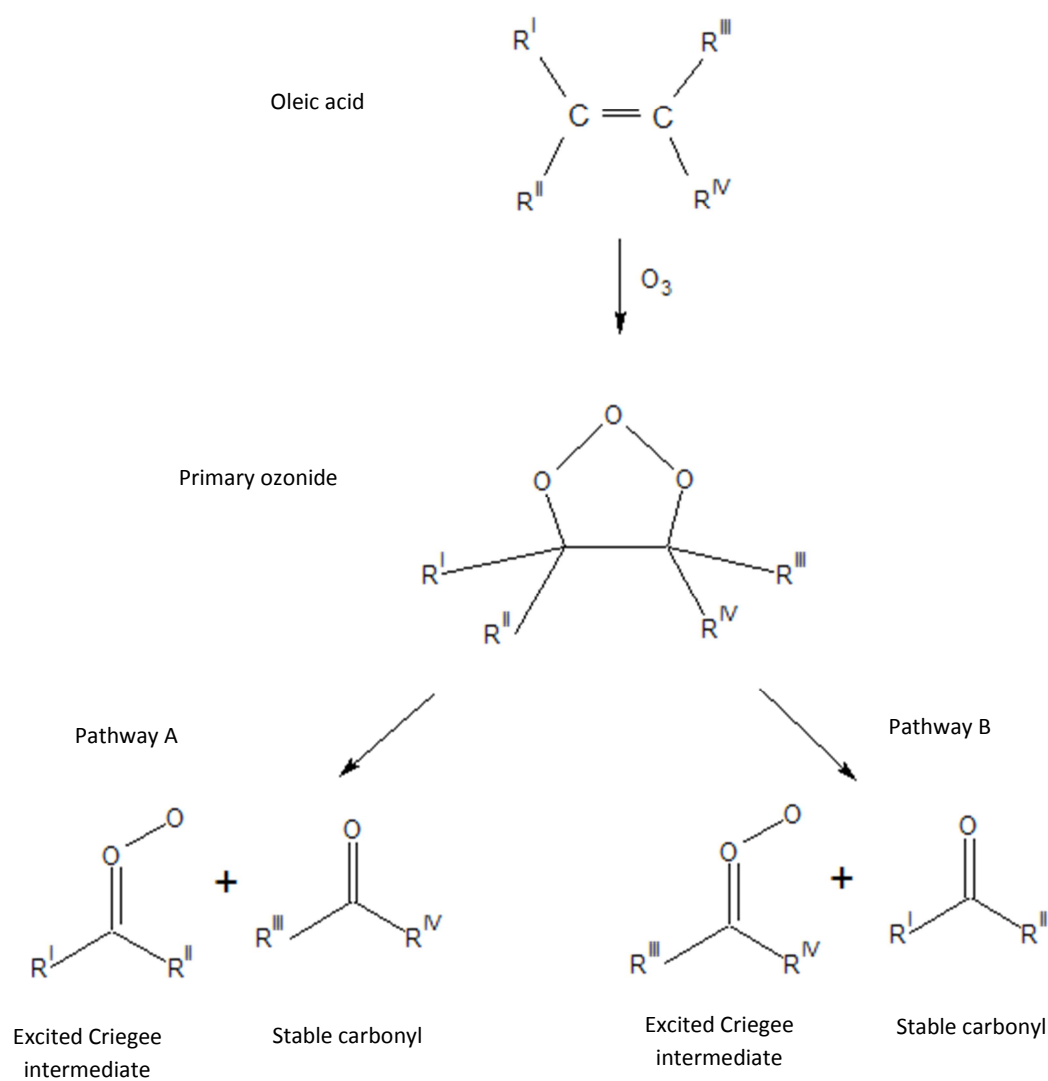
1. Ozone adds oxygen to the double bond of the oleic acid molecule forming an unstable primary ozonide.

Figure 3.43 Formation of a Primary Ozonide from Oleic Acid and Ozone



- The primary ozonide decomposes cleaving the molecule at the site of the double bond in the original oleic acid molecule forming an excited Criegee intermediate and a carbonyl as depicted in figure 3.44.

Figure 3.44 *The Decomposition of the Primary Ozonide Adapted from Vollhardt and Shore, 2003*



n.b. $R^I = CH_3(CH_2)_7$
 R^{II} and $R^{III} = H$
 $R^{IV} = (CH_2)_7CO_2H$

3. Depending on where the molozonide structure in the primary ozonide is cleaved there are two subsequent reaction pathways denoted as pathway A and pathway B.

Figure 3.45 Pathway A. The Cleavage of the Primary Ozonide Produces a Criegee Intermediate (I) and 9-oxononanoic Acid

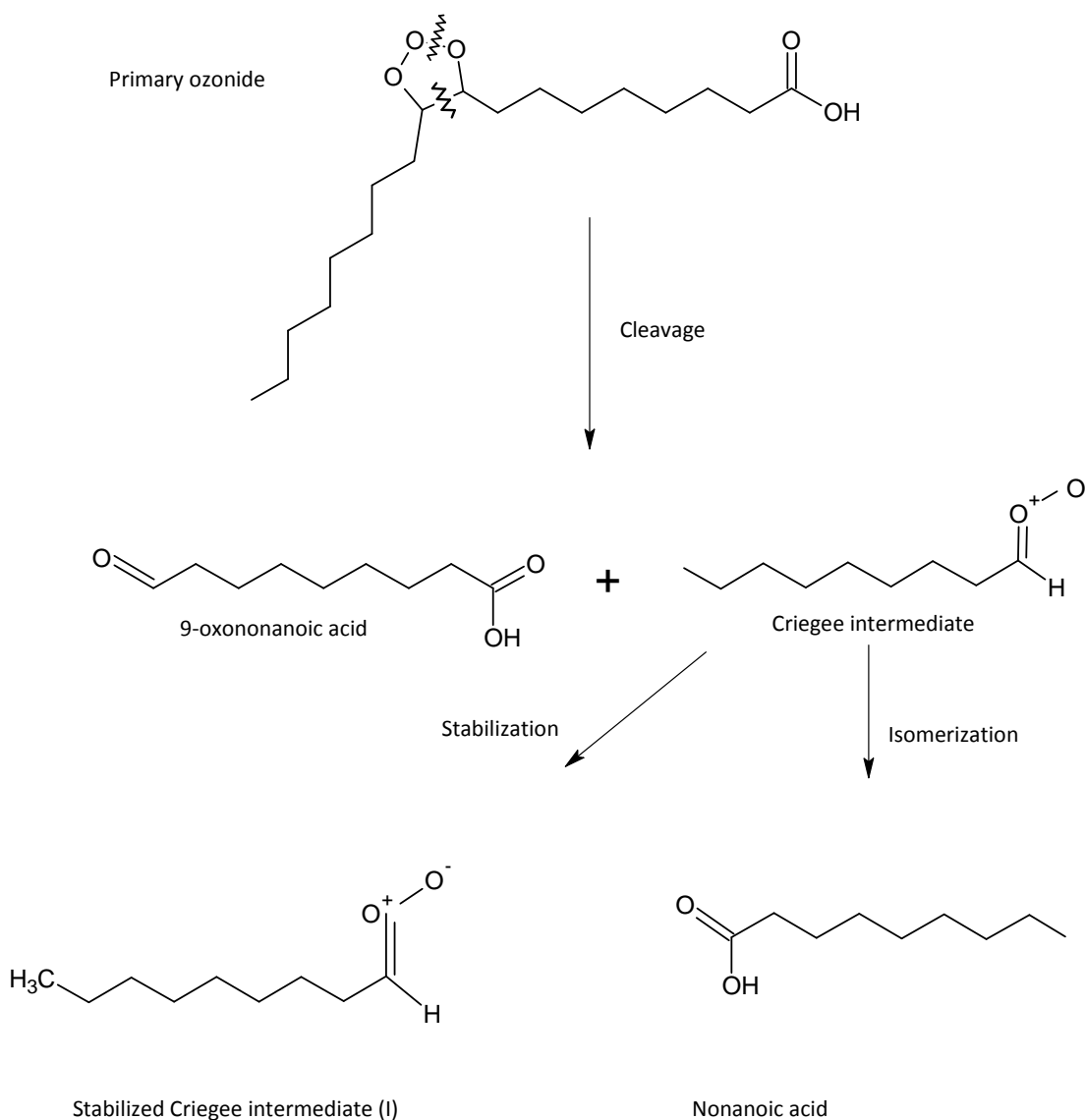
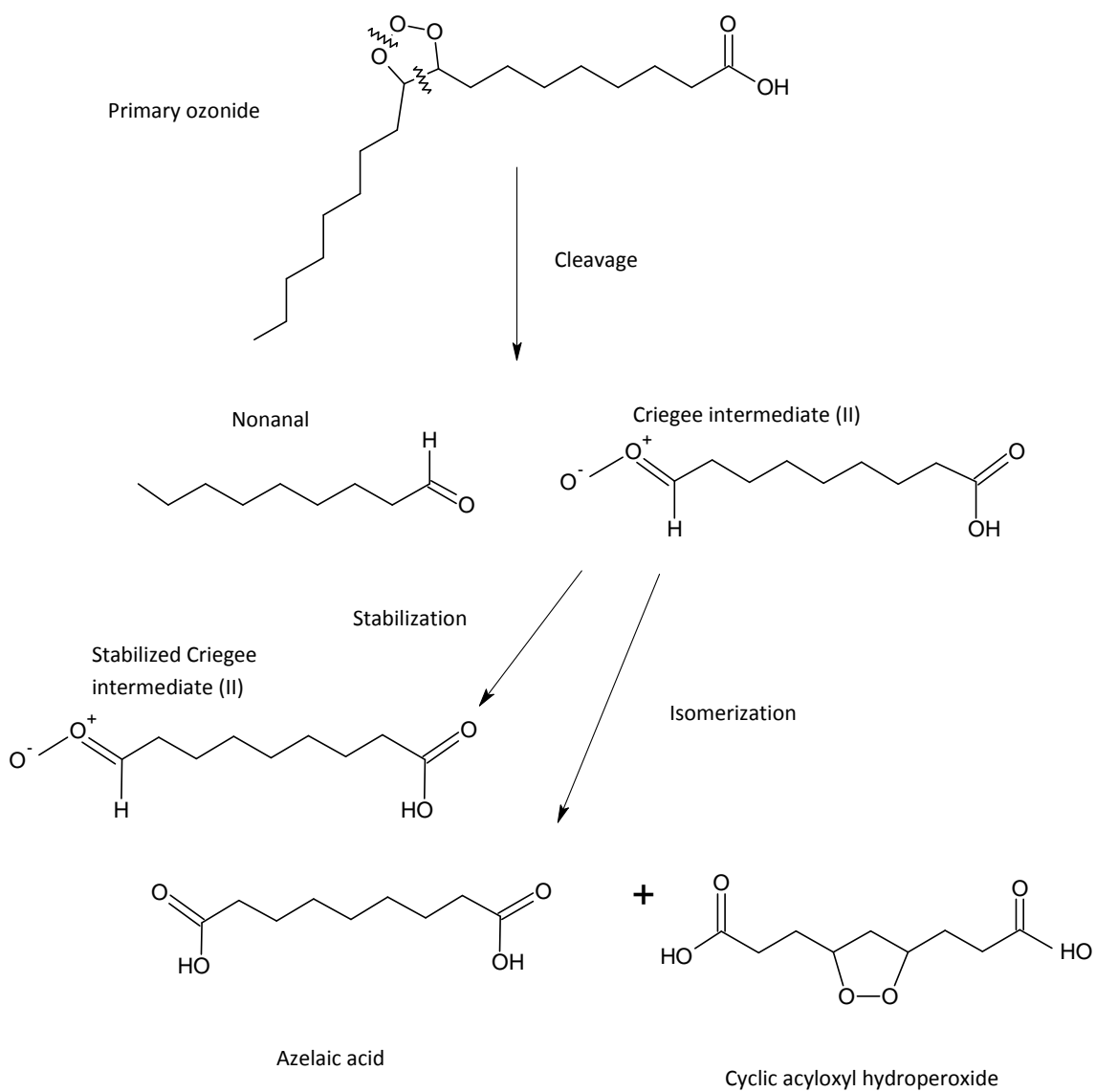


Figure 3.46 Pathway B. The Cleavage of the Primary Ozonide Produces a Criegee Intermediate (II) and Nonanal



The Criegee intermediates I and II are in a thermally excited state. The Criegee intermediates can be stabilized from collisions with the subphase solvent giving a stabilized product molecule which can then react with other product molecules or the subphase solvent, isomerised (change structural configuration) or decompose.

The combination of a stable carbonyl molecule and a stabilized Criegee intermediate forms a secondary ozonide molecule as depicted in figure 3.47. The diperoxide then decomposes forming two carbonyl molecules and oxygen as depicted in figure 3.48 and figure 3.53. The combination of stabilized Criegee intermediates could form oligomers (Zahardis et al., 2006) but the oligomer would be present as islands rather than a monolayer so would not be seen in the reflectivity data collected for this work.

Figure 3.47 *The Formation of Secondary Ozonides from Criegee Intermediates and a Stable Molecule*

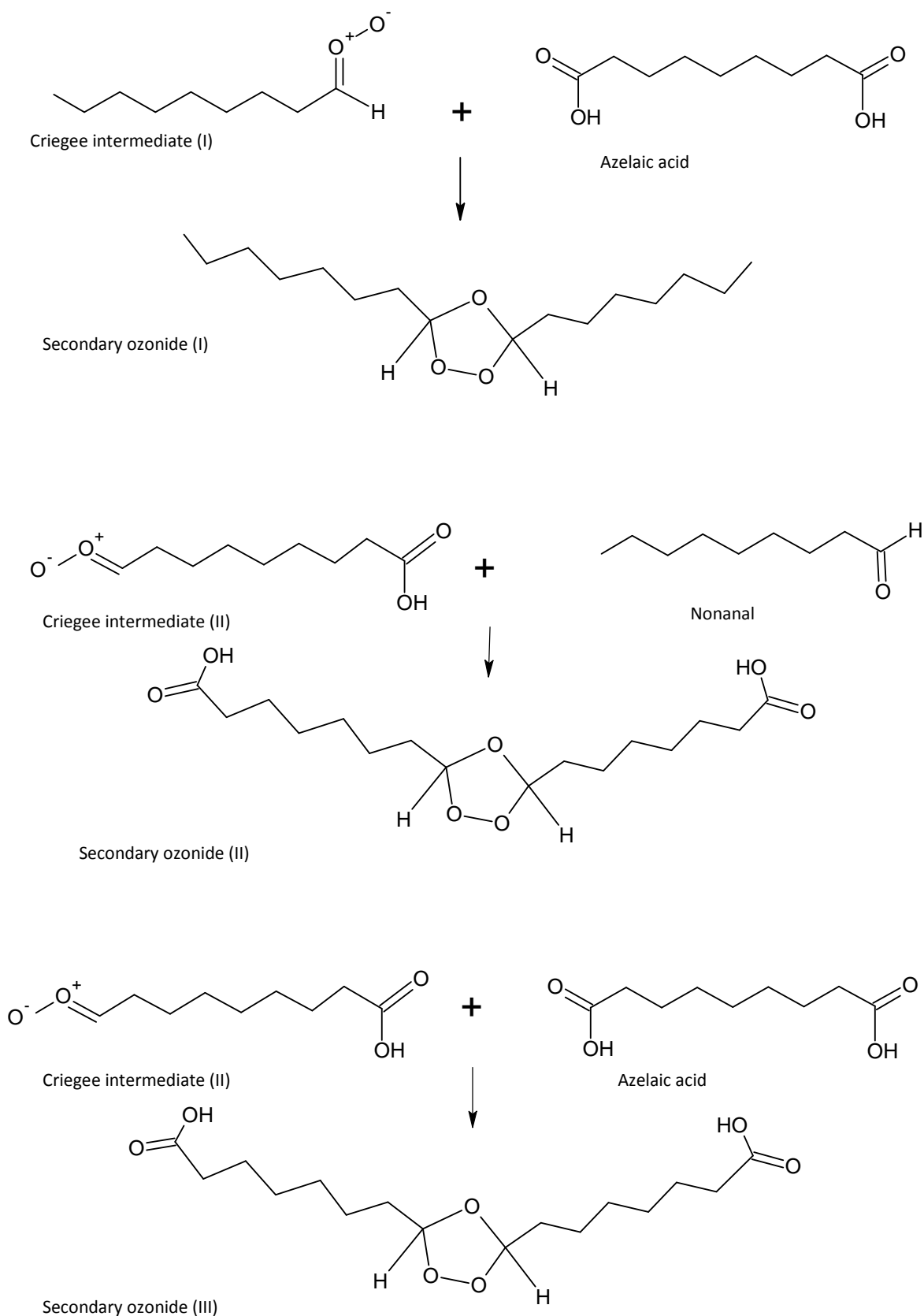


Figure 3.48 *The Formation of Diperoxide from Two Stabilized Criegee Intermediate (II) Molecules. The Diperoxide Decomposes into 9-oxononanoic Acid and Oxygen*

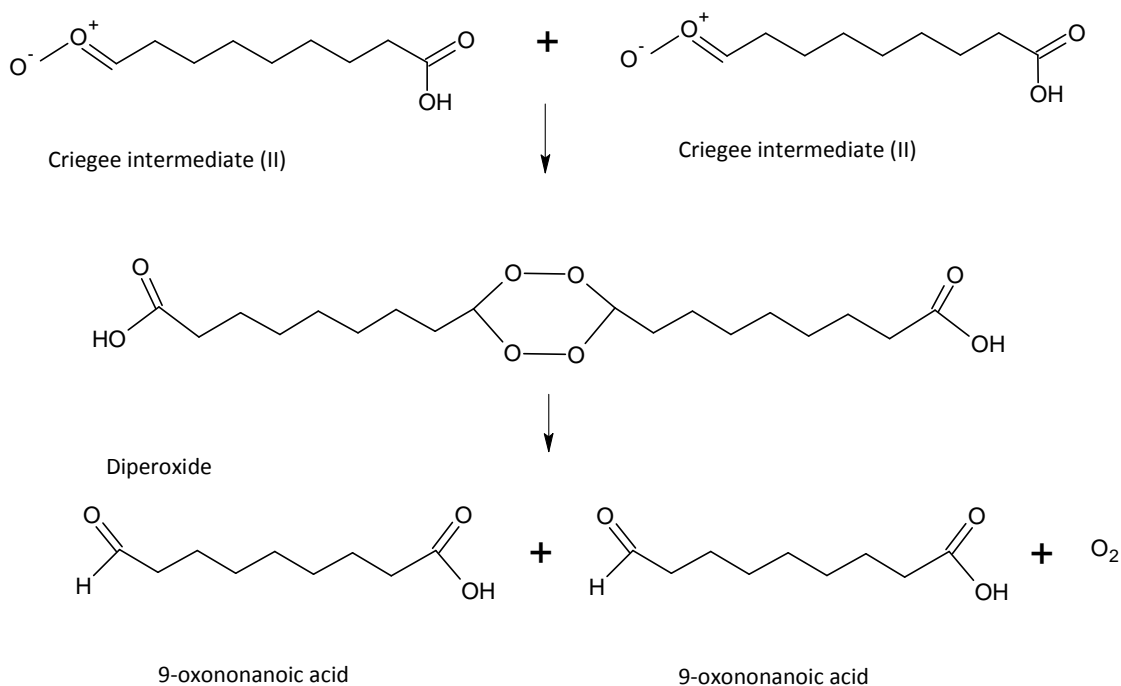
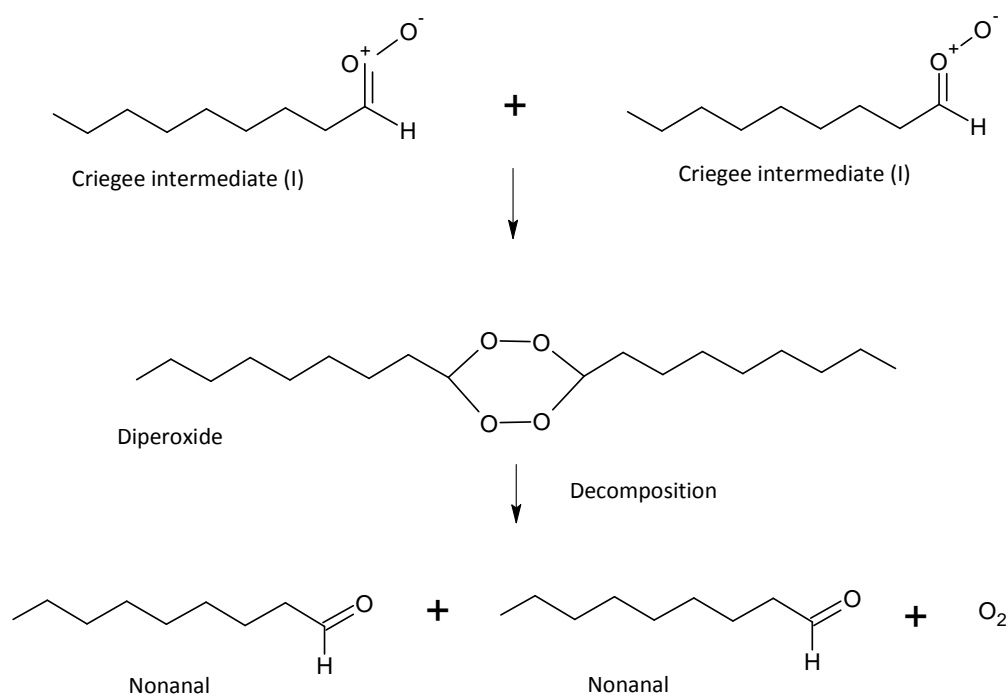


Figure 3.49 *The Formation of Diperoxide from Two Stabilized Criegee Intermediate (I) Molecules. The Diperoxide Decomposes into Two Nonanal Molecules*



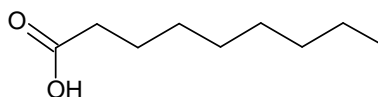
If a stabilized Criegee intermediate reacts with an aldehyde a secondary Criegee intermediate II is formed. The secondary Criegee intermediate undergoes decomposition to form a diperoxide. The diperoxide decomposes forming two 9-oxononanoic acid molecules which are volatile.

Following stabilization of isomerisation the resulting potential products would be nonanal, azelaic acid, nonanoic acid, α -acyloxyalkyl hydroperoxides, or oligomers.

3.9.4 The Fate of the Potential Reaction Products

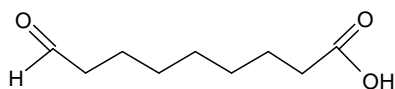
After considering the reaction mechanisms the stable reaction products will be highlighted and an explanation given for why there is no material remaining at the air-water interface after the reaction of an oleic acid monolayer with gas-phase ozone.

Figure 3.50 Nonanoic Acid (C_9) [$CH_3(CH_2)_7CO_2H$]

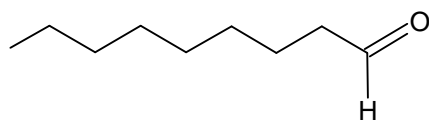


Nonanoic acid has a vapour pressure of 6.2×10^{-4} Torr at 20°C (Gilman et al. 2004 after Yaws 1994, Lide, 2004) and a solubility of 2.8×10^{-1} g L^{-1} at 20°C (Voss et al. 2007; Yalkowsky and He. 2003). Gilman et al., (2004) found that in the presence of a longer chained saturated molecule such as stearic acid (vapour pressure 1×10^{-6} Torr, solubility 0.00029 g L^{-1} at 20°C (Gilman et al. 2004 after Yaws 1994, Lide, 2004)), more volatile species could have a prolonged residence time at the air-liquid interface. Voss et al., (2007) concluded that nonanoic acid was soluble in an aqueous subphase. Nonanoic acid would not be expected to reside at the air-water interface.

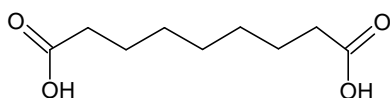
Figure 3.51 9-oxononanoic Acid [$OCH(CH_2)_7CO_2H$]



9-oxononanoic acid has a solubility of 19 g L^{-1} at 20°C (Voss et al. 2007; King, 1938). Voss et al., 2007 concluded that 9-oxononanoic acid would be soluble in an aqueous subphase of water and saline water due to its solubility, however did not test the theory with 9-oxononanoic acid. There is little data available on this chemical at the air-water interface but from its structure it would not be expected to reside at the air-water interface.

Figure 3.52 *Nonanal* [$CH_3(CH_2)_7CHO$]

Nonanal has a solubility of $9.6 \times 10^{-2} \text{ g L}^{-1}$ at 25°C (Voss et al. 2007; Yalkowsky and He. 2003). Voss et al., (2007) report that nonanal would evaporate and not persist at the air-water interface. Wadia et al., (2000) measured nonanal in the gas phase after reacting ozone with the lipid OPPC which has a cis configuration tail which is composed of oleic acid, on a Langmuir trough. Our observation is that if it was a product in the neutron experiments it did not persist at the air-water interface thus this study is in agreement with Voss et al., (2007) and Wadia et al., (2000).

Figure 3.53 *Azelaic Acid* [$HO_2C(CH_2)_7CO_2H$]

Azelaic acid has a solubility of 2.4 g L^{-1} at 20°C (Voss et al. 2007; Yalkowsky and He. 2003). It is very soluble and would not persist at the air-liquid interface; it would dissolve into the subphase of the Langmuir trough if formed.

The stable reaction products, based upon their physical data would be either soluble or volatile thus are lost from the air-water interface.

3.9.5 Discussion of the Mechanism

King et al., (2004) studied the loss of an oleic acid film from a water droplet using Raman spectroscopy. The results of the work presented in this chapter are in agreement with the findings of King et al., (2004) in that the monolayer of oleic acid in the experiment explained in this chapter was lost from the air-liquid interface, as the oleic acid was lost from the Raman spectra in the King et al., (2004) experiments, also that the products of the reaction of O_3 and oleic acid were either volatile or soluble. The fully deuterated oleic acid monolayer was lost from the air-liquid interface of the Langmuir trough in approximately 3000 to 4000 seconds. The ozone concentration was given as sub-picomolar in the King et al., (2004) study so was much lower than in this experiment. The oleic acid film would have been much thicker than a monolayer yet the signal declined more rapidly. The King et al., (2004) study gives evidence for the product nonanal being initially soluble as it gave spectra from the droplet phase.

Voss et al., (2007) observed no significant variation in the results of oxidation of an oleic acid monolayer on a water subphase or that of a 0.6 M sodium chloride solution using sum frequency generation vibrational spectroscopy to observe the reaction products and a Langmuir trough to study surface pressure at the air-water interface. In the Langmuir trough experiments an ozone concentration of $477 \pm 201 \times 10^{12}$ molecule cm^{-3} was reacted with the film. The Voss et al., (2007) kinetic decay of oleic acid on a subphase of water took 1500 seconds to reach a surface pressure of zero when reacted with ozone. The monolayer used for the neutron experiments presented here was exposed to far lower O_3 concentrations and took 2000 to 3000 seconds for the surface pressure to decay to zero. Voss et al., (2007) found no oleic acid remained at the air-water interface following exposure of the monolayer to ozone a result which our work is in agreement with. Voss et al., (2007) observed a change in the spectra from that of oleic acid after a few seconds of ozone exposure. The change in signal was found to be a result of a change in the order of the monolayer and was not due to products of the reaction residing at the air-liquid interface, this finding is in agreement with the inflection feature observed in the experiments detailed in this chapter. Voss et al., (2007) point out an implication of the reaction causing disorder in a cloud droplet film as this would allow the underlying aqueous subphase of a droplet to evaporate or separate into smaller droplets. Morris et al., (2002), noted that smaller droplets have a larger uptake coefficient, so clouds which have a smaller droplet size distribution may have a more rapid kinetic regime for the reaction of an organic film with gas phase ozone. This could be one of the pathways by which a cloud scavenges ozone in the troposphere.

Voss et al., (2006) studied the reaction of gas-phase ozone with a deuterated oleic acid monolayer spread in a petri dish observing the reaction with sum frequency generation spectroscopy where overlapping laser pulses of a broad wavelength are used to produce a spectrum of signal intensity versus incident infrared signal which shows peaks of C-D groups and C-H groups, the peak is sensitive to the molecular orientation and the number density of molecules at the interface. This study found that the products formed from the reaction of oleic acid and ozone were soluble or volatile and did not persist at the air liquid interface. A further study by Voss et al., (2007) found that when oleic acid was oxidised at the air-water interface and the air-saltwater interface that loss of oleic acid and its products occurred from the interface to the gaseous phase or the bulk liquid phase. The work presented in this chapter supports these findings as we also observed the loss of oleic acid from the air-water interface concluding that any products formed must be volatile or soluble. Voss et al., (2007) did not observe nonanoic acid or azelaic (nonanedioic) acid as they are highly soluble and are expected to dissolve into the aqueous subphase.

Zahardis et al., (2006) measured the high molecular weight products from the reaction of particle phase oleic acid with gas phase ozone by photoelectron resonance capture ionization spectrometry (PERCI-MS). The PERCI-MS measures the composition of the particle surface. The reaction products measured were secondary ozonides, and diperoxides, polymer formation at the particle surface was also observed. Zahardis et al., (2006) propose that the polymer formation occurs when a Criegee intermediate combines with oleic acid forming α -acyloxyalkyl hydroperoxide which then receives further additions of Criegee intermediates resulting in the formation of a polyanhydride when the intermediate molecule dehydrates. The addition of four Criegee intermediates to an oleic acid molecule was observed by Zahardis et al., (2006) which increases the polarity of the molecule, so it could potentially persist at the surface of the oleic acid particle in contrast to the findings of this work and that of King et al., (2009) with an oleic acid monolayer on an aqueous subphase.

Tedetti et al., (2007) investigated the atmospheric phenomenon of sensitized photooxidation of unsaturated hydrocarbons and fatty acids where ozone produced by photochemistry with volatile organic carbon and nitrogen oxides, initiates the oxidation process, then aqueous phase OH radical continues the oxidation of the products produced by oleic acid reacting with ozone. The secondary products were dicarboxylic acids which Tedetti et al., (2007) measured with gas chromatography and flame ionization spectroscopy. The dominant secondary product was a stable C₉ dicarboxylic acid, the secondary products ranged from C₂ to C₉. Tedetti et al., (2007) note that there was no bromide present and that this would inhibit the aqueous OH production in a saline droplet or aerosol but the chemistry shown is relevant to fresh water droplets such as rain droplets. In this work oxidation by OH radical was not observed in the experiments where the pH was altered which would inhibit OH radical production the decay of the monolayer and the pseudo first order rate constant was not markedly different from that where OH radical production would occur.

The change in the uptake of water in the presence of an oleic acid thin film subjected to gas phase ozone was investigated by Asad et al., (2004). The uptake of water by a thin film of oleic acid deposited on a gold coated quartz crystal surface was measured using a quartz microbalance which measured mass at the crystal face. The crystal was held in a chamber within a controlled atmosphere where the relative humidity could be increased so that the particle mass increased as water uptake took place, the crystal with film was then exposed to a flow of ozone in a separate chamber. After ozone exposure the particle became more hydrophilic, uptaking more water suggesting that the chain length of the molecule had decreased. With increasing exposure times to ozone a rapid uptake of water was observed followed by a plateau, after an exposure time of 10¹⁶ seconds to a concentration of 10¹⁴ to 10¹⁶ molecules cm⁻³ ozone Asad et

al., (2004) concluded that all the oleic acid would have reacted and increasing the exposure time did not lead to an increase in the water uptake. The products measured in the work of Asad et al., (2004) were consistent with cleavage of the double bond of the oleic acid molecule producing volatile nonanal with lower vapour pressure products which would remain in the condensed phase and that these product react more slowly with ozone producing the plateau behaviour. Asad et al. measured an infrared spectrum which indicated that azelaic acid was not a dominant condensed phase product and that the condensed phase product(s) were more oxidised suggesting that 9-oxononanoic acid (Katrib et al. 2004, Asad et al. 2004) was the dominant condensed phase product from the reaction of ozone and oleic acid.

The lipid OPPC (1-oleoyl-2-palmitoyl-*sn*-glycero-3-phosphocholine) has one *d*-33 unsaturated chain which in isolation has the structure of oleic acid. The other chain has a saturated structure which does not react with ozone. Wadia et al., (2000) used a Langmuir trough to measure the surface pressure and an atmospheric pressure ionization mass spectrometer (API-MS) to analyse the gas phase products of the reaction of ozone with OPPC at the air-water interface. In the Wadia et al., (2000) study the monolayer was not exposed to ozone until 5 to 30 minutes from spreading as the equipment set-up dictated. The reaction product nonanal was measured in the gas phase from the decomposition of the unsaturated chain of OPPC, a peak consistent with hydroxyhydroperoxide was also observed, gas phase OH was not observed. Flow tube measurements of the reaction of oleic acid with ozone by Broekhuizen et al., (2004) showed a loss in volume of the aerosol droplet consistent with the evaporation of nonanal.

Wadia et al., (2000) suggest a more rapid reaction of ozone with OPPC, at high ozone concentrations of 1880×10^{12} molecule cm^{-3} to 2510×10^{12} molecule cm^{-3} ozone the reaction is over in 5 minutes. Wadia et al., (2000) suggest that the production of products from the monolayer, in comparison to studies in the gas phase could be a result of the penetration and retention of ozone in the monolayer structure which could make reaction with the double bond more favourable. No trend in the data was observed with altered area per molecule / packing of the film, at an ozone concentration of 627×10^{12} molecule cm^{-3} the reaction time was slower at 11 minutes. In the experiments comprising this chapter the packing, which changed as the oleic acid film reacted, did affect the kinetics as at lower ozone concentrations that reaction was slower, however further experiments would be required to reliably establish this behaviour. It is probable that a lipid monolayer would react differently to a monolayer of a fatty acid as the head group of the lipid is more hydrophilic and the film would pack differently at the air-water interface.

In my work the inflection feature which was likely due to the orientation of the molecules which could be lying at a more horizontal angle to the air-liquid interface as the chain is shortened, appeared only at lower ozone concentrations. This may be because at a higher concentration of ozone the inflection is not measured as it would be more rapid and may be missed in the neutron measurement of surface coverage on the time order at which FIGARO had been set up to sample at. Alternatively it could have been that the higher ozone concentration was causing a different chemical mechanism to be followed however the similar bimolecular rate constants before and after the inflection does not support this. It would be possible to test this hypothesis in a future experiment.

3.9.6 Discussion of the Ozone Uptake Coefficient

In the experiments presented in this chapter an uptake coefficient was calculated by the method of Hearn et al., (2005), for the reactive uptake of ozone in a layer and that dissolved into the bulk which then reacts with a layer, this analysis as shown in equation 3.18 was used by González-Labrada et al., (2007) and by King et al., (2009) for the reaction of gas phase ozone with an oleic acid monolayer. The uptake coefficient for ozone reacting with a monolayer of oleic acid was 1.72×10^{-6} in the experiment detailed in this chapter. King et al., (2009) calculated an uptake coefficient of 4×10^{-6} for gas phase ozone reacting with a monolayer of oleic acid which was higher than that observed in this work. The difference in the finding of King et al., (2009) and this subsequent work may be a result of the saturated impurity in the molecule used by King et al., (2009) which would have a straighter tail potentially allowing faster penetration of the tail region of the monolayer to ozone molecules prior to ozone reacting with the unsaturated molecules in the monolayer. The concentration of ozone delivered to the reaction chamber was lower (4.2 to 16×10^{12} molecule cm^{-3}) and the starting values of the monolayer surface coverage were also lower (0.896 ± 0.125 to $2.06 \pm 0.227 \times 10^{18}$ molecule cm^{-2}), and the measured thickness of the layer was $19 \sim 20$ Å in the King et al., (2009) study compared to 15 Å in this work. The King et al., (2009) study was conducted in a Teflon bag rather than an aluminium reaction chamber. It is possible that there would be different flow conditions within a bag that would be more difficult to model so the ozone concentration in the monolayer region could be inaccurate. A larger uptake coefficient implies a more reactive system, it would be expected that a monolayer with more saturated molecules would be less reactive, this will be investigated in chapter 4 with mixed monolayer's of stearic and oleic acid.

The study of a monolayer of oleic acid on an aqueous pendant drop by González-Labrada et al., (2007) gave an uptake coefficient of 2.6×10^{-6} which is in agreement with the results of the work in this chapter and with that of King et al., (2009).

The study of submicron aerosol droplets of oleic acid reacting with ozone was measured with aerosol flow mass spectroscopy by Morris et al., (2002). The mass spectrometry techniques measure the loss of the organic substrate (Zahardis and Petrucci, 2007) from which an uptake coefficient can be calculated. Moise and Rudich, (2002) calculated an uptake coefficient of $8.3 \pm 0.2 \times 10^{-4}$ for ozone reacting with liquid oleic acid coating on the walls of a flow reactor/tube, a similar experiment by Thornberry and Abbatt, (2004) produced an uptake coefficient of $8.0 \pm 1.0 \times 10^{-4}$ for ozone reacting with an oleic acid coating, both these studies related the magnitude of the reactive uptake coefficient to the presence of unsaturated bonds (Zahardis and Petrucci, 2007). Morris et al., (2002) calculated the reactive uptake probability for ozone on oleic acid of $1.6 \pm 0.2 \times 10^{-3}$ based on the measurement of the consumption of oleic acid from particles of size 200, 400 and 600 nm. Morris et al., (2002) showed that oleic acid was consumed more rapidly by ozone in a population of smaller particles and that the consumption of oleic acid is slower when the aerosol is of a larger size. The study notes that it is difficult for oleic acid to replenish at the surface of a droplet if there are also saturated molecules present such as in an atmospheric droplet setting so the atmospheric validity of the uptake coefficient is limited, there was no water present in the Morris et al., (2002) study. The work presented here in chapter 3 will show the effect of the presence of saturated molecules on the uptake coefficient.

The effect of ozone oxidation on droplets of 2-propanol and oleic acid droplets in an aerosol flow tube coupled with single particle mass spectrometry was measured by Smith et al., (2002). The particle size decreased through reaction with gas phase ozone. Smith et al., (2002) concluded that the rate of oleic acid diffusion did not limit the reaction rate. Smith et al., (2002) used a size range of particles ($2.45\mu\text{m}$ to 680 nm) which was similar to that in the Morris et al., (2002) study. Smith et al., (2002) obtained uptake coefficients for individual particles of $0.99 \pm 0.09 \times 10^{-3}$ to $7.3 \pm 1.5 \times 10^{-3}$.

The uptake coefficients obtained from particle based experiments are larger than those obtained from monolayer experiments. Zahardis and Petrucci, (2007) note that particle based methods that do not account for secondary chemistry and produce an artificially large uptake coefficient. The monolayer neutron surface coverage method does not take into account the secondary chemistry of species that would react with oleic acid which may explain the difference in the uptake coefficient value when compared with aerosol particle studies which do giving a larger figure as the potential for reaction is greater in the presence of a secondary reactant species such as a Criegee intermediate. It may also be that the curved aerosol particle/droplet surface allows an orientation of molecules in the film which makes the double bond more accessible to the gas phase ozone molecules allowing more rapid reaction, as the films in the particle studies are not a monolayer there would also be rapid replacement of oleic acid at the air-droplet interface. Any

replacement of oleic acid molecules at the air-water interface is unlikely to be as efficient in an atmospheric droplet as it would be expected that the majority of amphiphiles would already reside at the air-water interface and the presence of saturated amphiphiles would potentially lower the uptake coefficient although this was not seen in the work of King et al., (2009) where a saturated impurity was present, it may be that the impurity was a small mole fraction, in the atmosphere it is likely that the saturated component of a monolayer would be more abundant depending on the abundance of OH radical which reacts with the saturated molecules. Moise and Rudich, (2000) studied the reactive uptake of ozone with self-assembled monolayers and with organic liquids showing that the uptake coefficient for ozone reacting with an alkene per reactive site was $9 \times 10^{-19} \text{ cm}^2 \text{ molecule}^{-1}$.

Atmospherically aged aerosol has a higher saturated component but oleic acid has been observed in aerosol that is a few days old. Smoydzin and von Glasow, (2007) state that only a small fraction of the organic surfactants found in marine aerosol react with ozone and that the majority reacts with hydroxyl radical and nitrate based on the modelling of organic surfactant films on marine aerosol. The same work states that an issue to be resolved to accurately model organic films on atmospheric aerosol is to study how closely packed the molecules are to influence the mass exchange of material into the droplet phase. Without this being quantified the uptake behaviour cannot be accurately modelled so knowing the density of the film is essential to model the mass exchange which indirectly governs the rate of loss of gas phase oxidant species reacting with the organic film (Smoydzin and von Glasow, 2007). A Langmuir trough and neutron reflectometry study of the effect of monolayer packing on reactive uptake could provide this information although the results of my work showed that once the monolayer was re-orientated by compression of the barriers the subsequent decay kinetics were not significantly affected.

It should also be noted that the time scale of measurements is important as the reactive uptake coefficient will decrease with time as the reactive sites are depleted and as water adsorbs competitively at the air-liquid interface (Smoydzin and von Glasow, 2007). This work and that King et al., (2009) has a measurement period of minutes whereas the particle studies using mass spectrometry takes measurements on a time scale of seconds. The measurement of surface pressure by González-Labrada et al., (2007) would be on a similar time scale to that of the mass spectrometry yet this study had a result that was in agreement with the work in this chapter and that of King et al., (2009).

3.10 The Atmospheric Monolayer Lifetime

The lifetime of a cloud droplet film is an important component in atmospheric modelling. A calculation of the lifetime of an oleic acid monolayer when exposed to a concentration of 40 ppb gas phase ozone, the background level in the troposphere which translates to 1.76×10^8 molecule cm^{-2} ozone in the monolayer, was made according to equation 3.18.

$$\tau_{oleic} = \frac{1}{k [O_3]_{film}} \quad (E. 3.18)$$

The bimolecular rate constant for the loss of oleic acid is k . When calculated with the tropospheric ozone concentration in the film a lifetime for an oleic acid monolayer on a cloud droplet exposed to gas phase ozone from outside the droplet is 3.54 hours based on the kinetic data obtained in this chapter at an ozone concentration of 40 ppb.

For comparison, using the value of the bimolecular rate constants from King et al., (2009) in equation 4.26 yields a lifetime of ~ 1.3 hours for an atmospheric ozone concentration of 50 ppb. The data in King et al., (2009) was taken from the decay of an oleic acid sample which contained a saturated impurity and which was calculated to have been exposed to a higher ozone concentration in the monolayer tail region. The molecule was calculated as being 20 Å in length in the King et al., (2009) study, for the data in this chapter the molecular length was taken as 15 Å from a structural neutron measurement. Should the King et al., (2009) data have been calculated for a molecular length of 15 Å the film lifetime value would be closer to that achieved in this study. The King et al., (2009) study also used a higher ozone concentration in the film region.

Oleic acid has been found in aged atmospheric aerosol in meat cooking emissions by Rogge et al., (1991) days after emission. The results of this experiment show that oleic acid is rapidly removed from the air-liquid interface meaning that the longer lifetimes reported for particles of atmospheric aerosol must be the result of partitioning to the bulk of the aerosol where the oleic acid is protected from oxidation or due to the presence of more resistant saturated film components. This work has shown that the rate of decay of oleic acid as a monolayer leads to an atmospheric lifetime of hours and that in consistency with the work of Wadia et al., (2000) that the decay of a monolayer is more rapid than that observed in particle phase experiments.

Morris et al., (2002) attribute the longer lifetimes found in atmospheric samples to the mixture of oleic acid with saturated fatty acids such as stearic and palmitic acid after the findings of Schauer et al., (1999) that ozone reacts rapidly and diffuses at a length of <10 nm and the diffusion of oleic acid to the surface of a particle is slow (Morris et al., 2002). Ozone reacts with

the molecules at the interface meaning those that are further into the particle or tightly packed with saturated molecules could be less vulnerable to oxidation by ozone (Morris et al., 2002) and could replenish the film at the interface. Oleic acid and stearic acid are emitted from many of the same sources so it is feasible that the two compounds will be found together. This theory was tested in chapter 4 where ozonolysis of a mixed stearic acid and oleic acid film was undertaken.

3.11 Conclusions

The oxidation of an oleic acid monolayer on an aqueous subphase by gas phase ozone resulted in the removal of the monolayer from the air-water interface. The kinetic decay of the oleic acid monolayer was exponential with a repeatable inflection feature at lower ozone concentrations. The inflection feature in the decay of the oleic acid monolayer was related to the packing of the film at the interface as the feature could be repeated by recompressing the monolayer. In an atmospheric setting the lifetime of a cloud droplet film composed of oleic acid would be approximately 2 minutes based on this experiment, which is shorter than that calculated from particle phase studies.

3.12 Suggestions for Further Work

To further investigate whether the inflection region observed in the decay of fully deuterated oleic acid at 16.1 ± 2.20 molecule cm^{-3} O_3 was a structural phenomenon caused by the orientation of the molecules of oleic acid at the air-liquid interface or a chemical phenomenon caused by the shortening of the chain of the oleic acid molecule, a series of structural neutron measurements with a wide range of momentum transfer values could be taken before and after exposure to O_3 . These measurements would show the effect of ozone on the thickness of the film. Studies of the reactive uptake coefficient for ozone with the monolayer of oleic acid taken with neutron reflectometry at different surface pressures to investigate the effect of the molecular packing on the uptake coefficient would provide useful data for aerosol modelling.

References

- Abelès, F. 1950. La théorie générale des couches minces. *Journal of Physics*. Radium, 11, pp. 307-309.
- Adam, N.K. 1968. *The Physics and Chemistry of Surfaces*. Dover Publications, New York, USA. (interlib loan)
- Adam, N.K., and Jessop, G. 1926. The Structure of Thin Films. Part VIII. Expanded Films. *Proceedings of the Royal Society* (London), A112, pp. 363-375. (interlib loan)
- Asad, A., Mmereki, B.T., Donaldson, D.J. 2004. Enhanced uptake of water by oxidatively processed oleic acid. *Atmospheric Chemistry and Physics*, 4, pp. 2083-2089.
- Barger, W.R. and Garret, W.D. 1970. Surface Active Material in the Marine Atmosphere. *Journal of Geophysical Research*, 75, 24, pp. 4561-4566.
- Barger, W.R. and Garret, W.D. 1976. Surface Active Organic Material in Air Over the Mediterranean and Over the Eastern Equatorial Pacific. *Journal of Geophysical Research*, 81, 18, pp. 3151-3157.
- Blanchard, D.C. 1963. The electrification of the atmosphere by particles from bubbles in the sea. *Progress in Oceanography*, 1, pp. 73 – 112.
- Blanchard, D.C. 1964. Sea-to-Air Transport of Surface Active Material. *Science*, 146, 3642, pp. 396-397.
- Blasing, T.J. 2011. Recent Greenhouse Gas Concentrations.
http://cdiac.esd.ornl.gov/pns/current_ghg.html. Accessed 14/06/2011. DOI:10.3334/CDIAC/atg.032.
Carbon Dioxide Information Analysis Centre, US Department of Energy.
- Bezdek, H.F. and Carlucci, A.F. 1974. Concentration and removal of liquid microlayers from a seawater surface by bursting bubbles. *Limnology and Oceanography*, 19, 1, pp. 126-132.
- Broekhuizen, K.E., Thornberry, T., Kumar, P.P., Abbat, J.P.D. 2004. Formation of cloud condensation nuclei by oxidative processing: Unsaturated fatty acids. *Journal of Geophysical Research*, 109, pp.1-8.
- Campbell, R. 2010. Web pages on the Figaro instrument as accessed on September 5th 2010
<http://www.ill.eu/instruments-support/instruments-groups/instruments/figaro/characteristics/>
- Campbell, R., Wacklin, H.P., Sutton, I., Cubitt, R., Fragneto, G. 2011. FIGARO: The new horizontal neutron reflectometer at the ILL. *European Journal Physical Journal Plus*, 126, 107.
- Chandra, S., Ziemke, J.R., Tie, X., Brasseur, G. 2004. Elevated ozone in the troposphere over the Atlantic and Pacific oceans in the Northern Hemisphere. *Geophysical Research Letters*, 31, pp 1-4.
- Cheng, Y., Li, S-M, Leithead, A., Brickell, P.C., Leaitch, W.R. 2004. Characterizations of *cis*-pinonic acid and n-fatty acids on fine aerosols in the Lower Fraser Valley during Pacific 2001 Air Quality Study. *Atmospheric Environment*, 38, 34, pp. 5789-5800.

- Chumpitaz, L.D.A., Coutinho, L.F., Meirelles, A.J.A. 1999. Surface Tension of Fatty Acids and Triglycerides. *Journal of the American Oil Chemists Society*, 76, 3, pp. 379-382.
- Climate Monitoring and Diagnostics Laboratory (CMDL). 2004. Summary Report 26. National Oceanic and Atmospheric Association; Climate Monitoring and Diagnostics Laboratory, Boulder, Colorado, USA. Available at <http://www.esrl.noaa.gov/gmd/publications/annrpt26/> as accessed on 25/08/2011.
- Cotton, W.R., Alexander, G.D., Hertenstein, R., Walko, R.L., McAnelly, R.L., Nicholls, M. 1995. Cloud venting – A review and some new global annual estimates. *Earth Science Reviews*, 39, pp. 169-206.
- Fang, J., Kawamura, K., Ishimura, Y., Matsumoto, K. 2002. Carbon Isotopic Composition of Fatty Acids in the Marine Aerosols from the Western North Pacific: Implication for the Source and Atmospheric Transport. *Environmental Science and Technology*, 36, pp. 2598-2604.
- Finlayson-Pitts, B. Pitts J.N. 2000 Chemistry of the Upper and Lower Atmosphere, Theory, Experiments and Applications. Academic Press, California, USA.
- Finlayson-Pitts, B., and Pitts, J.N. 1997. Tropospheric air pollution: Ozone, Airborne Toxics, Polycyclic Aromatic Hydrocarbons, and Particles. *Science*, 276, pp.1045-1052.
- Gaines, G.L. 1966. Insoluble Monolayers at Liquid-gas Interfaces. John Wiley and Sons Inc, New York.
- Gill, P.S., Graedel, T.E., Weschler, C.J. 1983. Organic films on atmospheric aerosol particles, fog droplets, cloud droplets, raindrops and snowflakes. *Reviews of Geophysics*, 21, 4, pp. 903-920.
- Gilman, J.B., Elaison, T.L., Vaida, V. 2004. Selectivity and stability of organic films at the air-aqueous interface. *Journal of Colloid and Interface Science*, 280, pp. 234-243.
- Goerke, J. 1998. Pulmonary surfactant: functions and molecular composition. *Biochimica et Biophysica Acta*, 1408, pp. 79-89.
- González-Labrada, E., Schmidt, R., Dewolf, C.E. 2006. Real-time monitoring of the ozonolysis of unsaturated organic monolayers. *Chemical Communications*, 23, pp.2471-2473.
- González-Labrada, E., Schmidt, R., Dewolf, C.E. 2007. Kinetic analysis of the ozone processing of an unsaturated organic monolayer as a model of an aerosol surface. *Physical Chemistry Chemical Physics*. 9, pp. 5814-5821.
- Hall, N (editor). 2010. Renaissance. The ILL Millennium Programme 2001 to 2009. The Scientific Coordination Office at ILL, Grenoble, France.
- Harrison, H., and Martinez, J.L. The ILL Millennium Programme Enters a New Era. *Neutron News*, 20, 3, pp. 25-28.

- Hearn, J.D., Lovett, A.J., Smith, G.D. 2005. Ozonolysis of oleic acid particles: evidence for a surface reaction and secondary reactions involving Criegee intermediates. *Physics Chemistry Chemical Physics*, 7, pp. 501-511.
- Intergovernmental Panel on Climate Change. 2007. Fourth Assessment Report: Climate Change 2007: Working Group 1: The Physical Science Basis. Contribution of Working Group 1 to the Fourth Assessment Report of the Intergovernmental Panel on Climate Change. [Soloman S., Quin D., Manning M., Chen Z., Marquis M., Averyt K.B., Tignor M., Miller H.L. eds]. Cambridge University Press, Cambridge, United Kingdom and New York, NY, USA, 996 pp.
- Jacob, D.J., Gottlieb, E.W., Prather, M.J. 1989. Chemistry of a Polluted Cloudy Boundary Layer. *Journal of Geophysical Research*, 94, 10, pp. 12975-13002.
- Jacob, D.J., Logan, J.A., Murti, P.P. 1999. Effect of rising Asian emissions on surface ozone in the United States. *Geophysical Research Letters*, 26, 14, pp. 2175-2178.
- Jacob, D.J. 2000. Heterogeneous chemistry and tropospheric ozone. *Atmospheric Environment*, 34, pp. 2131-2159.
- Katrib, Y., Martin, S.T., Hung, H-M., Rudich, Y., Zhang, H., Slowik, J.G., Davidovits, P., Jayne, J.T., Worsnop, D.G. 2004. Products and Mechanisms of Ozone Reactions with Oleic Acid for Aerosol Particles Having Core-Shell Morphologies. *Journal of Physical Chemistry. A*, 108, pp. 6686-6695.
- Kattner G.G. and Brockmann U.H. 1978. Fatty-acid composition of dissolved and particulate matter in surface films. *Marine Chemistry*, 6, pp. 233-241.
- Kawamura, K. and Gagosian, R.B. 1987. Implications of ω -oxocarboxylic acids in the remote marine atmosphere for photo-oxidation of unsaturated fatty acids. *Nature*, 325, pp.330-332.
- King, G. 1938. The oxidation of the 9:10-dihydroxystearic acids with periodic acid. η -Aldehydo-octoic acid., *Journal of the Chemical Society*, pp.1826-1828.
- King, M.D., Thompson, K.C., Ward, A.D. 2004. Laser tweezers Ramen study of optically trapped aerosol droplets of seawater and oleic acid reacting with ozone: Implications for cloud-droplet properties. *Journal of the American Chemical Society*, 126, pp. 16710-16711.
- King, M.D., Rennie, A.R., Thompson K.C., Fisher, F.N., Chuan Dong, C., Thomas, R.K., Pfrang, C. Hughes, A.V. 2009. Oxidation of oleic acid at the air-water interface and its potential effects on cloud critical supersaturations. *Physical Chemistry Chemical Physics*, 11, pp. 7699-7707.
- King, M.D., Rennie, A.R., Pfrang, C.P., Hughes, A.V., Thompson, K.C. 2010. Interaction of a nitrogen dioxide (NO₂) with a monolayer of oleic acid at the air-water interface - A simple proxy for atmospheric aerosol. *Atmospheric Environment*, 44, pp. 1822-1825.
- King, M.D. 2012. Personal communication: verbal.

- Larsson, K., Odham, G., Södergren, A. 1974. On lipid surface films on the sea. 1. A simple method for sampling and studies of composition. *Marine Chemistry*, 2, pp. 49-57.
- Lelieveld, J., Crutzen, P.J. 1990. Influences of cloud photochemical processes on tropospheric ozone. *Nature*, 343, pp. 227-233.
- Lelieveld, J., Crutzen, P.J. 1994. Role of deep convective cloud convection in the ozone budget of the Troposphere. *Science*, News Series, 264, 5166, pp. 1759-1761.
- Lide, D.R. 2004. Handbook of Chemistry and Physics, CRC Press, Cleveland USA.
- Limbeck, A., Puxbaum, H. 1999. Organic acids in continental background aerosols. *Atmospheric Environment*, 33, pp. 1847-1852.
- Lohmann, U. and Feichter, J. 2005. Global indirect aerosol effects: a review. *Atmospheric Chemistry and Physics*, 5, pp. 715-737.
- Lu, J.R., Thomas, R.K., Penfold, J. 2000. Surfactant layers at the air/water interface: structure and composition. *Advances in Colloid and Interface Science*, 84, pp. 143-304.
- Marty, J.C., Saliot, A., Buat-Ménard, P., Chesselet, R., Hunter, K.A. 1979. Relationship between the Lipid Compositions of Marine Aerosols, the Sea Surface Microlayer, and Subsurface Water. *Journal of Geophysical Research*, 84, C9, pp. 5707-5716.
- McNeill, F.V., Wolfe, G.M., Thornton, J.A. 2007. The oxidation of Oleate in Submicron Aqueous Salt Aerosols: Evidence of a Surface Process. *Journal of Physical Chemistry A*, 111, 6, pp 1073-1083.
- Mochida, M., Kitamori, Y., Kawamura, K., Nojiri, Y., Suzuki, K. 2002. Fatty acids in the marine atmosphere: Factors governing their concentrations and evaluation of organic films on sea-salt particles. *Journal of Geophysical Research*, 107, D17, pp. 4325-4334.
- Moise T. and Rudich, Y. 2002. Reactive Uptake of Ozone by Aerosol-Associated Unsaturated Fatty Acids: Kinetics, Mechanism and Products. *Journal of Physical Chemistry. A*, 106, 27, pp. 6469-6476.
- Monod, A. and Carlier, P. 1999. Impact of clouds on the tropospheric ozone budget: Direct effect of multiphase photochemistry of soluble organic compounds. *Atmospheric Environment*, 33, pp. 4431-4446.
- Morris, J.W., Davidovits, P., Jayne, J.T., Jimenez, J.L., Shi, Q., Kolb, C.E., Worsnop, D.R., Barney, W.S., Cass, G. 2002. Kinetics of submicron oleic acid aerosols with ozone: A novel aerosol mass spectrometric technique. *Geophysical Research Letters*, 29, 9.
- O'Dowd, C.D., de Leeuw, G. 2007. Marine aerosol production: a review of the current knowledge. *Philosophical Transactions of the Royal Society A*, 365, 1856, pp. 1753-1774.

- Penfold, J., and Thomas, R.K., 1990. The application of the specular reflection of neutrons to the study of surfaces and interfaces. *Journal of Physics: Condensed Matter*, 2, pp. 1369-1412.
- Pio, C.A., Alves, C.A., Duarte, A.C. 2001. Identification, abundance and origin of atmospheric organic particulate matter in a Portuguese rural area. *Atmospheric Environment*, 35, 8, pp. 1365-1375.
- Popendorf, K., Lomas, M.W., Van Mooy, B.A.S. 2011. Microbial sources of intact polar diacylglycerolipids in the Western North Atlantic Ocean. *Organic Geochemistry*, 42, pp. 803-811.
- Read, K.A., Mahajan, A. S., Carpenter, L.J., Evans, M.J., Faria, B.V.E., Heard, D.E., Hopkins, J.R., Lee, J.D., Moller, S.J., Lewis, A.C., Mendes, L., McQuaid, J.B., Oetjen, H., Saiz-Lopez, A., Pilling, M.J., Plane, J.M.C. 2008. Extensive halogen-mediated ozone destruction over the tropical Atlantic Ocean. *Nature*, 453, pp.1232-1235.
- Rennie, A. 2011. Personal communication: email.
- Rogge, W.F., Hildemann, L.M., Mazurek, M.A., Cass, G.R. 1991. Sources of Fine Organic Aerosol. 1. Charbroilers and Meat Cooking Operations. *Environmental Science and Technology*, 25, pp. 1112-1125.
- Rogge, W.F., Hildemann, L.M., Mazurek, M.A., Cass, G.R., Simoneit, B.R. 1993^a. Sources of Fine Organic Aerosol. 4. Particulate Abrasion Products from Leaf Surfaces and Urban Plants. *Environmental Science and Technology*, 27, pp. 2700-2711.
- Rogge, W.F., Hildemann, L.M., Mazurek, M.A., Cass, G.R. 1993^b. Sources of fine organic aerosol, 2. Noncatalyst and catalyst-equipped automobiles and heavy duty diesel trucks. *Environmental Science and Technology*, 27, 636-651.
- Rudich, Y., Donahue, N.M., Mentel, T.F. 2007. Aging of Organic Aerosol: Bridging the Gap between Laboratory and Field Studies. *Annual Reviews of Physical Chemistry*, 58, pp. 321-352.
- Rues, (de) M., Dentener, F., Thomas, A., Borrmann, S., Ström, J., Lelieveld, J. 2000. Airborne observations of dust aerosol over the North Atlantic Ocean during ACE 2: Indications for heterogeneous ozone destruction. *Journal of Geophysical Research*, 105, D12, pp. 15263-15275.
- Schauer J.J., Kleeman M.J., Cass G.R., Simoneit B.R.T. 1999. Measurement of Emmissions from Air Pollution Sources. 1. C₁ to C₂₉ Organic Compounds from Meat Charbroiling. *Environmental Science and Technology*, 33, 10, pp. 1566-1577.
- Seinfeld, J.H., and Pandis, S. N. 2006. Atmospheric Chemistry and Physics From Air Pollution to Climate Change. Second Edition. Wiley and Sons, New York, USA.
- Simoneit, B.R. and Mazurek, M. A. 1982. Organic Matter of the Troposphere-II. Natural background of biogenic lipid matter in aerosols over the rural western United States. *Atmospheric Environment*, 16, 9, pp. 2139-2159.

- Simoneit, B.R., Cox, R.E., Standley, L.J. 1988. Organic Matter of the Troposphere-IV Lipids in Harmattan Aerosols of Nigeria. *Atmospheric Environment*, 22, 5, pp. 983-1004.
- Simoneit, B.R., Sheng, G., Chen, X., Fu, J., Zhang, J., Xu, Y. 1991. Molecular Marker Study of Extractable Organic Matter in Aerosols from Urban Areas of China. *Atmospheric Environment*, 25A, 10, pp. 2111-2129.
- Simoneit, B.R., Kobayashi, M., Mochida, M., Kwamura, K., Huebert, B.J. 2004. Aerosol particles collected on aircraft flights over the northwestern Pacific region during the ACE-Asia campaign: Composition and major sources of the organic compounds. *Journal of Geophysical Research*, 109, pp. D19S09.
- Smith, G.D., Woods III, E., DeForest C.L., Baer, T., Miller, R.E. 2002. Reactive Uptake of Ozone by Oleic Acid Aerosol Particles: Application of Single-Particle Mass Spectrometry to Heterogeneous Reaction Kinetics. *Journal of Physical Chemistry A*, 106, pp. 8085-8095.
- Smoydzin, L. and von Glasow, R. 2007. Do organic surface films on sea salt aerosol influence atmospheric chemistry? – A model study. *Atmospheric Chemistry and Physics*, 7, pp. 5555-5567.
- Smoydzin, L. and von Glasow, R. 2007. Interactive comment on ‘Do organic surface films on sea salt aerosol influence atmospheric chemistry? – A model study’. *Atmospheric Chemistry and Physics Discussions*, 6, pp. S7241-S7254.
- Södergren, A. 1987. Origin and composition of surface slicks in lakes of differing trophic status. *Limnology and Oceanography*, 32, 6, pp. 1307-1316.
- Squires, P. 1958. The Microstructure and Colloidal Stability of Warm Clouds Part II. *Tellus X*, II, pp.262-271.
- Srisankar, E.V. and Patterson, L.K. 1979. *Archives of Environmental Health*, 34, 5, pp. 346-349.
- Tedetti, M., Kawamura, K., Narukawa, M., Joux, F., Charrière, B., Sempéré, R. 2007. Hydroxyl radical-induced photochemical formation of dicarboxylic acids from unsaturated fatty acid (oleic acid) in aqueous solution. *Journal of Photochemistry and Photobiology A: Chemistry*, 188, 1, pp. 135-139.
- ^aTervahattu, H., Hartonen, K., Kerminen, V-M., Kupiainen, K., Aarnio, P., Koskentalo, T., Tuck, A.F., Vaida, V. 2002. New evidence of an organic layer on marine aerosols. *Journal of Geophysical Research*, 107, D7, pp. 4053- 4061.
- ^bTervahattu, H., Juhanoja, J., Kupiainen, K. 2002. Identification of an Organic Coating on Marine Aerosol Particles by TOF-SIMS. *J Geophys. Res.*, 107.

- Tervahattu, H., Juhanoja, J., Vaida, V., Tuck, A.F., Niemi, J.V., Kupiainen, K., Kulmala, M., Vehkamäki, H. 2005. Fatty acids on continental sulphate aerosol particles. *Journal of Geophysical Research*, 110.
- Thornberry, T., Abbatt, J.P.D. 2004. Heterogeneous reaction of ozone with liquid unsaturated fatty acids: detailed kinetic and gas-phase product studies. *Physical Chemistry Chemical Physics*, 6,1, pp. 84-93.
- Tseng, R-S., Viechnicki, J.T., Skop, R.A., Brown, J.W. 1992. Sea-to-Air Transfer of Surface –Active Organic Compounds by Bursting Bubbles. *Journal of Geophysical Research*, 97, C4, pp. 5201-5206.
- Twomey, S. 1974. Pollution and Planetary Albedo. *Atmospheric Environment*, 8, 12, pp. 1251-1256.
- United Kingdom Photochemical Oxidants Review Group. 1997. Edited by Fowler, D. Published by the Department for Environment, Food and Rural Affairs (DEFRA) Available online at http://uk-air.defra.gov.uk/library/reports?report_id=108 as accessed 21/05/2011.
- Vingarzan, R. 2004. A review of surface ozone background levels and trends. *Atmospheric Environment*, 38, pp. 3431-3442.
- Voss, L.F., Bazerbashi, M.F., Beekman, C.P., Hadad, C.M., Allen, H.C. 2007. Oxidation of oleic acid at air/liquid interfaces. *Journal of Geophysical Research*, 112, pp. 1-9.
- Wadia, Y., Tobias, D.J., Stafford R., Finlayson-Pitts B.J. 2000. Real-Time Monitoring of the Kinetics and Gas-Phase Products of the Reaction of Ozone with an Unsaturated Phospholipid at the Air-Water Interface. *Langmuir*, 16, pp. 9321-9330.
- Walcek, C.J., Yuan, H-H., Stockwell, W.R. 1997. The Influence of Aqueous-Phase Chemical Reactions on Ozone Formation in Polluted and Nonpolluted Clouds. *Atmospheric Environment*, 31, 8, pp. 1221-1237.
- Warneck, P. 1988. Chemistry of the Natural Atmosphere. International Geophysics Series. Volume 41. Academic Press Inc, San Diego, USA.
- Yalkowsky, S.H. and He, Y. 2003. Handbook of Aqueous Solubility Data, CRC Press, Boca Raton, Florida, USA.
- Yaws, C.L. 1994. Handbook of Vapor Pressure, Gulf Publications, Houston USA.
- Zahardis, J., LaFranchi, B.W., Petrucci, G.A. 2006. Direct observation of polymerization in the oleic acid – ozone heterogeneous reaction system by photoelectron resonance capture ionization aerosol mass spectrometry. *Atmospheric Environment*, 40, pp. 1661-1670.
- Zahardis, J. and Petrucci, G.A. 2007. The oleic acid-ozone heterogeneous reaction system: products, kinetics, secondary chemistry, and atmospheric implications of a model system – a review. *Atmospheric Chemistry and Physics*, 7, pp.1237-1274.

Ziemann, P.J. 2005. Aerosol products, mechanisms, and kinetics of heterogeneous reactions of ozone with oleic acid in pure and mixed particles. *Faraday Discussions*, 130, pp. 460-490.

4 The Oxidation of Mixed Composition Monolayers

4.0 Abstract

Thin films on atmospheric aerosol are likely to be composed of a mixture of insoluble surface active molecules. In the chapter presented here the oxidation of oleic is studied in the presence of other insoluble surface active molecules. The surface coverage and surface pressure of mixed composition monolayers composed of stearic acid and oleic acid, one molecule deuterated and one non-deuterated, were monitored at the air-water interface of a Langmuir trough as the monolayer was exposed to gas-phase ozone. The deuterated stearic acid, mixed with non-deuterated oleic acid, monolayer did not decay when exposed to gas-phase ozone, a finding which contrasted with a very similar study of reactions occurring within the tail region of the POPC molecule. An atmospheric monolayer of a mixed composition of both saturated and unsaturated molecules could be resistant to ozone initiated oxidation, but OH radical as shown in chapter 2 will remove such a film.

4.1 Introduction

A monolayer on an atmospheric cloud droplet monolayer would have a mixed composition of surface active organics at the air-water interface due to the highly varied composition of such compounds in the troposphere. Experiments were conducted with mixed stearic acid and oleic acid monolayers of varying mole fractions of each organic acid. The mixed monolayer oxidation experiments enable a better understanding of the way in which a cloud droplet monolayer would be oxidised by ozone initiated processes when both saturated and un-saturated molecules were present at the air-water interface and to study the kinetics of this process.

4.2 Aims

The aims of this experimental work were:

- To monitor how the reaction between ozone and a mixed film composed of saturated and unsaturated fatty acids proceeded at the air-water interface.
- To measure the surface pressure and surface coverage of the monolayer in real time to enable kinetic analysis.

4.3 Background

The model of a cloud droplet film as defined by many authors (e.g. Ellison et al. 1999; Vaida et al. 2000; Elaison et al. 2003; Gilman et al. 2004,2006; Donaldson and Vaida 2006; Tervahattu et al. 2002^{a,b}, 2005) is always comprised of a mixed composition film of surface active compounds found in the atmosphere. To study the ozone initiated oxidation of a mixed composition monolayer as a proxy for a cloud droplet film, stearic and oleic acid monolayers were studied with neutron reflectometry under exposure to gas-phase ozone. Stearic acid $\text{CH}_3(\text{CH}_2)_{16}\text{COOH}$ was chosen as a saturated molecule and oleic acid (cis-9-octadecanoic acid) $\text{CH}_3(\text{CH}_2)_7\text{CH}=\text{CH}(\text{CH}_2)_7\text{COOH}$ was chosen as representative of an unsaturated molecule film component as both fatty acids have been sampled from the troposphere and they occur in the same location and had been independently studied at the air-water interface in chapter 2 and 3. Zahardis and Petrucci, (2007) stated that the study of internally mixed particles and coatings in the field of aerosol science represents ‘the next stage in the progression towards more realistic proxies of tropospheric organic aerosols’. The two molecules are simple, well characterised molecules that are miscible in a monolayer, thus the experiment is not excessively complex as to complicate the analysis beyond the capabilities of the project.

Oleic acid is created in animal cells and it is a constituent of animal and plant fats, (Daintith, 2008) and is found in many cooking oils (Rogge et al. 1991; Frankel, 1998). Tervahattu et al., (2002^{a, b}, 2005) found oleic acid to be the dominant unsaturated acid found in marine aerosol organic films. Oleic acid in a cloud droplet setting is subject to oxidation from OH and NO_3 as well as O_3 (Zahardis and Petrucci, 2007). The saturated stearic acid molecule, which was the subject of chapter 2, is unreactive with ozone. It is reasonable to assume that stearic and oleic acid can be emitted to the atmosphere from the same source. One of the primary sources of such compounds in urban areas is the combustion of cooking oils (Rogge et al. 1991). To illustrate how cooking is a combined source of stearic and oleic acid to the atmosphere, table 4.1 adapted from Frankel, (1998) shows the relative weight percentages of stearic acid and oleic acid in common cooking oils and fats. Both stearic acid and oleic acid are also emitted to the atmosphere from land plant emissions (Rogge et al. 1993^a), vehicle exhaust (Rogge et al. 1993^b) and from the sea surface microlayer (Marty et al. 1979) which is the dominant source of surface active organic material to warm marine cloud.

Table 4.1 *The Weight Percentage of the Stearic Acid and Oleic Acid Components of Common Cooking Fats and Oils*

Source	Stearic acid (weight %)	Oleic acid (weight %)
Corn	3	31
Peanut / Groundnut	3	38
Olive	2	78
Palm	4	40
Rapeseed / Canola	2	56
Sunflower	5	20
Lard	11	44
Beef Tallow	7	48

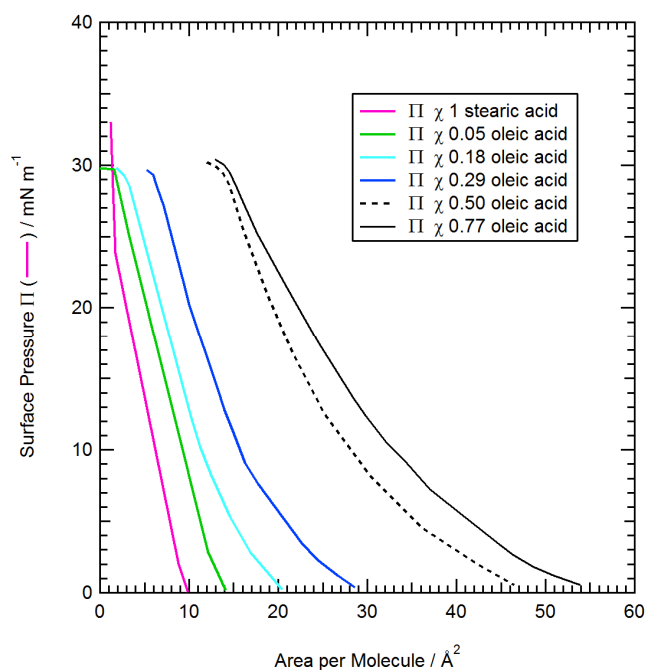
The solubility of oleic acid in water is $1.15 \times 10^{-5} \text{ gL}^{-1}$ (Howard and Meylan, 1997; Voss et al. 2006), the solubility of stearic acid in water is 0.0029 gL^{-1} (Weast, 1977), thus although stearic acid is more soluble in water than oleic acid, both acids form insoluble monolayers. In a mixed monolayer at room temperature and pressure, both molecules are miscible and would both be present at the air-water interface.

The monolayer formed by spreading oleic and stearic acid together from the same spreading solution will form a mixed monolayer of stearic acid and oleic acid molecules present at the air-water interface. The surface pressure measurement of a mixed film will be the average (but equal in sum) surface pressure of both molecules comprising the monolayer (equation 4.1).

$$\Pi_{monolayer} = \Pi_{stearic} + \Pi_{oleic} \quad (E 4.1)$$

The oleic acid molecule occupies a larger area than its saturated counterpart due to the *cis* form double bond in the hydrocarbon chain (Harkins and Florence, 1938). The bent shape of the oleic acid molecule increases the intermolecular distance in the monolayer thus oleic acid has a lower binding energy to the surrounding molecules than a saturated fatty acid (Harkins and Florence, 1938).

Figure 4.1 *The Surface Pressure versus Surface Area per Molecule Isotherms of Oleic and Stearic Acid Mixed Monolayers*



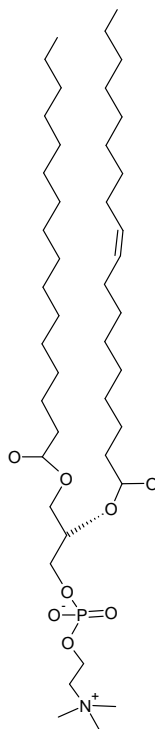
The data in figure 4.1 was sourced from Feher et al., (1977).

In a mixed stearic and oleic acid monolayer under compression the oleic acid is squeezed out of the monolayer at high surface pressures of $25\text{--}30\text{ mN m}^{-1}$ (Harkins and Florence, 1938) and $29\text{--}30\text{ mN m}^{-1}$ (Feher et al. 1977). With an increasing mole fraction of oleic acid the isotherm of a mixed stearic and oleic acid monolayer is shifted to a higher area per molecule and has a smoother appearance without defined phase changes in the slope of surface pressure versus area per molecule as shown in figure 4.1 (Feher et al. 1977).

4.4 Previous Studies of Mixed Composition Saturated with Unsaturated Molecular Constituent Monolayers Reacting with Ozone

Thompson et al., (2010) used neutron reflectometry to monitor the surface coverage of a POPC phospholipid monolayer at the air-water interface of a Langmuir trough as the monolayer was exposed to gas phase ozone. The POPC molecule shown in figure 4.2 has one saturated and one unsaturated tail. Isotopologues of POPC were used with the tails only deuterated, the head group only deuterated and the saturated tail individually as the only deuterated component. The surface coverage was measured over reaction time to show where the molecule was degrading due to reaction with ozone. Although the decay of the unsaturated tail only was not studied, it was concluded from the decay of the saturated tail (which was deuterated individually) that the gas-phase ozone attacked the double bond in the unsaturated tail group then the saturated tail group was subsequently broken down by a product of the reaction of ozone and the CH₂ double bond which produced OH radical which reacted with the saturated tail group in an intramolecular reaction.

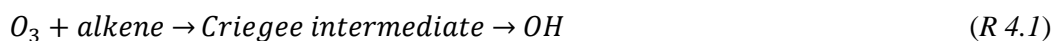
Figure 4.2 *The POPC Molecule Used in the Work of Thompson et al., (2010)*



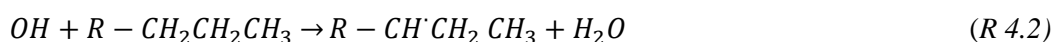
It is hypothesised that for a mixed monolayer of stearic and oleic acid exposed to gas-phase ozone the same decay mechanism may occur within the monolayer, this will be tested in this

chapter. Further studies involving mixed composition particles and thick films will be discussed in section 4.7.2.

The reaction which produces the OH radical which reacts with the saturated tail of the lipid at the air-water interface is shown in reaction 4.1.



Subsequently the OH radical can react with the CH₂ groups.



4.5 Experimental Methodology

The experimental section will be presented in the following order:

- Experimental objectives (4.5.1).
- A description of the oleic acid and stearic acid samples used for the neutron reflectometry experiments (4.5.2).
- The methodology of the neutron reflectometry measurement of a kinetic decay in the surface coverage measured simultaneously with the kinetic decay in the monolayer surface pressure (4.5.3).
- The generation of gas phase ozone (4.5.4) and the modelling of the ozone concentration in the reaction chamber (4.5.4.1).

4.5.1 Experimental Objectives

The experiments to monitor the surface coverage and surface pressure of the mixed composition monolayers were conducted using the Langmuir trough coupled with neutron reflectometry as has been described in the preceding chapters. The experiments were undertaken to investigate the following:

- To measure how oxidation of a mixed composition film would affect the surface coverage of each compound at the air-water interface.
- To investigate whether the oxidation of oleic acid would initialize a radical chain reaction with a saturated surfactant in the same film that does not react with ozone.

4.5.2 The Oleic Acid and Stearic Acid Samples

Fully deuterated stearic acid was purchased from Sigma Aldrich. The oleic acid sample used for this experimental work was the first fully deuterated oleic acid sample synthesised by the Oxford Isotope Facility. It should be noted that at the time of this experiment the fully deuterated oleic acid now available from Sigma Aldrich was not commercially available. The spreading solutions were made up with one component fatty acid deuterated and the other fatty acid component non-deuterated in chloroform so that the oxidation over time of the individual species reacting in the mixed composition monolayer could be observed. The mixed solutions consisted of a saturated and un-saturated fatty acid. The deuterated component had a strong scattering length density ($\rho = 6.57 \times 10^{-6} \text{ \AA}^{-2}$ for fully deuterated oleic acid) which is in contrast with the non-deuterated component which had a smaller scattering length density ($\rho = -6.71 \times 10^{-8} \text{ \AA}^{-2}$ for non-deuterated stearic acid) thus the surface coverage measurement is valid for the deuterated molecule in the presence of the non-deuterated compound as the majority of the neutron reflectivity signal is due to the deuterated component. The approximation is made that all neutron reflection is due to the deuterated component of the monolayer and thus the calculated surface coverage is that of the deuterated component.

The undiluted compounds were kept in a freezer at -18°C in the original containers under dark conditions as oleic acid degrades in light and air. The oleic acid was liquid at room temperature and pressure, the stearic acid was a powder at room temperature and pressure, each spreading solution was made up as a separate stock solution at a concentration of 10 mg mL^{-1} and mixed together in chloroform using a syringe to titrate out the correct quantity. The syringe was cleaned 6 times with chloroform between solutions. No plastic laboratory equipment was used with the chloroform, flasks with glass lids and glass Pasteur pipettes were used at all times. The spreading solutions were made up to a concentration of 1 mg mL^{-1} of organic acid in 10 mL chloroform and were stored in amber glassware and refrigerated to minimize degradation. The spreading solution concentrations are listed in table 4.2 with the respective mole fractions.

Table 4.2 *The Mole Fractions of Oleic and Stearic Acid in the Spreading Solutions*

Deuterated compound	Non-deuterated compound	Concentration mg mL⁻¹ in chloroform	Mole fraction
Stearic acid		0.591	0.64
	Oleic acid	0.291	0.35
Stearic acid	-	0.977	1
Oleic acid	-	1.022	1
Oleic acid		0.816	0.76
	Stearic acid	0.226	0.24
Oleic acid		0.206	0.20
	Stearic acid	0.721	0.80
Oleic acid		0.555	0.52
	Stearic acid	0.466	0.48
Oleic acid		0.580	0.52
	Stearic acid	0.490	0.48
Stearic Acid		1.278	0.50
	Oleic acid	1.118	0.50

The oleic acid sample used for this experimental work was also used for later experimental work in chapter 3 during which it was discovered that there was a saturated, deuterated impurity present from the synthesis of the sample. When the experimental work in this chapter took place the impurity had not been discovered and it had been assumed that the sample was oleic acid. The implications for the experiment are discussed in section 4.6.4.

4.5.3 Experimental Method

The experimental method was as described in chapter 2 for a neutron reflectometry experiment on the instrument SURF with a Langmuir trough. A monolayer was created by adding 30 μ L of a spreading solution containing a deuterated fatty acid and a different non-deuterated fatty acid, to the surface of the Langmuir trough drop wise. The film was compressed to a surface pressure, Π , of 20 mN m⁻¹. The Langmuir trough temperature was controlled at 20 °C. The kinetic decay of the surface pressure versus time was a measurement of the contribution of both the deuterated and non-deuterated components of the monolayer; measured simultaneously to the neutron reflectivity measurements. The neutron reflectivity surface coverage, Γ , measurement was dominated by the deuterated component of the monolayer and was thus a sensitive measurement of just one component of the mixed composition film.

The neutron reflectivity versus momentum transfer data was fit to the scattering length of the deuterated component of the monolayer and a value of the area per head group from the Langmuir trough data, to obtain a value of surface coverage which was valid for the mixture. Using an area per head group valid for the mixture improved the fit from that made to a value of area per head group calculated for the deuterated component of the monolayer only. The scattering length values to which the reflectivity versus momentum transfer data was fitted, using an Abelès optical matrix methodology are given in table 4.3.

Table 4.3 *The Scattering Lengths to which the Neutron Reflectivity versus Momentum Transfer Data was Fitted*

Compound	Scattering length density for neutrons (ρ) \AA^{-2}	Scattering length for neutrons (b) fm
Non-deuterated oleic acid	7.77×10^{-8}	4.11
Fully deuterated oleic acid	6.57×10^{-6}	348
Non deuterated stearic acid	-6.71×10^{-8}	-3.37
Fully deuterated stearic acid	7.19×10^{-6}	361

For the short range of Q used in these studies (~ 0.005 to 0.055 \AA^{-1}) the Abelès data fitting method allows one to sensitively fit the product of the scattering length density, ρ , and the thickness of the organic layer, δ . Measuring R over a larger range of Q (at 2 angles of incidence of the neutron beam) would give a structural variation of R with Q which would allow ρ and δ to be fitted independently with confidence. The Abelès regime fits equation 4.2 to the reflectivity versus momentum transfer data. In order to obtain a rapid measurement time for studying the kinetics of a reacting system, δ cannot be individually fitted. The surface coverage measurement is sensitive to $\rho\delta$ but not to each term individually. With care it was possible to resolve ρ and δ in the fitting process, but there is a large uncertainty on any thickness measurement performed at a small range of Q . A plot of the thickness data which did have reasonable errors is included within the results section for interest although the majority of the thickness data was not used as the error in the fit was too great for the data to be valid.

$$\Gamma = \frac{\rho\delta}{b_m} \quad (E 4.2)$$

$$\delta = \frac{b_m\Gamma}{\rho} \quad (E 4.3)$$

The surface coverage is determined by equation 4.2, re-arranging this in terms of thickness gives equation 4.3.

In the results it can be seen that the errors in the calculated thickness are very large. The bimolecular rate constants, are calculated using the ozone concentration within the monolayer, monolayer thickness is a term in the calculation of the ozone concentration within the monolayer as explained in chapter 3. As the thickness data errors were so large, a thickness of 15 \AA was used in the calculation of the ozone concentration within the monolayer; this thickness was obtained from the structural measurements of an oleic acid monolayer in chapter 3 and allows comparison of the rate constants between chapter 3 and 4.

4.5.4 Ozone Generation

The method of gas-phase ozone generation was as described in chapter 3 however the experiment was conducted on the SURF reflectometer, using the reaction chamber described in chapter 2. A brief description of the generation process is given here.

The ozone was generated by a mercury pen-ray lamp ozonizer manufactured by UVP (model 97-0067-01 (02)) and therefore a plain glass lid was fitted to the reaction chamber containing the Langmuir trough, without the integral photolysis lamp. The lid was sealed so as to be impervious to gas. The reaction chamber had a Swagelok inlet and outlet fitted at the top of the

aluminium reaction chamber. All fittings were stainless steel and all tubing was PTFE. The ozonizer was calibrated by Christian Pfrang by measuring the absorption spectrum of the ozone over a path length of 10cm, from 200 to 450 nm. The Beer-Lambert law was then applied to calculate the concentration of ozone.

Technical grade oxygen was circulated from a cylinder through a flow meter set to 1L min^{-1} at a backing pressure of 1 bar. The oxygen flowed along $\frac{1}{4}$ inch diameter Teflon tubing into the ozonizer where the oxygen was exposed to the mercury discharge lamp which utilizes shortwave (185nm) UV radiation to photolyse the molecular oxygen to produce a continuous flow of ozone in oxygen into the reaction chamber. The ozoniser power source was wired into the SURF instrument control panel so that the ozone supply could be triggered from the SURF command line automatically as part of the instruments procedure file.

4.5.4.1 Calculating the Concentration of Gas-phase Ozone

The ozone concentration within the reaction chamber and within the monolayer was calculated according to the method described in chapter 3, section 3.7.4.1. The gas-phase ozone concentration was $(2.4 \pm 0.6) \times 10^{12}$ molecules cm^{-3} and the concentration of ozone in the monolayer was $(4.3 \pm 1.1) \times 10^6$ molecules cm^{-2} .

The characteristic mixing time, t_{mix} , for ozone within the SURF reaction chamber was calculated according to equation 3.2 in chapter 3, section 3.7.4.1 as 2250 seconds.

4.5.5 The Method of Kinetic Analysis

The experiments which were conducted with a deuterated oleic acid monolayer or with a deuterated oleic acid component and a non-deuterated stearic acid component monolayer were fitted to the decay mechanism described in chapter 3, section 3.7.6.1. The surface coverage data was fitted to equation 4.4 (from chapter 3, section 3.7.6.2 equation 3.11). The kinetic fitting of equation 4.4 to the surface coverage data was started after 2250 seconds into the reaction after the characteristic mixing time.

$$\Gamma_t = \Gamma_{\text{final}} + \Gamma_0 e^{-k'(t-t_0)} \quad (\text{E } 4.4)$$

Where Γ_t was the surface coverage at the air-liquid interface at time t , Γ_{final} was the surface coverage at the air-liquid interface at the end of the reaction, t_0 was the start time of the reaction which corresponds to the time that, Γ_0 , the initial surface coverage at the air-liquid interface was

performed. k' was the pseudo first-order rate constant for the decay in the surface coverage of the deuterated material at the air-liquid interface.

The exponential kinetic fitting to the surface coverage data is plotted over the surface coverage data in the results section (4.6).

It was not possible to fit a kinetic decay mechanism to the experiments with deuterated stearic acid and non-deuterated oleic acid as no decay was noted as shall be shown.

4.6 Results

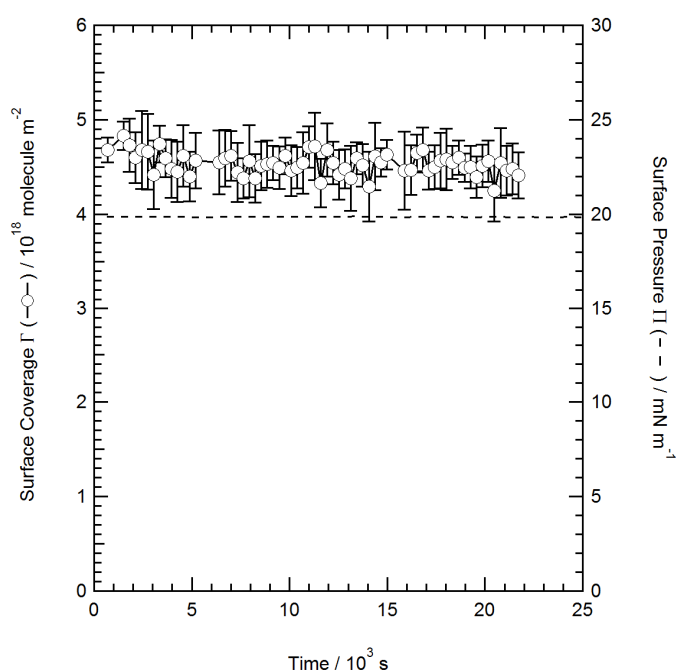
The results will be presented in the following order:

- Deuterated stearic acid only (4.6.1).
- Deuterated oleic acid only (4.6.2).
- Deuterated stearic acid and non-deuterated oleic acid monolayers from high to low ozone concentrations (4.6.3).
- Deuterated oleic acid and non-deuterated stearic acid monolayers from high to low ozone concentrations (4.6.4).

4.6.1 A Deuterated Stearic Acid Monolayer Decaying in the Presence of Gas-phase Ozone

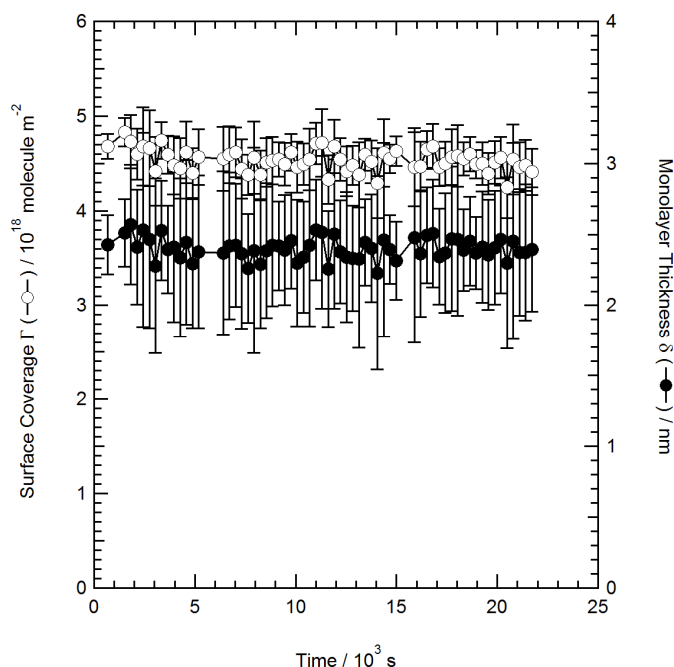
Stearic acid showed no reaction with gas-phase ozone as shown by figure 4.3. The fully deuterated stearic acid monolayer was exposed to a concentration of $(2.4 \pm 0.6) \times 10^{12}$ molecule cm^{-3} gas-phase ozone for over 6 hours during which time the loss in the surface coverage of stearic acid from the air-water interface was less than $(1 \pm 1) \times 10^{18}$ molecule m^{-2} . For all experiments the ozone supply was switched on at the beginning of the counting for the second data point (~ 200 seconds into the decay when the neutron beam was stable). The surface pressure also remained at ~ 20 mN m^{-1} over the same period.

Figure 4.3 *The Kinetic Decay in the Surface Coverage of a Monolayer of Deuterated Stearic Acid in an Atmosphere of $(2.4 \pm 0.6) \times 10^{12}$ molecule cm^{-3} O_3 in the Gas-Phase ($(4.3 \pm 1.1) \times 10^6$ molecule cm^{-2} O_3 in the Monolayer)*



The reflectivity data can be fitted to constrain the thickness of the monolayer once the surface coverage has been constrained. The monolayer thickness data is plotted in figure 4.4. The error bars are large on the thickness data obtained in this way and it is not of comparable quality to that which can be obtained by taking multi-angle reflectivity measurements. In figure 4.4 the thickness does remain generally flat and uniform during the measurement period. The gap in the reflectivity surface coverage and thickness data at 15000 seconds was due to a loss of the neutron beam at ISIS during the experiment.

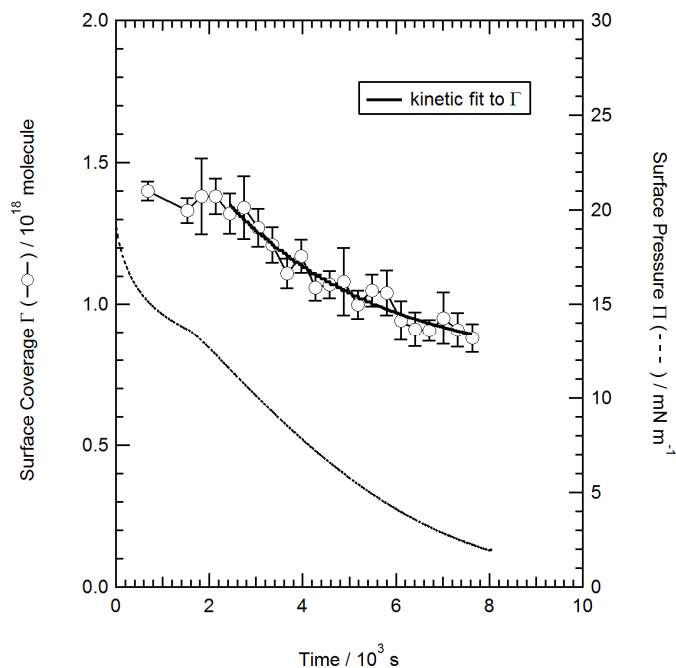
Figure 4.4 *The Monolayer Thickness at the Air-water Interface of a Monolayer of Deuterated Stearic Acid Exposed to $(2.4 \pm 0.6) \times 10^{12}$ molecule cm^{-3} O_3 in the Gas-Phase ($(4.3 \pm 1.1) \times 10^6$ molecule cm^{-2} O_3 in the Monolayer)*



4.6.2 A Deuterated Oleic Acid Monolayer Decaying in the Presence of Gas-phase Ozone

Ozone reacts with oleic acid. Over a time period of 2.2 hours the oleic acid monolayer decayed from a surface coverage of 1.4×10^{18} molecule m^{-2} to 0.9×10^{18} molecule m^{-2} in the absence of stearic acid (figure 4.5). The surface pressure decayed from 19 to 2 mN m^{-1} during the reaction with ozone. Equation 4.6 was fitted to the surface coverage data to give a rate constant for the decay in the monolayer surface coverage during the reaction with ozone. The ozone supply was switched on at the beginning of the surface pressure measurement.

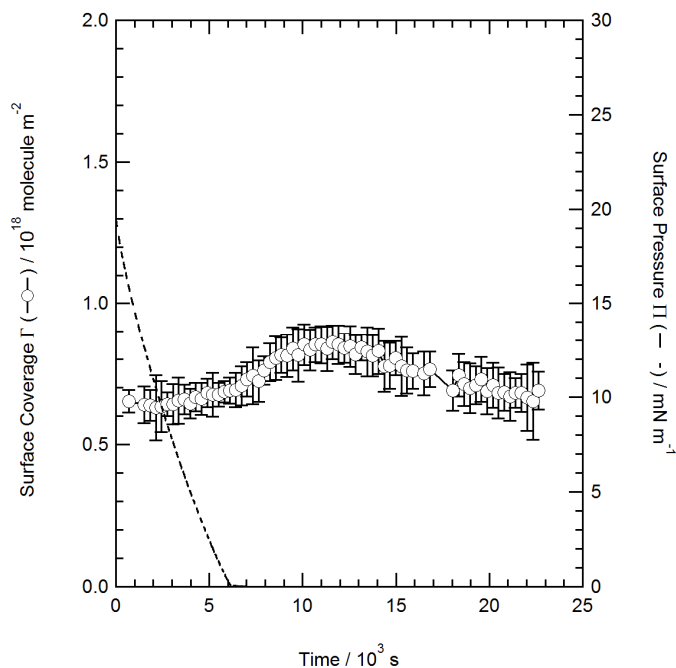
Figure 4.5 *The Kinetic Decay in the Surface Coverage of a Monolayer of Deuterated Oleic Acid in an Atmosphere of $(2.4 \pm 0.6) \times 10^{12}$ molecule cm^{-3} O_3 in the Gas-Phase ($(4.3 \pm 1.1) \times 10^6$ molecule cm^{-2} O_3 in the Monolayer)*



4.6.3 Monolayers of Deuterated Stearic Acid Mixed with Non-deuterated Oleic Acid

For mixed monolayers of deuterated stearic acid and non-deuterated oleic acid the surface coverage did not decay. When exposed to $(2.4 \pm 0.6) \times 10^{12}$ molecule cm^{-3} gas-phase ozone the surface coverage measurement increased slightly in value for a monolayer of deuterated stearic acid and non-deuterated oleic acid. The surface coverage rise is small and will be explained in section 4.7. What is clear is that the monolayer persists at the air-water interface over a period of over >20000 seconds (5.5 hours). The monolayer surface pressure decayed to 0 mN m^{-1} over ~6000 seconds as the oleic acid is being oxidised away but this cannot be seen in the surface coverage measurement as this measurement is valid just for the stearic acid. The oxidation of oleic acid had no effect on the deuterated stearic acid.

Figure 4.6 *The Kinetic Decay in the Surface Coverage of a Monolayer of Deuterated Stearic Acid and Non-deuterated Oleic Acid, Mole Fraction 0.5:0.5 in an Atmosphere of $(2.4 \pm 0.6) \times 10^{12}$ molecule cm^{-3} O_3 in the Gas-Phase ($(4.3 \pm 1.1) \times 10^6$ molecule cm^{-2} O_3 in the Monolayer)*



To confirm that the surface coverage rise was genuine the same experiment was repeated (figure 4.7 and 4.8). The surface coverage measurement did not repeat in the same way, the initial surface coverage was not consistent so it was difficult to judge whether the surface coverage rise due to increased reflectivity of the monolayer was structural or not as a lower surface coverage at the beginning of the experiment suggests the monolayers could have been packed differently. The surface coverage still increased towards the end of the experiment in figure 4.7.

Figure 4.7 *A Repeat Measurement of the Kinetic Decay in the Surface Coverage of a Monolayer of Deuterated Stearic Acid and Non-deuterated Oleic Acid, Mole Fraction 0.5:0.5 in an Atmosphere of $(2.4 \pm 0.6) \times 10^{12}$ molecule cm^{-3} O_3 in the Gas-Phase ($(4.3 \pm 1.1) \times 10^6$ molecule cm^{-2} O_3 in the Monolayer)*

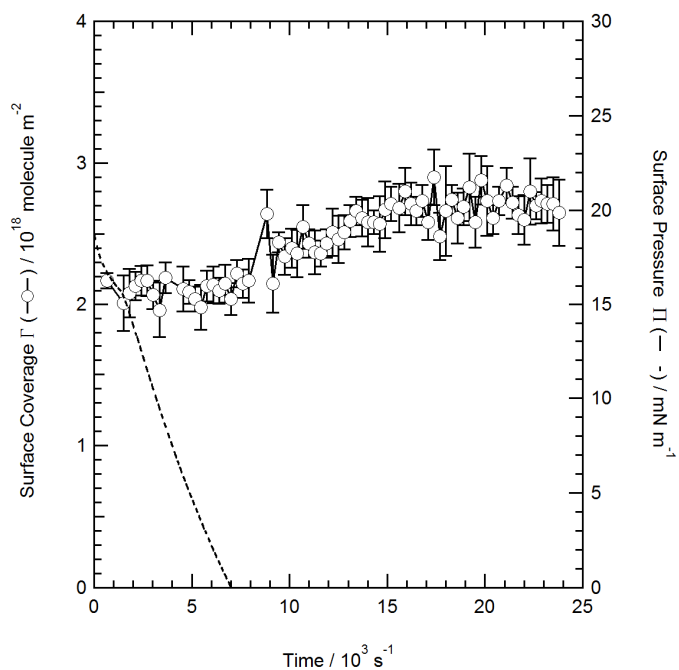
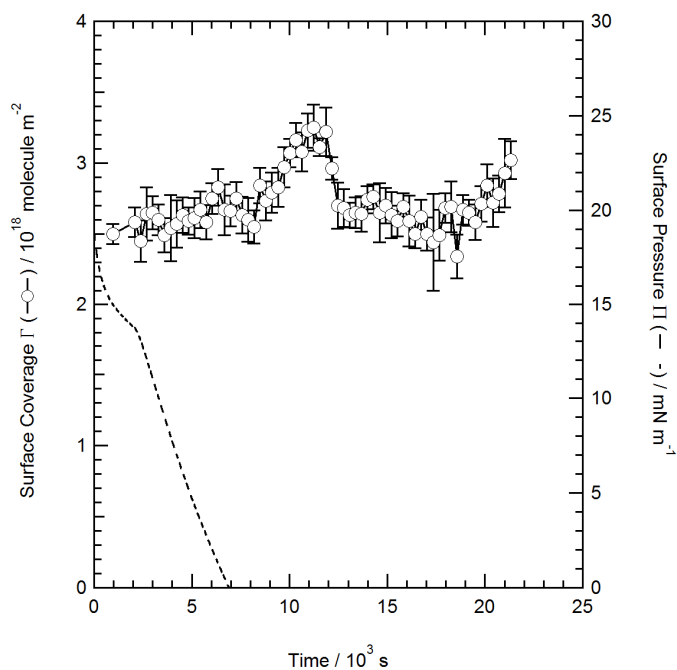
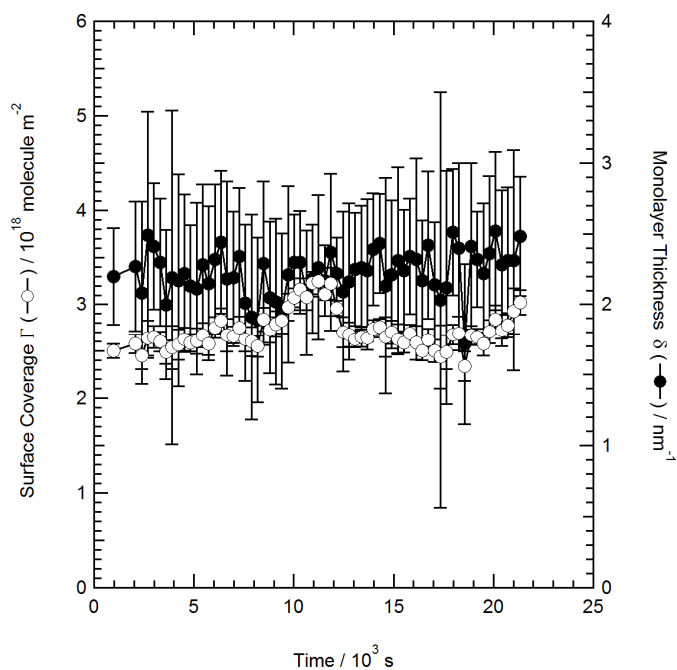


Figure 4.8 *A Further Repeat of the Kinetic Decay in the Surface Coverage of a Monolayer of Deuterated Stearic Acid and Non-deuterated Oleic Acid, Mole Fraction 0.5:0.5 in an Atmosphere of $(2.4 \pm 0.6) \times 10^{12}$ molecule cm^{-3} O_3 in the Gas-Phase ($(4.3 \pm 1.1) \times 10^6$ molecule cm^{-2} O_3 in the Monolayer)*



The rise in the surface coverage of a monolayer of deuterated stearic acid and non-deuterated oleic acid was repeated. The surface coverage rise is the result of a change in the scattering length density of the monolayer for example by the addition of oxygen to the film as a result of the reaction of ozone with the double bond in the oleic acid molecule.

Figure 4.9 *The Kinetic Decay in the Surface Coverage and the Thickness of a Monolayer of Deuterated Stearic Acid and Non-deuterated Oleic Acid, Mole Fraction 0.5:0.5 in an Atmosphere of $(2.4 \pm 0.6) \times 10^{12}$ molecule cm^{-3} O_3 in the Gas-phase ($(4.3 \pm 1.1) \times 10^6$ molecule cm^{-2} O_3 in the Monolayer)*

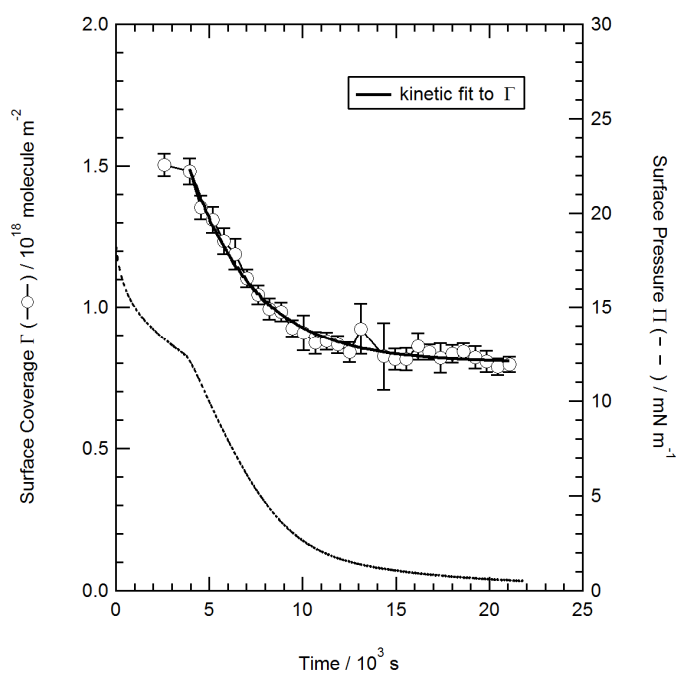


The monolayer thickness for the data in figure 4.8 is shown in figure 4.9, the thickness of the monolayer did not change during the reaction.

4.6.4 Monolayers of Deuterated Oleic Acid Mixed with Non-deuterated Stearic Acid

The reaction of ozone with a monolayer of deuterated oleic acid and non-deuterated stearic acid produced a decay in the surface coverage at the air-water interface. Figure 4.10 shows the kinetic decay for a monolayer composed of approximately three quarter deuterated oleic acid and one quarter non-deuterated stearic acid. It can be seen that the decay is very different to the rise in surface coverage seen in the majority deuterated stearic acid with non-deuterated oleic acid monolayers.

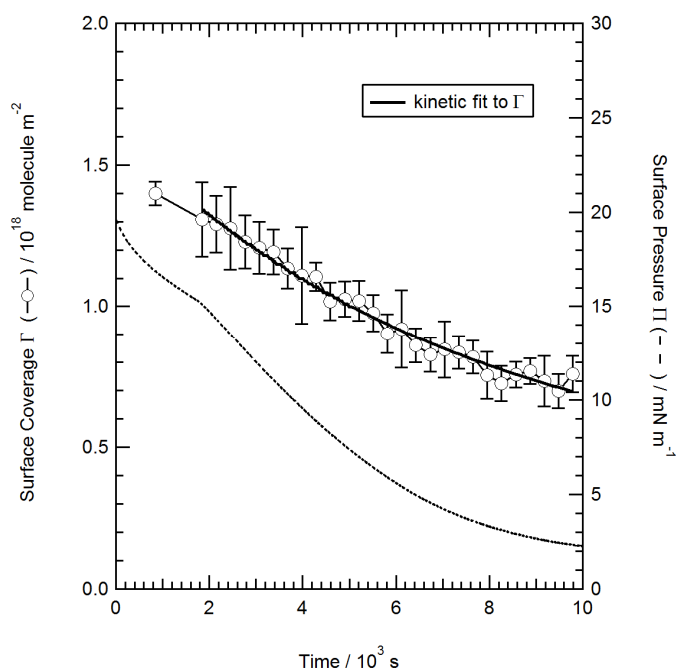
Figure 4.10 *The Kinetic Decay in the Surface Coverage of a Monolayer of Deuterated Oleic Acid and Non-deuterated Stearic Acid, Mole Fraction 0.76:0.24 in an Atmosphere of $(2.4 \pm 0.6) \times 10^{12}$ molecule cm^{-3} O_3 in the Gas-phase ($(4.3 \pm 1.1) \times 10^6$ molecule cm^{-2} O_3 in the Monolayer)*



At the greatest mole fraction of deuterated oleic acid to non-deuterated stearic acid the surface coverage decayed by 0.8×10^{18} molecule m^{-2} over 20000 seconds. The surface coverage data has large error bars in places where the neutron beam fluctuated and there was little signal thus the counting statistics were poor. The surface pressure data shows a phase change at 12 mN m^{-1} which was seen at higher surface pressures ($\sim 18 \text{ mN m}^{-1}$) in the kinetic decay of oleic acid alone in chapter 3. It should be noted that the oleic acid sample used for the experiments in this chapter had a saturated deuterated impurity as discussed in chapter 3 so the surface pressure and surface coverage behaviour in figure 4.10 to 4.13 may be influenced by the impurity. The residual surface coverage seen at the end of the experiments with deuterated oleic acid and non-

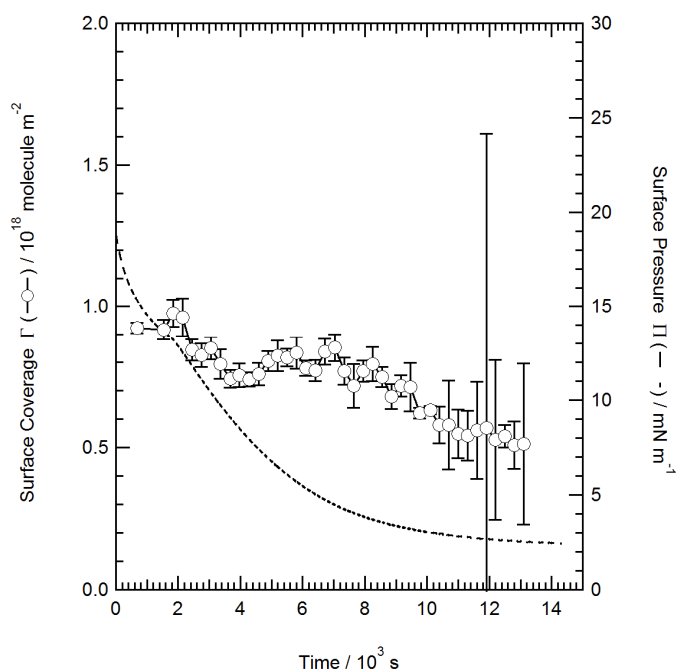
deuterated stearic acid monolayers could be the result of the impurity in the deuterated oleic acid sample which was shown in chapter 3 to leave a non-reacted, surface active, deuterated component at the air-water interface after exposure to gas-phase ozone.

Figure 4.11 *A Repeat of the Kinetic Decay in the Surface Coverage of a Monolayer of Deuterated Oleic Acid and Non-deuterated Stearic Acid, Mole Fraction 0.76:0.24 in an Atmosphere of $(2.4 \pm 0.6) \times 10^{12}$ molecule cm^{-3} O_3 in the Gas-Phase ($(4.3 \pm 1.1) \times 10^6$ molecule cm^{-2} O_3 in the Monolayer)*



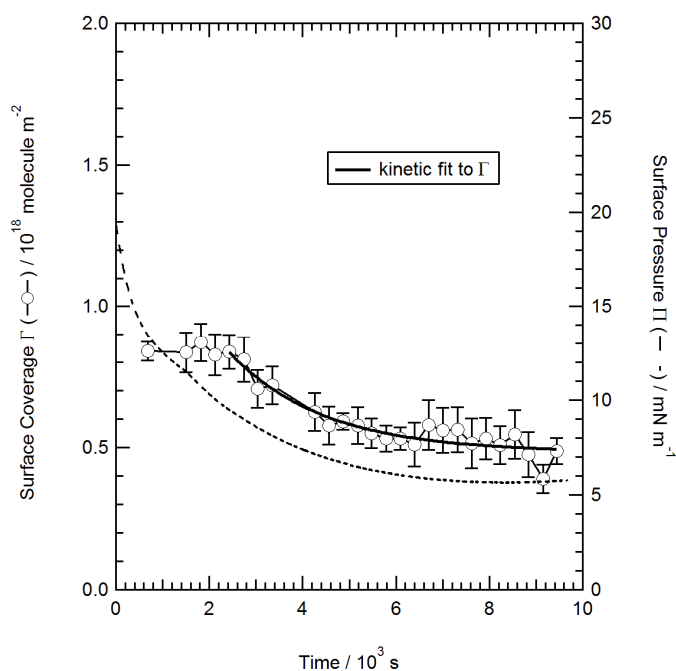
A failure in the delivery of the proton beam to the neutron producing target occurred at ~10,000 seconds during the repeat experiment shown in figure 4.11 so the data given is for the decay up to that point. The surface pressure and surface coverage values were similar to those shown in figure 4.10 for the same spreading solution.

Figure 4.12 *The Kinetic Decay in the Surface Coverage of a Monolayer of Deuterated Oleic Acid and Non-deuterated Stearic Acid, Mole Fraction 0.52:0.48 in an Atmosphere of $(2.4 \pm 0.6) \times 10^{12}$ molecule cm^{-3} O_3 in the Gas-Phase ($(4.3 \pm 1.1) \times 10^6$ molecule cm^{-2} O_3 in the Monolayer)*



In figure 4.13 the surface coverage fluctuates, rising slightly then decaying repeatedly, with an overall decay of 0.4×10^{18} molecule m^{-2} . It was not possible to fit equation 4.6 to the surface coverage data in figure 4.12. The surface pressure data did not reflect the fluctuating surface coverage. The concentration of stearic acid was higher at $\sim 50\%$ in this experiment than that shown in figures 4.10 and 4.11 however in figure 4.13 where the concentration of stearic acid was highest the surface coverage did not increase dramatically as it had in figure 4.12.

Figure 4.13 *The Kinetic Decay in the Surface Coverage of a Monolayer of Deuterated Oleic Acid and Non-deuterated Stearic Acid, Mole Fraction 0.20:0.80 in an Atmosphere of $(2.4 \pm 0.6) \times 10^{12}$ molecule cm^{-3} O_3 in the Gas-Phase ($(4.3 \pm 1.1) \times 10^6$ molecule cm^{-2} O_3 in the Monolayer)*



When the non-deuterated stearic acid content of the monolayer was higher than the concentration of deuterated oleic acid the surface coverage of the deuterated oleic acid still decayed as it reacted with ozone. The surface coverage did not reach a value of zero in any of the experiments with mixed monolayers of stearic and oleic acid exposed to gas-phase ozone.

4.6.5 Summary of the Experimental Results

- Deuterated stearic acid did not decay in the presence of oleic acid; therefore the Criegee intermediate produced by ozone reacting with oleic acid did not attack the stearic acid molecules in the monolayer.
- It can clearly be seen that the behaviour of the mixed stearic acid and oleic acid film is different to that of stearic acid alone.
- The effect of the inclusion of non-deuterated oleic acid in a monolayer with deuterated stearic acid is that as the oleic acid undergoes oxidation, the surface coverage remains of a significant value after prolonged exposure to ozone and does not reach the low values of $\sim 0.2 \times 10^{18}$ molecule m^{-2} in contrast to the oleic acid only monolayers shown in chapter 3.
- The surface coverage rise mid-experiment for deuterated stearic acid and non-deuterated oleic acid occurs in one instance only of oxidation of the same composition spreading solution suggesting that different products may be found depending on which molecular path the reaction takes.

4.6.6 Kinetic Results

The kinetic fits of equation 4.4 to the surface coverage versus reaction time data yielded the reaction rate constants for the mixed monolayers of deuterated oleic acid and non-deuterated stearic acid given in table 4.4.

Table 4.4 *The Reaction Rate Constants for the Reaction of Deuterated Oleic Acid and Deuterated Oleic Acid with Non-deuterated Stearic Acid with Gas-Phase Ozone*

Monolayer Mole Fraction of Oleic and Stearic Acid	$[O_3]_{film}$ / 10^{-6} molecule cm^{-2}	k' / s^{-1} / $10^{-4} s^{-1}$	k / (10^{-10}) $cm^2 molecule^{-1}$ s^{-1}
This study			
D-oleic χ 1	2.47 ± 0.34	3 ± 0.1	1.21 ± 0.56
D-oleic χ 0.76:	2.47 ± 0.34	2 ± 0.2	0.89 ± 0.19
H-stearic χ 0.24		3 ± 0.2	1.14 ± 0.07
D-oleic χ 0.20:	2.47 ± 0.34	5 ± 0.1	2 ± 0.74
H-stearic χ 0.80			
King et al., (2009)			0.73 ± 0.09
Gonzalez-Labrada et al., (2007)			0.49
Chapter 3	24 ± 3.9	20 ± 6	0.36 ± 0.1

The bimolecular rate constants for the reaction of the mixed oleic acid and stearic acid monolayers are comparable to those obtained for oleic acid in other studies and in chapter 3 of this thesis. The rate constant for the majority non-deuterated stearic mixed monolayer (D-oleic χ 0.20: H-stearic χ 0.80) is not in agreement with the work of King et al., (2009). Further experiments would be required to understand any correlation between the saturated component and the bimolecular rate constant.

4.7 Discussion

The following discussion will concentrate on:

- The effect of a non-deuterated component of a mixed monolayer on the measurement of surface coverage at the air-water interface (4.7.1)
- The experimental results in the context of other work on mixed films (4.7.2).

4.7.1 Discussion of the Contribution of Hydrogen Scattering of Neutrons to the Surface Coverage Measurements

The surface coverage and thickness did not change much during the reaction of a mixed monolayer of deuterated stearic acid and non-deuterated oleic acid showing that the reaction of oleic acid with ozone did not cause a subsequent decay of the stearic acid component of the film. The surface coverage increased a little, as shown in figure 4.7 to 4.9 where a mixed monolayer of deuterated stearic acid and non-deuterated oleic acid was reacting with ozone, could be explained by the loss of hydrogen atoms from the oleic acid component as the oxidation reaction proceeds. Hydrogen has a scattering length of -3.74 fm and its removal from the interface produces a lower reflectivity versus momentum transfer signal as hydrogen has a negative scattering length meaning that the non-deuterated component of a mixed film will still influence the reflectivity signal depending on its constituent atoms and their scattering length, as hydrogen is lost from the interface the reflectivity would increase raising the value of the derived surface coverage. The neutron reflectivity versus momentum transfer data was fitted assuming all the specular reflection was from the deuterated component of the monolayer, however the hydrogen (^1H) has a small negative effect on the scattering of neutrons and the deuterated fatty acid component of the monolayer has a large dominating contribution to the reflectance of neutrons in the monolayer.

The influence of the loss of hydrogen on the scattering from the monolayer can be estimated for a mole fraction of 0.5:0.5 deuterated stearic acid: non-deuterated oleic acid monolayer by:

The scattering length density, ρ , of a single component in the monolayer is defined as:

$$\rho = \frac{\sum n_i b_i}{V_i} \quad (E 4.5)$$

The neutron scattering length (b_m) of deuterated stearic acid ($\text{C}_{18}\text{D}_{35}\text{O}_2\text{H}$) is 3.61×10^{-13} m, the scattering length density (ρ) is $7.19 \times 10^{-6} \text{ \AA}^{-2}$. The neutron scattering length (b_m) of non-deuterated oleic acid ($\text{C}_{18}\text{H}_{34}\text{O}_2$) is 4.11×10^{-15} m, the scattering length density (ρ) is 7.77×10^{-8}

\AA^{-2} . The calculation of scattering length is dependent on the volume per molecule which is greater for non-deuterated oleic acid than for deuterated stearic acid.

The scattering length density (ρ) for a mixed monolayer is defined as:

$$\rho_{mixed\ monolayer} = \chi_1 \left(\frac{\sum n_i b_i}{V_i} \right) + \chi_2 \left(\frac{\sum n_i b_i}{V_i} \right) \quad (E\ 4.6)$$

Where in this instance the mole fraction of deuterated stearic acid (χ_1) is 0.5 and the mole fraction of non-deuterated oleic acid (χ_2) is 0.5.

$$\rho_{mixed\ monolayer} = 0.5\chi\ 7.19 \times 10^{-6} + 0.5\chi\ 7.77 \times 10^{-8} \text{\AA}^{-2} \quad (E\ 4.7)$$

$$\rho_{mixed\ monolayer} = 3.63 \times 10^{-6} \text{\AA}^{-2}$$

To explain why there is a rise in the monolayer surface coverage during the reaction of a mixed monolayer of deuterated stearic acid and non-deuterated oleic acid the effect of the addition of ozone to the double bond in the oleic acid monolayer on the scattering length density of the monolayer can be calculated by the addition of three oxygen atoms (b for oxygen is 1.8×10^{-16} m) which have a positive scattering effect to the non-deuterated oleic acid scattering term in equation 4.8.

$$\rho_{mixed\ monolayer} = 0.5\chi\ 7.19 \times 10^{-6} + 0.5\chi\ 34.8 \times 10^{-8} \text{\AA}^{-2} \quad (E\ 4.8)$$

$$\rho_{mixed\ monolayer} = 3.77 \times 10^{-6} \text{\AA}^{-2}$$

The increase in scattering from the addition of ozone to the double bond is $\sim 3.7\%$. The increase in surface coverage during the reaction in figure 4.7 to 4.9 was greater than the increase which could be caused by ozone addition to the double bond. The addition of ozone does not explain the increased surface coverage, the cause of the increase was not resolved. When fitting a curve to the reflectivity data to determine the monolayer surface coverage (the product of $\rho \times \delta$) the thickness is assumed to be constant. A more accurate thickness could be obtained to fit to and obtain a better surface coverage measurement with multi angle reflectivity versus momentum transfer data.

When a monolayer of deuterated stearic acid and non-deuterated oleic acid was exposed to gas-phase ozone a rise in surface coverage was observed then the value of surface coverage returned to the initial level suggesting that the scattering length density of the monolayer had increased then subsequently decreased again during the reaction of non-deuterated oleic acid with ozone (as stearic acid is inert to ozone). The analysis reflects the increased scattering length density as an increase in surface coverage (Γ) at the air-water interface in equation 4.2.

$$\Gamma = \frac{\rho\delta}{b_m} \quad (E 4.2)$$

b_m = total scattering length

ρ = scattering length density

δ = thickness (i.e. 15 Å or 1.5 nm)

The scattering from the deuterated stearic acid should not change as stearic acid is unreactive in the presence of ozone. If the signal owing to the specular reflection of neutrons changes that is an indication of an intra-molecular reaction where the ozone reacting with the oleic acid component of a mixed monolayer produces a reaction product which then affects the scattering by the deuterated stearic acid. As the surface coverage of the monolayer of deuterated stearic acid and non-deuterated oleic acid does not decay with time the deuterated stearic acid is not reacting with an oleic acid plus ozone reaction product, such as a Criegee intermediate formed from the reaction of oleic acid with ozone (the reader is referred to chapter 3 for this mechanism). The reactive products from oleic acid reacting with ozone must be consumed rapidly as it is not diffusing away from the reaction centre to react with stearic acid. This result is in contrast to that of Thompson et al., (2010) whom showed that a POPC molecule tail performs an intermolecular reaction on the same molecule where the saturated tail of the POPC molecule is consumed by a reactive intermediate formed from the reaction of ozone with the unsaturated tail.

The increase in surface coverage of the 0.5 mole fraction deuterated stearic acid, 0.5 mole fraction non-deuterated oleic acid could be investigated by obtaining thickness measurements of the mixed monolayer as it reacts with ozone. On the SURF reflectometer such measurements would take approximately 20 minutes per data point as it is necessary to count for longer for lower values of momentum transfer at the second angle and the detector must be moved. A twenty minute time resolution may miss the feature of the surface coverage rise, a higher time resolution would be desirable such as that achievable on the FIGARO reflectometer.

Figure 4.14 *The χ 0.52:0.48 D-Oleic Acid: Stearic Acid Monolayer and the χ 0.50:0.50 D-Stearic Acid: Oleic Acid Monolayer Relative Surface Coverage Plotted with the D-Stearic Acid Only and the D-Oleic Acid Only Monolayer Relative Surface Coverage*

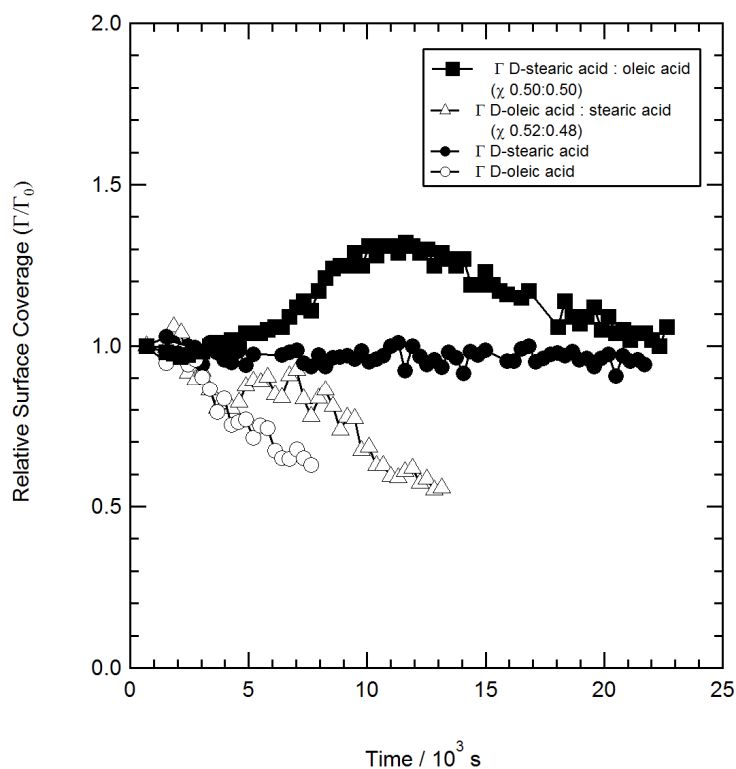


Figure 4.14 shows the relative change in surface coverage at the air-water interface for different monolayer compositions. The mixture of non-deuterated stearic acid with deuterated oleic acid appears to slow down the decay of the monolayer. It can be very clearly seen that there is little loss from deuterated stearic acid alone exposed to ozone. When deuterated stearic acid was mixed with oleic acid the surface coverage increased due to what is hypothesised to be a reaction product forming at the interface. The mechanism for ozone reacting with a monolayer containing stearic acid and oleic acid is expected to be the same as that of ozone reacting with oleic acid as the stearic acid is inert to ozone on the timescale studied.

4.7.2 Discussion of the Results in the Context of Other Studies

The work of King et al., (2009) showed that a monolayer of deuterated oleic acid held at the air-water interface of a Langmuir Trough over 14,000 seconds when exposed to a flow of oxygen was stable and did not decay and therefore was not oxidised. King et al., (2009) showed a halving of the surface coverage of deuterated oleic acid when exposed to a flow of ozone.

Ozone reacted with the oleic acid carbon-carbon double bonds generating primary ozonides and subsequent Criegee biradical intermediates (King et al. 2009) as explained in chapter 3. The addition of stearic acid to the monolayer in the experiments for this chapter where the surface coverage of the deuterated oleic acid within the monolayer was measured gave the same result. The rate constant k for the loss of deuterated oleic acid in a mixed monolayer was the same within error for a majority oleic acid mixed monolayer, when deuterated oleic acid was the minor component k' was slightly larger than that measured by King et al., (2009) for an oleic acid monolayer however more data would be required to conclusively confirm this finding. It may be that the contrast in chain length between the reaction product of oleic acid and the stearic acid changes the thickness of the monolayer.

Voss et al., (2006) studied the reaction of ozone with a deuterated oleic acid monolayer spread in a petri dish monitoring the composition at the air-water interface with sum-frequency generation (SFG) spectroscopy where overlapping laser pulses of a broad wavelength are used to produce a spectrum of signal intensity versus incident infrared signal which shows peaks of C-D groups and C-H groups, the peak is sensitive to the molecular orientation and the number density of molecules at the interface. Voss et al., (2006) found that the products formed from the reaction of oleic acid and ozone were soluble or volatile and did not persist at the air liquid interface. Experiments on mixed monolayers were undertaken with the saturated deuterated palmitic acid molecule ($C_{15}H_{31}COOH$) which was spread at the air-water interface with an oleic acid monolayer already in situ, the monolayer was spread to an area per molecule of 20\AA^2 . The palmitic acid signal was measured at the surface as the oleic acid monolayer was oxidised with ozone, showing palmitic acid replacing the oleic acid at the interface as the oleic acid reacted with ozone. The least soluble species was observed at the surface, as the oleic acid reacted its reaction products were soluble or volatile and it was lost from the interface and replaced by the palmitic acid. The solubility of oleic acid in water is $1.15 \times 10^{-5} \text{ g L}^{-1}$ at 25°C , the solubility of palmitic acid is higher ($8.21 \times 10^{-4} \text{ g L}^{-1}$ at 25°C) due to the shorter chain length (Howard and Meylan, 1997; Voss et al. 2006). Voss et al., (2006) state that unoxidised species from the subphase would replace oxidation products at the surface followed by oxidised species if the reservoir of unoxidised species is exhausted and that following oxidation the core of the aerosol droplet would be more likely to degrade. In the experiment described in this chapter there was no reservoir of surface active material to replace molecules at the air-water interface but the experiments on deuterated stearic acid with oleic acid did potentially show reaction product formation of oxidised species at the interface as the surface coverage increased during the reaction with ozone.

Self-assembled monolayers (SAMs) of alkenes and alkanes reacting with gas-phase ozone were used as atmospheric proxies by Moise and Rudich, (2000) as reviewed by Rudich (2003), infrared adsorption spectroscopy was used to characterize the double bonds and the alkyl chains present in the monolayer. Ozone reacted with the double bond causing the surface layer of alkenes allyltrimethylchlorosilane (C_3) and octenyltrimethylchlorosilane (C_8) to become disordered. A C_8 alkane monolayer did not react with ozone. Following ozonolysis the alkene monolayer coated surface became more hydrophilic with a more varied thickness described by Rudich (2003) as corrugated. Using total reflection infrared spectroscopy carbonyls and carboxylic acids were detected at the surface following the reaction of alkene self-assembled monolayers with gas-phase ozone. It is likely that a mixed composition oleic and stearic acid monolayer at the air-water interface would also through ozonolysis contain similar reaction products and would change in thickness as a result of the reaction with ozone.

The results of the current monolayer studies show that stearic acid will not react with gas-phase ozone at the air-water interface. Ozone readily dissolves in an organic liquid according to Henry's Law where the Henry's Law constant is high, for this reason there is likely to be a concentration of ozone within the monolayer. A lipid monolayer of mixed composition can show enhanced kinetics as the ozone is trapped in the tail region of the monolayer making interaction with the double bond more favourable compared to gas-phase collisions, (Wadia et al. 2000), and intramolecular reactions can take place (Thompson et al. 2010), this behaviour was not evident in the experiments presented here in this chapter with fatty acids which have greater spacing between the chains as the chains are positioned on separate molecules whereas the lipids have multiple chains on the same molecule.

The mixed composition particle phase studies show the formation of crystals of the saturated component of the droplet which could occur in a monolayer but would not have been detected in the work presented here.

It would be advantageous to repeat this experiment with a very high time resolution on the FIGARO reflectometer using the Sigma Aldrich deuterated oleic acid which subsequently to the experiment detailed in this chapter became commercially available and was used for the experiments in chapter 3. Taking structural reflectometry measurements at a greater Q range at points along a kinetic decay where the surface coverage was increasing would also give a better understanding of the mechanism by which the monolayer is oxidised.

4.8 Conclusions

The surface coverage of deuterated stearic acid monolayers did not decay in the presence of the oxidation of oleic acid, this was in contrast to the POPC lipid molecule with one saturated and one unsaturated chain used in the study by Thompson et al., (2010) in which the POPC stearic acid configured lipid tail did react with what was hypothesised to be a Criegee radical produced by the reaction of the oleic acid configured tail with gas-phase ozone, in an intra-molecular reaction where the reaction was taking place on the same molecule. As the stearic acid in this experiment did not decay there would still be an atmospheric film if the double bond in an unsaturated molecule was broken as a component of a mixed fatty acid composition cloud droplet film, it is OH radical that would remove saturated compounds from the air-water interface of a cloud droplet.

References

- Daintith J., 2008. A Dictionary of Chemistry. 6th Edition. Oxford University Press. Oxford. England. pp. 383.
- Donaldson, D.J., and Vaida, V. 2006. The Influence of Organic Films at the Air-aqueous Boundary on Atmospheric Processes. *Chemical Reviews*, 106, pp. 1445-1461.
- Eliason, T.L., Aloisio, S., Donaldson, D.J., Cziczo, D.J., Vaida, V. 2003. Processing of unsaturated organic acid films and aerosol by ozone. *Atmospheric Environment*, 37, pp. 2207-2219.
- Ellison, G.B., Tuck, A.F., Vaida, V. 1999. Atmospheric processing of organic aerosol. *Journal of Geophysical Research*, 104, D9, pp. 11,633-11,641.
- Feher, A.L., Collins, F.D., Healy, T.W. 1977. Mixed monolayers of simple saturated and unsaturated fatty acids. *Australian Journal of Chemistry*, 30, 3, pp. 511-519.
- Frankel, E.N. 1998. Lipid Oxidation, Chapter 1. The Oily Press, Dundee, Scotland.
- Gaines, G.L. 1966. Insoluble Monolayers at Liquid-gas Interfaces. Wiley Interscience, New York, USA.
- Gillman, J.B., Eliason, T.L., Vaida, V. 2004. Selectivity and stability of organic films at the air-aqueous interface. *Journal of Colloid and Interfacial Science*, 280, pp. 234-243.
- Gillman, J.B., Tervahattu, H., Vaida, V. 2006. Interfacial properties of mixed films of long-chain organics at the air-water interface. *Atmospheric Environment*, 40, pp. 6606-6614.
- Harkins, W.D., and Florence, R.T. 1938. Molecular Interaction in Mixed Monolayers on Aqueous Substitutions I. Mixtures of Alcohols, Acids and Amines. *Journal of Physics and Chemistry*, 6, pp. 856-870.
- Howard P.H. and Meylan, W.M. 1997. Handbook of Physical Properties of Organic Chemicals, Lewis Publishers, New York.
- Katrib, Y., Biskos, G., Buseck, P.R., Davidovits, P., Jayne, J.T., Mochida, M., Wise, M.E., Worsnop, D.R., Martin, S.T. 2005. Ozonolysis of Mixed Oleic-Acid/Stearic-Acid Particles: Reaction Kinetics and Chemical Morphology. *Journal of Physical Chemistry, A*, 109, pp. 10910-10919.
- King, M.D., Rennie A.R., Thompson K.C., Fisher F.N., Dong, C.C., Thomas R.K., Pfrang C., Hughes A.V. 2009. Physical Chemistry Chemical Physics. 11. pp. 7699-7707.
- Marty, J.C., Saliot, A., Buat-Ménard, P., Chesselet, R., Hunter, K.A. 1979. Relationship Between the Lipid Compositions of Marine Aerosols, the Sea Surface Microlayer, and Subsurface Water. *Journal of Geophysical Research*, 84, C9, pp. 5707-5716.

- Moise, T. and Rudich, Y. 2000. Reactive uptake of ozone by proxies for organic aerosols: Surface versus bulk processes. *Journal of Geophysical Research*, 105, D11, pp. 14667-14676.
- Rogge W.F., Hildemann, L.M., Mazurek, M.A., Cass, G.R. 1991. Sources of Fine Organic Aerosol. 1. Charbroilers and Meat Cooking Operations. *Environmental Science and Technology*, 25, pp. 1112-1125.
- Rogge, W.F., Hildemann, L.M., Mazurek, M.A., Cass, G.R., Simoneit, B.R. 1993^a. Sources of Fine Organic Aerosol. 4. Particulate Abrasion Products from Leaf Surfaces and Urban Plants. *Environmental Science and Technology*, 27, pp. 2700-2711.
- Rogge W.F., Hildemann, L.M., Mazurek, M.A., Cass, G.R. 1993^b. Sources of fine organic aerosol, 2. Noncatalyst and catalyst-equipped automobiles and heavy duty diesel trucks. *Environmental Science and Technology*, 27, pp.636-651.
- Rudich, Y. 2003. Laboratory Perspectives on the Chemical Transformations of Organic Matter in Atmospheric Particles. *Chemical Reviews*, 103, 12, pp. 5097-5124.
- Sigma Aldrich. 2011. Cell Culture Tuition Web Pages available at: <http://www.sigmaaldrich.com/life-science/cell-culture/learning-center/media-expert/oleic-acid.html>, as accessed on 19/1/2011.
- ^aTervahattu, H., Hartonen, K., Kerminen, V-M., Kupiainen, K., Aarnio, P., Koskentalo, T., Tuck, A.F., Vaida, V. 2002. New evidence of an organic layer on marine aerosols. *Journal of Geophysical Research*, 107, D7, pp. 4053- 4061.
- ^bTervahattu, H., Juhanoja, J., Kupiainen, K. 2002. Identification of an Organic Coating on Marine Aerosol Particles by TOF-SIMS. *J Geophys. Res*, 107.
- Tervahattu, H., Juhanoja, J., Vaida, V., Tuck, A.F., Niemi, J.V., Kupiainen, K., Kulmala, M., Vehkamäki, H. 2005. Fatty acids on continental sulphate aerosol particles. *Journal of Geophysical Research*, 110.
- Thompson, K.C.T., Rennie, A.R., King, M.D., Hardman, S.J.O., Lucas, C.O.M., Pfrang, C., Hughes, B.R., Hughes, A.V. 2010. Reaction of a Phospholipid Monolayer with Gas-Phase Ozone at the Air-Water Interface: Measurement of Surface Excess and Surface Pressure in Real Time. *Langmuir*, 26, 22, pp. 17295-17303.
- Vaida, V., Tuck, A.F., Ellison, G.B. 2000. Optical and Chemical Properties of Atmospheric Organic Aerosols. *Physics and Chemistry of the Earth*, 25, 3, pp. 195-198.
- Voss, L.F., Hadad, C.M., Allen, H.C. 2006. Competition between Atmospherically Relevant Fatty Acid Monolayers at the Air/Water Interface. *The Journal of Physical Chemistry, B*, 110, 39, pp. 19487-19490.

Wadia, Y., Tobias, D.J., Stafford R., Finlayson-Pitts B.J. 2000. Real-Time Monitoring of the Kinetics and Gas-Phase Products of the Reaction of Ozone with an Unsaturated Phospholipid at the Air-Water Interface. *Langmuir*, 16, pp. 9321-9330.

Weast, R.C. (editor) 1977. Handbook of Chemistry and Physics. 57th edition. Chemical Rubber Publishing Company, Ohio, USA.

Zahardis, J. and Petrucci, G.A. 2007. The oleic acid-ozone heterogeneous reaction system: products, kinetics, secondary chemistry, and atmospheric implications of a model system – a review. *Atmospheric Chemistry and Physics*, 7, pp.1237-1274.

Ziemann, P.J. 2005. Aerosol products, mechanisms, and kinetics of heterogeneous reactions of ozone with oleic acid in pure and mixed particles. *Faraday Discussions*, 130, pp. 460-490.

The Oxidation of Methyl Oleate Monolayers by Ozone

5.0 Abstract

A monolayer of methyl oleate, an insoluble amphiphile with a methyl ester head group as opposed to a fatty acid with a carboxylic acid head group, was oxidised at the air-water interface with gas-phase ozone generated by the photolysis of oxygen. The rate of the oxidation of the monolayer was monitored with neutron reflection on a Langmuir trough. The monolayer of deuterated methyl oleate ($C_{19}D_{36}O_2$), serves as a proxy for an organic film at the air-water interface of a cloud droplet in the atmosphere. The surface pressure of the monolayer was measured with a Wilhelmy plate and the surface coverage of the deuterated material at the air-water interface was measured with neutron reflection. The surface pressure and surface coverage of the deuterated monolayer declined with reaction time. A second-order rate constant for the reaction at the interface was calculated and used to determine an atmospheric lifetime for a methyl oleate monolayer at the air-water interface of a cloud droplet.

5.1 Introduction

Atmospheric cloud droplet films are likely to contain organic esters as they contain the fatty acids from which esters are derived and organic esters have been sampled in fog waters (Raja et al. 2009). Methyl oleate, a derivative of oleic acid is found in biodiesel and in cooking oil emissions; it is also naturally emitted to the atmosphere from vegetation (Flath et al. 1973; Ikeda et al. 1994; Knothe et al. 2006). The oxidation of the methyl oleate molecule by gas-phase ozone provides a proxy for the kinetics of the reaction of an unsaturated methyl ester component of a cloud droplet film. As the methyl oleate molecule is of a similar size and chain length to the oleic acid molecule an assessment of the effect of the head group on the reaction can be made by studying both systems.

5.2 Aims

1. To measure the effect on the monolayer lifetime of gas-phase ozone on an organic ester monolayer of methyl oleate and to simulate the ozonolysis of the ester component of a cloud droplet monolayer at the air-liquid interface.
2. To provide an insight into the kinetics and the potential reaction products of a methyl oleate monolayer reacting with gas-phase ozone.
3. To assess the differences in the rate of the reaction of gas-phase ozone with a monolayer possessing an ester head group and a monolayer with an acidic head group.

3. To calculate the atmospheric lifetime of a methyl oleate monolayer on a cloud droplet and compare the lifetime to a typical aerosol lifetime of 3 days to show whether the oxidation process is important in changing the lifetime of an aerosol particle to < 3 days.

5.3 Background

Methyl oleate is an organic ester of oleic acid where the head group has the configuration $RC(O)OR$ as opposed to $RC(O)OH$ for the oleic acid molecule. The methyl oleate molecule has a long alkyl chain which gives the molecule the properties of a wax where multiple molecules of methyl oleate can form a hydrophobic coating (Vollhardt and Schore, 2002). Emissions of methyl oleate to the troposphere are increasing due to the use of biofuels as increasingly fuels are blended to contain a proportion of renewable biofuel (Knothe et al. 1997), it can be predicted that these emissions will increase from current levels.

Studying methyl oleate provides a means of further understanding the ozonolysis of a monolayer than the study of oleic acid alone as the methyl oleate molecule, in contrast to the oleic acid molecule does not have a free carboxylic acid group, (Mochida et al. 2006).

The reader is referred to chapter 3 for information on the formation and concentration of gas-phase ozone in the troposphere.

Figure 5.1 *The Structure of the Methyl Oleate Molecule*

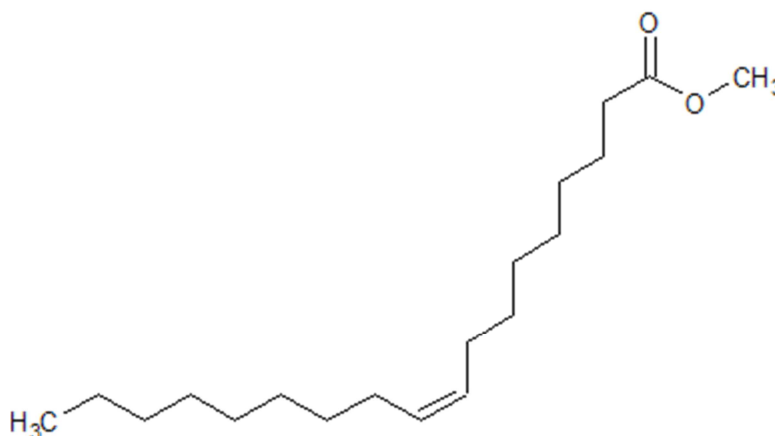
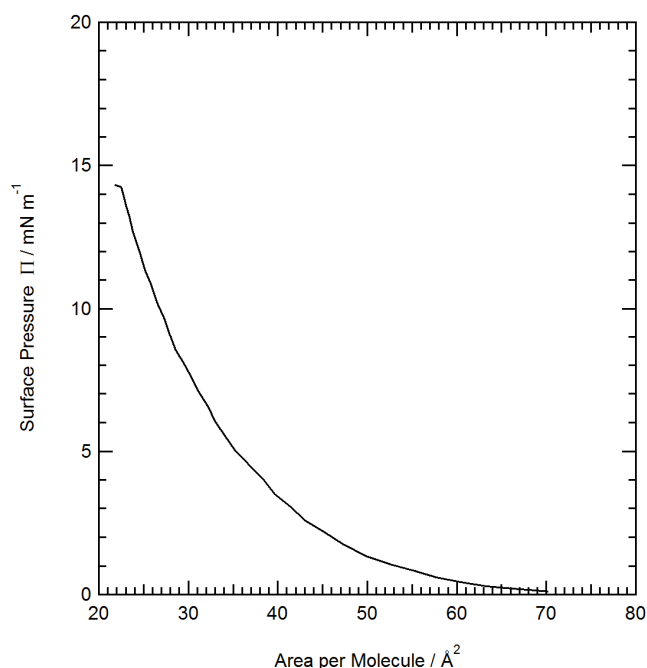


Figure 5.2 *A Comparison of the Surface Pressure Versus Surface Area per Molecule Isotherm for a Methyl Oleate Monolayer at the Air-water Interface*



The surface pressure versus surface area isotherm for methyl oleate shown in figure 5.2 was measured with non-deuterated methyl oleate purchased from Sigma-Aldrich. A concentration of 1 mg methyl oleate in chloroform was spread on a sub-phase of pure water (18 MΩ resistivity), the subphase temperature was maintained at 20°C. The methyl oleate monolayer collapsed at a surface pressure of 14.5 mN m⁻¹. Starting the neutron reflectivity measurements at a comparably low surface pressure of ~ 8 mN m⁻¹ compared to the other chapters ensured that the collapse of the monolayer was avoided when collecting kinetic data.

5.4 Methyl Oleate and Cloud Droplets

Methyl oleate has not been directly sampled in the troposphere or in rain or fog waters however other esters have been reported in fog waters samples from the US Gulf Coast by Raja et al., (2009). Recovery of methyl esters from atmospheric samples for analysis is poor for the commonly used techniques such as GCMS as methyl esters are readily lost from the sample during evaporative extraction (Pinxteren and Herrmann, 2007) or are deliberately created from fatty acids to aid their detection and measurement thus the original composition of the organic ester in a sample is lost.

5.5 Previous Atmospheric Studies of Methyl Oleate Reacting with Ozone

There are few studies of gas-phase ozone reacting with methyl oleate. Mochida et al., (2006) exposed mixed particles composed of methyl oleate, dioctyl adipate and myristic acid to gas-phase ozone within a flow tube. The flow tube was coupled with an Aerodyne quadrupole mass spectrometer to characterize the reaction products. Mochida et al., (2006) note that the reaction pathway for methyl oleate would be expected to be simpler than that of oleic acid ozonolysis as methyl oleate does not have a free carboxylic acid group (-C(O)OH) which can promote polymerization. Hearn et al., (2005) measured the loss of condensed phase methyl oleate from liquid particles exposed to gas-phase ozone, with chemical ionization mass spectrometry. Hearn et al., (2005) noted some differences between the reaction of methyl oleate and that of oleic acid with ozone. Methyl oleate reacted with ozone in the bulk of the particle in contrast to oleic acid particles which reacted with ozone at the surface of the particle (Hearn et al. 2005), and that methyl oleate does not react with the Criegee intermediates produced when the primary ozonide formed by ozone reacting with the double bond in the molecule decomposes as efficiently as oleic acid reacts with the Criegee intermediate (Hearn et al. 2005). Hearn et al., (2005) concluded that the reaction of methyl oleate with ozone was limited by diffusion of ozone within the particle.

The surface pressure behaviour of methyl oleate at the air-water interface was investigated by Clark and Robinson, (1940) and Gaines (1966). The isotherm is as that of oleic acid with indistinct phases of a liquid character until a surface pressure of $\sim 15 \text{ mN m}^{-1}$ where collapse occurs. The head group of the methyl oleate is relatively large and not particularly soluble compared to that of its parent fatty acid. For a monolayer of methyl oleate reacting with ozone it can be inferred that as is the case with oleic acid monolayers that methyl oleate would be photo-sensitive, and that the surface pressure would gradually decay in oxygen due to its unsaturated structure.

The kinetics of the ozonolysis of a methyl oleate monolayer at the air-water interface has not been previously determined. Previous atmospheric studies by Mochida et al., (2006) and Hearn et al., (2005) have used bulk liquid particles of methyl oleate. In this chapter new data will be presented which can be incorporated into future modelling of aerosol and cloud droplet film behaviour and reactivity.

5.6 Experimental Methodology

The experimental section is presented in the following order:

- Experimental objectives (5.6.1).
- A description of the methyl oleate sample used to acquire neutron reflectivity experiments (5.6.2).
- The generation of gas-phase ozone and the calculation of the ozone concentration in the chamber and within the monolayer (5.6.3).
- The methodology of a typical neutron reflectivity surface coverage measurement and simultaneous surface pressure measurement of methyl oleate reacting with ozone at the air-water interface (5.6.4).
- The kinetic fitting regime used to ascertain rate constants for the decay in the methyl oleate monolayer surface coverage as a result of ozone initiated oxidation (5.6.5).

The experiments were conducted on the FIGARO reflectometer with the corresponding reaction chamber as shown in chapter 3.

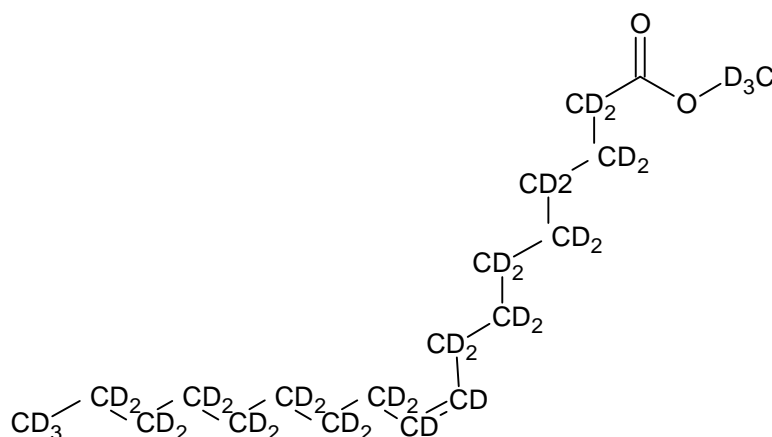
5.6.1 Experimental Objectives

In this experiment, the objectives were:

1. To ascertain whether the methyl oleate monolayer is lost from the air-liquid interface when oxidised by ozone. It is expected that ozone will react at the site of the *cis* double bond in the hydrocarbon chain of the molecule as it did in the case of an oleic acid monolayer.
2. To determine whether the decay of methyl oleate from the air-water interface as it reacts with ozone has a bimolecular rate constant similar to that for ozone reacting with oleic acid at the air-liquid interface.

5.6.2 The Deuterated Methyl Oleate Sample

A single, fully deuterated methyl oleate ($C_{19}D_{36}O_2$), sample was custom synthesised at the Oxford University Isotope Facility for this work. The deuterated methyl oleate sample was made up with chloroform into a spreading solution at a concentration of 1 mg mL^{-1} methyl oleate in chloroform. The chloroform used for the spreading solution and for cleaning the Langmuir trough was Chromosolv plus for HPLC 99.9% with ethanol stabilizer which will evaporate or go into solution and is not surface active, as manufactured by Sigma Aldrich, catalogue number: 650471.

Figure 5.3 *The Structure of the D₃₆ Methyl Oleate Molecule***5.6.3 Generating and Determining the Concentration of Gas-phase Ozone**

The production of gas-phase ozone and its delivery to the reaction chamber was as described in chapter 3. The bottled oxygen was manufactured by Air Products and was of a purity of 99.5%. The flow of oxygen was controlled with a ball and valve flow meter with a capacity of 5 L⁻¹ min⁻¹, manufactured by Cole Palmer. All tubing was Teflon with Swagelok stainless steel connectors. The oxygen was flowed through a pen ray ozoniser: model 97-0067-02 manufactured by UVP. The ozone was then flowed into the aluminium reaction chamber surrounding the Langmuir trough. The ozoniser generates ozone through reaction 5.1 and 5.2.



The gas-phase concentration of ozone in the reaction chamber differed from that in the oleic acid ozonolysis experiment described in chapter 3 as the volume of the reaction chamber was reduced to an available volume of 13.3 L⁻¹ using hollow aluminium boxes which were inserted into the chamber around the Langmuir trough; these were fitted so as not to impede the neutron beam or the surface pressure measurement apparatus. The function of the inserts was to reduce the mixing time taken for ozone entering the chamber to become well mixed and gradient free.

As described in chapter 3, the gas-phase ozone concentration was modelled as a well-mixed reactor. The gas-phase ozone concentration was determined using equation 5.1.

The efficiency of the ozoniser was calibrated by our collaborator Christian Pfrang at the Department of Chemistry, University of Reading, by measuring the absorbance at a wavelength of 254 nm of the ozone produced by the ozonizer in a cell with a UV visible spectrometer.

The concentration of ozone in the reaction chamber was determined by calculating the flux of ozone into and out of the reaction chamber allowing calculation of the concentration within the chamber according to equation 5.1.

To calculate the concentration of ozone in the reaction chamber, $[O_3]_{chamber}$, the following equation is used where F_{rate} is the flow rate of ozone from the ozonizer (5 L min^{-1}). The value F_{rate} was kept constant for each experiment. $[O_3]_{ozonizer}$ is the concentration of ozone in the flow (F), taken from the ozoniser calibration, which was varied for different experiments. V, is the volume of the reaction chamber minus the volume of the Langmuir trough and fittings ($V = 13.3 \text{ L}^{-1}$). The concentration of ozone within the reaction chamber during the experiments is given in table 5.1.

$$[O_3]_{chamber} = F[O_3]_{ozonizer} \left(1 - e^{-\frac{F_{rate}t}{V}}\right) \quad (E 5.1)$$

The gas-phase ozone concentrations for the methyl oleate neutron experiment are detailed in table 5.1. Based on the work of Smith et al., (2002) it is presumed that the gas-phase ozone dissolves into the monolayer and subsequently reacts. The concentration of ozone in the monolayer region ($[O_3]_{film}$), was calculated using Henry's law in the form of equation 5.2, taken from Smith et al., (2002).

$$[O_3]_{film} = \delta([O_3]_{chamber}H) \quad (E 5.2)$$

The values input to equation 5.2 were as follows:

δ = film thickness in cm, a value of $\sim 1.5 \text{ nm}$

$H = 11.75 \text{ M atm}^{-1}$, the Henrys law solubility coefficient for ozone in oleic acid (a figure for methyl oleate was not available however it would be expected to be similar to that for oleic acid)

$[O_3]_{chamber}$ = the concentration of ozone in the gas-phase of the reaction chamber in molecules cm^{-3} as listed in table 5.1.

Table 5.1 *The Gas-Phase Ozone Concentration in the Reaction Chamber and the Corresponding Ozone Concentration in the Monolayer Region*

Intervals set on ozoniser	Concentration of O ₃ from ozoniser [O ₃] _{ozonizer} / 10 ¹² molecule cm ⁻³	Concentration of O ₃ in chamber [O ₃] _{chamber} / 10 ¹² molecule cm ⁻³	Concentration of O ₃ in film [O ₃] _{film} / 10 ⁸ molecule cm ⁻²
1	53.2 ± 7.4	16.7 ± 2.3	0.39 ± 0.05
1.5	92.8 ± 22.7	29.1 ± 7.1	0.67 ± 0.16
1.7	130 ± 37	40.8 ± 11.6	0.94 ± 0.27
2	169 ± 57.4	53 ± 18	1.23 ± 0.42
2.5	301 ± 13	94.3 ± 4.1	2.18 ± 0.09
3	387 ± 49.2	121 ± 15.4	2.80 ± 0.36
4	566 ± 108	177 ± 34	4.10 ± 0.41
5	749 ± 22.4	235 ± 7	5.32 ± 0.16

5.6.4 The Experimental Methodology of a Typical Neutron Reflectivity Experiment to Measure the Surface Coverage and Surface Pressure of a Methyl Oleate Monolayer Reacting with Gas-phase Ozone

The neutron reflectivity measurements of the monolayer surface coverage were taken on the neutron reflectometer FIGARO at the Institute Laue Langevin, ESRF, Grenoble, France. The FIGARO beamline Langmuir trough, described in chapter 3 was used for all measurements. The Langmuir trough accessories used in this experiment were:

- Surface Pressure Sensor: model IU4, manufactured by Nima Technology.
- Chromatography paper for Wilhelmy plates: 1cm width reel, manufactured by Whatman, catalogue number: 3001604. The paper thickness was 0.18 mm. The paper was cut to form a Wilhelmy plate of a length of 20mm.

The aluminium reaction chamber housing the Langmuir trough was as described in chapter 3 but with the addition of aluminium box inserts fitted around the Langmuir trough which reduced the volume of the chamber by to 13.3 L⁻¹.

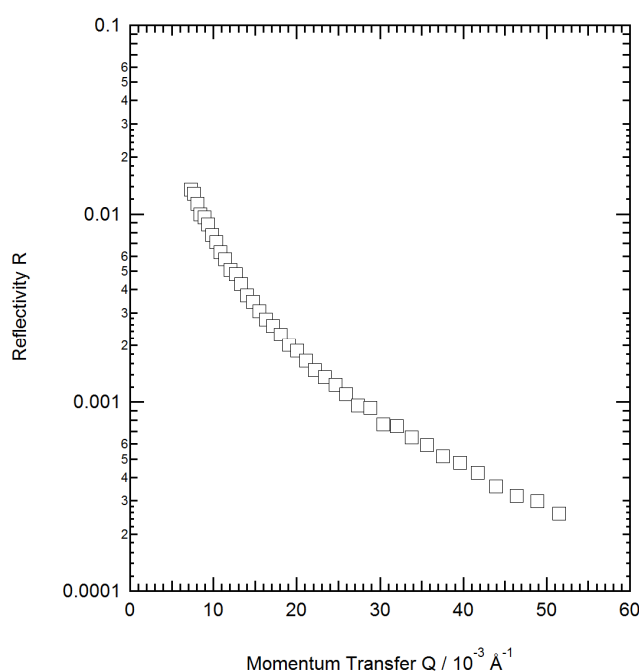
Both surface measurements of surface pressure (Π), and of surface coverage (Γ), the amount of deuterated material at the air-liquid interface were undertaken on a Langmuir trough simultaneously. Measurement of the surface pressure (Π), was conducted with a Wilhelmy plate

suspended from a balance as explained in the preceding chapters. The surface coverage data was obtained using the neutron reflectometer FIGARO to collect time of flight measurements of neutron reflectivity versus momentum transfer, as explained in chapter 3. The 0.6° angle of incidence was used for all the measurements in this chapter. The counting period for the accrual of neutrons on the FIGARO detector was shorter at ~ 10 seconds per point in this experiment. Widening of the instrument slits and adjustment of the choppers allowed a very high flux of neutrons to the instrument enabled a short measurement time.

The cleaning and calibration of the Langmuir trough was as described in chapters 2 and 3. When the sub-phase was clean and no rise in surface pressure was seen upon the closing of the barriers the monolayer was applied to the surface. With the Langmuir trough barriers open the film was applied drop wise to the surface of the Langmuir trough sub-phase. A micro-litre syringe was used to spread $50 \mu\text{L}$ of the deuterated methyl oleate spreading solution to the interface, the initial surface pressure reading was $\sim 7 \text{ mNm}^{-1}$. The area per molecule was $\sim 70 \text{ \AA}^2$ prior to compression. The temperature of the Langmuir trough sub-phase was maintained at $\sim 20^\circ\text{C}$ using a temperature controlled, circulating water bath. The Langmuir trough was housed in an aluminium reaction chamber, custom made by the University of Reading and based on the design of the SURF reaction chamber described in chapter 2. The chamber dimensions were: height 18.5 cm maximum, width 39 cm, length 64 cm. As described in chapter 4 the Langmuir trough sub-phase was made up to a mole ratio of 0.088 mole D_2O in H_2O to produce null reflecting water with a scattering length of zero to neutrons.

The treatment of the reflectivity data to obtain a value of surface coverage was as described in chapter 2 and the data format was as described for the FIGARO reflectometer in section 3.7.3.1 of chapter 3. The scattering length of D_{36} methyl oleate used to calculate the surface coverage was 380 fm. A plot of the reflectivity of the D_{36} methyl oleate monolayer at a surface pressure of 7 mNm^{-1} without ozone is shown in figure 5.4.

Figure 5.4 *The Reflectivity Profile for an Un-reacted Monolayer of Fully Deuterated Methyl Oleate in an O₂ Atmosphere at a Surface Pressure of 7 mNm⁻¹*



The error bars in figure 5.4 represent the error in the measurement of reflectivity (R), based upon the statistical error in the counting of neutrons at the detector as explained in chapter 2. The size of the error bars decreases with higher momentum transfer / Q as at a low range of Q there are fewer counts on the detector so there is a smaller population to measure producing a higher variance.

5.6.5 The Reaction Kinetics of a Methyl Oleate Monolayer Reacting with Gas-phase Ozone

5.6.5.1 The Decay Mechanism

The shape of the decay in the surface coverage of a monolayer of methyl oleate at the air-water interface exposed to gas-phase ozone was similar to that observed with deuterated oleic acid in chapter 3 where the surface coverage of the monolayer decayed exponentially.

The rate expression for the reaction of a deuterated methyl oleate monolayer with gas-phase ozone is:



$$\frac{-d[C_{19}D_{36}O_2]}{dt} = k[C_{19}D_{36}O_2][O_3] \quad (E\ 5.3)$$

The reaction was pseudo first-order. In chapter 3 the kinetic fitting was initiated after a calculated mixing time, for methyl oleate an equation was fit to which incorporated the mixing time for ozone in the chamber as a variable in the fit to the surface coverage data.

The change in the surface coverage of methyl oleate is described by equations 5.4 to 5.10 which also incorporate the ozone mixing time in equation 5.9 onwards.

$$\frac{-d[\text{methyl oleate}]}{dt} = \frac{d\Gamma_{MO}}{dt} \quad (E 5.4)$$

$$\frac{-d\Gamma_{MO}}{dt} = k\Gamma[O_{3(\text{chamber})}] \quad (E 5.5)$$

H is the Henrys law coefficient for ozone in oleic acid (11.75), the value for oleic acid has been used as there was not a published value for methyl oleate, and δ is the monolayer thickness, these terms are incorporated into equation 5.5 giving equation 5.6. The monolayer thickness was not measured for methyl oleate; it is expected to be approximately 15 to 20Å (~15 nm) similar to that of oleic acid.

$$\frac{-d\Gamma_{MO}}{dt} = kH\delta\Gamma[O_{3(\text{chamber})}] \quad (E 5.6)$$

The ozone concentration in the chamber is related to the ozone concentration produced by the ozonizer as calculated in equation 5.7.

$$[O_3]_{\text{chamber}} = [O_3]_{\text{ozonizer}} \left(1 - e^{-\frac{Ft}{V}}\right) \quad (E 5.7)$$

Incorporating the ozone concentration into equation 5.6 gives equation 5.8.

$$\frac{-d[\Gamma_{MO}]_t}{dt} = kH\delta\Gamma_{MO}[O_3]_{\text{ozonizer}} \left(1 - e^{-\frac{Ft}{V}}\right) \quad (E 5.8)$$

Equation 5.8 was solved analytically (the steps taken in solving equation 5.8 to produce equation 5.9 are given in the appendix, item 4). The surface coverage data was fit to equation 5.9 to obtain the rate of change in the surface coverage with reaction time.

$$-\ln \frac{[\Gamma_{MO}]_t}{[\Gamma_{MO}]_{t=0}} = k[O_3]_{\text{ozonizer}}H\delta \left(t - \frac{V}{F} \left(1 - e^{-\frac{Ft}{V}}\right)\right) \quad (E 5.9)$$

Equation 5.9 is fitted to the surface coverage versus time data in the following format:

$$y = \gamma \left(x - \frac{1}{\beta} (1 - e^{-\beta x})\right) \quad (E 5.10)$$

Where the result of the fit γ is equal to $k[O_3]_{\text{ozonizer}}H\delta$, the bimolecular rate of the reaction, k , multiplied by the gas concentration of gas-phase ozone produced by the ozonizer, $[O_3]_{\text{ozonizer}}$, the Henry's law constant for ozone in oleic acid (Smith et al., 2002), H , and the monolayer thickness, δ (1.5 nm).

Equation 5.9 contained a term which modelled the ozone concentration in the monolayer tail region β which was equivalent to the reciprocal of the mixing time for ozone in the reaction chamber ($\frac{1}{\tau_{\text{mix}}}$). Equation 5.10 was fitted to the surface coverage data with a parameter of the fit being the characteristic mixing time of the gas-phase ozone within the reaction chamber which was held constant. The equations describing the ozone concentration are included in the appendix, item 5.1. The results of the fit of equation 5.10 to the surface coverage versus reaction time data and the resulting bimolecular rate constant calculated from the fit are given in section 5.7.6.

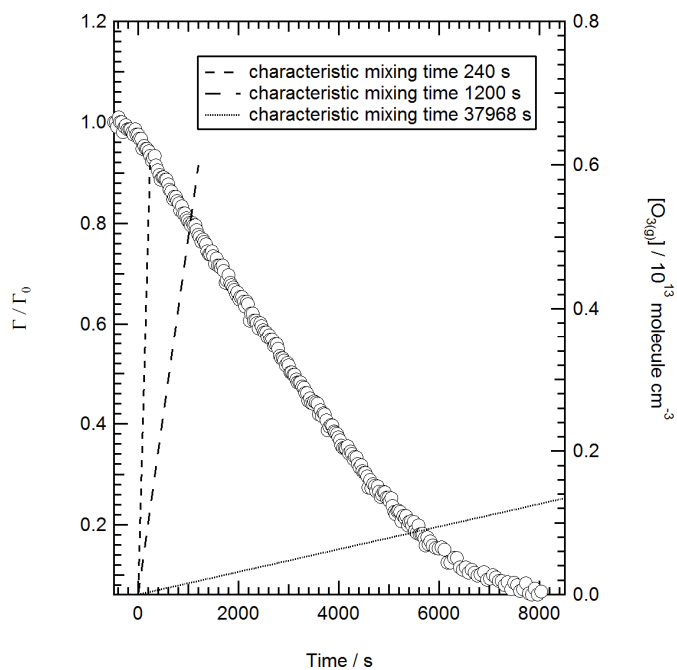
The characteristic mixing time was calculated according to equation 5.11, in the same manner as used in chapter 3. This calculation gave a mixing time of 160 seconds for the ozone concentration in the chamber to reach 37%. Fitting equation 5.10 using the independently calculated mixing time of 160 seconds as a fixed parameter produced a poor fit to the surface coverage data.

$$t_{\text{mix}} = \frac{V}{F_{\text{rate}}} \quad (E 5.11)$$

To obtain a better fit to the surface coverage data the kinetic fitting was subsequently processed with 3 mixing times of 240, 1200 and 37968 seconds. A mixing time of 240 seconds was in closer agreement with the modelling of the mixing time for ozone within the reaction chamber but did not produce an adequate fit to the decay. The best fits were produced using a mixing time of 37968 seconds but this was an unrealistic mixing time given the size of the chamber and duration of the kinetic decay. The mixing time used to calculate k was 1200 seconds as this was more realistic to the experiment and still gave a good fit to the surface coverage data.

Figure 5.5 shows the example of a surface coverage measurement of a methyl oleate monolayer over time under exposure a concentration of $(16.7 \pm 2.3) \times 10^{12}$ molecule cm^{-3} gas-phase ozone, the surface coverage data is shown with the ozone concentration over time for three different mixing times.

Figure 5.5 *The Decay in Surface Coverage of a Monolayer of Methyl Oleate Exposed to $(16.7 \pm 2.3) \times 10^{12}$ molecule cm^{-3} Gas-Phase O_3 Versus the Modelled O_3 Concentration from Equation 5.10*



5.7 Experimental Results

The surface pressure data was obtained from Wilhelmy plate measurements as described in chapter 2. The surface pressure measurements were taken simultaneously with the surface coverage measurements. The surface coverage measurement was the priority as it had been shown in chapter 2 that the surface pressure data did not reliably define the kinetics at the interface. Due to the set-up of the gas-phase reactant, with a flow of 5 L min^{-1} into a smaller volume chamber than in chapter 3 and 4, the surface pressure data was noisier than would be desirable for a publication because of gas turbulence in the cell.

Nine successful experiments were undertaken in the beam time designated on the neutron reflectometer FIGARO for study of the methyl oleate monolayer and gas-phase ozone system. The ozone concentration ranged from $(0.39 \pm 0.05) \times 10^8 \text{ molecule cm}^{-3}$ to $(5.32 \pm 0.16) \times 10^8 \text{ molecule cm}^{-2}$.

The results are presented in the following order:

- The surface coverage and surface pressure of a methyl oleate monolayers reacting with gas-phase ozone (5.7.1).
- The surface coverage and surface pressure of a methyl oleate monolayer in an oxygen only atmosphere (5.7.2).
- A summary of the experimental surface coverage and surface pressure measurement results (5.7.3).
- Kinetic analysis and results (5.7.4).

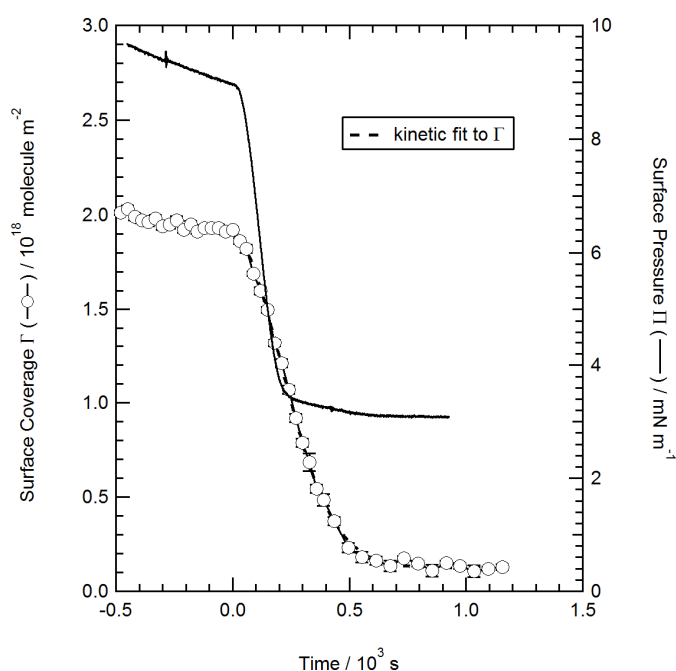
All experiments were conducted on a sub-phase of null reflective water. The kinetic fits of the surface coverage data to equation 5.10 are included on the plots in the results section of this chapter and will be discussed after the presentation of the results in section 5.7.4.

Time zero is shown as reaction time zero when the ozoniser was switched on. The monolayer surface pressure of deuterated methyl oleate decayed from 15 mN m^{-1} giving a starting pressure of $\sim 7 \text{ mN m}^{-1}$, the decrease in surface pressure took place whilst the neutron instrument interlock was taking effect, the interlock is a safety feature that restricts delivery of the neutron beam to the instrument until the sample area is clear of personnel.

5.7.1 The Surface Coverage and Surface Pressure of Methyl Oleate Monolayers Exposed Gas-phase Ozone

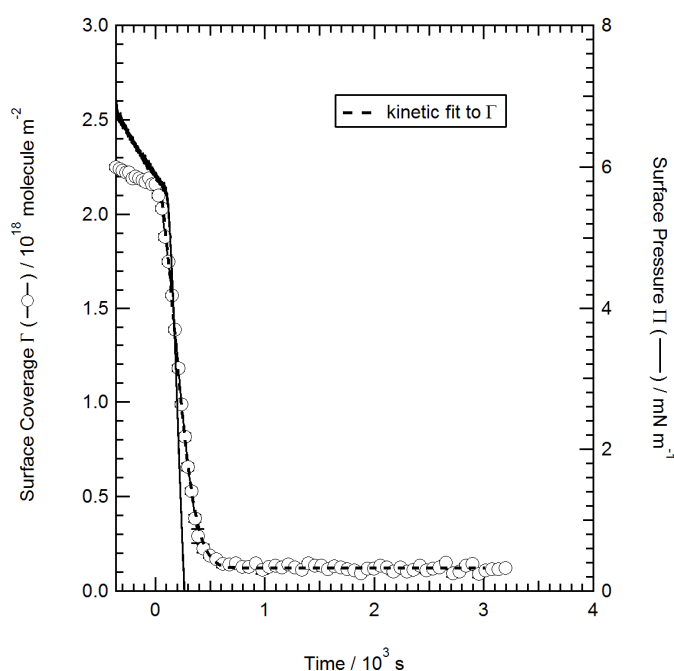
The ozone concentration for the ozone experiments was from $(235 \pm 7.0) \times 10^{12}$ to $(16.7 \pm 2.3) \times 10^{12}$ molecule cm^{-3} . The results are presented in descending order of ozone concentration. Reaction time zero in the plots is the point at which the ozoniser was switched on.

Figure 5.6 *The Kinetic Decay of a D_{36} Methyl Oleate Monolayer Exposed to a Gas-Phase Ozone Concentration of $(235 \pm 7) \times 10^{12}$ molecule cm^{-3}*



The surface coverage decayed rapidly to a residual surface coverage of $\sim 0.2 \times 10^{18}$ molecule m^{-2} . The error in the surface coverage data was within point for many of the measurements and rapid kinetic measurements were achieved with 300 second neutron counting period per individual reflectivity measurement, the errors are small as the efficiency of the set-up of the instrument by the instrument scientist was optimal so the error the reflectivity measurement was small and the data fitting was good so the corresponding error in the surface coverage is small. The surface pressure did not decay to zero in figure 5.6, however the measurement of surface pressure did reach a value of zero in the following experiments.

Figure 5.7 *The Kinetic Decay of a D_{36} Methyl Oleate Monolayer Exposed to a Gas-Phase Ozone Concentration of $(177 \pm 34) \times 10^{12}$ molecule cm^{-3}*



At an ozone concentration of $(177 \pm 34) \times 10^{12}$ molecule cm^{-3} as shown in figure 5.7 the monolayer surface pressure decayed to zero over a duration of 500 seconds O_3 exposure, and the surface coverage decayed to a residual value of $\sim 1.5 \times 10^{18}$ molecule m^{-2} . The highest ozone concentration experiment was conducted at $(235 \pm 7) \times 10^{12}$ molecule cm^{-3} , the monolayer decayed by 2×10^{18} molecule m^{-2} over 650 seconds, here within error the decay in surface coverage was slower than at the slightly higher O_3 concentration of at $(235 \pm 7) \times 10^{12}$ molecule cm^{-3} .

There were two experiments undertaken at an ozone concentration of $(121 \pm 15.4) \times 10^{12}$ molecule cm^{-3} . As shown in figure 5.8 and 5.9 in both cases the monolayer decayed away by 2×10^{18} molecule m^{-2} over 800 seconds to a residual value of $\sim 1.5 \times 10^{18}$ molecule m^{-2} .

Figure 5.8 *The Kinetic Decay of a D_{36} Methyl Oleate Monolayer Exposed to a Gas-Phase Ozone Concentration of $(121 \pm 15.4) \times 10^{12}$ molecule cm^{-3}*

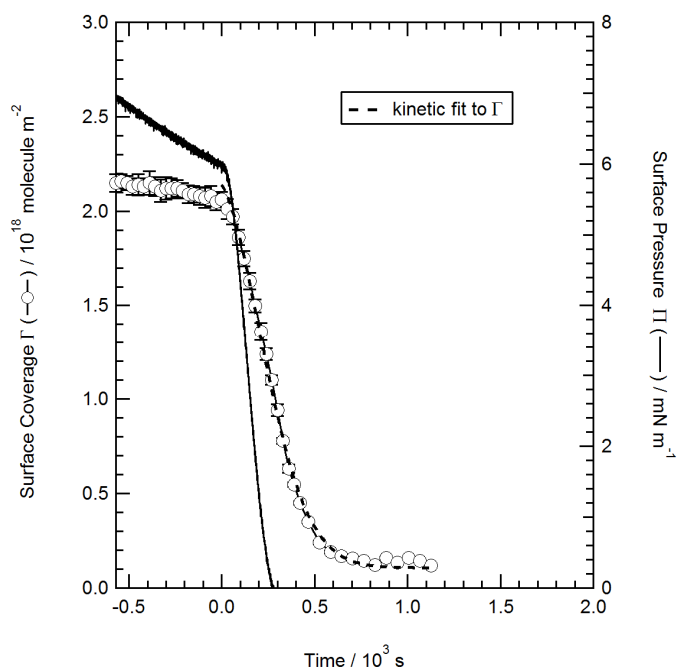
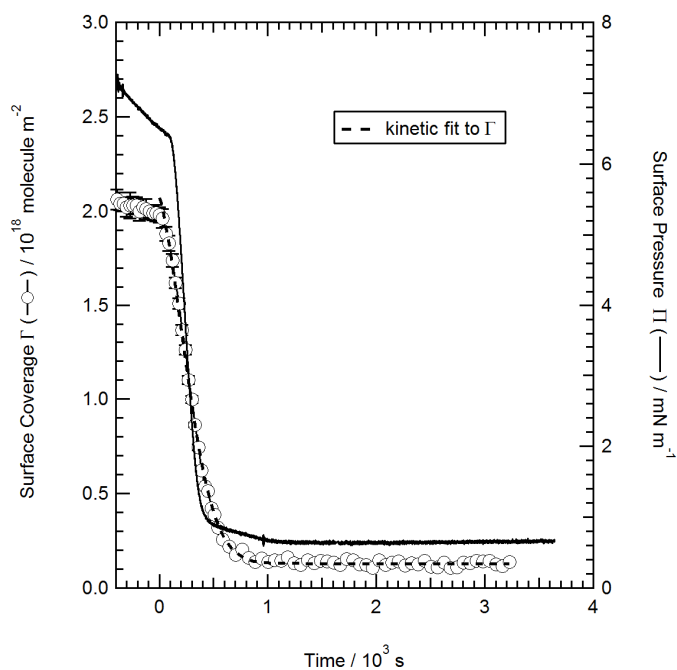
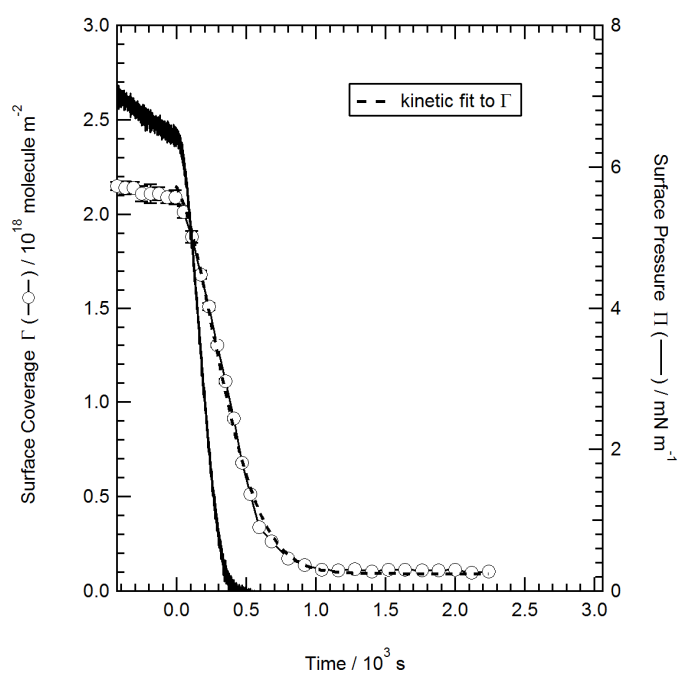


Figure 5.9 A Repeat of the Kinetic Decay of a D_{36} Methyl Oleate Monolayer Exposed to a Gas-Phase Ozone Concentration of $(121 \pm 15.4) \times 10^{12}$ molecule cm^{-3}



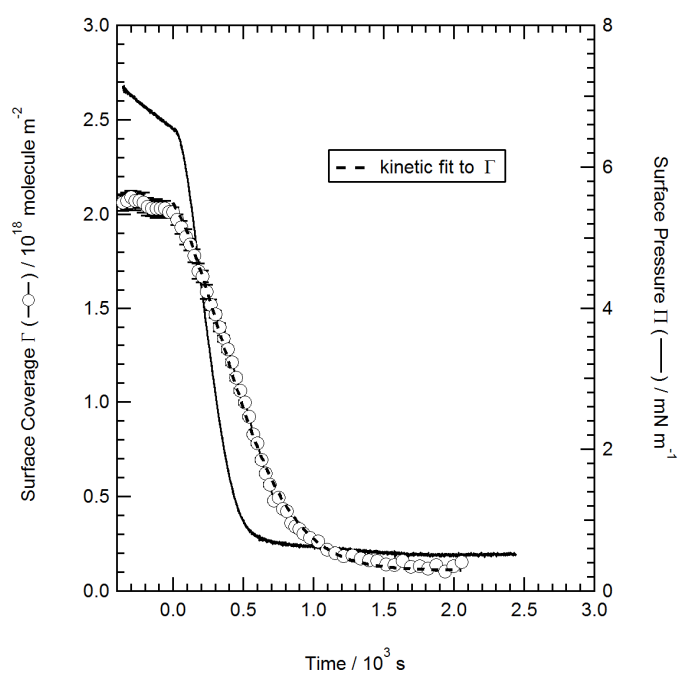
The repeat surface coverage measurement was conducted over a longer time period to show whether the monolayer surface coverage would reach a value of zero under sustained exposure to ozone. There remained a steady residual surface coverage of $\sim 1.5 \times 10^{18}$ molecule m^{-2} for 2500 seconds (41 minutes).

Figure 5.10 *The Kinetic Decay of a D_{36} Methyl Oleate Monolayer Exposed to a Gas-Phase Ozone Concentration of $(94.3 \pm 4.1) \times 10^{12} \text{ molecule cm}^{-3}$*



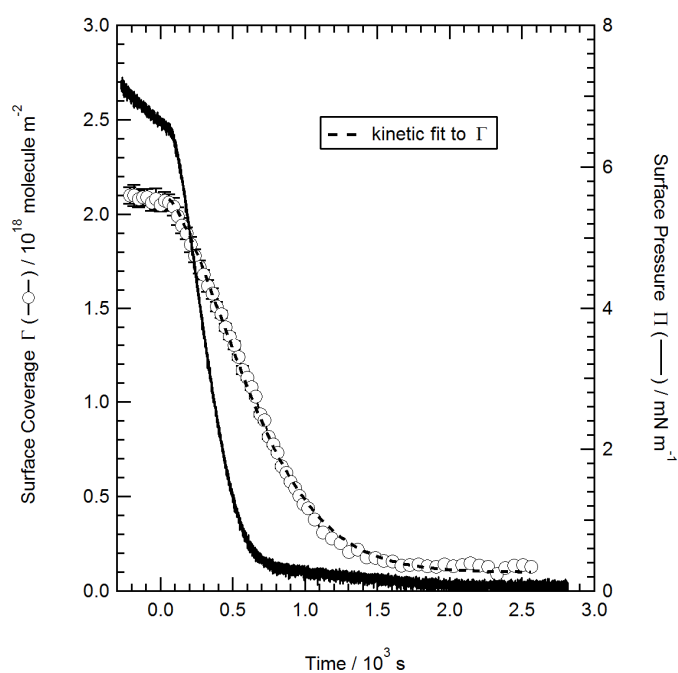
When exposed to an ozone concentration of $(94.3 \pm 4.1) \times 10^{12} \text{ molecule cm}^{-3}$ the methyl oleate monolayer decayed by $2 \times 10^{18} \text{ molecule m}^{-2}$ over 1050 seconds.

Figure 5.11 *The Kinetic Decay of a D_{36} Methyl Oleate Monolayer Exposed to a Gas-Phase Ozone Concentration of $(53 \pm 18) \times 10^{12}$ molecule cm^{-3}*



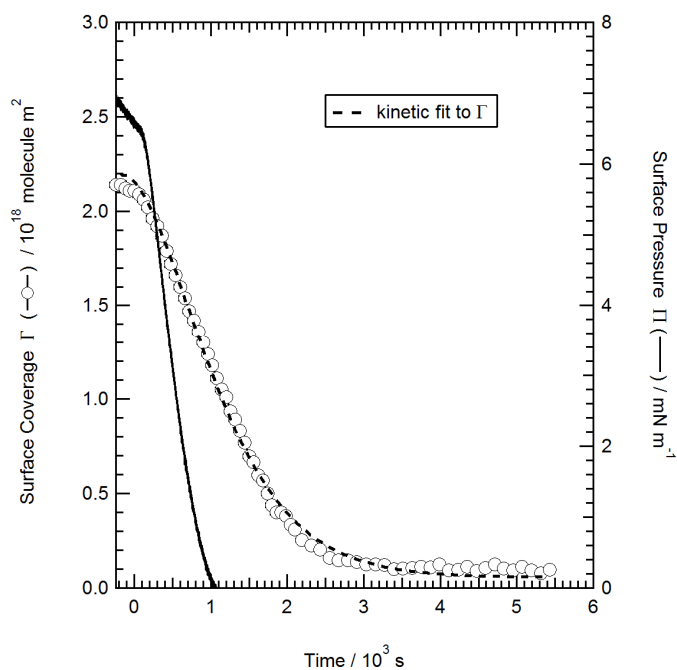
The kinetic decay in the monolayer at a gas-phase ozone concentration of $(53 \pm 18) \times 10^{12}$ molecule cm^{-3} in the monolayer tail region produced a loss of 2×10^{18} molecule m^{-2} over 2000 seconds, the time taken for the film to decay to a surface coverage of zero decreased with increasing ozone concentration.

Figure 5.12 *The Kinetic Decay of a D_{36} Methyl Oleate Monolayer Exposed to a Gas-Phase Ozone Concentration of $(40.8 \pm 11.6) \times 10^{12}$ molecule cm^{-3}*



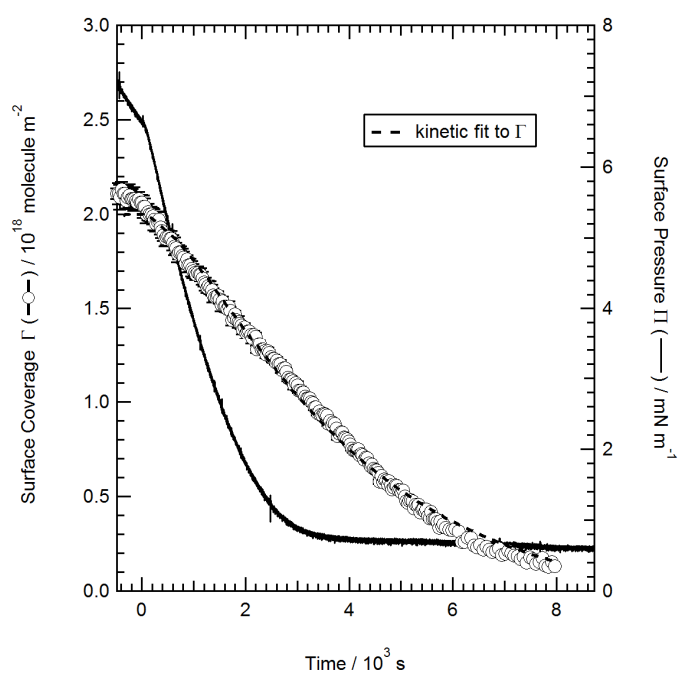
When exposed to a gas-phase ozone concentration of $(40.8 \pm 11.6) \times 10^{12}$ molecule cm^{-3} the surface coverage of the monolayer declined by 2×10^{18} molecule m^{-2} over a period of 1700 seconds.

Figure 5.13 *The Kinetic Decay of a D_{36} Methyl Oleate Monolayer Exposed to a Gas-Phase Ozone Concentration of $(29.1 \pm 7.1) \times 10^{12} \text{ molecule cm}^{-3}$*



In figure 5.13 the data points from 1000 seconds onwards have larger spacing as the reflectivity data was co-added into larger time bins to produce a higher signal to fit to with better signal to noise statistics in the reflectivity measurement. At an ozone concentration of $(29.1 \pm 7.1) \times 10^{12} \text{ molecule cm}^{-3}$ the surface coverage decayed by approximately $2 \times 10^{18} \text{ molecules m}^{-2}$ over 3000 seconds.

Figure 5.14 *The Kinetic Decay of a D_{36} Methyl Oleate Monolayer Exposed to a Gas-Phase Ozone Concentration of $(16.7 \pm 2.3) \times 10^{12}$ molecule cm^{-3}*



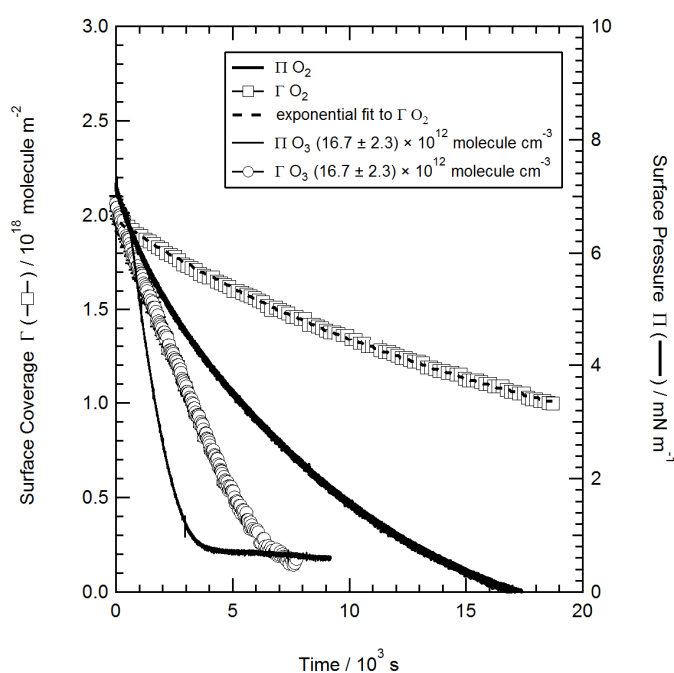
At the lowest gas-phase ozone concentration the methyl oleate monolayer decay became shallower in gradient at 6000 seconds as the residual concentration of $\sim 1.5 \times 10^{18}$ molecule m^{-2} was reached at 8000 seconds (>2 hours).

5.7.2 The Surface Coverage and Surface Pressure of Methyl Oleate Monolayers in an Oxygen Atmosphere

Methyl oleate monolayers were found to decay in a pure oxygen atmosphere. The rate of decay in oxygen was slower than the reaction in an ozone atmosphere as shown in figure 5.15. The decay in surface coverage recorded in an oxygen only atmosphere was fitted to equation 5.12.

$$\Gamma = \Gamma_0 e^{-kt} \quad (E 5.12)$$

Figure 5.15 *The Decay in the Surface Pressure (Π) and the Surface Coverage (Γ) of a D_{36} Methyl Oleate Monolayer at the Air-liquid Interface over Time in an Oxygen Atmosphere with an Exponential Fit to the Surface Coverage Data Plotted with a Low Ozone Concentration Experiment*



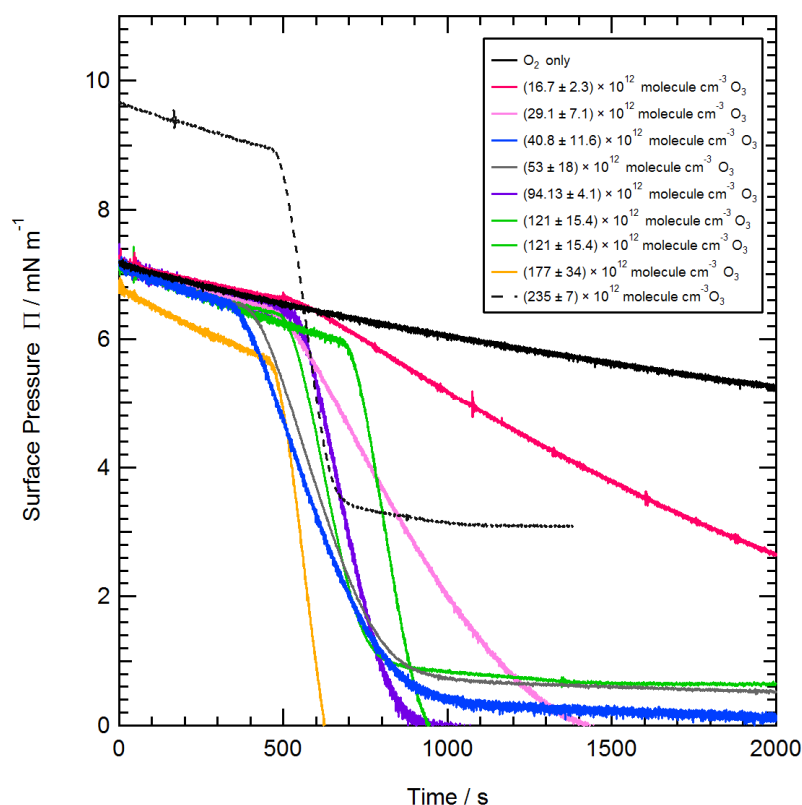
A monolayer of D_{36} methyl oleate on a sub-phase of null reflective water, without exposure to ozone took approximately 17000 seconds to decay to zero surface pressure, at which point any remaining molecules at the air-liquid interface were too far apart to exert a measurable surface pressure above that of the sub-phase. The surface coverage decayed to 1.1×10^{18} molecule m^{-2} over 19000 seconds (~ 5.2 hours), a loss of 0.9×10^{18} molecule m^{-2} . Figure 5.15 shows the difference in the decay in the methyl oleate monolayer surface coverage when exposed to oxygen and to a low concentration of ozone. The decay in an ozone atmosphere is more rapid, over 8000 seconds the surface coverage decays to a value of $\sim 0.1 \times 10^{18}$ molecule m^{-2} . In contrast to the decay of methyl oleate in oxygen where 0.5×10^{18} molecule m^{-2} of deuterated methyl oleate was lost from the air-water interface over 8000 seconds (figure 5.15) the lowest

O_3 concentration of $(16.7 \pm 2.3) \times 10^{12}$ molecule cm^{-3} shown in figure 5.14 gave a loss of 2×10^{18} molecule m^{-2} from the air-water interface over 8000 seconds, the film was not entirely removed by exposure to ozone or loss of molecules at the surface going into solution or beneath the barriers on the Langmuir trough.

5.7.3 A Summary of the Surface Pressure and Surface Coverage Results

Figure 5.16 *The Decay in the Surface Pressure (Π) of a D_{36} Methyl Oleate Monolayer at the Air–Water Interface over Time in an Atmosphere of Varied Concentrations of Gas-Phase Ozone*

Time zero is the time at which the ozoniser was activated.



As demonstrated in figure 5.16 the surface pressure data broadly shows a steeper decay in surface pressure with increasing ozone concentration. The highest ozone concentration of $(235 \pm 7) \times 10^{12}$ molecules cm^{-3} caused the monolayer to decay to a surface pressure of zero within 620 seconds. At the lowest ozone concentration of $(16.7 \pm 2.3) \times 10^{12}$ molecules cm^{-3} the surface pressure exerted by the methyl oleate monolayer reduced to a low surface pressure of 0.4 mNm^{-1} zero in 4100 seconds, the measurement did not reach zero for this concentration,

however recompression of the Langmuir trough barriers did not produce a reading thus it was inferred that the measurement had drifted during the duration of the experiment for example due to evaporation changing the height of the meniscus and that this reading was effectively zero. The surface pressure decayed to a zero value more rapidly than the surface coverage at the air-water interface.

Figure 5.17 *The Kinetic Decay in the Surface Coverage of Methyl Oleate Monolayers Exposed to Varied Concentrations of Gas-phase Ozone*

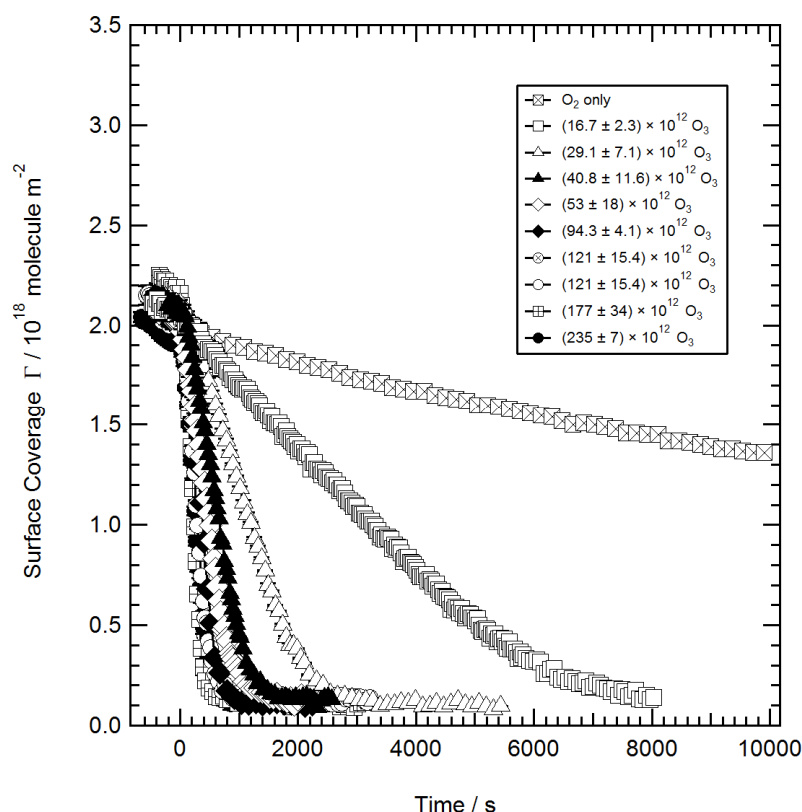
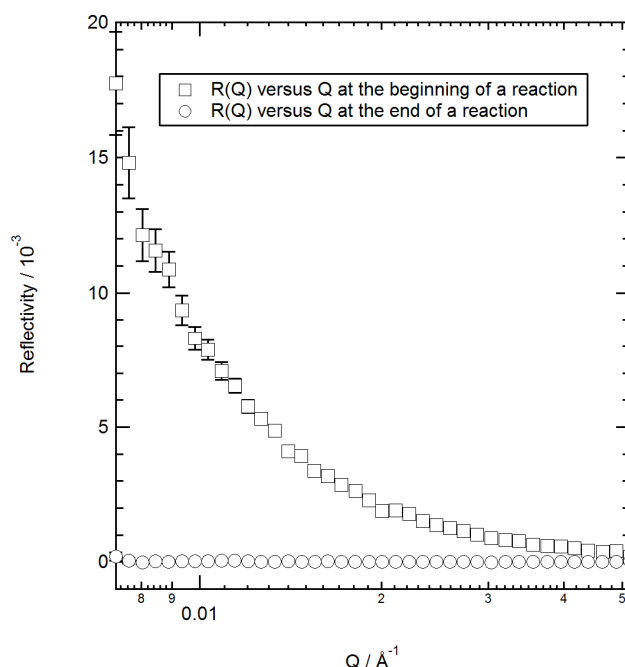


Figure 5.17 shows the decay in surface coverage (Γ) over time for methyl oleate monolayers exposed to various concentrations of gaseous ozone. It can be seen that the higher the ozone concentration the more rapid the decay in the surface coverage and that the reaction with oxygen produced a shallower decay in the surface coverage of deuterated material at the air-water interface. It can be seen in figure 5.17 that in an oxygen only atmosphere the decay in surface coverage was of a much slower rate than when the methyl oleate monolayer reacted with ozone. The change in the rate of decay when the monolayers of oleic acid in chapter 3 were exposed to low concentrations of gas-phase ozone (~ 11 to $\sim 100 \times 10^{12}$ molecule cm^3) was not seen for methyl oleate although the experiments were started at a lower surface pressure so if the change in decay rate was a feature of the packing of the film then it may have been missed

in this experiment. The surface coverage did not decay to a zero value over the timescales and range of ozone concentrations studied, a small residual surface concentration was observed of $\sim (0.1 \pm 0.025) \times 10^{18}$ molecule m^{-2} at the end of some of the experiments. Figure 5.18 shows that the $R(Q)$ versus Q signal is zero at this point, the measurement is in the instrumental noise at this low value of surface coverage so it cannot be stated whether there is any deuterated material remaining at the interface or not, if there was it would be a very small amount, the corresponding surface coverage measurements are given in figure 5.14.

Figure 5.18 Reflectivity versus Momentum Transfer for a Methyl Oleate Monolayer at the Air-water Interface Exposed to a Gas-phase Ozone Concentration of $(16.7 \pm 2.3) \times 10^{12}$ molecule cm^{-3}



In summary the experimental results for monitoring the surface coverage at the air-water interface and the monolayer surface pressure of methyl oleate monolayers during exposure to gas-phase ozone which was subsequently absorbed into the organic film, were that:

- The surface pressure of methyl oleate does decay exponentially under exposure to ozone in the same manner as the surface coverage data but the surface pressure decays more rapidly so would not yield a useful rate constant for determining the presence of an intact film at the air-liquid interface accurately.
- The decay in the monolayer surface coverage with time was faster with exposure to increasing ozone concentrations.

5.7.4 Kinetic Results

The fitting of equation 5.10 to the surface coverage data gave a value of $k[\text{O}_3]_{\text{ozoniser}}\text{H}\delta$, the values of the surface coverage at the start of the reaction and the mixing time were kept constant during the fitting process, $k[\text{O}_3]_{\text{ozoniser}}\text{H}\delta$ was plotted against the concentration of ozone produced by the ozoniser, $[\text{O}_3]_{\text{ozoniser}}\text{H}\delta$, as shown in figure 5.19 and a line was fit to obtain the slope of $k[\text{O}_3]_{\text{ozoniser}}\text{H}\delta$ with increasing $[\text{O}_3]_{\text{ozoniser}}$, the slope gives the bimolecular rate constant, k . The results of the fitting of equation 5.10 are summarised in table 5.2. The values of $k[\text{O}_3]_{\text{ozoniser}}\text{H}\delta$ are valid for a null reflective water sub-phase of pH 5.5 at a temperature of 20 °C.

Table 5.2 *The Pseudo First Order Rate Constants and Second Order Rate Constants for Methyl Oleate Monolayers Reacting with Gas-phase Ozone*

$[\text{O}_3]_{\text{ozoniser}} \times 10^{12} \text{ cm}^{-3}$	$[\text{O}_3]_{\text{chamber}} \times 10^{12} \text{ molecule cm}^{-3}$	$[\text{O}_3]_{\text{film}} \times 10^8 \text{ molecule cm}^{-2}$	$\frac{I_{\text{final}}}{I_{\text{initial}}}$	$[\text{O}_3]_{\text{ozoniser}} \text{H}\delta \times 10^8 \text{ molecule cm}^{-2}$	$k[\text{O}_3]_{\text{ozoniser}} \text{H}\delta \text{ s}^{-1}$	Bimolecular $k / 10^{-11} \text{ cm}^{-2} \text{ molecule}^{-1} \text{ s}^{-1}$
749 ± 22.4	235 ± 7	4.1 ± 0.12	0.0672	13.2 ± 0.40	0.004549 ± 0.000093	2.72 ± 0.44
566 ± 108	177 ± 34	3.1 ± 0.32	0.0408	9.98 ± 1.90	0.0003 ± 0.0000032	
387 ± 49.2	121 ± 15.4	2.1 ± 0.27	0.0623	6.82 ± 0.87	0.006435 ± 0.00017	
387 ± 49.2	121 ± 15.4	2.1 ± 0.27	0.0648	6.82 ± 0.87	0.0274 ± 0.001	
301 ± 13	94.3 ± 4.1	1.7 ± 0.07	0.0493	5.31 ± 0.23	0.0179 ± 0.00042	
169 ± 57.4	53 ± 18	0.93 ± 0.32	0.0756	2.98 ± 1.01	0.0214 ± 0.00094	
130 ± 37	40.8 ± 11.6	0.72 ± 0.2	0.0621	2.29 ± 0.65	0.0122 ± 0.0005	
92.8 ± 22.7	29.1 ± 7.1	0.51 ± 0.12	0.0448	1.64 ± 0.4	0.0016 ± 0.00004	
53.2 ± 7.4	16.7 ± 2.3	0.29 ± 0.04	0.0616	0.94 ± 0.13	0.037 ± 0.001	
O ₂ only	n/a	n/a	n/a	n/a	0.00005 ± 0.002	

Figure 5.19 The 2nd Order Kinetic Plot for the Decay in the Surface Coverage of a Monolayer of D₃₆ Methyl Oleate Under Conditions of Ozonolysis

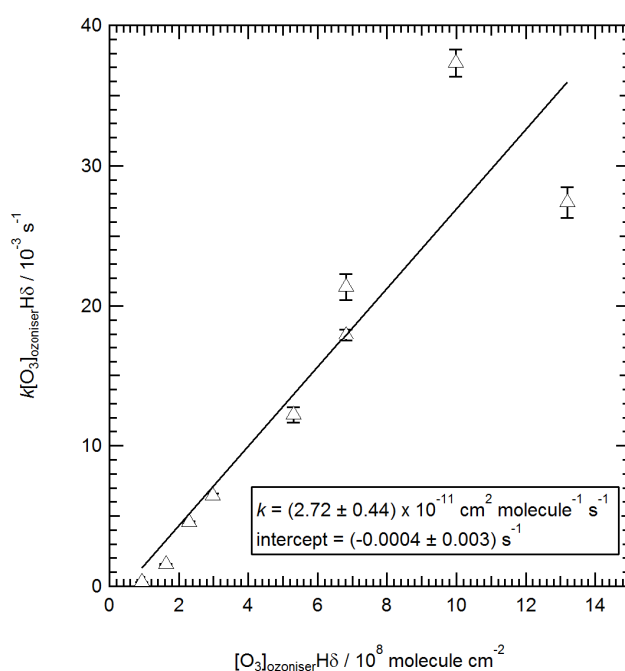


Figure 5.19 shows a straight line fit to the experimentally obtained values of $k[O_3]_{\text{ozoniser}} H\delta$ for methyl oleate ozonolysis with varied concentrations of ozone. The intercept of the line has a very low value consistent with a value of zero as the error is bigger than the value. A value for bimolecular rate constant, k , of $(2.72 \pm 0.44) \times 10^{-11} \text{ cm}^2 \text{ molecule}^{-1} \text{ s}^{-1}$ was achieved for the reaction of a methyl oleate monolayer with gas-phase ozone which had dissolved into the organic film then reacted with the methyl oleate. This value is in agreement with that for oleic acid monolayer reacting with gas-phase ozone. The bimolecular rate constant for gas-phase ozone reacting with an oleic acid monolayer was $(4.5 \pm 0.7) \times 10^{-11} \text{ s}^{-1}$ (see chapter 4); a value of $(7.3 \pm 0.9) \times 10^{-11} \text{ s}^{-1}$ was obtained by King et al., (2009).

To consider if the surface coverage measurements are valid for the reaction of ozone with methyl oleate or if transport of ozone is contributing to the kinetics, the following mechanisms must be constrained:

- Diffusion of gas phase ozone from the bulk into the surface region near to the monolayer ($\tau_{\text{diffusion}}$).
- Accommodation of the gas-phase ozone into the organic film ($\tau_{\text{interfacial}}$).
- The reaction of the methyl oleate monolayer film with the ozone accommodated within the monolayer (τ_{reaction}).

The time taken for ozone to diffuse to the monolayer and to reach a stable concentration (for mixing to complete) was calculated. The characteristic time for the diffusion of ozone ($\tau_{diffusion}$) in the gas-phase was calculated from equation 5.13 (Seinfeld and Pandis, (2006); King et al, (2009)) where d is the thickness of the monolayer, ($\sim 15 \text{ \AA}$) also known as the characteristic distance, D_g is the gas-phase diffusion constant for ozone ($1.80 \times 10^{-5} \text{ m}^2 \text{ s}^{-1}$) (Seinfeld and Pandis, 2006; King et al. 2009).

$$\tau_{diffusion} = \frac{d^2}{4D_g} \quad (E. 5.13)$$

The characteristic diffusion time for ozone to diffuse to the monolayer was $5.56 \times 10^{-14} \text{ s}$ for a 20 \AA thickness monolayer and $3.13 \times 10^{-14} \text{ s}$ for a monolayer thickness of 15 \AA .

The characteristic time taken for the accommodation of ozone at the interface or interfacial equilibrium was calculated according to equation 5.14 where D_l denotes the diffusion constant for ozone in an organic liquid ($1 \times 10^{-9} \text{ m}^2 \text{ s}^{-1}$) (Seinfeld and Pandis. 2006; King et al. 2009).

$$\tau_{interfacial} = \frac{d^2}{\pi^2 D_l} \quad (E. 5.14)$$

The accommodation time was $2.28 \times 10^{-10} \text{ s}$ for a monolayer thickness of 15 \AA and $4.05 \times 10^{-10} \text{ s}$ for a thickness of 20 \AA .

The characteristic time taken for the reaction of ozone with methyl oleate, $\tau_{reaction}$ was determined by the following equation 5.15, where k is the bimolecular surface reaction rate constant between methyl oleate and ozone, the value k ($2.7 \times 10^{-11} \text{ cm}^2 \text{ molecule}^{-1} \text{ s}^{-1}$) was converted to units of m mol s^{-1} ($1.6 \times 10^9 \text{ m mol s}^{-1}$). The surface concentration of methyl oleate (surface coverage) $\Gamma_{methyl\ oleate}$ of $2 \times 10^{18} \text{ molecules m}^{-2}$ was taken from the experimental data and converted to units of mol ($3.3 \times 10^6 \text{ mol}$).

$$\tau_{reaction} = \frac{1}{k \Gamma_{methyl\ oleate}} \quad (E. 5.15)$$

As equation 5.15 is dependent on the starting value of Γ which was not consistent it has been calculated for a surface coverage of methyl oleate ($\Gamma_{methyl\ oleate}$) of $2 \times 10^{18} \text{ molecules m}^{-2}$ and for $3 \times 10^{18} \text{ molecules m}^{-2}$ giving results of $1.8 \times 10^{-4} \text{ s}$ and $1.2 \times 10^{-4} \text{ s}$ respectively.

What this analysis shows is that as with oleic acid in chapter 3, the characteristic lifetime of the reaction of an methyl oleate monolayer with gas-phase ozone is much slower than the diffusion of ozone to the air-water interface and the interfacial accommodation of ozone therefore the measured results of surface coverage are valid for the reaction between the monolayer and

ozone and are not measuring the process of diffusion or accommodation rather than the reaction of the ozone with the monolayer.

The uptake coefficient (γ) for ozone on a cloud droplet or aerosol particle possessing a monolayer of methyl oleate can be estimated using equation 5.16 from Hearn et al., (2005). Where H is the Henry's law constant of $480 \text{ mol m}^{-3} \text{ atm}^{-1}$, R is the gas constant of $8.204 \times 10^{-5} \text{ atm m}^3 \text{ mol}^{-1} \text{ K}^{-1}$, T is the temperature at cloud base height in the troposphere, \bar{c} is the average molecular speed of gas-phase ozone (360 m s^{-1}), δ is the thickness of the film ($20 \times 10^{-10} \text{ m}$).

$$\gamma = \frac{4HRT}{\bar{c}} \delta k \Gamma_{\text{methyl oleate}} \tag{E 5.16}$$

The uptake coefficient γ calculated for different temperatures are given in table 5.3. The uptake coefficient was calculated at a temperature of 293 K for comparison with other studies (Hearn et al. 2005; King et al. 2009) and at 273 K and 278 K as temperatures representative of the cloud base temperature for a warm marine cloud (Snider, 1999). To enable comparison to the uptake coefficient calculated in chapter 3 the uptake coefficient was also modelled for a monolayer thickness of 15 \AA .

The uptake coefficients calculated for different temperatures are given in table 5.3.

Table 5.3 *Uptake Coefficients for Ozone into a Cloud Droplet/ Aerosol with a Methyl Oleate Monolayer at the Air-water Interface*

$\Gamma / 10^{18}$ molecule m^{-2}	$\Gamma / 10^{-6}$ mole m^{-2}	$\delta / \text{\AA}$ Methyl Oleate Film	γ at T = 293 K (~20°C) $/ \times 10^{-6}$	γ at T=278 K (~5°C) $/ \times 10^{-6}$	γ at T=273 K (~0°C) $/ \times 10^{-6}$
2	3.32	15	1.1	0.99	0.97
2	3.32	20	1.4	1.3	1.3
3	4.98	15	1.6	1.5	1.5
3	4.98	20	2.1	2	1.9

5.8 Discussion

The discussion will focus on the following aspects of this work;

- The surface coverage and surface pressure measurements and the kinetic results of the decay of methyl oleate monolayers over time during the reaction with gas-phase ozone will be compared to other studies.
- Discussion of the reaction mechanism for a methyl oleate monolayer reacting with gas-phase ozone at the air-water interface.

5.8.1 Discussion of the Surface Coverage and Surface Pressure Results

The decay in the surface coverage of methyl oleate at the air-water interface during a reaction with ozone did not feature the plateau seen at a surface coverage of $\sim 2 \times 10^{18}$ molecule m^{-2} in the decay in the surface coverage of oleic acid monolayers reacting with ozone. The plateau in the decay in the surface coverage of oleic acid at the air-water interface was probably the result of the reorganization of the packing of the monolayer at a surface coverage of $\sim 2 \times 10^{18}$ molecule m^{-2} . The methyl oleate experiments were started at a lower surface coverage than the oleic acid ozonolysis experiments so the packing of the monolayer during the reaction may have meant that the plateau was not seen. The difference in the surface pressure at the beginning of the experiments between the oleic acid monolayer (~ 20 to 22 mN m^{-1}) and the methyl oleate monolayer (~ 7 to 10 mN m^{-1}) was due to the rapid decay of methyl oleate at the start of the experiment.

The final surface coverage of deuterated material remaining at the air-water interface after sustained ozone exposure was within the region of measurement noise for the neutron reflectivity measurements of the methyl oleate monolayers. In the work of Mochida et al., (2006) methyl oleate was also observed to almost completely oxidise away from particles monitored with quadrupole aerosol mass spectrometry, under sustained ozone exposure. The surface pressure of the methyl oleate monolayer decreased rapidly from the initiation of the ozone supply to the chamber and reached a value of zero in advance of the surface coverage.

A monolayer of methyl oleate at the air-water interface of a cloud droplet would be oxidised away by ozone from the air surrounding the droplet. The reaction products, as demonstrated in chapter 3 for the ozonolysis of oleic acid, did not remain at the air-water interface thus must be volatile or soluble.

5.8.2 Discussion of the Kinetic Results

For comparison the values relating to the mixing of ozone and its uptake to the monolayer are given in table 5.4 for the King et al., (2009) oleic acid ozonolysis study and for the oleic acid experiment in chapter 3 together with the values from this chapter. The decay of an oleic acid monolayer as it reacts with ozone would be expected to be similar to that of methyl oleate as methyl oleate is the methyl ester of oleic acid, thus the structure of the molecule beyond the head group is very similar and ozone is expected to initially react with the double bond in the tail of the methyl oleate molecule so the initial step of the reaction would be the same as for oleic acid.

Table 5.4 *The Gas-phase Ozone Diffusion and Uptake Characteristic Time for Oleic Acid and Methyl Oleate Monolayers*

Parameter	δ (Å)	Γ_{initial} ($\times 10^{18}$ molecule m^{-2})	Oleic Acid and Ozone (King et al. 2010)	Oleic Acid and Ozone (chapter 3)	Methyl Oleate and Ozone
$\tau_{\text{diffusion}}$	20	-	$\sim 6 \times 10^{-14}$	-	5.56×10^{-14}
(s)	15	-	-	3.13×10^{-14}	3.13×10^{-14}
$\tau_{\text{interfacial}}$	20	-	$\sim 3 \times 10^{-10}$	-	4.05×10^{-10}
(s)	15	-	-	2.28×10^{-10}	2.28×10^{-10}
τ_{reaction}		2	10^3	1×10^{-4}	1.8×10^{-4}
(s)		3	-	6.8×10^{-5}	1.2×10^{-4}
k ($\text{cm}^2 \text{ molecule}^{-1} \text{ s}^{-1}$)			$(7.3 \pm 0.9) \times 10^{-11}$	$(4.5 \pm 0.7) \times 10^{-11}$	$(2.7 \pm 0.4) \times 10^{-11}$
γ at 293 K	20	2	$\sim 4 \times 10^{-6}$	2.3×10^{-6}	1.4×10^{-6}
	20	3	-	3.5×10^{-6}	2.1×10^{-6}
	15	2	-	1.7×10^{-6}	1.1×10^{-6}
	15	3	-	2.6×10^{-6}	1.6×10^{-6}

From table 5.4 it can be seen that there is a discrepancy in the value of τ_{reaction} as published by King et al., (2009) and that which I have calculated. This is due to a mistake in the published paper where the τ_{reaction} was calculated with a first order rate constant of $k = 10^{-3} \text{ s}^{-1}$ instead of using bimolecular k . Repeating the calculation of τ_{reaction} with bimolecular k from the King et al., (2009) paper gives a value of $6.8 \times 10^{-5} \text{ s}$. The values of the bimolecular rate constant and for the time taken for ozone to diffuse to the film, be accommodated in the organic film and react for methyl oleate are in good agreement with those for oleic acid monolayers reacting with gas-

phase ozone at the air-water interface. The agreement is a pleasing result as the measurements in the work of King et al., (2009) were taken on a different reflectometer to the work in this thesis and the reaction chamber volume was reduced for the methyl oleate ozonolysis experiments from the volume of the chamber in chapter 3 yet the results are in good agreement showing that the experimental method produces reliable results. The uptake coefficients are slightly smaller for ozone to a methyl oleate film than for ozone to a film of oleic acid.

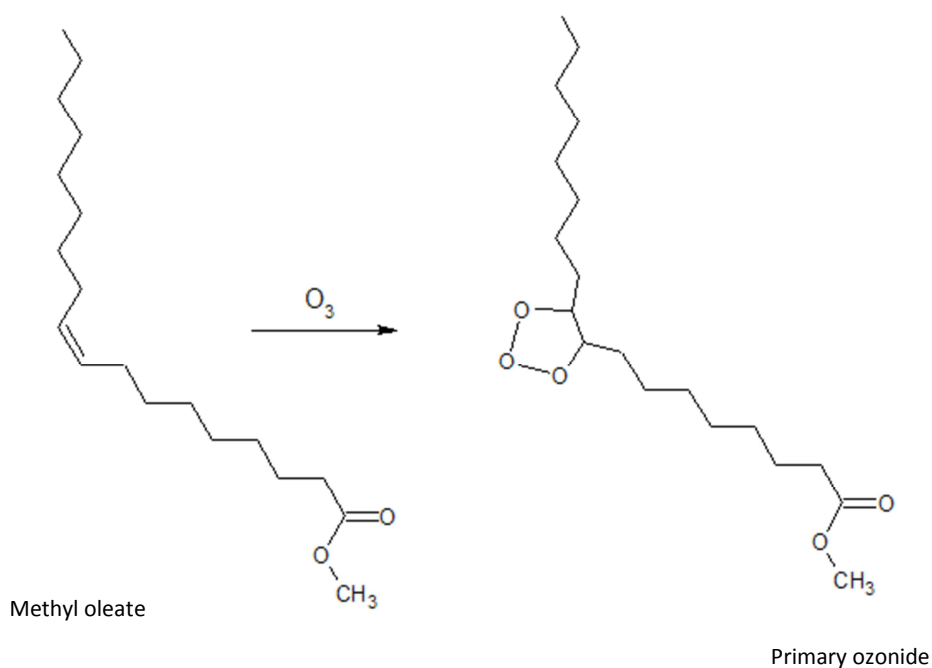
5.8.3 A Proposed Mechanism for the Reaction of Ozone with a Methyl Oleate Monolayer

The following pages give a possible mechanism for the ozonolysis of methyl oleate at the air-liquid interface based on literature. The work of Ziemann (2005) and the work of Zahardis and Petrucci, (2007) on the ozonolysis of oleic acid form the basis of the chemical mechanism of decay detailed here, together with the work Mochida et al., (2006). The reaction of methyl oleate with ozone takes several steps which are detailed here as individual steps in figure 5.20 to 5.27. Zahardis and Petrucci, (2007) and give an overview of the process of unsaturated alkene ozonolysis as follows;

- A primary ozonide is formed by addition of O_3 to the double bond.
- Cleavage produces aldehydes (ketones) and carbonyl oxides (Criegee intermediates).
- The carbonyl oxide/ Criegee intermediate and the aldehyde / ketone recombine forming secondary ozonides.
- The secondary ozonides gradually decompose to lower molecular weight products such as nonanal, 9-oxo-methyl nonanoate, nonanoic acid and the azelaic acid methyl ester (Shilling et al. 2007).
- The Criegee intermediates can attack other stable species.

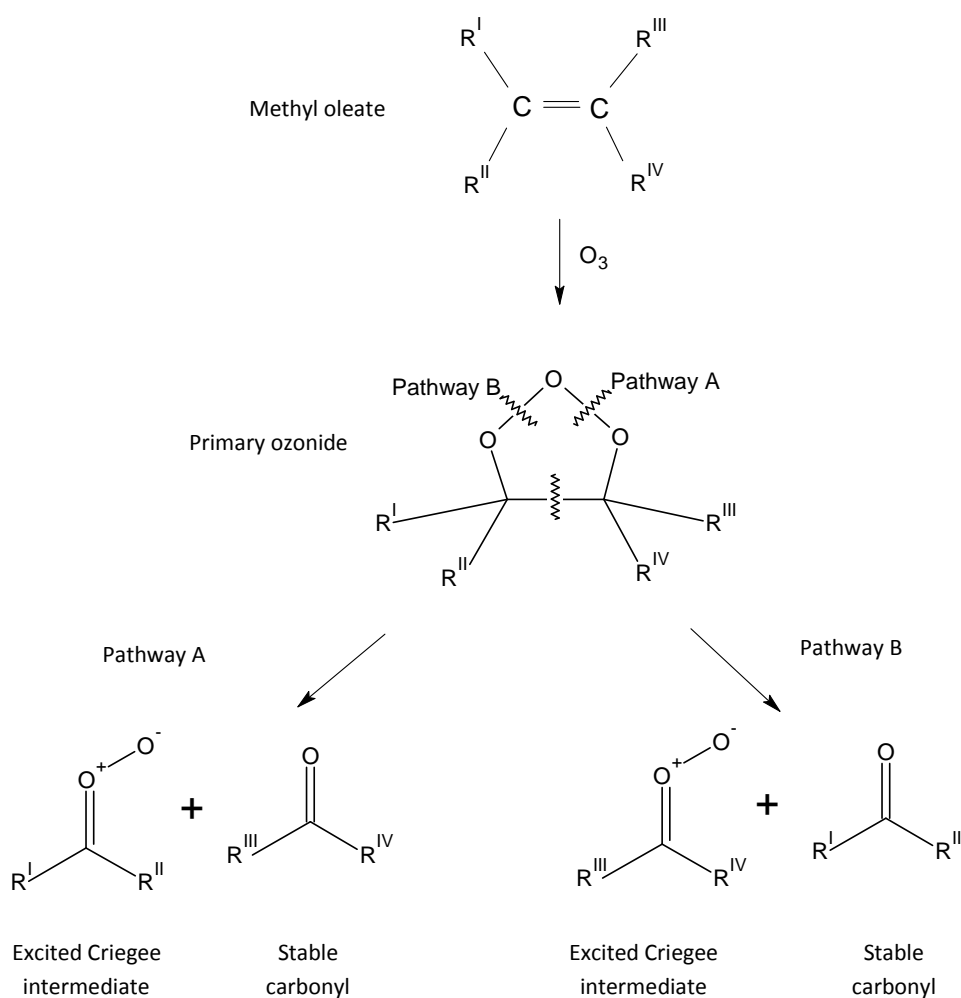
1. Ozone adds to the double bond of the oleic acid molecule in a 1,3 cycloaddition forming a primary ozonide. The primary ozonide is unstable and would not be formed in a large enough concentration to contribute to the reflectivity signal in the measurements taken for this work.

Figure 5.20 *Formation of a Primary Ozonide from Methyl Oleate and O₃*



- The primary ozonide decomposes cleaving the molecule at the site of the double bond in the original methyl oleate molecule forming an excited Criegee intermediate and a stable carbonyl. This results in 2 sets of different reaction products which follow different pathways detailed here as pathway A and B.

Figure 5.21 *The Decomposition of the Primary Ozonide Adapted from Vollhardt and Shore, (2003)*



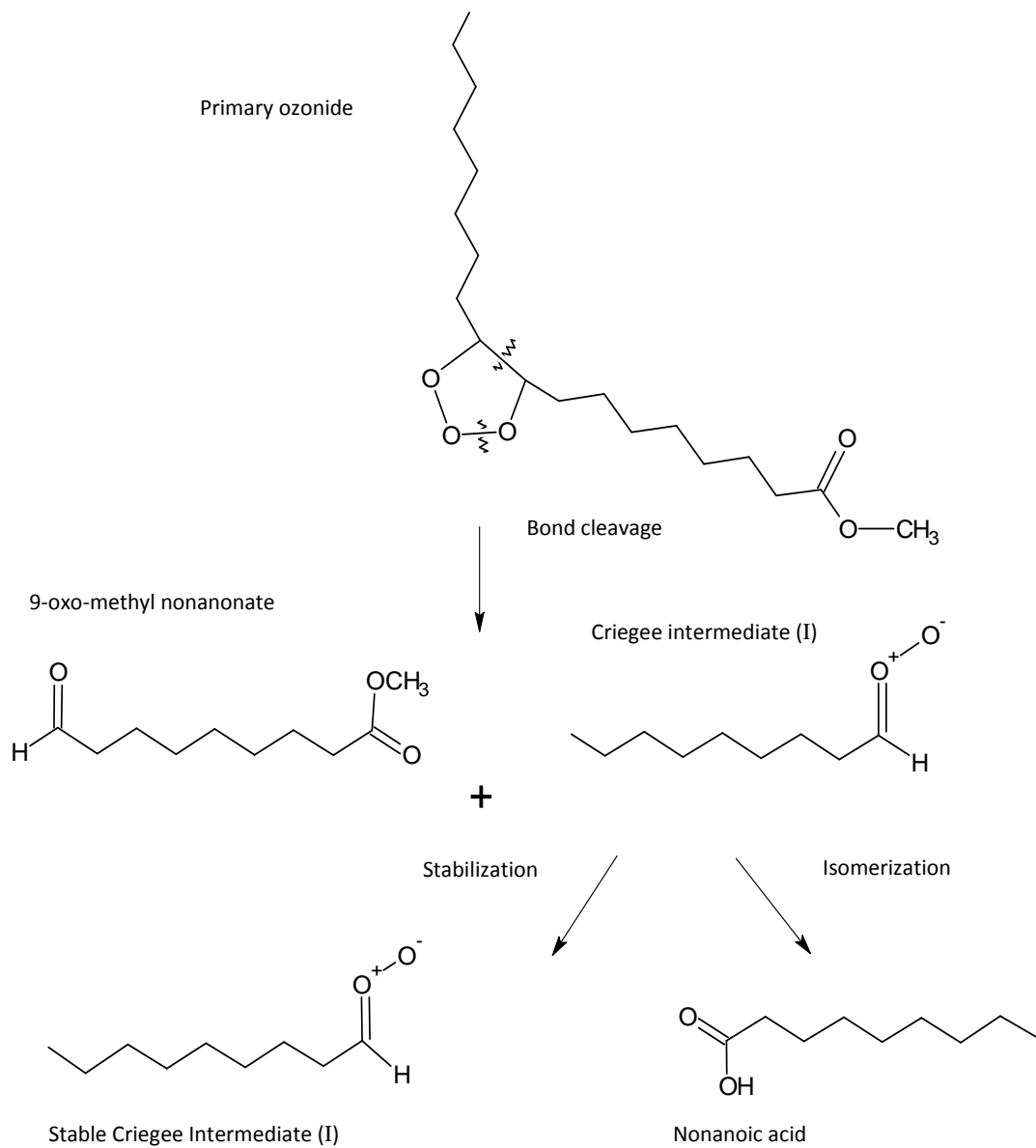
3. Depending on where the molozonide structure in the primary ozonide is cleaved there are two subsequent reaction pathways denoted as pathway A and pathway B.

Pathway A

The primary ozonide is cleaved between the oxygen atoms in the molozonide structure and at the carbon-carbon bond site.

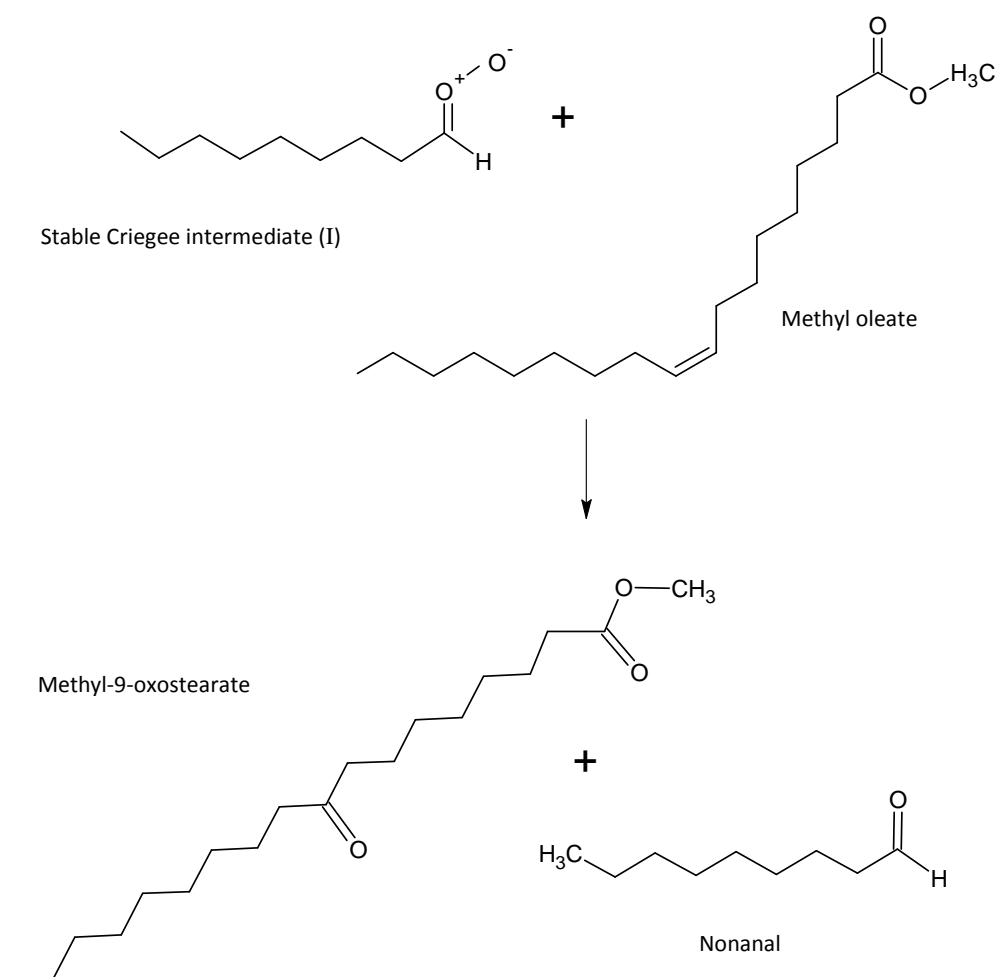
The Criegee intermediate (I) is an unstable, excited intermediate which would not be observed with neutron reflectometry due to its very short lifetime under the conditions of the experiment. The Criegee intermediate can stabilize fulfilling the charge on the oxygen atom forming stable Criegee intermediate (I). Alternatively the excited Criegee intermediate (I) can isomerize forming nonanoic acid.

Figure 5.22 *The Cleavage of the Primary Ozonide Produces a Criegee Intermediate (I) and 9-oxo-methyl Nonanonate. The Criegee Intermediate (I) then Stabilizes or Isomerises*



The reaction of stabilized Criegee intermediate I and methyl oleate can produce Methyl-9-oxostearate, methyl-10-oxostearate, nonanal or 9-oxo-nonanoic acid. Figure 5.23 shows methyl-9-oxostearate as an example.

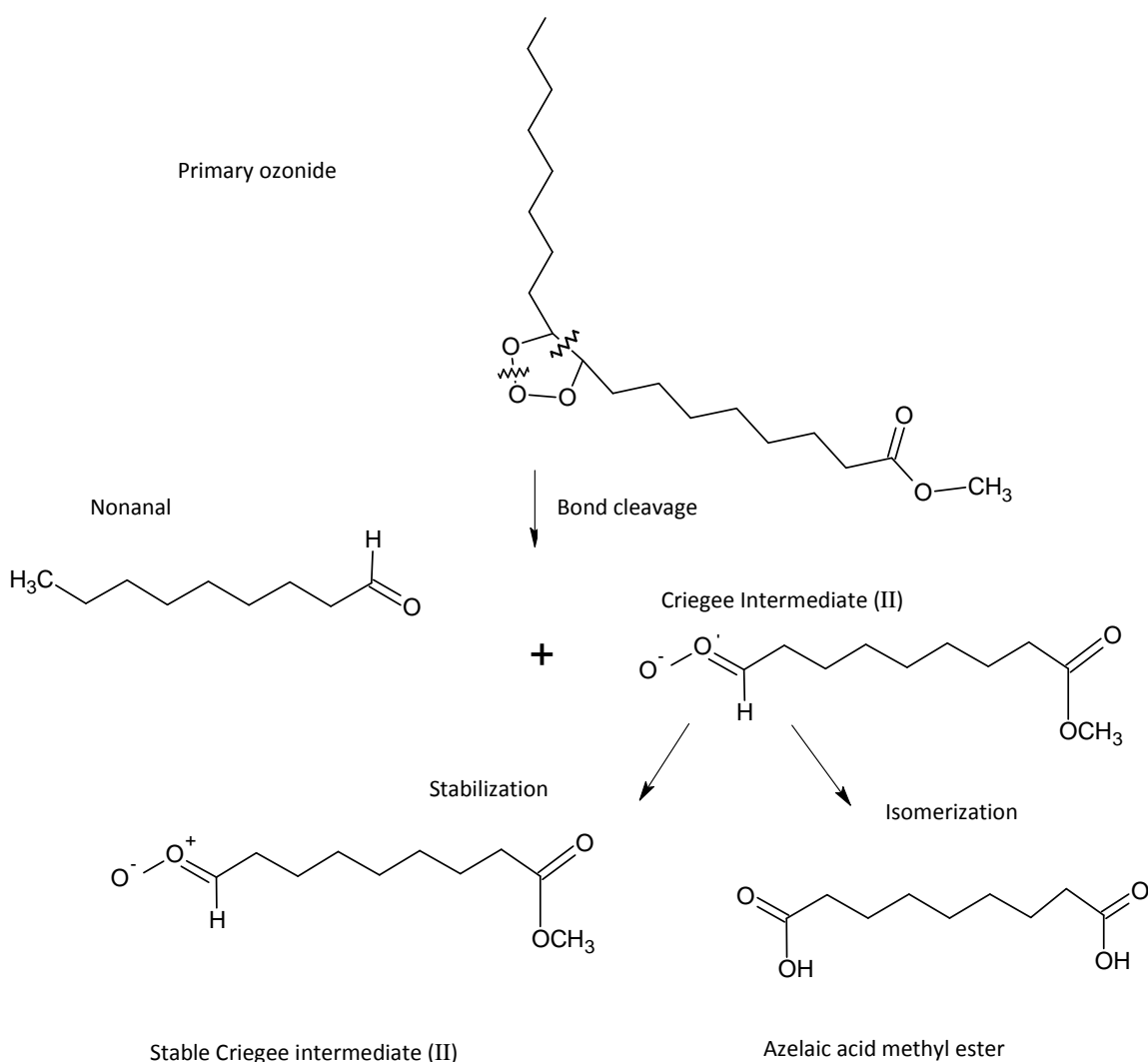
Figure 5.23 *The Formation of Methyl-9-oxostearate and Nonanal from Criegee Intermediate (I) and Methyl Oleate*



Pathway B

The Criegee intermediate (II) is an unstable, excited intermediate which would not be observed with neutron reflectometry due to its very short lifetime under the conditions of the experiment. The Criegee intermediate can stabilize by fulfilment of the charge on the oxygen atom forming stable Criegee intermediate (II). Alternatively the excited Criegee intermediate (II) can isomerize where forming the methyl ester of azelaic acid.

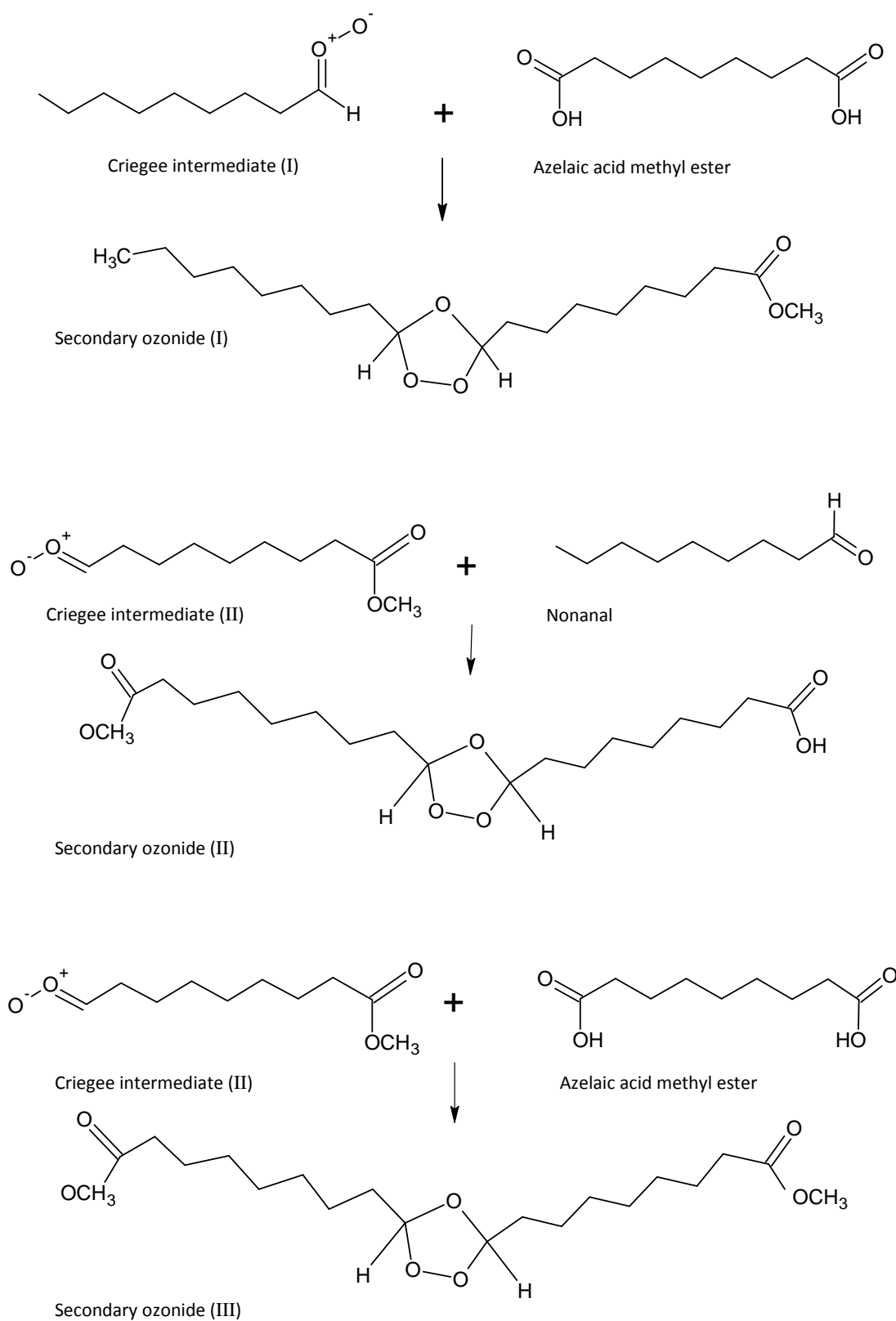
Figure 5.24 *Pathway B. The Cleavage of the Primary Ozonide Produces a Criegee Intermediate (II) and Nonanal. The Excited Criegee Intermediate (II) can Stabilize or Isomerise to the Methyl Ester of Azelaic Acid*



The stabilized Criegee intermediates can react with the products of isomerization (azelaic acid methyl ester) and the product of the reaction of Criegee intermediate (I) with methyl oleate

(nonanal) producing secondary ozonides (figure 5.24) which subsequently decompose to lower molecular weight species such as nonanal, 9-oxo-methyl nonanolate, nonanoic acid and the azelaic acid methyl ester (Shilling et al. 2007). Alternatively the combination of two stabilized Criegee intermediates can form a diperoxide which decomposes to 9-oxo-methyl nonanolate (figure 5.26) or nonanal (figure 5.27).

Figure 5.25 *The Formation of Secondary Ozonides from Criegee Intermediates and a Stable Molecule*



The stabilized Criegee intermediates could also react producing diperoxide molecules which decompose into 9-oxo-methyl nonanate (figure 5.25) or nonanal (figure 5.26).

Figure 5.26 *The Formation of Diperoxide from Two Stabilized Criegee Intermediate (II) Molecules. The Diperoxide Decomposes into Two 9-oxo-methyl Nonanate Molecules and Oxygen*

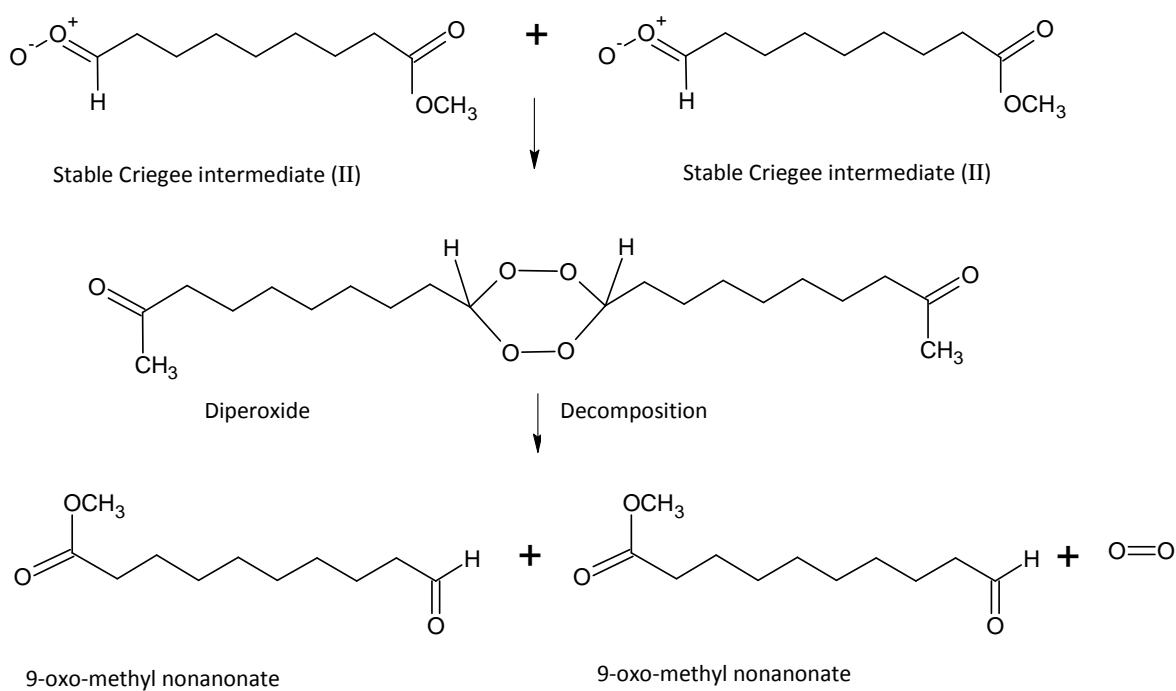
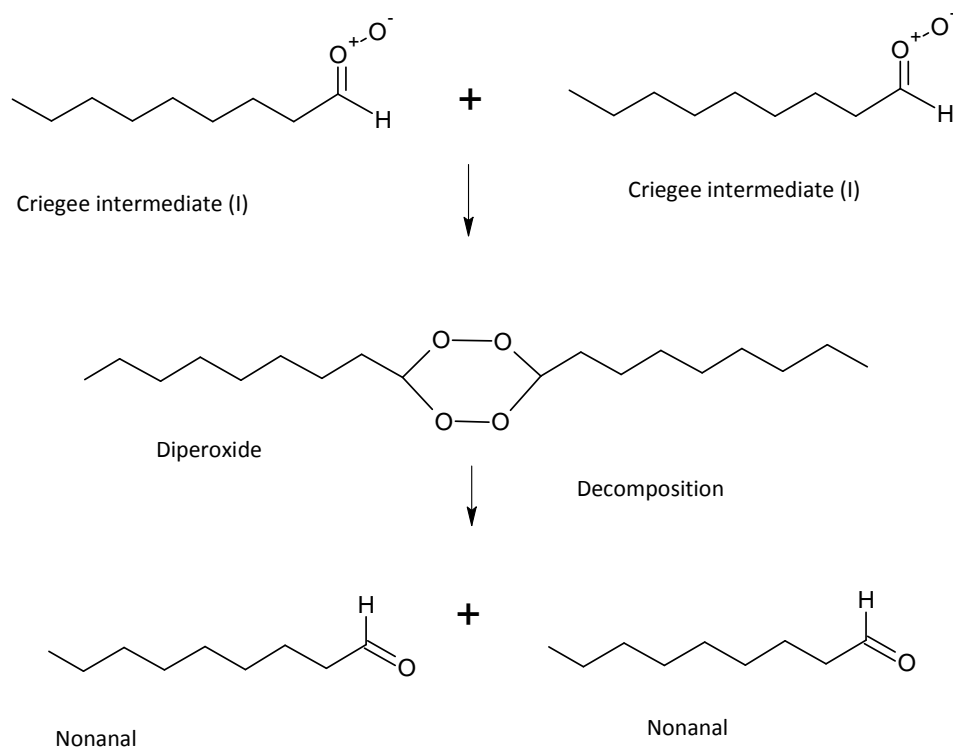






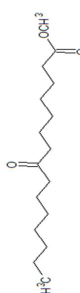
Figure 5.27 *The Formation of Diperoxide from Two Stabilized Criegee Intermediate Molecules (I). The Diperoxide Decomposes into Two Nonanal Molecules*



5.8.3.1 Reaction Products Formed by the Ozonolysis of Methyl Oleate

The stable products which may be seen in the time resolution of the neutron reflectivity technique are listed and a brief characterisation of each species propensity for the air-water interface is given in table 5.5 and the subsequent discussion based on literature.

Table 5.5 *The Solubility and Volatility of the Possible Products from the Ozonolysis of a Methyl Oleate Monolayer at the Air-water Interface*

Compound Name	Image of Molecule	Aqueous Solubility g / L	Henry's Law Coefficient	Vapour Pressure mmHg	Likely to Reside at Interface
Nonanoic Acid $\text{CH}_3(\text{CH}_2)_7\text{CO}_2\text{H}$		2.8×10^{-1} (Voss et al. 2007; Yalkowsky and He. 2003)	4.13×10^{-8} atm m ³ / mole (RSC, 2011 as generated from the EPI Suite of software)	6.2×10^{-4} at 20°C (Gilman et al, 2004 after Yaws 1994, Lide, 2004)	No - too soluble
Nonanal $\text{CH}_3(\text{CH}_2)_7\text{CHO}$		9.6×10^{-2} (Voss et al. 2007; Yalkowsky and He. 2003)	8.02×10^{-4} atm m ³ / mole (RSC, 2011 as generated from the EPI Suite of software)	3.7×10^{-1} at 25°C (RSC, 2011 as generated from the EPI Suite of software)	No - too volatile
Methyl ester of azelaic acid (azelaic monomethyl ester, mono-methyl azelate, IUPAC name: 9-methoxy-9-oxononanoic acid) $\text{C}_{10}\text{H}_{18}\text{O}_4$ / $\text{HOOC}(\text{CH}_2)_7\text{COOCH}_3$		0.6703 at 25°C (RSC, 2011 as predicted by the EPI Suite software from the US Environmental Protection Agency)	9.09×10^{-10} atm m ³ / mole (RSC, 2011 as generated from the EPI Suite of software)	6.72×10^{-5} at 25°C (RSC, 2011 as generated from ACD/Labs software) 0.000239 at 25°C (RSC, 2011 as generated from the EPI Suite software).	No - too soluble
Methyl ester of 9-oxononanoic acid 9-oxo-methyl nonanoate $\text{C}_{10}\text{H}_{18}\text{O}_3$		3.201 at 25°C (RSC EPI suite calculation)	3.468×10^{-10} atm m ³ /mole (RSC EPI suite calculation)	6.92×10^{-6} at 25°C (RSC/ACD Labs)	No - too soluble
Methyl-9-oxo-stearate and Methyl-10-oxo-stearate $\text{C}_{19}\text{H}_{36}\text{O}_3$		5.461×10^{-5} mg L at 25°C (RSC/ EPI Suite)	4.089×10^{-05} atm m ³ /mole (RSC EPI suite calculation)	7.34×10^{-7} at 25°C (RSC /ACD Labs)	Not known

Gilman et al., (2004) found that in the presence of a longer chained saturated molecule such as stearic acid (C_{18} , vapour pressure 1×10^{-6} , solubility 0.00029, Gilman et al. 2004 after Yaws 1994, and Lide, 2004), more volatile species such as nonanoic acid could have a prolonged residence time at the air-liquid interface. However Voss et al, 2007 concluded that nonanoic acid was soluble in an aqueous sub-phase.

Voss et al. 2007 report that nonanal would evaporate and not persist at the air-water interface. Wadia et al, 2000 measured nonanal in the gas-phase after reacting ozone with the lipid OPPC, (which has a cis configuration tail which is composed of oleic acid), on a Langmuir trough. Our observation is that if it was a product in the neutron experiments it did not persist at the air-water interface thus this study is in agreement with Voss et al., 2007 and Wadia et al., 2000.

If Criegee intermediate (I) and methyl oleate react nonanal and methyl-9-oxo-stearate or methyl-10-oxo-stearate are produced. Methyl-9-oxo-stearate and methyl-10-oxo-stearate are not volatile, nor soluble so could be present at the air-liquid interface, if a large number of these molecules were present then oligomer formation could occur however it would be unlikely to show in this study as it would be present as patches, should these form a pattern then it could potentially be seen with off specular neutron reflectivity measurements (Rennie, 2009). There is very little experimental data relating to these compounds and none specifically related to their behaviour at the air-water interface at present.

Mochida et al., (2006) studied the gas-phase formation of high molecular weight organic peroxides from the reaction of methyl oleate with ozone via the formation of stabilized Criegee intermediates in the context of organic aerosol particles. Measurements were taken of particle composition after exposure to ozone using an aerosol flow tube with a quadrupole aerosol mass spectrometer. The methyl oleate was mixed in dioctyl adipate and myristic acid at different mole fractions. Pure methyl oleate particles and those with 0.04 mole fraction methyl oleate in the dioctyl adipate which is inert but does vary the concentration of double bonds when subjected to ozonolysis gave two secondary ozonides as major products. A mixture of methyl oleate and myristic acid gave α -acyloxyalkyl alkyl peroxides resulting from the attack of myristic acid by the secondary Criegee intermediates. The secondary Criegee intermediates and aldehydes react to produce secondary ozonides but when the mole fraction of myristic acid was higher the reaction of the secondary Criegee intermediate with the carboxylic group competes with this process changing the product chemistry and more high molecular weight organic peroxides are produced. The same study states that the methyl oleate and ozone reaction is less likely to produce polymers than the oleic acid and ozone system as the methyl oleate does not have the free carboxylic acid head group which enables polymerisation as oleic acid does. The

reaction pathway for methyl oleate with ozone is very similar to that of oleic acid (Ziemann, 2005, Hung et al. 2005, Mochida et al. 2006). Mochida et al.,(2006) showed that for the reaction of methyl oleate with ozone the stabilization of Criegee intermediates is favoured over their isomerization, which would form nonanoic acid and the azelaic acid monomethyl ester. The mixture of myristic acid which possesses the carboxylic acid group and methyl oleate which does not, shows that α -acyloxyalkyl peroxides were the dominant high molecular weight reaction product from ozonolysis of a particle of mixed fatty acid and methyl ester composition which could lead to the reaction of saturated molecules by hydrogen abstraction in an atmospheric particle (Mochida et al. 2006). Mochida et al., (2006) also note that in the presence of water which was minimal in their work, then low molecular weight products would be more favourable formed by the reaction of the secondary Criegee intermediate with water. Thus we conclude that oligomerization is not prevalent in our system.

5.9 The Atmospheric Monolayer Lifetime

As with the oleic acid work in the same manner as in chapter 3, an atmospheric lifetime for a methyl oleate monolayer at the air-water interface when exposed to gas-phase ozone from outside the cloud droplet was calculated for an atmospheric ozone concentration of 40 ppb which translates to a concentration of 1.73×10^6 molecule cm^{-2} in the tail region of the monolayer. The lifetime, $\tau_{\text{methyl oleate}}$ was calculated from equation 5.17.

$$\tau_{\text{methyl oleate}} = \frac{1}{k_{[\text{O}_3]}} \quad (E.5.17)$$

The calculated lifetime for a methyl oleate monolayer at the air-water interface exposed to a background concentration of ozone of 40 ppb is ~5 hours and 53 minutes. The length of the molecule was modelled as 20 Å. The methyl ester, methyl oleate in monolayer form has a slightly longer lifetime than that of oleic acid which was ~3.54 hours when exposed to a background concentration of ozone of 40 ppb as calculated in chapter 3.

5.10 Suggested Further Research

The Mochida et al., study of the ozonolysis of particles of methyl oleate with myristic acid ($\text{C}_{14}\text{H}_{28}\text{O}_2$) which has a free $-\text{COOH}$ group, could be adapted if myristic acid could be used as a component of a mixed monolayer with methyl oleate, making an interesting kinetic study for comparison with the Mochida et al., (2006) work on the ozonolysis mechanism for unsaturated compounds in an atmospheric droplet or aerosol setting and a valuable contribution to the

understanding of the reactions in mixed particles as it would provide an alternative model system to the mixed oleic and stearic acid films studied in chapter 4.

Xiao and Bertram, (2011) estimated that a methyl oleate particle under exposure to gas-phase NO_3 which reacts with the double bond as ozone does; at the surface of the liquid particle had a lifetime a lifetime of 8 to 28.5 minutes which was calculated, based on data for methyl oleate mixed with squalane, diethyl sebacate and dioctyl sebacate. The uptake coefficient for NO_3 onto methyl oleate was $(1.4 \pm 8.6/-0.5) \times 10^{-1}$. Thus it would appear that NO_3 would oxidise methyl oleate more rapidly than ozone, this could be tested for the air-water interface by repeating the experiment in this chapter with NO_3 as the reactant in place of ozone, the author took part in an experiment which attempted to do this as a collaboration with Christian Pfrang (University of Reading) but the data was not available for this thesis and had not been analysed to the point of calculating an atmospheric lifetime when this thesis was completed. Diurnal concentrations of reactive gasses could make one reactant more important than another during hours of darkness as the concentration of ozone is dependent on photochemistry.

5.11 Conclusions

The second order rate constant is in good agreement with that of oleic acid obtained in chapter 4 and by King et al., (2009) suggesting that it is the double bond in the hydrocarbon chain of the film species which is determining the reaction rate and that the interaction of dissolved ozone in the sub-phase which may occur in this system and any reaction with the head group of the amphiphile is not determining the rate of the reaction.

References

- Akamatsu, Y. and Law, J.H. 1970. The Enzymatic Synthesis of Fatty Acid Methyl Esters by Carboxyl Group Alkylation. *The Journal of Biological Chemistry*, 245, 4, pp. 709-713.
- Altieri, K.E., Seitzinger, S.P., Carlton, A.G., Turpin, B.J., Klein, G.C., Marshall, A.G. 2008. Oligomers formed through in-cloud methylglyoxyl reactions: Chemical composition, properties, and mechanisms investigated by ultra-high resolution FT-ICR mass spectrometry. *Atmospheric Environment*, 42, 7, pp. 1476-1490.
- Clark, G.L. and Robinson, J.V. 1940. A Study of Some Esters and Chlorinate Derivatives Possibly Useful as Lubricating Addition Agents. *Journal of the American Chemical Society*, 62, 8, pp. 1948-1951.
- Flath, R.A., Forrey, R.R., Guadagni, D.G. 1973. Aroma components of olive oil. *Journal of Agricultural and Food Chemistry*, 21, 6, pp. 948-952.
- Gaines, G.L. 1966. Insoluble Monolayers at Liquid-gas Interfaces. Wiley Interscience, New York, USA.
- Gilman, J.B., Elaison, T.L., Vaida, V. 2004. Selectivity and stability of organic films at the air-aqueous interface. *Journal of Colloid and Interface Science*, 280, pp. 234-243.
- Hearn, J.D., Lovett, A., Smith, G.D. 2005. Ozonolysis of oleic acid particles: evidence for a surface reaction and secondary reactions involving Criegee intermediates. *Physical Chemistry Chemical Physics*, 7, pp. 501-511.
- Ikeda, N., Ishihara, M., Tsuneya, T., Kawakita, M., Yoshihara, M., Suzuki, Y., Komaki, R., Inui, M. 1994. Volatile components of honeysuckle. *Flavour and Fragrance Journal*, 9, 6, pp. 325-331.
- Kalberer, M., Paulson, D., Sax, M., Steinbacher, M., Dommen, J., Prevot, A.S.H., Fisseha, R., Weingartner, E., Frankevich, V., Zenobi, R., Baltensperger, U. 2004. Identification of Polymers as Major Components of Atmospheric Aerosol. *Science*, 303, pp. 1659-1662.
- King, M.D., Rennie, A.R., Thompson, K.C., Fisher, F.N., Chaun Dong, C., Thomas, R.K., Pfrang, C., Hughes, A.V. 2009. Oxidation of oleic acid at the air-water interface and its potential effects on cloud critical supersaturations. *Physical Chemistry Chemical Physics*, 11, pp. 7699-7707.
- Knothe, G., Dunn, R.O., Bagby, M.O. 1997. Chapter 10 in Fuels and Chemicals from Biomass edited by B.C. Saha and J. Woodward. ACS Symposium Series. pp. 172-208.
- Knothe, G., Sharp, C.A., Ryan, T.W. 2006. Exhaust Emissions of Biodiesel, Petrodiesel, Neat Methyl Esters, and Alkanes in a New Technology Engine. *Energy and Fuels*, 20, 1, pp. 403-408.
- Lide, D.R. 2004. Handbook of Chemistry and Physics, CRC Press, Cleveland USA.

- Mochida, M., Katrib, Y., Jayne, J.T., Worsnop, D.R., Martin, S.T. 2006. The relative importance of competing pathways for the formation of high-molecular-weight peroxides in the ozonolysis of organic aerosol particles. *Atmospheric Chemistry and Physics*, 6, pp.4851-4866.
- Raja, S., Raghunathan, R., Kommalapati, R..R., Shen, X., Collett, Jr. J.L., Valsaraj, K.T. 2009. Organic composition of fogwater in the Texas-Louisiana gulf coast corridor. *Atmospheric Environment*, 43, pp. 4214-4222.
- Rennie, A. 2009. Personal communication: verbal discussion of ozonolysis products.
- Royal Society of Chemistry. 2011. Chemspider web resource of chemical physical data available at: <http://www.chemspider.com/Chemical-Structure.67563.html> (Azelaic acid monomethyl ester, mono-methyl azelate), compile from software including ACS Labs and EPI Suite. As accessed on 20/10/2011.
- Seinfeld, J.H., and Pandis, S. N. 2006. *Atmospheric Chemistry and Physics From Air Pollution to Climate Change*. Second Edition. Wiley and Sons, New York, USA.
- Shilling, J.E., King, S.M., Mochida, M., Worsnop, D.R., Martin, S.T. 2007. Mass Spectral Evidence That Small Changes in Composition Caused by Oxidative Aging Processes Alter Aerosol CCN Properties. *Journal of Physical Chemistry:A*, 111, pp. 3358-3368.
- Smith, G.D., Woods, E., DeForest, C.L. 2002. Reactive uptake of ozone by oleic acid aerosol particles: application of single-particle mass spectrometry to heterogeneous reaction kinetics, *Journal of Physical Chemistry, A*, 106, pp. 8085.
- Snider, J.B. 1999. Long-Term Observations of Cloud Liquid, Water Vapour, and Cloud Base Temperature in the North Atlantic Ocean. *Journal of Atmospheric and Oceanic Technology*, 17, pp. 928-939.
- Pinxteren, van D. and Herrmann, H. 2007. Determination of functionalised carboxylic acids in atmospheric particles and cloud water using capillary electrophoresis/mass spectroscopy. *Journal of Chromatography A*, 1171, 1-2, pp. 112-123.
- Vollhardt, K.P.C. and Schore N.E. 2002. *Organic Chemistry Structure and Function*. 4th edition. W.H. Freeman and Company, New York, USA.
- Voss, L.F., Bazerbashi, M.F., Beekman, C.P., Hadad, C.M., Allen, H.C. 2007. Oxidation of oleic acid at air/liquid interfaces. *Journal of Geophysical Research*, 112, pp. 1-9.
- Wadia, Y., Tobias, D.J., Stafford R., Finlayson-Pitts B.J. 2000. Real-Time Monitoring of the Kinetics and Gas-Phase Products of the Reaction of Ozone with an Unsaturated Phospholipid at the Air-Water Interface. *Langmuir*, 16, pp. 9321-9330.

- Xiao, S and Bertram, A.K. 2011. Reactive uptake kinetics of NO_3 on multicomponent and multiphase organic mixtures containing unsaturated and saturated organics. *Physical Chemistry Chemical Physics*, 13, pp. 6628-6636.
- Yalkowsky, S.H. and He, Y. 2003. Handbook of Aqueous Solubility Data, CRC Press, Boca Raton, Florida, USA.
- Yaws, C.L. 1994. Handbook of Vapor Pressure, Gulf Publications, Houston USA.
- Ziemann, P.J. 2005. Aerosol products, mechanisms, and kinetics of heterogeneous reactions of ozone with oleic acid in pure and mixed particles. *Faraday Discussions*, 130, pp. 469-490.
- Zahardis, J., LaFranchi, B.W., Petrucci, G.A. 2006. Direct observation of polymerization in the oleic acid – ozone heterogeneous reaction system by photoelectron resonance capture ionization aerosol mass spectrometry. *Atmospheric Environment*, 40, pp. 1661-1670.
- Zahardis, J., and Petrucci, G.A. 2007^a. Review of oleic acid-ozone heterogeneous chemistry. *Atmospheric Chemistry and Physics*, 7, pp. 1237-1274.
- Zahardis, J. and Petrucci, G.A. 2007^b. The oleic acid-ozone heterogeneous reaction system: products, kinetics, secondary chemistry, and atmospheric implications of a model system – a review. *Atmospheric Chemistry and Physics*, 7, pp.1237-1274.

The Oxidation of Phospholipid Monolayers

6.0 Abstract

The surface coverage and surface pressure of a monolayer of the phospholipid 1,2-dipalmitoyl-*sn*-glycero-3-phosphocholine (DPPC) reacting with aqueous hydroxyl radical was studied using three deuterated isotopologues of DPPC, fully deuterated (d75) DPPC, head group deuterated (d13) DPPC and tail group deuterated (d62) DPPC. The use of three different deuterations of DPPC allowed neutron reflectivity measurements to be taken showing the surface coverage of different parts of the molecule with reaction time to show where material was being lost from the air-water interface. The surface coverage of the head group deuterated monolayer declined most rapidly in the presence of OH, but OH generated in the subphase beneath the monolayer also penetrated the tail group of the DPPC molecule and reacted with the CH₂ groups within the saturated tail group. The loss in the surface coverage of the tail deuterated DPPC proceeded at a slower rate than the head group and the surface coverage of a fully deuterated DPPC monolayer reacting with OH declined at a rate which between the deuterated head group DPPC and the deuterated tail group DPPC as the decay of the fully deuterated DPPC monolayer surface coverage was the combination of the head and tail group reacting.

6.1 Introduction

In chapter 2 it was shown that aqueous OH radical initiated the oxidation of a stearic acid monolayer at the air-water interface. It was not clear where on the stearic acid molecule the OH radical reacted in the initial step of the reaction with stearic acid. To better understand the mechanism by which aqueous OH radical reacts with a monolayer at the air-water interface the experiment in this chapter was designed to show if OH would penetrate the lipid tails of the DPPC molecule or just attack the head group.

A neutron reflectometry experiment was conducted to monitor the oxidation of a DPPC (1,2-dipalmitoyl-*sn*-glycero-3-phosphocholine) phospholipid monolayer at the air-water interface by aqueous-phase OH radical to mimic the breakdown of a surface active phospholipid as a component of a cloud droplet or aerosol film. DPPC was selected for study as it is commercially available as three different isotopologues with the whole molecule deuterated, deuterated tails only and deuterated head only. The DPPC isotopologues were used to demonstrate where the lipid molecule was attacked by aqueous OH radical in its initial step; neutron reflectometry was used to selectively follow the loss of deuterium in specific parts of the molecule. It was hypothesised that if the OH radical penetrated the monolayer tail region the monolayer would

persist for longer at the air-water interface than if the OH radical attacked the head group of the lipid as loss of the phosphocholine head group would greatly increase the aqueous solubility of the lipid.

6.2 Aims

The aims of studying the oxidation of a DPPC monolayer by aqueous OH radical were:

1. To show how the phospholipid molecule is lost from the air-water interface during a reaction with aqueous OH radical using isotopologues of DPPC in fully deuterated and partially deuterated form (heads deuterated and tails deuterated).
2. To measure the site specific kinetics of the initial reaction step as aqueous OH radical attacks a saturated phospholipid monolayer.

6.3 Background

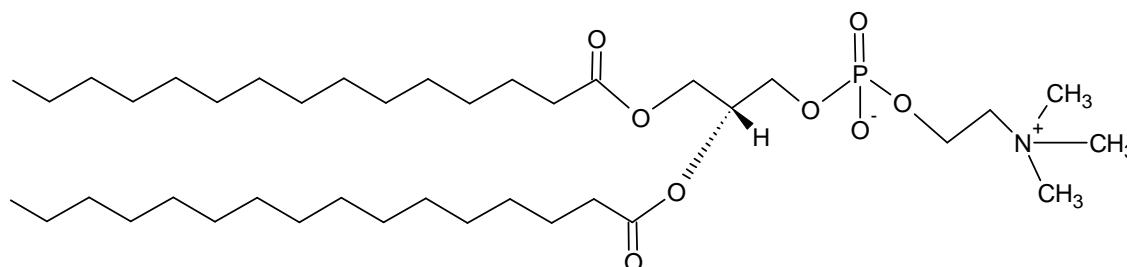
6.3.1 Phospholipids and the Atmosphere

When waves break and collide, jets of small droplets become airborne, these droplets contain components of the sea surface microlayer, the top 1 to 1000 μm of the water column which is enriched in organic substances such as the lipid DOPC (dioleoyl phosphatidylcholine) (Gašparović et al. 2008), the fatty acid content of the sea surface microlayer comes from the degradation of planktonic lipid material (Marty et al. 1979). Lipids break down through oxidation to smaller molecules such as fatty acids, methyl esters and dicarboxylic acids which are routinely sampled in atmospheric waters, Marty et al., (1979) compared the composition of the sea surface microlayer to marine aerosol samples finding that the pattern of fatty acid lipids in marine aerosol samples reflected the distribution of planktonic fatty acid lipids in the sea surface microlayer but that the aerosol contained a higher fraction of low molecular weight fatty acids ($< C_{12}$) than the sea surface microlayer (Marty et al. 1979).

Oxidation of the DPPC lipid molecule will be discussed in this chapter. The DPPC molecule studied here and the POPC molecule used in the work of Thompson et al., (2010) form part of the mammalian lung surfactant (Rooney et al. 1994). The POPC (1-palmitoyl-2-oleoyl-*sn*-glycero-3-phosphocholine) molecule is a natural unsaturated lipid, the DPPC (1,2-dipalmitoyl-

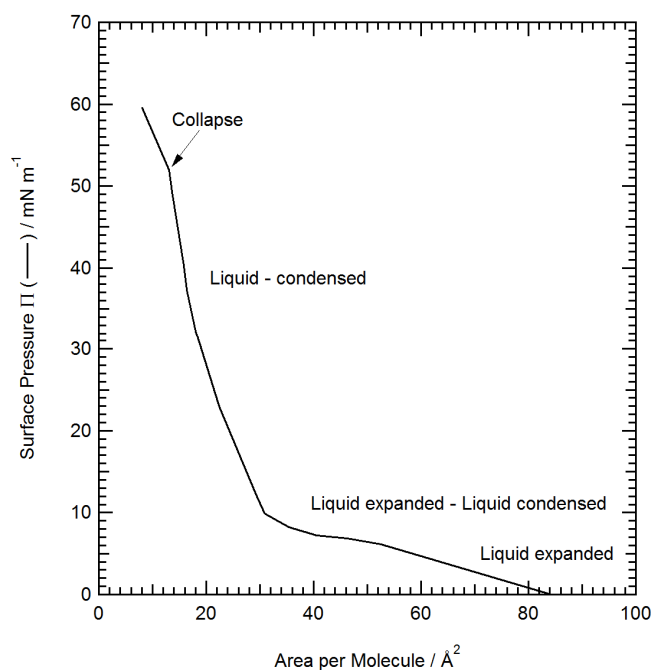
sn-glycero-3-phosphocholine) molecule is a lipid possessing two saturated palmitic acid tails, the POPC lipid has two unsaturated tails.

Figure 6.1 Structure of the DPPC Molecule ($C_{40}H_{80}NO_8P$)



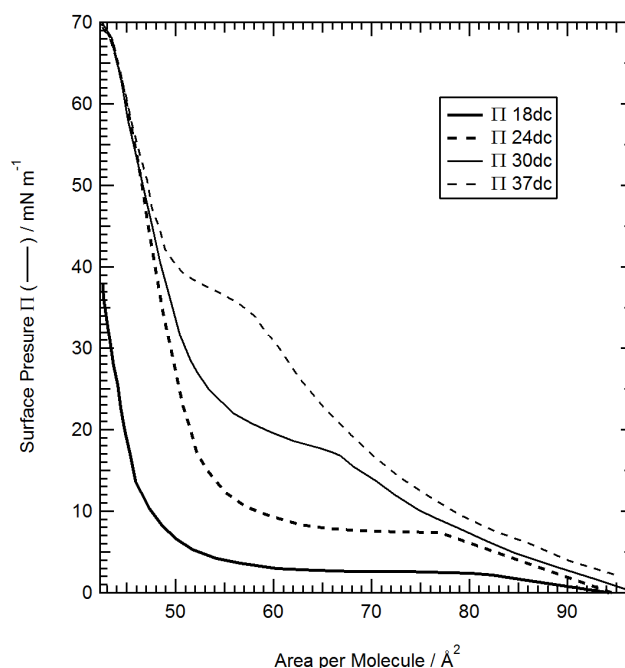
The surface pressure versus area per molecule isotherm of a monolayer of DPPC under compression at a rate of $20 \text{ cm}^2 / \text{minute}$ is given in figure 6.2. The monolayer collapses at a surface pressure of ~ 50 to 60 mN m^{-1} depending on the subphase temperature. The monolayer phases are labelled. The experiments in this chapter were conducted at a starting surface pressure of $<37 \text{ mN m}^{-1}$ at a temperature of 18°C within the liquid condensed phase of the isotherm away from regions of phase transition. The DPPC monolayer phase transitions are highly temperature dependent as demonstrated in figure 6.3.

Figure 6.2 The Surface Pressure versus Surface Area Isotherm of DPPC at the Air Water Interface at 22°C on a Subphase of Pure Water



The isotherm in figure 6.2 was adapted from Can et al., (2008).

Figure 6.3 *The Surface Pressure versus Surface Area Isotherm of DPPC at the Air Water Interface at Varied Temperatures on a Subphase of Pure Water*



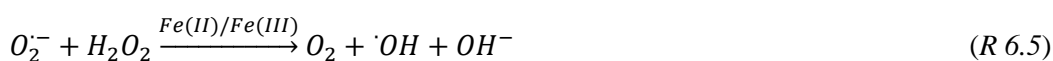
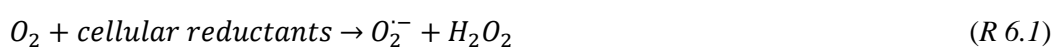
The isotherms in figure 6.3 were adapted from Yang et al., (1994), Crane et al., (1999) and Ma and Allen, (2006).

6.3.2 Lipid Oxidation

The oxidation of surface-active lipids has both a potential physical effect on cloud droplet monolayers as well as toxicological effects on the human body presenting an illustration of the impact of atmospheric chemistry on health. In many countries the ozone levels are subject to statutory regulation through limits on the levels of precursor species due to evidence of ill effects on health (Finlayson-Pitts and Pitts, 2000). The health effects of ozone on the lung have been intensively studied and the health implications of exposure to air pollution are summarised by Kampa and Castanas, (2008). The lining of alveoli in the mammal lung contains a monolayer of lipids which lower the surface tension at the air-liquid interface within the lung allowing the alveoli to expand and contract when an organism breathes (Wadia et al. 2000; Hawgood and Clements, 1990; Goerke, 1998). The pulmonary surfactant which is composed of ~80% phosphatidylcholines (Veldhuizen et al. 1998,) starts as tightly packed multiple layers which are secreted into the alveoli where they are hydrated and then expand into tubular myelin which is a lattice like structure. The lung surfactant spreads from the tubular myelin forming an interfacial

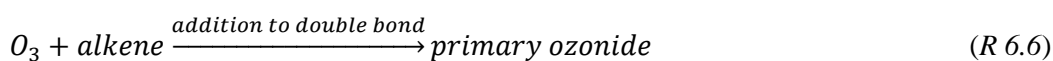
monolayer (Hawgood and Clements, 1990). The phosphocholines which form the interfacial monolayer in the lung have fatty acid components in the tail region, such as OPPC (1-oleoyl-2-palmitoyl-*sn*-glycero-3-phosphocholine) which has an oleic acid and a palmitic acid strand in the tail region of the molecule. The unsaturated oleic acid strand can be broken down by ozone producing products which inflame the lung (Wadia et al. 2000).

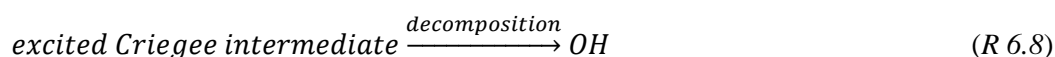
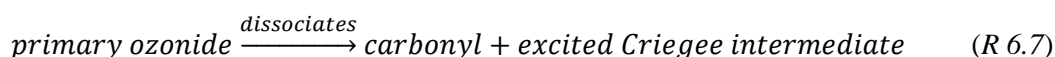
Reaction of saturated phospholipids with aqueous hydroxyl radical can be expected based on the findings in chapter 2 where a monolayer of the saturated fatty acid, stearic acid was oxidised and lost from the air-water interface conforming to a degraded chain mechanism where lower molecular weight surface active product molecules formed and were subsequently reacted away from the air-water interface. The reaction of lipids with hydroxyl radical is associated with damage to cells (Mello Filho et al. 1984). The saturated DPPC molecule is the dominant phospholipid in red blood cells (Lockwood and Lee, 1984; Vance and Vance, 1985; Can et al. 2008). Hydroxyl radical is inhaled into the lung in air as well as being produced within the lung lining as the result of an immune response to thermal injury (Till et al. 1985). OH radical can be formed in the lung by the following process in the presence of transition metals (Valleyathan and Shi, 1997).



The OH radical can initiate oxidative damage such as the breakdown of cell walls by lipid peroxidation (molecular breakdown in a chain reaction), a process which can cause cell death (Valleyathan and Shi, 1997). OH radical can also cause strand breakage in DNA, damage proteins rendering them inactive and unable to catalyse processes within the body, and disrupt the activity of the mitochondria which fuel cell growth (Valleyathan and Shi, 1997).

OH can be produced from ozone reacted with alkenes such as oleic acid or the unsaturated tail group of certain phospholipids by the following reaction confirmed by Atkinson and Aschmann (1993):





There are multiple mechanisms by which the generation of OH could occur as a result of the reaction of ozone with an alkene, the mechanisms are summarised by Finlayson-Pitts and Pitts (2000).

During collaborative work the reaction of POPC (1-palmitoyl-2-oleoyl-*sn*-glycero-3-phosphocholine) monolayers with gas-phase ozone was investigated using neutron reflectometry, this work has been published by Thompson et al., (2010). The POPC molecule possesses two tail strands, one of which is saturated, the other unsaturated. Thompson et al., (2010) showed that gas-phase ozone reacts with the unsaturated strand attacking the double bonds in the unsaturated tails of the molecule (Lai et al. 1994; Pryor et al. 1996; Thompson et al. 2010) and a subsequent reaction occurs which oxidises the saturated tail strand. The secondary intramolecular reaction was attributed to the formation of OH radical. These findings provided the basis for an experiment where a deuterated DPPC monolayer was exposed to aqueous-phase OH radical and the surface coverage of the monolayer was monitored with reaction time. Reactions 6.6 to 6.8 give a mechanism by which ozone could initiate the production of OH which could subsequently react with saturated alkanes within a monolayer so studying the mechanism of OH oxidation of phospholipid monolayers will provide additional data to support the findings of Thompson et al., (2010). The experiment in this chapter will confirm whether aqueous OH radical can penetrate a phospholipid monolayer and oxidise the saturated tail strands of the DPPC molecule.

6.4 Experimental

The experimental section is presented in the following order:

- Experimental objectives (6.4.1).
- A description of the DPPC samples used for the neutron reflectivity experiments (6.4.2).
- The generation and concentrations of aqueous-phase hydroxyl radical used in the neutron reflectivity experiments (6.4.3).
- The methodology of the neutron reflectivity experiments (6.4.4).
- The neutron reflectivity data fitting (6.4.5).

6.4.1 Experimental Objectives

The experiment was designed to monitor the properties of surface pressure, Π , and surface coverage, Γ , of a monolayer of the phospholipid DPPC at the air-water interface in real time as the monolayer was oxidised with aqueous hydroxyl radical.

The objectives of the experiment conducted on the SURF reflectometer were;

1. To measure the decay in the surface pressure and the surface coverage of a DPPC monolayer at the air-water interface simultaneously whilst the monolayer reacted with aqueous-phase hydroxyl radical.
2. To ascertain whether a DPPC monolayer would persist at the air-water interface under sustained exposure to aqueous-phase hydroxyl radical.
3. To measure the decay of a monolayer of DPPC molecules which were fully deuterated, had deuterated head groups only and which had deuterated tail groups only in order to study where the hydroxyl radical was reacting with the DPPC molecule and how far it was penetrating the monolayer.

6.4.2 DPPC Samples

Three deuterated DPPC samples were used in this work, each had a different degree of deuteration which provided a label which when the results were compiled would show where the hydroxyl radical was breaking apart the DPPC molecule.

Figure 6.4 *The Fully Deuterated (d75) DPPC Molecule ($C_{40}H_5NO_8PD_{75}$)*

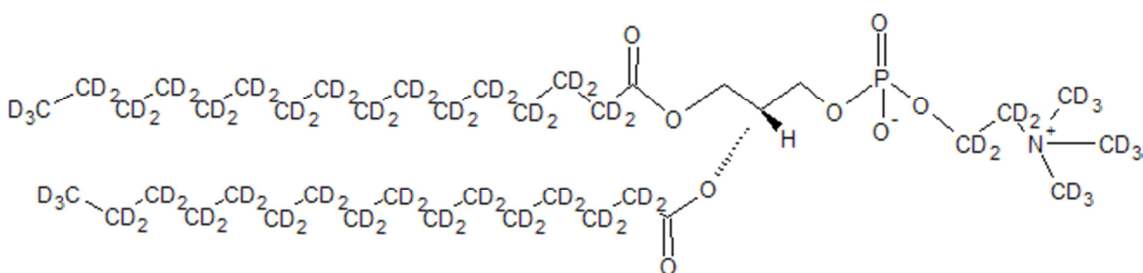


Figure 6.5 *The Head Group Deuterated (d13) DPPC Molecule ($C_{40}H_{67}NO_8PD_{13}$)*

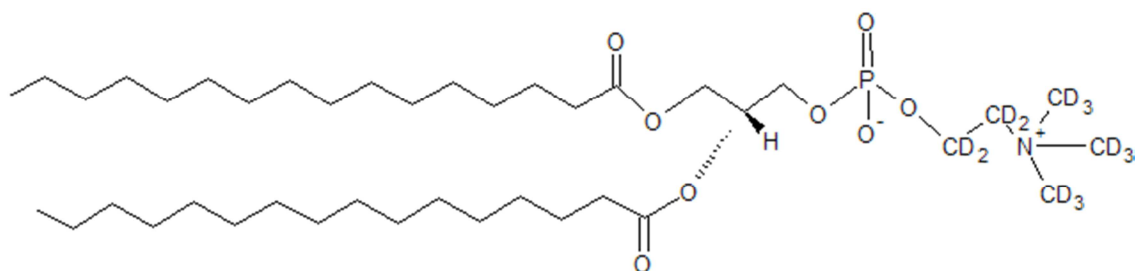
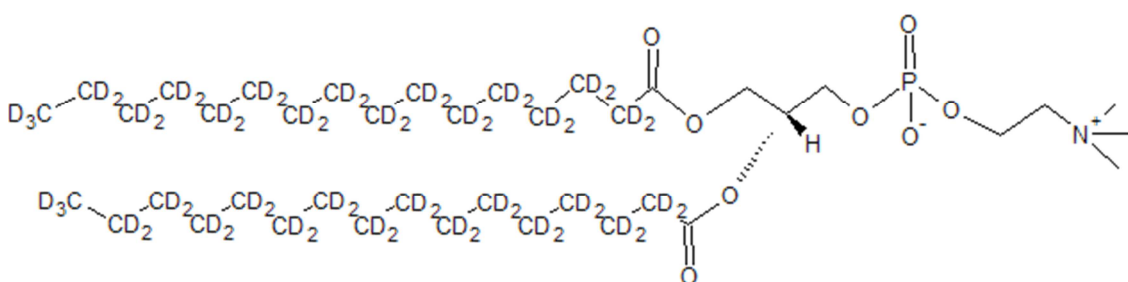


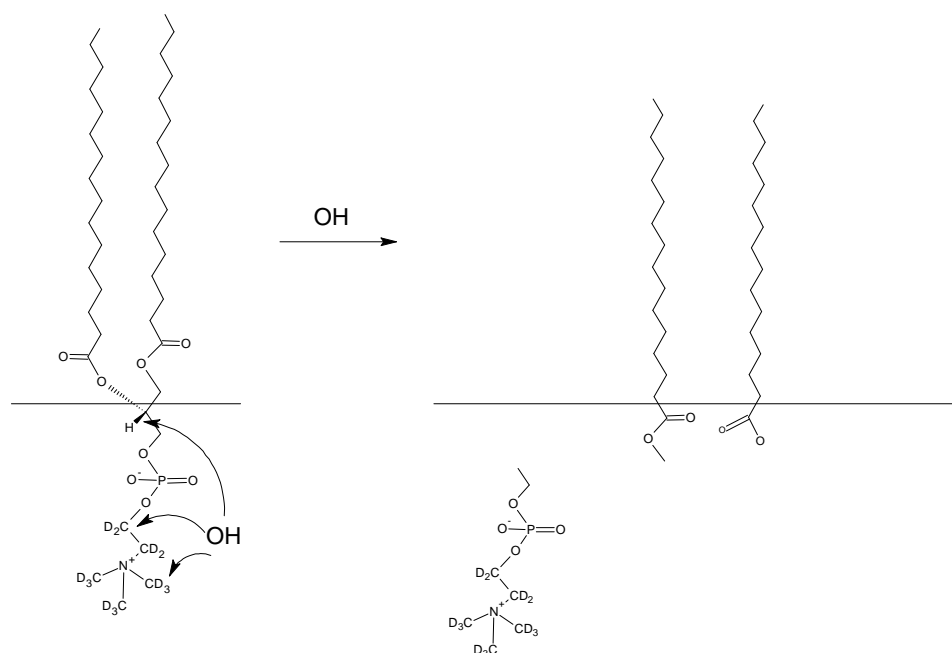
Figure 6.6 *The Tail Group Deuterated (d62) DPPC Molecule ($C_{40}H_{18}NO_8PD_{62}$)*



The deuterated DPPC samples were purchased from Avanti Polar Lipids. Partial deuteration of the DPPC molecule allows a measurement of the surface coverage of the deuterated part of the molecule giving a label with which to measure of the persistence of a particular part of the DPPC molecule at the air-water interface during a reaction. In this case partial deuteration was

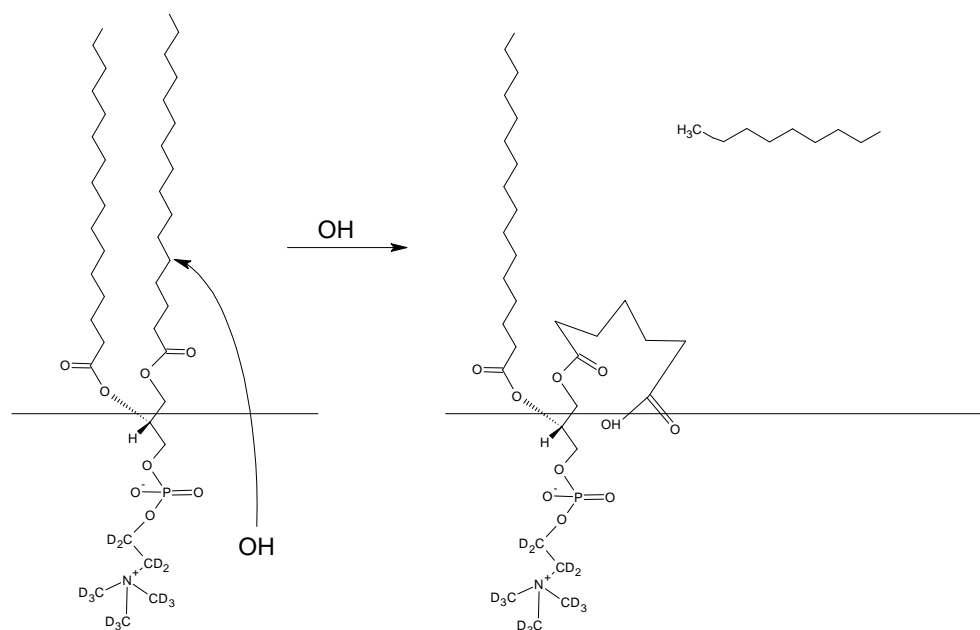
used to see where the aqueous OH radical would attack the DPPC monolayer. There are two scenarios for where the OH radical could react which are shown in figure 6.7 and figure 6.8 as an example using the head group deuterated DPPC molecule.

Figure 6.7 *Reaction Scenario I: Aqueous OH Radical Reacting with the Head Group. The Head Group Reflectivity Signal is Rapidly Lost from the Air-water Interface*



The OH radical can abstract any hydrogen in the head group, the DPPC head group would subsequently decompose in the subphase. The remaining products would potentially remain at the air-water interface. The surface coverage of deuterated material at the air-water interface would decline rapidly for the head only deuterated DPPC isotopologue once the head group had reacted and decomposed.

Figure 6.8 *Reaction Scenario II: Aqueous OH Radical Reacting with the Tail Group. The Head group Reflectivity Signal Persists at the Air-water Interface*



In scenario I the surface coverage signal from the deuterated head group would rapidly be lost from the air-water interface with reaction time as the OH would abstract the hydrogen in the head group leaving soluble product molecules that would not persist at the interface. The same rapid loss in surface coverage would be observed for the tail group deuterated DPPC molecule and the fully deuterated DPPC molecule.

In scenario II the OH would diffuse into the gas-phase tail region of the monolayer and abstract hydrogen from the CH₂ groups comprising the DPPC molecules tail. Where the tail of the molecule is deuterated the surface coverage signal would remain at the air-water interface for longer than in scenario I but at a different rate of loss to the head group deuterated molecule as some of the deuterated product of OH reacting with the tail would remain surface active with an intact head group.

6.4.3 The Generation of Aqueous-phase Hydroxyl Radical

Aqueous-phase hydroxyl radical was generated within the Langmuir trough subphase by photolysis of H₂O₂ using the method described in chapter 2, section 2.4.5 using a 254 nm wavelength ultra violet lamp integral to the lid of the reaction chamber which housed the Langmuir trough during the reflectometry experiments. The calibration of the lamp is described in chapter 2, the lamp was calibrated to find the photolysis rate constant, J using chemical

actinometry, and titrations of H_2O_2 were performed to determine the concentration of H_2O_2 consumed during the photolysis reaction as described in chapter 2. The lamps were configured with the same two bulbs as photolysis lamp configuration B in figure 2.16, chapter 2 so the same calibration is valid for this experiment. The subphase contained $0.32 \text{ mol dm}^{-3} \text{ H}_2\text{O}_2$. The OH concentration during the photolysis experiments was estimated based on the temporal decay of hydrogen peroxide due to photolysis as $15.8 \times 10^{12} \text{ mol dm}^{-3}$ (see chapter 2 section 2.4.7.1 for a description of the model used to determine the concentration of aqueous OH).

6.4.4 The Neutron Reflectivity Experimental Method

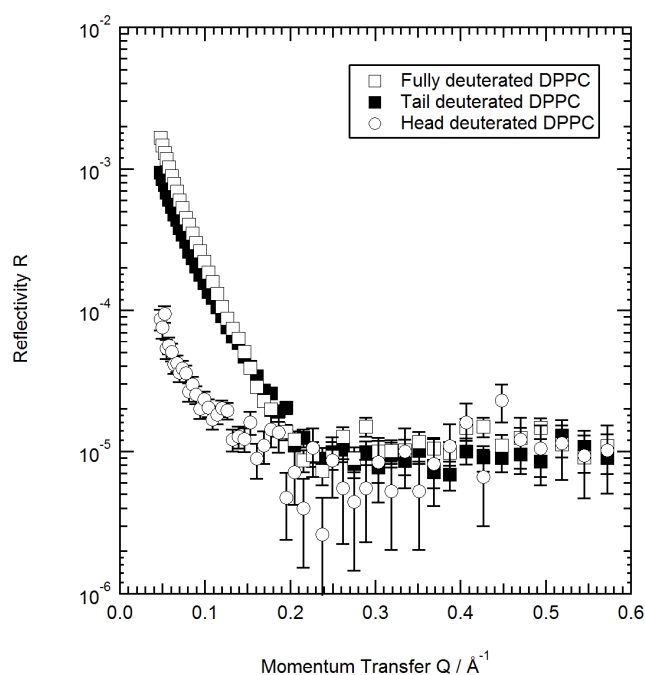
The monolayer surface pressure (Π) and surface coverage (Γ) measurements were taken on the SURF reflectometer coupled with the ISIS Langmuir trough following the procedure and techniques described in chapter 2. The set-up of the reaction chamber surrounding the Langmuir trough was as described in chapter 2 for an aqueous-phase ozone oxidation experiment, using the reaction chamber shown in chapter 2 as this was made to fit to the SURF reflectometer. The lid of the reaction chamber contained the photolysis lamp used to generate OH radical from H_2O_2 in the subphase beneath the monolayer.

The spreading solutions for the Langmuir trough were made up to a concentration of 1 mg / mL DPPC in chloroform. In a typical experiment 100 μL of the spreading solution was spread at the surface of the Langmuir trough on a subphase of null reflective water containing $0.32 \text{ mol dm}^{-3} \text{ H}_2\text{O}_2$ and the monolayer was compressed by closure of the Langmuir trough barriers to a surface pressure of 38 mN m^{-1} . The pH of the subphase was 5.2, the subphase temperature was maintained at $18 \text{ }^\circ\text{C}$ using a circulating water bath attached to a cooling system in the base of the Langmuir trough, it was important to control the temperature to ensure that the measurements were repeatable as the DPPC surface pressure isotherm is greatly altered by changes in temperature as shown in figure 6.3. Once the DPPC monolayer had been compressed to a surface pressure of 38 mN m^{-1} the Langmuir trough barriers were held still, and the Langmuir trough Wilhelmy plate balance was set to record the surface pressure of the DPPC monolayer at the air-water interface over time (the kinetic decay in surface pressure). The neutron beam to the SURF reflectometer was started simultaneously with the recording of the surface pressure kinetic decay measurement.

The SURF reflectometer was set to count neutrons at intervals of 300 seconds per reflectivity (R) versus momentum transfer (Q) data point after counting to an initial current of $50 \mu\text{A}$ to accrue the first bin of reflectivity versus momentum transfer measurements which is fitted to

equation 6.6 (page 386) to form the initial surface coverage data point. The photolysis lamp was switched on, beginning the generation of OH radical when the measured current at the SURF reflectometer detector reached a value of $50\mu\text{A}$ just before the counting of neutrons for the second data point was initiated in each experiment. The reaction lasted >3 hours. Figure 6.9 shows R versus Q plots for monolayers of the three isotopologues of DPPC on an H_2O_2 subphase prior to the photolysis lamp being switched on to generate OH radical. It can be seen that the head group deuterated DPPC gives the lowest reflectivity as there is less deuterated material to measure at the air-water interface.

Figure 6.9 *Reflectivity versus Momentum Transfer Measurement of a DPPC Monolayers on a Subphase of Null Reflective Water Containing $0.32\text{ mol dm}^{-3}\text{ H}_2\text{O}_2$ Prior to Exposure to OH*



Six experiments, two for each isotopologue of DPPC, were achieved in the neutron time available. The neutron beam was unreliable during this work; it has been noted in the results section where this affected the data acquisition. Blank measurements of the reflectivity versus momentum transfer of neutrons from a monolayer of $d72$ DPPC over time on a subphase of null reflective water with H_2O_2 , without photolysis and of a $d72$ DPPC monolayer on a subphase of null reflective water with photolysis (no H_2O_2), were taken to show the difference in the loss of material due to photolysis and due to any reaction of DPPC with H_2O_2 compared with the loss in deuterated material as a result of the reaction of OH radical with DPPC. The experiments were conducted at a single OH concentration of $15.8 \times 10^{12}\text{ mol dm}^{-3}$ in the subphase. The OH

concentration was controlled by the lamp intensity (photolysis rate constant J) and this was not altered. The initial surface coverage at the beginning of the experiments varied as the monolayers were spread by different members of the experimental team and some material was lost from the interface during this process.

6.4.4.1 Stability of the Neutron Beam

The neutron beam at ISIS was not very stable during the time awarded on the SURF instrument to perform the experiments in this chapter. When the neutron beam was functioning the number of neutrons being received at the instrument was low and the current of the beam was variable. The variability in the neutron beam resulted in time gaps in the surface coverage measurements in some of the experiments where there were no neutrons to measure with. At times when the beam current was low points have been co-added together by the instrument scientist Arwel Hughes so that a 300 second count to produce a single surface coverage measurement became a 600 second count to produce a single surface coverage data point and the middle time of the two periods of counting provides the time at which the measurement is plotted.

6.4.5 The Neutron Reflectivity Data Fitting

The DPPC reflectivity versus momentum transfer data was fitted to equation 6.6 using a conceptual model of three layers constrained by their scattering length to neutrons (the air above an interfacial monolayer, the monolayer and the subphase beneath the monolayer), the scattering of neutrons within the model is solved using an Abelès equivalent optical matrix method (Abelès 1950) optical matrix methodology. The model treats the monolayer as the area of interest as in these experiments the subphase of null reflective water and the air above the trough do not contribute to the measurement. The data fitting method is described in detail in chapter 2. The thickness of the monolayer (τ) was varied and the scattering length density (ρ) was varied to obtain a value of area per head group (Å^2), the scattering length of the monolayer (b) was a constant in the model.

The scattering lengths for the different isotopologues of DPPC which were spread at the air-water interface are given in table 6.1. The reflectivity data was fitted to the relevant scattering length (a constant) from table 6.1 and a thickness of $\sim 20 \text{ Å}$ (which is varied to fit the model) to obtain a value of the monolayer surface coverage according to equation 6.6.

Table 6.1 *The Scattering Length of the Different Isotopologues of DPPC used in the Neutron Reflectivity Experiments*

Molecule	Scattering Length $b / \text{Å}$	Scattering Length Density $\rho / \text{Å}^{-2}$
Fully deuterated d75 DPPC	808×10^{-5}	6.56×10^{-6}
Head group deuterated d13 DPPC	163×10^{-5}	1.32×10^{-6}
Tail group deuterated d62 DPPC	673×10^{-5}	5.46×10^{-6}

As explained in chapter 2 the surface coverage is equal to the scattering length density (ρ) multiplied by the thickness (τ) divided by the scattering length (b) (E 6.6) which is the same as one divided by the area per molecule (APM) (E 6.7).

$$\Gamma = \frac{\rho\tau}{b} \tag{E 6.6}$$

$$\Gamma = \frac{1}{APM} \tag{E 6.7}$$

6.5 Results

The aim of the experiment was to look for site specific kinetics so a change in OH concentration was not necessary to monitor this. The decay in the surface coverage and the surface pressure of fully deuterated and partially deuterated DPPC monolayers was monitored over reaction time in order to determine whether the aqueous-phase OH was attacking the head group first or the tail group of the DPPC molecule by comparing the decay in surface coverage and surface pressure of the partially deuterated molecules to the fully deuterated molecule.

The simultaneous neutron surface coverage (Γ) and monolayer surface pressure (Π) measurements will be presented in the following order:

- Fully deuterated DPPC monolayers exposed to aqueous OH radical (6.5.1).
- Head deuterated DPPC monolayers exposed to aqueous OH radical (6.5.2).
- Tail deuterated DPPC monolayers exposed to aqueous OH radical (6.5.3).
- The photolysis only decay of a fully deuterated DPPC monolayer on a subphase of null reflective water (6.5.4).
- The decay of a fully deuterated DPPC monolayer on a subphase of H₂O₂ without photolysis (6.5.5).
- A summary of the results (6.5.6).

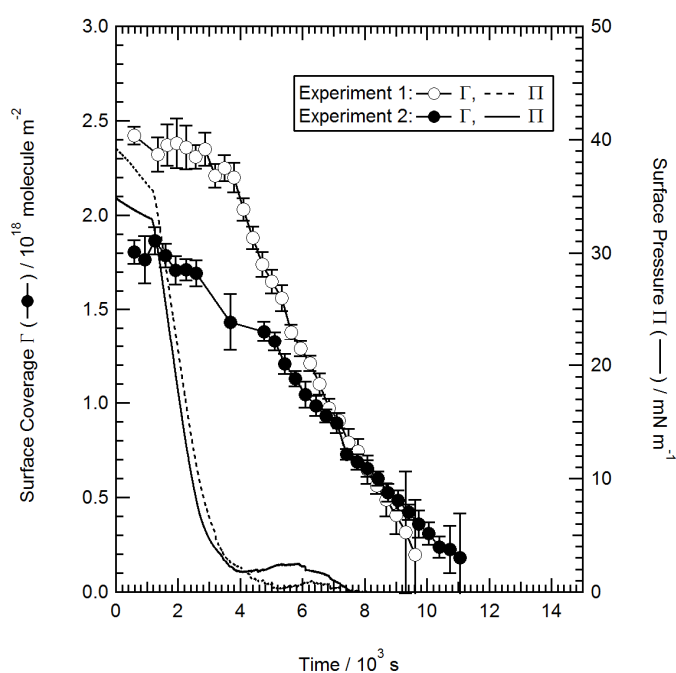
6.5.1 The Decay of the Fully Deuterated DPPC Monolayers Reacting with Aqueous OH Radical

Two experiments were conducted to measure the decay in the surface coverage of fully deuterated DPPC monolayers as they reacted with aqueous OH radical are shown in figure 6.8. The photolysis lamp was switched on when a neutron count of 50 μ A was reached at the detector of the SURF instrument, for all the OH radical experiments the second surface coverage point onwards was measured under conditions of OH generation. After a loss of approximately 1×10^{18} molecule m⁻² the slope of the decay in surface coverage changes to a slightly shallower gradient. The monolayer surface pressure decays to ~ 0.5 mN m⁻¹ then a slight rise occurs before the surface pressure reaches zero, this behaviour is similar to that exhibited by stearic acid reacting with aqueous OH radical in chapter 2.

The gap in the surface coverage measurement frequency at 2500 to 5000 seconds is the result of a low current of protons to the target which produces the neutron beam at the ISIS facility. The beam did not fail completely but was not of a sufficient strength to accrue a rapid measurement thus the surface coverage point at ~ 3600 seconds was obtained from the low reflectivity versus

momentum transfer signal over 2000 seconds, it can be seen that the error bar on this point is large. The reflectivity versus momentum transfer data was fitted to equation 6.6 as individual points to avoid the conceptual model taking iterations based on the previous measurement so that this point did not influence the subsequent surface coverage measurements in the experiment.

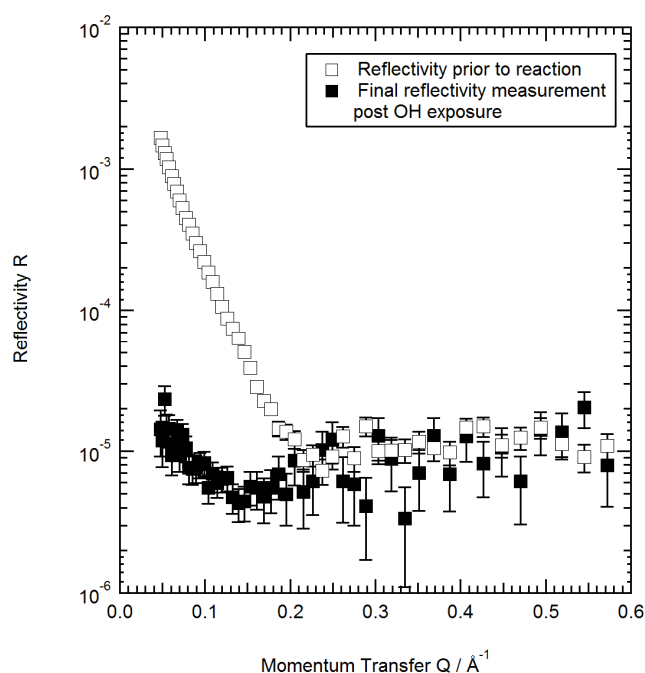
Figure 6.10 *The Decay in the Surface Coverage of Fully Deuterated DPPC Monolayers Exposed to Aqueous-phase OH Radical*



The surface coverage data in figure 6.10 and in subsequent figures is shown in the figure key with the corresponding surface pressure data to distinguish between repeat experiments.

Figure 6.11 shows the reflectivity versus momentum transfer of neutrons which have been reflected by the fully deuterated DPPC monolayer at the air-water interface at the beginning (first point) and the end of the experiment (last point) for which the surface coverage versus time measurement is shown in figure 6.10 as open circles. It can be seen that there was a signal of reflectivity above the instrumental noise at the end of the experiment indicating that at the point where the experiment ended there was still a small amount of deuterated material remaining.

Figure 6.11 *The Neutron Reflectivity versus Momentum Transfer Measurement of a Monolayer of Fully Deuterated DPPC at the Air-water Interface*



6.5.2 The Decay of the Head Group Deuterated DPPC Monolayers Reacting with Aqueous OH Radical

Two measurements of d13 DPPC monolayers composed of molecules with the head group deuterated are shown in figure 6.12. The gaps in the surface coverage data sets are where the neutron beam was lost temporarily during the experiment. The surface pressure at the air-water interface decayed to a value of $\sim 3 \text{ mN m}^{-1}$ before rising by 1 mN m^{-1} and subsequently decaying to zero. The surface coverage signal from the deuterated head group decayed to zero in the presence of OH in < 7000 seconds. Figure 6.13 shows the R versus Q data for a head deuterated DPPC monolayer at the air-water interface prior to reaction, which formed the first surface coverage value plotted in figure 6.12 as a filled in circle, and the final surface coverage point of the same data set once the monolayer had reacted with OH. It can be seen that there are gaps in the final R versus Q data set where the neutron beam was fluctuating and that the data is noisy as there was little deuterated material remaining to measure.

Figure 6.12 *The Decay in the Surface Coverage of Head Group Deuterated DPPC Monolayers Exposed to Aqueous-phase OH Radical*

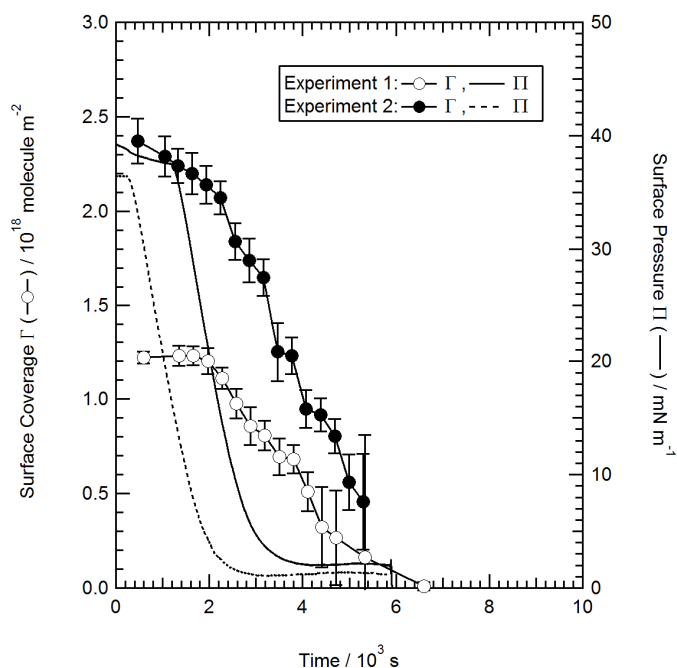
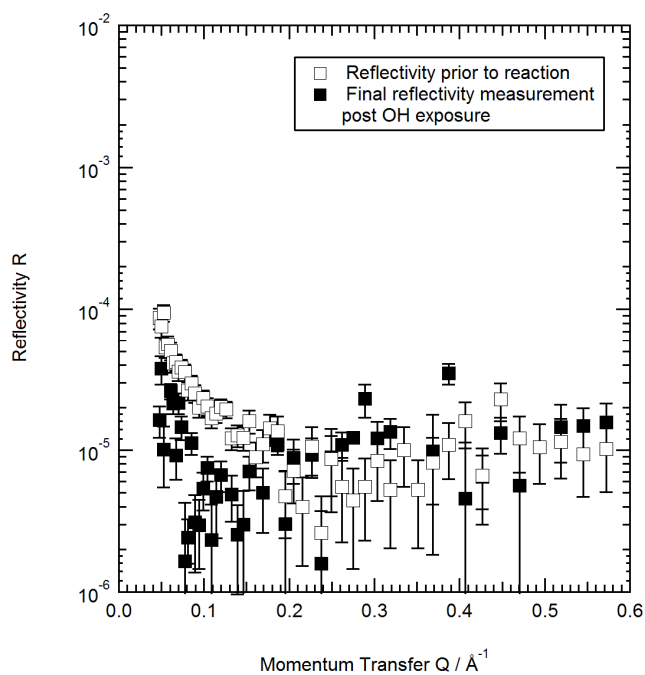


Figure 6.13 *The Neutron Reflectivity versus Momentum Transfer Measurement of a Monolayer of Head Group Deuterated DPPC at the Air-water Interface*



6.5.3 The Decay of the Tail Group Deuterated DPPC Monolayers Reacting with Aqueous OH Radical

Figure 6.14 shows the decay in surface coverage of a monolayer of d62-DPPC with the tail group deuterated when exposed to aqueous OH radical. OH radical did react with the tail as a gradual decay can be seen. The measurement repeated well, the repeat measurement was taken for a longer time period as the neutron beam was lost at the end of the initial experiment. In the repeat at low values of surface coverage $< 0.5 \times 10^{18}$ molecule m^{-2} the surface coverage appeared to rise again. It can be seen from figure 6.15 which shows the R versus Q data collected for the last surface coverage point as filled in squares that there are gaps in the reflectivity signal and that the errors were larger on this data thus the apparent rise in surface coverage of the last point in figure 6.14 is not genuine.

The surface pressure decayed to a value of ~ 0.2 mN m^{-1} then increased slightly before decaying as in previous experiments. The surface pressure did not decay to zero at the end of the experiment due to the formation of bubbles beneath the Wilhelmy plate.

If the temporal profile (Γ versus time) of d62-DPPC and d13-DPPC matches then it shows that OH was reacting indiscriminately with hydrogen at any point along the molecule regardless of distance from the subphase where the OH was generated. If the decay of the d62-DPPC and d13-DPPC are different then the experiments show that the OH radical preferentially abstracts hydrogen from a specific position on the DPPC molecule. It can be seen by comparing figure 6.12 and figure 6.14 that the surface coverage of the d13-DPPC decays more rapidly than the surface coverage of d62-DPPC in the presence of OH.

Figure 6.14 *The Decay in the Surface Coverage of Tail Group Deuterated DPPC Monolayers Exposed to Aqueous-phase OH Radical*

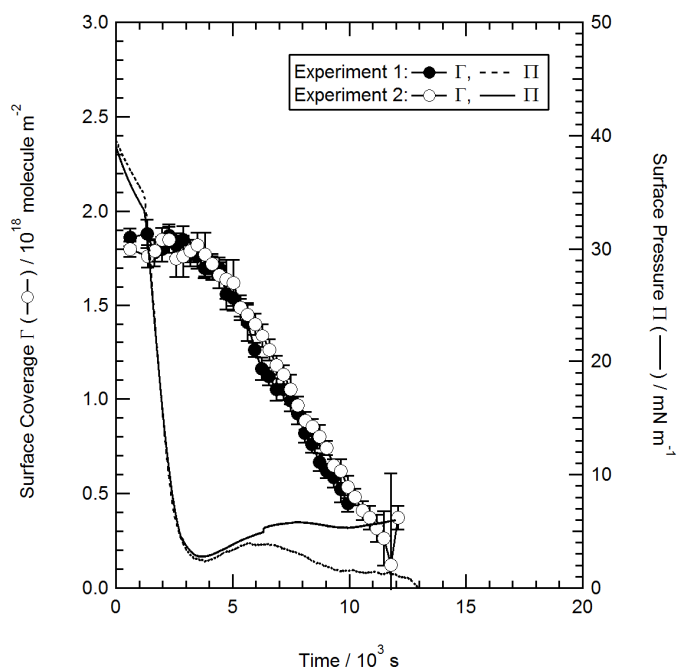
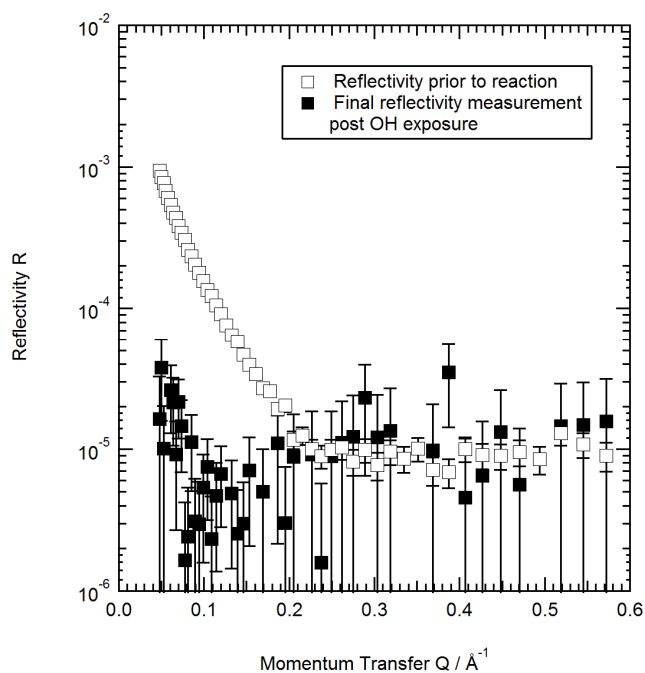


Figure 6.15 *The Neutron Reflectivity versus Momentum Transfer Measurement of a Monolayer of Tail Group Deuterated DPPC at the Air-water Interface*



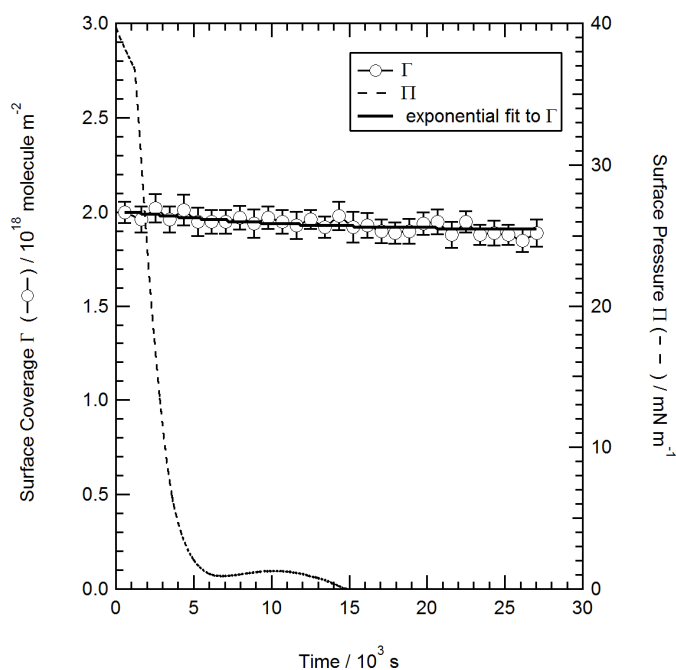
6.5.4 The Photolysis Only Decay of a Fully Deuterated DPPC Monolayer on a Subphase of Null Reflective Water

The DPPC sample did not appear to photolyse. There was little loss in the surface coverage of the DPPC monolayer over >25000 seconds when exposed to the photolysis lamp without H₂O₂. The monolayer surface pressure decayed to a value of 0 mN m⁻¹ over 15000 seconds, for the fully deuterated and head deuterated DPPC monolayers in the presence of OH the surface pressure decayed to zero in < 8000 seconds, the measurement of the decay in the surface pressure of the tail deuterated DPPC was affected by bubble formation beneath the Wilhelmy plate. The decay in the surface pressure versus time features a slight rise at low surface pressures before decaying to zero.

The surface coverage data was fitted to an exponential decay (equation 6.8)

$$\Gamma = \Gamma_0 e^{-kt} \quad (E 6.8)$$

Figure 6.16 *The Decay of a Fully Deuterated DPPC Monolayer with Photolysis on a Subphase of Null Reflective Water with an Exponential Decay Fitted to the Surface Coverage over Time*



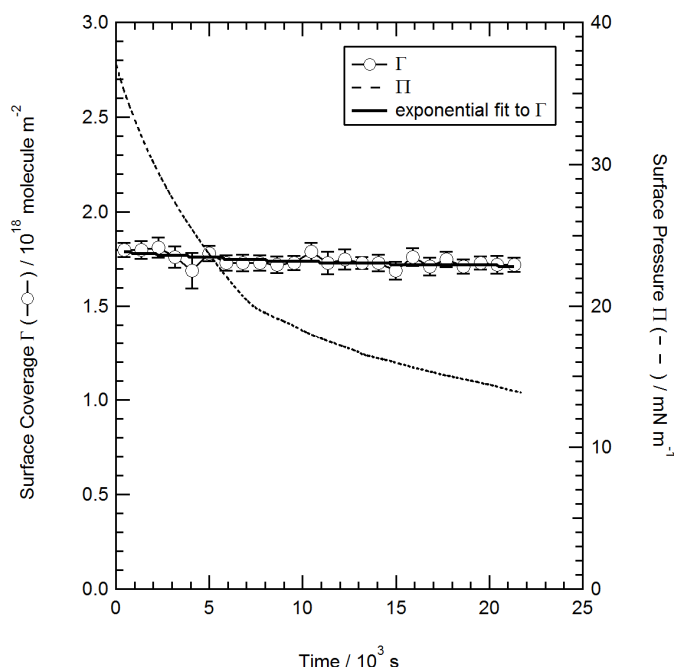
The pseudo first order rate of decay for the photolysis of a fully deuterated DPPC monolayer (k) was $(9.7 \pm 2.3) \times 10^{-5} \text{ s}^{-1}$. The photolysis of a stearic acid monolayer in chapter 2 gave a value of k of $(6.35 \pm 0.69) \times 10^{-6} \text{ s}^{-1}$.

The average value of $k[\text{OH}]$ at 17°C for OH reacting with a stearic acid monolayer was $4.71 \times 10^{-4} \text{ s}^{-1}$. It was not possible to fit kinetics to the decay of DPPC as a result of reaction with aqueous OH given that the purpose of the experiment was to measure the site specific loss due rather than the overall decay of fully deuterated DPPC. Thus for comparison it can be seen that the rate constant for the loss of DPPC due to photolysis of $(9.7 \pm 2.3) \times 10^{-5} \text{ s}^{-1}$ was slower than the reaction rate constant for stearic acid reacting with aqueous OH of $4.71 \times 10^{-4} \text{ s}^{-1}$.

6.5.5 The Decay of a Fully Deuterated DPPC Monolayer on a Subphase of H_2O_2 without Photolysis

The effect of any dark reaction between H_2O_2 and DPPC is shown in figure 6.17; the surface coverage remained constant within $0.2 \times 10^{18} \text{ molecule m}^{-2}$ for $> 20,000$ seconds indicating that there was no dark reaction taking place between the DPPC monolayer and the H_2O_2 in the subphase beneath the monolayer on the timescale of the measurements taken in this work. The surface pressure decayed by 23 mN m^{-1} over $> 20,000$ seconds. Equation 6.8 was fitted to the kinetic decay of surface coverage versus time.

Figure 6.17 *The Decay of a Fully Deuterated DPPC Monolayer with No Photolysis on a Subphase of H_2O_2*



The pseudo first order rate of decay for the dark reaction of a fully deuterated DPPC monolayer with a subphase containing $0.32 \text{ mol dm}^{-3} \text{ mol dm}^{-3} \text{ H}_2\text{O}_2$ (k) was $(8.8 \pm 2.6) \times 10^{-5} \text{ s}^{-1}$ which was slightly faster than the photolysis only experiment (figure 6.16). The dark reaction of stearic acid and $2.352 \text{ mol dm}^{-3} \text{ H}_2\text{O}_2$ in chapter 2 gave a value of k of $(1.44 \pm 0.45) \times 10^{-6} \text{ s}^{-1}$.

6.5.6 Summary of Experimental Results

The kinetic decay in the surface coverage versus time of the three different deuterations of DPPC monitored during the reaction with aqueous OH radical at the air-water interface are given together in figure 6.18 showing the surface coverage divided by the initial surface coverage before the photolysis lamp was switched on to make OH, which gives the relative loss due to the reaction of DPPC with OH plotted against reaction time.

The surface coverage of the deuterated head group is lost from the interface most rapidly thus the head group is being preferentially attacked by OH radical from the subphase. The rate of decay in the surface coverage of the fully deuterated DPPC monolayer lies between the rate of decay of the head and the tail deuterated DPPC.

Figure 6.18 *A Comparison of the Kinetic Decay in the Relative Surface Coverage of DPPC Isotopologue Monolayers at the Air-water Interface Exposed to $15.8 \times 10^{12} \text{ mol dm}^{-3}$ Aqueous OH Radical*

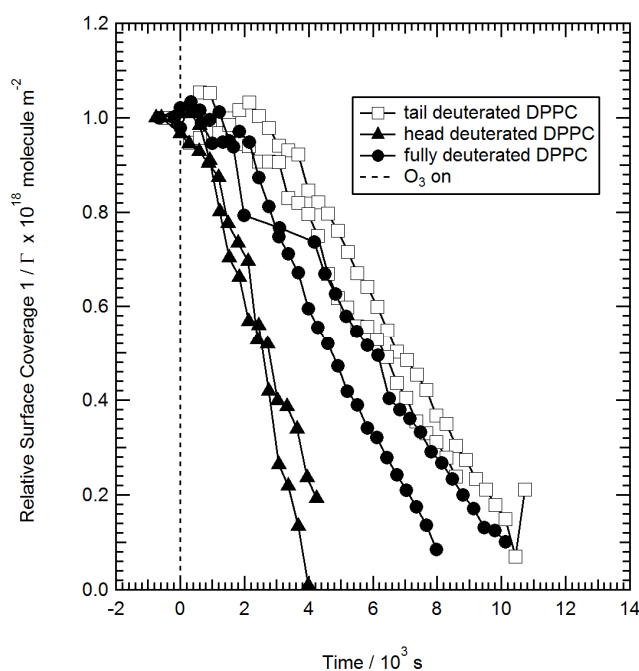
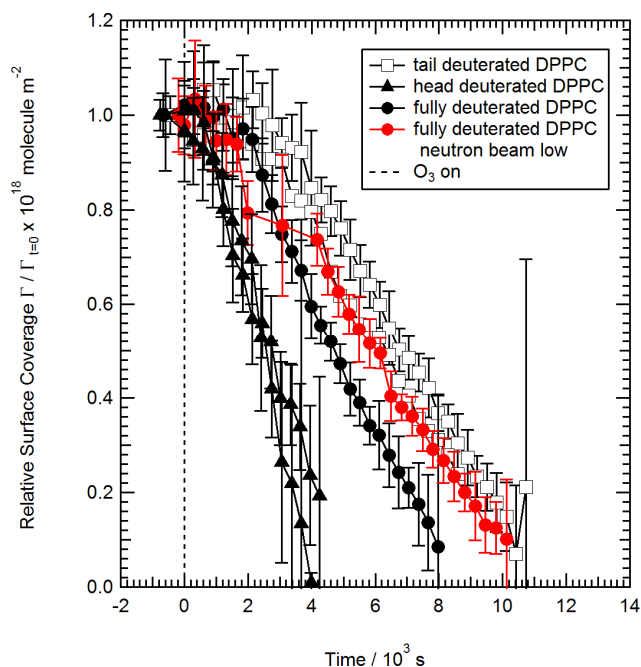


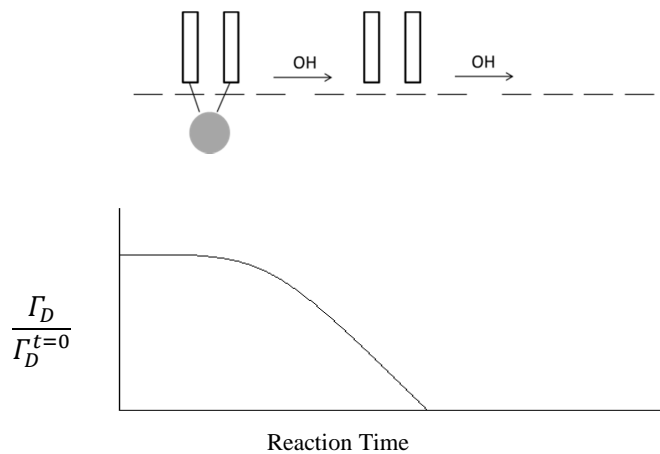
Figure 6.19 *A Comparison of the Kinetic Decay in the Relative Surface Coverage of DPPC Isotopologue Monolayers at the Air-water Interface Exposed to $15.8 \times 10^{12} \text{ mol dm}^{-3}$ Aqueous OH Radical with an Interrupted Experiment Highlighted*



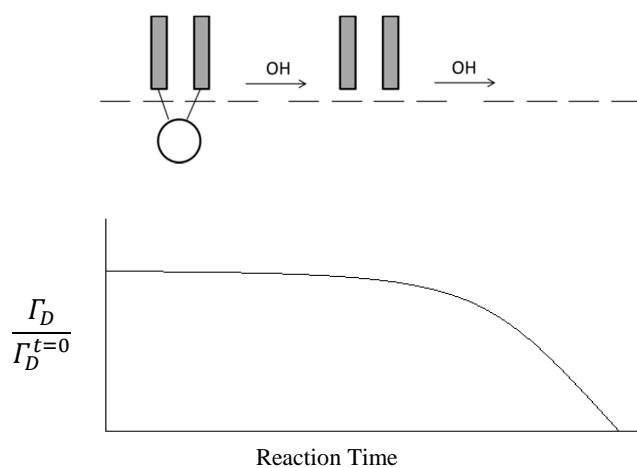
The following figure shows two reaction scenarios in cartoon form of how the decay over time of the surface coverage of deuterated material at the air-water interface would look. Scenario one is that OH is not diffusing into the organic layer of DPPC and is preferentially reacting with the head group of the molecule and the lower tail. Scenario two is that OH is diffusing into the tail of the DPPC molecules in the organic layer at the air-water interface and reacting with the tail and head group at the same rate.

Figure 6.20 *Reaction Scenario One. OH Preferentially Reacting with the DPPC Head Group*

Deuterated Head Group DPPC



Deuterated Tail Group DPPC



Fully Deuterated DPPC

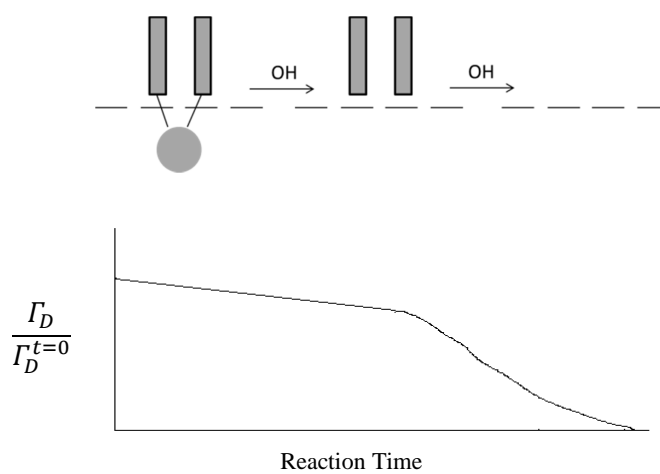
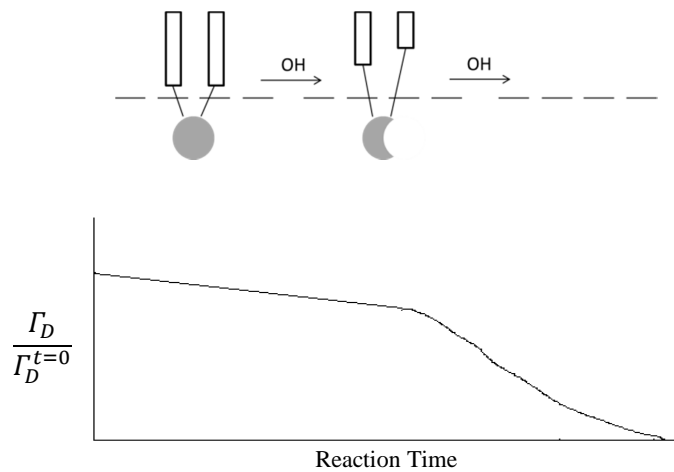
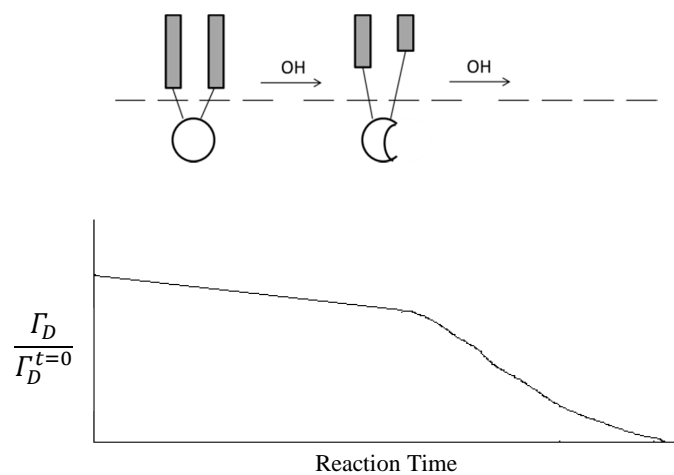


Figure 6.21 *Reaction Scenario Two. OH Diffusing into the DPPC Tails and Reacting and also Reacting with the Head Group*

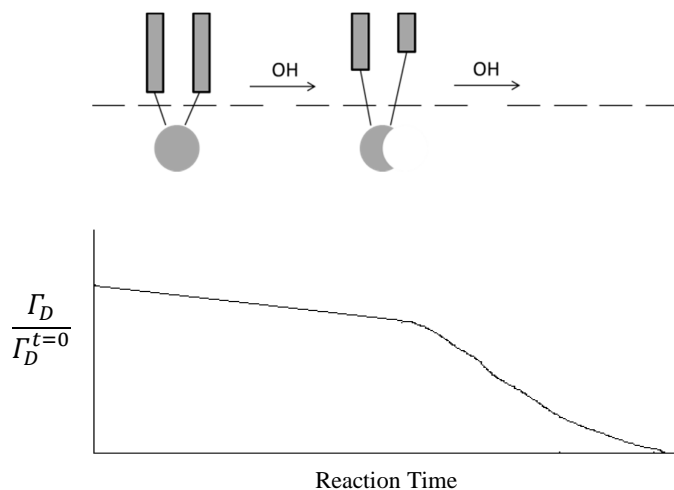
Deuterated Head Group DPPC



Deuterated Tail Group DPPC



Fully Deuterated DPPC



It can be seen that the surface coverage measurements from this experimental work reflect reaction scenario one.

In summary the experimental results were as follows:

- The surface coverage of all three isotopologues of DPPC decayed in the presence to a low value consistent with loss of the monolayer. The surface coverage decay showed degradation kinetics as seen for stearic acid monolayers reacting with OH in chapter 2.
- The surface pressure measurement of the three isotopologues of DPPC decayed to a value of zero in the presence of aqueous OH radical.
- The tail group persisted for longer than the head group of the DPPC molecule at the air-water interface, the head and tail group react at different rates. The head group is attacked preferentially.
- There was no dark reaction between aqueous H₂O₂ and DPPC at the air-water interface.
- The DPPC monolayer did not appear to photolyse on a subphase of null reflective water based on the surface coverage measurements. The surface pressure of the DPPC monolayer was affected by photolysis although the decay was slower than in the presence of OH.

6.6 Discussion of the Atmospheric Implications of the Oxidation of Phospholipids at the Air-water Interface

A brief discussion of the experimental results is given with comparison to other studies of the oxidation of phospholipid monolayers at the air water interface.

In chapter 2 the kinetics of the decay in surface coverage of a stearic acid monolayer as it was oxidised by aqueous OH radical generated in the subphase were investigated. The decay of the surface coverage versus time and the surface pressure versus time of stearic acid was of a similar shape to that of DPPC exposed to OH seen in this chapter suggesting that degradation kinetics may be appropriate to both systems. As with stearic acid the surface pressure measurement did not reflect the amount of material residing at the air-water interface when compared to the surface coverage measurements.

The experimental results show that aqueous OH radical generated within the subphase beneath a monolayer of the DPPC phospholipid can diffuse into the tail region of the monolayer and react with the CH₂ groups comprising the hydrocarbon tail. Aqueous OH radical in the core of a cloud droplet could by the same mechanism enter the tail region of a cloud droplet film and contribute to the oxidation of monolayers in an atmospheric setting. Phospholipid oxidation can

produce shorter surface active product molecules which are present in aged samples of atmospheric aerosol. The oxidation of a lipid coating (1-oleoyl-2-palmitoyl-*sn*-phosphocholine, OPPC) on a solid substrate $\text{NaNO}_2/\text{NaCl}$ by OH from the substrate, referred to as bottom up oxidation was reported by Karagulian et al., (2008) as monitored with diffuse reflection infrared Fourier transform spectrometry. The OH travelled into the tail region of the lipid and reacted with the double bond in the OPPC tail group. The work reported here confirms this behaviour of OH initiated oxidation from within a droplet or particle of a monolayer at the air-water interface and in addition this work shows that the phospholipid head group is preferentially attacked and is lost from the interface before the tail group.

In a monolayer POPC (a phospholipid with one saturated and one unsaturated tail), gas-phase ozone reacted with the double bond in the tail region of the POPC molecule starting an intramolecular reaction where the saturated palmitoyl tail strand of the POPC molecule was subsequently oxidised (Thompson et al. 2010), this oxidation was attributed to OH radical formation in the monolayer tail region by the decomposition of an excited Criegee intermediate in the presence of water. The experiments in this chapter show that OH radical formed in the subphase can also penetrate the tail of a phospholipid molecule and react. Thompson et al., (2010) showed that ozonolysis of an unsaturated strand could initiate reaction of the saturated tail strand on the same molecule; it has not been resolved as to whether the same reaction would occur on a neighbouring fully saturated molecule within a monolayer. The experiments in this chapter show that a DPPC monolayer will react with OH radical, which is a reaction product of the ozonolysis of an alkene, which could oxidise a cloud droplet or aerosol droplet film comprised of saturated phospholipids, a mixed film of saturated and unsaturated phospholipids would also be oxidised based on this work, and that of Wadia et al., (2000) and Thompson et al., (2010) on ozone reacting with OPPC and POPC.

It is likely that following the cleavage of a DPPC molecule after hydrogen abstraction that the reaction products may contain a saturated fatty acid component. From chapter 2 where a monolayer of saturated stearic acid was oxidised by OH radical it can be hypothesised that such a product molecule at the air-water interface would break down into shorter chain products which could still initially have a surface active component. The decay of the tail deuterated DPPC in this chapter showed that the tail was present at the air-water interface for longer than the head group of the molecule. The decay in surface coverage over time for the tail deuterated DPPC reacting with aqueous OH radical appears to have some small features in the surface coverage decay and to give the surface pressure rise as was seen in some of the stearic acid oxidation experiments, the kinetics of the oxidation of the DPPC tail strands could be investigated further with a higher time resolution neutron experiment on the FIGARO

reflectometer to see if the reaction has degradation kinetics as exhibited by the OH-stearic acid monolayer system.

With regards to future work it would be advantageous to repeat the photolysis reaction of the DPPC monolayer on a subphase of null reflective water to confirm the result and to take further repeated measurements of each experiment in order to perform a kinetic analysis. Expansion of the experiment to include mixed phospholipid monolayers and mixed phospholipid with shorter chain fatty acid molecules would provide a better proxy for a cloud droplet film once a kinetic study of the phospholipid has been completed. Using the neutron reflectometry technique with time resolution which allows kinetic analysis of the reaction at the air-water interface as demonstrated in this thesis and the work of King et al., (2009, 2010) and Thompson et al., (2010) to study the interaction of ozonolysis products of lung surfactant molecules (including hydroxyl radical generated by ozone reacting with alkenes) with the original phospholipid monolayer for example with mixtures of different concentrations of each molecule forming a monolayer could provide valuable multidisciplinary data of relevance to both an atmospheric setting and to understanding the effect of ozone on lung surfactant.

References

- Abelès, F. Investigations of the propagation of sinusoidal electromagnetic waves in stratified media. Application to thin films. *Annals of Physics, Paris*, 5, pp. 596-598.
- Can, S.Z., Chang, C.F., Walker, R.A. 2008. Spontaneous formation of DPPC monolayers at aqueous/vapor interfaces and the impact of charged surfactants. *Biochimica et Biophysica Acta*, 1778, pp. 2368-2377.
- Crane, J.M., Putz, G., Hall, S.B. 1999. Persistence of Phase Coexistence in Disaturated Phosphatidylcholine Monolayers at High Surface Pressures. *Biophysical Journal*, 77, pp. 3134-3143.
- Finlayson-Pitts, B.J. and J.N. Pitts, 2000. Chemistry of the Upper and Lower Atmosphere. Academic Press.
- Gašparović, B., Frka, S., Kozarac, Z., Nelson, A. 2008. A method for the characterization of sea surface microlayer based on monolayer properties in presence and absence of phospholipids. *Analytica Chimica Acta*, 620, 1-2, pp. 64-72.
- Goerke, J. 1998. Pulmonary surfactant: functions and molecular composition. *Biochimica et Biophysica Acta (BBA)- Molecular Basis of Disease*, 1408, 2-3, pp. 79-89.
- Hawgood, S. and Clements, J.A. 1990. Pulmonary Surfactant and Its Apoproteins, *Journal of Clinical Investigation*, 86, pp. 1-6.
- Kampa, M and Castanas, E. 2008. Human health effects of air pollution. *Environmental Pollution*, 151, 2, pp. 362-367.
- Karagulian, F., Dilbeck, C.W., Finlayson-Pitts, B.J. 2008. Unusual Oxidation of Organics at Interfaces from the Bottom Up and Atmospheric Implications. *Journal of the American Chemical Society*, 130, pp.11272-11273.
- King, M.D., Rennie, A.R., Thompson, K.C., Fisher, F.N., Chaun Dong, C., Thomas, R.K., Pfrang, C.P., Hughes, A.V. 2009. Oxidation of oleic acid at the air-water interface and its potential effects on cloud critical supersaturations. *Physical Chemistry Chemical Physics*, 11, pp. 7699-7707.
- King, M.D., Rennie, A.R., Pfrang, C., Hughes, A.V., Thompson, K.C. 2010. Interaction of nitrogen dioxide (NO₂) at the air-water interface – A simple proxy for atmospheric aerosol. *Atmospheric Environment*, 44, 14, pp. 1822-1825.
- Lai, C.C., Yang, S.H., Finlayson-Pitts, B.J. 1994. Interactions of Monolayers of Unsaturated Phosphocholines with Ozone at the Air-Water Interface. *Langmuir*, 10, pp. 4637-4644.
- Lockwood, A.P.M., and Lee, A.G., The Membranes of Animal Cells. 3rd edition, E. Arnold, London.

- Ma, G., and Allen, H.C. 2006. DPPC Langmuir Monolayers at the Air-Water Interface: Probing the Tail and Head Groups by Vibrational Sum Frequency Generation Spectroscopy. *Langmuir*, 22, pp.5341-5349.
- Marty, J.C., Saloit, A., Buat-Ménard, P., Chesselet, R., Hunter, K.A. 1979. Relationship Between the Lipid Compositions of Marine Aerosols, the Sea Surface Microlayer and Subsurface Water. *Journal of Geophysical Research*, 84, C9, pp. 5707-5716.
- Mello Filho, A.C., Hoffman, E., Meneghini, R. 1984. Cell killing and DNA damage by hydrogen peroxide are mediated by intracellular iron. *Journal of Biochemistry*, 218, pp. 273-275.
- Pryor, W.A., Bermúdez, E., Cueto, R., Squadrito, G.L. 1996. Detection of Aldehydes in Bronchoalveolar Lavage of Rats Exposed to Ozone. *Fundamentals of Applied Toxicology*, 34, pp. 148- 156.
- Rooney, S.A., Young, S.L., Mendelson, C.R. 1994. Molecular and cellular processing of lung surfactant. *The Journal of the Federation of American Societies for Experimental Biology*, 8, pp. 958-970.
- Thompson, K.C., Rennie, A.R., King, M.D., Hardman, S.J.O., Lucas, C.O.M., Pfrang, C., Hughes, B.R., Hughes, A.V. 2010. Reaction of a Phospholipid Monolayer with Gas-Phase Ozone at the Air-Water Interface: Measurement of Surface Excess and Surface Pressure in Real Time. *Langmuir*, 26, 22, pp. 17295-17303.
- Till, G.O., Hatherill, J.R., Tourtellotte, W.W., Lutz, M.J., Ward, P.A. 1988. Lipid Peroxidation and Acute Lung Injury after Thermal Trauma to the Skin. *American Journal of Pathology*, 119, 3, pp. 376-384.
- Valleyathan, V. and Shi, X. 1997. The Role of Oxygen Free Radicals in Occupational and Environmental Lung Diseases. *Environmental Health Perspectives*, 105, 1, pp. 165-177.
- Vance, D.E., Vance, J.E. 1985. *Biochemistry of Lipids and Membranes*. Benjamin Cummings Publishing Corporation California.
- Veldhuizen, R., Nag, K., Orgeig, S., Possmayer, F. 1998. The role of lipids in pulmonary surfactant. *Biocemica et Biophysica Acta- Molecular Basis of Disease*, 1408, 2-3, pp. 90-108.
- Wadia, Y., Tobias, D.J., Stafford, R., Finlayson-Pitts, B.J. 2000. Real-Time Monitoring of the Kinetics and Gas-Phase Products of the Reaction of Ozone with an Unsaturated Phospholipid at the Air-Water Interface. *Langmuir*, 16, 24, pp. 9321-9330.
- Yang, X.M., Xiao, D., Xiao, S.J., Wei, Y. 1994. Domain structures of phospholipid monolayer Langmuir-Blodgett films determined by atomic force microscopy. *Applied Physics A: Solids and Surfaces*, 59, pp. 139-143.

Synthesis of the Experimental Results

The purpose of this chapter is to provide an executive summary of the results of the experimental work in this thesis in an atmospheric context and to suggest how the work could be improved upon and further developed. I shall begin with a summary of the main results for each system studied followed by a summary of the atmospheric implications of these results. The advantages and disadvantages of the techniques employed and the work which could have been carried out with further time will then be noted.

7.1 A Summary of the Key Results

7.1.1 The Oxidation of Stearic Acid Monolayers by Aqueous Phase OH Radical

The investigation of the oxidation of stearic acid monolayers by aqueous OH radical generated by photolysis within the subphase, served as a proxy for the oxidation of a saturated monolayer at the air-water interface of an atmospheric droplet from a radical species generated within the droplet.

A monolayer of stearic acid at the air-water interface was degraded by aqueous hydroxyl radical. The monolayer was removed under sustained exposure to aqueous hydroxyl radical. The measurement of surface pressure and the surface coverage of the stearic acid monolayer decayed with reaction time, however the surface pressure measurement did not reflect the surface coverage of material at the interface; this showed that the neutron reflectometry technique gives more accurate information on the persistence of an amphiphile at the air-water interface from which measurements of the reaction kinetics can be performed. The surface pressure measurement decayed then increased in value during oxidation by aqueous OH radical and subsequently decayed again. The surface coverage measurement did reflect this behaviour showing a subtle change in the decay slope. It would be advantageous to repeat this work at a higher time resolution on the FIGARO reflectometer to further investigate the region in the decay of the monolayer where the surface pressure rise occurred. The region where the surface pressure increased was inferred to be where a surface active product of the cleavage of the stearic acid molecule was building up at the air-water interface. The decay in the surface coverage over reaction time was fitted to a sequential decay mechanism which incorporated the decay of stearic acid which was cleaved by hydroxyl radical, then the build-up of surface active reaction products at the air-water interface which were subsequently cleaved by hydroxyl radical forming soluble products which lack the length of hydrocarbon chain required to persist at the interface. There was no increase in the rate of the reaction between the stearic acid monolayer and hydroxyl radical when the hydrogen peroxide concentration was increased,

increasing the hydrogen peroxide concentration had only a slight effect of the hydroxyl radical concentration but a higher hydroxyl radical concentration did not alter the rate constant significantly. The effect of temperature on the reaction between hydroxyl radical and stearic acid was investigated and no direct correlation between the temperature and the rate constant was found. It would be advantageous to repeat the experiment as much of the data could not be used due to failure of the neutron beam which left large time gaps in the surface coverage measurements.

The experiment's primary aim was to investigate the oxidation of a saturated fatty acid monolayer of stearic acid at the air-water interface by aqueous hydroxyl radical as a proxy for a cloud droplet monolayer being oxidised by species from the droplet phase. When modelled for a concentration of hydroxyl radical found in atmospheric waters, such a reaction takes place on a time scale of ~550 days which is longer than the lifetime of a cloud droplet or aerosol particle (~ < 14 days) thus the reaction will not be of importance in an atmospheric setting. However the experiment shows that a saturated fatty acid monolayer will break down when exposed to hydroxyl radical and such a reaction is likely to take place in the gas-phase, this has not been investigated here but would be expected to be a rapid process (Textor et al., 2006). The rate constants and modelled atmospheric lifetimes from the experiments are summarised in section 7.2.

7.1.2 The Oxidation of Oleic Acid Monolayers Initiated by Gas-phase Ozone

The investigation of the oxidation of oleic acid monolayers initiated by gas-phase ozone served as a proxy for the oxidation of an unsaturated monolayer at the air-water interface of an atmospheric droplet by a gas-phase reactive species.

A monolayer of fully deuterated oleic acid at the air-water interface was degraded by gas-phase ozone. The surface pressure of the monolayer and the surface coverage of deuterated material at the air-water interface both decayed exponentially however the time order of the surface pressure and surface coverage decay were different showing the need for neutron reflectivity measurements to accurately determine how much material persisted at the air-water interface. The monolayer was removed under sustained exposure to gas-phase ozone, the monolayer was also unstable in an oxygen atmosphere but decayed much more rapidly in the presence of ozone than oxygen alone. Ozone is known to react with oleic acid at the site of the carbon-carbon double bond in the tail of the molecule. To better understand the mechanism of decay of the oleic acid monolayer, a monolayer of partially deuterated oleic acid which was deuterated beyond the double bond in the tail of the molecule was also studied as it reacted with gas-phase ozone. Based on the earlier work of King et al., (2009), it was thought that a surface active

reaction product produced by ozone reacting with the double bond in the oleic acid molecule would remain at the interface however the two deuterations of oleic acid decayed with the same behaviour, the rate constants for the decay of the deuterated portion of the tail were of a similar rate. The concentration of ozone above the organic film was varied and at lower concentrations of $(16.1 \pm 3.89) \times 10^{12}$ molecule cm^{-3} , the decay in the surface coverage changed and two distinct regions of decay could be seen during the reaction with a region of inflection between them. Upon recompression of the monolayer by closing the Langmuir trough barriers the inflection was repeated suggesting that this was a structural feature of the packing of the monolayer at the air-water interface and the orientation of the oleic acid molecules as the area per head group increases when neighbouring molecules are reacted away from the air-water interface. By slowing the reaction down using a low ozone concentration the inflection feature was visible; it is likely that at the higher ozone concentrations the time resolution of the surface coverage measurement misses the inflection. To test whether the formation of hydroxyl radical formation in the aqueous subphase beneath the monolayer was a factor in determining the decay of the oleic acid monolayer initiated by gas-phase ozone, the pH of the subphase was altered to dis-favour hydroxyl radical formation, no change in the decay of the monolayer was observed indicating that hydroxyl radical was not influencing the decay of the oleic acid monolayer.

The atmospheric implication of the decay of an oleic acid monolayer film at the air-water interface due to a reaction with gas-phase ozone is that an oleic acid monolayer as a proxy for unsaturated organic molecules is that a cloud droplet or aerosol organic film would decay away forming products which were not surface active. The lifetime of an oleic acid monolayer in the atmosphere exposed to an ozone concentration of 40 ppb would be ~ 3.5 hours thus the reaction of gas-phase ozone with oleic acid will be significant in the removal of cloud droplet and aerosol organic films in the atmosphere.

7.1.3 The Oxidation of Mixed Oleic and Stearic Acid Monolayers Initiated by Gas-phase Ozone

To demonstrate the decay kinetics of a more complex and atmospherically realistic organic film under oxidation by gas-phase atmospheric oxidants, a mixed monolayer of oleic and stearic acid was created and exposed to gas-phase ozone. The surface pressure of the mixed film decayed exponentially from the point of exposure to gas-phase ozone. It was found that in the presence of oleic acid the stearic acid component of the monolayer did not decay when exposed to gas phase ozone at a concentration of $(2.4 \pm 0.6) \times 10^{12}$ molecules cm^{-3} . It was concluded that the Criegee intermediate produced by the reaction of ozone with oleic acid was not performing an inter-molecular reaction and attacking the stearic acid molecules in the film. The oleic acid

component of the monolayer decayed away as it reacted with the gas-phase ozone leaving the stearic acid component behind as was evident from the residual surface coverage which was still seen after prolonged reaction times. With further data collection it would be possible to estimate an atmospheric lifetime for a mixed composition monolayer at the air-water interface of a cloud or aerosol droplet however a judgement can be made that ozone would remove the unsaturated component of such a film leaving the saturated species which would be oxidised by hydroxyl radical.

7.1.4 The Oxidation of Methyl Oleate Monolayers Initiated by Gas-phase Ozone

To demonstrate the decay kinetics of a further organic molecule category found in cloud waters a monolayer of the methyl ester of oleic acid, methyl oleate was exposed to gas-phase ozone. The surface pressure of the monolayer and the surface coverage of deuterated material at the air-water interface both decayed exponentially however the time order of the surface pressure and surface coverage decay were different. The monolayer decayed to a very low surface coverage at which it would not be intact when exposed to gas-phase ozone. The rate of the decay in the surface coverage of deuterated material at the air-water interface increased with exposure to increasing concentrations of gas-phase ozone. The atmospheric lifetime for a methyl oleate monolayer exposed to a gas-phase ozone concentration of 40 ppb would be ~ 2.4 hours which is shorter than the lifetime of a cloud or aerosol droplet thus the reaction could be a significant pathway in the removal of a cloud droplet film.

7.1.5 The Oxidation of Phospholipid Monolayers Initiated by Aqueous Phase OH Radical

To demonstrate the decay kinetics of a further organic molecule category found in cloud waters and the sea-surface microlayer a monolayer of the phospholipid, DPPC which has two saturated tails, was exposed to hydroxyl radical. Three deuterations of DPPC were used, a fully deuterated DPPC molecule, a head group only deuterated DPPC molecule and a tail group deuterated DPPC molecule. The decay in the monolayer surface pressure of DPPC exposed to aqueous hydroxyl radical was more rapid than the decay in the surface coverage of the deuterated material at the air-water interface. Under sustained exposure to hydroxyl radical the surface coverage of the DPPC monolayer decayed to a very low value at which the monolayer would not be intact. The tail group persisted at the air-water interface for longer than the head group showing that the head group is attacked preferentially. The decay of the surface coverage of the tail deuterated molecule shows that the hydroxyl radical can penetrate the tail region of the monolayer. The atmospheric implication of these results is that a phospholipid monolayer

could be removed by oxidation by aqueous phase species however if the head group is lost at a faster rate. The work of Thompson et al., (2010) showed that the POPC phospholipid molecule which has one saturated and one unsaturated tail was broken down by gas-phase ozone, which initiated an intra-molecular reaction which broke down the saturated tail, thus in the atmosphere a phospholipid monolayer can be broken down by both aqueous hydroxyl radical and gas-phase ozone. This is an important result as saturated phospholipids are one of the largest and most resistant candidate compounds for an atmospheric monolayer film.

7.2 A Summary of the Kinetic Results

The reaction rate constants for the reaction of monolayers with aqueous OH radical and with gas-phase ozone absorbed to the monolayer, with the corresponding uptake coefficients are given in table 7.1 and 7.2 together with the calculated lifetime for oxidised monolayers based on the bimolecular rate constants obtained in this work.

Table 7.1 *A Summary of the Reaction Rate Constants and Monolayer Atmospheric Lifetimes Resulting from the Experimental Work in this Thesis*

Reaction system	Average k / s^{-1}	Bimolecular k	Monolayer atmospheric lifetime
Aqueous OH + stearic acid monolayer	4.71×10^{-4}	$5.5 \times 10^7 \text{ dm}^3$ $\text{mol}^{-1} \text{ s}^{-1}$	~553 days
Gas-phase O_3 + oleic acid monolayer	0.66×10^{-2}	$(4.5 \pm 0.68) \times$ 10^{-11} cm^2 $\text{molecule}^{-1} \text{ s}^{-1}$	~3 hours 32 minutes
Gas-phase O_3 + methyl oleate monolayer	0.014	$(2.72 \pm 0.44) \times$ 10^{-11} cm^2 $\text{molecule}^{-1} \text{ s}^{-1}$	~5 hours 53 minutes

Table 7.2 *Uptake Coefficients for Ozone by a Monolayer of Oleic Acid and a Monolayer of Methyl Oleate*

Reaction system	Γ $\times 10^{18}$ molecule m^{-2}	Uptake coefficient for ozone at 20°C $\times 10^{-6}$	Uptake coefficient for ozone at 5°C $\times 10^{-6}$	Uptake coefficient for ozone at 0°C $\times 10^{-6}$
Gas-phase O ₃ + oleic acid monolayer δ 15 Å	2	1.7	1.6	1.6
	3	2.6	2.5	2.4
Gas-phase O ₃ + oleic acid monolayer δ 20 Å	2	2.3	2.2	2.2
	3	3.5	3.3	3.2
Gas-phase O ₃ + methyl oleate monolayer δ 15 Å	2	1.1	0.99	0.97
	3	1.6	1.5	1.5
Gas- phase O ₃ + methyl oleate monolayer δ 20 Å	2	1.4	1.3	1.3
	3	2.1	2	1.9

The saturated species stearic acid has a long lifetime at the air-water interface when exposed to aqueous phase OH radical indicating that this oxidation mechanism does not have a significant role in the removal of cloud droplet and aerosol particle monolayers. The un-saturated species, oleic acid and methyl oleate had a much shorter lifetime at the air-water interface than stearic acid. The ozone initiated oxidation of the un-saturated species in a cloud droplet or aerosol particle monolayer at the air-water interface is significant in the removal of cloud droplet monolayers and the aging of atmospheric aerosol as the oxidation process removes the monolayer within the lifetime of an atmospheric droplet.

7.3 Atmospheric Implications of the Findings of this Work

The work in this thesis has shown that fatty acids, methyl esters and phospholipids are subject to oxidation by common atmospheric radical species. The removal of a cloud or aerosol droplet monolayer by oxidation in situ in the atmosphere is highly likely given these results. The effects

of the removal of an interfacial monolayer at the air-water interface of a cloud droplet or aerosol particle on cloud droplet nucleation and growth are as follows:

The presence of an organic monolayer at the air-droplet interface of a cloud droplet increases the ability of a nucleating droplet growing to a sufficient size to become a rain droplet according to the modified form of Köhler theory (Shulman et al., 1996; Sorjamaa et al., 2004) as the monolayer will decrease the surface tension of the droplet in comparison to pure water, making uptake of water vapour to the droplet more favourable and thus lowering critical supersaturation of water vapour in air at which an aerosol particle (cloud condensation nuclei) can grow into a cloud droplet (King et al., 2009^a). The presence of a monolayer also limits evaporation from an atmospheric droplet and prolongs its lifetime in the atmosphere (Gill et al., 1983). The oxidation and removal of a monolayer at the air-droplet interface of a cloud or aerosol droplet increases the surface tension reducing the uptake of water vapour to a droplet at a given relative humidity and potentially increases the likelihood of evaporation from the droplet as the surface coverage of the monolayer is reduced.

Any soluble reaction products which enter the bulk droplet aqueous phase from the reaction of an organic monolayer at the air-droplet interface will contribute to the Raoult term of Köhler theory. The effect of a soluble reaction product from the reaction of ozone with a monolayer of oleic acid was modelled by King et al., (2009^a), showing that it was the contribution of soluble reaction products to the Raoult term which had a greater effect on the growth of a cloud droplet than any effects on surface tension, thus oxidation of the monolayer lowered the critical supersaturation required for droplet growth. King et al., (2009^b) showed that an oleic acid coated particle in an optical trap grew when exposed to gas-phase ozone. Oxidation of an interfacial monolayer makes the interface more chemically hydrophilic but with a higher surface tension than in the presence of a monolayer. The effect of monolayer oxidation on a cloud droplet will depend on many factors including the relative humidity of the air in which the droplet resides and the size of the droplet, what is clear is that a droplet with a monolayer behaves differently upon oxidation of the monolayer. This work has shown that during a reaction with atmospheric radical species a monolayer breaks down forming products some of which are potentially soluble and may enter the bulk of an atmospheric droplet contributing to chemical aging and alteration in the evolution of the droplet.

The atmospheric lifetimes calculated for the monolayers studied as they react with given species (table 7.1) show that the saturated stearic acid monolayer is more resistant to oxidation than the unsaturated species which readily react with gas-phase ozone. The reaction of gas-phase ozone with an unsaturated monolayer appears to proceed by the diffusion of ozone into the tail region

of the monolayer and subsequent reaction with the double bond which occurs rapidly, and the monolayer is subsequently lost from the air-water interface. Gas-phase ozone reacts with an unsaturated methyl ester at a similar rate and via a similar mechanism to a reaction with the corresponding fatty acid showing it is the destruction of the tail group of the amphiphile which dominates the kinetics.

The phospholipid DPPC was shown to be lost from the air-water interface during a reaction with aqueous phase OH radical. It is likely that phospholipid material, as a component of the sea surface microlayer, will be found in atmospheric aerosol and that such lipid content could potentially form cloud and aerosol droplet films which would subsequently react with aqueous hydroxyl radical to produce lower molecular weight surface active products which would react and subsequently lost from the air-water interface.

7.4 Ideas for Further Development of This Work

In reality a monolayer present on an atmospheric droplet will be composed of a multitude of different species. Here I have investigated simple systems in order to understand some of the kinetic processes that would take place in such a setting. The ultimate goal of such work given unlimited time and resources would be to gradually build up the proxy system to a level of complexity which was more realistic to the chemistry a genuine atmospheric droplet having investigated the reactions involved individually by the same technique thus having directly comparable measurements to compare to a complex mixed system. The subphase beneath the monolayer could be altered to reflect the chemistry of different atmospheric aerosol species. It would be beneficial to repeat some of the experiments at different pH and temperature in order to better quantify the reaction rate constants which are valid in certain atmospheric conditions.

The project could be further developed by the identification of the reaction products from oxidation of the monolayers, which would allow the effect of monolayer oxidation on cloud droplet growth to be better quantified as modelling of the behaviour of an oxidised coated droplet using Köhler theory could be completed. It was hoped in the scope of this work to conduct sampling of the reacted and unreacted monolayer using the Langmuir Blodgett technique where a treated slide is dipped through the monolayer and the monolayer is deposited onto the slide providing a substrate on which further chemical techniques such as atomic force microscopy could be conducted. There are several different substrates which could be used which mimic the chemistry of an aerosol particle. This experiment was not achieved as it was

felt that the reactants involved such as ozone and OH radical may damage expensive equipment which did not belong to the university.

Ellipsometry may provide an inexpensive method of determining the surface coverage of the monolayer rather than neutron reflectometry, an initial attempt at this was unsuccessful but with more time this should be possible however it would require the construction of a custom built reaction chamber to fit onto an ellipsometer if the measurements were to be taken in real time to use for kinetic analysis and again there is the concern that oxidant species may damage equipment so the chamber would require extensive testing before this work could go ahead.

7.5 Conclusions

The reaction rate constants and uptake coefficients measured in this work provide new data to the atmospheric science community for reactions of monolayers at the air-water interface that were not previously available. The mechanism for the reaction of a stearic acid monolayer with aqueous OH radical reacting in a degraded chain mechanism shows a route by which shorter chain saturated surface active molecules can be generated at the air-water interface of atmospheric droplets. The experimental work has shown that the neutron reflectometry technique provides a measurement of the average surface concentration of a one molecule thick organic film during a reaction in real time, which is suitable for kinetic analysis and that the technique of selective deuterations to highlight different parts of a molecule can also be used at a single angle with rapid real time neutron reflectivity measurements to successfully follow the structural breakdown of an organic film.

References

Gill, P.S., Graedel, T.E., Weschler, C.J. 1983. Organic Films on Atmospheric Aerosol Particles, Fog Droplets, Cloud Droplets, Raindrops and Snowflakes. *Reviews of Geophysics*, 21, 4, pp. 903-920.

Shulman, M.L., Jacobson, M.C., Carlson, R.J., Synovec, R.E., Young, T.E. 1996. Dissolution behaviour and surface tension effects of organic compounds in nucleating cloud droplets. *Geophysical Research Letters*, 23, 3, pp. 277-280.

Sorjamaa, R., Svenningsson, B., Raatikainen, T., Henning, S., Bilde, M., Laaksonen, A. 2004. The role of surfactants in Köhler theory reconsidered. *Atmospheric Chemistry and Physics*, 4, pp. 2107-2117.

King, M.D., Rennie, A.R., Thompson, K.C., Fisher, F., Chaun Dong, C., Thomas, R.K. Pfrang, C.P., Hughes, A.V. 2009^a. Oxidation of oleic acid at the air-water interface and its potential effects on cloud critical supersaturations. *Physical Chemistry Chemical Physics*, 35, pp. 7699-7707.

King, M.D., Thompson, K.C., Ward, A.W. 2009^b. Laser Tweezers Ramen Study of Optically Trapped Aerosol Droplets of Seawater and Oleic Acid Reacting with Ozone: Implications for Cloud-Droplet Properties. *Journal of the American Chemical Society*, 126, pp. 16710-16711

The equation and figure numbers are a continuation of those in the relevant chapter.

Appendices to Chapter 3

Item 1 *The Differential Equations Used to Calculate the Concentration of Gas-phase Ozone in the Reaction Chamber during an Experiment*

The following variables were included in the calculation of the concentration of gas phase ozone in the reaction chamber, $[O_3]_{chamber}$:

Flux into the reaction chamber from the ozoniser (the number of molecules per second),

$$F[O_3]_{ozonizer}$$

Flux out of the reaction chamber via the exhaust (the number of moles per second),

$$F[O_3]_{chamber}$$

The volume of the reaction chamber,

$$V_{chamber}$$

$$\frac{d[O_3]_{chamber}}{dt} = \frac{F[O_3]_{ozonizer}}{V_{chamber}} - \frac{F[O_3]_{chamber}}{V_{chamber}} \quad (E 3.19)$$

$$\frac{d[O_3]_{chamber}}{dt} = \frac{F}{V_{chamber}} [[O_3]_{ozonizer} - [O_3]_{chamber}] \quad (E 3.20)$$

$$\frac{d[O_3]_{chamber}}{dt} = \frac{F}{V_{chamber}} ([O_3]_{ozonizer} - [O_3]_{chamber}) \quad (E 3.21)$$

$$\frac{d[O_3]_{chamber}}{dt} = \frac{F}{V_{chamber}} Z \quad (E 3.22)$$

$$Z = [O_3]_{ozonizer} - [O_3]_{chamber} \quad (E 3.23)$$

$$\frac{dZ}{dt} = 0 - \frac{d[O_3]_{chamber}}{dt} \quad (E 3.24)$$

$$\frac{dZ}{dt} = \frac{F}{V_{chamber}} Z \quad (E 3.25)$$

$$\frac{dZ}{dt} = \frac{F}{V_{chamber}} Z \Rightarrow \int \frac{dZ}{Z} = \frac{-F}{V_{chamber}} \int dt \quad (E 3.26)$$

$$\ln\left(\frac{Z}{Z_0}\right) = \frac{-F}{V_{chamber}} t \quad (E 3.27)$$

$$Z_0 = [O_3]_{ozonizer} - 0 \quad (E 3.28)$$

$$\ln\left(\frac{[O_3]_{\text{ozonizer}} - [O_3]_{\text{chamber}}}{[O_3]_{\text{ozonizer}}}\right) = \frac{F}{V_{\text{chamber}}} t \quad (E 3.29)$$

$$\ln\left(1 - \frac{[O_3]_{\text{chamber}}}{[O_3]_{\text{ozonizer}}}\right) = -\frac{F}{V_{\text{chamber}}} t \quad (E 3.30)$$

$$1 - \frac{[O_3]_{\text{chamber}}}{[O_3]_{\text{ozonizer}}} = e^{-\frac{F}{V}t} \quad (E 3.31)$$

$$\frac{[O_3]_{\text{chamber}}}{[O_3]_{\text{ozonizer}}} = 1 - e^{-\frac{F}{V}t} \quad (E 3.32)$$

The final equation for calculating the gas phase ozone concentration in the reaction chamber is:

$$[O_3]_{\text{chamber}} = [O_3]_{\text{ozonizer}} \left(1 - e^{-\frac{Ft}{V}}\right) \quad (E 3.1)$$

The terms represent the following parameters.

$[O_3]_{\text{chamber}}$ = The concentration of gas phase ozone in the chamber

$[O_3]_{\text{ozonizer}}$ = The concentration of ozone being delivered to the chamber from the ozonizer

F = The flow rate

V = The volume of the chamber

t = Time

Item 2 *An Explanation of the Choice of Kinetic Fitting Regime for Oleic Acid Monolayers Reacting with Gas-Phase Ozone Absorbed to the Monolayer Region*

The surface coverage data in this chapter was fitted to equation 3.11. The initial point for the fit was chosen to be after the mixing time as calculated by the equations in appendix item 3.0. In a later chapter (5) for the reaction of gas-phase ozone with methyl oleate a different fitting equation was used which estimated the mixing time as part of the fit, this equation is given below.

$$-\ln\frac{\Gamma_{\text{oleic}t}}{\Gamma_{\text{oleic}t=0}} = k[O_3]_0 H\delta \left(t - \frac{V}{F} \left(1 - e^{-\frac{F}{V}t}\right)\right) \quad (E 3.33)$$

Where k and k' are related by:

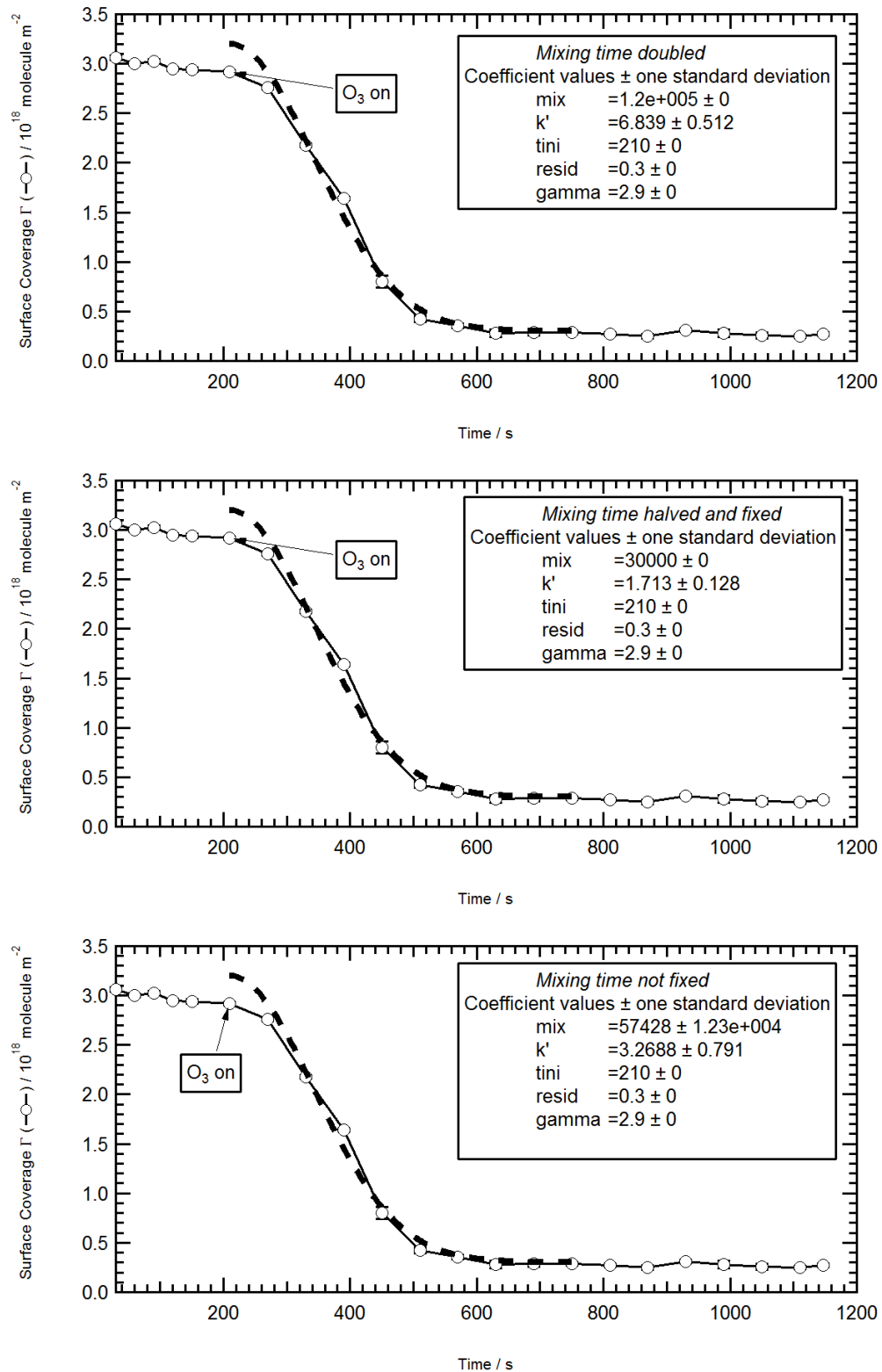
$$k' = k[O_3]_{\text{ozoniser}} H\delta$$

Item 3 *The Application of Mixing Time to the Decay of Oleic Acid Monolayers Exposed to Gas Phase Ozone*

The following figure shows why the equation with the mixing time term (E 3.33) was not used for the oleic acid monolayer reacting with gas-phase ozone. The shape of the kinetic decay in surface coverage is different for methyl oleate and for oleic acid reacting with ozone. For the oleic acid the mixing integral equation did not calculate k' effectively. The figures show that by increasing the value of the mixing term as a parameter in the fit that k' also grew, the two terms behaved in a linked manor when fitting to the oleic acid surface coverage data; this was not the case for the methyl oleate experiments.

For the reaction of oleic acid with gas-phase ozone the fit was controlled by the mixing time for the majority of the decay curve with the lower portion being controlled by k . For methyl oleate the majority of the fit was controlled by k .

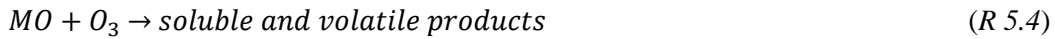
Figure 3.56 Kinetic Fitting of Equation 5.12 With Various Mixing Times For Ozone In the Reaction Chamber



Appendices to Chapter 5

Item 4 *The Derivation of the Rate Expression for a Methyl Oleate Monolayer Reacting with Gas-phase Ozone*

The reaction of a methyl oleate monolayer, MO, with gas-phase ozone, O₃, produces product molecules which are not surface active.



The following kinetic equation is formed with the kinetic variable being the surface concentration (measured surface coverage) of methyl oleate.

$$\frac{-d[\Gamma_{MO}]}{dt} = k[\Gamma_{MO}][O_3]_{chamber} \quad (E 5.18)$$

The gas-phase ozone diffuses, accommodates and dissolves into the thin organic film readily at a much faster rate than the reaction with the methyl oleate so the equation is adapted to incorporate the modelled concentration of ozone in the monolayer, [O₃]_{film}, rather than the gas-phase. The ozone concentration in the monolayer is calculated assuming a Henry's Law relationship with a general organic.

$$H = \frac{[O_3]_{chamber}}{[O_3]_{film}\delta} \quad (E 5.19)$$

Where H is the Henry's law coefficient for ozone and δ is the thickness of the monolayer, the monolayer thickness was not directly measured in the experiment. It is expected to be approximately 20 Å.

The incorporation of [O₃]_{film} results in the following kinetic equation.

$$\frac{-d[\Gamma_{MO}]}{dt} = kH\delta[\Gamma_{MO}][O_3]_{film} \quad (E 5.20)$$

The kinetic fitting to the surface coverage of methyl oleate versus reaction time will need to take into account the mixing time for the concentration of ozone within the reaction chamber to equilibrate. To do this another term is added to the rate equation above. The additional term is as explained in chapter 4 for the modelling of the concentration of gas-phase ozone in the monolayer region which took into account the mixing time in the reaction chamber.

$$[O_3]_{film} = [O_3]_{chamber}H\delta \quad (E 5.21)$$

$$[O_3]_{chamber} = [O_3]_{ozonizer} \left(1 - e^{-\frac{Ft}{V}}\right) \quad (E 5.7)$$

or

$$[O_3]_{film} = \left(1 - e^{-\frac{Ft}{V}}\right) \quad (E 5.22)$$

$$\frac{-d[\Gamma_{MO}]}{dt} = kH\delta[\Gamma_{MO}][O_3]_{ozone} \left(1 - e^{-\frac{Ft}{V}}\right) \quad (E 5.8)$$

The above equation was analytically solved by Martin King to produce a kinetic equation which could be fit to the neutron reflectivity surface coverage data in one step rather than separately modelling the ozone concentration as shown in chapter 4. The steps for solving the rate equation are given here.

The format of the rate expression was altered to the following for ease of tabulation.

$$\frac{-dy}{dx} = Ay(1 - e^{-\beta x}) \quad (E 5.23)$$

$$A = k[O_3]_{ozone}H\delta$$

$$\beta = \frac{F}{V}$$

$$x = t$$

$$y = [\Gamma_{MO}]$$

To solve the rate expression analytically the following steps were taken. The expression was substituted in terms of functions of x and y .

$$\frac{-dy}{dx} = f(x)f(y) \quad (E 5.24)$$

The above terms were integrated.

$$-\int \frac{dy}{f(y)} = \int f(x)dx \quad (E 5.25)$$

$$-\int_{y_0}^{y_t} \frac{dy}{y} = \int_0^t A(1 - e^{-\beta x})dx \quad (E 5.26)$$

$$-\int_{y_0}^{y_t} \frac{dy}{y} = A \int_0^t dx - A \int_0^t e^{-\beta x} dx \quad (E 5.27)$$

$$-[\ln y]_{y_0}^{y_t} = A[x]_0^t - \frac{A}{\beta} [e^{-\beta x}]_0^t \quad (E 5.28)$$

$$-\ln\left(\frac{y_t}{y_0}\right) = At + \frac{A}{\beta}(e^{-\beta t} - 1) \quad (E 5.29)$$

$$-\ln\left(\frac{y_t}{y_0}\right) = At + \frac{A}{\beta}(1 - e^{\beta t}) \quad (E 5.30)$$

$$-\ln\frac{r_{MO}^t}{r_{MO}^{t=0}} = k[O_3]_{ozonizer}H\delta t - \frac{-k[O_3]_{ozonizer}H\delta V}{F}\left(1 - e^{-\frac{Ft}{V}}\right) \quad (E 5.31)$$

The surface coverage data was fitted to the following equation.

$$y = \gamma\left(x - \frac{1}{\beta}(1 - e^{-\beta x})\right) \quad (E 5.32)$$

Where $\gamma = k[O_3]_{ozonizer}H\delta$ and $\beta = \frac{F}{V} = \frac{1}{\tau_{mix}}$. β was held constant during the fitting of equation 5.32 to the decay in the monolayer surface coverage versus reaction time.